

---

---

ON THE ADHESION FORCES  
OF BACTERIAL MEMBRANES  
AND DERIVATIVES

---

---

THESIS SUBMITTED TO OBTAIN THE DEGREE OF  
DOCTOR OF PHILOSOPHY

SHEFFIELD, ENGLAND  
JULY 30<sup>TH</sup>, 2014

WRITTEN BY

ANA LORENA MORALES-GARCÍA  
*Department of Physics and Astronomy*

SUPERVISED BY

PROF. MARK GEOGHEGAN  
*Department of Physics and Astronomy*

DR STEPHEN A. ROLFE  
*Department of Animal and Plant Sciences*

2014  
THE UNIVERSITY OF SHEFFIELD

# Contents

<b>Abstract</b>	<b>vi</b>
<b>Resumen</b>	<b>vii</b>
<b>Nomenclature</b>	<b>viii</b>
<b>List of Figures</b>	<b>xiv</b>
<b>List of Tables</b>	<b>xxii</b>
<b>Presentations and publications</b>	<b>xxiii</b>
<b>Acknowledgements</b>	<b>xxiv</b>
<b>1 Foreword</b>	<b>1</b>
<b>2 Background</b>	<b>6</b>
2.1 Introduction . . . . .	6
2.1.1 The Gram stain . . . . .	6
2.2 Biological perspectives of bacterial adhesion . . . . .	9
2.2.1 Biofilm formation in different species . . . . .	12

---

2.2.2	<i>Rhodococcus</i> in nature . . . . .	19
2.2.3	<i>Pseudomonas</i> in nature . . . . .	24
2.3	Conditioning film formation . . . . .	27
2.3.1	Protein adsorption to surfaces . . . . .	29
2.4	Physical perspectives of bacterial adhesion . . . . .	31
2.4.1	xDLVO forces and bacterial adhesion . . . . .	36
2.4.2	Hydrophobicity . . . . .	36
2.4.3	Factors that influence bacterial adhesion . . . . .	37
2.5	Macroscopic methods to measure bacterial surface properties . . . . .	42
2.6	Scanning force microscopy . . . . .	44
2.6.1	Introduction . . . . .	44
2.6.2	Feedback Loop . . . . .	47
2.6.3	Modes of operation . . . . .	49
2.6.4	SFM cantilevers . . . . .	51
2.6.5	Force mode . . . . .	55
2.6.6	SFM probe functionalisation . . . . .	55
<b>3</b>	<b>Bacterial immobilisation for SFM</b>	<b>64</b>
3.1	Introduction . . . . .	64
3.1.1	Imaging bacteria in air and liquid . . . . .	65
3.2	Background on immobilisation methods . . . . .	70
3.2.1	Mechanical entrapment . . . . .	70
3.2.2	Biofilm formation for immobilisation . . . . .	71
3.2.3	Polydopamine adhesives . . . . .	73
3.2.4	Electrostatic attraction . . . . .	76
3.2.5	Covalent immobilisation . . . . .	82
3.3	Immobilisation of <i>Rhodococcus</i> spp. and <i>Pseudomonas</i> spp. . . . .	86
3.3.1	General experimental protocol for bacterial growth . . . . .	86
3.3.2	Mechanical entrapment through or on filter pores . . . . .	90
3.3.3	Attachment via hydrophobic interactions . . . . .	92

---

3.3.4	Attachment via electrostatic interactions . . . . .	97
3.3.5	Adhesion enhanced by polyphenolic proteins . . . . .	106
3.3.6	Covalent immobilisation of bacteria . . . . .	109
3.4	Concluding remarks . . . . .	116
<b>4</b>	<b>Mapping the hydrophobicity of bacterial surfaces</b>	<b>119</b>
4.1	Application of CFM to the study of bacteria . . . . .	120
4.1.1	Chapter overview . . . . .	123
4.2	Experimental protocols . . . . .	124
4.2.1	Bacterial growth, substrate preparation and covalent linking	124
4.2.2	SFM cantilever functionalisation . . . . .	124
4.2.3	SFM imaging and force measurements . . . . .	127
4.3	Imaging . . . . .	130
4.3.1	Imaging <i>Pseudomonas</i> . . . . .	133
4.3.2	Imaging <i>Rhodococcus</i> . . . . .	138
4.4	Force measurements . . . . .	142
4.5	Data Analysis . . . . .	152
4.5.1	Statistical analysis . . . . .	152
4.5.2	R and finite mixture models . . . . .	155
4.5.3	Force-volume data fits . . . . .	176
4.5.4	Tip-cell interactions . . . . .	178
4.5.5	Differences between groups . . . . .	187
4.6	Heterogeneity in bacterial cell surfaces . . . . .	192
4.7	Concluding remarks . . . . .	196
4.7.1	Bacterial adhesion in context . . . . .	196
4.7.2	The chemical maps of the future . . . . .	197
4.7.3	The statistics of heterogeneity . . . . .	198
<b>5</b>	<b>DNA interactions with mineral surfaces</b>	<b>200</b>
5.1	Chapter overview . . . . .	208

---

5.2	Deoxyribonucleic acid . . . . .	209
5.3	Polymer physics of nucleic acids . . . . .	213
5.4	Single-molecule force spectroscopy . . . . .	217
5.4.1	SFM as a tool for single molecular analysis . . . . .	221
5.5	Experimental protocols . . . . .	222
5.5.1	dsDNA fragment preparation . . . . .	222
5.5.2	Cantilever functionalisation . . . . .	223
5.5.3	SFM experiments . . . . .	224
5.6	SMFS results . . . . .	227
5.6.1	WLC fitting . . . . .	228
5.6.2	Force-distance curve analysis . . . . .	245
5.7	Concluding remarks . . . . .	249
5.7.1	Future work in SMFS . . . . .	251
<b>6</b>	<b>Conclusions</b>	<b>253</b>
6.1	Future work . . . . .	262
	<b>Appendix A: Cell viability experiments</b>	<b>265</b>
	<b>Appendix B: Force-volume maps</b>	<b>269</b>
	<b>Appendix C: R code for bimodal fits</b>	<b>273</b>
	<b>Appendix D: Influence of preparation protocols</b>	<b>277</b>
	<b>Appendix E: Growth curves</b>	<b>281</b>
	<b>Appendix F: Miscellaneous force-mapping experiments</b>	<b>285</b>
	<b>Appendix G: SFM images of adhesion surfaces</b>	<b>287</b>
	<b>Bibliography</b>	<b>326</b>

## Abstract

Bacterial adhesion is a multifactorial process, an understanding of which is key in environmental bioremediation and the design of materials for medical applications. The mechanisms that govern cell adhesion must be analysed from the physics point of view in order to obtain quantitative descriptors.

The genera *Rhodococcus* and *Pseudomonas* are widely spread in nature, forming biofilms. Their adhesion was studied by means of chemical force microscopy (CFM), a technique that relies on the functionalisation of scanning force microscopy (SFM) tips.

A pre-requisite of SFM is to have the cells firmly anchored to the surface in order to obtain images and measurements in physiological conditions. A range of immobilisation approaches was attempted, concluding that covalent bonding was the ideal method to attach the studied strains.

Force-volume maps of two pseudomonads (Gram negative, hydrophilic) and two rhodococci (Gram positive, hydrophobic) were acquired using four different cantilever functionalities ( $\text{Si}_3\text{N}_4$ , Au, hydrophobic and hydrophilic self-assembled monolayers) and the results were analysed statistically and fitted using a number of Gaussian curves. The comparisons revealed that the data were highly heterogeneous and that there were small differences between the adhesion forces generated by different combinations of cantilevers and cells. Force-volume maps revealed that, on a given cell, the majority of the bacterial membrane interacted with small adhesion forces with the cantilevers and sparse nanodomains interacted with larger forces. This heterogeneity was explained in terms of biological and chemical differences on the bacterial membrane.

Extra-cellular polymeric substances (EPS) form a matrix that encases bacterial cells and promotes their adhesion to surfaces, protecting them from environmental threats. EPS in *Pseudomonas* contain extra-cellular DNA, but its role in adhesion remains poorly understood. SFM cantilevers were functionalised with DNA strands and probed against Si surfaces under a variety of solutions ( $\text{H}_2\text{O}$ ;  $\text{Na}^+$  2, 20 mM;  $\text{Ca}^{2+}$  1, 10 mM). Specific interactions between the DNA molecule and the surface were detected in a number of force curves, and were usually seen with a higher frequency in the sodium solutions, but the adhesion forces were greater under the calcium solutions. Both observations are in agreement with molecular dynamic simulations that predict a large energy barrier for the attachment and detachment of DNA under calcium (and not so great for sodium) and a bridging effect of the divalent cation between the nucleotide and the surface. It was concluded that eDNA is involved in the biofilm formation process of Pse1, which is mediated by  $\text{Ca}^{2+}$ .

## Resumen

La adhesión bacteriana es un proceso multifactorial, cuya comprensión es clave en el desarrollo de la biorremediación ambiental y en el diseño de materiales para aplicaciones médicas. Los géneros *Rhodococcus* y *Pseudomonas* se hallan ampliamente distribuidos en la naturaleza, formando biopelículas. Su adhesión ha sido estudiada por medio de la Microscopía de Fuerza Química (CFM), técnica que esta basada en la funcionalización de las sondas del Microscopio de Barrido de Fuerza (SFM). Un requisito previo a los estudios llevados a cabo en el SFM, es fijar las células firmemente a una superficie, para que estas sean estudiadas en condiciones fisiológicas. En este proyecto se aplicaron diversas técnicas de inmovilización y se concluyó que la adhesión por medio de enlaces covalentes es ideal para fijar a las especies estudiadas.

Se obtuvieron mapas de volumen de fuerzas de dos *Pseudomonas* (Gram negativas, hidrofílicas) y dos *Rhodococcus* (Gram positivas, hidrofóbicas) usando cuatro sondas diferentes ( $\text{Si}_3\text{N}_4$ , Au, y monocapas autoensambladas con terminaciones hidrofílicas e hidrofóbicas) y los resultados se analizaron estadísticamente y se modelaron usando varias funciones Gaussianas. Las comparaciones revelaron que los datos eran altamente heterogéneos y que existían pequeñas diferencias entre las fuerzas adhesivas generadas por las distintas combinaciones de sonda y cepa. Los mapas de volumen de fuerza revelaron que, en un organismo dado, la mayor parte de la membrana interactúa con poca fuerza con la sonda, mientras que ciertas nanoregiones distribuidas aleatoriamente en la membrana, interactúan con fuerzas mayores. Esta heterogeneidad se explicó en términos de diferencias químicas y biológicas en la membrana bacteriana.

Las sustancias poliméricas extra-celulares (EPS) forman una matriz que envuelve a las células bacterianas y promueve su adhesión a superficies, protegiéndolas de diversas amenazas ambientales. Las EPS en *Pseudomonas* contienen ADN extracelular, cuyo papel adhesivo aún no se comprende perfectamente. Las sondas del SFM fueron funcionalizadas con cadenas de ADN, y se hicieron interactuar con superficies de silicón en diversas soluciones ( $\text{H}_2\text{O}$ ;  $\text{Na}^+$  2, 20 mM;  $\text{Ca}^{2+}$  1, 10 mM). Interacciones específicas entre la molécula de ADN y la superficie fueron detectadas en varias curvas de fuerza, las cuales se vieron con mayor frecuencia en las soluciones sódicas, aunque las fuerzas de adhesión fueron mayores en las soluciones cálcicas. Ambas observaciones corresponden con las predicciones hechas por simulaciones moleculares, las cuales predicen una gran barrera de adsorción y desorción entre ADN y silica en soluciones de sodio, mientras que la barrera en calcio no es tan alta. Este hecho se atribuye a la formación de enlaces puente entre el nucleótido y la superficie. Se concluyó que el ADN extracelular juega un papel importante en la formación de biopelículas de Pse1, proceso que es mediado por iones divalentes.

## Nomenclature

$\alpha$	Angle between bond vectors
$\alpha$	Angle of cantilever
$\epsilon_i$	Signal at time $i$
$\epsilon_t$	Error signal
$\kappa$	Debye length
$\mu$	Bacterial growth rate
$\vec{r}_i$	Individual monomer position
$\vec{R}$	Vector sum of the position of individual monomers
$\Psi$	Surface potential
$\Sigma$	Total intensity of the SFM laser
$k_B$	Boltzmann constant
$A$	Hamaker constant
$A_\lambda$	Absorbance
$C_\infty$	Flory characteristic ratio
$d$	Cell-surface separation distance

$d$	Distance to the tip from the end of the cantilever
$E$	Young's modulus
$F_L$	Lateral deflection
$F_N$	Vertical deflection
$g_n$	Standard gravity
$k_r$	Spring constant of a rectangular cantilever
$k_v$	Spring constant of a V-shaped cantilever
$l$	Length
$L_1$	Semi-length of cantilever
$l_K$	Kuhn length
$l_p$	Persistence length
$n$	Number of bonds in a chain
$N_0$	Initial number of cells in a culture
$Q$	Quality factor
$r$	Radius of cell
$t$	Time
$t_c$	Thickness
$w$	Width
$Z_t$	$z$ -piezo position at time $t$
<b>L</b>	Langevin function
L-DOPA	L-3,4-dihydroxyphenylalanine
A	Ampere
AB	Polar acid-base interactions
Adhesion Buffer	$K_3PO_4$ , KCl, $CaCl_2$

AHLs	Acyl homoserine lactones
APTES	(3-aminopropyl)triethoxysilane
B	Bending modulus
BHI	Brain heart infusion
BM	Brownian motion
bp	Base pairs in DNA
C	Colonies
CAM	Contact angle measurements
CDF	Cumulative distribution function
CFM	Chemical force microscopy
CSH	Cell surface hydrophobicity
DDT	1-dodecanethiol
DLVO	Derjaguin Landau Verwey Overbeek theory of colloidal stability
DNA	Deoxyribonucleic acid
DNase	Deoxyribonuclease
dsDNA	Double-stranded DNA
DSP	Digital signal processor
eDNA	Extra-cellular DNA
EDTA	Ethylenediaminetetraacetic acid
EGTA	Ethylene glycol tetraacetic acid
EL	Electrostatic interactions
EM	Expectation-maximisation algorithm
EPS	Extra-cellular polymeric substances
F	Force

FD curve	Force-distance curve
FJC	Freely-jointed chain
gnDNA	Genomic DNA
HEPES	4-(2-hydroxyethyl)-1-piperazineethanesulfonic acid (a Good's buffer)
HIV	Human immunodeficiency virus
HPLC grade	Solvent suitable for high-performance liquid chromatography
InvOLS	Inverse optical lever sensitivity
IQR	Inter-quartile range
L	Contour length
LB	Luria-Bertani broth
LPS	Lipopolysaccharides
LW	Lifshitz-van der Waals interactions
M	Monolayer
MATH	Microbial adhesion to hydrocarbons
MC	Micro-colonies
MES	2-(N-morpholino)ethanesulfonic acid (a Good's buffer)
MLE	Maximum likelihood estimation
MOPS	3-(N-morpholino)propanesulfonic acid (a Good's buffer)
MUA	11-mercaptoundecanoic acid
MUL	1-mercapto-1-undecanol
N	Newtons
N	Number of cells after division
OD <sub>600</sub>	Optical density at 600 nm

---

ODT	1-octadecanethiol
PBS	Phosphate buffered saline
pdf	Probability density function
PDL	Poly-D-lysine
PEG	Polyethylene glycol
PEI	Polyethyleneamine
PID	Proportional, integral and differential terms of the control signal
pK	Negative logarithm of a chemical dissociation constant
PLL	Poly-L-lysine
PS	Polystyrene
Pse1	<i>Pseudomonas</i> strain 1
Pse2	<i>Pseudomonas</i> strain 2
PSTC	Tissue culture-treated polystyrene
PUNIAS	Protein unfolding and nano-indentation analysis software
Q	Quartz
Q1, Q2, Q3, Q4	Quartiles
QS	Quorum sensing
R2A	Reasoner's agar
Rc291	<i>Rhodococcus spp.</i> strain 291
Rc92	<i>Rhodococcus spp.</i> strain 92
SAM	Self-assembled monolayers
SFM	Scanning force microscopy
SPM	Scanning probe microscope
ssDNA	Salmon sperm DNA

STM	Scanning tunneling microscope
sulfo-NHS	N-hydroxysulfosuccinimide
SWB	Super-wide band filter
T	Absolute temperature
TE buffer	10 mM Tris and 1 mM EDTA at pH 8.0
Tris	Tris(hydroxymethyl)aminomethane
WB	Wide band filter
WLC	Worm-like chain model
x	Chain extension
xDLVO	Extended DLVO theory

## List of Figures

1.1	Relative scale of biological and chemical structures. . . . .	4
2.1	Gram positive membrane structure. . . . .	7
2.2	Gram negative membrane structure. . . . .	8
2.3	Representation of the structure of a mature <i>P. aeruginosa</i> biofilm. .	10
2.4	Biofilm formation of <i>Pseudomonas</i> Pse1 and Pse2. . . . .	14
2.5	<i>Rhodococcus ruber</i> C208 biofilm formation. . . . .	15
2.6	Biofilm formation of <i>Rhodococcus</i> spp. 291 and 92 . . . . .	16
2.7	Confocal microscopy images of <i>Rhodococcus</i> 92 and 291. . . . .	17
2.8	<i>Rhodococcus</i> cell wall membrane. . . . .	20
2.9	Mycolic acid formula. . . . .	21
2.10	Trehalose dimycolate. . . . .	21
2.11	Alginate structure. . . . .	26
2.12	Biofouling at different length and time scales. . . . .	28
2.13	Adsorption competition of two different proteins . . . . .	30
2.14	Geometry of the vdW interaction between a sphere and a plane. . .	32
2.15	Diffuse electric double layer. . . . .	33
2.16	Energy profile of the combined DLVO interactions. . . . .	34

---

2.17	Factors that influence bacterial adhesion. . . . .	38
2.18	SFM cantilever as a sphere in a spring. . . . .	45
2.19	Scanning force microscope setup. . . . .	46
2.20	SFM electronics. . . . .	48
2.21	Feedback loop for contact mode. . . . .	50
2.22	Dynamic, amplitude-modulated SFM mode. . . . .	51
2.23	Feedback loop for AC Mode. . . . .	52
2.24	Triangular cantilever geometric parameters. . . . .	53
2.25	SFM cantilever. . . . .	54
2.26	Diagram of a force-distance curve. . . . .	56
2.27	Repulsive part of a force-distance curve. . . . .	57
2.28	Attractive part of a force-distance curve. . . . .	57
2.29	Thiol SAMs grafted to Au coated tips. . . . .	59
2.30	CFM of <i>Mycobacterium bovis</i> cells. . . . .	60
2.31	SFM images and forces of <i>Rhodococcus erythropolis</i> . . . . .	61
3.1	Bacterial adhesion by cell drying. . . . .	66
3.2	SFM images of <i>E. coli</i> . . . . .	67
3.3	Force-distance curves in air and water. . . . .	68
3.4	Meniscus between a sphere and a plane. . . . .	69
3.5	Tip-sample meniscus formation. . . . .	70
3.6	Physical entrapment methods of immobilisation . . . . .	72
3.7	Byssus of <i>Mytilus edulis</i> . . . . .	74
3.8	Adhesion of DOPA to substrates . . . . .	75
3.9	Chemical formulae of L-DOPA and hydroxyproline. . . . .	76
3.10	Immobilisation of bacterial cells using polydopamine adhesives. . . . .	77
3.11	Bacterial immobilisation via electrostatic interactions. . . . .	79
3.12	Bacterial adhesion using APTES. . . . .	80
3.13	APTES layer on silicon. . . . .	81
3.14	EDC/NHS crosslinking reaction. . . . .	84

---

3.15 EDC/NHS crosslinking reaction mechanism. . . . .	85
3.16 Agar plates. . . . .	87
3.17 Bacterial growth procedure. . . . .	90
3.18 Bacterial immobilisation on polycarbonate membranes. . . . .	92
3.19 24 h Rc291 biofilm on polystyrene. . . . .	93
3.20 46 h Rc291 biofilm on polystyrene. . . . .	94
3.21 Rc291 attached to polystyrene. . . . .	95
3.22 Rc291 attached to polystyrene. . . . .	95
3.23 Rc291 attached to polystyrene. . . . .	96
3.24 Rc291 attached to polystyrene. . . . .	96
3.25 Rc291 attached to polystyrene. . . . .	97
3.26 24 h Rc291 biofilm on glass coated with APTES . . . . .	98
3.27 Rc291 attached to an APTES coated surface . . . . .	99
3.28 Rc291 attached to an APTES coated surface . . . . .	100
3.29 24 h Rc291 biofilm on glass coated with PEI. . . . .	100
3.30 Rc291 attached to PEI . . . . .	102
3.31 Rc291 attached to PEI . . . . .	102
3.32 Rc92 attached to PEI . . . . .	103
3.33 Rc291 attached to PEI . . . . .	104
3.34 Rc92 attached to PEI . . . . .	105
3.35 Rc92 attached to PEI . . . . .	105
3.36 24 h Pse2 biofilm on glass coated with Cell-Tak <sup>®</sup> . . . . .	106
3.37 Blood smear technique. . . . .	108
3.38 Bacteria attached to a Cell-Tak <sup>®</sup> coated surface . . . . .	108
3.39 Effect of EDC/NHS in cell viability after 3 h. . . . .	113
3.40 Viability of the bacterial strains, as determined via fluorescence. . .	114
3.41 <i>Pseudomonas</i> 1 imaged with a DDT-coated tip. . . . .	115
3.42 <i>Pseudomonas</i> 1 imaged with a DDT-coated tip. . . . .	116
3.43 Immobilisation methods decision chart . . . . .	118

---

4.1	Comparative adhesion forces between SAMs . . . . .	121
4.2	Diagram of an ideal SAM on Au. . . . .	126
4.3	Force-volume mode . . . . .	128
4.4	Cell and background forces. . . . .	129
4.5	Iterative mask . . . . .	130
4.6	MOPS structure . . . . .	130
4.7	Relationship between the size of the probe and bacterium. . . . .	132
4.8	Double tip effect. . . . .	132
4.9	<i>Pseudomonas</i> 1 imaged with a $\text{Si}_3\text{N}_4$ tip. . . . .	134
4.10	<i>Pseudomonas</i> 1 imaged with an Au tip. . . . .	134
4.11	<i>Pseudomonas</i> 1 imaged with a DDT tip . . . . .	135
4.12	<i>Pseudomonas</i> 1 imaged with a DDT tip . . . . .	135
4.13	<i>Pseudomonas</i> 1 imaged with a MUA tip . . . . .	136
4.14	<i>Pseudomonas</i> 2 imaged with a $\text{Si}_3\text{N}_4$ tip. . . . .	136
4.15	<i>Pseudomonas</i> 2 imaged with an Au tip. . . . .	137
4.16	<i>Pseudomonas</i> 2 imaged with a DDT tip. . . . .	137
4.17	<i>Rhodococcus</i> 291 imaged with a $\text{Si}_3\text{N}_4$ tip. . . . .	139
4.18	<i>Rhodococcus</i> 291 imaged with an Au tip. . . . .	139
4.19	<i>Rhodococcus</i> 291 imaged with a MUA tip. . . . .	140
4.20	<i>Rhodococcus</i> 92 imaged with a $\text{Si}_3\text{N}_4$ tip. . . . .	140
4.21	<i>Rhodococcus</i> 92 imaged with a $\text{Si}_3\text{N}_4$ tip. . . . .	141
4.22	<i>Rhodococcus</i> 92 imaged with a DDT tip. . . . .	141
4.23	<i>Rhodococcus</i> 92 imaged with a MUA tip. . . . .	142
4.24	Pse1 mapped with a $\text{Si}_3\text{N}_4$ tip. . . . .	143
4.25	Pse1 mapped with a $\text{Si}_3\text{N}_4$ tip. . . . .	143
4.26	Pse1 mapped with a $\text{Si}_3\text{N}_4$ tip. . . . .	144
4.27	Pse1 mapped with a $\text{Si}_3\text{N}_4$ tip. . . . .	144
4.28	Pse1 mapped with an Au tip. . . . .	145
4.29	Pse1 mapped with an Au tip. . . . .	145

4.30 Pse1 mapped with an Au tip. . . . .	146
4.31 Pse1 mapped with a DDT tip. . . . .	146
4.32 Pse1 mapped with a DDT tip. . . . .	147
4.33 Pse1 mapped with a DDT tip. . . . .	147
4.34 Pse1 mapped with a MUA tip. . . . .	148
4.35 Pse1 mapped with a MUA tip. . . . .	148
4.36 MUA-MUA and MUA-Si control experiments . . . . .	149
4.37 Adhesion forces for MUA/MUA and MUA/Si interactions . . . . .	150
4.38 DDT-DDT and DDT-Si control experiments . . . . .	151
4.39 Adhesion forces for DDT/DDT and DDT/Si interactions . . . . .	152
4.40 Bimodal adhesion histograms . . . . .	154
4.41 Gaussian pdfs generated using R . . . . .	156
4.42 Two and twenty five mixture models . . . . .	159
4.43 Histogram fitted with two Gaussian curves . . . . .	160
4.44 Means and deviations of Si <sub>3</sub> N <sub>4</sub> log forces . . . . .	164
4.45 Means and deviations of Au log forces . . . . .	164
4.46 Means and deviations of DDT log forces . . . . .	165
4.47 Means and deviations of MUA log forces . . . . .	165
4.48 Means of the mixture components of Pse1 . . . . .	166
4.49 Means of the mixture components of Pse2 . . . . .	166
4.50 Means of the mixture components of Rc92 . . . . .	167
4.51 Means of the mixture components of Rc291 . . . . .	167
4.52 Collection of force-volume maps of Pse1 with a Si <sub>3</sub> N <sub>4</sub> tip . . . . .	170
4.53 Colour-coded maps of Pse1 probed with Au . . . . .	171
4.54 Colour-coded maps of Pse1 probed with MUA . . . . .	172
4.55 Colour-coded maps of Pse2 probed with MUA . . . . .	173
4.56 Colour-coded maps of Rc92 probed with MUA . . . . .	174
4.57 Colour-coded maps of Rc291 probed with Au . . . . .	175
4.58 Bimodal fits for five Pse1 cells with a Si <sub>3</sub> N <sub>4</sub> tip. . . . .	176

---

4.59	Bimodal fits for five Pse1 cells with an Au tip. . . . .	177
4.60	Bimodal fits for five Pse1 cells with a DDT tip. . . . .	177
4.61	Bimodal fits for five Pse1 cells with an MUA tip. . . . .	178
4.62	Typical defects found in SAMs . . . . .	179
4.63	Molecular interactions between the tip and the surface . . . . .	181
4.64	Potential energy profile for the tip-sample interaction . . . . .	183
4.65	Interaction between a CFM tip and bacterial exopolymers . . . . .	184
4.66	Rc291 and Au force interactions . . . . .	184
4.67	Force-distance curve of a Pse1 cell, using a silicon nitride probe. . .	185
4.68	Pse1 force-distance curve . . . . .	186
4.69	Pse1 extension curves . . . . .	186
4.70	Comparative adhesion forces of Pse1 cells with Si <sub>3</sub> N <sub>4</sub> tips . . . . .	188
4.71	Comparative adhesion forces of Pse1 cells with Au tips . . . . .	188
4.72	Comparative adhesion forces of Pse1 cells with DDT tips . . . . .	188
4.73	Comparative adhesion forces of Pse1 cells with MUA tips . . . . .	189
4.74	Enhanced adhesion with Au-coated cantilevers . . . . .	192
4.75	Interaction between a bacterium and a surface . . . . .	194
4.76	Sources of bacterial heterogeneity . . . . .	195
5.1	Growth of Pse1 with and without DNase . . . . .	202
5.2	<i>Pseudomonas</i> biofilms treated with DNase . . . . .	204
5.3	Pse1 attachment to fused quartz silica with and without DNase . .	205
5.4	Influence of DNA sources and sizes on cell adhesion . . . . .	206
5.5	Pse1 attachment under different Ca <sup>2+</sup> concentrations . . . . .	207
5.6	Structure of nucleotides . . . . .	210
5.7	Location and interaction between base pairs . . . . .	211
5.8	B-DNA Structure . . . . .	212
5.9	Polymer chain models . . . . .	215
5.10	Azimuthal rotation of bonds . . . . .	217
5.11	DNA studies using optical tweezers . . . . .	219

---

5.12	DNA studies using magnetic tweezers . . . . .	220
5.13	Force resolution of SMFS techniques . . . . .	220
5.14	Thiolation reaction . . . . .	223
5.15	DNA-functionalised cantilever . . . . .	224
5.16	Typical areas in the retraction part of a force-distance curve. . . . .	226
5.17	Force distance curve of DNA functionalised tip . . . . .	228
5.18	DNA force experiments under water . . . . .	229
5.19	DNA force experiments under electrolytes . . . . .	230
5.20	Contour lengths in water . . . . .	232
5.21	Contour lengths in $\text{Na}^+$ 2 mM . . . . .	233
5.22	Contour lengths in $\text{Na}^+$ 20 mM . . . . .	233
5.23	Contour lengths in $\text{Ca}^{2+}$ 1 mM . . . . .	234
5.24	Contour lengths in $\text{Ca}^{2+}$ 10 mM . . . . .	234
5.25	Scatter plot of forces in water . . . . .	235
5.26	Scatter plot of forces in sodium solutions . . . . .	235
5.27	Scatter plot of forces in calcium solutions . . . . .	236
5.28	Z-density for the system in calcium, without DNA. . . . .	237
5.29	Molecular dynamics simulations in $\text{Ca}^{2+}$ . . . . .	238
5.30	Energy configurations for DNA in $\text{Ca}^{2+}$ . . . . .	239
5.31	Z-density for the system in sodium, without DNA. . . . .	240
5.32	Molecular dynamic simulations in $\text{Na}^+$ . . . . .	241
5.33	Energy configurations for DNA in $\text{Na}^+$ . . . . .	242
5.34	Contour lengths . . . . .	244
5.35	Molecular conformation during polymer detachment . . . . .	246
5.36	Molecular conformation during polymer detachment (Continuation)	247
6.1	Effect of EDC/NHS in cell viability after 6 h. . . . .	266
6.2	Cell viability after 3 h of washing in PBS. . . . .	267
6.3	Cell viability after 6 h of washing in PBS. . . . .	268
6.4	Force-volume maps of Pse2 . . . . .	270

---

6.5	Force-volume maps of Rc92 . . . . .	271
6.6	Force-volume maps of Rc291 . . . . .	272
6.7	Contact angle measurements as a function of the washing medium .	279
6.8	Contact angle measurements . . . . .	280
6.9	Typical bacterial growth curve appearance. . . . .	282
6.10	Growth curve of <i>Pseudomonas</i> Pse1 . . . . .	283
6.11	Growth curve of <i>Pseudomonas</i> Pse2 . . . . .	283
6.12	Growth curve of <i>Rhodococcus</i> Rc92 . . . . .	284
6.13	Growth curve of <i>Rhodococcus</i> Rc291 . . . . .	284
6.14	<i>Rhodococcus</i> 291 imaged with a Si <sub>3</sub> N <sub>4</sub> tip. . . . .	286
6.15	Rc291 adhesion forces in water . . . . .	286
6.16	PEI surface. . . . .	287
6.17	APTES surface. . . . .	288

## List of Tables

2.1	Taxonomy of <i>Rhodococcus</i> . . . . .	18
2.2	Taxonomy of <i>Pseudomonas</i> . . . . .	24
2.3	MATH scores of the studied strains. . . . .	43
3.1	Composition of R2A agar. . . . .	88
3.2	Composition of AB10 medium. . . . .	89
3.3	Cell viability experiments using BacLight®. . . . .	112
4.1	Adhesion forces with hydrophobic and hydrophilic tips (Vadillo) . .	122
4.2	Adhesion forces with hydrophobic and hydrophilic tips (Dorobantu)	123
4.3	Statistical descriptors of mixture model fits . . . . .	162
4.4	Statistical descriptors of mixture model fits (Cont.) . . . . .	163
4.5	Median values of adhesion in <i>Pseudomonas</i> . . . . .	191
4.6	Median values of adhesion in <i>Rhodococcus</i> . . . . .	191
5.1	Percentage of occurrence of multiple peaks . . . . .	227
5.2	Retraction profiles occurrence . . . . .	248

## Presentations and publications

The contents of this thesis were presented at the following conferences:

- **Morales-García, A.L.**, SFM studies of bacterial cell walls. Oral presentation, XI Symposium of Mexican Students and Studies in UK 2013, Sheffield, UK.
- **Morales-García, A.L.**, Walton, R., Rolfe, S.A. and Geoghegan, M. SFM study of bacterial cell walls. Poster presented at PhysCell 2012, Hyères, France and Annual SFM User Meeting 2012, Louvain-la-Neuve, Belgium.
- **Morales-García, A.L.**, Hall, A.R., Althagafi, T., Rolfe, S. and Geoghegan, M. SFM study of bacterial cell walls. Oral presentation, 8th EBSA European Biophysics Congress, Budapest, Hungary; *Eur. Biophys. J.* 2011, **40** (Suppl. 1), S151, abstract O-430.
- **Morales-García, A.L.**, Kailas, L., Andrews, J.S., Rolfe, S.R., Hobbs, J.K. and Geoghegan, M. Mapping the Hydrophobicity of Bacterial Cell Surfaces. Poster presented at Nanomeasure 2010, Krakow, Poland (Best poster award); Physics Meets Biology 2010, Oxford, UK; Physical Aspects of Polymer Physics, Bristol, UK, 2009; INASCON 2009, Sursee, Switzerland.

The contents of this thesis will be included in the following publications:

- Pen, Y., Zhang, Z., **Morales-García, A.L.**, Mears, M., Tarmey, D., Edyvean, R.G., Banwart, S.A. and Geoghegan, M. “Conformational and mechanical properties of rhodococcal extracellular polymeric substances” (Manuscript in review).
- Walton, R., Freeman, C.L., **Morales-García, A.L.** Harding, J., Rolfe, S.A., Geoghegan, M. and Banwart, S.A., “The Role of Extracellular DNA in Cellular Adhesion to Silica” (Manuscript in preparation).

## Acknowledgements

*Success consists of going from  
failure to failure without the loss  
of enthusiasm*

---

*Winston Churchill*

This thesis encompasses more than four years of intense work, happy productive days, and often, disappointing ones. Now that I stand almost at the end of this journey, it is a time reflect back to the course of my PhD and remember all the people who helped me succeed in my endeavours.

Firstly I would like to express my sincere thanks to my supervisors, Prof. Mark Geoghegan and Dr Steve Rolfe. Thanks a lot Mark, for believing in me and in this project. Your kind words always inspired me and motivated me to keep trying, despite all the adversities. Thanks a lot, Steve, for all your support in the lab and with the analysis of the data. You always had a very different perspective on my experiments, which enriched this thesis substantially. Thank you both for your continued interest on this project and for making my PhD an experience of growth and personal development.

Thanks to Prof. Cameron Alexander (School of Pharmacy of the University of Nottingham) and to Prof. Catherine Biggs (ChELSI, Chemical and Biological Engineering, The University of Sheffield) for having reviewed this thesis and for your helpful comments in the viva. This document was vastly improved after a careful consideration of all your comments.

I would also like to thank all the members (past and present) of the Polymer Physics group, from whom I learnt a great deal of experimental techniques and who shared their wisdom without restriction. My appreciation goes to Dr Rhoda Hawkins, Dr Ateyyah Al-Baradi, Dr Maryam Raftari, Youmna Mouhamad, Dr Yu Pen, Chris Clarkson, Sarah Canning, Dr Mike Weir, Latifah Alfaid, Masaharu Ibaragi, Tom Kennelly, Dr Andrew Dennison, Dr Andy Parnell, Dr Rita La Spina, Dr Parvaneh Mokarian-Tabari, Dr Tao Wang, Fabio Pontecchiani and Alessandra Petrolì. Special thanks go to Dr Zhenyu (Jason) Zhang, Dr Matt Mears and Dr Rachel Walton, who played a key role in this learning process and helped me develop all the experiments on this thesis. My appreciation also goes to Amy Hall, who has always been there to share my joys and problems. Thanks for being my friend!

My recognition also goes to all the members (past and present) of the SPM group, who were always there to help me with diverse technical issues. Thanks to Prof. Jamie Hobbs, Dr Becca Savage, Dr Christa Weber, Dr Lekshmi Kailas, Dr Ehtsham-ul-Haq, Dr Tsvetelin Vasilev, Paul Chapman, Jonathan Burns, Nusrat Sajid and my lovely flatmate, Elisa Laera. Special thanks go to Ross Carter, Jake Albon and Dr Nic Mullin for all the helpful discussions, and for putting their work aside to assist me in my moments of need.

My sincere thanks to all the people in the Department of Animal and Plant Sciences, Molecular Biology and Biotechnology and the Medical School, who made this project possible. Thanks to Maggi Killion, Jody Smith, Nichola Price, Irene Johnson, Malcolm Crookes, J. J. Potter, Dr Dave Johnson, Dr Asuka Kuwabara, Dr Rodrigo Echevoyén, Dr Robert Malinowski, Serina Akhtar, Alex McFarlane, Dr Robert Turner, Dr Gemma Montagut, Dr Lorena Preciado and Dr Jesús Pérez. I would also like to acknowledge Esther J. Karunakaran from Chemical and Biological Engineering for her helpful advice about contact angle determination.

In the Chemistry Department I would like to thank Prof. Graham Leggett, for kindly providing the facilities for gold evaporation and to Ali Johnson for technical help in the lab. I would also like to extend my sincere thanks to Lara James and Dr Peter Portius, for their help with the APTES purification and to Prof. Charles Stirling, for his support with my outreach projects.

In the Kroto Research Centre, I would like to thank Prof. Steve Banwart, Dr Colin Freeman, Dr Wei Wang, Dr Maria Romero, Dr Johanna Andrews, Dr Jesus Ojeda, Dr Harry Langford, Dr Dayi Zhang, Dr Hamid Pouran, Prof. Sir Harry Kroto and Lady Margaret Kroto.

I would also like to thank the members of the nanobiophysics group at the Université catholique de Louvain, namely Prof. Yves Dufrêne, Dr David Alsteens, Dr Audrey Beaussart, Dr Sofiane El Kirat and Prachi Tripathi for allowing me to

visit their labs in Belgium and sharing their knowledge and experiences with me. I am also grateful to Dr Drew Tarmey in the Medical School of the University of Nottingham, for his valuable input in the development of some of my experimental protocols.

Special thanks for Dr Philippe Carl for having made the software PUNIAS adequate to analyse my data, and for his continuous support during the past year.

I would also like to thank all the people at the Sheffield International College, who supported me during the course of my PhD, specially Carolyn Gibbs, Richard Davies, Kevin Smith and Susan Handford-Styring.

It is also important to acknowledge all the people that day to day made my PhD experience an unforgettable one. Thanks to all the members of the Physics and Astronomy Department in which I have found very valuable friendships. Thanks to Chris Rosslowe, Darren White, Emile Doran, Rikki Coles, John Quilter, Dr Daniel Sercombe, Dr Saida Caballero, Patricia Bessiere, Dave Sahman, Dr David Hubber, Dr Krisada Rawiraswattana, Liam Hardy, Stefan Schwarz, Richard Webb, Dr Stathes Paganis and Dr Tim Richardson (†). Special thanks to Jad and Robert, who accompanied me in every experiment.

I thank CONACyT for their continuous financial support to my studies, since my BSc years working in research in Chemistry, my MSc in Nanotechnology and the PhD project that I am presenting in this thesis.

Furthermore, I would like to dedicate this thesis to all the people back at home in Mexico, which have supported me all my life and made it possible for me to be here, almost at the end of my studies. Gracias Papá por haberme enseñado la importancia del conocimiento desde una temprana edad. Gracias Ma por tu esfuerzo diario, sin tí no estaría donde estoy yo. Gracias Nu por cuidar tan bien de todos allá en casa. Espero que algún día tu también puedas conocer el mundo. Gracias a mis abis y abuelitos por su cariño y apoyo, y aunque algunos de ustedes ya falten, siempre estarán en mi corazón. Gracias al Dr. Oscar Suárez y a la Dra. Myriam Meléndez por haberme impulsado a continuar con el doctorado. A Marisol López por tu amistad y a J. R., mi amor por siempre.

Last, but not least, I would like to thank my beloved boy, Rik Bailey, who has supported me a lot during the experimental and writing-up process, and has proof-read this thesis (and perhaps even, these acknowledgements). Thanks a lot for helping me achieve my goals, I could not have done it without you. My success is yours as well!. Extended thanks go to his family, Kevin, Wendy and Nicky, for making me feel at home here, where I am so far away from home.

The following thesis deals with the study of bacteria and bacterial product adhesion. Why bacteria? As Sebastian Amyes' excellent introduction to this subject [1] states in its introductory lines: we are, and we have always lived, in the "Age of Bacteria". Bacteria are the most successful and numerous of all organisms that have lived on Earth. Their biomass surpasses that of the rest of the living organisms combined. Even within our body, the number of bacterial cells exceeds the number of human cells. Bacteria are adaptable organisms that can be found in every environment, even the most inhospitable, like the barren Atacama desert soil, volcanic vents and the bottom of Antarctic lakes. It is thought that they will be the last survivors on Earth, billions of years from now, where the life supporting characteristics of our Sun change (i.e. it leaves its main sequence), and the weather becomes too extreme for us to inhabit the Earth [2].

As exotic and appealing as they might sound, the present thesis does not deal with extremophiles or post-apocalyptic organisms, but with two almost omnipresent and versatile species, namely *Rhodococcus spp.* and *Pseudomonas spp.* The adhesive characteristics of their membranes will be studied by means of scanning force microscopy (SFM), with the aim of complementing our current knowledge of the molecular basis of their adhesion and ultimately design surfaces with increased (or decreased) preference for bacterial cells, that could be used for a variety of applications.

The study of bacterial surfaces is of prime importance in the understanding of their adhesion to mineral substrates and living tissues. Bacteria have a selective advantage while attached to surfaces and are well adapted to life in a sessile form [3]. Bacterial adhesion finds its biggest impact in medicine, pharmaceutical sciences, biotechnology and environmental bioremediation. Due to the nature of the interactions between the outermost layers of these organisms and the surfaces

encountered in nature, it is necessary to employ state of the art biophysical techniques to help us elucidate the molecular mechanisms of these cellular processes.

Bacterial adhesion is paramount in medicine for a variety of reasons. Among them we can highlight the interaction of pathogenic bacteria with living mammalian cells and the adherence of pathogens to medical devices and implants. Biofilm formation poses a threat to patients that suffer from very diverse ailments. Biofilm is the term given to a number of microorganisms embedded in a polysaccharide matrix, an association that protects them against environmental threats, making it more difficult to eradicate them. It has been estimated that around 80% of the microbial infections in the human body have their roots in a microbial consortium or biofilm [4]. More will be said about the importance of biofilm formation and the mechanisms of this process in Section 2.2.

Bacterial adhesion is also central to environmental studies. Sessile microbes are capable of catalytically transforming chemical compounds containing C,H,O,N and dissolving minerals containing Fe [5], Mn, Ni, Zn and Cu [6], thus being key in biogeochemical cycles. Falkowski *et al.* deems microorganisms as the “biogeochemical engineers of life” because during the early history of our planet Earth, microbes largely drove the chemical speciation of elements on the planet’s crust, enabling the evolution of more complicated life forms through their red-ox machinery [7]. Environmental engineers have exploited the adaptable metabolism of bacteria and used it in soil bioremediation and industrial manufacture processes [8]. More will be said about the application of rhodococci and pseudomonads in Section 2.2.

Bacterial interactions are mediated by the cell wall polymers, which nature spans across many different types of chemical compounds. Examples include extra-cellular polysaccharides, surface proteins, lipopolysaccharides, fimbriae and lipoteichoic acids. The particular characteristics and ratios of these constituents depend on the growth stage of the cells and the particular genus of bacteria. One obvious distinction is the division between Gram positive and Gram negative bacteria (§2.1.1) [9]. A comparison between these two types of bacteria is therefore interesting, and having as many examples as possible of biologically distinct types of bacteria enhances our current knowledge about the relationship between membrane structure and adhesive properties. Furthermore, the more it is discovered about the attachment of diverse strains of bacteria to varied surfaces, the more will be known about the *basic* mechanisms of bacterial adhesion. The fact that there is a myriad of attachment strategies in the microbial world appears to make the problem of the understanding of these mechanisms, frankly overwhelming. It is only logical to assume that the more data are gathered and assimilated, the more tools there are to construct the framework of bacterial adhesion. Based on this, it was decided to select the Gram negative strains *Pseudomonas* 1 and *Pseudomonas*

2 and the Gram positive strains *Rhodococcus* 92 and *Rhodococcus* 291. In Sections 2.2.2 and 2.2.3 the nature and uses of these strains will be revised.

Cell surface physicochemical properties, such as electrical potential and hydrophobicity, are thought to direct the degree of adhesion between the organisms and surfaces. Traditionally, these properties have been estimated using macroscopic methods, like zeta potentials and bacterial contact angles (§2.5). Through these techniques, average measurements of a consortium of thousands of cells can be obtained. Nonetheless, microbial cell surfaces are highly heterogeneous and furthermore, the individuals may differ considerably, even when they belong to the same colony. With the advent of scanning force microscopy (SFM) in the mid-eighties, and its application to microbiological surfaces, now it is possible to image and probe not only individual cells, but specific areas of the cell membrane.

Scanning force microscopy (§2.6) can assess the contribution of the different physicochemical properties to bacterial adhesion. Since the attachment of cells to surfaces is mediated by specific and non-specific forces, the molecular organisation of the interfaces and the nature of the surrounding solvent, play a key role in the strength of these interactions (§2.4). In order to understand this phenomenon, a technique called chemical force microscopy (CFM) (§2.6.6), was developed [10]. Chemically modified tips are mounted on the high precision machinery of the SFM. The well characterised surfaces of the chemically modified probes, enable the microscope to also become a tool for molecular recognition. The well-defined chemistry of the SFM probe, with hydrophilic and hydrophobic groups, targets specific interactions between the selected molecules, and the surface of the bacterial cells, which also have hydrophobic and hydrophilic components all throughout their cell walls. Chemical force microscopy was used to investigate the interaction forces between hydrophobic and hydrophilic tips, as well as control silicon nitride ( $\text{Si}_3\text{N}_4$ ) and gold (Au) tips, versus the rhodococci and pseudomonads. These experiments are explained in Chapter 4.

The SFM is capable of obtaining high resolution images of bacterial cells in air and in physiological conditions (Chapter 3), thus being able to obtain topographic maps of cell surfaces with nanoscale resolution (Figure 1.1). From a biologist's perspective, this technique is more advantageous than electron microscopies, because live organisms can be studied, and damaging mounting techniques can be avoided. Nonetheless, imaging cells in liquid is a very challenging technique, because the cells need to withstand the lateral dragging forces exerted by the microscope tip, and amplified by the surrounding liquid. Several attempts to immobilise bacterial cells are detailed in Chapter 3 and a collection of images of cells belonging to the aforementioned strains will be presented in this chapter.

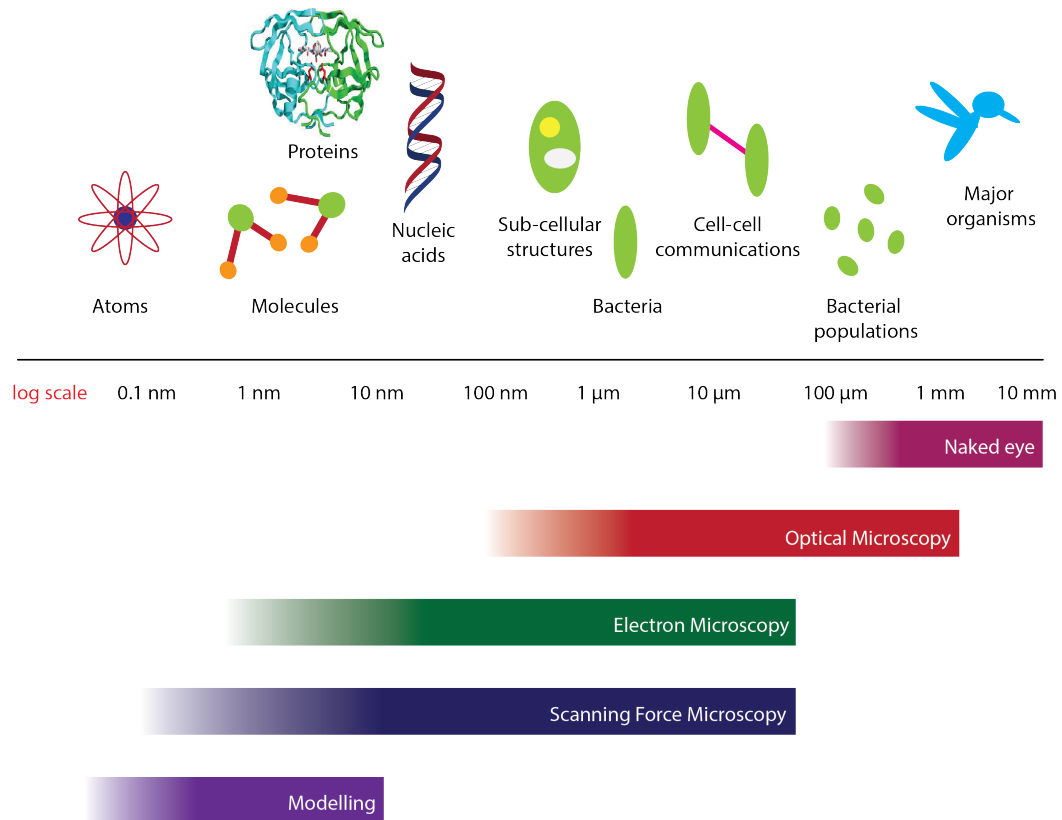


**Figure 1.1:** The relative scale of chemical and biological structures and processes alongside the experimental techniques used to study these phenomena. Although light microscopy is useful in cell counting and identification, the nanoscale realm remains beyond its scope. With electron and scanning force microscopies, the study of sub-cellular structures and cell-membrane details has advanced immeasurably. Still, atomic and molecular behaviour are better studied with the aid of computational modelling. The present thesis, although based on SFM, makes use of optical techniques and aims to relate the experimental findings to current mathematical models. The advance of science will undoubtedly be seen as a seamless integration of these techniques, joined for a common end.

For some species, like *Pseudomonas*, extra-cellular DNA (eDNA) is an important component of the EPS matrix. eDNA is directly involved in the adhesion of *Pseudomonas* to surfaces. It has been seen that in *Pseudomonas* Pse1, the addition of the enzyme deoxyribonuclease (DNase), which hydrolyses the DNA present in the extra-cellular matrix, promotes the detachment of *Pseudomonas* cells from a fused quartz slide [11]. Moreover, it has been found that eDNA is not different from chromosomal DNA [12], although the mechanism of its production remains unclear. Several bacterial species, like *Pseudomonas* have an evolutionary advantage, as they have learned to use this nucleotide to enhance their adhesion to surfaces. Even though polysaccharides are the most common adhesives for bacteria [13], it is known that they can also use lipids, proteins and nucleic acids [12]. Since eDNA seems to interact with an adhesive surface in a similar way in which other exo-polymers do, it became interesting to investigate the adhesion of individual strands of DNA with mineral surfaces. That is why gold coated SFM cantilevers were functionalised with thiolated DNA and were probed against silicon surfaces under a variety of ionic solutions. The results of these experiments are presented in Chapter 5.

The cell membrane and the extra-cellular polymers that encase the microbe are the elements in contact with the external environment, determining its adhesive properties. Consequently, it is interesting to perform measurements that are representative of the natural environment [14]. However, it is common to prepare and clean the cells before the analysis, in order to get rid of unwanted debris and contaminants introduced by the growth media. The standard sample preparation for SFM studies involves several cycles of centrifugation of the bacterial cells and washing the obtained bacterial pellet with a buffer, saline solution or pure water. Some authors [15, 16] claim that the delicate nature of the microbial cell surface can be damaged through the preparation techniques, making it difficult to extrapolate the experiences witnessed in a laboratory with the actual natural processes of adhesion. Based on the assumption that the preparation methods could be affecting the quantity or quality of the EPS layer, it was decided to assess this loss and the viability of the bacterial cells through contact angle experiments for *Rhodococcus* 291. The results of these analyses will be exposed in Appendix D.

## 2.1 Introduction

This introductory chapter will deal with the biological and physical aspects of bacterial adhesion and the different existing methodologies that assess the degree of attachment of bacterial cells to surfaces. A brief portrayal of biofilm formation will be included, emphasising the existing differences between the biofilms produced by *Pseudomonas* and *Rhodococcus* species. Some details about the biology, uses, and pathogenicity of these bacteria will be explained.

Later on, this review will analyse the physical models that are often applied to describe the attachment of bacterial cells to surfaces, like thermodynamic and colloidal approaches.

This chapter will finish with a description of experimental techniques that relate the biological behaviour of the cells to the framework of the physical models. These techniques will include macroscopic methods, like contact angle and microbial adhesion to hydrocarbons, and microscopic methods, like scanning force microscopy, to study the topography and behaviour of single organisms.

### 2.1.1 The Gram stain

This literature review will start by explaining some key distinctions between Gram negative and Gram positive bacteria, since the present thesis deals with organisms that belong to both categories.

In the 1880's, the Danish scientist Hans Christian Gram, while studying bacterial colonies attached to lung samples, devised a method to visualise bacteria more

easily, by staining them with crystal violet. He observed that after washing some samples with ethanol, the organisms retained the violet dye, whereas in others the dye faded away with the treatment. At that time, the results of this study were not appreciated or understood, and it took several years to realise that the differential uptake of the crystal violet dye was related to a fundamental difference between the cells. Even though H. C. Gram did not design this staining protocol to distinguish between different classes of cells, nowadays the Gram stain is a typical and widely used method, used to classify bacteria according to the properties of their cell walls [17].

Those organisms that retain the purple dye are known as Gram positive bacteria. They have thick peptidoglycan layers, rich in lipoteichoic acids or lipoglycans. Lipoteichoic acids predominate in the Firmicutes lineage (e.g. *Bacillus spp.*, *Streptococcus spp.* and *Staphylococcus spp.*), whereas lipoglycans predominate in Mollicutes and Actinobacteria (e.g. *Rhodococcus spp.*) A cross section of the Gram positive cell wall is depicted in Figure 2.1.

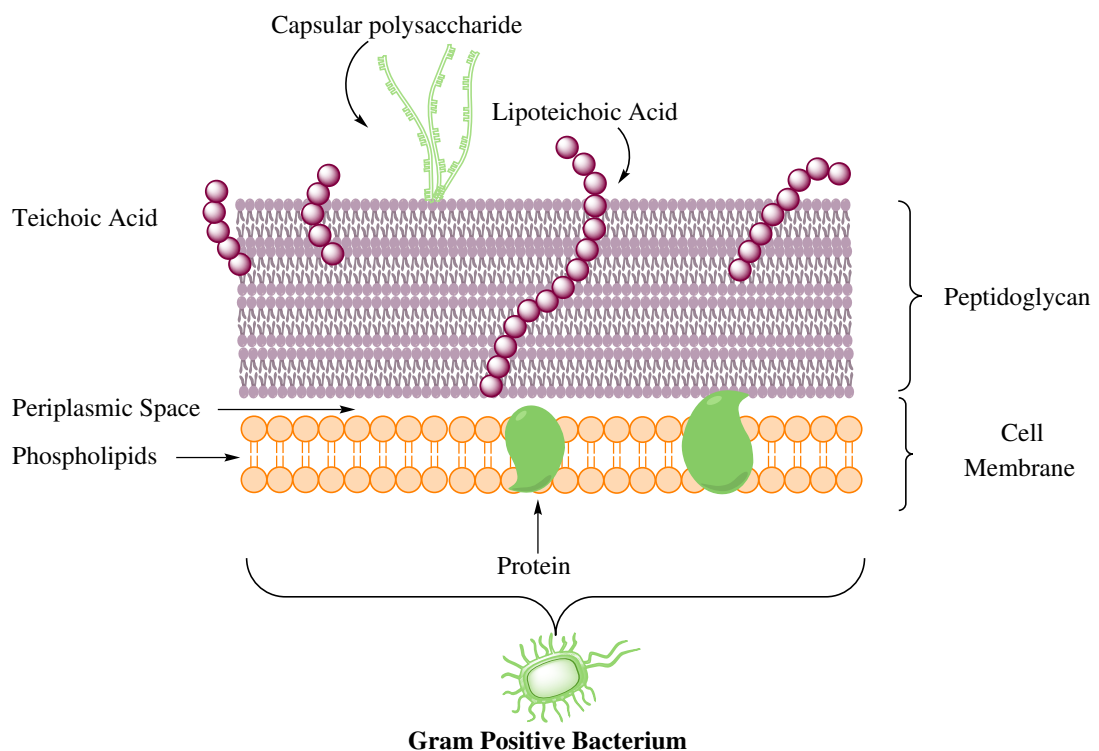


**Figure 2.1:** Example of the structure of a Gram positive membrane. n.b. Not all Gram positive cells have lipoteichoic acids, some have lipoglycans instead. Similarly, teichoic acids are not present in all the Gram positive species.

The organisms that do not retain the crystal violet during the Gram stain, are said to be Gram negative. After the crystal violet has been washed away with ethanol or acetone, the cells appear colourless, thus being difficult to visualise. To improve visibility, a counterstain, like safranin is added, making the cells red or pink. Gram negative cells have a much thinner peptidoglycan layer, as compared to Gram positive cells. They possess a more complicated cell structure that includes inner and outer membranes, separated by the periplasmic space. The outer membrane contains lipopolysaccharides (LPS) in the outer region and phospholipids in the inner region. Lipoproteins can be found attached to a polysaccharide backbone. In addition, porins can be found, which are barrel proteins that allow passive diffusion of molecules. In Gram negative cells, no lipoteichoic acids or lipoglycans are present. Common examples of this type of cells are *Haemophilus influenzae*, *Vibrio cholerae*, *Escherichia coli* and *Pseudomonas aeruginosa*. Details of the cell wall of this organisms can be seen in Figure 2.2.

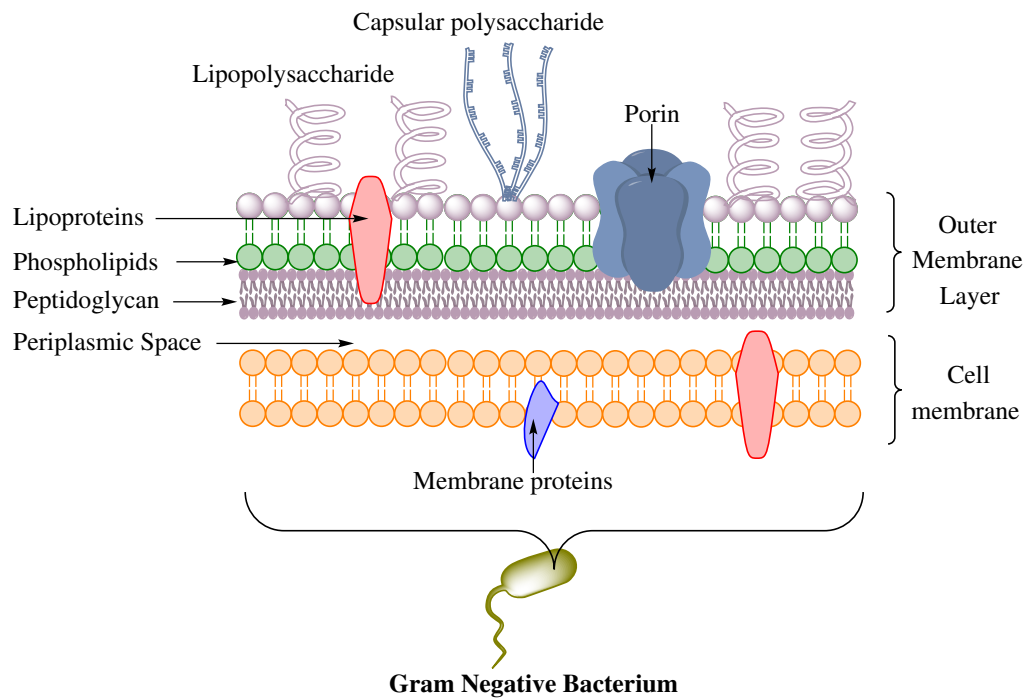


**Figure 2.2:** Gram negative membrane structure.

The present thesis deals with the study of the Gram negative organisms *Pseudomonas* Pse1 and Pse2, and the Gram positive bacteria *Rhodococcus* spp. Rc92 and Rc291. Particular details about the biology of these microbes can be found in Sections 2.2.2 and 2.2.3.

## 2.2 Biological perspectives of bacterial adhesion

For most of the history of microbiology, microorganisms have been thought of as free floating, planktonic organisms, growing independently from each other in a suspended form. However, microbes accumulate at surfaces and interfaces forming conglomerates known as biofilms. Biofilms can be defined simply and broadly as communities of microorganisms that are attached to a surface, by means of a matrix composed by water and biopolymers. A concerted effort to study microbial biofilms began only few decades ago with the discovery that, in natural aquatic systems, bacteria are found predominately attached to surfaces [18].

In the first half of the XX century, Heukelekian and Heller found that the metabolic activities of marine microorganisms were improved when they were attached to surfaces, enabling bacteria to grow in situations where otherwise nutrients are too dilute for them to assimilate [19]. Some years later, ZoBell reinforced this idea by discovering that there were many more microorganisms attached to solid surfaces than floating freely in marine environments [20].

The term biofilm was first introduced by Costerton in 1978 [21], and since then, the presence of biofilms has been identified in many natural environments, where nutrients and surfaces are available. Biofilms comprise organisms that differ from their planktonic counterparts in terms of the genes that they transcribe. Their association to the biofilm confers them an increased protection against environmental stresses. This mode of life is so successful that it has been estimated that over 99% of microorganisms on Earth can be found within the confines of a biofilm [22].

In most biofilms, the microbes account for less than 10% of the total mass of the biofilm. The rest is made of a nutrient rich matrix known as extra-cellular polymeric substances (EPS). The EPS matrix supports the life of a bacterial community and plays a wide variety of roles. This slime keeps the cells together, and the close proximity between them allows intercellular communication, in the form of exchange of genetic information and quorum sensing (i.e. ability of bacteria to sense the cell density in the vicinity, through the accumulation of signalling molecules). The biofilm matrix is also very rich in nutrients and enzymes, that can be utilised by the members of the community.

Inside a biofilm, often a very complex architecture can be found, giving mechanical stability to the conglomerate, and thus being able to resist shear forces in flowing water environments. The matrix will also protect against external threats, like antibiotics, phagocytosis, and disinfectants [23].

The mechanism of bacterial biofilm formation can be exemplified by describing one of the most studied surface-associated organisms, *Pseudomonas aeruginosa* [18]. Figure 2.3, shows the mechanism in which biofilms are formed in an aquatic environment. The cycle starts with free swimming cells (Figure 2.3a)

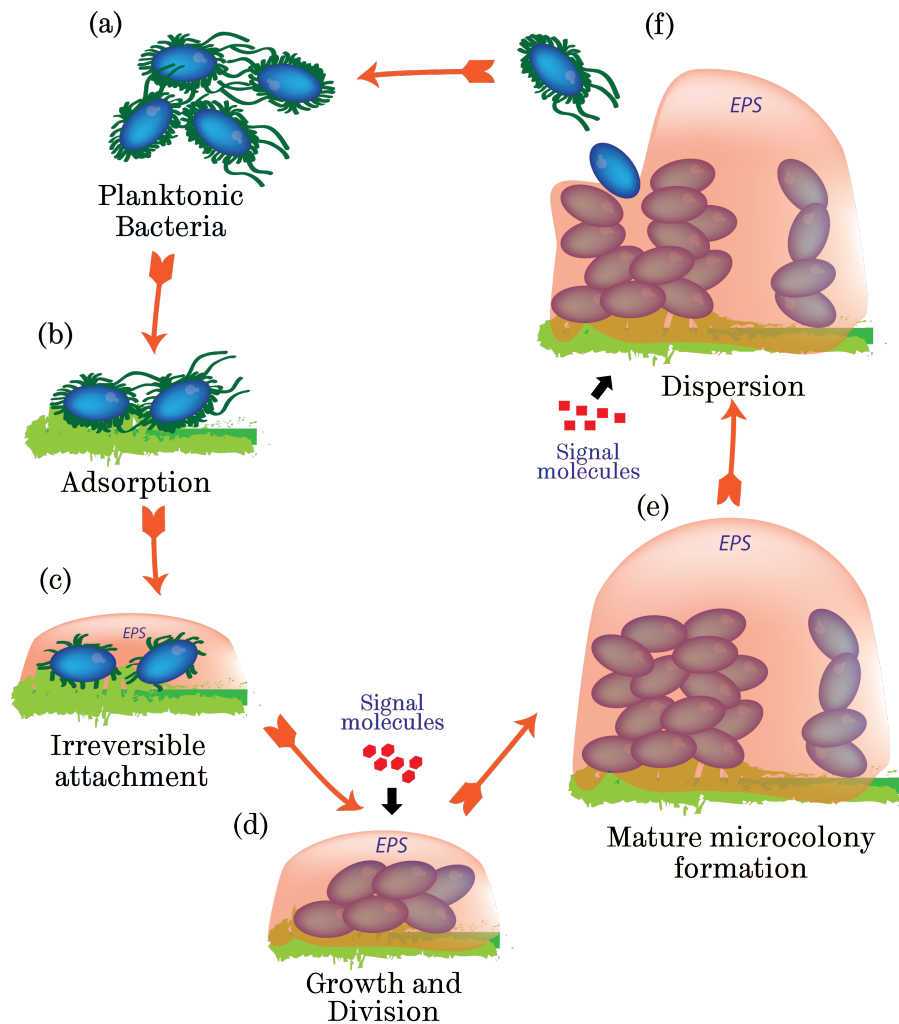


**Figure 2.3:** Representation of the structure of a mature *P. aeruginosa* biofilm. The mature biofilm comprises mushroom-shaped micro-colonies of bacteria that are surrounded by an extra-cellular polysaccharide matrix and separated by fluid-filled channels [18].

swarming towards a solid surface, triggered by certain environmental cues, like a high concentration of nutrients in the surrounding medium. The cells will then mobilise, aided by their flagella, Brownian motion or a chemotactic process, towards

the surface. This surface might not be bare, but coated in organic compounds and conditioned for the reception of the cells. It is known that carbohydrate-coated substrates facilitate the attachment of marine microbes to surfaces, and that salivary films promote the attachment of oral bacteria to glass slides [24]. When the cells approach, their motility is reduced and their surface polymers establish a temporary contact with the substrate. This step is known as *docking* or *secondary minimum adhesion* (Figure 2.3b).

The cells are now physically adsorbed to the surface and are able to roll, creep and move laterally aided by their appendages, or they might even resume their planktonic life. The adhesion is only consolidated when they get very close to the surface and they overcome electrostatic repulsions; microbes bear normally negative charges and mineral surfaces often also possess a negative charge. This repulsion might be overcome by specific molecular interactions, and be aided by the appendages, which have a different chemical composition, shifting the equilibrium towards adhesion.

In this attached form, the bacteria will creep laterally, aided by either their flagella or pili, until they find more cells to form a microcolony. At this point they will begin to exude a slime or EPS. This viscoelastic matrix will surround the cells and consolidate the adhesion process. The cells are now irreversibly bound to a surface through a series of steps known as *locking* or *primary minimum adhesion* (Figure 2.3c). At this point the cells are clustered together, in close proximity with each other and with the surface, and they start to establish specific receptor-ligand bonds with the material. Some studies suggest that while undergoing permanent attachment to the surface, the cells start a physiological transformation that enables them to settle in a place where they are not free floating any more, but they have close contact with many neighbours. They differentiate into an associated form, expressing large quantities of exopolysaccharides and repressing the synthesis of flagella, to create a more stable biofilm (Figure 2.3d).

Once the micro-colony is formed, the bacteria start to grow in a three dimensional fashion, until they reach structural maturity, a process that can take many days. A mature biofilm has a complex architecture that includes channels and pores, in which water, ions, nutrients and signalling molecules, circulate. There is an optimum flow through the channels that allows the perfusion of substances rather than the erosion of the matrix (Figure 2.3e). It has been through the advancement of confocal microscopy that it has been possible to elucidate the three dimensional structure of biofilms.

A biofilm is not a motionless pile of attached cells, but a dynamic microbial community, where many dynamic processes occur, like enzymatic reactions, genetic exchange, accumulation of substances, red-ox reactions, signalling and chemotactic

processes, due to gradients of pH,  $pO_2$  and nutrients. The nature of the cells inside the biofilm is heterogeneous; while the cells on the surface are more exposed to oxygen, the cells in the centre might even switch to an anaerobic mode of growth.

The presence of an EPS layer is very advantageous for survival, because it protects the cells against ultraviolet radiation, antibiotics and other external threats. It also modifies the biodegradative capabilities and the production of metabolites.

When the environment ceases to support the biofilm, due to a scarcity of nutrients or excess of waste, the bacteria will respond to the detachment signals, and the equilibrium will shift in favour of dispersal. The outermost layer begins to generate planktonic organisms, which once again will switch on the genes responsible for the alteration of their phenotype, to be in optimal conditions for a free floating life (Figure 2.3f).

The signals that lead to the detachment of cells need to be studied in more detail. Starvation is thought to be the major cause for the detachment of cells to the planktonic form, but other signals might also influence the dispersal of the biofilm. For instance, in *P. aeruginosa* the overexpression of the enzyme alginate lyase triggers detachment. In *P. fluorescens*, the quantity of EPS is reduced after extended periods of time, leading to a slow dispersal of the biofilm [18].

The aforementioned process is applicable to the formation of biofilms in water-saturated or aquatic systems. Biofilm formation where the presence of water is transient, like in soils or mineral surfaces, will vary from this description [25].

## 2.2.1 Biofilm formation in different species

### Biofilm formation in *Pseudomonas*

Not all bacteria will form biofilms on the same conditions and with the same ease; whereas strains like *P. aeruginosa* and *P. fluorescens* readily associate to surfaces, even in the scarcity of nutrients, species like *E. coli* K-12 and *V. cholerae*, do not form a biofilm in a minimum medium, unless supplemented with amino acids. Conversely, the *E. coli* O517:H7 strain, which is widely studied due to its pathogenicity, only associates to surfaces when the nutritional content of the media is minimum [18]. It is clear that the study of biofilm formation needs to take into account the biology of the organism, as well as the environmental factors.

Diverse studies of *P. aeruginosa* have shown that their attachment is dependent on their flagella and type-IV or motile pili [26,27]. The attachment can also vary according to the nature of the lipopolysaccharides (LPS). *P. aeruginosa* makes two types of LPS, named A and B band structures. Makin and Beveridge [28]

showed that mutants defective in the B band of the LPS preferentially adhere to hydrophobic substrates, and their predilection for hydrophilic surfaces is reduced.

It has been seen that pseudomonads scan the surface, looking for an appropriate anchoring point. Once the cell is attached, it will continue to propel itself on the surface, aided by its type-IV pili in a twitching fashion. The twitching motility leads to the formation of the initial micro-colonies, when many cells congregate in an optimal location. Once the cells are attached, their gene expression changes. In *P. aeruginosa*, the synthesis of the exopolysaccharide alginate is up-regulated five times more in sessile organisms compared to their planktonic counterparts [18,29].

In *P. fluorescens* attachment proteins seem to play a key role in biofilm formation; it has been seen that adding proteases triggers the detachment of cells from the film and that the protein synthesis is needed in the early stages of biofilm formation [26].

*Pseudomonas putida* biofilms are very sensitive to starvation signals, quickly dispersing in response to global carbon deprivation. In the rhizosphere (i.e. the soil zone surrounding the roots of plants), the natural habitat of these bacteria, the ability to quickly rearrange in response to a change in the environmental conditions is beneficial, as bacteria can efficiently reach better niches. The adhesion in this pseudomonad is controlled by a regulatory protein which is necessary for biofilm formation in this strain. [30]. Confocal microscopy studies of biofilm formation in *P. putida* reveal that during the early stages of biofilm formation single cells and micro-colonies dominate the surface. After 24 h, small and irregular micro-colonies transform into neatly arranged circular colonies, which during the following days extend vertically to form pillars. After 48 h, about 80% of the available surface has been covered [31].

Andrews *et al.* [24] studied the biofilm formation behaviour of *Pseudomonas* Pse1 and Pse2 on polystyrene, tissue culture-treated polystyrene and quartz, which are substrates that have a different value of hydrophobicity. In Figure 2.4 it can be appreciated that Pse1 adheres to surfaces considerably more than Pse2; Pse1 adheres primarily to hydrophobic polystyrene. Pse1 is hydrophilic (MATH score, adherence to n-decane of 17.53%), and Pse2 is more hydrophobic (MATH score, adherence to n-decane of 33.13%) so it is clear that hydrophobicity does not relate to adhesion to substrates in every case. Raman spectroscopy showed multiple peaks associated with the presence of nucleic acids for the sessile organisms, and these peaks had increased with respect to their planktonic counterparts, suggesting that DNA might play a role in biofilm formation. More on the role of extra-cellular DNA in the biofilm forming abilities of *Pseudomonas* species will be said in Chapter 5.

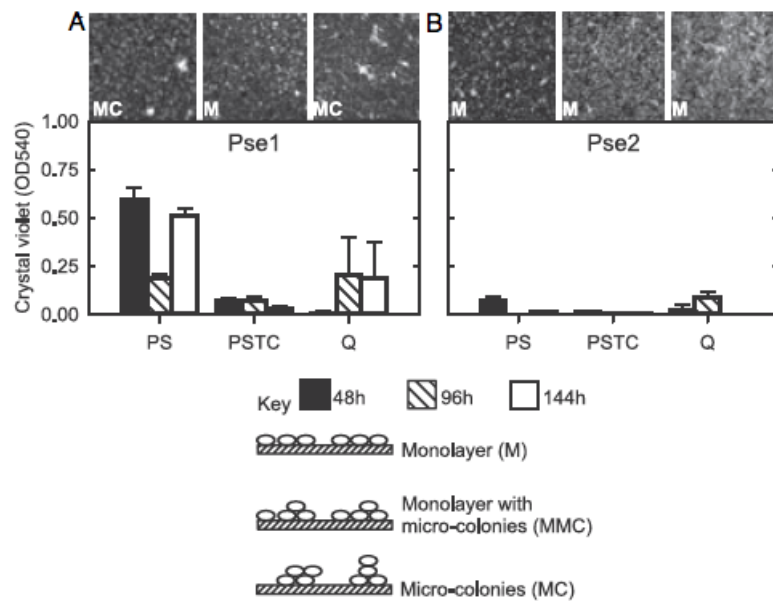


**Figure 2.4:** Attachment of *Pseudomonas* Pse1 and Pse2 to three surfaces with different hydrophobicities. Cells were grown for 48, 96 and 144 h in 96-well plates made of PS: polystyrene, PSTC: tissue culture-treated polystyrene and Q: quartz. The cells were grown at 20 °C in AB10 medium with 2 mM glucose as a carbon source. The graphs show the retention of crystal violet, and the micrographs are confocal microscopy images of the biofilms dyed with SYTO9 at 96 h of growth. The colony morphology is indicated as M: monolayer, MC: micro-colonies and C: colonies. Image adapted with permission of [24]. Copyright (2010) John Wiley and Sons.

### Biofilm formation in *Rhodococcus*

According to Sivan *et al.* [32], the biofilm architecture of Rhodococcal biofilms is not that different from the model that has already been explained for *Pseudomonas aeruginosa*. *R. ruber* has been seen to form three dimensional, mushroom-shaped colonies on polyethylene after a few hours of incubation. In this experiment, the plastic polyethylene was used not only as a substrate, but also as a carbon source, yielding a complex biofilm in less than 24 h. The biofilm extra-cellular matrix was rich in polysaccharides and proteins; the former had a maximum concentration after 20 days of incubation, whereas the latter peaked at 10 days. The viability of the cells was monitored for these experiments, showing that even after 60 days of incubation the majority of the cells were alive. The cells were highly hydrophobic, and it is thought that they increased hydrophobicity in response to starvation signals, and to enhance their attachment to the surface. The bacteria degraded

the polyethylene at a rate of 0.86% per week, making this strain a valuable tool for plastic biodegradation in natural environments (Figure 2.5).

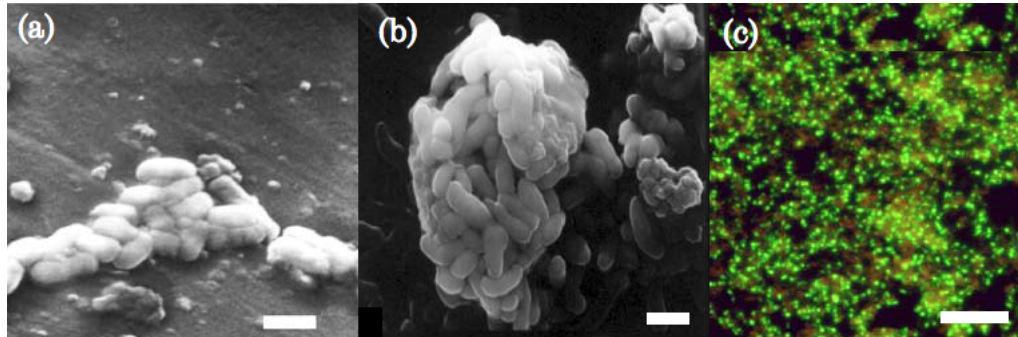


**Figure 2.5:** *Rhodococcus ruber* C208 biofilm formation on a polyethylene surface. (a) Micro-colonies formed on polyethylene after 8 h incubation. Scale bar = 1  $\mu\text{m}$  (b) Mature biofilm after 20 h of incubation, showing a mushroom shaped pillar. Scale bar = 1  $\mu\text{m}$ . (c) Biofilm after 60 days of incubation, stained with SYTO9/propidium iodide, Live/Dead BacLight<sup>®</sup> incubation kit. The green cells are alive, and the red cells are dead. Scale bar = 5  $\mu\text{m}$ . Images adapted with permission of [32]. Copyright (2006) Springer .

Andrews *et al.* [24] studied the formation of biofilms of *Rhodococcus spp.* 92 and 291 on polystyrene, tissue culture-treated polystyrene and quartz, substrates selected due to their differences in hydrophobicity. These bacteria were obtained from polluted aquifers, and the surfaces were selected for their hydrophobic and electrostatic properties, with the aim to understand potential properties of rock-forming minerals, which are the principal habitats of bacterial cells in groundwater systems. As seen in Figure 2.6, Rc291 attached to surfaces more substantially than Rc92. Rc291 showed an increased preference to hydrophobic polystyrene.

Van Loosdrecht *et al.* [33] pointed out that bacterial adhesion is controlled by the hydrophobic interactions between the surface of bacterial cells and their substratum. Since rhodococci are hydrophobic organisms, due to their mycolic acid rich cell wall, and hydrophobic bacteria tend to adhere to hydrophobic materials [34, 35], it was thought that a difference in hydrophobicity might explain the differential behaviour of these two strains. The hydrophobicity of Rc92 and Rc291 was measured using the MATH score (microbial adhesion to hydrocarbons), partitioning the bacterial cells between an aqueous phase and n-decane. Rc291 (76.9% adherence to n-decane) was somewhat more hydrophobic than Rc92 (47.9% adherence to n-decane) [36]. Such a difference cannot account for the very dissimilar behaviour in the presence of polystyrene.

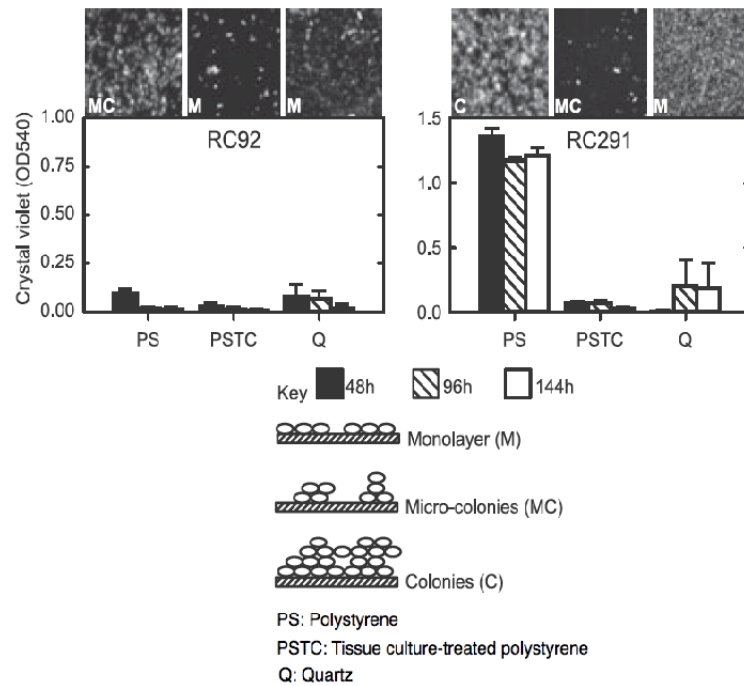


**Figure 2.6:** Attachment of *Rhodococcus* spp. 92 and 291 to three surfaces with different hydrophobicities. Cells were grown for 48, 96 and 144 h in 96-well plates made of PS: polystyrene, PSTC: tissue culture-treated polystyrene and Q: quartz. The cells were grown at 20 °C in AB10 medium with 2 mM glucose as a carbon source. The graphs show the retention of crystal violet, and the micrographs are confocal microscopy images of the biofilms dyed with SYTO9 at 96 h of growth. The colony morphology is indicated as M: monolayer, MC: micro-colonies and C: colonies. Image adapted with permission of [24]. Copyright (2010) John Wiley and Sons.

With the aim of understanding the role of lipophilic compounds on the attachment of these two strains and to visualise hydrophobic compounds, the stain Nile Red was used. Nile Red fluoresces in red in the presence of polar lipids, and fluoresces yellow with non-polar lipids. Confocal images of the biofilms formed by Rc92 and Rc291 and stained by Nile Red, and the nucleic acid stain SYTO9 are shown in Figure 2.7.

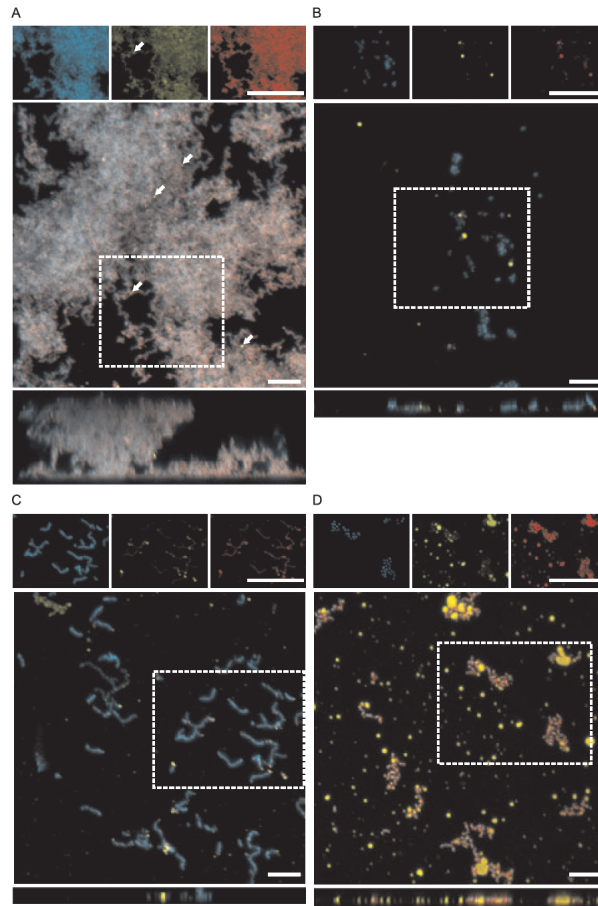


**Figure 2.7:** Confocal microscopy images of *Rhodococcus* 92 and 291. Images A and B show biofilm and planktonic cells, respectively, of Rc291. Images C and D show biofilm and planktonic cells, respectively, of Rc92. The images were acquired after 96 h of incubation. The insets on top of the colour composites show, from left to right, the individual emission channels as follows: the cyan inset shows the DNA stained with SYTO9. The yellow inset shows the non-polar lipids, stained with Nile Red. The red inset shows the polar lipids, stained with Nile Red. The arrows in A show non-polar lipids enriched regions. Scale bars: 10  $\mu\text{m}$ . Image adapted with permission of [24]. Copyright (2010) John Wiley and Sons.

<b>Taxonomy of <i>Rhodococcus</i></b>	
Kingdom	Bacteria
Phylum	Actinobacteria
Order	Actinomycetales
Suborder	Corynebacterineae
Family	Nocardiaceae
Genus	<i>Rhodococcus</i>
Strains	92, 291

**Common species:** *R. equi*, *R. erythropolis*, *R. fascians*, *R. globerulus*, *R. luteus*, *R. maris*, *R. opacus*, *R. rhodochrous*, *R. ruber*

**Table 2.1:** Taxonomy of *Rhodococcus*.

Rc291 formed extensive biofilms on polystyrene which included 20–30  $\mu\text{m}$  pillars of cells (Figure 2.7a). The Nile Red stain revealed that both types of lipids are closely associated to the surfaces, and only few regions are predominantly rich in non-polar lipids, as shown by the arrows. Figure 2.7b, shows the Rc291 planktonic cells appearing as small clusters with few regions of non-polar lipids.

Rc92 (Figure 2.7c) showed little biofilm formation, with the cells appearing as long chains. These chains have areas of non-polar lipids in one of their ends. On the other hand, it is possible to appreciate the striking difference with the planktonic cells depicted in Figure 2.7d: the cells are surrounded by large amounts of lipophilic material and yellow clusters of non-polar lipids.

Figure 2.7 proves that despite having the two strains similar hydrophobicity, they produce distinct lipophilic materials that are associated to the cells in different manners. This seems to influence their biofilm forming behaviour. Rc291, which has both polar and non-polar lipids closely associated, attaches extensively to surfaces and to other bacterial cells. Rc92, on the other hand, produces vast amounts of these lipids, but they are released into the medium as they are not tightly associated. This facilitates the formation of clusters in suspension and avoiding their attachment to the polystyrene surface. Raman spectroscopy of the bacterial cells supports the idea that the strains produce different types of lipids, which also varied markedly between sessile and free floating cells.

## 2.2.2 *Rhodococcus* in nature

Rhodococci are nocardioform actinomycetes, non-motile, aerobic organisms generally found in either a coccoid or short rod form. They are Gram positive bacteria and as such their cell wall is characterised by an outer thick peptidoglycan layer abundant in lipoglycans (e.g. lipoarabinomannan) that covers the cell membrane. Lipoglycans are amphiphatic lipids with a neutral polysaccharide core and a negatively charged lipid anchor. The taxonomical description of *Rhodococcus* can be found in Table 2.1 and a diagram of their cell wall in Figure 2.8.

*Rhodococcus* also belong to the suprageneric bacterial group *Mycolata*, which is characterised by the presence of mycolic or  $\alpha$  - branched-  $\beta$  - hydroxylated fatty acids in the cell walls. These aliphatic long chain molecules (depicted in Figure 2.9) are, in most cases, the ones that confer hydrophobicity to the cells, providing them with low permeability to hydrophilic biocides and a superb protection against dehydration and environmental injuries.

The cell envelope of *Rhodococcus* is made up of mycolic acids connected to arabinogalactan moieties; these cell wall polysaccharides are covalently attached to peptidoglycan on their other end. The outer cell wall of rhodococci bears surfactant groups, like trehalose dimycolate, which confer them assimilatory capabilities (Figure 2.8).

The peptidoglycan is A1 $\gamma$  type (i.e. the peptides are directly crosslinked with the mesodiaminopimelic acid) and the arabinogalactan is linked to the peptidoglycan by an L-rhamnose-D-N-acetylglucosamine phosphate. Proteins are also anchored to the peptidoglycan.

The mycolic acid-arabinogalactan-peptidoglycan assembly confer special characteristics to *Rhodococcus* and other mycolata [39]. The size and branching of the mycolic acids differs with the species, growth stage and conditions of culturing [35, 38, 40]. Mycolic acids of *Rhodococcus* typically have lengths of 28–54 carbons in total. The side alkyl chain is typically saturated, spanning from 10 to 16 carbons, whereas the main meromycolate chain is typically longer, having up to four unsaturation sites (Figure 2.9).

*Rhodococcus* species are known to produce trehalose-containing glycolipid biosurfactants (Figure 2.10), which reduce the surface tension of water and allow the permeabilisation of the lipid barrier, for the uptake of long chain hydrocarbons by the bacterial cell [41]. The type and quantity of these surfactants depend on the growth conditions and the carbon source. Their role has been primarily associated with the pseudo-solubilisation of alkanes, for them to be used as carbon sources, but also are known to be released into the culture medium, modifying the cell surface hydrophobicity of the cells, and enhancing their attachment to hydrocar-

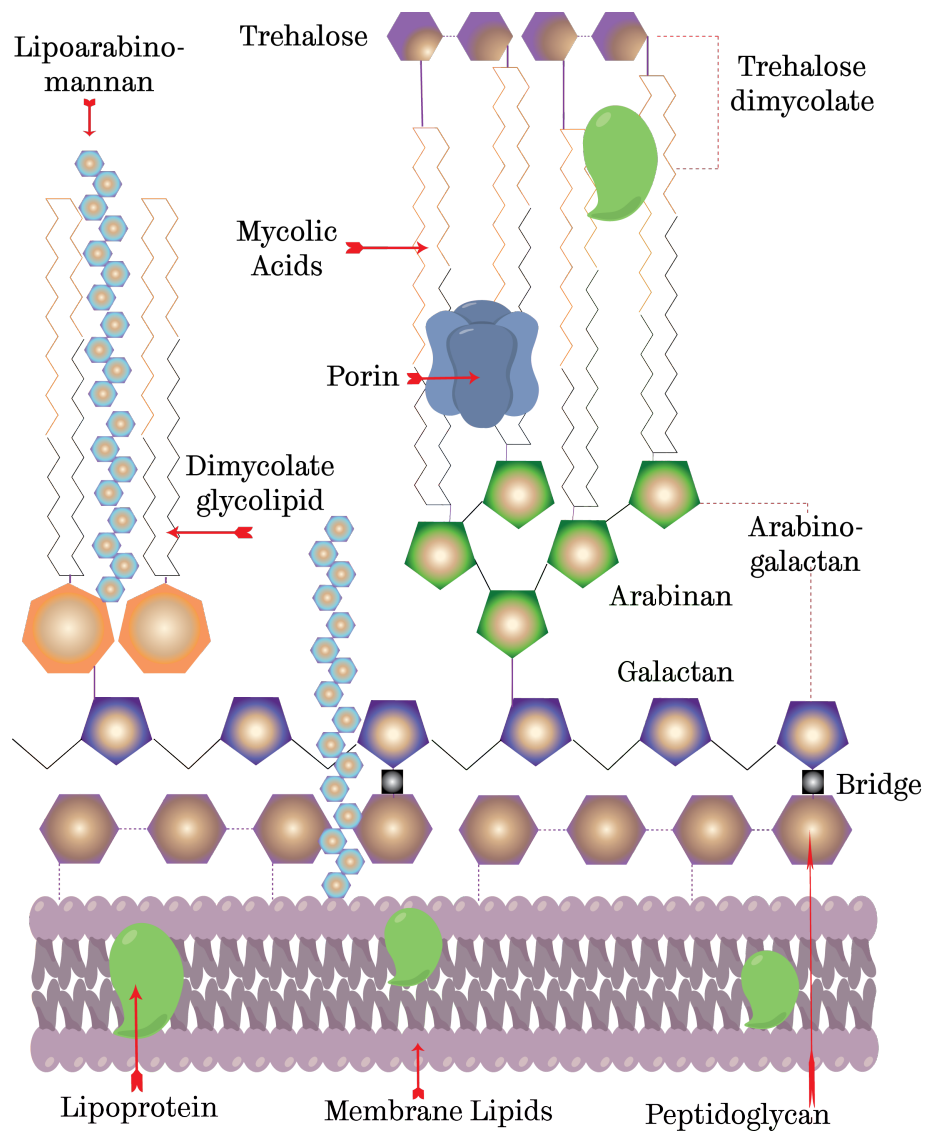


**Figure 2.8:** *Rhodococcus* cell wall membrane. The squares labelled as *bridge* represent the L-rhamnose-D-N-acetylglucosamine phosphate bonds. Image inspired from references [37,38].

bons. The trehalose dimycolates themselves, have found application in the fields of medicine, bioremediation and industry [42–46].

The rhodococcal cell wall also has non-covalently linked elements embedded on the cell walls, like porins, lipoglycans and lipoproteins, among others (See details in Figure 2.8). Channel forming porins allow the accumulation of hydrophilic

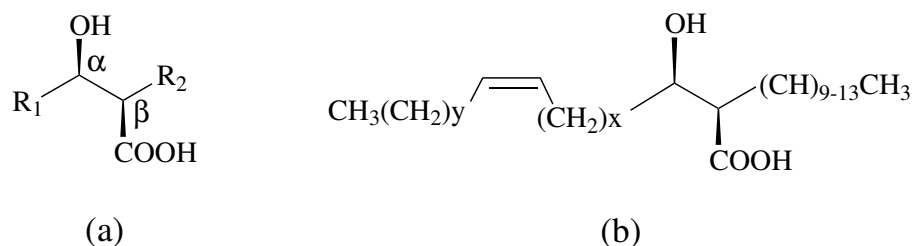


**Figure 2.9:** General formula of a mycolic acid (b) Mycolic acid present in *R. erythropolis*.  $x + y = 18 - 40$  carbons [37].

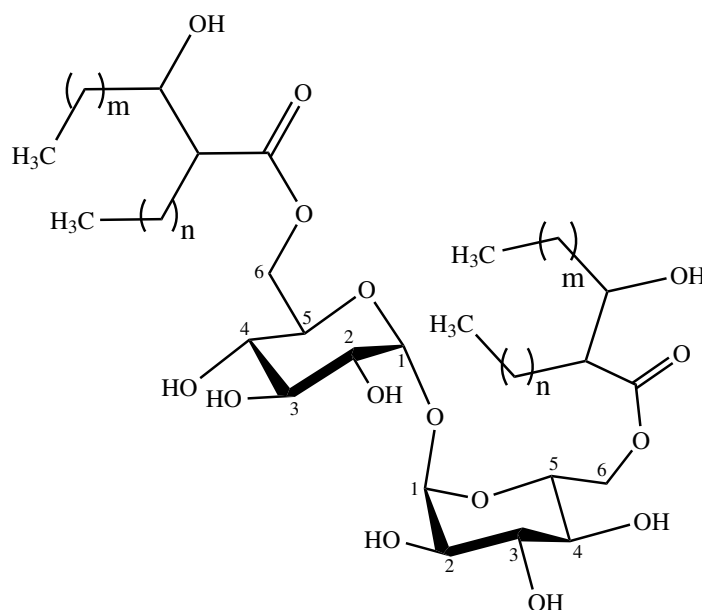


**Figure 2.10:** Trehalose dimycolate present in *R. erythropolis*.  $m+n = 27-31$  [47].

solutes that need to cross the lipid permeability barrier. *Rhodococcus* organisms have lipoglycans, in the form of lipoarabinomannan, whose role has been related to the optimal growth of the cells. Lipoproteins can also be found embedded into the inner cell wall or associated to the outer wall. They are related to mechanisms of transportation and red-ox reactivity of the cell.

The genus *Rhodococcus* is widespread in nature and includes species capable of metabolising a vast range of hydrophobic compounds, such as aromatic and aliphatic hydrocarbons, heterocyclic compounds, nitriles, herbicides, chlorinated phenolic compounds, lignin, coal and petroleum, among others. This is why bio-

processing systems employ *Rhodococcus* for several environmental applications. The ability to degrade this wide variety of compounds is due to the chemical armamentarium that this organism is equipped with, like enzymes (e.g. steroid ring opening enzymes [48] and dechlorination proteins [49] to name a couple) and surface active glycolipids [42]. *Rhodococcus* is therefore regarded as one of the most promising organisms in bioremediation [43], microbial enhanced oil recovery [50] and a useful aid in chemical synthesis in industry [51].

On the other hand, some members of this genus are known to be opportunistic pathogens for animals, plants and humans. Of special importance is *Rhodococcus equi*, which causes pneumonia in horses, goats and pigs. Other veterinary conditions associated to these bacteria are enteritis, lymphadenitis and abortion. It can also infect immunodeficient humans such as HIV patients, causing pulmonary infections, peritonitis and skin infections [52].

In waste-water treatment plants, the genus *Rhodococcus* is partly responsible for foaming and scum formation, which affect the proper functioning of the water tanks [35]. The cell surface hydrophobicity and filamentous growth of this genus are responsible for the formation of very stable foams that increase operating costs and reduce the performance of these plants. Similarly, it has been seen that in the presence of hydrocarbons, the colonies of *Rhodococcus* undergo colony morphotype changes that have been associated with the formation of scum [34, 53]. It is vital to understand the role of cell surface hydrophobicity and the effects of growth conditions, in order to develop the best control strategy and maximise the remediation output [35, 54, 55].

Diverse colony morphotypes have been observed for *Rhodococcus*. Iwabuchi *et al.* [53] investigated the distinction between rough and smooth colonies. Rough colonies show an increased preference for surface adhesion. They are normally hydrophobic (more than 70° in the contact angle measurement (CAM)) organisms, which adhere to liquid hydrocarbons as well as hydrophobic (Teflon, 108° CAM) and hydrophilic surfaces (Quartz, 30° CAM). Mucoidal strains are hydrophilic (25–45° CAM) and prefer to stay in suspension and produce EPS with hydrophilic characteristics. The authors found that the overproduction or addition of EPS to rough hydrophobic *Rhodococcus* strains hindered the attachment of the cells to surfaces. They hypothesise that this process might be relevant in natural environments, where the temporal overproduction of EPS hinders the adhesion to substrates and translocates the cells to more favourable niches [53].

The fact that in some cases EPS seem to aid the bacterial attachment to surfaces, and in some case hinder it, might be due to the fact that a loose terminology is used in the description of the extra-cellular substances; they can vary substantially in composition, hydrophobicity and degree of association to the cell. Tightly bound EPS behave differently than a diffuse EPS layer.

Microbial adhesion is understood as the process of attaching bacterial cells that are in an aqueous suspension onto a solid or liquid substrate. This process can be reversible in the first stages of adhesion, and irreversible, once complicated chemical interactions between the cell and the surface have taken place [56,57].

Adhesion to solid or liquid hydrocarbons is a common strategy that microbes use in conditions of nutrient deficiency. Certain microbes, with the aid of biosurfactants, can metabolise long-chain hydrocarbons. In order for a microbe to assimilate these compounds efficiently, it has to attach to the oil-water interface, by reducing the effective distance between the cell and its nutrient source. Since the degradation of nutrients takes place inside the cell, the bacterium needs to integrate these long molecules to the cell by a process of diffusion. Hence, the bacterium needs to have an adequate cell envelope that facilitates the adhesion to hydrophobic surfaces. It has already been stated that bacterial cells possess in their outermost membrane an array of lipids, proteins, polysaccharides, as well as extra-polymeric substances with varied composition and adhesive appendages, that can bridge the gap between the cells and the substrates [58].

The presence and chain length of mycolic acids in coryneform bacteria, including hydrocarbon degrading *Rhodococcus* spp., was found, in this case, to correlate well with cell surface hydrophobicity [40]. Other authors [35], however, failed to see a clear relationship between mycolic acid length and overall cell surface hydrophobicity.

Rhodococci are well adapted to the presence of hydrocarbons in the environment. Some strains can emulsify hydrocarbons by producing biosurfactants. The emulsification of long-chained carbon compounds makes them available to the bacterial cells, and allows them to be included inside the cell membrane and used as carbon sources. Rhodococcal cells, being hydrophobic, can adhere to the interface between water and liquid hydrocarbons; if they are not hydrophobic enough, they can tailor their surfaces by changing the degree of saturation of their cell membranes, modifying the *cis/trans* ratio or modifying the length of the carbonated chains [34]. For instance, Sivan *et al.* [32] have studied the biofilm formation of the strain *Rhodococcus ruber* C208, whose sole carbon source is polyethylene. This is very advantageous, as this plastic is a common soil pollutant.

<b>Taxonomy of <i>Pseudomonas</i></b>	
Kingdom	Bacteria
Phylum	Proteobacteria
Class	Gammaproteobacteria
Order	Pseudomonadales
Family	Pseudomonadacea
Genus	<i>Pseudomonas</i>
Species	1, 2
<b>Common species:</b> <i>P. aeruginosa</i> , <i>P. syringae</i> , <i>P. fluorescens</i> , <i>P. fragi</i> , <i>P. gessardi</i> , <i>P. jessenii</i> , <i>P. corrugata</i> , <i>P. stutzeri</i> , <i>P. oleovorans</i>	

**Table 2.2:** Taxonomy of *Pseudomonas*.

### 2.2.3 *Pseudomonas* in nature

Pseudomonads are Gram negative  $\gamma$ -proteobacteria, with a very versatile metabolism. They are chemoorganotrophs, with a respiratory metabolism but in some cases they can adapt to anoxic conditions, using  $\text{NO}_3^-$  and  $\text{NO}_2^-$  as terminal electron acceptors [59]. They are straight or curved rods, with dimensions 1.5– 4  $\mu\text{m}$  by 0.5– 1  $\mu\text{m}$ . They are motile by means of polar flagella. Some strains produce pigments that are of particular interest as they are highly coloured or fluorescent [60]. Their taxonomic description can be found in Table 2.2.

Pseudomonads have been studied since the XIX century. The term *Pseudomonas* was given by Migula [61] because of the resemblance of this bacteria with the nanoflagellate protists *Monas*. Since they were first systematically studied by den Dooren de Jong [62] it was discovered that they had a remarkable nutritional versatility; they can use a wide variety of carbon, nitrogen and phosphate sources, even if these proceed from toxic xenobiotic substances [63]. Pseudomonads are easy to grow in lab conditions, even in nutrient-poor media, or at low temperature.

The literature is particularly rich in references to *Pseudomonas aeruginosa*, *P. fluorescens* and *P. putida*. *Pseudomonas aeruginosa* is a metabolically diverse opportunistic pathogen that is among the leading causes of nosocomial (i.e. hospital acquired) infections, along with the bacteria *S. aureus*, *Enterococci* spp., *Enterobacter* spp., *Klebsiella pneumoniae*, *E. coli* and the fungus *Candida albicans* [64].

*P. aeruginosa* is found in terrestrial and aquatic environments. It is a common opportunistic pathogen that infects immunocompromised patients, causing urinary tract infections, respiratory problems, bacteremia and infection in compromised tissues (i.e. burnt or scarred), infections in joints and tissues and gastrointestinal infections, among others.

*P. aeruginosa* is particularly pernicious in cystic fibrosis patients, where it provokes chronic infections. Cystic fibrosis is a genetic disorder that affects most critically the lungs, but it can also affect other parts of the body, like the gastrointestinal system. It is characterised by an abnormal transport of  $\text{Cl}^-$  across the epithelial cells, which leads to an increased secretion of a thick mucus and an inflammation of the airways. This mucus is readily and chronically infected by several strains of bacteria, of which *P. aeruginosa* has the highest prevalence, particularly in adult hosts. The pseudomonal infection contributes to the inflammation and damage of the lungs of the patient, which might ultimately need to be replaced by a transplanted organ [65].

*Pseudomonas* anchors firmly to the surface of the mucoid tissue or the lung cells by means of adhesion promoting structures, like pili and flagella. Once the infection is well established and a mature biofilm has developed on the lung, these structures are lost. Other structural and chemical changes occur as a result of the maturation of the biofilm, that enables them to survive, despite the host defence strategies and repeated courses of antibiotics. Pseudomonads produce extra-polymeric substances that include enzymes that cleave immunoglobulines and exotoxins that prevent phagocytosis. Moreover, the cells adhered to cystic fibrosis patients' lungs are hypermutable and as such they have the ability to adapt quickly to the environment and switch genes on and off. If the cells are found in anoxic conditions, or if the nutrients are scarce, the production of the polysaccharide alginate (Figure 2.11) is increased, encasing them and protecting them against the host defence mechanisms. This exacerbates the inflammation and causes the deterioration of the health of the carrier. *Pseudomonas* biofilms on the lungs ensure the persistence of the cells in the organism and thus the understanding of the mechanisms of adhesion is key in the alleviation of the infection in cystic fibrosis patients [65].

The growth and initial formation of *Pseudomonas* biofilms is regulated by a process known as *quorum sensing* (QS). QS involves the production of chemical signals that allow the communication between cells, regulate the expression of genes, control the population density, and promote phenotypic changes. In *P. aeruginosa* QS is essential for adhesion and for the development of virulence factors. These bacteria, like other Gram negative ones, are known to produce acyl homoserine lactones (AHLs) signal molecules, which diffuse freely through the bacterial cell

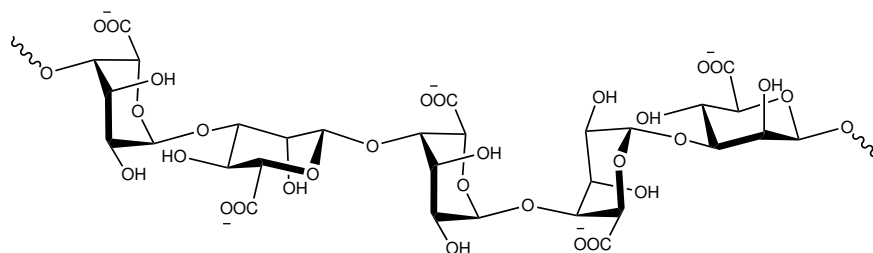


**Figure 2.11:** Alginate structure. Alginate is a polysaccharide produced by many types of bacteria, including *Pseudomonas*. It is a linear copolymer of 1–4-linked  $\beta$ -D-mannuronic acid and C-5-epimer  $\alpha$ -L guluronic acid. It is used in industry as a common gelling agent.

membrane; due to this process, the concentration of the AHLs inside and outside the cell is the same, allowing the bacteria to sense other organisms in the vicinity [66]. The mechanisms of virulence and biofilm formation in *P. aeruginosa* are regulated by an intricate network, composed by signalling molecules and receptor proteins [67]. These regulatory mechanisms make this strain a very successful organism, often resistant to common antibiotics.

*Pseudomonas putida* is a saprophytic species, which has a more diverse transport and metabolic systems than *Pseudomonas aeruginosa*, being able to use a wider variety of C and N sources. These two species have very similar genomes, but the former lacks the aggressive virulent factors of *P. aeruginosa*, like the exotoxin A and type III secretion systems [68]. Its safety and metabolic diversity, allow its use in many areas of human interest, like bioremediation, biocatalysis, agriculture and in the production of biodegradable plastics [69].

Of particular notoriety is the strain *P. putida* KT2440, which has been declared as a certified biosafety strain (i.e. a non-preferred host, generally regarded as safe, that lacks virulent factors) and can be used as a host for cloning and gene expression of other Gram negative bacteria. This strain has an exceptional metabolic diversity due to a very high number of enzymes and transporters of metabolites [68].

*P. putida* is ubiquitous in the environment, and is often associated to soils and aquatic biomes, but can also be found in clinical specimens. Even though it is part of the human oropharyngeal flora, it can infect immunocompromised cancer patients, causing septicaemia [70].

*P. putida* finds a lot of uses in bioremediation, due to its fast growth kinetics, the ability to grow in a wide range of temperatures and pH and in very polluted

environments. This strain thrives in aquifers contaminated with phenolic effluents produced by industries that produce textiles, dyes, petroleum derivatives, explosives, plastics, and pharmaceuticals. Phenol and some of its derivatives are toxic for the aquatic fauna, even in low concentrations and are known to be carcinogenic in humans. *P. putida* is known to degrade phenol by enzymatically cleaving the phenyl ring [71–73].

## 2.3 Conditioning film formation

Surface biofouling is described as the build-up of organic and inorganic compounds that are either present in a particular environment, or actively secreted by microorganisms with the intention of strengthening the microbes' bonds with the surface. Before cells start adhering to the surface, a process known as conditioning occurs, in which molecules coat the majority of the surface.

In natural aquatic environments, the aqueous media contains a great variety of chemical substances that include polysaccharides, proteins, ions, fatty acids and other products of decomposition. Every solid surface that forms part of this ecosystem will undoubtedly be covered by a myriad of substances. If a clean solid surface is introduced, the biofouling process readily starts. If this surface bears a charge, an electric double layer will immediately be formed, minimising the surface's interfacial energy.

According to Compère *et al.* [76] proteins are the next to approach the surface, and constitute the majority of the conditioning layer. Protein coverage will shortly be followed by polysaccharides. Other substances have been found to be present in this primary film, spanning from lipids to nucleic and humic acids (n.b. humic acids are a mixture of carboxylic acids with phenolic functionalities which are the major constituents of natural organic matter in soil, lakes and ocean water).

The conditioning film will change the surface's characteristics, including its roughness and chemical properties. Specific microbial receptors (e.g. lectin/carbohydrates) might be part of the conditioning films and these can select for the colonisers and trigger biological responses in them. For instance, films covered by alginate, which is a polysaccharide and a polyelectrolyte, stimulate biological changes in bacterial cells in the plankton (e.g. in *Pseudomonas*).

Once the surface has been coated by proteins, carbohydrates and other macromolecules, bacteria are able to attach to the surface. Finally, in marine and other aquatic environments, the highest scale of biofouling will be characterised by the attachment of major organisms, like barnacles and mussels. The evolution of biofouling at different time and length scales is portrayed in Figure 2.12.

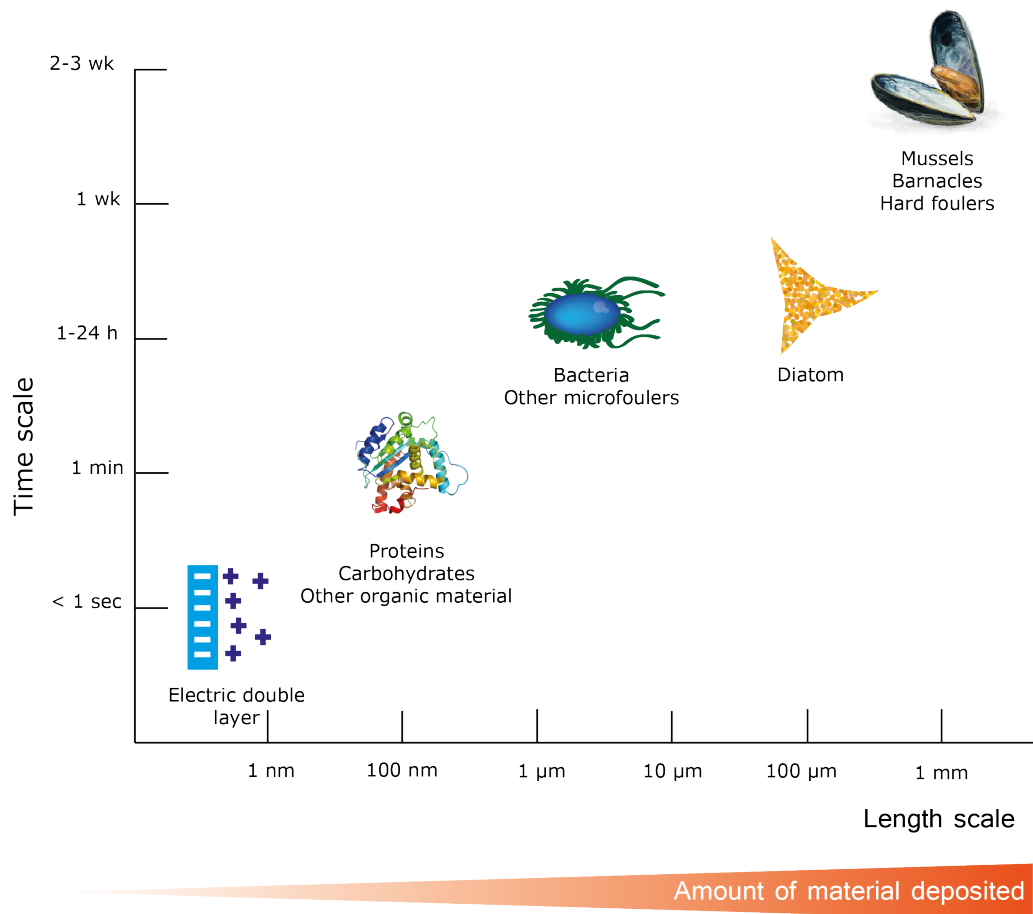


**Figure 2.12:** Biofouling at different length and time scales. The first entities to arrive to a surface are ions, followed closely by proteins, carbohydrates and other organic substances like lipids and humic acids. Bacterial colonisation follows and if present other soft foulers like diatoms or algae will be adhered in a matter of hours. The last organisms to adhere will be hard foulers like mussels, barnacles and bryozoans. Image adapted from reference [74]. Image of protein taken from [75] and used under the Creative Commons Licence.

### 2.3.1 Protein adsorption to surfaces

Since proteins are the primary constituents of conditioning films, it is important to mention some aspects of protein layer formation. Initially proteins that are in suspension might approach the surface; if the interactions are attractive and overcome the present hydrodynamic effects, the protein is transiently or permanently bound to it. The protein at this point might be able to change its conformation in order to maximise its attachment to the surface, only if by doing so, gains structural stability. If it changes its conformation its “footprint” extends over time. The rate at which proteins spread depends on the supply rate and the surface characteristics. There will be an equilibrium between the supply rate and the protein spreading rate, that will determine the kinetics of surface coverage.

If the suspension contains more than one type of protein, other factors come into play. The size of the various proteins and their preference for the substrate will determine which protein will adsorb more favourably. This phenomenon is called the “Vroman effect”, which describes the phenomenon in which the most motile proteins arrive first to a surface, but then they are displaced by others which have a higher affinity for the substrate. Hirsh *et al.* [77] proposed a mechanism for this displacement, which has been illustrated in Figure 2.13. In this model a second protein arrives to a surface coated originally by Protein 1 and embeds itself. The two proteins form a complex in which the aggregate changes conformation and exposes Protein 1 to the liquid medium. Protein 2, which has a higher preference for the substrate attaches, displacing Protein 1 and releasing it into the medium. To this day this is the most accepted mechanism behind the Vroman effect.

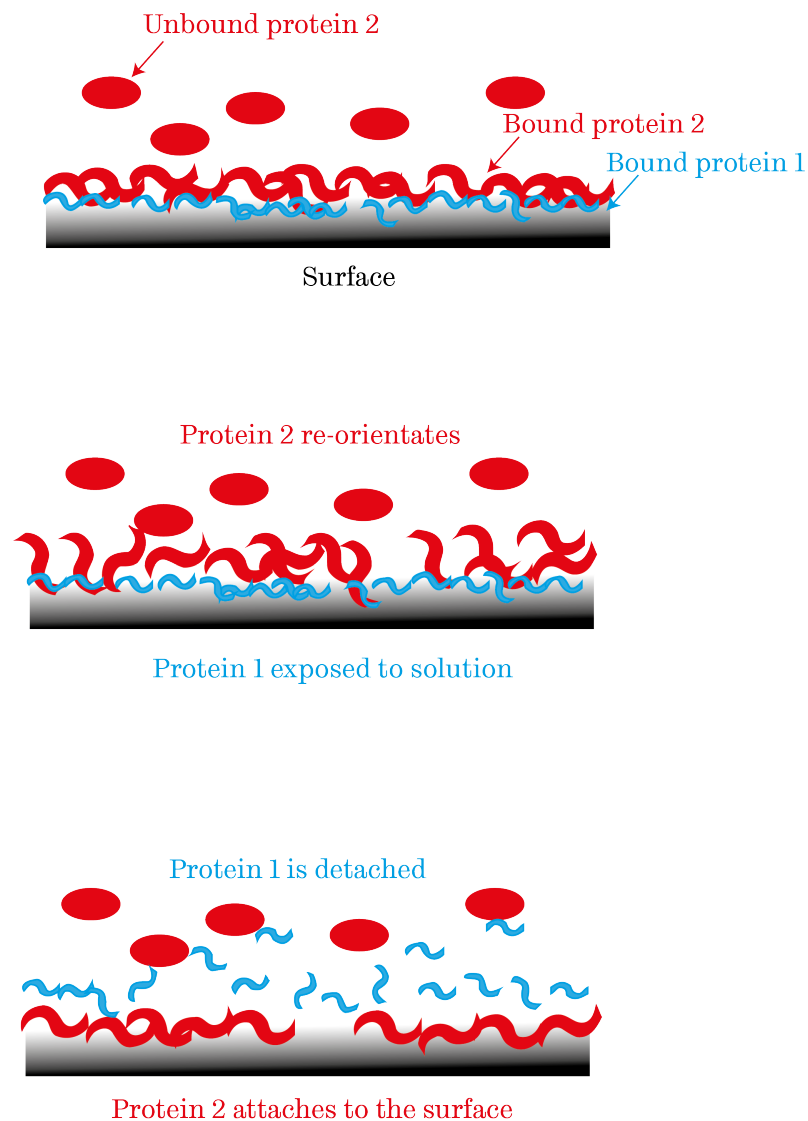


**Figure 2.13:** Adsorption competition of two different proteins, as proposed using the transient complex mechanism. The top figure shows the latecomer Protein 2 (red) in its un-adsorbed conformation (spherical) and in its adsorbed conformation (elongated). Initially the protein embeds itself in the layer of the originally adsorbed Protein 1 (blue). A complex between the two proteins is formed, which turns and exposes Protein 1 to the liquid phase. The lowermost image shows Protein 1 detaching from the surface, and Protein 2 adsorbing to it. Image adapted from reference [77].

## 2.4 Physical perspectives of bacterial adhesion

Bacterial cell adhesion, both between cell-to-cell and cell-to-surface, is a very common phenomenon. Since these microorganisms are only a few microns in size, the same theories that in physics are used to describe colloids, can be extrapolated to understand the movement, sedimentation and adhesion of the individuals of a bacterial suspension. This approach is valid only to a certain extent, since bacteria are “living particles” which tend to change their physicochemical properties over time, since they have metabolic resources at their disposal [78].

The deposition of a colloidal bacterial suspension will be governed mainly by Brownian motion (BM) and hydrodynamic forces, while the adhesion to a surface will depend on electrostatic (EL), electrodynamic or Lifshitz-van der Waals (LW) and polar acid-base interactions (AB) [79].

Lifshitz-van der Waals forces comprise three different interactions that are closely related in nature: (1) Keesom forces, in which dipole-dipole interactions are randomly orienting, (2) Debye forces, in which dipole-induced dipole forces are randomly orienting and (3) London dispersion forces that describe fluctuating dipole-induced dipole forces. Keesom and Debye forces are present in molecules with permanent dipoles, while London forces occur in all atoms and are due to the instantaneous non-uniform distribution of electronic density in the molecule. These three interactions decay rapidly with increasing distance with a factor of  $\lambda^{-6}$  [80] and thus are considered long-range interactions [3].

Hugo C. Hamaker, in the 1930’s proposed his theory of the stability of hydrophobic colloids based on these long-range attractive forces and explained it as a balance between attractive van der Waals forces and repulsive electrostatic forces. This theory was complemented by Boris V. Derjaguin, Lev D. Landau, Evert J. W. Verwey and Theo Overbeek, and became to be known as the DLVO theory, after the last four authors’ surname initials [80]. This theory has been used since the 1940’s to explain colloidal stability, and since Marshall’s [81] pioneering work in the 1970’s, as a basis to study the mechanisms of bacterial adhesion. The classical DLVO theory explains the total interaction between a cell and a substrate (Eq. 2.1) ( $\Delta E_{\text{TOT}}$ ), which is the balance between the normally attractive van der Waals force ( $\Delta E_{\text{LW}}$ ) and the generally repulsive electrical double layer interaction ( $\Delta E_{\text{EL}}$ ):

$$\Delta E_{\text{TOT}} = \Delta E_{\text{LW}} + \Delta E_{\text{EL}}, \quad (2.1)$$

where  $\Delta E_{\text{LW}}$  can be defined as:

$$\Delta E_{\text{LW}} = -\frac{Ar}{6d}, \quad (2.2)$$

where  $A$  is the Hamaker constant,  $r$  is the radius of the cell, and  $d$  is the separation distance, as illustrated by Figure 2.14.

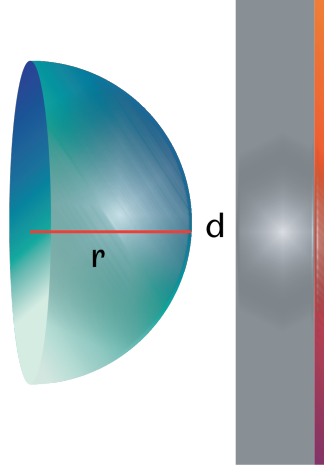


**Figure 2.14:** Geometry of the van der Waals interaction between a sphere and a planar surface.

The double layer interaction is caused by Coulombic forces. In the vicinity of a charged surface, which is immersed in an ionic solution, there is a build-up of counter-ions in a section called *Stern layer*. Outside this region, the neutralisation diminishes, but there is still a depletion of co-ions. With increasing distance, the charge accumulation diminishes asymptotically until the electric balance of the bulk is reached (Figure 2.15). When two objects, which bear a diffuse double layer are put into close contact, they repel each other. The double layer interaction can be expressed in terms of the surface potential  $\Psi$ , the distance between the surfaces  $d$ , and the Debye length  $\kappa$ , which is related to the ionic strength of the media:

$$\Delta E_{EL} \propto \Psi^2 e^{-\kappa d} \tag{2.3}$$

Bacteria have an inherent electrical surface charge, due to the ionic end-groups of the surface macromolecules, and their interaction with the external aqueous media. When immersed in water, these polymers, if they have the same charge, will repel each other, with a force that can surpass LW and AB attraction. The rate of decay of EL interactions depends strongly on the ionic strength of the surrounding media. If the ionic strength of the medium increases, the thickness of the double layer decreases, and as a consequence the cells can approach the surface with sufficient proximity to the surface in a point where the attractive

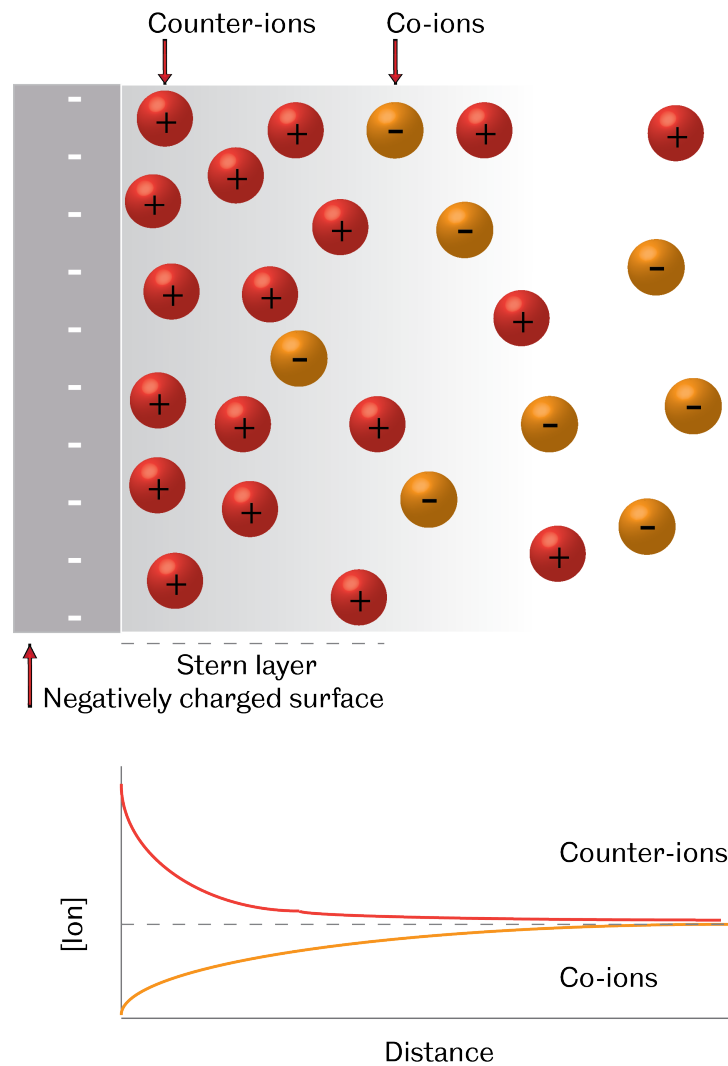


**Figure 2.15:** Aqueous electrolyte near a charged surface, showing a non-uniform distribution of the electric charges in the vicinity of the surface. The counter-ions are not rigidly held, but diffuse into the liquid phase until they reach the concentration of the bulk, as shown in the graph. The Stern model is the most accurate representation of the diffuse double layer. It assumes that the ions have a finite size, and thus they can only approach the surface at a certain minimum distance. The Stern layer is a plane in which the counter-ions are specifically adsorbed by the surface. Image adapted from [82].

van der Waals forces overcome the repulsive electrostatic interactions [83]. Under physiological conditions, like NaCl 0.9%, ( $\sim 0.15$  M) EL forces can be felt up to a distance of 8–10 nm [80] and thus, they are considered long-range interactions [3].

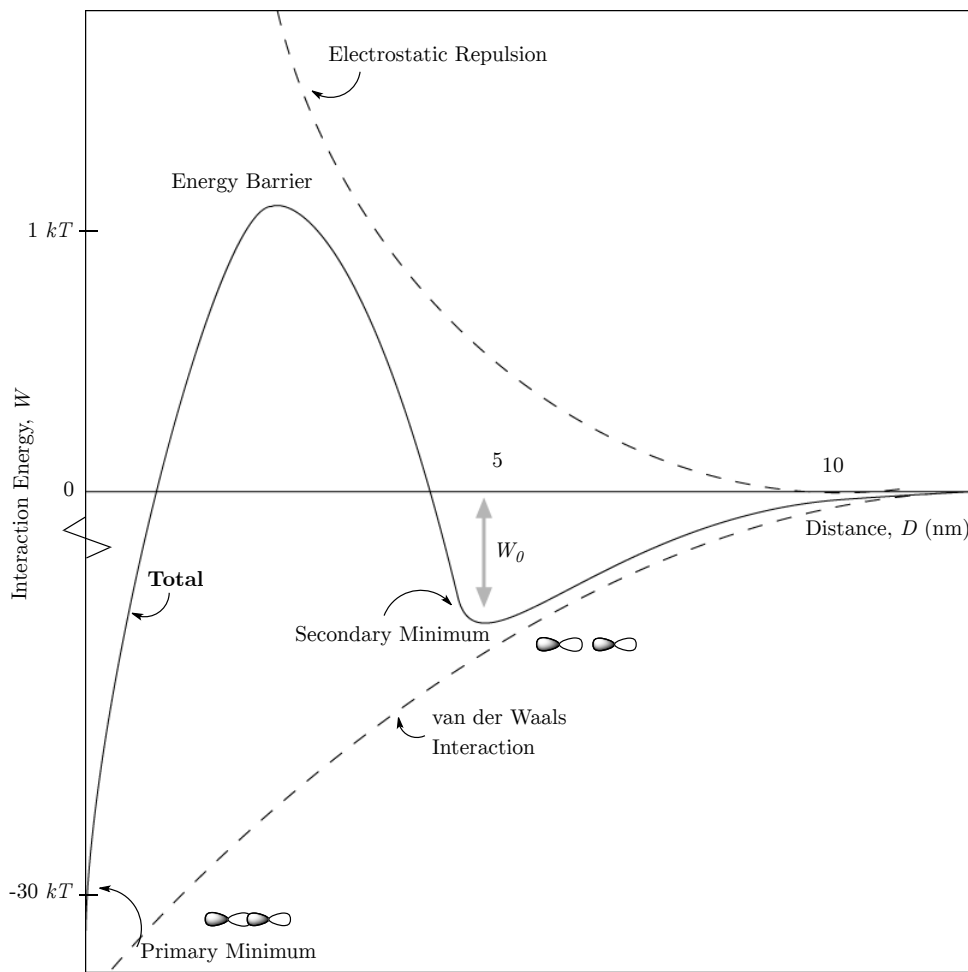


**Figure 2.16:** Energy profile of the combined DLVO interactions. Image adapted from [82].

It has been said that, for adhesion to happen the van der Waals attraction has to exceed the EL repulsion at small distances. Figure 2.16 shows the interaction potential that occur between two colloidal particles, or surfaces, combining LW forces and EL forces. The potential energy minimum at contact is dubbed the *primary minimum* which, as it can be seen in Figure 2.16, the energy barrier may be too high to overcome and attachment through this minimum difficult to attain. In this case, particles can become attached by reaching the *secondary minimum*, if this is low enough, and if not, remain in suspension.

It was later recognised that other forces also influenced colloidal interactions. Polar forces (AB), which are neither electrodynamic or electrostatic in nature, comprise the attractive hydrophobic interaction and its repulsive counterpart, hydration pressure. These energies can sometimes be two orders of magnitude larger than LW or EL forces, but their range of action is shorter than LW or EL interactions. These interactions are polar in nature, arising from the electron acceptor-donor forces, particularly in a polar medium, like water. Hydrophobic attraction has normally a decay length of 10–15 nm [80]. Other short-range interactions include steric forces, specific ion effects and hydrogen bonding.

Due to the size of the bacterial cells, Brownian motion (BM) has a noticeable effect on their suspensions. All particles at temperatures higher than 0 K have a free energy of  $3/2kT$  when they have three degrees of freedom. As mentioned before, BM will impact their rate of deposition [80].

Van Oss [80] considered the contribution of all of these forces and proposed an extension of the DLVO theory that accounted for the AB and Brownian motion, and this is known as the Extended DLVO theory (xDLVO). The AB component is directly related to attractive hydrophobic interaction and repulsive hydration effects, and for bacteria can be calculated by comparing their affinity to monopolar and apolar solvents [84]. The contributions to the xDLVO model can be seen in Equation 2.4.

$$\Delta E_{\text{TOT}} = \Delta E_{\text{LW}} + \Delta E_{\text{EL}} + \Delta E_{\text{AB}} + \Delta E_{\text{BM}}. \quad (2.4)$$

The profile of the additive effect of the xDLVO forces would have a somewhat different profile from that portrayed in Figure 2.16 [80]. Nonetheless, the xDLVO energy profile, would still have a primary and a secondary minimum. Adhesion through the primary minimum is irreversible, but difficult to attain. In order to reach this potential well, it is necessary to go up the electrosteric barrier or reduce it significantly. This can be achieved by lowering the surface potential or charge; if the ionic strength of the medium is increased, the electrostatic double layer will decrease in thickness. If this surface charge remains high, even after raising the ionic strength of the medium, the surfaces will adhere on the shallow and reversible, secondary minimum.

### 2.4.1 xDLVO forces and bacterial adhesion

Bacteria have other ways to overcome the energy barrier for adhesion. For example, there might be specific interactions between specific cell-wall components and substrates, through extra-cellular polysaccharides, membrane macromolecules or appendages [3].

A colloidal model proposes to treat bacterial cells as bare spheres, but this is far from accurate, as bacterial cells have an envelope with heterogeneous properties. For instance, it has been seen in *P. fluorescens* that lipopolysaccharides (LPS), major components of the outer membrane of Gram negative cells, aid in the adhesion to surfaces via the formation of hydrogen bonds. When these macromolecules are truncated, their adhesive properties are changed, making them less adherent to hydrophilic substrates and more to hydrophobic surfaces [3]. Similarly, the presence of appendages can modify the overall hydrophobicity of the cell. Fimbriae, for instance, contain a larger proportion of hydrophobic amino-acid residues, making them more adhesive to other hydrophobic substrates. Moreover, fimbriae overcome the initial energetic barrier, facilitating the adhesion of a cell to a substrate, due to their high affinity for the substrate [85].

In other words, when macromolecules or appendages, like the aforementioned LPS or fimbriae are present, non specific long-range interactions can be obscured by specific short-range forces, thus modifying the normal balance of forces that a DLVO-like model predicts [3].

Similarly, the surfaces of the bacteria in media are not necessarily the same as the surface of bacteria adhered to another surface. Since microbes change in response to their environment, the application of a first principles colloidal model must be treated with care.

Notwithstanding these limitations, the xDLVO theory has been applied successfully to the modelling of microbial adhesion by many authors [86–92]. For instance, Dorobantu *et al.* [87] used the xDLVO theory as a framework for the interpretation of the adhesion of *Rhodococcus erythropolis*, and accounted for the presence of extracellular adhesive structures.

### 2.4.2 Hydrophobicity

The hydrophobic effect plays a key role in many biological phenomena, like protein folding, enzyme-substrate interactions, cell attachment, antigen-antibody interactions, lectin-carbohydrate and the stability of lipid membranes, among others [93]. Since 1973, Marshall and Cruickshank [94] recognised the influence of cell surface

hydrophobicity (CSH) in bacterial attachment. According to R.J. Doyle is thought that hydrophobicity is one of the main driving forces for bacterial adhesion, being perhaps more important than LW or EL interactions [95].

Hydrophobicity is related to the inability of water to dissolve non-polar liquids. The name hydrophobicity is suggestive of the *fear of water* and might be misleading, since the London forces between polar and non-polar liquids are important and favourable. For the dissolution in water of a non-polar liquid to occur, the former must penetrate a liquid with a strong cohesive energy, by virtue of the hydrogen bonds that water has. Water molecules would rather keep their very stable hydrogen bonds, which causes a re-orientation of water molecules at the interface with the apolar liquid [93]. Hence hydrophobic bonds, are not bonds *per se*, just a tendency of apolar molecules to remain in contact with each other, rather than in contact with water.

For a microbe, if it has enough hydrophobic sites on its surface, then it is possible for it to adhere to a hydrophobic substrate in the presence of water. Microorganisms rarely possess a completely hydrophobic envelope; they have heterogeneous surfaces that might include hydrophobic elements, such as the spore coats in *Bacillus* species, peptidoglycan and mycolic acids in *Corynebacterium*, *Mycobacterium* and *Rhodococcus* species, fimbrial proteins in *E. coli*, and phospholipids in *Vibrio cholerae* [95].

### 2.4.3 Factors that influence bacterial adhesion

Traditionally, bacterial adherence and detachment to surfaces has been determined by macroscopic methods, which use flow chambers, detachment by air bubbles, spinning disks or a direct count of adhered cells using stained or labelled cells. The SFM can be used to assess the adherence of microbes to substrates by either calculating the lateral detachment force or by investigating the adhesive properties between the tip and the cell surface. Collectively, it has been seen that there are a number of factors that influence the degree of attachment of microorganisms, and these have been summarised in Figure 2.17.

#### Environmental factors

1. **Temperature:** Di Bonaventura *et al.* [96] cultured several strains of the Gram positive bacteria *Listeria monocytogenes* in an interval of 4 – 37 °C and found out that the cell surface hydrophobicity increased with temperature, being up to three times higher at 37 °C than at 4 °C. Higher hydrophobicity values were also correlated with an increased attachment to polystyrene, a hydrophobic material. This is because a change in temperature can alter the

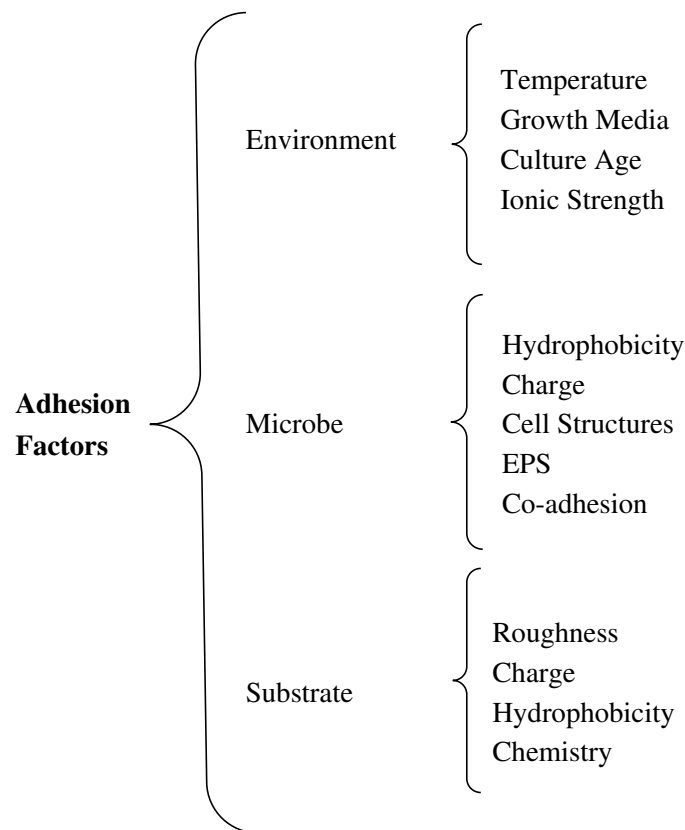


**Figure 2.17:** Factors that influence bacterial adhesion.

saturation, length and distribution of cell-membrane bound fatty acids. A similar effect has been seen for other strains [97].

2. **Growth time and media:** The studies conducted by Stratton *et al.* [54], de Carvalho [98] and Lang and Philp [42] revealed that in *Rhodococcus* species, the mycolic acid composition, and hence, the hydrophobicity are affected by culture age, culture media and carbon source. For instance, Bredholt *et al.* [45] studied a strain of *Rhodococcus* that has been known to degrade oil. They observed that the hydrophobicity of the cells varied considerably with culture time, peaking in the exponential phase. Highly hydrophobic cells adhere better to oil droplets and release emulsifiers, that contribute to alkane degradation.
3. **Ionic strength:** Pouran [99] investigated the effects of the increase of ionic strength in the adhesion of *Sphingomonas* spp. to mineral surfaces, finding that the number of cells attached is considerably larger at low salt concentrations (20 mM NaCl) than at high concentrations (200 mM). It is hypothesised

that at high ionic strengths the membrane biopolymers recoil, making them less capable of interacting with the surface.

### **Bacterial Factors**

1. **Cell surface hydrophobicity and charge:** Cells acquire an electric charge in aqueous media, due to the ionisation of the surface macromolecules; generally bacteria have a negative charge at the pH of natural environments. The surface charge does not correlate directly with hydrophobicity, as both hydrophobic and hydrophilic cells can have high surface charges. Nonetheless it is more common to find highly charged hydrophilic cells [100]. Bendinger *et al.* [40] studied several *Rhodococcus* strains and other Corynebacterineae with and without mycolic acids. Their study showed that the length of the mycolic acid chains was related to the cell surface hydrophobicity; the shorter the chains, the less hydrophobic the cells are. This study also showed that the *Rhodococcus* strains have a relatively high negative surface charge, compared to other mycolic acid containing bacteria. The negative charges might arise from the free carboxyl end of peptidoglycan, and from the phosphate and carboxylate end of lipoarabinomannan [40]. Other authors [35] found the correlation between carbon source, mycolic acid composition and hydrophobicity not to be as clear. It seems that the production of EPS by some strains, modifies their hydrophobicity and changes their adhesion to substrates. Studies on other bacterial strains [101] have shown that the cell surface charge and hydrophobicity are highly dependent on the time of harvest and on the culture conditions; cell adhesion and aggregation are multifactorial processes, rendering the comparisons between experiments a complicated issue.
2. **Cell structures:** Surface structures such as fimbriae, capsules, flagella and other polymeric protrusions have remarkable effects in bacterial adhesion. Although they are not considered in the classical or extended DLVO theories, which assume cells are spherical smooth particles, they often explain deviations from the theory. Due to the small diameter of appendages and unique chemistry, they can pierce the repulsive energetic barriers and promote irreversible adhesion through the primary minimum. This has been suggested by analysing the attachment of smooth particles and cells with appendages, both having the same hydrophobicity and charge, finding that the latter attach much better to surfaces [102].
3. **EPS:** EPS are a complex, hierarchically organised and highly hydrated matrix of proteins, polysaccharides, nucleic acids, lipids, humic substances and

soluble factors. They contribute to attach the cells into the primary minimum, by lowering the adhesion barrier. The effect of this glue cannot easily be accounted for in the current physical models, but its importance to biofilm formation is indisputable.

The properties of the extra-cellular matrix depend on the environmental conditions and the age of the biofilm. The extra-cellular matrix adapts to changes in the concentration of nutrients, oxygen, temperature, pH and desiccation. Likewise, the EPS composition will depend on the properties of the surface that the microorganisms are attaching to, like its roughness, hydrophobicity and charge.

The composition of the EPS matrix will vary according to the type of organism: in Gram negative bacteria, EPS often bear a negative charge, due to the presence of anionic polysaccharides, uronic acids or ketal-linked pyruvates. In some cases the association of these functionalities with cations fortifies the binding of the matrix. Conversely, the EPS of Gram positive bacteria often contains cationic groups [18]. Furthermore, EPS can be classified according to their proximity and degree of association with the bacterium: cell-bound EPS is tightly linked to the cell via covalent or non-covalent bonds, whereas free EPS or slime is loosely attached. Different extraction methods can differentiate between these two types of polymers [101].

EPS are thought to bridge the gap between the secondary minimum (reversible attachment) and the primary minimum (irreversible attachment), as described by the DLVO theory [34].

4. **Co-adhesion:** In a natural environment bacteria live in mixed communities, where very diverse organisms inhabit in a mixed biofilm. In these consortia, intricate symbiotic processes take place. The presence of a particular strain attached to a substratum can remarkably enhance or weaken the adhesion of a second strain [103].

### Substratum factors

1. **Roughness:** Rough areas and substratum heterogeneities have been found to increase cellular adhesion [104–108]. Roughened areas, although not accounted for in the DLVO models, might explain the fact that in some cases cells are not washed away from a substrate, even while resting on the secondary minimum. Rough surfaces have a greater surface area (i.e. increased number of contact points with the cell) and their troughs are ideal sites for colonisation and deposition of nutrients. Some research groups have devised

methods to create patterned *nanorough* substrates that immobilise cells in a desired orientation [109–111].

It is also noteworthy the fact that the maximum degree of fouling does not necessarily correlate with the highest roughness values; the shape and the size of the bacteria need to be taken into account [112]. These parameters are interesting for the creation of *hygienic* surfaces: in food processing, surfaces must have an average roughness  $R_a \leq 0.8 \mu\text{m}$  to prevent bacterial attachment [113], but this parameter might not be accurate for all strains and conditions.

- 2. Charge and Hydrophobicity:** Microbial adhesion depends on the hydrophobicity and charge of both bacterium and substratum. As a general trend, very hydrophilic and negatively charged substrata are very resistant to the attachment of bacteria, whereas neutral, hydrophobic substrates attract a larger number of cells. The literature on bacterial adhesion has many examples of multifactorial experiments, where the hydrophobicity and charge of the substrate are varied systematically, to assess the influence that they have on the attachment. Pouran [99] and Andrews *et al.* [24] studied the attachment of *Rhodococcus* Rc291 and Rc92, as well as *Pseudomonas* Pse1 and Pse2. Their studies show that polystyrene surfaces will be preferentially colonised by the hydrophobic Rc291, and in lesser degree by Rc92. The hydrophilic Pse1 and Pse2 colonise mineral surfaces of iron and aluminium oxides, but also adhere to hydrophobic polystyrene. This proves that bacterial adhesion cannot be explained simply in terms of hydrophobicity, and many other factors contribute to the adhesion.
- 3. Chemistry:** It is possible to tailor the chemical properties of the surfaces to enhance bacterial adhesion. For example, Gu *et al.* [114] formed square patterns of self-assembled monolayers with  $\text{CH}_3$  terminations, separated by OH-SAM channels. The bacteria attach to the hydrophobic regions and interact with bacteria in the vicinity, through the hydrophilic gaps. Other methods to coat solid surfaces for bacterial adhesion will be amply reviewed in Chapter 3.

## 2.5 Macroscopic methods to measure bacterial surface properties

There are many methods that can be used to assess the adhesion of bacteria to substrates. A simple way to assess the preference of a bacterial suspension for a solid substratum is to count the number of cells adhered to a surface, after a defined washing step, where unbound cells are removed. A simple flow cell system can be devised, in which the influence of the shear stress on cell detachment can be measured [115].

Many studies of adhesion focus particularly on the measurement of hydrophobicity. Two of the most common macroscopic methods to assess the hydrophobicity of microbial cells are presented in the following paragraphs.

### MATH

Bacterial strains that possess hydrophobic surfaces characteristics are known to adhere to liquid hydrocarbons. Hence, microbial adhesion to hydrocarbons (MATH) has been proposed as a technique to measure bacterial cell hydrophobicity. A simple approach to this experiment consists in vortexing an aqueous cell suspension of bacteria with a liquid hydrocarbon (e.g. n-hexadecane) for a given time, allowing the separation of the phases, and then measuring the decrease in turbidity in the aqueous phase, as a result of the bacterial organisms moving into the organic phase [116]. The hydrophobicity is estimated from the formula:

$$\% \text{ Hydrophobicity} = 100 \times \frac{A_{\lambda\text{-initial}} - A_{\lambda\text{-final}}}{A_{\lambda\text{-initial}}} \quad (2.5)$$

where  $A_{\lambda\text{-initial}}$  and  $A_{\lambda\text{-final}}$  are the initial and final absorbances measured at 540 nm. Despite the simplicity of this experiment, and the general criticism about this method as an accurate representation of the cell hydrophobicity [117], MATH is still widely used in the microbiological community. Andrews *et al.* [118] measured the hydrophobicity of this thesis' studied strains, Pse1, Pse2, Rc92, and Rc291 using *n*-decane as the organic phase. The results from this analysis are presented in Table 2.3.

### Contact angle measurements

Contact angle measurements (CAM) are classic experiments that determine the free energy of solid surfaces. They do not directly give a measure of hydrophobicity,

MATH scores of the studied strains	
Strain	% Adherence
Pse1	$17.528 \pm 1.589$
Pse2	$33.134 \pm 1.108$
Rc92	$47.906 \pm 1.474$
Rc291	$76.900 \pm 1.950$

**Table 2.3:** MATH scores of the studied strains. The MATH test was carried out using *n*-decane as the hydrocarbon phase. The bacterial cells were grown at 20°C, supplemented with glucose 2 mM [118].

but they measure a related set of properties, as the wettability depends on the surface energy properties of the cell.

Normally, the working procedure involves the assembly of a bacterial lawn and the careful deposition of a water droplet on the surface of the lawn. The lawn formation can easily be achieved by filtering a bacterial suspension onto a filter membrane with the aid of vacuum, and the measurement using a goniometer. The success of this experiment relies on the achievement of an homogeneous, reasonably flat and rather dry surface. This is experimentally difficult, as the water from the lawn needs to be eliminated as much as possible, to avoid deviations in the measurements, but not too much, as dessication might affect the properties of the cells. It is expected that hydrophobic cell surfaces will force the water drop to deposit with angles superior to 45°, whereas hydrophilic cell surfaces are expected to be more wettable [119].

Thermodynamic properties can be assessed through the measurement of the contact angles of bacterial lawns, with polar and apolar liquids.

Even though this experiment is relatively simple to interpret, there are many reasons as to why the results generated might be doubtful. Firstly, the ideal conditions to measure contact angles are on homogeneous, dry, smooth and flat surfaces. This is not the case for a bacterial cell lawn. Secondly, after the water droplet has been placed on top of the lawn, the water might seep through the lawn, changing the measured angle. There is still disagreement as to when the angle is stable and can be measured. Nowadays high resolution cameras can be adapted to goniometers, so that the evolution of the water droplet can be recorded through time; the measured angle will be derived from an statistical analysis of hundreds of pictures, thus diminishing the uncertainty in the measurements. Finally, the cells might not reveal their true hydrophobic layer if they are covered in hydrophilic

EPS. Careful consideration on the washing procedures should be made, in order to determine what actually has been measured. The results of our own contact angle measurements will be detailed in Appendix D.

### **ζ-potentials**

As previously stated before, the electric charge in bacteria can affect the adhesion of cells to other charged surfaces. Charges in cells arise from anionic groups in the bacterial macromolecules, like phosphates and carboxylates. The cell surface charge can be assessed through the measurements of zeta ( $\zeta$ ) potentials, which are the electric potentials at the bacteria-water interface.  $\zeta$ -potentials can be assessed, for instance, by measuring the electrophoretic mobility of a cell suspension. [120]

CAM, MATH and  $\zeta$ -potentials, although useful and descriptive, represent an averaged measurement of the properties of a consortium of bacterial cells. Every cell can have an heterogeneous cell surface, and a macroscopic method will neglect this distinction. Therefore, microscopic methods are needed to complement the existing knowledge of the adhesive properties of bacteria, and their hydrophobicity. One of these methods is scanning force microscopy, which will be reviewed in the following section.

## **2.6 Scanning force microscopy**

### **2.6.1 Introduction**

In March 1986 Gerd Binnig and Calvin Quate from Stanford University and their IBM collaborator, Christoph Gerber, published a classic paper entitled ‘Atomic Force Microscope’ [121], and introduced a new kind of microscope that was described as ‘a combination of the principles of the scanning tunneling microscope and the stylus profilometer’. They reported the use of a probe that did not damage the surface, that had a vertical resolution of less than 1 Å and a lateral resolution of 30 Å, capable of measuring forces in the sub-pN range. This new microscope was based on the scanning tunnelling microscope (STM) developed by Binnig himself and Heinrich Rohrer four years before. Collectively, this family of instruments are called scanning probe microscopes (SPMs) and rely on the use of a very sharp probe that measures its distance-dependent interaction with a sample [122].

A microfabricated nanometre sharp-tip is grown at the end of a flexible cantilever, which transduces the interaction force between the tip and the sample.

Cantilevers obey simple Newtonian mechanics and are governed by Hooke's law:

$$F = kd \quad (2.6)$$

where  $F$  is the spring force,  $k$  is the spring constant of the cantilever, and  $d$  is the spring deflection. A representation of an SFM cantilever as a simple spring can be seen in Figure 2.18.

Figure 2.25 on page 54 shows a diagram of an SFM probe with 5 cantilevers; four triangular and one rectangular. The cantilever to be used is chosen by the experimenter, depending of the sample needs. At the end of these cantilevers, a conical tip can be seen. The apex of the cantilever will sense the sample surface when it is lowered down close enough to be in the bonding range, by bending upwards or downwards in response to the interaction. Figure 2.25b, shows the largest of the triangular cantilevers being bent as it comes close to a surface [122].

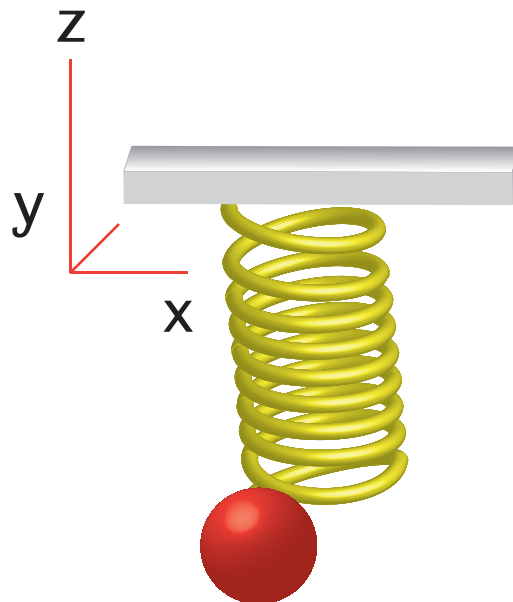


**Figure 2.18:** Representation of an SFM cantilever as a small sphere held by a Hookean spring. Image adapted from reference [123].

The reflection of a laser beam focused on the back side of the cantilever is used to monitor the movement of the probe. A laser diode produces a beam that is shone over the cantilever and reflected onto a 4-quadrant photodiode, with the aid of a mirror. The photodiode produces a voltage that depends on the position of the laser beam in its quadrants. A vertical displacement is generated by normal

forces, whereas a lateral displacement is caused by a twist of the lever, due to friction forces. Figure 2.19 on page 46 shows a diagram of the setup of an SFM.

The movements of the tip can be finely adjusted, with sub-nanometre precision, by means of piezoelectric materials. The tip is scanned over a surface and at each position, the cantilever deflection is measured and translated into a topographic map by the computer.

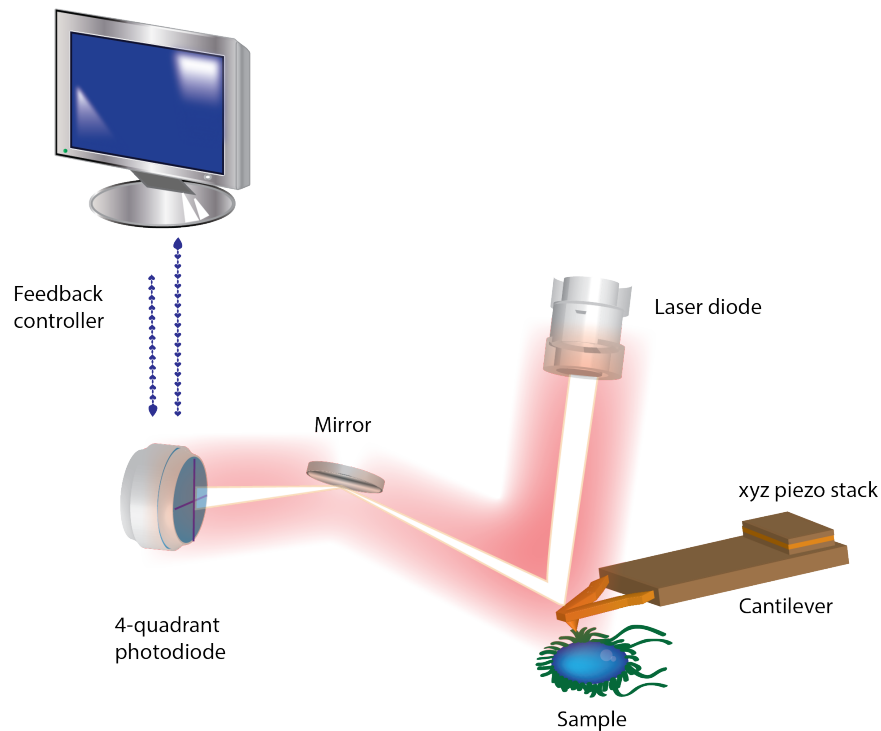


**Figure 2.19:** Simple diagram (not to scale) that includes the main elements of a scanning force microscope.

Figure 2.20 shows a more detailed scheme of the electronic system of the SFM. The setup depends on the particular model of microscope. In some, the sample is scanned over the tip, in which case the sample stage contains a piezoelectric tube. In some, the tip is scanned over the sample. The latter model is called a stand-alone microscope, and it is often coupled with an inverted microscope and commonly used for biological applications. The SFM head of a stand-alone microscope also contains piezoelectric elements, the tip holder, laser, photodiode and positioning mechanisms to direct the laser beam on the back of the cantilever and the photodiode. The head also includes an electronic system capable of processing

the signals that come out of the photodiode, namely  $F_N$  and  $F_L$ , the vertical and lateral deflections of the laser and  $\Sigma$ , the total intensity.

The high voltage electronics amplify the XYZ low voltage signals generated by the digital signal processor (DSP) in order to operate the piezoelectric scanner with high voltages in the range of 100 V. The high voltage electronics transfer analog voltage signals  $F_N$ ,  $F_L$  and  $\Sigma$  that come out of the photodiode and direct them to the DSP. The role of the high voltage electronic system is to convert small signals from the computer to the hundreds of volts needed for the piezoelectric scanner to function.

The function of the DSP is to process all the signals and calculate the required parameters for real-time operation. The computer is loaded with software capable of acquiring, processing and analysing the signals and converting them into images and graphs.

The piezoelectric scanner, which has been augmented in Figure 2.20 for clarity, accurately positions the tip over the sample. The piezoelectric element relies on the application of a potential difference between the two phases of the tube, in order to change the dimensions of the material and extend and retract the piezo, or move it in the x, y axis. A piezoelectric ceramic element can position the tip or sample with sub-nanometre resolution.

## 2.6.2 Feedback Loop

The feedback loop is a control system that, during SFM scanning, keeps a variable constant, at a given set point value. This variable could be, for example, amplitude or deflection. The control system should be as fast as possible in order to obtain a wide bandwidth; the faster the feedback loop, the faster the acquisition of the images. The control signal is characterised by three terms, named proportional (P), integral (I) and differential (D) and is commonly regarded as *PID*. The *PID* feedback loop is part of the DSP electronic system. The values of these three parameters determine the position of the  $z$ -piezo at a time  $t$  ( $Z_t$ ), which is given by:

$$Z_t = P_{\varepsilon_t} + I \int_0^t \varepsilon_i + D \frac{\varepsilon_t - \varepsilon_{t-1}}{dt} \tag{2.7}$$

where  $\varepsilon_t$  is the error signal, or deviation between the set point and the measured value of the constant parameter at the time  $t$ .  $P$ ,  $I$ ,  $D$  are the proportional, integral and differential gains. In modern SFMs the differential gain tends not to

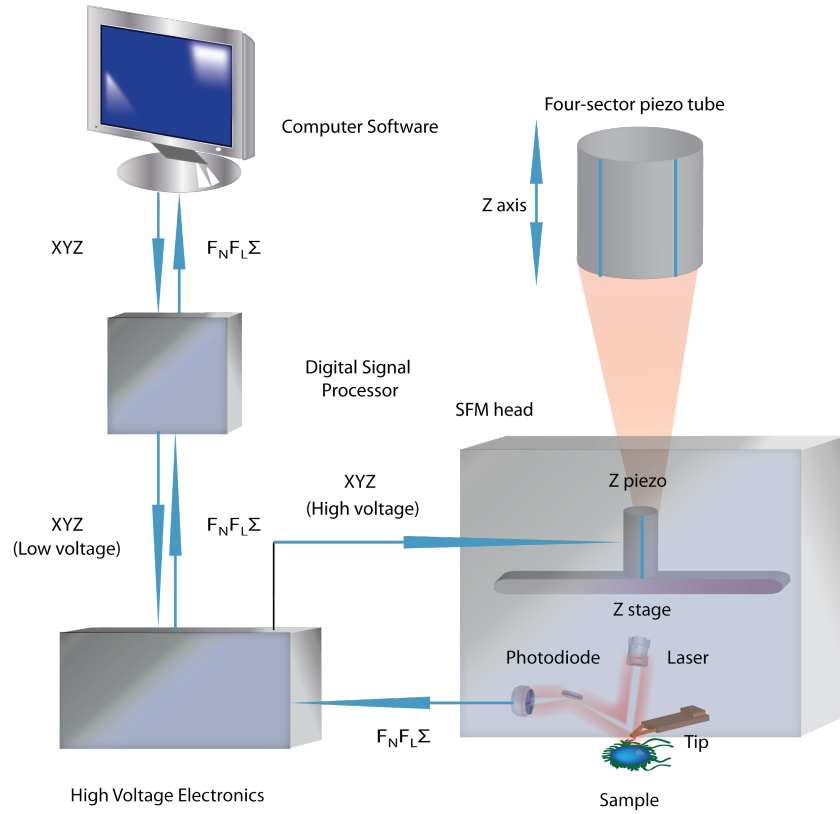


**Figure 2.20:** SFM electronic system.

be modified, and therefore equation 2.7 can be simplified to:

$$Z_{t-1} = P_{\varepsilon_{t-1}} + Idt \int_0^t \varepsilon_i, \quad (2.8)$$

which can be rewritten as:

$$Z_t = Z_{t-1} + a\varepsilon_t + b\varepsilon_{t-1}, \quad (2.9)$$

where  $a = P + Idt$  and  $b = -P$ .

The SFM electronics compare the measured force with the set point value, and the difference is called the error signal  $\varepsilon_t$ .  $\varepsilon_t$  is then sent to the feedback controller to correct the position of the  $z$ -piezo. When the  $P$  and  $I$  gains are optimal, the value of  $\varepsilon_t$  is minimal, and the probe tracks the surface features optimally.

The feedback loop output can be improved by adjusting the value of gain or gains and the set point. One can visually see, on the forward and backward traces

during imaging, the degree of overlapping of the traces; if they have very different profiles, the parameters need to be adjusted. As  $a$  and  $b$  in Equation 2.9 are increased, the feedback loop response becomes faster, and the images are seen with increased clarity. If the gains have a very high value, noise is observed in the system (often accompanied by a high-pitched noise), as the  $z$ -piezo oscillates at high frequency. The user needs to find the right medium, to optimise the scanning process [122].

### 2.6.3 Modes of operation

The SFM can image either in static or dynamic modes. This classification is related to the oscillation of the tip during scanning; in static modes, the tip does not oscillate, whereas in the latter category it does. The most important form of static scanning is contact mode, while the most popular form of dynamic imaging is amplitude-modulation mode (often used as synonym of AC mode, intermittent contact mode, or tapping mode).

In contact mode, the tip is brought into contact with the sample, scanning at a fixed value of vertical deflection of the cantilever, determined by the set point. If the feedback mechanism is working optimally, a constant force is applied to the sample throughout the scan. As the scan goes by, the  $z$ -piezo is continually adjusted so that it maintains a value of deflection equal to the set point, as explained in Section 2.6.2.

In reality, even though a constant deflection is maintained, a constant force might not be kept, as the photodiode signal, which is related to the selection of the set point, usually drifts with time.

In contact mode, two common outputs are produced: height images, which are colour-coded representations of the distance that the  $z$ -piezo needs to travel to maintain a constant applied force, and deflection images, which arise from small variations of the cantilever deflection, caused by delays in the feedback loop, as it cannot trace changes in topography too quickly, giving rise to an error signal.

The deflection signal is related to the angle of the cantilever. If no feedback is applied during the scan, then the height of the probe is not adjusted and its angle, and deflection signal, are modified every time it encounters on the surface a feature of a different height. Conversely, if the feedback loop is on, then the height of the probe is adjusted to keep the deflection constant at the desired set point, as illustrated by Figure 2.21.

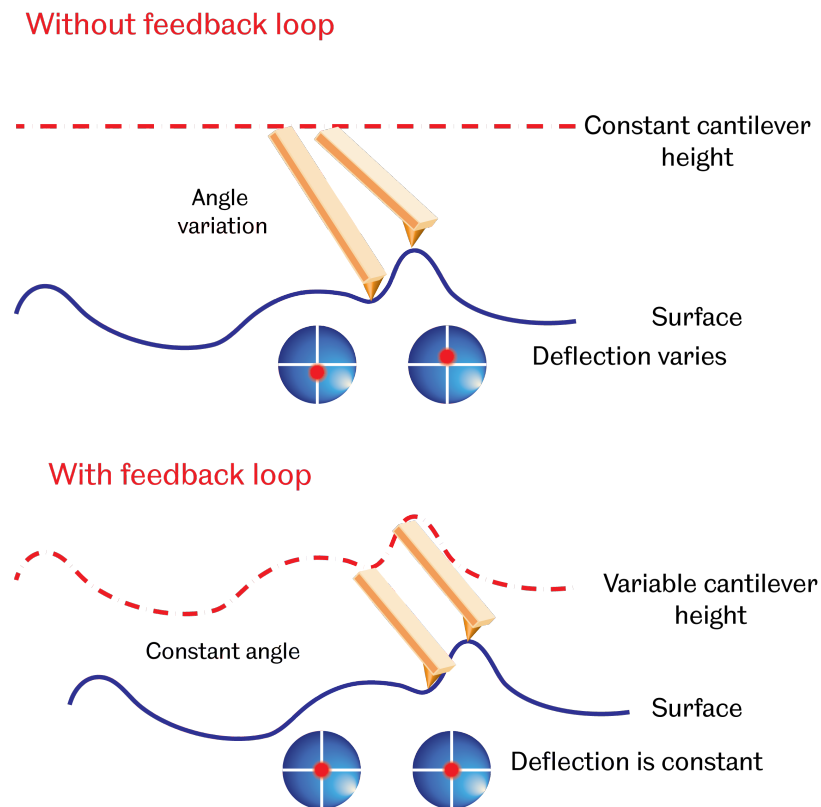


**Figure 2.21:** Feedback loop for contact mode. The top section of the diagram depicts the change in the scanning angle, as a result of keeping the height of the cantilever constant. Such angle variation is reflected in a movement of the laser signal on the photodiode. The lower section shows the  $z$ -movement of the piezo, which keeps the angle and the position of the laser on the photodiode constant. Image adapted from reference [124].

In amplitude-modulated SFM mode, the cantilever is oscillated away from the surface near its resonant frequency,  $f_0$  with a given oscillation  $A_0$ . As the probe comes near to the surface, the amplitude signal  $A$  is recorded (Figure 2.22).

The feedback loop used in amplitude-modulated SFM mode is quite similar to the contact mode one, except that in this case the cantilever is oscillated near its resonant frequency, causing the angle of the cantilever and the value of deflection to oscillate as well. As seen in Figure 2.23, if the SFM is operated without a feedback loop, when the probe encounters tall features, the amplitude of the oscillation is reduced, whereas troughs in the sample would provoke its increase. Conversely, if the AC feedback loop is on, the amplitude is kept constant at a certain set point

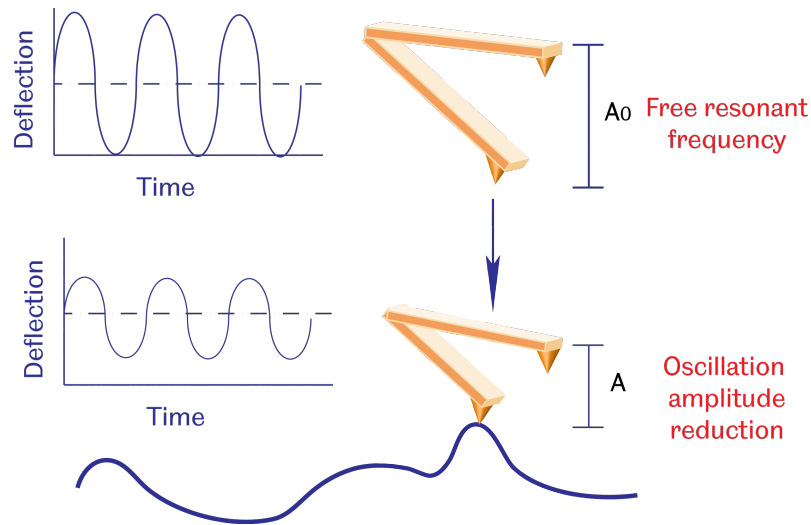


**Figure 2.22:** Dynamic, amplitude-modulated SFM mode. In the top of the figure, we observe the cantilever driven at its free-air resonant frequency, with an amplitude  $A_0$ . When the cantilever approaches the surface, the amplitude of the oscillation is reduced to  $A$ . Image adapted from reference [122].

value, whereas the height of the probe is adjusted according to the surface feature's height. The  $z$ -position is stored and used to generate the height data.

For biological samples, the dynamic methods of scanning are preferred over the static ones, due to a reduction of the vertical applied forces and the elimination of the lateral forces, which can detach the samples with ease.

#### 2.6.4 SFM cantilevers

The spring constant of the SFM probes can be calculated, for rectangular cantilevers  $k_r$ , if the dimensions and properties of the materials are known, according to:

$$k_r = \frac{Et_c^3 w}{4l^3} \quad (2.10)$$

where  $E$  is the Young's modulus of the material, in this case,  $\text{Si}_3\text{N}_4$  and is equal to  $1.5 \times 10^{11}$  N/m,  $t_c$  is the thickness,  $w$  is the width and  $l$  is the length. For a

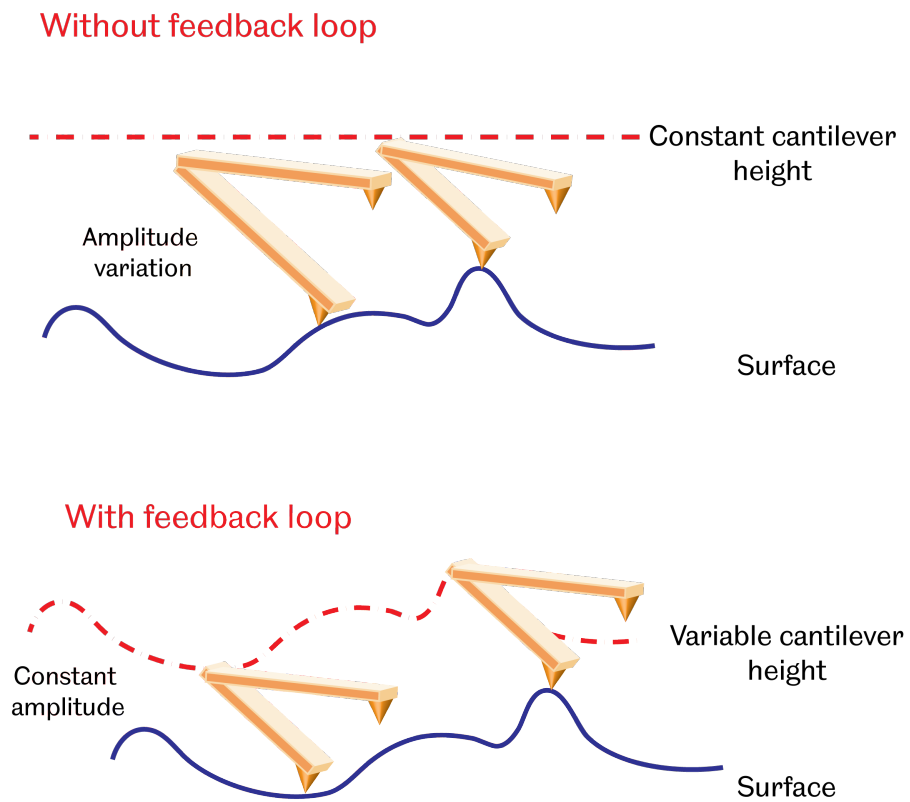


**Figure 2.23:** Feedback loop for AC Mode.

V-shaped or triangular cantilever, the stiffness  $k_v$  can be approximated by:

$$k_v = \left\{ \frac{Et_c^3 w}{2L_1^3} \cos\alpha \left\{ 1 + \frac{w^3}{2\left(L_1 \tan\alpha + \frac{w}{\cos\alpha}\right)^3} \times (3\cos\alpha - 2) \right\}^{-1} \right\} \left( \frac{L_1}{L_1 - d} \right)^3, \quad (2.11)$$

where  $L_1$ ,  $\alpha$  and  $d$  are defined by Figure 2.24.

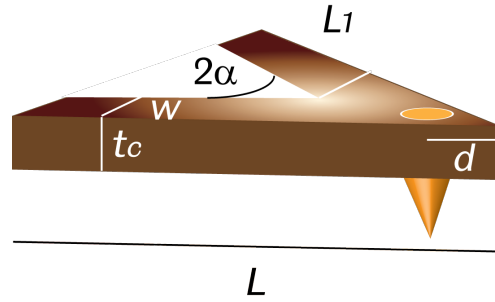


**Figure 2.24:** Triangular cantilever geometric parameters for the calculation of the spring constant. Image adapted from [125, 126].

The probes used for biological applications require low spring constants, and high resonant frequencies, to avoid damaging the delicate structures of cells and biomolecules. Cantilevers made of Si have a Young's modulus value  $E_{\text{Si}} = 169$  GPa [127], whereas  $\text{Si}_3\text{N}_4$  cantilevers are slightly more compliant, having a value of  $E_{\text{Si}_3\text{N}_4} = 150$  GPa [122]. Moreover,  $\text{Si}_3\text{N}_4$  tips are blunter, which is more advantageous, as they might not puncture the delicate bacterial membranes so easily [128].

Some companies have expressly developed cantilevers for biological applications. For instance, the Olympus Biolever has been designed to acquire contact and AC mode images and measurements under water. The rectangular Biolever has a 60  $\mu\text{m}$  long  $\text{Si}_3\text{N}_4$  cantilever, Au coated on both sides, with a tall and thin tip (40 nm radius of curvature, 5  $\mu\text{m}$  height) on a very thin cantilever (180 nm), with a high resonant frequency (37 kHz) and a low spring constant (0.03 pN/nm). For this research project, the more versatile and inexpensive, Bruker MLCT  $\text{Si}_3\text{N}_4$  cantilevers were used [129]. The second largest triangular cantilever (the third from left to right, Figure 2.25) was selected, which has a length of 225  $\mu\text{m}$ , Au coating only on the backside, a 2.5–8.0  $\mu\text{m}$  tip with a maximum radius of curvature of 60 nm. The cantilever is slightly thicker than the Olympus Biolever, being 550 nm, with a resonant frequency between 10-20 kHz and a low spring constant of

(0.03 pN/nm) [130]. Occasionally, the SNL-10 Veeco (now Bruker) silicon nitride cantilevers were also used. The longest and thinnest cantilever was often employed, which has a length of 205  $\mu\text{m}$ , Au coating only on the backside, a 2.5–8.0  $\mu\text{m}$  tip with a maximum radius of curvature of 12 nm. Its spring constant is around 0.06 N/m.

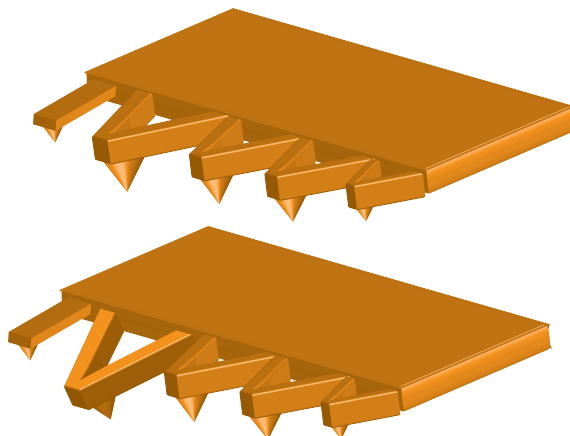


**Figure 2.25:** Diagram of a  $\text{Si}_3\text{N}_4$  chip with 5 cantilevers with different lengths and spring constants. An MLCT non-conductive silicon nitride cantilever distributed by Bruker. The chip has, from left to right, probes of 0.02, 0.01, 0.03, 0.10 and 0.50 N/m nominal spring constants. These probes have a back side coating of 60 nm of Au on top of a 15 nm adhesive layer of Cr [130]. The lower diagram shows the bending of the second cantilever as it approaches the surface.

As can be seen from Equations 2.10 and 2.11, the spring constant of cantilevers solely depends on their geometry and material and is not dependent on the surrounding media. However, the viscosity of the media does affect the mechanical response of the cantilever

Upon immersion in water, the resonant frequency of the cantilever will be reduced, as the probe has an increased effective mass. Its behaviour can be described as a damped harmonic oscillator. The quality factor  $Q$  (i.e. parameter which describes the damping of an oscillator) is also reduced in liquid, as a result of the hydrodynamic forces in the tip-media system. This decreases the performance of the dynamic modes.

In principle, an SFM could measure forces ranging from weak van der Waals forces, in the pN region to strong covalent bonds of hundreds of nN, but in practice the sensitivity is limited by thermal noise and vibrations of the electronic components. Moreover, if the measurement is acquired inside a fluid the cantilever quality factor is strongly diminished due to hydrodynamic damping [131].

### 2.6.5 Force mode

The SFM is not only capable of recording images with nanoscale resolution; it can also be used as a tool for force spectroscopy, an experiment whose output is a force-distance curve. A force-distance curve represents the force on an SFM probe as a result of its position in reference with the sample surface. As seen in Figure 2.26a, the measurement starts away from the surface, where surface forces are absent and the cantilever is not deflected. Then the probe is lowered down (b) until it starts interacting with the surface. There is a sudden small attractive force, due to capillary forces that is denoted jump-to-contact (c). The probe goes into the repulsive regime (d), due to electrostatic forces, as shown in Figure 2.27, until it reaches a maximum point. The probe is then lifted away from the surface (Figure 2.26e) (jump-off contact), but the  $z$ -motor has to overcome the adhesion force between the tip and the sample, caused by attractive van der Waals forces, as shown in Figure 2.28. In the final step, the probe is disengaged from the surface (Figure 2.26f). Force spectroscopy experiments are useful in the determination of adhesive forces, elasticity or stiffness of bacterial membranes, measurement of chemical bonds and specific interactions, determination of capillary forces, among others.

### 2.6.6 SFM probe functionalisation

The chemical modification of SFM probes enables the measurement of forces between specific molecular groups as well as the creation of a map of the spatial distribution of such groups on a sample. Chemical force microscopy is the term given to the use of chemically modified probes in order to measure specific interactions. This term was conceived by a team led by Charles M. Lieber from Harvard [131, 132].

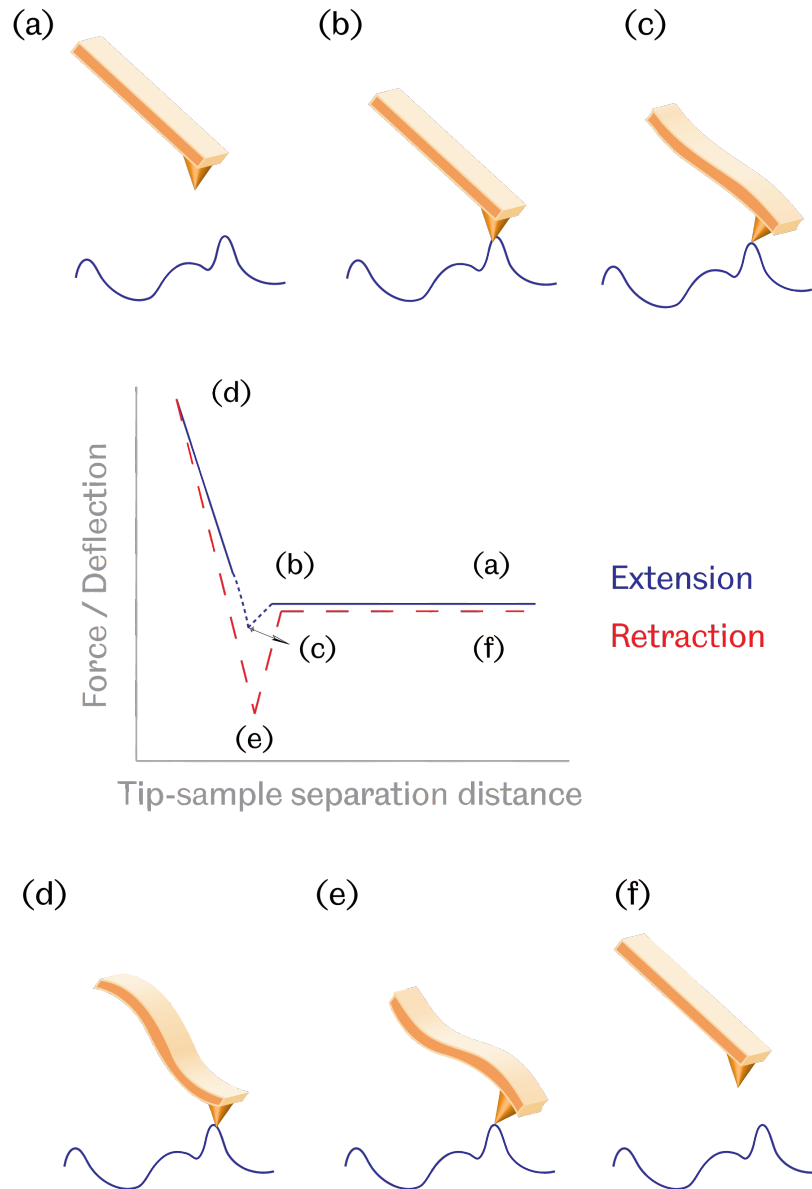


**Figure 2.26:** Diagram of a force-distance curve, showing the different steps of the extension and retraction of the tip. Image inspired by reference [123].

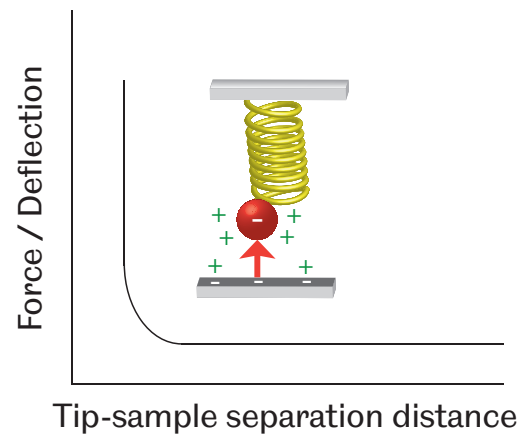


**Figure 2.27:** Electrostatic double-layer repulsion as seen in a force-distance curve. Image inspired by reference [123].

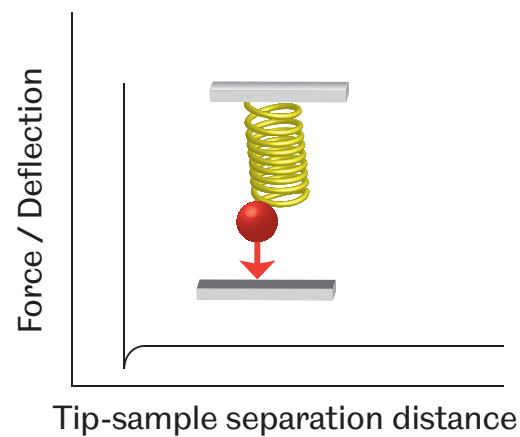


**Figure 2.28:** van der Waals attraction influence on a force-distance curve. A jump-to-contact event can be seen in the lower left end of the curve. Image inspired by reference [123].

Chemical force microscopy aims to extract chemically valuable information about the samples, by controlling the composition of the SFM probes, thus expanding the scope of the experiments. Although the data are still physical in nature, with a clever chemical or biological control of the tips it is possible to obtain relevant compositional information. As stated in §2.6.4, the cantilevers are usually made of silicon nitride, but the composition is not carefully controlled and varies from  $\text{Si}_3\text{N}_4$  to  $\text{Si}_{15}\text{N}_4$  [133], a situation that might interfere with the reproducibility of the experiments.

By ensuring the homogeneity of the tip composition, and giving it a desired functionality, it is possible to map local variations of hydrophobicity and other properties. The tips can be functionalised by modifying the silicon itself, using silanisation or hydrosilation reactions, in which is possible to graft aliphatic chains onto the cantilevers, using trichlorosilane groups. These methods, although cheap and straightforward, yield air-sensitive and often thick and unevenly coated tips [134].

Nowadays one of the most used methods involves the vapour deposition of a thin adhesive chromium layer and a gold layer over a commercial silicon nitride cantilever. A tip coated with gold has a less hydrophilic character than its  $\text{Si}_3\text{N}_4$  precursor, giving rise to different interactions with the surface and thus reducing the capillary condensation force in ambient air. Since gold reacts readily with sulfur compounds, the tip is immersed in a thiol ethanolic solution and a self-assembled monolayer (SAM) of alkanethiols is easily formed within a few hours. Thiols are commonly used because the wide range of end groups that is possible to have and because of their stability and ease of handling. The alkanethiols have, in the non-sulfur end, a functional group that gives the tip the desired chemical behaviour: if it has a methylated end, it has a hydrophobic character, whereas an alcohol or acid end will make the tip hydrophilic (Figure 2.29).

It is important to form the monolayer as soon as the coating process is finished, to avoid the contamination of Au. It is also recommended to use the functionalised cantilevers as soon as possible, to avoid further decomposition of the carefully controlled chemistry of the tip that has just been created.

On the downside of CFM, the radius of curvature of the tip might increase with the coating process, diminishing the sensitivity of the tip to small features [135].

Chemical force microscopy has been used by Dufrêne *et al.* to map the hydrophobicity of fungal samples like *Aspergillus fumigatus* [136], *Phanaerochaete chrysosporium* [137], as well as the bacteria *Mycobacterium bovis* [138] and *Mycobacterium tuberculosis* [139]. The group led by Dufrêne validated their results testing the effectivity of their tips on substrates covered by SAMs of known composition (Figure 2.30).

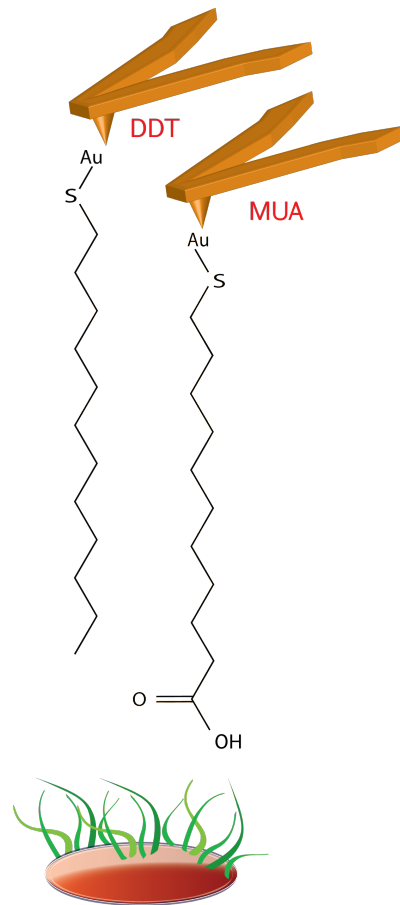


**Figure 2.29:** Thiol SAMs grafted to Au coated tips. A hydrophobic termination can be achieved by anchoring 1-dodecanethiol (DDT), whereas a hydrophilic behaviour would be seen when 11-mercaptoundecanoic acid (MUA) is grafted to the tip.

In the same way, Vadillo *et al.* [140,141] have used hydrophobic and hydrophilic tips to map the hydrophobicity of *Lactobacillus* strains, finding a heterogeneous cell surface. Dorobantu *et al.* [87,142] have conducted force experiments on *Rhodococcus erythropolis* and explained them in the frame of the xDLVO model. Their studies reveal heterogeneity in the measurements of these cells, while probing them with hydrophilic and hydrophobic tips. The presence of EPS and bacterial capsules were accounted for during the analysis. The measurement of adhesion forces in many points of the cell surface, reveal that the highest forces are concentrated in one pole of the cell (Figure 2.31).

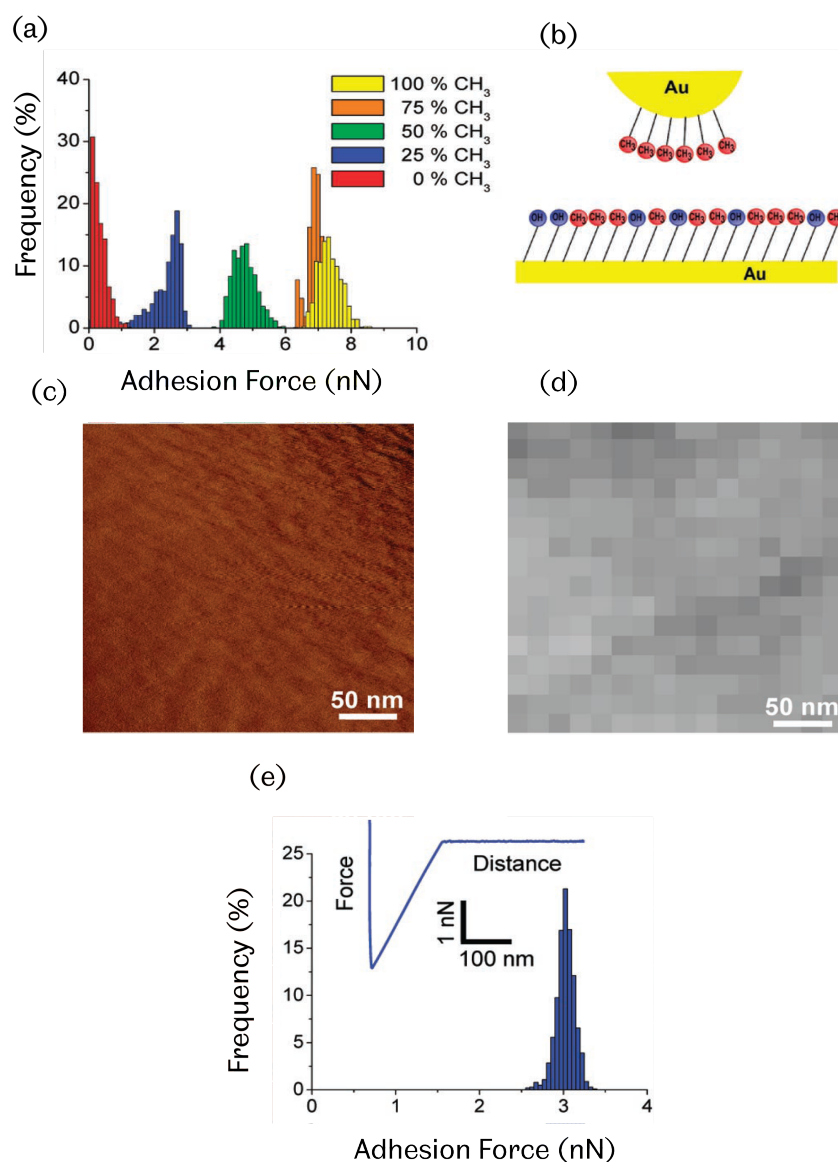


**Figure 2.30:** CFM of *Mycobacterium bovis* cells. (a) Histograms of adhesion of reference SAMs of known molar fractions. (b) Hydrophobic coated tip versus a SAMs of a known  $\% \text{CH}_3$  molar composition. (c) Topographic image of a bacterial membrane region. (d) Force-volume map of the same area. (e) Statistical analysis of the forces of the force-volume map. Images adapted with permission from [138]. Copyright (2007) American Chemical Society.

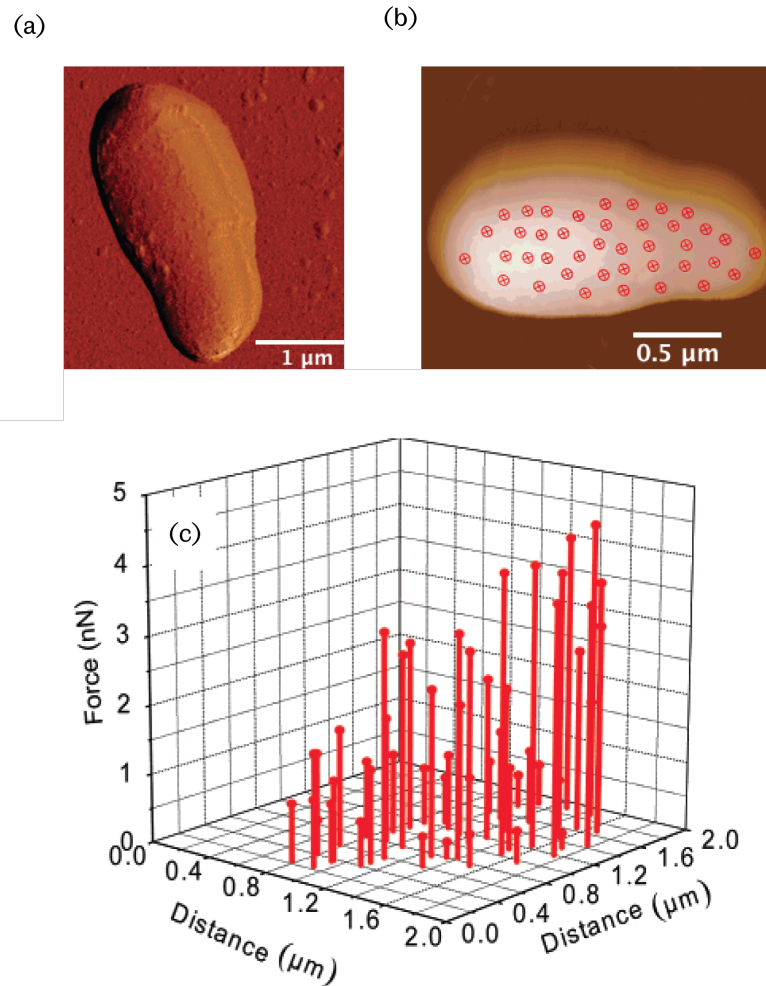


**Figure 2.31:** SFM images and forces of *Rhodococcus erythropolis*. (a) AC Mode, amplitude image of a *R. erythropolis* cell. (b) Map that shows the location of the acquired force distance measurements. (c) Distribution and measurement of the forces that shows higher values towards one pole of the cell. Images adapted with permission of [142]. Copyright (2008) American Chemical Society.

## Single Molecule Force Spectroscopy

Advanced functionalisation of SFM tips can be used for molecular recognition spectroscopy, in which the binding of molecules on SFM tips towards on-substrate receptors is measured by applying a force to the molecule-receptor bond until the bond breaks. A number of molecules must remain permanently attached to the SFM probe usually by covalent bonds via flexible linker spacer molecules. This technique is known as single molecule force spectroscopy (SMFS) [143].

SMFS has been used in the past few years to measure the adhesion of nucleic acid strands [144], enzymes and substrates [145], antigens and antibodies [146], proteins [147], lectins and carbohydrates [146], ligands and cell surface receptors and cell adhesion proteins [148]. It is sensitive enough to detect conformational transitions, reveal functional heterogeneity and determine the number of molecules involved in a chemical reaction [149].

To ensure single molecule events, it is important that only a small number of interacting molecules are attached to the SFM probe. For that to happen, the concentration of the biomolecules must be very low and they should be attached with a favourable orientation.

To that end, spacers are often employed, by tethering flexible and distensible linker molecules, which aim is to separate the biological probe from the tip surface by some nanometres and allow the bioprobe to orient freely. Moreover, the use of spacers permits the distinction between specific and non-specific interactions. Polyethylene glycol (PEG) is often the linker of choice [150, 151].

For example, the group led by G. Francius [152] used the lectin Concanavalin-A SMFS probes, to probe polysaccharides present on the surfaces of planktonic *P. fluorescens* cells. The conformation of the polysaccharides was studied through the measurement of the interaction forces using SFMS and analysed through the freely-jointed chain (FJC) model.

Our own efforts in SMFS can be seen in Chapter 5, where thiolated DNA fragments were tethered to gold coated SFM cantilevers and the interaction between them and model silicon surfaces, under a variety of ionic solutions, was measured.

## Single cell force spectroscopy

Chemical force microscopy and single molecule force spectroscopy give a valuable insight into the chemical properties of bacterial cells. However, these approaches are limited to the properties of the attached molecules, which might not behave in the same way as they do when they are embedded on cell surfaces. The lack

of molecular context could be producing data that is not reproducible in natural environments.

To this end, *bioprobes* can be created, in which the tip of the SFM cantilever is replaced with one or few microbial organisms. A bioprobe will ensure that the molecules are in their native conditions.

Experimentally, the idea of single cell force spectroscopy (SCFS) is not easy to convey. Some authors [153, 154] have coated colloidal probes with bacterial cells, and make them interact with surfaces, while others attach single cells to tipless cantilevers. For example, Cail and Hochella [155] attached *Enterococcus faecalis* to the apex of an SFM cantilever using APTES functionalised cantilevers. Such methodologies can be used to study the interaction between mineral surfaces and bacterial cells.

Perhaps more challenging, is the use of SCFS to measure cell-cell interactions. To this date, there are very few examples in the literature where this has been achieved. Benoit *et al.* [156] attached a cell of the eukaryotic slime mould *Dictyostelium discoideum* to a tipless cantilever, and studied the its interaction with another cell deposited on a Petri dish. The two cells were left in contact for some time, and the detachment force was estimated to be around 20 pN. In terms of bacterial interactions, Younes *et al.* studied the interaction between *Staphylococcus* cells attached to a tipless cantilever, and *Lactobacillus* cells attached to a solid substrate and compared them with the interaction between a pair of staphylococci, revealing that the mixed pair had stronger interactions. Although the present thesis does not deal with SCFS experiments it is important to highlight this technique, since it might revolutionise the field of bacterial interactions and adhesion. Currently SCFS experiments are very challenging and time-consuming, but it is expected that when this technique matures, it will enhance our physical comprehension of complex biological processes.

## Bacterial immobilisation for SFM

### 3.1 Introduction

Microscopy techniques, such as optical, electron and scanning force microscopy, have had a tremendous impact in our understanding of the components, topography and interaction forces of bacteria. The invention of the optical microscope opened the investigation into microbiology, but its applicability has remained somewhat limited, due to its intrinsic limits in resolution. Electron microscopy, which uses electrons instead of light, has been able to overcome the diffraction limit of light, producing outstanding images. Scanning and transmission electron microscopies (SEM and TEM, respectively) have allowed us to visualise the cytoplasmic arrangement of thin sections of bacterial cells. When coupled with immunostaining, they can provide information about specific molecular components on the surface and inside of the cell [9].

Sample preparation for electron microscopy is not an easy task. Both TEM and SEM employ heavy metal stains that enhance contrast between different sections. Often, the samples need to be frozen, sectioned or fixed, depending on the particular requirements of the object of study and the technique. So, although these forms of microscopy provide very detailed information about the structure of bacterial cells and their surface, the complex preparation techniques limit its applicability in the study of bacterial organisms and bacterial interactions *in vivo*.

Scanning force microscopy does not require freezing, sectioning or embedding the sample in heavy metal layers for imaging. The only requirement is to have the biological sample firmly attached to a flat surface. Microbes spontaneously adsorb to substrata and thus, imaging in air using an SFM presents few challenges. The main concerns in attaining a successful SFM scanning are to remove the residues

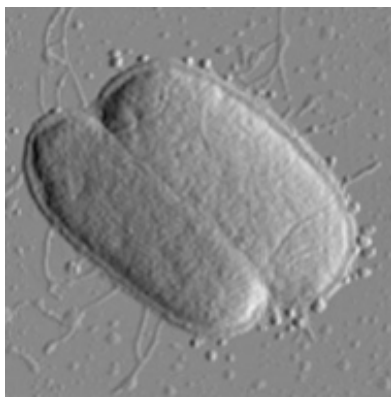
of the culture medium and the secretions produced by the organisms and to avoid the crystallisation of salts on the surface. However, if the imaging is to take place under liquid, further steps are required in order to make sure the cells will withstand the scanning.

It has been acknowledged by many researchers that cell immobilisation under a liquid is a significant barrier to the applicability of SFM to the study of bacterial organisms [157–167]. The methods to immobilise bacteria cannot be applied to all types of bacterial cells due to their intrinsic variations in size, shape, rigidity and surface chemistry. Bacterial organisms, unlike eukaryotic cells, do not spread on the substrate, thus having a very small contact area for attachment.

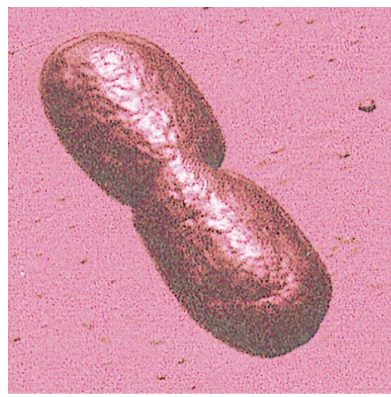
The adhesive properties of bacterial surfaces depend on the nature of the surface proteins, polysaccharides and appendages, whose presence is dictated by the genetic code of the strain. The ionic strength, pH and chemistry of the imaging media can be tailored to enhance the adhesion of the bacterial cells to the substrate, provided the behaviour of the cells is not modified in such a way that falls beyond the subject of study. When selecting the imaging medium one must be sure that the physiology or the organism is not compromised by the immobilisation technique and imaging conditions. In any case, the measured properties will be dependent on the environment: for example Gabouriad *et al.* [168] showed that there were considerable differences between the nanomechanical properties of *S. putrefaciens* at pH 4 and 10. Similarly Pen *et al.* [153] showed that the adhesion profiles of *Rhodococcus* Rc291 varied with pH, as shown by SFM force curves.

### 3.1.1 Imaging bacteria in air and liquid

Air drying is a quick and simple method of immobilisation of bacterial cells. This method works best with strains that are resistant to dehydration, otherwise they can die or appear deflated or shrivelled, even if they are re-hydrated later with water or buffer. Even transient drying can trigger signals that affect the cell surface properties. Moreover, the interaction force of adhesion is rather feeble, making the sample often impossible to be studied under liquid [169, 170]. Figure 3.1 shows a couple of examples of bacterial cells attached onto solid substrates after they have been dried. It is possible to appreciate fine appendages and delicate membrane features, like the rim of the cell capsule. Thus, imaging in air is preferred in some cases, where the resolution of the cell topography is essential [171].



(a) *E. coli* K12 J62.



(b) *E. coli* ATCC 25922.

**Figure 3.1:** Bacterial adhesion by cell drying. Both images were acquired in air. Figure 3.1a was used with permission from [169]. Copyright (2004) John Wiley and Sons. Figure 3.1b was used with permission from [170]. Copyright (1998) American Society for Microbiology.

Figure 3.2 shows an example from the literature [172], in which *E. coli* cells imaged in air show a breadth of surface features and appendages, whereas the ones imaged under PBS appear fuzzy and less resolved.

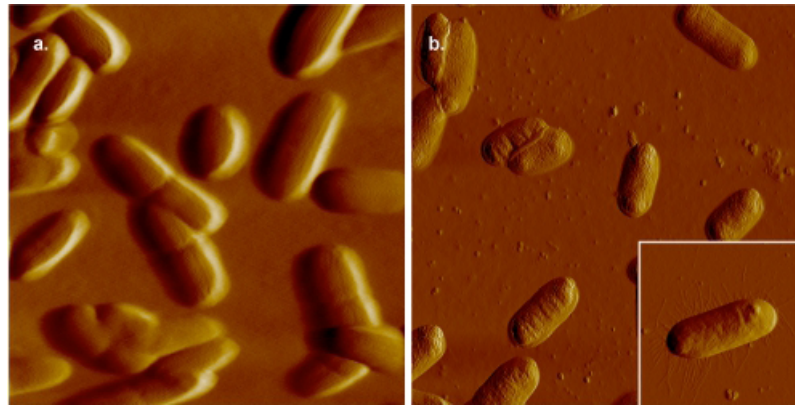


**Figure 3.2:** SFM images of *E. coli*. (a) Imaged under PBS, (b) Imaged in air. Note how in panel (b) more surface features can be observed, including appendages, like the ones highlighted in the inset. Image used with permission from [172]. Copyright (2011) JoVE.

Imaging in liquid is preferred over imaging in air in order to keep the cells hydrated, alive and even capable of reproduction if kept with nutrients. Additionally, keeping the cells under a liquid is essential for force-distance measurements, as this reduces the meniscus forces. Since one of the main goals of the present thesis is the measurement of the adhesive forces present on cell membranes, it was imperative to find a reliable immobilisation method to attach bacterial cells under liquid.

### Meniscus forces

Adhesive forces can be very sensitive to the presence of even trace amounts of water vapour in the atmosphere and as a consequence can be easily modified with changing relative humidity [82]. This has a considerable impact on the appearance of force-distance curves. As explained before in Section 2.6.5 and in Figure 2.26 on page 56, the area under the generated curve (i.e. the *jump-off contact* section of the force curve) is related to the measurement of the tip-sample detachment force. Figure 3.3 shows a force-distance curve of a silicon sample acquired in air and in liquid. In air, a large adhesion force or jump-off contact is evident, whereas in liquid the interaction force is greatly diminished [173].

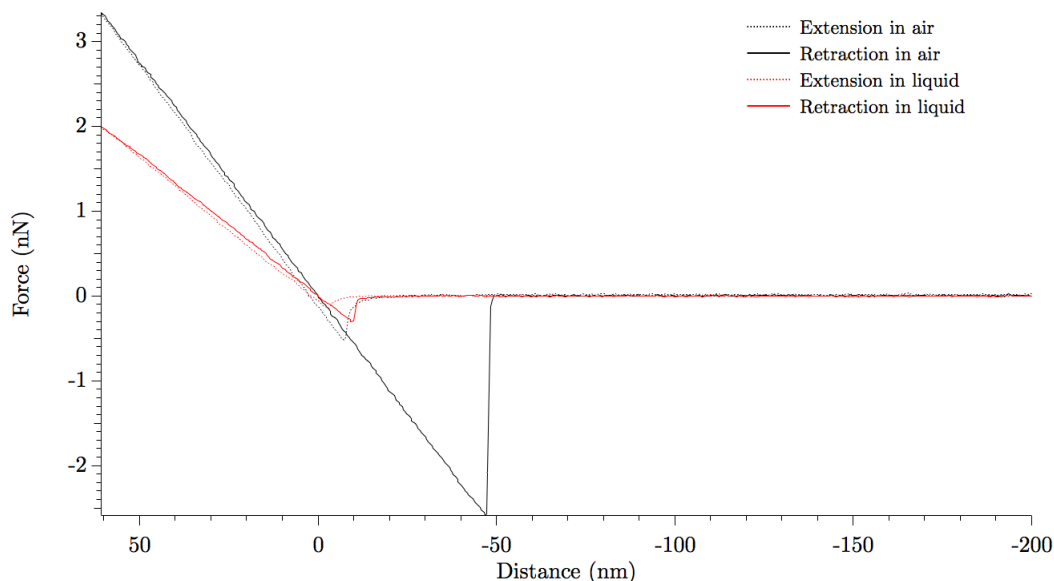


**Figure 3.3:** Force-distance curves in air and water between a clean silicon surface and a  $\text{Si}_3\text{N}_4$  tip.

Meniscus forces are capillary in nature and are a consequence of water vapour condensation in surface contact points of the tip (e.g. cracks and pores). The formation of a meniscus arises from an increased number of van der Waals interactions between water molecules in a confined space, like in the gap between an SFM tip and a substrate. A thin layer of liquid is formed on the tip surface, as schematically shown in Figure 3.4 for the simplified case of a sphere and a planar surface. The thin water layer prevents the tip from pulling off the surface due to an increased surface energy, whereas it only has a small effect in the attractive range of the force-distance curve [173].

The formation of menisci can be understood from a thermodynamics point of view. If the radius of curvature of a micro-contact is below a critical radius, a meniscus will be formed. At equilibrium, the size of this critical radius is related to the vapour pressure and can be defined by the Kelvin radius:

$$r_k = \frac{\gamma_L V}{RT \log(p/p_s)} \quad (3.1)$$

where  $\gamma_L$  is the surface tension,  $R$  is the gas constant,  $T$  is the temperature,  $V$  the molar volume and  $p/p_s$  the relative vapour pressure or relative humidity. For water, the surface tension at 293 K is 0.074 N/m, thus the van der Waals distance of water is  $\gamma_L V / RT = 5.4 \text{ \AA}$ . For a value of  $p/p_s = 0.9$  a Kelvin radius of 100  $\text{Å}$  is obtained. So it follows that the smaller the relative humidity (i.e.  $p/p_s$ ), the smaller

the size of the critical radius for the formation of the meniscus, and thus, the more difficult it is to form a meniscus between two surfaces. This can be clearly seen in Figure 3.5, where environmental SEM pictures of menisci formed between SFM tips and silicon surfaces. At a relative humidity of 40% no meniscus is visible, but at a humidity of 99%, the meniscus is clearly noticeable.

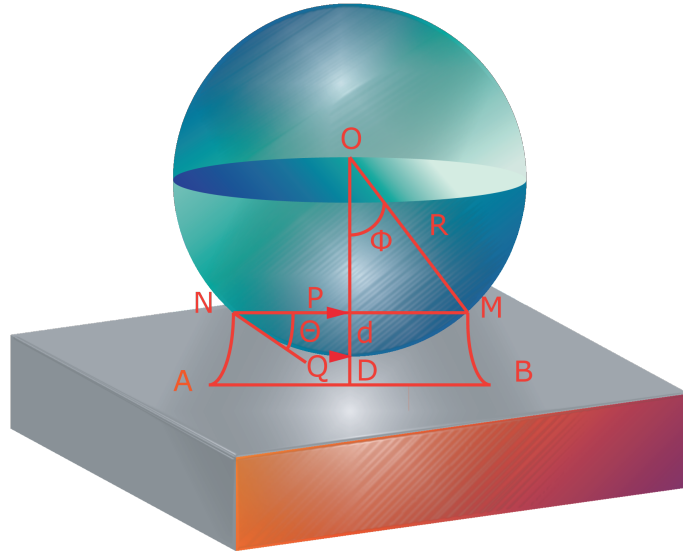


**Figure 3.4:** Meniscus formed between a planar substrate and a spherical object: model of the tip-sample interaction in humid air. Image adapted from [82].

For a sphere and a planar surface (Figure 3.4), the meniscus forces can be approximated for  $R \gg D$ :

$$F^{R \gg D} = \frac{4\pi R \gamma_L \cos \theta}{1 + D/d} \tag{3.2}$$

where  $R$  is the radius of the sphere,  $d$  the length of the segment  $\overline{PQ}$ ,  $D$  the distance between the sphere and the planar surface and  $\theta$  the meniscus contact angle [82].

The water meniscus force exceeds other surface interactions, like van der Waals. In order to measure the contribution of the latter type of forces it is imperative to eliminate the meniscus force. This can be achieved by working in a low humidity environment (e.g.  $N_2$  or vacuum) or by submerging the tip-sample system in a liquid. This is why force measurements are typically performed under water,

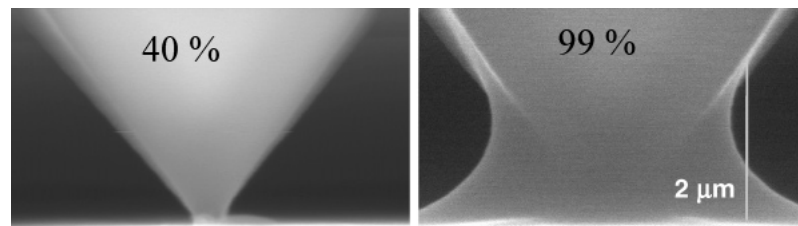


**Figure 3.5:** Images of the menisci formed between an SFM cantilever and a silicon substrate at two different relative humidities. Image adapted with permission from [174]. Copyright (2005) American Chemical Society.

buffer or media, not only to eliminate the meniscus forces, but to keep the cells in physiological conditions, hydrated and potentially viable. While working in a liquid environment solves some experimental issues, it can present other challenges. As has been stated above, the dragging forces of a cantilever under liquid can easily detach the cells, and imaging of bacterial cells under liquid is frequently an arduous experiment with poor repeatability. In the next section, the work of some researchers that effectively imaged bacterial cells under liquid, will be reviewed.

## 3.2 Background on immobilisation methods

The methods to immobilise bacteria for SFM scanning, can roughly be divided into five categories: mechanical entrapment, biofilm formation, use of polydopamine adhesives, use of cationic surfaces and covalent bonding between the cells and substrates. A description of these protocols and the efforts of researchers in this field will be reviewed in the following sections.

### 3.2.1 Mechanical entrapment

Mechanical entrapment into polycarbonate membranes is an ideal system for the immobilisation of rigid and spherical organisms such as yeast and fungal spores. The membrane pores have to be selected in such a way that they are slightly smaller than the cells to probe, so that these can be firmly immobilised. This methodology was developed by Kasas and Ikai in 1995 [157] and explored further by Dufrêne ever since [175–178] (Figure 3.6a). Turner *et al.* [160] improved this methodology by etching the membranes with a concentrated alkaline solution, evening the size of the pores and thus maximising the chances of getting a cell trapped. Using this methodology, they studied live *S. aureus* using PBS to to image non-dividing cells and brain heart infusion (BHI) broth to study dividing cells (Figure 3.6b).

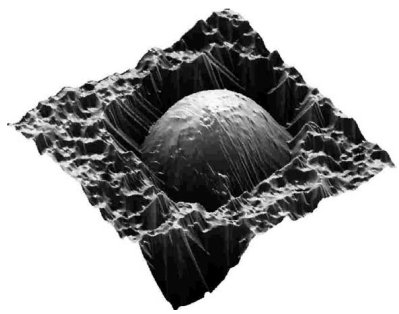
Kailas *et al.* [164] presented an alternative method to trap spherical shaped *S. aureus* by immobilising them in holes made on photoresists by laser interference lithography. This method has the advantage of removing the constriction on the cells. This method has been explored further by Bailey *et al.* [179] who applied this technique to rod shaped cells using pillars with successful results. Dupres *et al.* [180] and Alsteens *et al.* [138] immobilised rod-shaped cells, depositing them onto polycarbonate membranes; the cells did not go inside the holes, but instead rested on top of the membrane surface. This interaction was good enough for their study in liquid. Doktycz *et al.* [161,181] proposed another method to entrap cells mechanically; they used a gelatin coating, which yielded successful results in SFM imaging. Gelatin immobilisation has elements of mechanical and also chemical immobilisation; gelatin is denatured collagen and some bacteria, like *E. coli* bind to collagen via specific adhesive sites. These interactions, added to electrostatic and hydrophobic forces, immobilise the cell for SFM scanning. The presence of ions in the imaging media can affect the attachment to gelatin coated mica and not all bacterial species have affinity for this substrate (Figure 3.6c).

In general, mechanical immobilisation has many limitations: polycarbonate membranes, although inexpensive and easy to use, are mostly limited to spherical organisms. On the other hand, lithographically etched supports are expensive to produce, and need to be tailored to the specific measurements of a particular species. On this account, there has not been a wider presence of these protocols in the literature. Novel ways of mechanical entrapment are needed, since this method has all the elements to be ideal for the study of microorganisms in natural conditions.

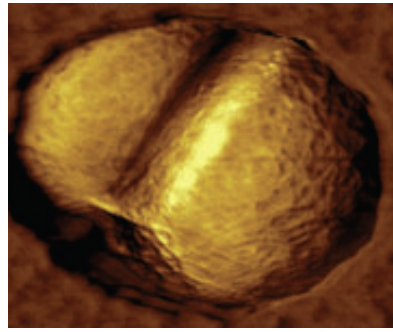
### 3.2.2 Biofilm formation for immobilisation

In some cases the interactions between the microbes and the substrate are strong enough that the cells do not need to be constricted in any way and the substrate does not need to be modified, but examples of this immobilisation approach are rather scarce. Bagchi *et al.* [184] reported the attachment of the hyphae of the soil-dwelling Gram positive *Streptomyces coelicolor* to muscovite mica. The interaction is strong enough for them to take contact mode images in liquid and force-volume maps. The hyphae-substrate interaction is presumed to be of electrostatic nature (Figure 3.11c).

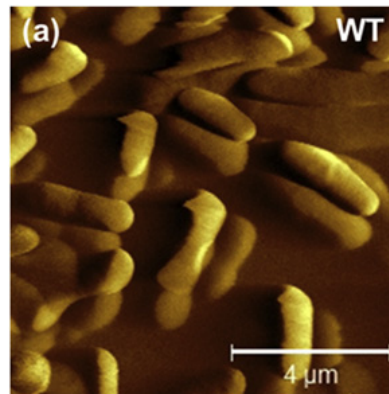
Another way to achieve a strong cell-substrate interaction, without the need of pre-conditioning the substrate, is to form a biofilm for several days. Bacteria themselves produce polymers that condition the substrate and aid in cell attachment. Nonetheless, a close-packed arrangement of a cell multi-layer, might make



(a) *A. oryzae* LMTC 2.14 in a polymer membrane.



(b) *S. aureus* NTC 85 32 in an etched polymer membrane.



(c) *E. coli* K-12 in gelatin.

**Figure 3.6:** Physical entrapment. Figure 3.6a was used with permission from [182]. Copyright (2002) Elsevier. Figure 3.6b was used with permission from [160]. Copyright (2009) John Wiley and Sons. Figure 3.6c was used with permission from [183]. Copyright (2012) Elsevier.

it challenging to observe individual organisms adequately. As reviewed in §2.2, biofilms are complex three-dimensional networks of cells, which are adhered to surfaces and among each other by means of extra-cellular polymeric substances. Hence, through this approach, only microbial conglomerates can be observed and such observations have been amply reported in the literature. Ahimou *et al.* [185] studied the biofilm formed by a mixed culture of bacteria that came from an activated sludge. Mangold *et al.* [186] incubated pyrite coupons in an *Acidithiobacillus ferrooxidans* suspension for 4 days, to allow attachment and biofilm formation. Other biofilm studies by SFM include the papers published by Oh *et al.* [187] and Tsofigkas *et al.* [188] on *E. coli*, Volle *et al.* [189] on *Bacillus subtilis*, *Micrococcus luteus*, *E. coli* and *Pseudomonas putida*, Otero *et al.* [190] and Whitehead *et al.* [112] on *Pseudomonas aeruginosa*, Hu *et al.* [191] and Liu *et al.* [192] on *Streptococcus mutans*, Lorite *et al.* [108] on *Xylella fastidiosa*, Díaz *et al.* [193] on the early stages of biofilm formation of *Pseudomonas fluorescens* and Abe *et al.* [194] on drinking water biofilm samples.

Some authors have used polystyrene to immobilise bacteria. Dufrêne and van der Aa [195] incubated small polystyrene squares in an *Azospirillum brasilense* suspension for 24 h. Although they were able to observe EPS adhered to the plastic, no bacterial cells were observed under liquid. Cell detachment appears to be a common problem in the study of bacterial biofilms under liquid, and consequently, a high number of surface coating techniques have been devised, in order to strengthen the bonds between the organisms and their support. A number of surface-modification protocols, to increase adhesiveness, will be presented in the following sections.

### 3.2.3 Polydopamine adhesives

A number of marine invertebrates have the ability to produce strong adhesive materials that help them adhere to under-water substrates, fighting buoyancy and currents in highly saline environments [196]. The mechanisms of their adhesion have been of interest to biologists, who seek to use their strategies and apply them to the immobilisation of biological samples under buffer. Of particular notoriety is the marine mussel *Mytilus edulis*, which adheres strongly to surfaces by means of a *byssus*, which is a bundle of threads composed by eight *mussel foot proteins* (Mfps). The main proteins are depicted in Figure 3.7; Mfp-3,5 and 6, which are in contact with the surface, contribute the most to the overall adhesion to the surface. These proteins use a catechol (i.e. benzenediol) containing substance, which is generated by a post-translational modification of the aminoacid tyrosine, to yield 3,4-dihydroxyphenilalanine (DOPA).

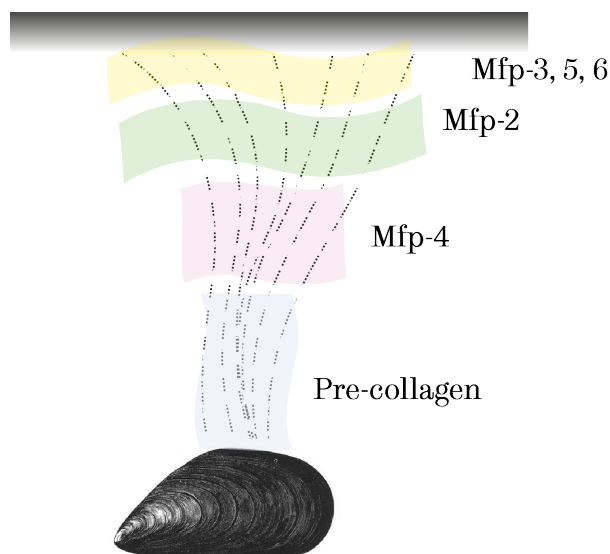


**Figure 3.7:** Byssus of *Mytilus edulis*, showing its component mussel foot proteins (Mfps). Mfp-3,5,6 are the most responsible for the mussel adhesion and are characterised by a high content of DOPA; Mfp-5 has over 30% of this substance. Image adapted from reference [197].

DOPA and its analogues are catecholic compounds, and their role as adhesion and crosslinking promoters has been investigated. A wide variety of surfaces can be conditioned using these compounds, a process that enhance the interaction between surfaces through the formation of hydrogen, ionic, covalent and coordination bonds between the catechol moieties and the substrates. For instance, Messersmith *et al.* [198] reported the formation of strong bidentate binuclear bridges on titania surfaces and other metal oxides, whereas only hydrogen bonding interactions occur between DOPA and mica (Figure 3.8) [199].

The group led by Messersmith uses synthetic forms of DOPA to enhance adhesion and for a variety of applications, including fetal membrane repair to prevent birth complications [200], antibacterial hydrogels based on DOPA that include silver nanoparticles [201] and catechol pH-responsive polymers for the targeted release of cancer drugs [202].

A mixture of proteins extracted from *Mytilus edulis* has been solubilised, and sold under the commercial name of Cell-Tak<sup>®</sup> [203]. These proteins are rich in L-3,4-dihydroxyphenylalanine (L-DOPA) (i.e. the precursor of polydopamine) and hydroxyproline [204] (Figure 3.9).

A Cell-Tak<sup>®</sup> neutral solution can be spread on glass slides and used as a support for mammalian cells and tissues. Ay *et al.* used Cell-Tak<sup>®</sup> to immobilise human

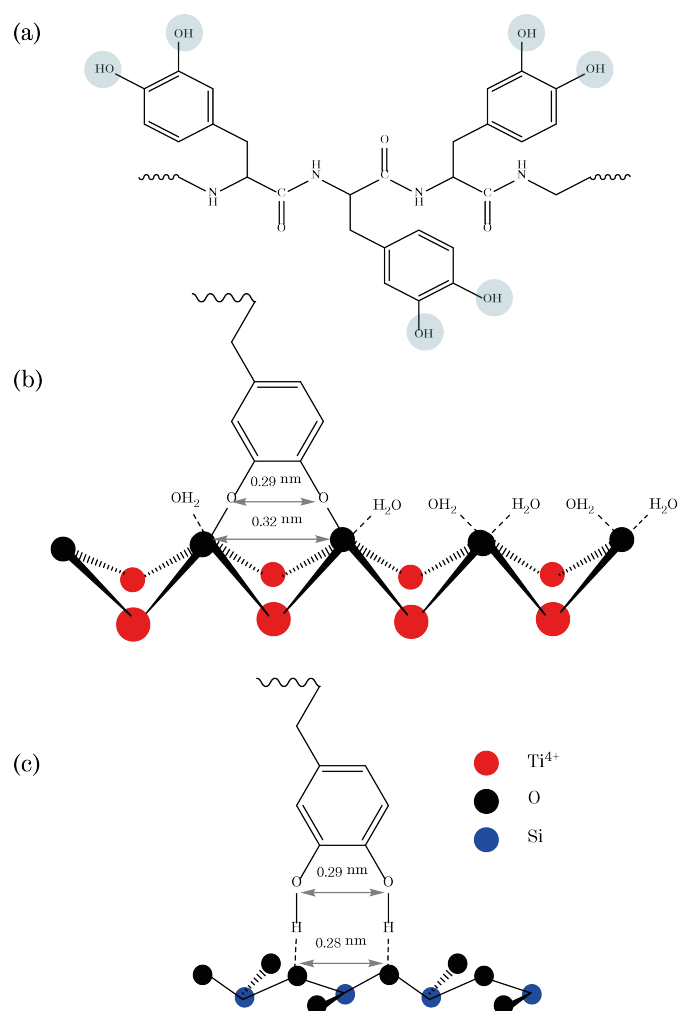


**Figure 3.8:** Adhesion of DOPA to substrates. (a) Chemical structure of a sequence of three DOPA units, highlighting the catechol groups. (b) Interaction between DOPA and a  $\text{TiO}_2$  surface via coordination bonds. (c) Interaction between DOPA and mica via hydrogen bonds. Image adapted from reference [199].

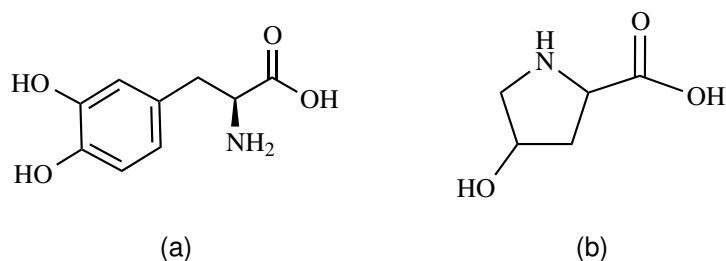


**Figure 3.9:** Chemical formulae of (a) L-3,4-dihydroxyphenylalanine (L-DOPA) and (b) hydroxyproline, main components of the polyphenolic proteins present in *Mytilus edulis* bioadhesives [204].

lymphoma cells for SFM scanning [205]. Similarly, Hwang *et al.* [206] immobilised chinese hamster ovary and HeLa cells (both are commonly used cell lines used in medical research) for optical microscopy essays.

The use of DOPA or Cell-Tak<sup>®</sup> in bacterial studies is more limited. Kang and Elimelech coated an SFM cantilever with polydopamine, and attached single *E. coli*, *B. subtilis* and *S. cerevisiae* bacterial cells. The resultant *bioprobes* were used in force experiments against quartz surfaces under different ionic solutions. The authors maintain that their preparation method is superior to chemically fixed cells, as it is non-invasive and does not require crosslinking. Meyer *et al.* [166] systematically studied diverse immobilisation methods for bacterial cells in SFM experiments, including those of mechanical, electrostatic and covalent nature, as well as Cell-Tak<sup>®</sup>; the majority of these methods have been also reviewed and tested in the present thesis. The authors of this paper claim that they successfully immobilised *E. coli*, *B. subtilis*, *S. sciuri* and *Mycobacterium sp.*, and imaged them in contact mode under a variety of liquids (Figure 3.10). They concluded that Cell-Tak<sup>®</sup> was the most successful method they tried, and they proposed it can be used as a general protocol for the preparation of Gram positive and Gram negative cells for SFM scanning in physiological conditions. Despite the authors' belief of the wide applicability of this method, only few publications describing the use of Cell-Tak<sup>®</sup> as a bacterial bioadhesive were found, suggesting that these results must be interpreted carefully and that this technique might not be the *panacea* that biophysicists are looking for.

### 3.2.4 Electrostatic attraction

Polycationic surfaces enhance the electrostatic interactions between the negatively charged ions present on the cell surface of microorganisms and the sample substrate. Bacteria generally have a superficial negative charge due to the presence of

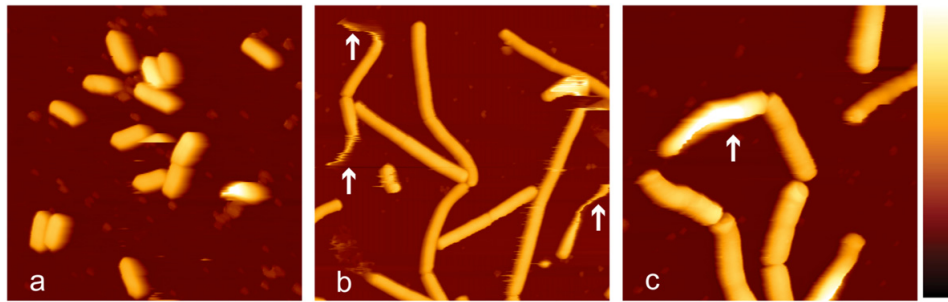


**Figure 3.10:** Immobilisation of bacterial cells using polydopamine adhesives. Cell-Tak<sup>®</sup> was used to image *E. coli* (a), *B. subtilis* (b) and *Mycobacterium sp.* (c) in contact mode under the buffer HEPES. The arrows show sections of the bacterial cell that detached or moved during scanning. Image taken with permission from [166]. Copyright (2010) Elsevier.

peptidoglycan, rich in carboxylate and amino groups. Teichoic acids, lipoglycans and lipopolysaccharides are phosphate rich groups that if present, also contribute to the overall negative charge. Polycationic surfaces include poly-L or poly-D-lysine (PLL, PDL), polyethyleneamine (PEI), and aminosilanes, out of which (3-aminopropyl)triethoxysilane (APTES), is the most commonly used (Figure 3.11).

### Poly-lysine

Poly-lysine has been used to immobilise a variety of microorganisms to flat substrates, including the fungus *Candida albicans* [207], and the bacterial strains *E. coli* [188,208–210], *Streptococcus mutans* [211,212], Lactobacilli [140,213], Staphylococci [212,214–217], *Pseudomonas aeruginosa* [218] and *Pseudomonas fluorescens* [219,220].

Similarly, it is also commonly used to attach microbial cells to the apex of a cantilever or tip. Atabek *et al.* [221] and Touhami *et al.* [222] used PLL to attach bacteria of the genus *Pseudomonas* to an SFM cantilever. Lower *et al.* [154] used poly-D-lysine to manufacture an *E. coli* colloidal cell probe (i.e. a micron-sized polystyrene bead coated with bacteria and attached to an SFM cantilever). Correspondingly, PDL has been used [36] to attach *Rhodococcus* 291 to colloidal probes. The advantage of using the optical isomer D over L resides on the fact that some cells can digest PLL [223].

Bacteria immobilised by poly-L-lysine can be imaged under media [171,188], buffers (PBS: phosphate buffered saline [207,216], MES: 2-(N-morpholino)ethane-

sulfonic acid, [217], MOPS: 3-(N-morpholino)propanesulfonic acid, [219], HEPES: 4-(2-hydroxyethyl)-1-piperazineethanesulfonic acid [213,221], adhesion buffer [105], deionised water [153,171], or inorganic salt solutions (NaCl [154], KCl [140]).

### Polyethyleneimine

Glass slides coated with polyethyleneimine have also been widely used to attach bacterial cells to glass substrates. Examples include *E. coli* K12 [224–227], *P. fluorescens* [152,227], *Acidithiobacillus ferrooxidans* [228,229] and *Bordetella pertussis* [230].

Correspondingly, cell probes have been manufactured employing PEI as an adhesive for the bacterial species *Lactococcus lactis* [231], *E. coli* [232–235], *Lactobacillus rhamnosus GG* [236] and *Streptococcus thermophilus* [237] among others.

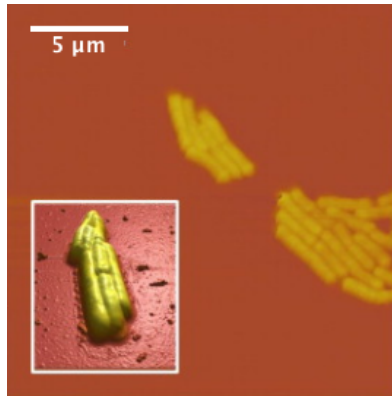
Bacteria linked to the surface by PEI have been imaged under deionised water [228,231], or buffers (PBS, [152,166,230,236,237] Tris: tris(hydroxymethyl)amino-methane [225,233,235,238]).

### 3-Aminopropyltriethoxysilane

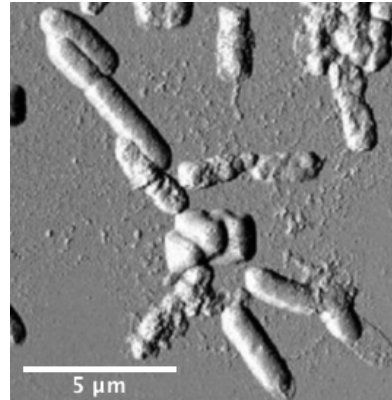
The use of 3-aminopropyltriethoxysilane (APTES) has also been reported in the literature as a way to immobilise bacteria, due to the polycationic nature of the aminosilanised functionality that is created [239]. Furthermore, the amino groups in APTES can potentially bind to the aldehyde and ketone groups that are present on the cell walls [155,240].

Liu *et al.* [163] attached and imaged *Xanthomonas campestris*, *Pseudomonas syringae* and *Bacillus subtilis* to APTES treated mica. Longo *et al.* [241] immobilised *E. coli* to acquire force-volume maps and measure elasticity. Anselmetti *et al.* [242] imaged *Corynebacterium glutamicum* ATCC14067 using intermittent contact mode in liquid using also silanised glass and mica (Figure 3.12).

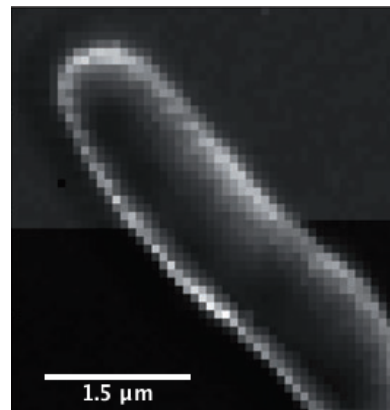
APTES is a relatively cheap and readily available aminosilane. As a trifunctional silane it crosslinks the surface through one of its alkoxy groups, while leaving the other two for the lateral crosslinking of molecules into a monolayer. The amine group that corresponds will ideally be pointing upwards, thus creating an array of positive charges under an aqueous solution [244] (Figure 3.13). If the aminosilanation reaction is not adequately controlled, then the molecular orientation of the amine moieties can vary, thus reducing the efficiency of the surface groups as bonding agents [245].



(a) *Lactobacillus rhamnosus* GG on PEI, imaged in air.



(b) *M. lysodeikticus*, *P. fluorescens* on PLL, imaged under medium.



(c) *S. coelicolor* hypha on mica, imaged under water.

**Figure 3.11:** Bacterial immobilisation via electrostatic interactions. Figure 3.11a used with permission from [236]. Copyright (2013) Elsevier. Figure 3.11b was used with permission from [220]. IOP Publishing. Copyright (2012). All rights reserved. Figure 3.11c used with permission from [184]. Copyright (2008) John Wiley and Sons.

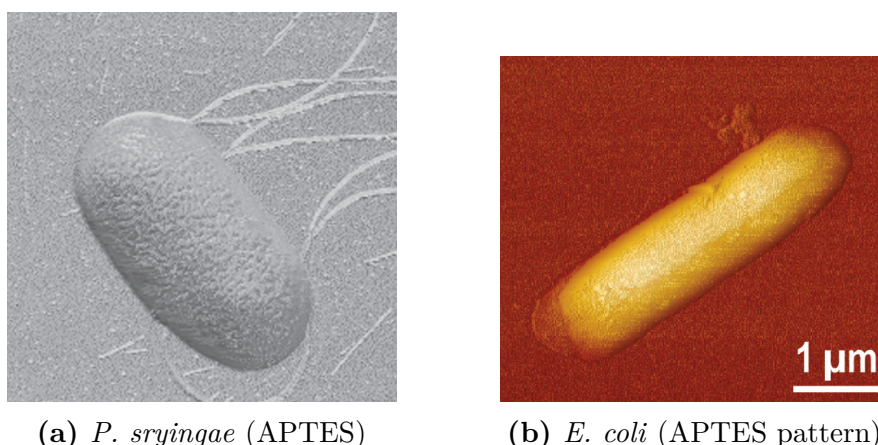


**Figure 3.12:** Bacterial adhesion using APTES. Both images were acquired in air. Figure 3.12a was used with permission from [163]. Copyright (2011) John Wiley and Sons. Figure 3.12b was used with permission from [243]. Copyright (2009) American Chemical Society.

The stability of an APTES layer comes from the lateral crosslinking rather than from direct surface crosslinking. The formation of these layers depends strongly on the method of synthesis, namely chemical vapour deposition or formed from an organic or aqueous solution [244].

APTES is known for its instability, and can polymerise inside its container bottle, reducing its effectivity in reactions. This can be prevented by keeping the siloxane in anoxic conditions. A polymerised APTES cannot give reproducible surface properties once it is attached to a silicon surface. Liquid phase polymerisation can lead to an uneven surface that is not suitable for molecular imaging, although, it can bind bacteria without noticeable deformations.

APTES surfaces have been carefully characterised. One can determine the number of  $\text{NH}_2$  groups in the aminated surface by using the ninhydrin reaction as used by Karrasch *et al.* [240] and Sarin *et al.* [247]. A 2% APTES solution in 95% acetone for 3 min, typically gives an average of 6 amino groups per  $\text{nm}^2$ . Similarly, Alexander *et al.* found an average of 3 amino groups per  $\text{nm}^2$  using a 1% APTES solution in 95% acetic acid (1 mM) in methanol and 4% water [239].

Bacteria attached to silanised glass can be imaged or measured under buffer (PBS [91, 219, 248, 248], HEPES, [189, 218, 249], MOPS [219, 250], acetate [176]) or water [251, 252].

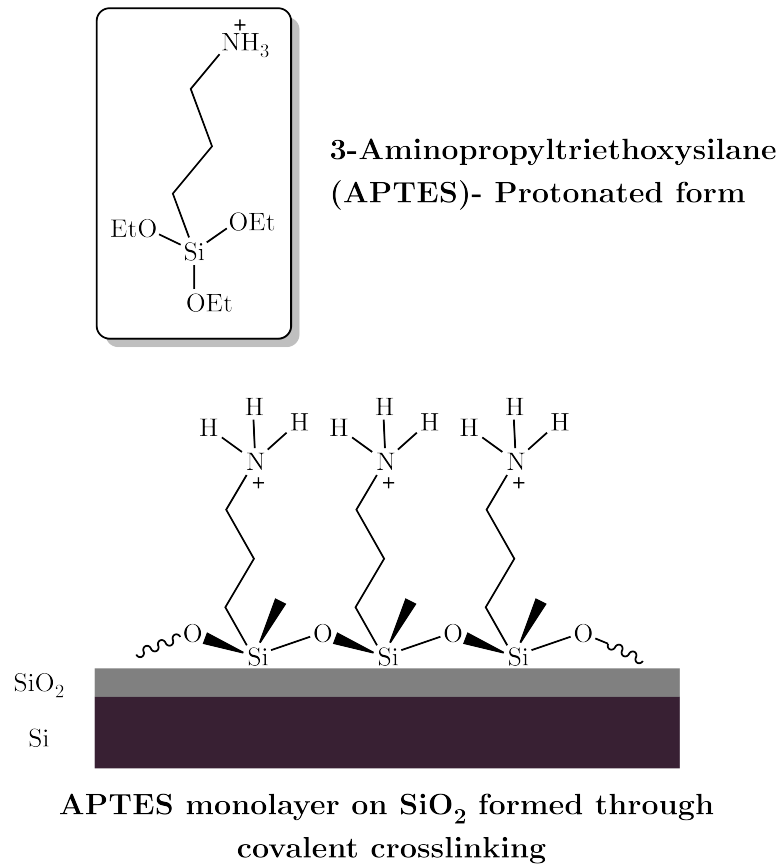


**Figure 3.13:** APTES structure and crosslinked monolayer on a SiO<sub>2</sub> substrate. The pKa of APTES is  $\sim 10$  [246], so in neutral buffer conditions, the amine groups are protonated. Image adapted from [244].

### Buffer selection

The selection of an adequate buffer for SFM imaging, when using electrostatic forces to bind cells to substrates, is of the utmost importance [253]. Often the imaging buffers must have a lower ionic strength than the one required for physiological conditions and even distilled water has been used. It is difficult to choose a universal buffer for SFM imaging and this needs to be selected carefully to avoid affecting the compressibility of the cells, due to changes in turgor pressure [160].

When the cells are bound to the surface using electrostatic interactions, the interaction is subject to the salt contents of the imaging media, which is weakened at high ionic strength. Hence, the imaging would be performed ideally in deionised

water, if not for the osmotic stress that this would cause to the cells [166]. In some cases even by rinsing the cells with DI water prior to imaging in buffer, the capsular EPS of the bacteria can be disrupted. For instance, Stukalov *et al.*, have reported the detachment of electrostatically immobilised cells during scanning while using buffer. They hypothesised that this might happen due to the weakening of the electrostatic interactions at high ionic strength, as stated in Section 2.4.3.

### 3.2.5 Covalent immobilisation

From the first early experiments in the early nineties of scanning force microscopy of bacteria, it became apparent that when the cells were firmly immobilised, the resolution of their surface features increased considerably [254]. Glutaraldehyde was one of the first choices for firm immobilisation, as it had been commonly used for electron microscopy fixation. Glutaraldehyde forms covalent bonds between the proteins on the bacterial cell wall [163]. Despite its potential use for cell fixing, the effect of this chemical has been widely researched, and it has been noted that it changes the conformation of the cell wall, modifies the morphology and dimensions of the cells, stiffens the bacterial cell wall and kills the organisms [226, 255]. Since this method limits the biological significance of the results, it is imperative to find other ways of immobilising cells that do not affect the cell envelope greatly.

#### APTES with EDC and NHS

Liu and Camesano [167, 256] have immobilised bacterial cells for SFM scanning by creating covalent bonds between the cells and molecules attached to a solid substrate. The bonding protocol involved the use of the zero-length crosslinker EDC (1-ethyl-3-(3-dimethylaminopropyl)carbodiimide) aided by NHS (N-hydroxysuccinimide) or sulfo-NHS (N-hydroxysulfosuccinimide); this is a zero-length crosslinker because it directly conjugates carboxylates to primary amines, without a spacer. This reaction couples the carboxylic groups on bacterial surfaces with amino groups on APTES coated glass slides, without modifying the bacterial surface, as the activated groups do not remain a part of the linkage. EDC reaction targets the carboxylic groups on the bacterial surface forming an unstable O-acylisourea intermediate complexes. In a second state, these transient species react with NHS, which creates succinimidyl ester functionalities that readily react with primary amino groups. If the activated groups do not find the amino groups of the APTES surface, they revert back to the original carboxylic acid form, leaving the bacterial top side unmodified, and only the underside of the cell crosslinked to the glass [218]. This process is illustrated in the general scheme

of reaction in Figure 3.14 and in the detailed reaction mechanism in Figure 3.15. Other researchers have reported that the cells remain viable and that the activity of bioactive molecules is not disrupted by the crosslinkers [257].

Atabek, Liu and Camesano [167,218] evaluated the attachment of the bacteria *E. coli*, *P. aeruginosa* and *S. epidermis* employing three different methods: poly-L-lysine, APTES/EDC/NHS and mechanical trapping. The authors claim that all three methods resulted in similar bacterial morphologies and force events. The authors also conducted  $\zeta$ -potential measurements on *Pseudomonas aeruginosa* before and after the EDC/NHS treatment and they found, in both situations, a similar value, concluding that the bacterial surface was not modified by this method. On the other hand, Volle *et al.* [189] fixed *E. coli* and *B. subtilis* for SFM studies using the EDC/NHS protocol as well as natively-formed biofilms on glass. They found differences between the two modes of attachment in the bacterial spring constants (i.e. elasticity) of the studied cells and in the adhesive properties of the cell surfaces. It is evident that the biological significance of the APTES/EDC/NHS method must be analysed carefully before any conclusions can be made.

Other researchers have successfully applied EDC/NHS/APTES to immobilise other biological samples for SFM. Chen *et al.* [248] immobilised the nitrogen fixing bacteria *Bradyrhizobium japonicum* and probed the bacterial cell surface polymers with soybean agglutinin-modified SFM probes. The authors found a considerably different behaviour between the adhesion forces acquired in the presence of  $Mg^{2+}$  and  $Ca^{2+}$  with those acquired in the presence of (Gal)/N-acetyl-galactosamine, a substance which blocks the soybean agglutinin receptor sites. Other biological samples like bacteriophages [162] and proteins [259] have been attached to surfaces using this methodology.

Since proteins can also be bound via the EDC/NHS methodology, it is important to consider if the presence of these in the cell suspension medium could affect the efficiency of the attachment of the cells to the substrate. Potentially, proteins with primary amine residues could compete with the APTES surface for the carboxylic acid binding sites on the cell surface. Ideally the buffer in which the reaction takes place, should be relatively free of proteins, apart from those which are being excreted by the cells or released by lysed cells. So far, the extent of this competition remains unknown.

When using APTES/EDC/NHS the imaging can be performed under water, PBS or any of the Good's buffers (e.g. MOPS, HEPES, MES etc. These are commonly used biological buffers, proposed by Good *et al.* in 1966 [260]), making it a very flexible method, that can study cells in physiological conditions.

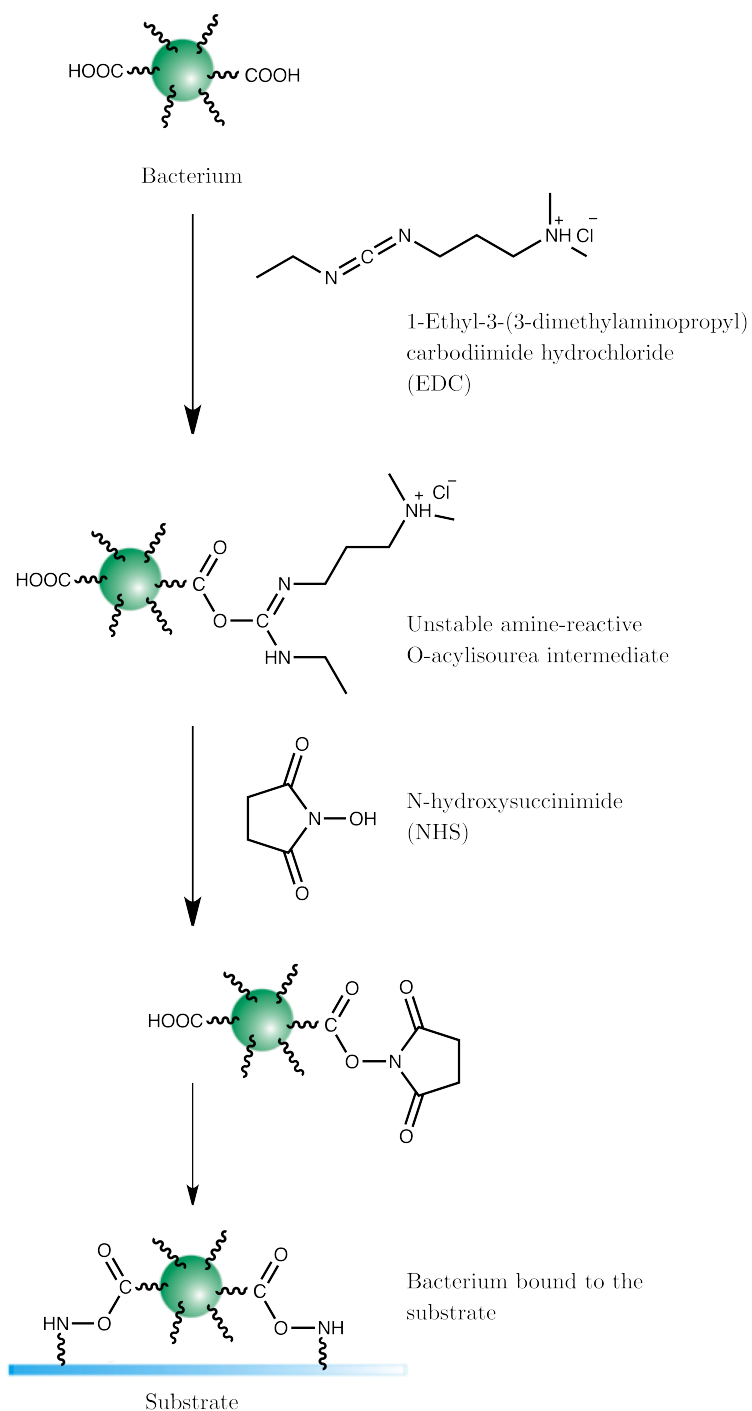


**Figure 3.14:** Reaction scheme of the immobilisation of bacterial cells using the zero-length EDC/NHS crosslinking reaction. Image adapted from [167].

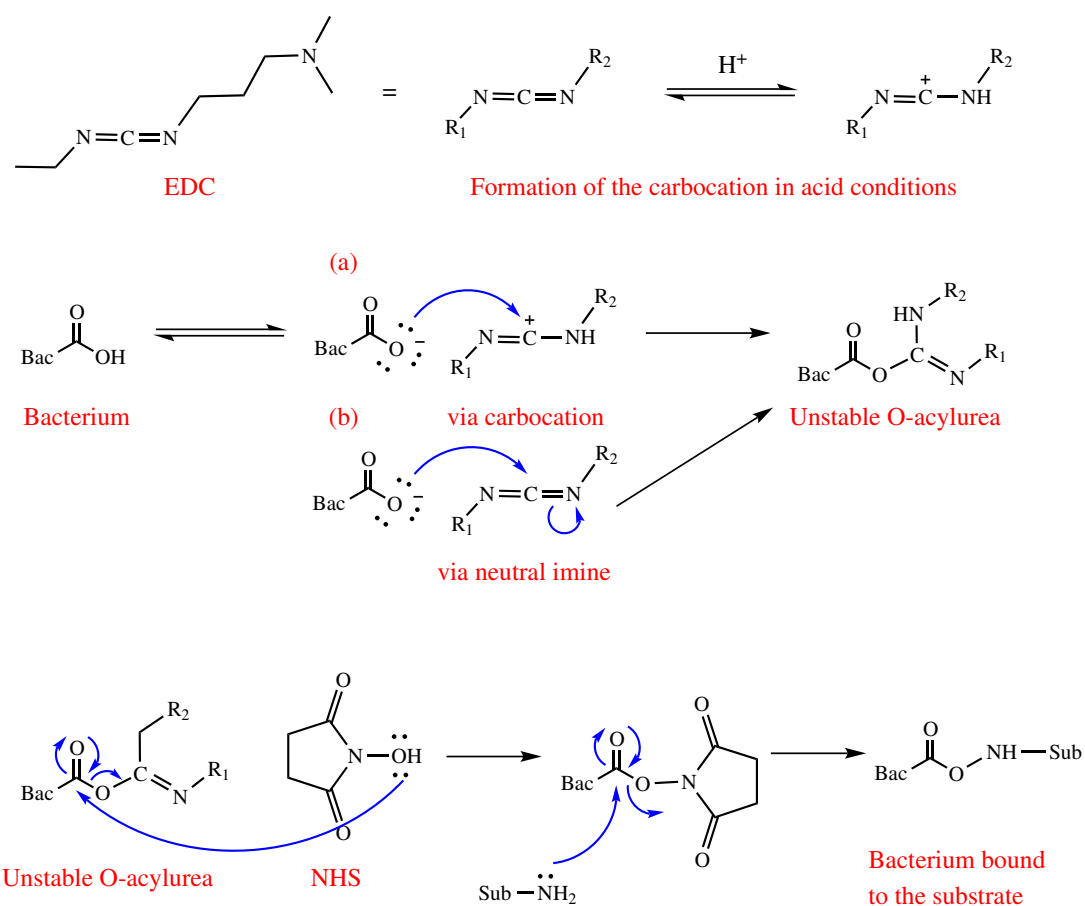


**Figure 3.15:** Reaction mechanism of the zero-length EDC/NHS crosslinking reaction. The reaction can proceed in acid conditions via a (a) carbocation intermediate or (b) the neutral imine. Bac: Bacterium, Sub: Substrate. Image adapted from [258].

### 3.3 Immobilisation of *Rhodococcus* spp. and *Pseudomonas* spp.

Having reviewed a wide choice of literary sources, and being aware of the challenges in the immobilisation of bacterial entities for SFM scanning, it was decided to experiment with different techniques, starting from the mild ones, like biofilm formation and mechanical entrapment, followed by electrostatic immobilisation and concluding with the formation of covalent bonds. In the following sections diverse immobilisation trials will be presented, discussing their suitability for rhodococci and pseudomonads.

#### 3.3.1 General experimental protocol for bacterial growth

*Rhodococcus* and *Pseudomonas* species have often been isolated from contaminated sites during screening programmes for pollutants [8, 261]; *Rhodococcus* spp. Rc291 and Rc92 were isolated from a gasworks site in Newcastle, England and were gifts from J.A.C. Archer of the University of Cambridge. *Pseudomonas* Pse1 and Pse2 were isolated from a phenol contaminated aquifer in the West Midlands, England. The bacterial strains strains from at  $-80\text{ }^{\circ}\text{C}$  frozen stocks (70% bacterial suspension, 30% glycerol) were plated onto Reasoner's (R2A) agar (Oxoid, Hampshire, England) plates (Table 3.1) for 3 days at  $20\text{ }^{\circ}\text{C}$ . The plates were stored at  $4\text{ }^{\circ}\text{C}$  and used for a maximum time of 1 month. R2A media is used for slow-growing species, the growth of which could be suppressed by a faster growing strain, and thus this media is scarce in nutrients. A picture of a set of these bacterial plates can be seen in Figure 3.16.

The cells were pre-cultivated in a culture tube containing 3 mL of AB10 medium (Table 3.2) for 12 h at  $20\text{ }^{\circ}\text{C}$  in an incubator (Sanyo MIR-153 refrigerated incubator, Sanyo-Panasonic, Loughborough, England) fitted with an orbital shaker (Luckham R1000 Orbital Shaker, Luckham Ltd. Burgess Hill, England) at 50 r.p.m. 100  $\mu\text{L}$  of this pre-culture were used to inoculate 100 mL of AB10 medium, in the aforementioned conditions, for 72 h.

Cells were pelleted by centrifugation at  $1200\text{ }g_n$  (MSE Centaur 2, MSE Ltd. London, England) and resuspended in sterile 0.9% (w/v) NaCl to an optical density at 600 nm ( $\text{OD}_{600}$ ) of 0.2. ( $\text{OD}_{600}$  is a common way to assess the concentration of bacterial cells in a suspension. The light scattering caused by the bacteria in suspension is measured using a spectrophotometer at a wavelength of 600 nm.)  $\text{OD}_{600}$  values were measured using a WPA light wave S2000 UV/Vis spectrophotometer (WPA, Cambridge, England).

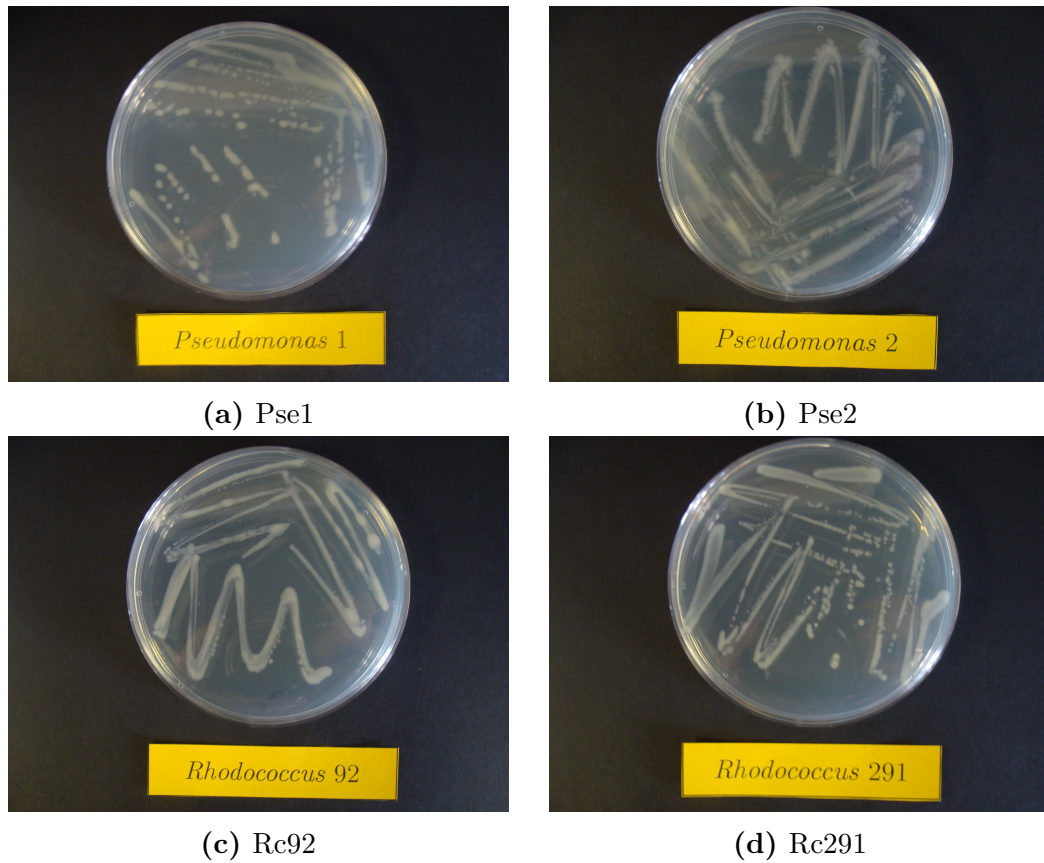


**Figure 3.16:** R2A plates in which the studied strains were grown. Fresh agar plates were prepared every month, taking fresh cells from the frozen glycerol stocks. The plates were grown at 20 °C for 3 days and kept at 4 °C thereafter.

---

Composition of R2A media	
Ingredient	Concentration (g/L)
Yeast extract	0.5
Proteose peptone	0.5
Casamino acids	0.5
Glucose	0.5
Soluble starch	0.5
Sodium pyruvate	0.3
K <sub>2</sub> HPO <sub>4</sub>	0.3
MgSO <sub>4</sub> · 7H <sub>2</sub> O	0.05
Agar	15.0

---

**Table 3.1:** Composition of R2A agar [262].

5 mL of the adjusted cell suspension were added to 45 mL of AB10 and grown under the same conditions to late exponential or early stationary phase, normally to an OD<sub>600</sub> of 0.3–0.4 (When the values of the absorbance of the cell suspension are correlated with the growth time, a *growth curve* can be plotted. More information about the growth curves can be found in Appendix E. For a visual summary of the preparation technique refer to Figure 3.17).

In the final step, the cells were harvested by centrifugation at 1200  $g_n$  and washed or resuspended according to the particular requirements of each technique.

Batch	Ingredient	Concentration
A	$(\text{NH}_4)_2\text{SO}_4$	1.51 mM
	$\text{Na}_2\text{HPO}_4$	3.37 mM
	$\text{KH}_2\text{PO}_4$	2.20 mM
	NaCl	179 mM
B	$\text{CaCl}_2$	10 mM
	$\text{MgCl}_2$	0.1 mM
	$\text{FeCl}_3$	1 mM
Trace	$\text{CaSO}_4$	0.2 mg/L
	$\text{FeSO}_4 \cdot 7\text{H}_2\text{O}$	0.2 mg/L
	$\text{MnSO}_4 \cdot \text{H}_2\text{O}$	20 $\mu\text{g/L}$
	$\text{CuSO}_4$	20 $\mu\text{g/L}$
	$\text{ZnSO}_4 \cdot 7\text{H}_2\text{O}$	20 $\mu\text{g/L}$
	$\text{CoSO}_4 \cdot 7\text{H}_2\text{O}$	10 $\mu\text{g/L}$
	$\text{NaMoO}_4 \cdot \text{H}_2\text{O}$	10 $\mu\text{g/L}$
	$\text{H}_3\text{BO}_3$	5 $\mu\text{g/L}$
Carbon Source	Glucose	2 mM

**Table 3.2:** Composition of AB10 medium [263]. A and B were autoclaved separately, to avoid precipitation, and mixed afterwards. The A and B mixture was kept refrigerated at 4 °C until use. The trace elements were mixed and filtered and were added along with the carbon source immediately before the preparation of the culture.

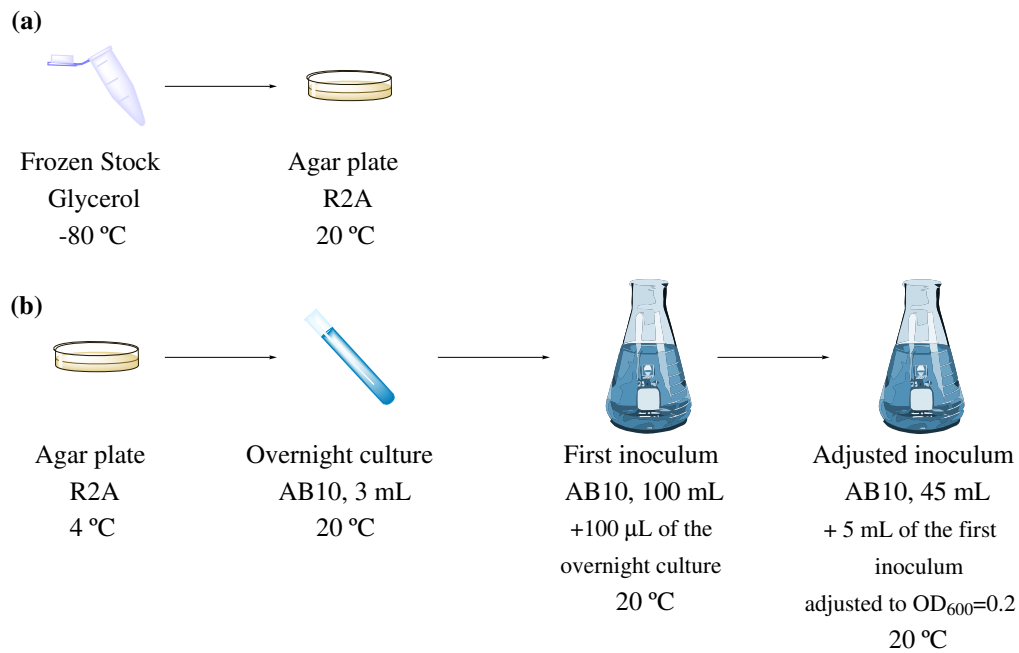


**Figure 3.17:** Bacterial growth procedure.

### 3.3.2 Mechanical entrapment through or on filter pores

#### Immobilisation of *Pseudomonas* on polycarbonate membranes

Our own efforts of immobilising the studied strains on membranes can be seen in Figure 3.18. In Figure 3.18b, Pse2 cells were filtered onto polycarbonate filters. The cells seem to be in close contact with each other, forming a monolayer deposited on top of the membrane. Details of the cell membrane can be appreciated as well as globules of organic material in the interstitial spaces between the cells. The cells appear somewhat deflated, due to the combined action of dehydration and suction. For the particular case of rod-shaped cells, this immobilisation technique is not ideal, because the cells are not properly trapped inside the holes. In the presence of a liquid medium, the cells immediately detach, as the interaction forces between the cells and the membrane are feeble.

As stated before, Turner *et al.* [160] used highly alkaline solutions to etch the membranes, increasing the diameter of the hole, and evening out their sizes. Since there are only a few available pore sizes in commercially available polycarbonate membranes, etching the pores until a desired hole diameter is achieved is highly advantageous. Furthermore, a possibility exists that two pores merge together into one that could accommodate a rod-shaped cell.

Ana Lorena Morales-García

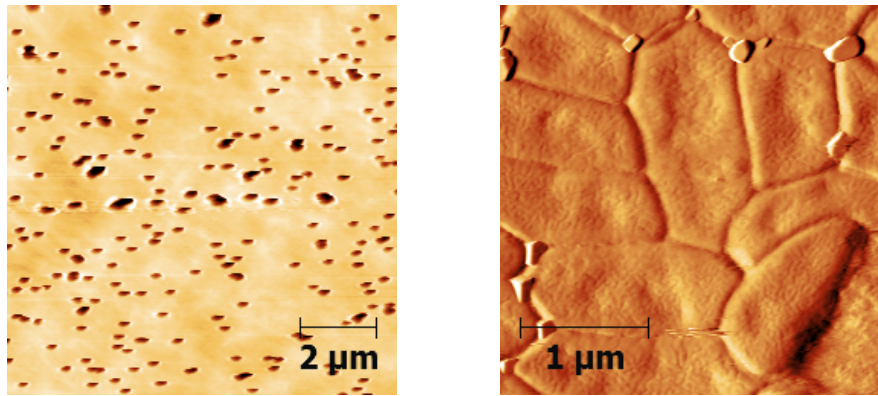
### Experimental conditions for the mechanical immobilisation technique

The bacterial cells shown in Figure 3.18 were grown and harvested as explained in Section 3.3.1. Bacterial cells were grown to early stationary phase and adjusted to an optical density of 0.2. 5 mL of the suspension were filtered through 1.2  $\mu\text{m}$  Millipore RTTP hydrophilic polycarbonate membranes (Millipore Germany) mounted on 25 mm syringe filter holders (Sartorius, Germany).

Some membranes were used as sold and others were etched for 3 h in NaOH 4 M, and washed thoroughly with water afterwards. The etched membranes were air-dried overnight.

The filters were attached to clean glass slides using double sided tape (Scotch 3M, England). The filters were imaged using a Veeco Dimension 3100 SFM (Nanoscope IV, Digital Instruments, Woodbury, NY, USA) encased in a protective acrylic box, where the humidity was measured to be 50% using a sensor (Sensirion Humidity Sensor, Hero Electronics Ltd. Ampthill, England). The samples were imaged in contact mode in air, using SNL-10 Veeco cantilevers, with a nominal spring constant of 0.06 N/m and nominal resonant frequency in the 12-24 kHz interval. Upon the addition of NaCl 0.9% the cells detached (Data not shown).

Mechanical entrapment was not a suitable method for the immobilisation of the studied strains, as both *Rhodococcus* and *Pseudomonas* are rod-shaped organisms. Even after etching the membranes with a 4 M NaOH solution for several hours, suitable holes that could accommodate these bacteria were not found (data not shown). Dupres *et al.* [180] and Alsteens *et al.* [138] both reported the immobilisation of rod-shaped *Mycobacterium bovis* on the surface of polycarbonate membranes. The bacterial cells shown in their reports do not seem to be lodged inside a hole, but seem to be resting inside a crevice of the membrane. After many attempts, using small and large pore sizes, and etched membranes, it was not possible to obtain cells that could withstand SFM scanning in liquid using this immobilisation technique.



(a) Non-etched polycarbonate membrane with a nominal pore size of 0.2  $\mu\text{m}$ .

(b) Pse2 on a polycarbonate membrane, imaged in air. The height scale is 220 nm.

**Figure 3.18:** Bacterial immobilisation on polycarbonate membranes. (a) Bare, non-etched, polycarbonate membrane as seen with an SFM. The nominal size of its pores is 0.2  $\mu\text{m}$ . (b) Pse2 cells filtered onto a 1.2  $\mu\text{m}$  alkaline etched polycarbonate membrane. The cells are not entrapped inside the holes, and rest on the membrane surface. The images were acquired in contact mode using an SNL-10 probe, using the 0.06 N/m cantilever.

### 3.3.3 Attachment via hydrophobic interactions

#### Immobilisation of *Rhodococcus* and *Pseudomonas* on polystyrene

Since previous studies [24, 36] revealed that Rc291 and Pse1 formed extensive biofilms on polystyrene, it was thought that this plastic would make a good support for SFM scanning.

Rc291 forms substantial biofilms on polystyrene inserts that have been left inside a growing bacterial suspension for 1–2 days, as seen in Figures 3.19 and 3.20.

Polystyrene also makes a very good support for SFM scanning in air. The strain Rc291 was selected for the trials, as it was known that it possesses a high value of hydrophobicity, of 76.9%, according to the MATH test (§2.5). It was found that Rc291 attached to polystyrene substrates, and was an excellent support for SFM scanning in air, even in contact mode. Figures 3.21 and 3.22 reveal sharply defined, whole cells, where some details of their surfaces can be appreciated. Figure 3.22 shows the presence of amorphous material surrounding the cells, which could be EPS, parts of lysed cells, or organic debris from the growth media. Since the

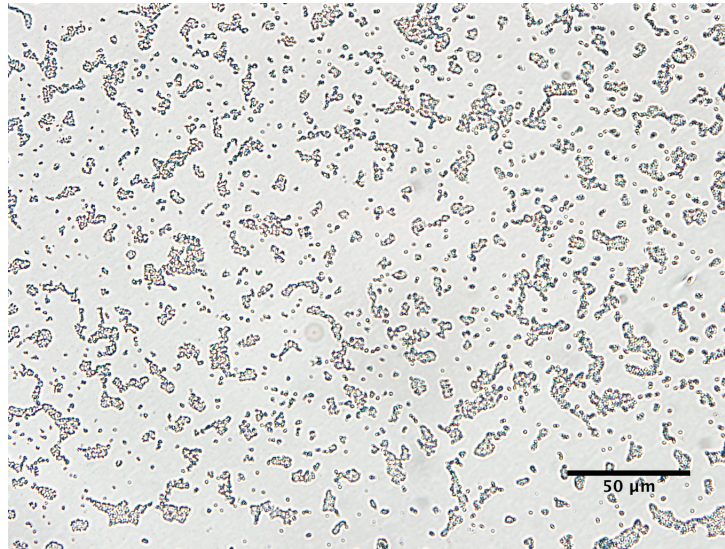


**Figure 3.19:** Rc291 biofilm on polystyrene, grown for 24 h. Cells grown at 25 °C in AB10, supplemented with 2 mM glucose. The cells were grown in the presence of a polystyrene insert. This image was taken with a 40× objective.

biofilms are in their first stages of formation, no three dimensional network has been formed yet and thus single bacterial cells can be imaged on polystyrene.

However, when the cells are imaged in water, media or buffer, the attachment is not strong enough, and the cells tend to detach with repeated scans, or appear fuzzy. Figures 3.23, 3.24 and 3.25 show the effect that water or media have on the attached biofilm. Some cells withstand the scanning, whereas others detach completely after several frames have been acquired. After many experiments in which the growth times, imaging medium and type of polystyrene were systematically varied, it was concluded that the sole use of hydrophobic interactions was not good enough to immobilise the cells for SFM scanning in physiological conditions.

### Experimental conditions for polystyrene immobilisation

Two different brands of Petri dishes were used: Sterilin (Sterilin, Teddington, UK) and ibidi (ibidi GmbH, Munich, Germany). The former are made out of virgin polystyrene, sterilised by  $\gamma$ -radiation and manufactured in mirror finished moulds to ensure optical clarity [264]. The ibidi dishes are made of hydrophobic polystyrene of the highest optical quality. These dishes have a refractive index and birefringence similar to those of glass. The optical quality of ibidi dishes ensures low roughness, making them suitable for high resolution microscopy [265].

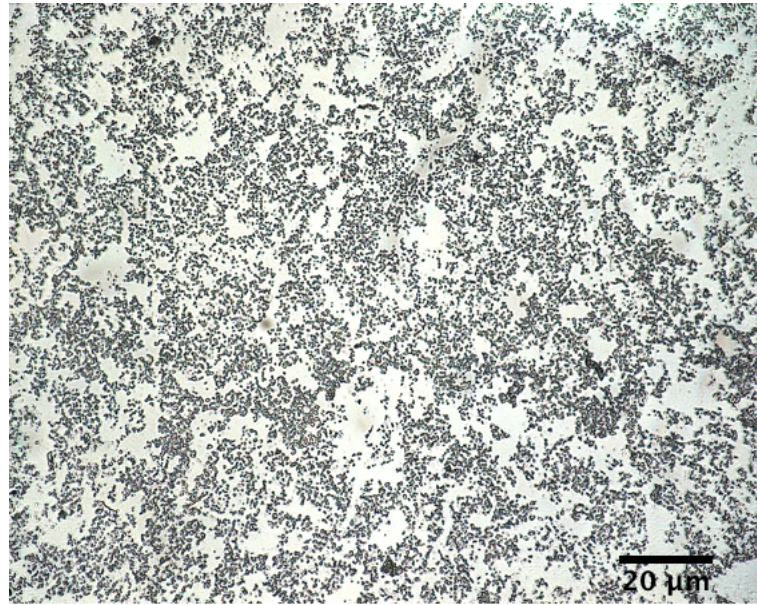
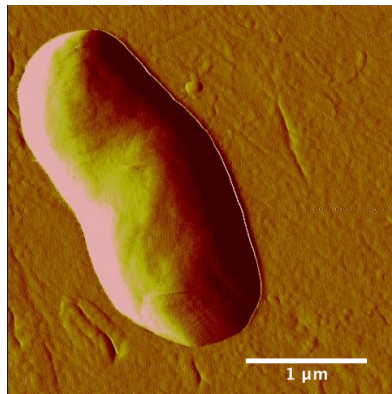


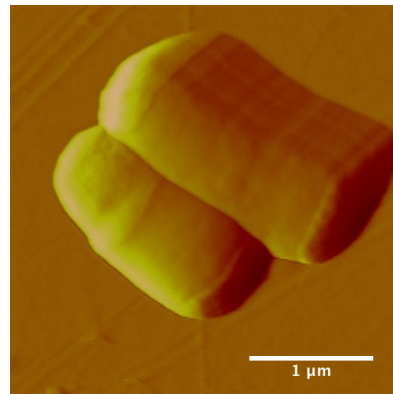
**Figure 3.20:** Rc291 biofilm on polystyrene, grown for 46 h. Cells grown at 25 °C in AB10, supplemented with 2 mM glucose. The cells were grown in the presence of a polystyrene insert. This image was taken using a 40× objective.

Rc291 cell colonies were taken from the agar plates and grown in AB10 liquid medium, supplemented with glucose 2 mM, inside of Sterilin or ibidi Petri dishes for 24 h at 20 °C. Once this time has lapsed, the culture medium was decanted and the bottom of the Petri dish, where the cells were attached, was carefully rinsed with ultra pure water (distilled and deionised to an electric resistivity of 18 MΩ·cm) and allowed to dry. The cells were then imaged in air, or under water or media.

The plates, shown in Figures 3.21 - 3.25 were imaged using a Dimension 3100 system (Nanoscope IV, Digital Instruments, NY, USA) in contact mode, using MLCT Si<sub>3</sub>N<sub>4</sub> SFM probes (Bruker AFM Probes, USA), with a spring constant of 0.01 N/m. The images were acquired using low scanning frequencies (0.5 Hz) to avoid cell detachment. Biofilm morphology was assessed visually using a light transmission microscope (Olympus BX50W1, Olympus Optical Ltd., Watford, UK) with a 40× objective, and representative images were captured using the CellB imaging software (Olympus Optical Ltd., Watford, UK) (Figures 3.19 and 3.20).

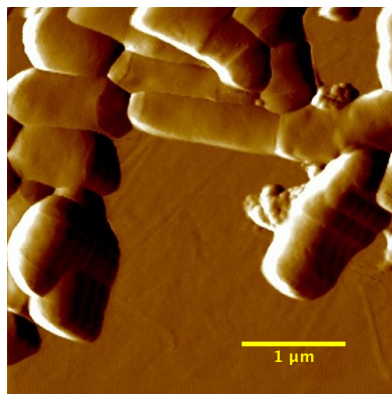


(a) Rc291 on polystyrene, imaged in air. The height scale is 800 nm.

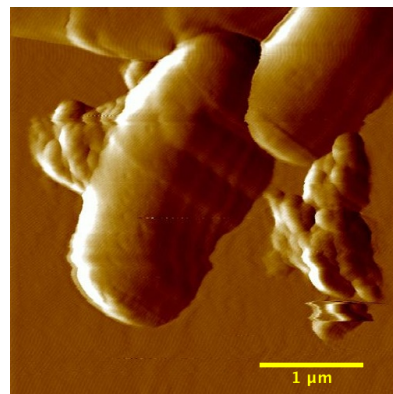


(b) Rc291 on polystyrene, imaged in air. The height scale is 1 μm.

**Figure 3.21:** Rc291 attached to polystyrene. Biofilms formed on Sterilin Petri dishes after 24 h. The images were acquired in contact mode using an MLCT probe, using the 0.01 N/m cantilever.

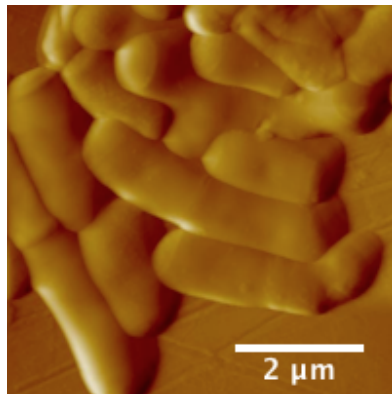


(a) Rc291 cell on polystyrene, imaged in air. The height scale is 800 nm.

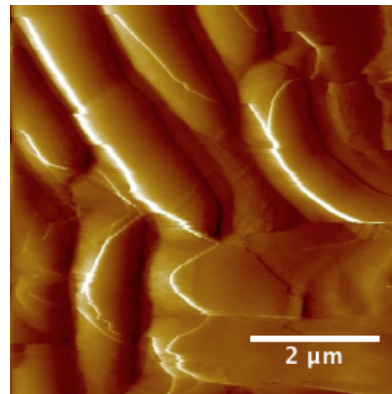


(b) Rc291 cells on polystyrene, imaged in air. The height scale is 800 nm.

**Figure 3.22:** Rc291 attached to polystyrene. Biofilms formed on ibidi Petri dishes after 24 h. The images were acquired in contact mode using an MLCT probe, using the 0.01 N/m cantilever.

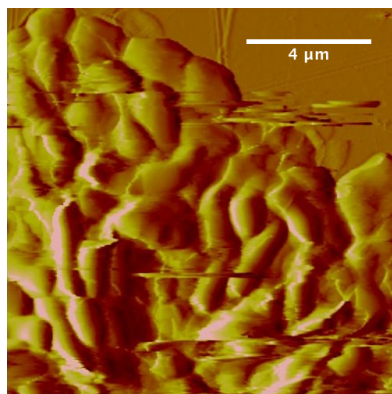


(a) Rc291 cells on polystyrene, imaged in air. The height scale is 1 μm.

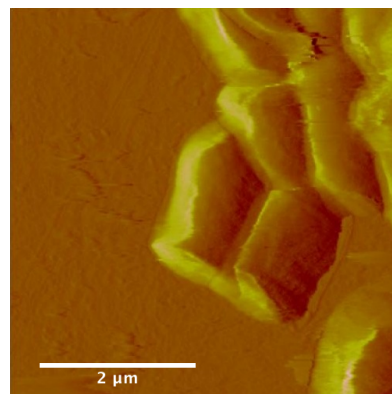


(b) Rc291 cells on polystyrene, imaged in water. The height scale is 1 μm.

**Figure 3.23:** Rc291 attached to polystyrene. Biofilms formed on Sterilin Petri dishes after 24 h. Fuzzy bacterial cell surfaces can be seen in Figure 3.23b. The images were acquired in contact mode using an MLCT probe, using the 0.01 N/m cantilever.

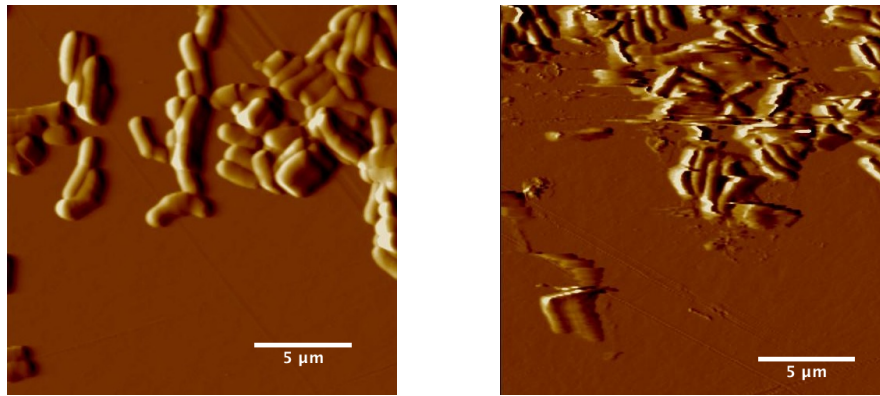


(a) Rc291 cells on polystyrene, imaged in water. The height scale is 1 μm.



(b) Rc291 cells on polystyrene, imaged in water. The height scale is 1 μm.

**Figure 3.24:** Rc291 attached to polystyrene. Biofilms formed on Sterilin Petri dishes after 24 h. Figure 3.24a shows horizontal lines produced either by the detachment of cellular fragments or by the drift of the cantilever and/or sample through time, generating tip dragging. The images were acquired in contact mode using an MLCT probe, using the 0.01 N/m cantilever.



(a) Rc291 cells on polystyrene, imaged in air. The height scale is 1  $\mu\text{m}$ .

(b) Rc291 cells on polystyrene, imaged in AB10. The height scale is 700 nm.

**Figure 3.25:** Rc291 attached to polystyrene. Biofilms formed on Sterilin Petri dishes after 24 h. Figure 3.25b shows horizontal lines produced either by the detachment of cellular fragments or by the drift of the cantilever and/or sample through time, generating tip dragging. The images were acquired in contact mode using an MLCT probe, using the 0.01 N/m cantilever.

### 3.3.4 Attachment via electrostatic interactions

#### APTES

APTES immobilisation promotes the formation of extensive biofilms, as seen in the optical microscopy image shown in Figure 3.26, for Rc291. APTES coated surfaces are also suitable for detailed SFM images in air, as seen in Figure 3.27, where some surface features, like capsular material and membrane rugosity are apparent. Occasionally, it was possible to image Rc291 cells under their growth medium (Figure 3.28), AB10, observing a fuzzy cell surface and some other fragments detaching under the action of the SFM probe. After many attempts where the contact time, imaging medium and APTES concentration were varied, without obtaining consistently satisfactory results, it was concluded that APTES-coated surfaces were not a reliable methodology for the immobilisation of our bacterial strains for SFM studies.

#### Experimental conditions for APTES immobilisation

The coating of the APTES surfaces started by thoroughly cleaning microscope glass slides. Firstly they were cleaned using an ultrasonic bath (Branson 2510 40

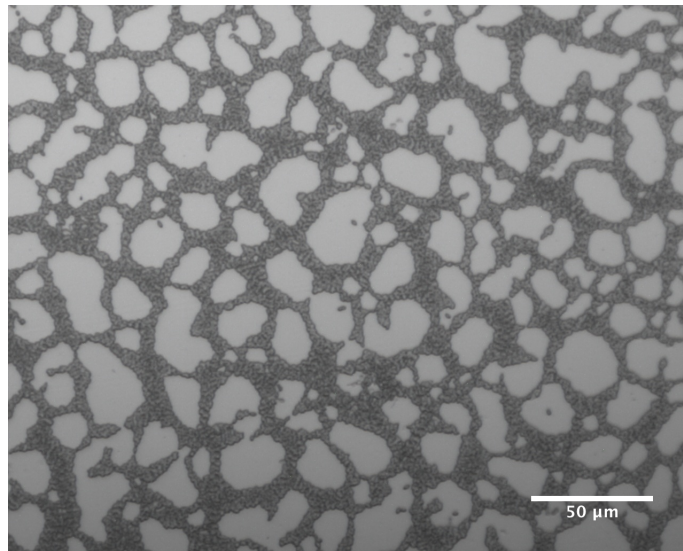


**Figure 3.26:** 24 h Rc291 biofilm on glass coated with APTES. Cells grown at 20 °C in AB10, supplemented with 2 mM glucose. The cells were grown inside a Petri dish containing a glass slide coated with APTES. Image taken with a 50× objective.

KHz, Branson Ultrasonics Co., Danbury, CT) with detergent (Decon Laboratories, Sussex), followed by water rinsing. The glass slides were then soaked in piranha solution (i.e. 70% H<sub>2</sub>SO<sub>4</sub>, 30% H<sub>2</sub>O<sub>2</sub>, both Sigma-Aldrich, Dorset, England) for 1 h. The acid-cleaned slides were then thoroughly rinsed with deionised water and methanol, dried with N<sub>2</sub> gas and kept in a sealed container.

The glass slides were then submerged into a slide chamber in a 10% APTES (Sigma-Aldrich, Dorset, England) methanolic (Methanol, Fischer, Leicestershire, England) solution for 15 min. The slides were then removed from the solution, rinsed with water and methanol and left to dry overnight in a vacuum oven at 40 °C to eliminate all traces of solvent. The slides were used immediately after preparation.

The bacterial cells were grown as in Section 3.3.1 until late exponential phase or early stationary phase. The suspension was centrifuged, the old medium poured out and the cells were resuspended in fresh AB10 medium. 500 µL of the bacterial suspension were deposited onto the APTES coated slide and spread over the surface. The bacteria were left to settle for 1 h before the SFM experiment, avoiding evaporation. The APTES slides were gently rinsed with water and left to dry, for scanning in air, or gently rinsed with AB10 for liquid imaging.

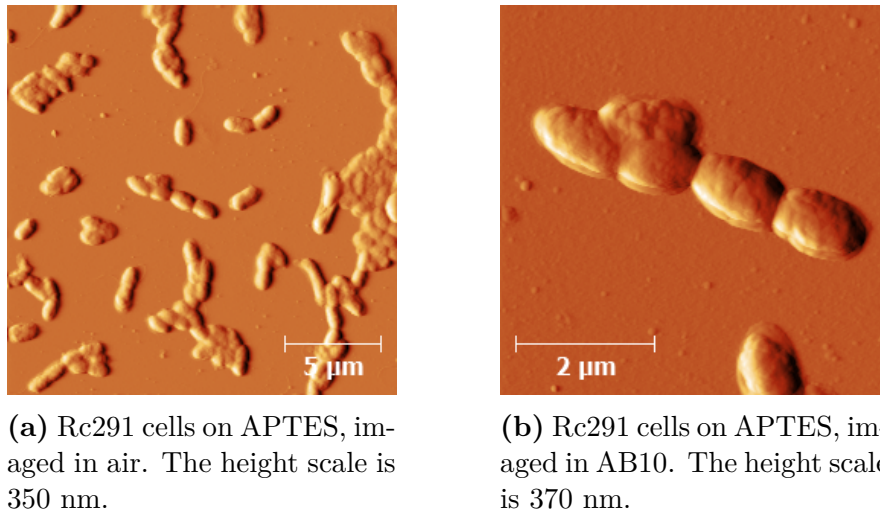
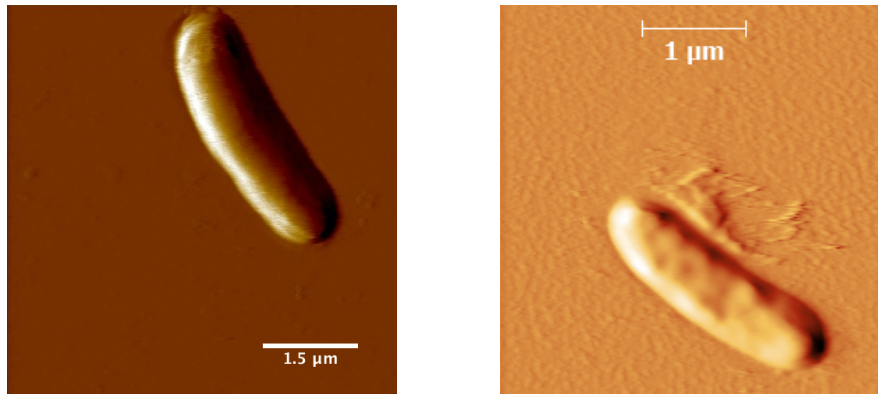


**Figure 3.27:** Rc291 attached to an APTES coated surface. The images were acquired in contact mode using an MLCT probe, using the 0.01 N/m cantilever.

The samples, shown in Figures 3.27 and 3.28 were imaged using a Dimension 3100 system (Nanoscope IV, Digital Instruments, NY, USA) in contact mode, using MLCT  $\text{Si}_3\text{N}_4$  SFM probes (Bruker AFM Probes, USA), with a spring constant of 0.01 N/m. The images were acquired using low scanning frequencies (0.5 Hz) to avoid cell detachment. The samples in Figure 3.28 were scanned under AB10 medium.

Biofilm morphology was assessed visually using a light transmission microscope Nikon Eclipse ME 600 (Nikon, Melville, NY) with a 50 $\times$  objective. The microscope was coupled to a Pixelink camera (Pixelink, Ottawa, Canada) and representative images were captured using the Pixelink OEM imaging software (Pixelink, Ottawa, Canada).



(a) Rc291 cell on APTES, imaged in AB10. The height scale is 1  $\mu\text{m}$ .

(b) Rc291 cell on APTES, imaged in AB10. The height scale is 180 nm.

**Figure 3.28:** Rc291 attached to an APTES coated surface. The images were acquired in contact mode using an MLCT probe, using the 0.01 N/m cantilever.

### Polyethyleneimine

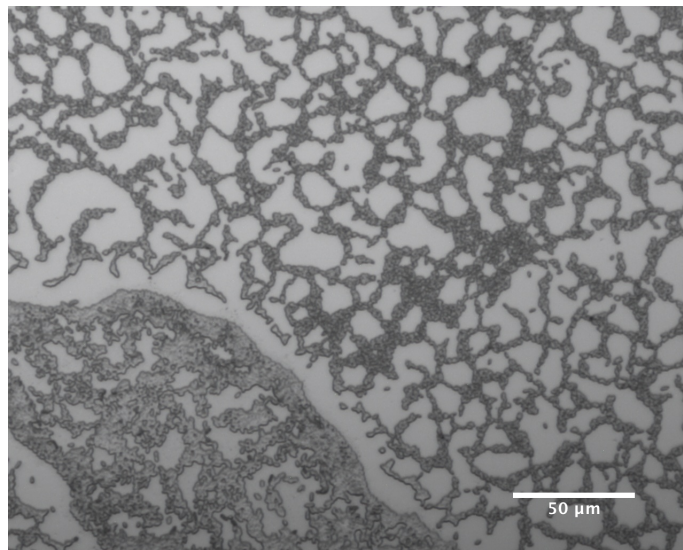


**Figure 3.29:** Rc291 biofilm on glass coated with PEI. Cells grown at 20 °C in AB10, supplemented with 2 mM glucose for 24 h. The cells were grown inside a Petri dish containing a glass slide coated with PEI. This image was taken with a 50 $\times$  objective.

### Experimental conditions for PEI immobilisation

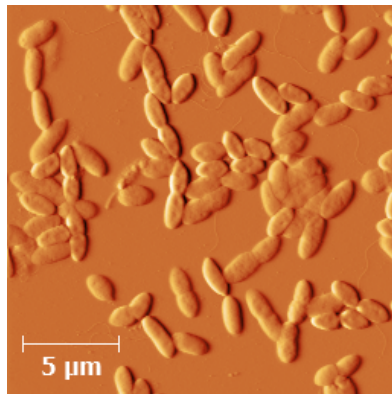
The coating of the PEI surfaces started by thoroughly cleaning microscope glass slides. Firstly they were cleaned using an ultrasonic bath (Branson 2510 40 kHz, Branson Ultrasonics Co., Danbury, CT) with Decon detergent (Decon Laboratories, Sussex), followed by water rinsing. The glass slides were then soaked in piranha solution for 1 h. The acid-cleaned slides were then rinsed with plenty of water and methanol, dried with N<sub>2</sub> gas and kept in a sealed Petri dish until use.

The glass slides were then submerged into a slide chamber in a 0.2% PEI (Sigma-Aldrich, Dorset, England) aqueous solution at pH 7 for 4 h. The slides were then removed from the solution, rinsed with water and left to dry overnight in a vacuum oven at 40 °C to eliminate all traces of solvent. The slides were used immediately after preparation.

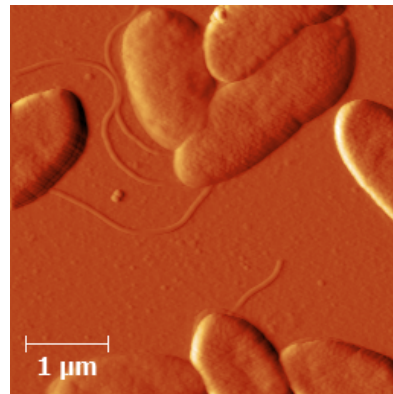
The bacterial cells were grown as in Section 3.3.1 until late exponential phase or early stationary phase. The suspension was centrifuged, the old medium poured out and the cells were resuspended in fresh AB10 medium. 500 µL of the bacterial suspension were deposited onto the PEI coated slide and spread over the surface. The bacteria were left to settle for 1 h before the SFM experiment, avoiding evaporation. The PEI slides were gently rinsed with water and left to dry, for scanning in air, or gently rinsed with AB10 for liquid imaging.

The samples, shown in Figures 3.30- 3.35 were imaged using a Dimension 3100 system (Nanoscope IV, Digital Instruments, NY, USA) in contact mode, using MLCT Si<sub>3</sub>N<sub>4</sub> SFM probes (Bruker AFM Probes, USA), with a spring constant of 0.01 N/m. The images were acquired using low scanning frequencies (0.5 Hz) to avoid cell detachment. The images shown in Figures 3.31b and 3.35 were acquired in water.

Biofilm morphology was assessed visually using a light transmission microscope Nikon Eclipse ME 600 (Nikon, Melville, NY) with a 50× objective, coupled to a Pixelink camera (Pixelink, Ottawa, Canada) and representative images were captured using the Pixelink OEM imaging software (Pixelink, Ottawa, Canada).

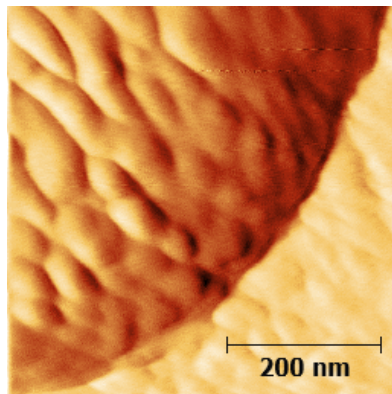


(a) Rc291 cells on PEI, imaged in air. The height scale is 250 nm.

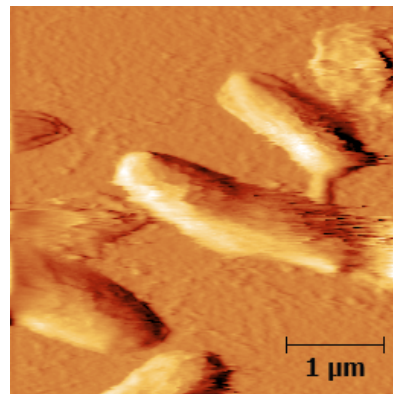


(b) Rc291 cells on PEI, imaged in air. The height scale is 380 nm.

**Figure 3.30:** Rc291 attached to PEI. The images were acquired in contact mode using an MLCT probe, using the 0.01 N/m cantilever.



(a) Rc291 cells on PEI, imaged in air. The height scale is 90 nm.



(b) Rc291 cells on PEI, imaged in water. The height scale is 420 nm.

**Figure 3.31:** Rc291 attached to PEI. The images were acquired in contact mode using an MLCT probe, using the 0.01 N/m cantilever.

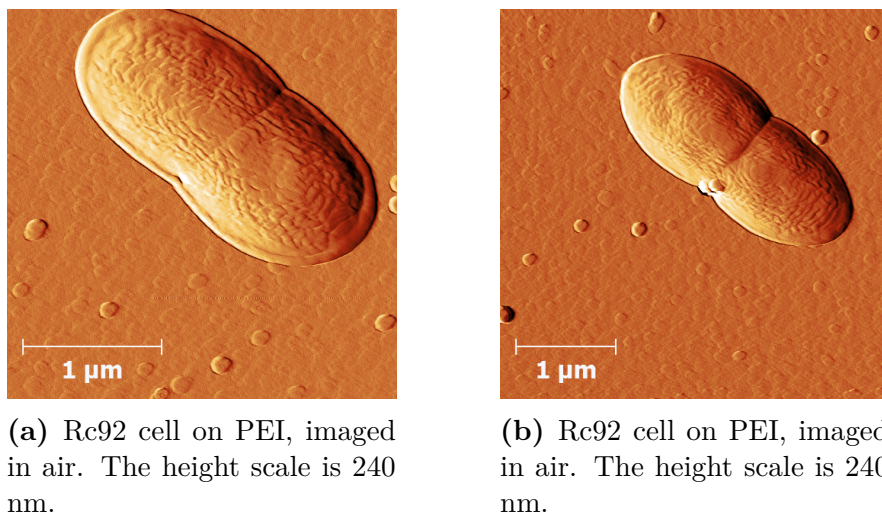
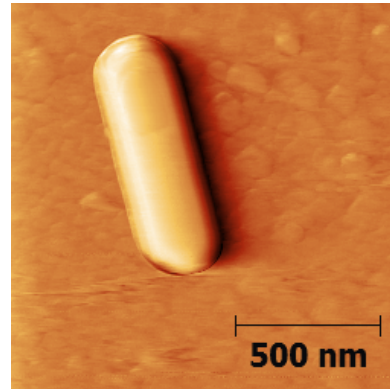
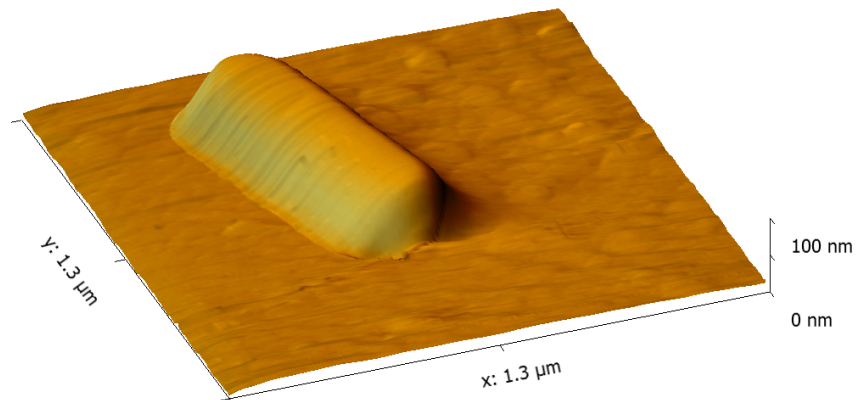


**Figure 3.32:** Rc92 attached to PEI. The images were acquired in contact mode using an MLCT probe, using the 0.01 N/m cantilever.

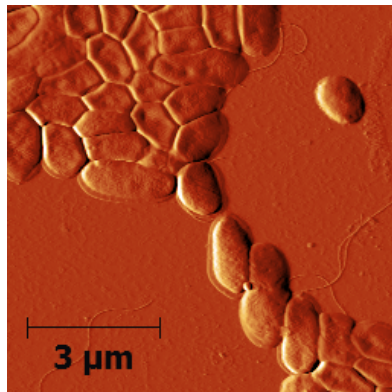


(a) Rc291 cell on PEI, imaged in air. The height scale is 100 nm.

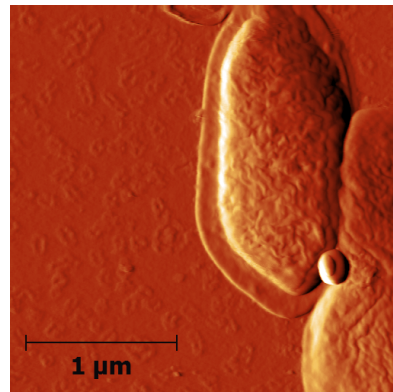


(b) 3D view of an Rc291 cell.  
The height scale is 100 nm.

**Figure 3.33:** Rc291 attached to PEI. The images were acquired in contact mode using an MLCT probe, using the 0.01 N/m cantilever.

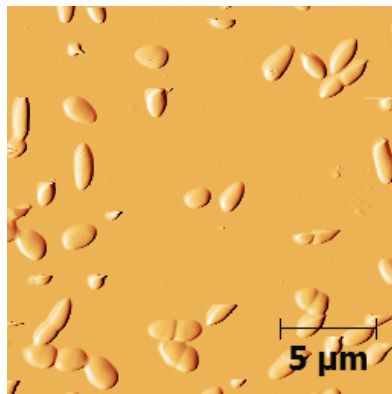


(a) Rc92 cells on PEI, imaged in air. The height scale is 300 nm.

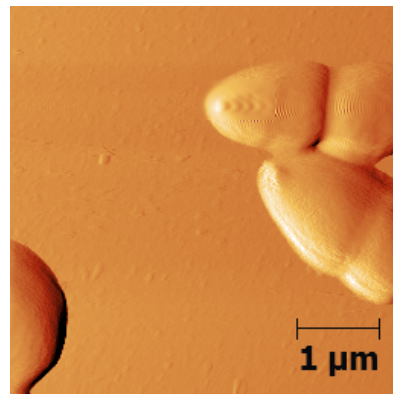


(b) Rc92 cells on PEI, imaged in air. The height scale is 300 nm.

**Figure 3.34:** Rc92 attached to PEI. The images were acquired in contact mode using an MLCT probe, using the 0.01 N/m cantilever.



(a) Rc92 cells on PEI, imaged in water. The height scale is 300 nm.



(b) Rc92 cells on PEI, imaged in water. The height scale is 300 nm.

**Figure 3.35:** Rc92 attached to PEI. The images were acquired in contact mode using an MLCT probe, using the 0.01 N/m cantilever.

### 3.3.5 Adhesion enhanced by polyphenolic proteins

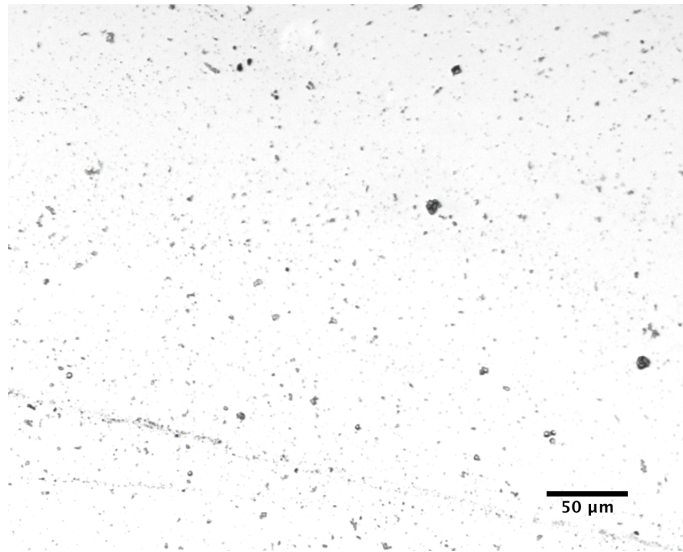


**Figure 3.36:** Pse2 biofilm on glass coated with Cell-Tak<sup>®</sup>, grown for 24 h. Cells grown at 20 °C in AB10, supplemented with 2 mM glucose. The cells were left to settle for 15 min on a glass slide coated with Cell-Tak<sup>®</sup>, with a coating density of 20 μg/slide. This image was taken with a 50× objective.

Cell-Tak<sup>®</sup> and polyphenolic proteins, and derivatives (e.g. L-DOPA) are well known in biology for being suitable adhesives for a wide variety of biological samples. Commonly these samples are eukaryotic cells [266] or proteins. Very few examples have been found in the literature where Cell-Tak<sup>®</sup> is used to attach bacteria for SFM scanning, and the attempts are not always successful. For instance, Razatos *et al.* [224] could not attach *E. coli* K-12 using Cell-Tak<sup>®</sup>, and employed glutaraldehyde instead. Similarly, Bailey *et al.* failed to see immobilised *S. aureus* SH1000 cells through polyphenolic proteins, and used mechanical trapping instead.

On the other hand, Meyer *et al.* [166] successfully immobilised a range of Gram positive and negative bacteria using this methodology, as shown in Section 3.2.3. Following their positive results, it was decided to pursue this technique. Unfortunately, this immobilisation method did not prove to be appropriate for the strains that we were using, which failed to withstand SFM scanning under liquid. The result of our efforts can be seen in Figure 3.38 where feebly immobilised Rc92 and Pse2 cells can be seen. Cellular material is being dragged by the action of the probe, and consequently the cells appear fuzzy and indistinct. It was concluded that polyphenolic proteins were not a suitable candidate for the immobilisation of the strains used in the present thesis.

Ana Lorena Morales-García

### Experimental conditions using polyphenolic proteins

Cell-Tak<sup>®</sup> is a solution of polyphenolic proteins patented by Benedict and Picciano in 1992 [267] and commercialised by BD Biosciences (Bedford, MA, USA). The adhesive is sold dissolved in a concentration of 1 mg/mL in 5% acetic acid. Cell-Tak<sup>®</sup> is taken to pH 8 using Na<sub>2</sub>CO<sub>3</sub> (Sigma-Aldrich, Dorset, England) 2M. 1–2% isopropyl alcohol (Sigma-Aldrich, Dorset, England) is added to the mixture to decrease the surface tension of the solution. Cell-Tak<sup>®</sup> is applied to glass surfaces at a concentration of 20 µL/slide and spread using the “blood smear technique” [203]. The blood smear technique is shown in Figure 3.37: a small drop of the polyphenolic protein solution is deposited on the glass slide using a micropipette. A second clean slide is held on top of the drop at a 30° angle. The spreader slide is pushed so that the edge barely touches the drop of Cell-Tak<sup>®</sup>, which by capillary action will wet the edge of the spreader slide. The spreader slide is then dragged across the surface of the sample slide, to create a thin film of even thickness. The slides are then left to settle for 20 min and are rinsed with water, air dried and left in the fridge until use. Typically the slides were prepared just before the SFM experiment.

The cells were grown as explained in Section 3.3.1. Once the cells were harvested, they were washed twice with PBS, and resuspended in PBS where they were kept until the experiment.

500 µL of the cell suspension were transferred and spread onto the Cell-Tak<sup>®</sup> coated slide and left to settle for 10 minutes and rinsed with MOPS 20 mM. MOPS is the common name for the buffer 3-(N-morpholino)propanesulfonic acid, a buffer type introduced by Good *et al.* in 1966 [260]. It has a pKa of 7.2, making it an excellent choice as a biological buffer in neutral conditions.

The cells shown in Figure 3.38 were imaged using a Dimension 3100 system (Nanoscope IV, Digital Instruments, NY, USA) in contact mode in MOPS 20 mM, using SNL-10 Veeco cantilevers, with a nominal spring constant of 0.06 N/m and nominal resonant frequency in the 12–24 kHz interval. The pictures were acquired with a slow scanning frequency of 0.25–0.5 Hz, to avoid cell detachment.

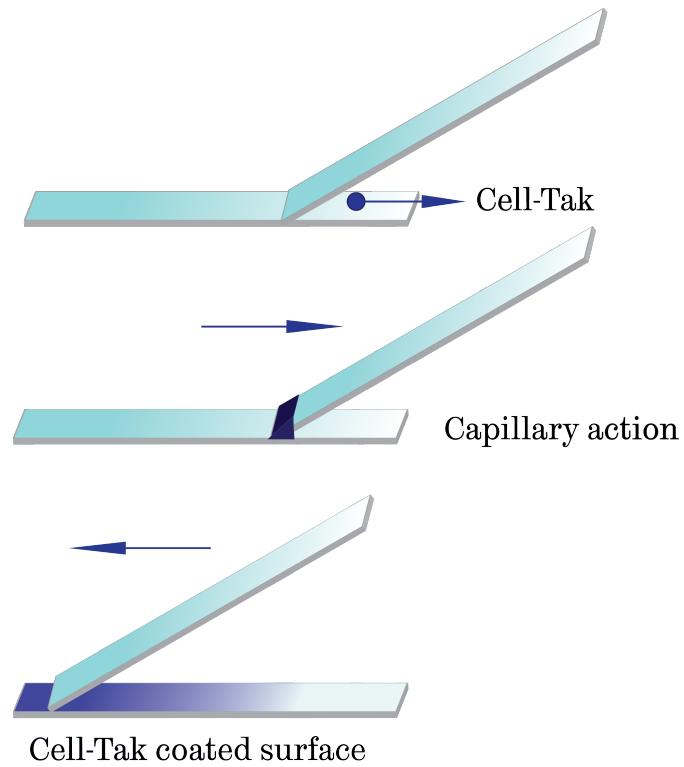
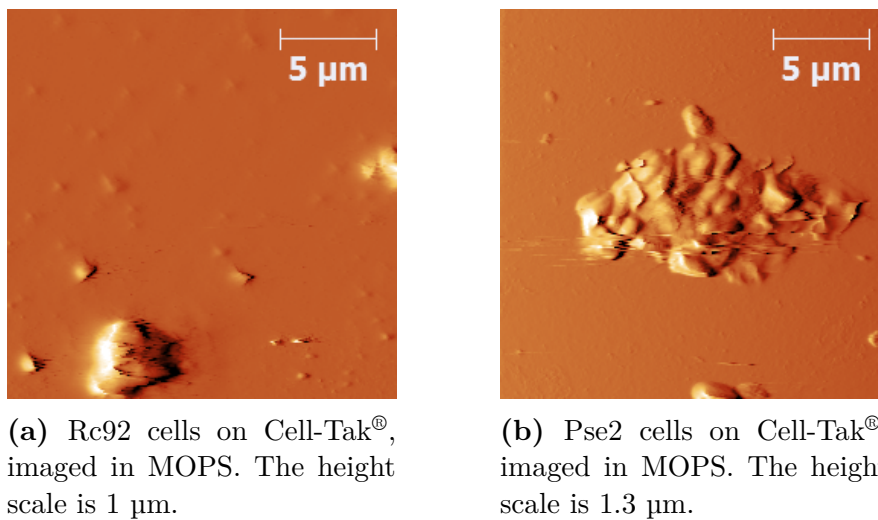


**Figure 3.37:** Blood smear technique used to spread a drop of Cell-Tak<sup>®</sup> on a microscope glass slide.



**(a)** Rc92 cells on Cell-Tak<sup>®</sup>, imaged in MOPS. The height scale is 1 μm.

**(b)** Pse2 cells on Cell-Tak<sup>®</sup>, imaged in MOPS. The height scale is 1.3 μm.

**Figure 3.38:** Bacteria attached to a Cell-Tak<sup>®</sup> coated surface. The images were acquired in contact mode using an SNL-10 probe, using the 0.06 N/m cantilever.

### 3.3.6 Covalent immobilisation of bacteria

The EDC/NHS/APTES methodology, described in Section 3.2.5 was implemented for the attachment of the working strains. Since none of the previously described methods yielded strong, repeatable samples that could be scanned in liquid for extended periods of time, it was decided to attach the cells to aminosilanised (APTES) substrates using covalent bonds (EDC/NHS). In the following sections, the preparation methods of the substrates and cells will be detailed, alongside characterisation methods of the APTES surfaces.

#### Substrate preparation

Silicon wafers of  $425 \pm 25$   $\mu\text{m}$  thickness, with a native oxide superficial layer, (Prolog Semicor, Kiev, Ukraine) were cut into rectangles of  $0.5 \times 1$  cm. The substrates were cleaned using piranha solution for 1 h (with a ratio of  $\text{H}_2\text{SO}_4:\text{H}_2\text{O}_2$  7:3) and then rinsed with copious amounts of deionised water. The wafers were then boiled in water for 1 h and the water was replaced 2–3 times during this process. Afterwards the wafers were rinsed with analytical grade ethanol (Sigma-Aldrich, Dorset, England) and sonicated in HPLC grade methanol (Fisher, Leicestershire, England). The wafers were kept in a sealed vial containing methanol until they were used.

The silicon wafers were immersed in 30% v/v of 3-aminopropyltriethoxysilane (Sigma-Aldrich, Dorset, England) in HPLC grade dry methanol (Fisher, Leicestershire, England) for 1 h. The reaction was conducted in a custom-made closed cell, previously flushed with  $\text{N}_2$  (g). The silane was previously distilled under an argon atmosphere. Dry conditions were kept to avoid the hydrolysis of the ethoxy groups in APTES, as it has been suggested that the presence of water leads to the polymerisation of the silane in the reaction vessel; this ultimately reduces the grafting efficiency which would consequentially lead to poor cell attachment [268–270].

After the reaction vessel was open, each wafer square was rinsed with 50 mL of methanol and 50 mL of analytical grade water (AnalaR Normapur, VWR, Fontenay-Sous-Bois, France). It is important to keep the wafers immersed in the APTES solution until they are ready to be washed with the solvents, otherwise the silane forms a very rough surface. Once they had been washed, the wafers were dried under a nitrogen stream and kept at  $4^\circ\text{C}$  until they were used. (They were never stored for more than 2 weeks.)

### Spectroscopic ellipsometry

Spectroscopic ellipsometry is used to measure the changes in light polarisation that occur when a light beam is reflected onto a thin film deposited upon a reflective substrate. The changes in polarisation are related to the nature of the layer material and its thickness. Thus, ellipsometry is a non-destructive optical technique, that allows the measurements of the thickness of thin transparent films.

Spectroscopic ellipsometry measurements were employed to investigate the thickness of the APTES layer. A M2000 V rotating compensator ellipsometer (J.A. Woollam Co., Inc., Lincoln, England) was used. Precautions were taken to avoid defective areas of the wafers. The measurements were taken at a fixed angle of incidence of  $70^\circ$  to the surface normal. The spectra generated were fitted with a multilayer model of Si + SiO<sub>2</sub> native layer (2 nm) + Cauchy, using the CompleteEase analysis software (J.A. Woollam Co., Inc., Lincoln, England). The refractive index  $n_p$  of the dry APTES layer was described using the Cauchy approximation,

$$n_p(\lambda) = A_n + \frac{B_n}{\lambda^2} + \frac{C_n}{\lambda^4} \quad (3.3)$$

with the starting parameters  $A = 1.555$ ,  $B = 0.4928 \mu\text{m}^{-2}$  and  $C = 0.01314 \mu\text{m}^{-4}$ , which were fitted by iteration. Using this model, the average thickness of APTES was determined to be  $10.22 \pm 5.44 \text{ nm}$  ( $n = 35$ ).

### Contact angle measurements

Measurements of the water contact angle on APTES surfaces were made using a Theta optical tensiometer (Attension, Biolin Scientific, Espoo, Finland) using the static sessile method. The experiments were made using water ( $18 \text{ M}\Omega \cdot \text{cm}$ ) dispensed from a syringe and freshly prepared APTES surfaces. Drop images were collected using a digital camera and analysed with a curve fitting method using the tangent approximation. A contact angle of  $68.54 \pm 0.10^\circ$  ( $n = 3$  slides) was obtained, after averaging 600 images per experiment.

### Zero-length crosslinking reaction

The underside of the bacterial cells was anchored to the APTES coated surface described in Section 3.3.6, via the EDC/NHS zero-length reaction.

EDC (Fluka, Dorset, England) and NHS (Sigma-Aldrich, Dorset, England) were dissolved in 0.1 M sodium phosphate (pH 7.1) buffer to form stock solutions at 0.5 M and 0.1 M, that were kept at  $4^\circ\text{C}$  and used within 2 weeks.  $100 \mu\text{L}$  EDC

were added to 700  $\mu\text{L}$  of the washed cell culture (washed  $2\times$  in PBS at 1200  $g_n$  and resuspended in phosphate buffer to a final  $\text{OD}_{600}$  in the range of 0.2–0.7) to a final concentration of 50 mM. This mixture was made in an 1.5 mL microcentrifuge tube and mixed on an orbital shaker at 225 rpm for 20 min. 200  $\mu\text{L}$  of NHS were then added to achieve a final concentration of 20 mM. A rectangular silicon wafer coated with APTES, was introduced into the microcentrifuge tube and was shaken for 6 h at 50 rpm at 20 °C. The pH of the suspension remained close to neutral because of the action of the phosphate buffer.

### Cell viability

The viability and morphology of bacterial cells has been reported not to be affected by the EDC/NHS treatment [252]. The Live/Dead BacLight<sup>®</sup> bacterial viability kit (Molecular Probes, Eugene, OR) was used to confirm the vital state of Pse1, Pse2, Rc92 and Rc291 before and after the covalent immobilisation. The BacLight<sup>®</sup> kit is a two-colour assay that uses a mixture of SYTO9, a green-fluorescent nucleic acid stain and the red-fluorescent nuclear acid stain propidium iodide. SYTO9 labels all bacteria in a population, including cells with intact membranes and cells with damaged membranes. Propidium iodide, on the other hand, penetrates only bacteria with damaged membranes, causing a reduction in the fluorescence of SYTO9. As a result of that, live or whole cells fluoresce green and damaged or dead cells fluoresce red. SYTO9 has an emission maximum at 500 nm and propidium iodide at 635 nm.

3.6  $\mu\text{L}$  of SYTO9 3.34 mM and 3  $\mu\text{L}$  of propidium iodide 20 mM were combined into 1 mL of phosphate buffer pH 7.1, to obtain final concentration of 12  $\mu\text{M}$  and 60  $\mu\text{M}$  respectively. The mixture was kept protected from light. 10  $\mu\text{L}$  of the dye mixture was added for each mL of cell suspension. The dyes were left to incubate for 10 minutes, before measuring 10  $\mu\text{L}$  of the stained cell suspension and putting it on a microscope slide, and covering it with a coverslip. The samples were analysed with an Olympus microscope (Olympus BX50W1, Olympus Optical Ltd., Watford, UK) equipped with SWB (super-wide band) and WB (wide band) filters. The first one allows a visualisation of the fluorescence of the green and red channels (i.e. alive and dead cells), whereas the second one only allows the visualisation of the red fluorescence. Representative images were captured using the CellB imaging software (Olympus Optical Ltd., Watford, UK).

The efficacy of the dyes on the bacterial strains was verified by killing tests, in which the sample is incubated in 70 % ethanol for 1 h, with the purpose of killing the cells; if all the majority of the cells fluoresce red after the killing test, then one can infer that the staining method worked appropriately.

Percentage of living cells (%)				
Experiment	Pse1	Pse2	Rc92	Rc291
Ethanol 70% (1 h)	$0 \pm 0$	$0 \pm 0$	$0 \pm 0$	$0 \pm 0$
No treatment (3 h)	$100 \pm 0$	$100 \pm 0$	$100 \pm 0$	$100 \pm 0$
EDC/NHS (3 h)	$91 \pm 0$	$73 \pm 14$	$88 \pm 5$	$84 \pm 7$
No treatment (6 h)	$100 \pm 0$	$100 \pm 0$	$98 \pm 0$	$100 \pm 0$
EDC/NHS (6 h)	$84 \pm 14$	$84 \pm 8$	$65 \pm 1$	$90 \pm 15$
EDC/NHS/APTES (6 h)	$48 \pm 6$	$38 \pm 17$	$50 \pm 8$	$40 \pm 8$

**Table 3.3:** Cell viability experiments using BacLight<sup>®</sup>. The quoted uncertainty corresponds to the standard deviation of 4 measurements.

Fluorescent images of the four strains stained with SYTO9/propidium iodide after 3 h of the EDC/NHS treatment can be seen in Figure 3.39 and in Figure 3.40 APTES-coated silicon wafers with crosslinked bacterial cells, after 6 h of EDC/NHS treatment can be appreciated.

The number of live (i.e. green) cells and red (i.e. dead) cells in Figure 3.40 and in Appendix A, were determined using the Fiji software [271]. Since there were too many cells on each frame, manual counting was not practical, and automated counting was used instead. To perform this operation, the images produced by the SWB filter (i.e. dual fluorescence) were converted to a 16-bit greyscale format. Then the threshold was adjusted to highlight all the cells, taking care not to include noise pixels inside this threshold. Assemblies of bacterial cells were separated from each other by watershed segmentation. Finally, the tool “Analyse Particles” was used to determine the total number of cells. To calculate the number of dead cells, the images produced by the WB filter (i.e. single red fluorescence) were analysed as in the aforementioned protocol. Finally, to determine the number of live cells, the number of particles calculated in the WB images was subtracted to the total number of particles in the frame, given by the SWB images. The results of such counts, converted to percentages, appear in Table 3.3. The values recorded are the average of 4 images of different sections of the same sample; the uncertainty values correspond to the standard deviations of the cell counts.

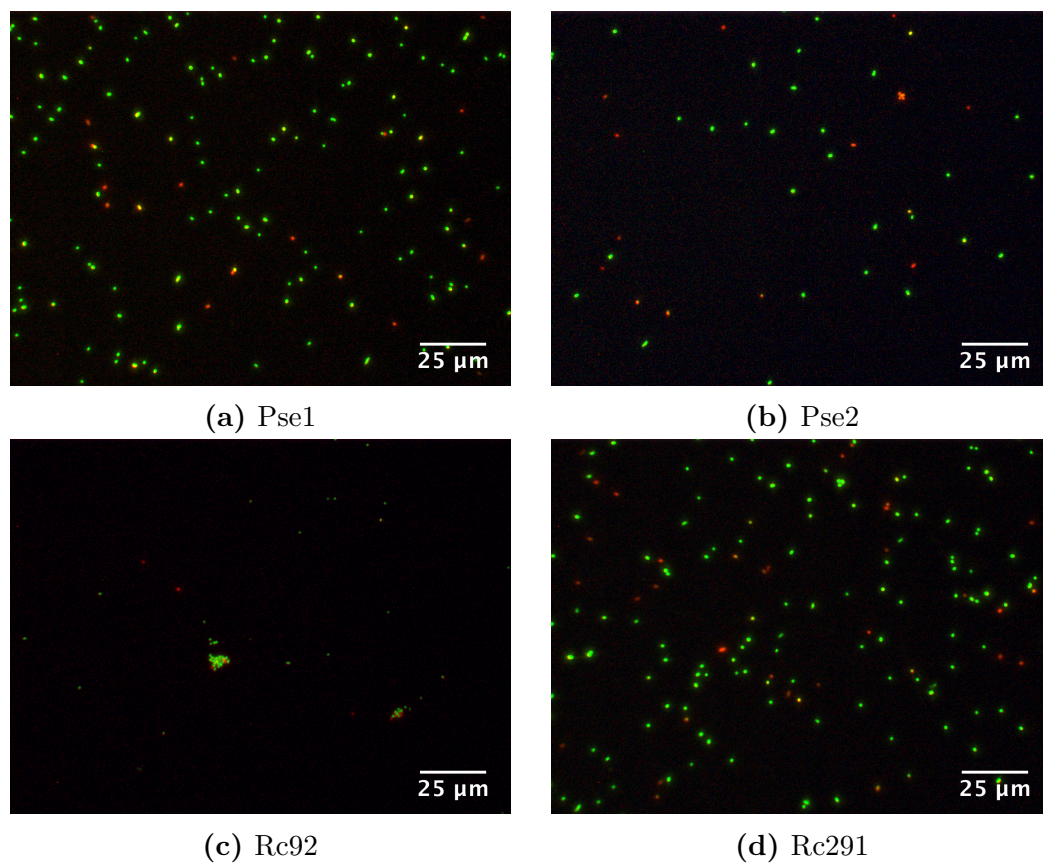


**Figure 3.39:** Bacterial cells after being treated with EDC/NHS, after 3 h of incubation. The cells were stained with BacLight<sup>®</sup>.

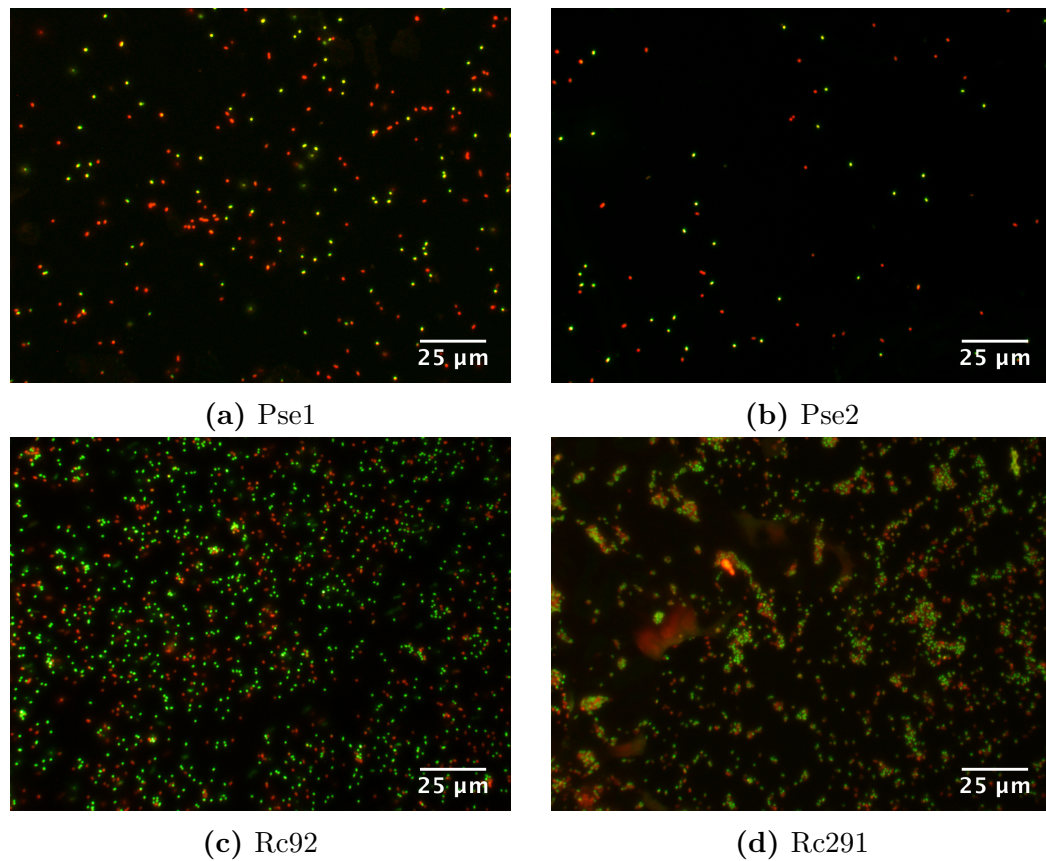


**Figure 3.40:** Bacterial cells attached to APTES substrates via the zero-length EDC/NHS crosslinking reaction, after 6 h of incubation. The cells were stained with SYTO9/propidium iodide and imaged with a super-wide band filter mirror unit that allows the passage of the emission wavelengths of both dyes.

### SFM scanning

A Molecular Force Probe 3D system (MFP-3D, Asylum Research, Santa Barbara, USA) was used for the imaging of bacterial cells attached via covalent bonds. MLCT  $\text{Si}_3\text{N}_4$  SFM probes (Bruker AFM Probes, Camarillo, USA) were employed, using the cantilever with a nominal spring constant of 0.03 N/m.

The images were obtained in intermittent contact mode under MOPS 20 mM, using slow scan frequencies (0.5–1 Hz). A couple of examples of bacterial cells imaged with this technique are shown in Figures 3.41 and 3.42. The cells were firmly immobilised the majority of the times, and details of the cell surfaces can be appreciated. It was concluded that the use of covalent bonding through the zero-length crosslinkers EDC and NHS on APTES was a reliable technique for the immobilisation of *Rhodococcus spp.* Rc291 and Rc92 and *Pseudomonas* Pse1 and Pse2. Consequently, this method was chosen for all the imaging and force experiments of these strains, as will be detailed in Chapter 4.

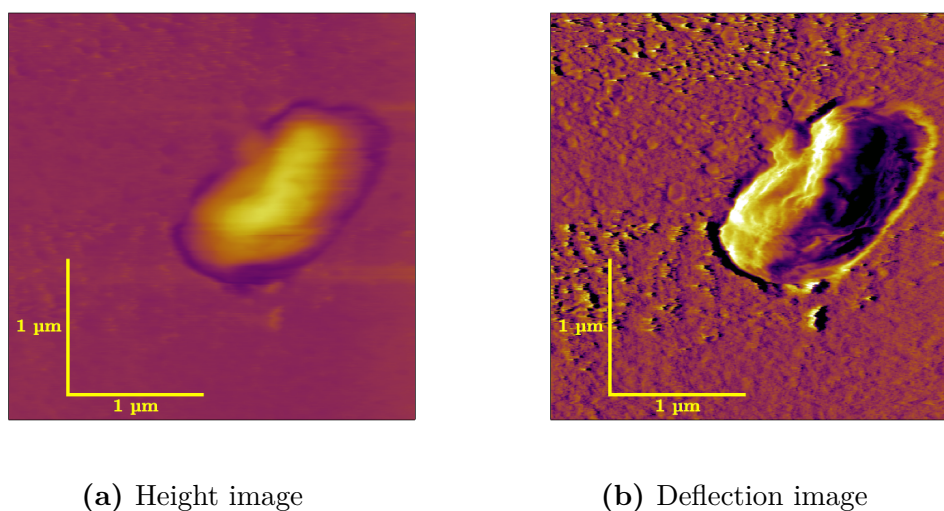


**Figure 3.41:** *Pseudomonas* 1 cells imaged with a DDT-coated tip. The height scale is 300 nm. The images were acquired in intermittent contact mode using an MLCT probe, using the 0.03 N/m cantilever. n.b. A *DDT tip* is a chemically functionalised tip used for chemical force microscopy; its use and preparation will be detailed in Chapter 4.

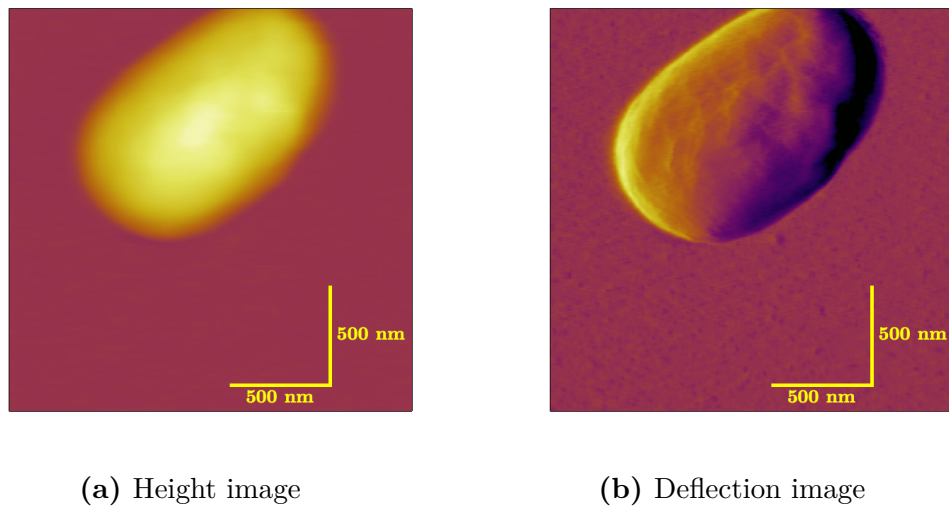


**Figure 3.42:** *Pseudomonas* 1 cells imaged with a DDT-coated tip. The height scale is 300 nm. The images were acquired in intermittent contact mode using an MLCT probe, using the 0.03 N/m cantilever.

### 3.4 Concluding remarks

In this chapter, many immobilisation strategies were described, along with the experimental conditions that were used in successful examples. The benefits and difficulties associated with each technique were discussed and representative examples were given. In the second part of this chapter, the techniques that were found in the literature were adapted and used for our bacterial systems. This exercise proved to be time-consuming, since the selection of the best method of immobilisation was not straightforward.

Based on the knowledge gathered during the course of these experiments, some conclusions can be drawn and a general plan for immobilisation of bacterial strains is presented in Figure 3.43. This plan is not universal and does not presume to cover all the possible hurdles encountered during microbial scanning with an SFM under liquid, but it is a starting point. The following paragraphs offer a quick summary of the reasoning behind the order of the immobilisation techniques in Figure 3.43; further details can be found all throughout the present chapter.

The first step is an obvious one, in which the experimenter should try to see if the cells attach without the need of any additives. Although extremely rare, some researchers have succeeded in doing this [272]. If the dragging force of the microscope is too great for the cells to withstand, then the experimenter should try to constrict them mechanically. The excellent approach taken by Kailas *et*

*al.* [164] was discussed in this chapter. They designed lithographic grids with the ideal measurements to constrict *S. aureus* cells. Since this was the only strain they were using, it made sense to have this state-of-the-art grid. In later experiments in the same research group [179], this technique was enhanced by increasing the hydrophobicity of the substrate by covering it with polystyrene, and thus the cells could be trapped more frequently and predictably.

In general, mechanical entrapment can be applied to immobilise spherical cells, making use of polycarbonate membranes, which have nearly circular pores. Although polycarbonate membrane manufacturers (e.g. Millipore) produce a variety of sizes, it is possible to increase the diameter of the holes by etching the membranes in a highly alkaline solution as in the publication by Turner *et al.* [160]. This method is excellent for stiff cells (e.g. *S. aureus*, *S. cerevisiae*), but the use of this technique might prove challenging for more compliant cells, like *Streptococcus pneumoniae* [273].

Hydrophobic cells, like *Rhodococcus* can often be immobilised onto hydrophobic substrates. If the substrate is rough it is more likely that the cells will be accommodated in crevices and resist being washed off by the hydrodynamic forces that surround the probe.

The majority of the cells possess a negatively charged envelope, and thus they display attractive interactions with polycationic surfaces. Indeed, this property has been exploited by many researchers who have successfully imaged and analysed cells attached with this methodology. Often they performed these scans under pure water to minimise screening by ions. This solution, however, could cause osmotic damage to the cells and therefore it should be used with care.

If all the previous techniques were unable to immobilise the cells reliably for continuous SFM imaging, then covalent bonds might be required. For the particular case of the cells studied in this thesis the EDC/NHS/APTES methodology was successfully applied and hence we can infer that the cell envelopes were rich in carboxylic acid groups to support bond formation with the substrate (see Figure 3.14). For bacterial cells that are poor in carboxylic acid groups but rich in amine terminal groups, Camesano *et al.* [167] suggest a similar crosslinking protocol that exploits the amino groups on the cell surfaces and binds them to surfaces rich in carboxylic acids (i.e. inverse crosslinking).

In every method, the experimenter should take special care to minimise the tip-cell interaction by an adequate selection of the scanning parameters, the SFM probe and the imaging liquid. A systematic approach like the one taken in this project and described on this diagram will increase the chances of getting repeatable samples in a short amount of time.

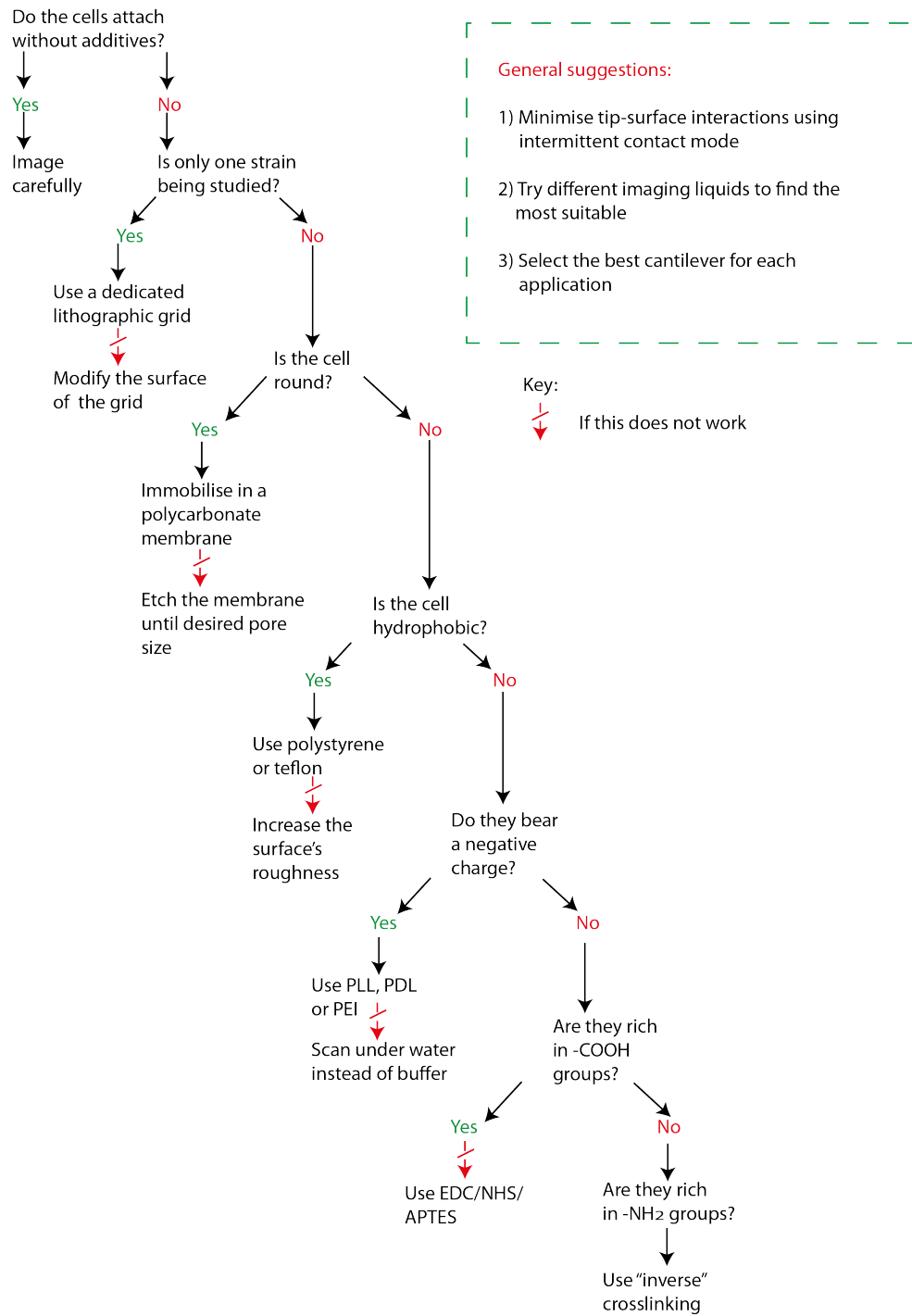


**Figure 3.43:** Decision chart for a rational selection of the best immobilisation method.

## Mapping the hydrophobicity of bacterial surfaces

As Israelachvili [82] beautifully narrates in the introduction to his classic book, “Intermolecular and Surface Forces”, the interest in the interactions between molecules dates back to the seventeenth century. Newton himself pondered about the relationship between the forces between molecules and the properties of matter, a subject that continued to be interesting to many other scientists in the years to come. With these musings, the field of intermolecular interactions was born. With the advent of the atomic era and quantum mechanics in the 20th century, soon it was established that all interactions between molecules arise from electrostatic forces between electrons and protons between neighbouring particles. Since the spatial distribution of electronic clouds in molecules still remains elusive to us due to the technical impossibilities to solve the Schrödinger equation for a large ensemble of atoms, we must settle for a less exact solution for the moment. So, despite the fact that all forces between molecules arise from these electrostatic attractions, we ought to simplify the problem and categorise the diverse intermolecular forces into subgroups. This is why we have the distinction between van der Waals forces, hydrophobic interactions, solvation forces, hydrogen bonds and other related forces.

The *molecules* that the author of this thesis is interested in studying, are located on the outer membrane of bacterial cell walls. The *intermolecular* forces that were measured, are between the molecules on the bacterial cell surface and probing molecules or surfaces, located in an SFM probe. The *type* of forces investigated are a combination of van der Waals, hydrophobic and electrostatic interactions. The *means* to study these chemical interactions are given by the use of the force-distance mode of the scanning force microscope (SFM), in its chemical force microscopy variant, which will be dealt with in the present chapter.

## 4.1 Application of CFM to the study of bacteria

As defined in §2.6.6, chemical force microscopy is a variant of the typical SFM in which the tip and/or the surface are derivatised in such a way that the interaction forces between different functional groups are clearly distinguished. CFM was developed by Charles Lieber and collaborators [132], in an attempt to selectively measure interaction forces between self assembled monolayers, grafted onto flat surfaces, and SFM probes. This publication opened a lot of possibilities in force spectroscopy research.

There are many ways in which the AFM cantilevers can be derivatised with a particular functionality. One of them consists in attaching aliphatic chains to the silica surface via silanisation reactions. This method, although cheap and uncomplicated, has the disadvantage of lacking an appropriate polymerisation control [134]. The most popular method to modify SFM tips relies on the self-assembly of thiol layers to gold coated cantilevers. These thiol molecules have long carbonated chains and in the non-sulfurated end they bear a functional group of hydrophobic or hydrophilic character (Figure 2.29 on page 59).

Chemical force microscopy has allowed a direct interrogation of surfaces of varied chemistries and under diverse conditions, and it was therefore a natural step to apply it to biological surfaces. A wide variety of physical, chemical and biological processes have been assessed through CFM, for example, spatially resolved determination of surface forces, local determination of pK values [274] and the mapping of the hydrophobicity [136,275] and adhesive properties [88] of bacterial cell surfaces.

The surface of bacterial cells is a very complex consortium of chemically distinct polymers, that bear hydrophobic or hydrophilic groups. Therefore it is interesting to analyse their behaviour towards probes that display hydrophobic and hydrophilic functionalities. As a rule of thumb, adhesion forces are generally larger between functional groups that are capable of forming hydrogen bonds than those that cannot form these interactions; for example, one would expect, in principle, larger interaction forces in a polar media between two acid groups  $-\text{COOH}/-\text{COOH}$  than between two methyl groups  $-\text{CH}_3/-\text{CH}_3$ , but this behaviour can be affected by the nature of the atmosphere, pH and electrolyte concentration.

It has been found that in ethanolic solution, the interaction between SAMs of hydrophilic character is higher than between hydrophobic SAMs, as seen in Figure 4.1. It was hypothesised that the ability of the acid terminations to form hydrogen bonds surpassed any possible interaction (e.g. dispersion or hydrophobic forces) that the methyl groups could have. The small adhesion between methyl and carboxylic acid groups was attributed to the large and unfavourable interfacial free energy that dominates these groups in ethanol [276].

Ana Lorena Morales-García

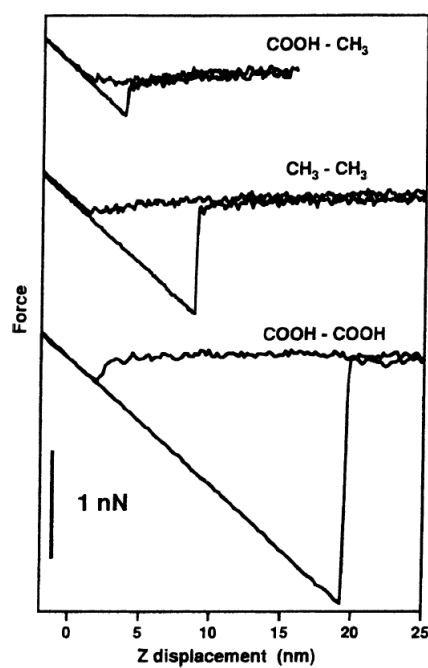


**Figure 4.1:** Comparative adhesion forces between SAMs of diverse functionalities. The mean adhesion values are: COOH/COOH:  $2.3 \pm 0.8$  nN; CH<sub>3</sub>/CH<sub>3</sub>:  $1.0 \pm 0.4$  nN; CH<sub>3</sub>/COOH:  $0.3 \pm 0.2$  nN. Image reproduced with permission of [277]. Copyright (1995) American Chemical Society.

Adhesion forces with hydrophobic and hydrophilic tips				
Strain	KCl (mM)	Contact angle (°)	Force (nN) ODT tip	Force (nN) MUL tip
<i>L. acidophilus</i>	10	76	-1.34	-0.11
<i>L. acidophilus</i>	100	47	-0.88	-2.14
<i>L. casei</i>	10	32	-0.91	-1.96
<i>L. casei</i>	100	35	-2.31	-0.47

**Table 4.1:** Adhesion forces with hydrophobic and hydrophilic tips. ODT stands for 1-octadecanethiol, which confers hydrophobic character to the tip. Hydrophilic tips were functionalised with 11-mercapto-1-undecanol (MUL). Data taken from [140].

Vadillo *et al.* [140] studied the adhesion forces between several *Lactobacillus* strains with diverse hydrophobicities (property that was estimated by their contact angle measurements) using methyl- and hydroxyl-terminated SFM probes. In accordance with the expected behaviour, those strains with a large contact angle had larger interaction forces with the hydrophobic tip than with the hydrophilic tip. Conversely, bacterial cells that had low water contact angles showed a marked preference for the hydrophilic tip. These measurements were found to be highly dependent on the ionic strength of the scanning medium: when the concentration of the imaging solution (KCl) was increased by a factor of ten times, the hydrophobic and hydrophilic strains reversed their behaviour and increased their adhesion force with the other cantilever. The authors attribute this behaviour to a change in conformation of the superficial macromolecules that provokes them to expose different regions that have a different chemistry. The results of the force measurements are summarised in Table 4.1.

In another classical example of CFM applied to the study of bacterial cell surfaces, Dorobantu *et al.* [87] studied the adhesion of *Rhodococcus erythropolis* and *Acinetobacter venetianus*. The former one was deemed highly hydrophobic due to its elevated oil/water contact angle ( $153^\circ$ ), while the latter one had a more hydrophilic character ( $56^\circ$ ). The bacterial cells were probed using MUL and ODT functionalised probes (Table 4.2).

In the study conducted by Dorobantu *et al.* the use of tips with different chemical functionality does not seem to have a marked effect on the generated adhesion forces. It should also be taken into account the fact that the treatment of the data (e.g. statistics, modelling) and the environmental conditions (e.g. scanning buffer)

Adhesion forces with hydrophobic and hydrophilic tips				
Strain	K <sub>3</sub> PO <sub>3</sub> (mM)	Contact angle (°)	Force (nN) ODT tip	Force (nN) MUL tip
<i>R. erythropolis</i>	100	153	0.55	0.48
<i>A. venetianus</i>	100	56	0.41	0.39

**Table 4.2:** Adhesion forces with hydrophobic and hydrophilic tips. ODT stands for 1-octadecanethiol, which confers hydrophobic character to the tip. Hydrophilic tips were functionalised with 11-mercapto-1-undecanol (MUL). Data taken from [87].

play a major role in the final output of the adhesion results, and thus, the values of adhesion reported in different publications might not be directly comparable (e.g. note the arbitrary change of sign in the adhesion values recorded on Tables 4.1 and 4.2).

Alsteens *et al.* [138] probed the mycolic-acid containing bacterial cells, *Mycobacterium bovis* using methyl terminated thiols grafted onto SFM probes. They found adhesion forces around 3 nN, evenly distributed throughout the cell. This high adhesion force is suggestive of the interaction between the hydrophobic mycolic acids and the methyl functionalities on the tip.

#### 4.1.1 Chapter overview

Having in mind the applicability of CFM probes to the study of hydrophobic and hydrophilic bacterial cells, it was decided to assemble a multivariate experiment. The hydrophobic *Rhodococcus* Rc92 and Rc291, and the hydrophilic *Pseudomonas* Pse1 and Pse2 (whose value of hydrophobicity was determined by their MATH scores presented in Table 2.3 on page 43) were studied by means of SFM and CFM. Four different tip functionalities were employed: silicon nitride (Si<sub>3</sub>N<sub>4</sub>), gold (Au), a hydrophobic SAM (DDT) and a hydrophilic SAM (MUA). In this chapter the results of these 16 different types of experiments will be described, compared and explained.

The bacterial cells were firstly located and imaged using intermittent contact mode, and many high resolution images were acquired. These pictures will be presented and discussed in the §4.3. The distribution of adhesion forces on the bacterial cell surfaces was determined using the force-volume mode of the SFM. In this mode, a series of force-volume maps were recorded; these maps relate the

topographic features of the cell with discrete measurements of their adhesion force. A gallery of force maps is presented in §4.4.

The generated maps are analysed in terms of the adhesion force in each point of the cell and such forces are compiled in histograms. The distributions were described using a finite mixture model, that fits a number of Gaussian curves to the force histograms. Details about these models and some examples of the aforementioned fits can be found in §4.5.

The finite mixture models, along with statistical descriptors such as the median and standard deviation, were used to assess the differences between (1) cells that belong to the same culture, (2) different strains of the same species and (3) different species of bacteria. The analysis revealed a high degree of heterogeneity in adhesive measurements that exist within the surface of a particular cell. Ideas about the heterogeneity of the measurements and a rationale about the difference between groups is understood in terms of tip-sample interactions, which are discussed at the end of the chapter.

## 4.2 Experimental protocols

### 4.2.1 Bacterial growth, substrate preparation and covalent linking

The bacterial cells Pse1, Pse2, Rc92 and Rc291 were grown according to the methodology written in (§3.3.1, p.86). The aminosilanised silicon substrates were prepared following the instructions in §3.3.6, (p.109) and characterised using spectroscopic ellipsometry (§3.3.6, p.110) and contact angle measurements (§3.3.6, p.110). The bacterial cells were firmly immobilised to the aminosililated substrates using the EDC/NHS chemistry as explained in §3.3.6, p.110. A good proportion of the cells were confirmed to be viable after 6 h of immobilisation, through the use of SYTO9/propidium iodide fluorescent dyes, data which are presented in §3.3.6 on p.111 and in Appendix A.

### 4.2.2 SFM cantilever functionalisation

Chemically well-defined, clean, flat functionalised surfaces were prepared via self-assembled monolayers. To start with, freshly-opened MLCT  $\text{Si}_3\text{N}_4$  SFM probes (Bruker AFM Probes, Camarillo, USA) were transferred to a clean glass Petri dish and cleaned using a homemade oxygen plasma cleaner. To remove further organic

contamination, the probes were introduced into piranha solution (i.e. 70% H<sub>2</sub>SO<sub>4</sub>, 30% H<sub>2</sub>O<sub>2</sub>, both Sigma-Aldrich, Dorset, England) for 1 h. The acid-cleaned probes were then thoroughly rinsed with deionised water and ethanol, dried with N<sub>2</sub> gas and kept in a clean sealed container until functionalisation. All of these precautions were taken because it has been found [278] that the poly(dimethylsiloxane) gel-packs, in which the cantilevers are shipped in, contaminates the tips with silicone oils. The presence of foreign substances might affect the coating process and the reliability of the results. Regrettably, it was found that the piranha treatment produced a low output of useful cantilevers, since the high temperatures this solution generates and the excessive handling of the probes in the subsequent washing steps, caused the fragile tips to break or to bend [279]. Other authors have opted for less aggressive UV/ozone treatments [226], exposure to UV light or more frequently use the cantilevers as they were sold.

Once the cantilevers have been cleaned, they are ready to be coated. Metal films were deposited onto the probes using an Auto 306 evaporator (BOC-Edwards, Crawley, UK). The evaporator was kept at a pressure of  $10^{-7} - 10^{-6}$  mbar prior to evaporation. Gold wire (99.99% purity, Goodfellow Metals, England) and chromium chips (99.99%, Agar Scientific, England) were deposited into designated evaporation boats: molybdenum boats for currents of 35 A for Au deposition, and tungsten for currents of 55 A for chromium. The cantilevers were fixed to a homemade support and introduced to the evaporator chamber. A 1 nm layer of Cr was deposited at a rate of  $\sim 0.3$  nm/s. This primer layer is necessary in the cases in which the top metal (Au) does not form oxides readily, in order to improve its adhesion. Once the desired thickness was obtained, the evaporator was left to purge the chromium vapour with the aid of vacuum for ten minutes. Consecutively, a 12-15 nm layer of Au was evaporated. Gold is often chosen as the substrate for SAMs due to its chemically inert behaviour, its ease of patterning and handling, the fact that it can be easily evaporated onto diverse substrates and its non-toxicity, which allows the study of living organisms. Once the gold layer was formed, the evaporator was vented and the cantilevers were taken out and they were ready to be used.

SAMs provide a very easy method to tailor the properties of metals. They are formed by the adsorption of molecules present in a liquid or gaseous solution onto a solid surface, in an ordered manner. The adsorbates arrange spontaneously in a regular fashion and can even form crystalline layers; such adsorption happens readily, as this process lowers the free energy at the metallic interface. These adsorbates are tailored in such a way that on one end they have a ligand head group, which presents high preference for the metallic substrate. The most common type of SAMs are created from the interaction between alkanethiols and Au, Ag, Cu, Pd, Pt, and Hg. The other end bears the functional group of interest [280].

An idealised SAM is depicted in Fig 4.2. As shown, the typical thickness of the layer is about 1-3 nm. The chains appear tilted with relation to the normal, because it allows them to adopt a close-packed structure in which the ligand head groups interact with the metal atoms at regular intervals.

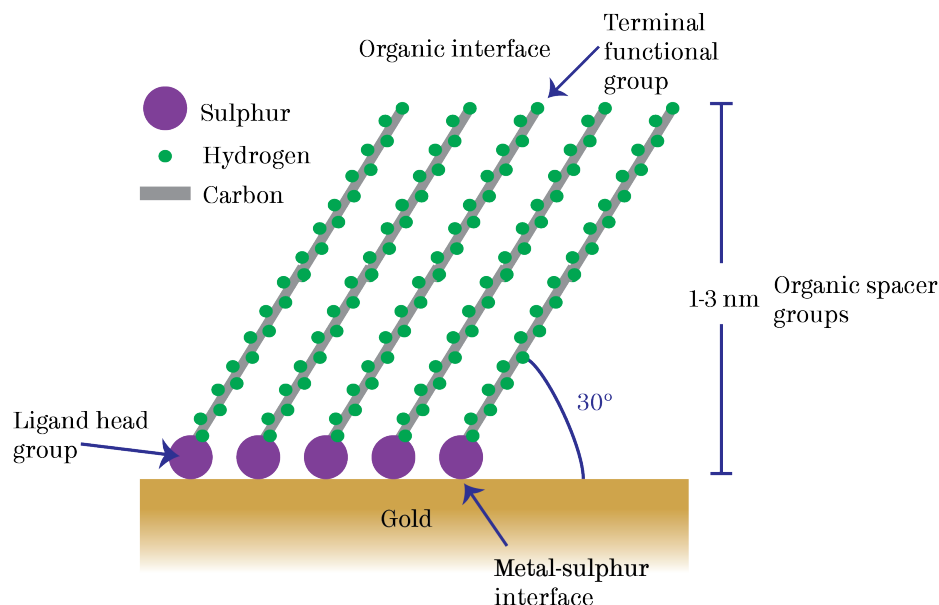


**Figure 4.2:** Diagram of an ideal SAM on Au. The chains are tilted  $30^\circ$  from the normal, to fill the space, because the van der Waals radii of the chains do not exactly match the sites of the gold (111) lattice. The chains are arranged in such a way that maximises the van der Waals interactions between atoms. In other words, the side chains are stabilised to a great degree by hydrophobic interactions. Image inspired from reference [280].

The self-assembled monolayers were prepared by immersing overnight the Au-coated cantilevers in 1 mM ethanolic solutions of 11-mercaptoundecanoic acid (MUA) (99% purity, Sigma-Aldrich, Dorset, England) or 1-dodecanethiol (DDT) ( $\geq 98\%$  purity, Sigma-Aldrich, Dorset, England), at room temperature. Even though a dense coverage of molecules is attained in a few seconds, more time is required to reorganise the molecules, in order to reduce the number of defects on the SAM. After the grafting time had elapsed, the cantilevers were extracted from the solution and carefully rinsed with analytical grade ethanol and air-dried. The functionalised probes were immediately mounted on the SFM cantilever holder and submerged into the scanning solution, to avoid contamination.

### 4.2.3 SFM imaging and force measurements

A Molecular Force Probe 3D system (MFP-3D, Asylum Research, Santa Barbara, USA) was used for the imaging of bacterial cells attached via covalent bonds. MLCT  $\text{Si}_3\text{N}_4$  SFM probes (Bruker AFM Probes, Camarillo, USA) were employed. Out of the six cantilevers that the MLCT probes have, the one dubbed “D” (second largest, see Figure 2.25 on page 54) was used. This cantilever has a resonant frequency of 10–20 kHz, a spring constant of 0.01–0.06 N/m, a length of 220–230  $\mu\text{m}$  and a width of 15–25  $\mu\text{m}$  as reported by the manufacturer. Force calibration was carried out, under buffer, following a two-step procedure established by Hutter and Bechhoefer [281]. Firstly, the photodetector sensitivity (InvOLS : inverse optical lever sensitivity) was measured by taking a force curve on a very stiff sample. A clean silicon wafer was the substrate of choice, since it is very hard and therefore it is assumed that any deflection detected during the measurement is due to the probe, rather than to the sample. The sensitivity measured is the gradient of the plot of photodetector signal against tip displacement. The slope of the retraction curve on the resulting force curve was fitted manually. The InvOLS was measured on three areas of the sample.

Once the InvOLS has been determined, the microscope head is retracted and a thermal spectrum is acquired. A thermal tune is a way to determine the natural frequency of the cantilever over a frequency range, by performing an iterative series of frequency sweeps and finding an average value. The cantilever in this case will behave like a harmonic oscillator, only driven by thermal noise. Usually 100-300 samples or sweeps were taken before fitting the fundamental resonance peak. On average, the spring constant was found to be  $0.040 \pm 0.003$  N/m ( $n = 17$ ).

The images were obtained in intermittent contact mode, using slow scan frequencies (0.5–1 Hz). The resonant frequency in liquid was determined by manually tuning the cantilever and it was estimated to be in the range of 12–14 kHz.

Once the bacterial cells were localised using intermittent contact mode, the microscope was switched to contact mode. A number of force-distance curves were acquired using the force-volume mode, inbuilt in the IgorPro software. Force-volume mapping is capable of recording force-distance measurements in a 2-dimensional array, correlating adhesive and mechanical parameters with the bacterial topography. The force maps were acquired using  $32 \times 32$  grids; each point on these grids corresponds to a force measurement and has associated a height and adhesion value. A diagram that depicts the way in which the force-volume mode of the SFM works, can be seen in Figure 4.3.

The area that each of the acquired maps comprised, included regions belonging to the bacterial cell and regions belonging to the APTES background. Both areas

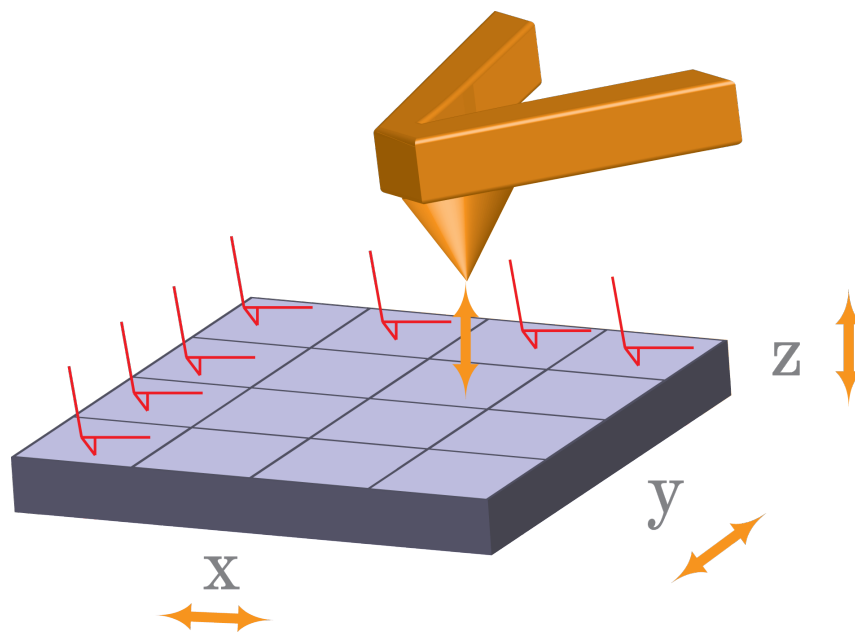


**Figure 4.3:** Force-volume mode on a  $4 \times 4$  grid. The SFM cantilever moves in the  $z$  direction, determining the force of adhesion and the height at a given point of the surface. Once recorded, it moves in  $x$  or  $y$  to a neighbouring point, where it takes another force-distance curve.

showed very different adhesion forces and adhesion histogram profile, as seen in Figure 4.4. Whereas the forces taken inside the cell have low values and a skewed distribution, the forces recorded on the APTES are higher and appear more normally distributed. In order to distinguish these two regions and select only the area pertaining the cell, a *mask* was employed (Figure 4.5). IgorPro is able to tell the two surfaces apart if a threshold value is given. This threshold value can be manually selected or it can be calculated using diverse methods. The masks were determined using the *iterative mask mode*, through a series of computations that have been described in reference [282].

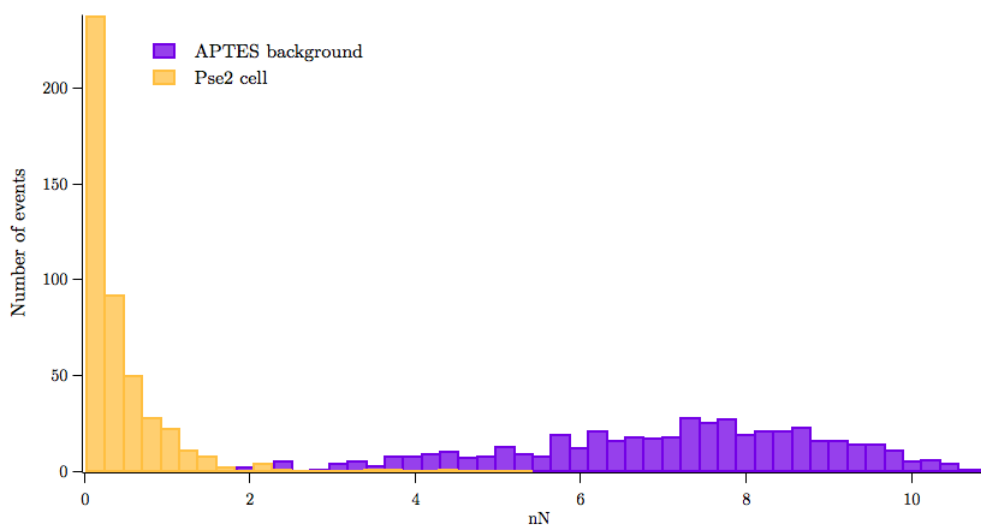


**Figure 4.4:** Comparison between the forces generated by probing a cell and its APTES background. The background is masked using an iterative mask, inbuilt in the IgorPro software.

The measurements were obtained using a force distance of 500 nm and an absolute trigger value of 100 nm, which is equivalent to a loading rate of approximately 40,000 pN/s (n.b. the loading rate is the change in the applied force with time). The force applied to the sample was around 4 nN (it varied slightly, depending on the value of the spring constant of the cantilever). The piezo  $z$ -velocity was kept at a standard of 0.99  $\mu\text{m/s}$  and the dwell time was kept at 0 s. Examples of force-volume maps taken on Pse1 cells using a silicon nitride tip can be seen in Figures 4.24-4.27 in §4.3 and other select examples of maps of Pse1 maps, acquired with different cantilevers, can be found on the same section.

The images and measurements were acquired under MOPS 20 mM. MOPS is one of the so-called Good's buffers [260], a group of buffers widely used in biology and biochemistry. MOPS has a pKa of 7.2, thus keeping the pH of the

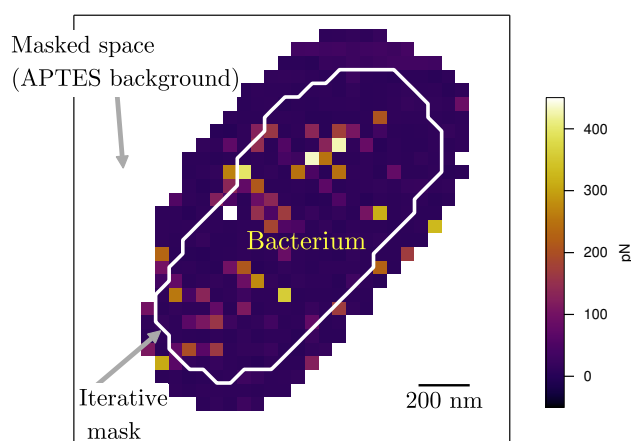


**Figure 4.5:** Mask used to separate the area belonging to the bacterial cell and the area belonging to the APTES background. The size of the mask was automatically generated by IgorPro, using an iterative algorithm.

solution close to neutral. MOPS is highly soluble in water, non-toxic, has limited interaction with mineral cations, does not affect biochemical reactions and has limited permeability through cellular membranes, making it an ideal candidate for our applications (Figure 4.6) [283].

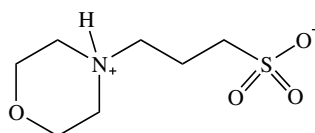


**Figure 4.6:** Chemical structure of 3-(N-morpholino)propanesulfonic acid (MOPS).

### 4.3 Imaging

As mentioned in Chapter 3, it is imperative to have the cells firmly anchored to the substrate, in order to have adequate images and reliable samples. If the sample fails to withstand the lateral force of the SFM tip, then the cells will detach halfway through the scanning. While describing common approaches to immobilise bacterial cells, it was made clear that for the particular case of the studied *Rhodococcus* and *Pseudomonas* strains, only covalent linking between the cells and the substrate seemed to consistently produce good samples, with

strong linkages and reproducible behaviour. Even though the use of poly-L-lysine, polyethyleneimine, polystyrene, polyphenolic proteins and polycarbonate membranes occasionally produced bacterial cells that withstood scanning under a liquid medium, these cells were extremely hard to find and much time was wasted looking for them. Consequently it was decided to use the EDC/NHS/APTES attachment protocol, that proved to have a considerably higher (albeit not 100%) success rate.

Another key condition to image the bacterial strains that concern this thesis, is to minimise the interaction between the tip and the sample through the use intermittent contact mode instead of contact mode. It was found that even the covalent linkages were not strong enough to hold the bacteria if they were being scanned with continuous contact from the tip. The use of intermittent contact mode ensured that the majority of the cells remained attached after they were being imaged.

In order to obtain any reliable information from SFM images it is important to be aware of the possibility of imaging artifacts. An experienced user will try to minimise their presence during the scanning itself, but if this is not possible, the images should be interpreted taking these artifacts into account, so that they do not give false impressions. As long as the apex of the tip is much smaller than the observed feature and is free of contaminants, the SFM will produce an accurate representation of the sample. Therefore, an adequate tip size should be selected prior to the experiments. A scale diagram of the tips used in this thesis and an average bacterium is depicted in Figure 4.7.

In general, there are common artifacts and technical difficulties that the user should be aware of:

### Tip artifacts

- **Object broadening:** The object will appear different if it is scanned with a sharp or a blunt tip. When the features are smaller than the tip radius they will appear broader than what they actually are. Furthermore, the geometry of the tip will also affect the shape of the sample. The pyramidal volume of the tip might not be able to access some regions of the scanned surface.
- **Damaged tips:** If the tip has been damaged or if it has been contaminated with the sample, it might give rise to the so called *double-tip effect*, depicted in Figure 4.8. Moreover, if the tip gets contaminated, the debris can get dragged along the sample and produce horizontal streaks. Often they can be erased during the image post-processing [284].

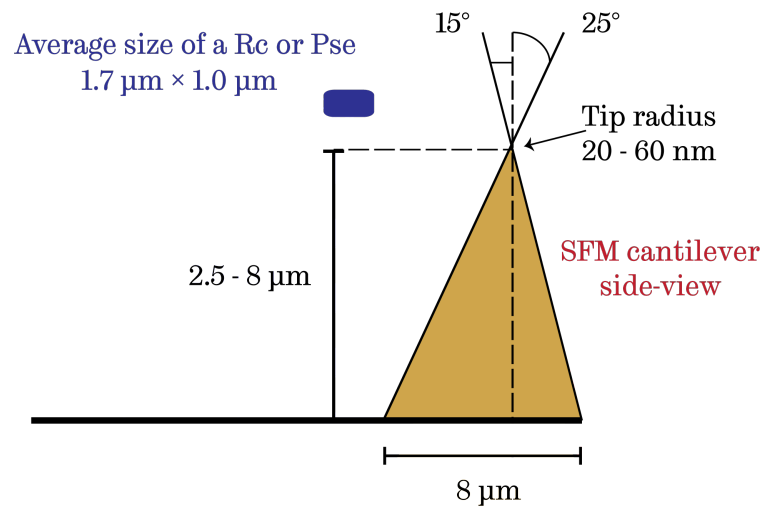


**Figure 4.7:** Relationship between the size of the probe and the average size of a bacterium. The probe dimensions were taken from [130] and the average size from the bacterium was calculated after having measured 48 bacterial cells.

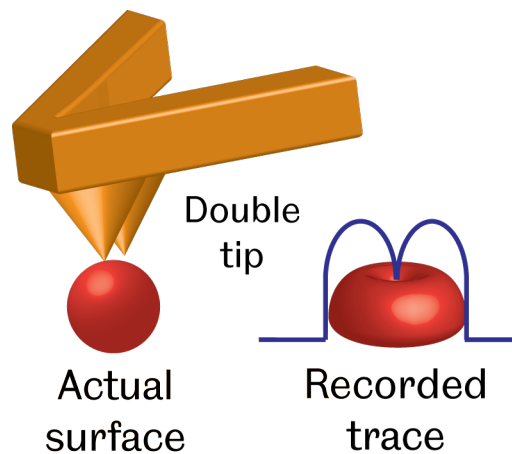


**Figure 4.8:** Double tip effect. Artifact caused by the contamination or degradation of the SFM tip. This explains the double features in Figures 4.18b and 4.22b. Image adapted from reference [122].

### Scanner artifacts

- **Feedback issues:** The feedback mechanism controls the response of the piezoelectric device towards changes in amplitude through the gains. If the gains are too low, the tip does not make proper contact with the surface, and the image appears blurry; if they are too high the image is distorted due to

a *ringing* effect. Often, the user has to find the right balance in the image by modifying the gains, but this might not be possible every time and artifacts might be present in some of the images.

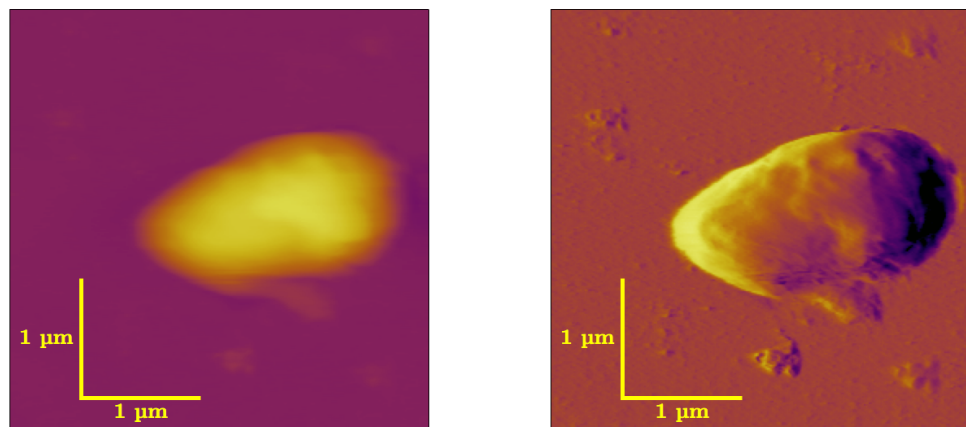
- **Thermal and mechanical noise:** External temperature changes might complicate the SFM setup, especially at the beginning of the experiment. Often it is convenient to allow the system to equilibrate before starting the experiment. Often the user has to keep zeroing the deflection between images, as the signal in the photodetector tends to drift. The measured room temperature while performing the mapping experiments presented in this chapter was 28 °C and thus thermal drift and solvent evaporation commonly presented technical difficulties. Acoustic and mechanical drift can also be an issue, although the majority of the times these sources of noise were effectively reduced by the air table on which the SFM is placed upon [284].
- **Non-linear response:** The response of the piezoelectric scanner to the driving signal is non-linear and thus correction factors must be applied. Additionally the images require post-processing to reduce the tilt of the sample in relation to the tip, in a procedure known as *flattening*. The images were flattened using the microscope software, IgorPro 6.22A, and other visible defects, like streak lines, were smoothed.

### 4.3.1 Imaging *Pseudomonas*

Figures 4.9-4.16 are representative examples of *Pseudomonas* Pse1 and Pse2 as imaged with Si<sub>3</sub>N<sub>4</sub>, Au, DDT and MUA cantilevers. The average length of *Pseudomonas* Pse1 was found to be  $1.84 \pm 0.54$  μm and the width  $0.92 \pm 0.11$  μm ( $n=9$ ). The average length of Pse2 was found to be  $1.48 \pm 0.24$  μm and the width  $0.84 \pm 0.08$  μm ( $n=9$ ).

There are some aspects of the images that are noteworthy. Figures 4.11-4.14 have particularly defined surface features and these are examples of good imaging conditions. Figure 4.14 clearly shows the presence of a great number of appendages that protrude from the Pse2 cell. Other authors [285] have confirmed the expression of pili and flagella in related *Pseudomonas* after the bacteria have adhered.

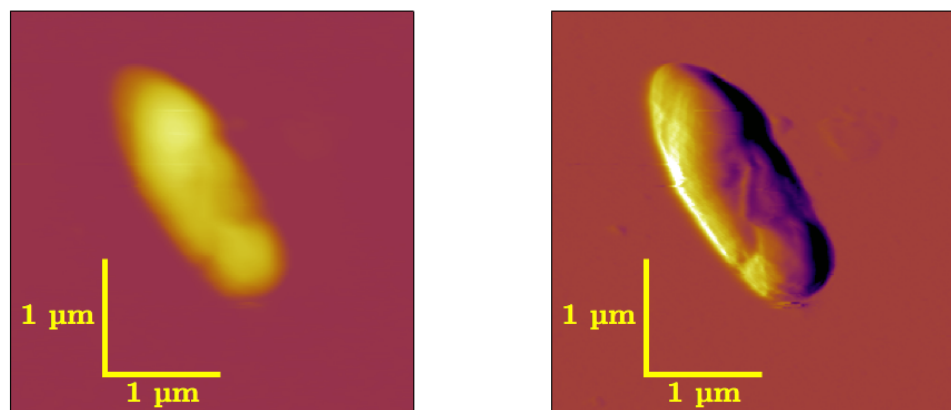
Images, like Figure 4.9 and Figure 4.12 contain globules of material of a few hundred nanometres that could either be cellular fragments of lysed cells or clusters of EPS.



(a) Height image

(b) Deflection image

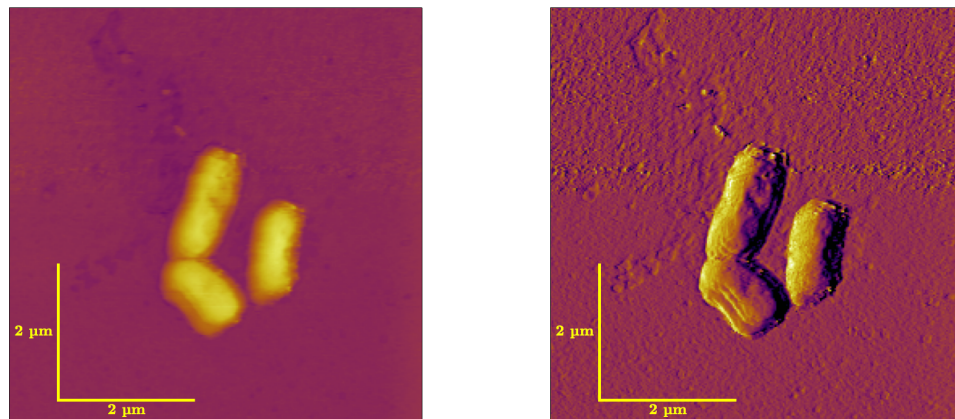
**Figure 4.9:** *Pseudomonas* 1 imaged with a  $\text{Si}_3\text{N}_4$  tip. The height scale is 250 nm. The imaging parameters for this bacterium were not ideal, since some small double features can be seen, and the image appears somewhat blurry.



(a) Height image

(b) Deflection image

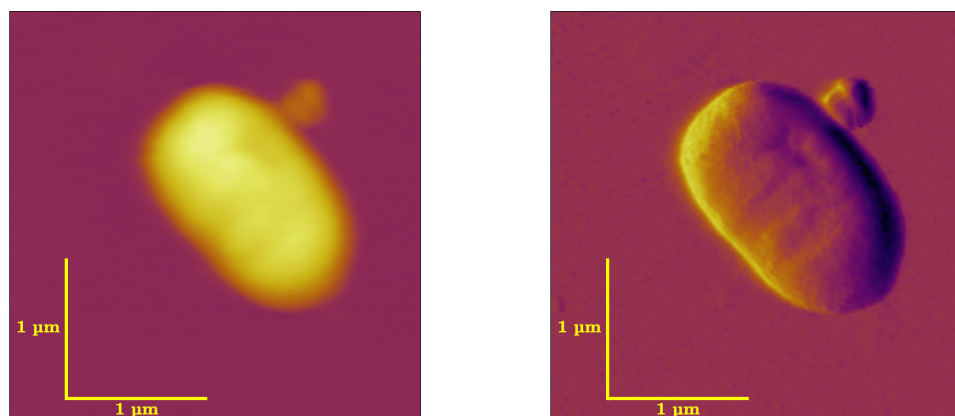
**Figure 4.10:** *Pseudomonas* 1 imaged with an Au tip. The height scale is 500 nm.



(a) Height image

(b) Deflection image

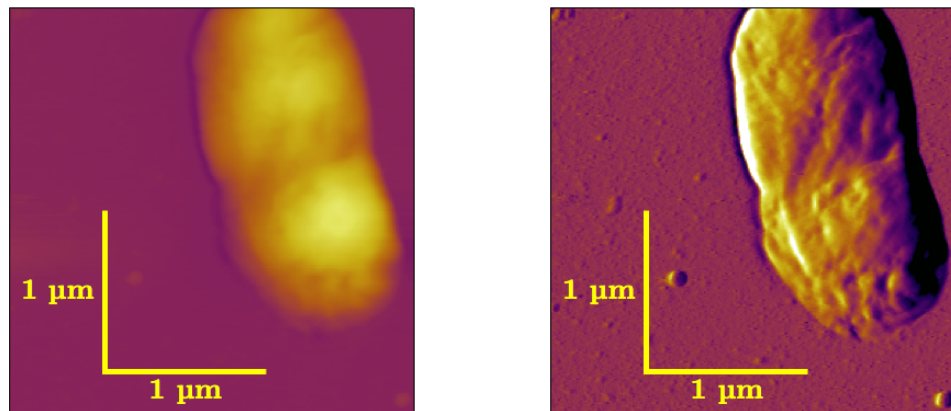
**Figure 4.11:** *Pseudomonas* 1 imaged with a DDT tip. The height scale is 400 nm.



(a) Height image

(b) Deflection image

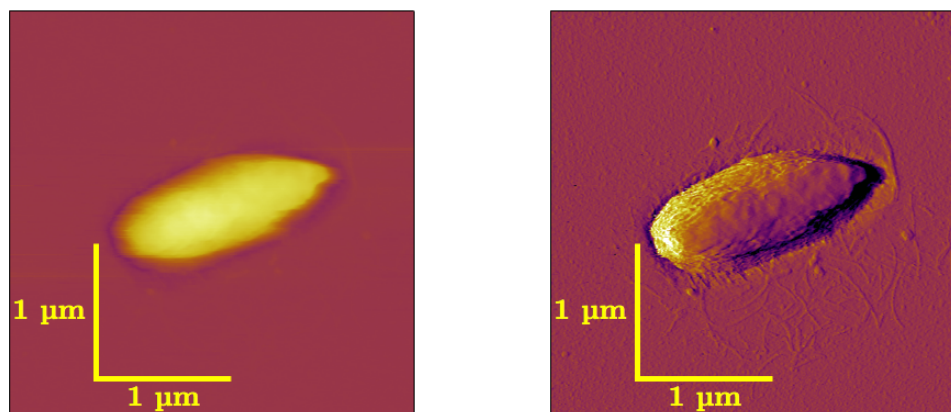
**Figure 4.12:** *Pseudomonas* 1 imaged with a DDT tip. The height scale is 300 nm. A globule of organic material is located next to the cell. Its provenance might be from EPS or cell debris.



(a) Height image

(b) Deflection image

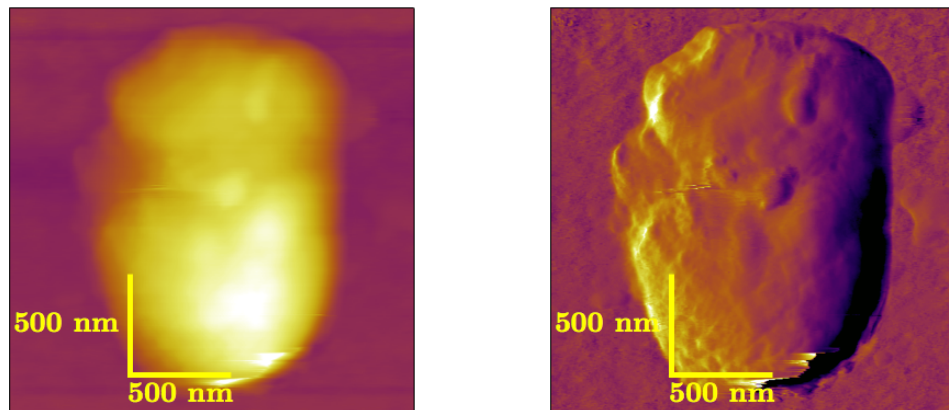
**Figure 4.13:** *Pseudomonas 1* imaged with a MUA tip. The height scale is 200 nm.



(a) Height image

(b) Deflection image

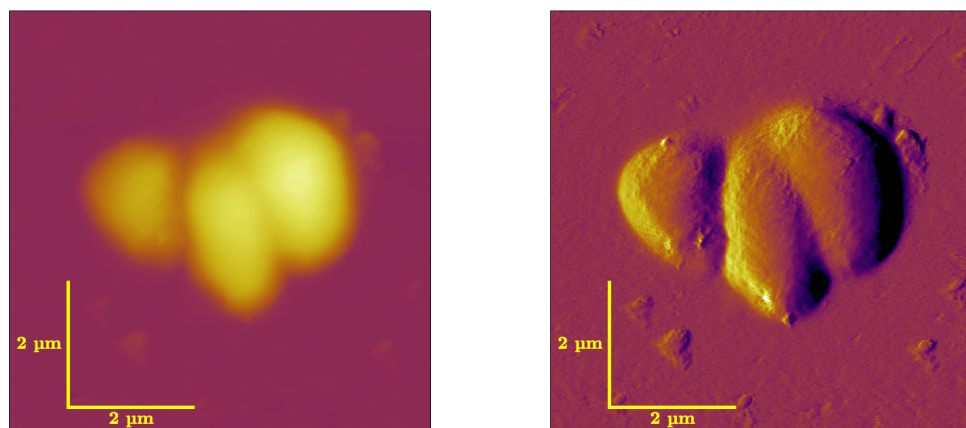
**Figure 4.14:** *Pseudomonas 2* imaged with a  $\text{Si}_3\text{N}_4$  tip. The height scale is 400 nm. Details of the cellular appendages can be clearly visualised.



(a) Height image

(b) Deflection image

**Figure 4.15:** *Pseudomonas 2* imaged with an Au tip. The height scale is 200 nm. The surface of the cell has many irregularities, perhaps due to EPS coverage.



(a) Height image

(b) Deflection image

**Figure 4.16:** *Pseudomonas 2* imaged with a DDT tip. The height scale is 400 nm.

### 4.3.2 Imaging *Rhodococcus*

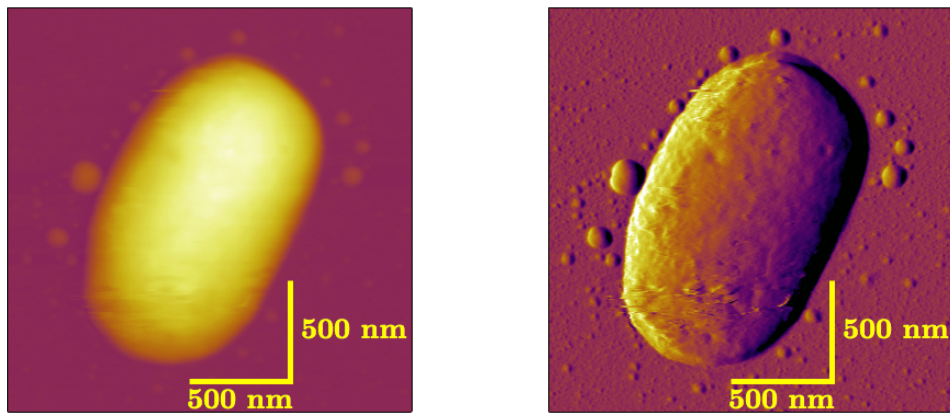
Figures 4.17-4.23 are representative examples of *Rhodococcus* Rc92 and Rc291 cells scanned using four different types of cantilevers: Si<sub>3</sub>N<sub>4</sub>, Au, DDT and MUA. *Rhodococcus* images depicted in Figures 4.17, 4.19 and 4.23 contain globular material that can be associated with EPS or with cellular fragments. There is some loose material associated to the cells and can be seen as horizontal streaks (Figures 4.17, 4.22 and 4.23). This phenomenon could be indicative of a feebly attached capsular layer of material that surrounds the bacterial cell.

Figure 4.20 shows an example of a cell that was captured in the process of division, showing a horizontal line across the cell. A detailed version of this feature can be seen in Figure 4.21, where the topographic variations of the cell can be appreciated.

In Figure 4.18, despite the evident double-tip artifact, the presence of an appendage can be confirmed. There is some evidence of scant pili on the surface of other strains of *Rhodococcus* but their significance has not been understood [286].

The average length of *Rhodococcus* Rc92 was found to be  $1.48 \pm 0.21$   $\mu\text{m}$  and the width  $0.99 \pm 0.09$   $\mu\text{m}$  ( $n = 9$ ). The average length of Rc291 was found to be  $1.88 \pm 0.51$   $\mu\text{m}$  and the width  $1.11 \pm 0.24$   $\mu\text{m}$  ( $n = 9$ ).

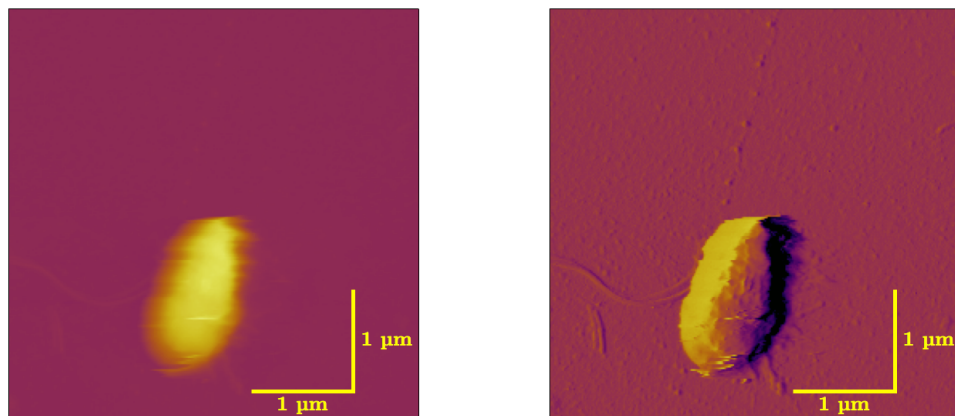
In Figures 4.18b and 4.22b certain features of the cells seem to be repeated twice. This is the result of the damage or contamination of the tip, that makes it have two apices, provoking this common imaging artifact, as shown in Figure 4.8 [122].



(a) Height image

(b) Deflection image

**Figure 4.17:** *Rhodococcus* 291 imaged with a  $\text{Si}_3\text{N}_4$  tip. The height scale is 200 nm. The bacterial cell is accompanied by a number of globules, perhaps clusters of EPS or cellular debris.



(a) Height image

(b) Deflection image

**Figure 4.18:** *Rhodococcus* 291 imaged with an Au tip. The height scale is 500 nm.

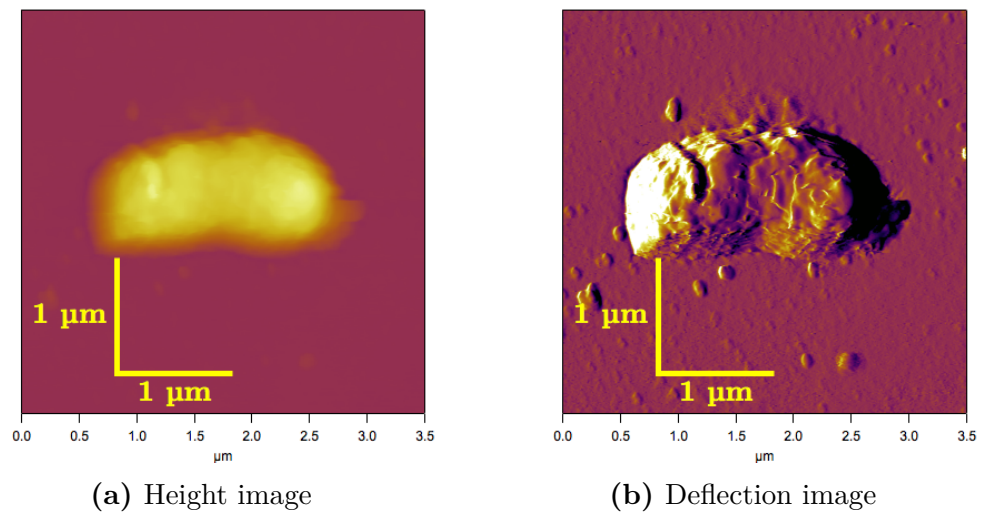


**Figure 4.19:** *Rhodococcus* 291 imaged with a MUA tip. The height scale is 600 nm.

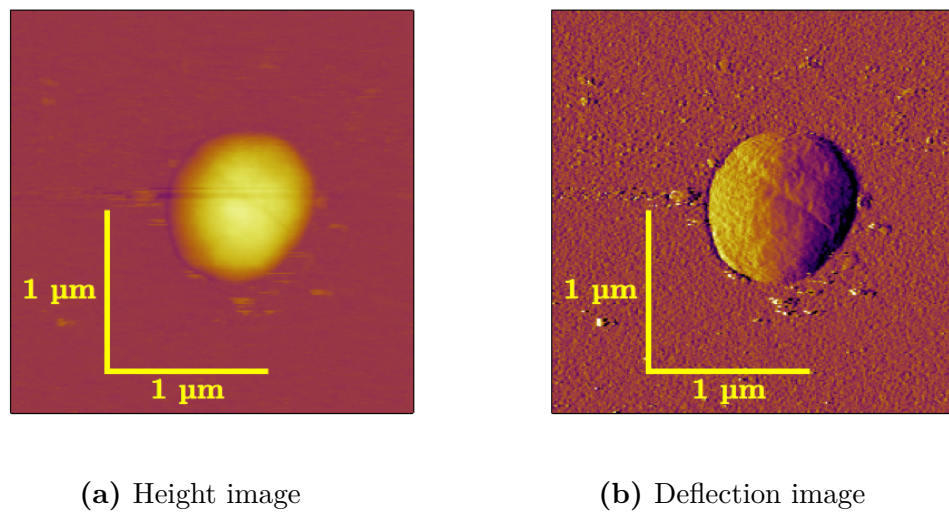
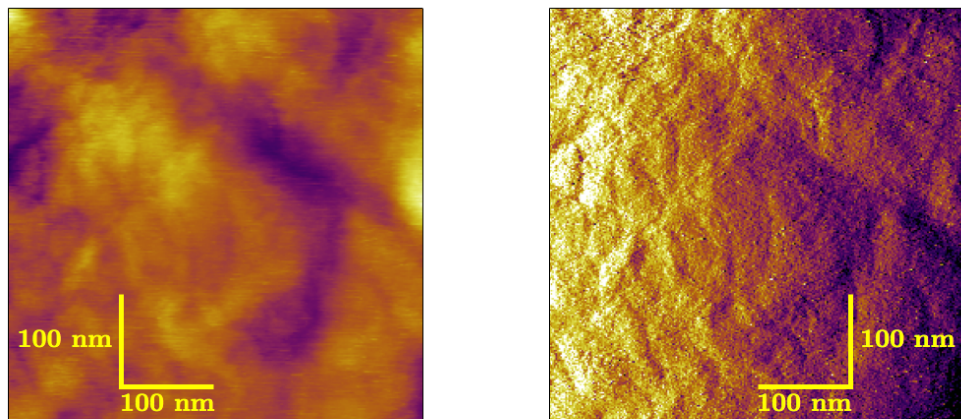


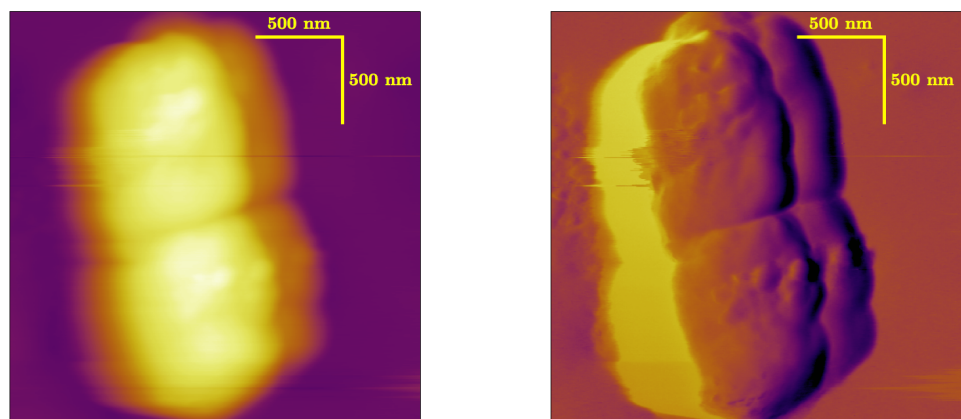
**Figure 4.20:** *Rhodococcus* 92 imaged with a  $\text{Si}_3\text{N}_4$  tip. The height scale is 250 nm.



(a) Height image

(b) Deflection image

**Figure 4.21:** Detail of the membrane of *Rhodococcus 92* imaged with a  $\text{Si}_3\text{N}_4$  tip. The height scale is 15 nm. Some details of the bacterial cell surface can be seen with nanoscale resolution. By only studying the morphology of such features it would be difficult to ascertain their chemical nature. The idea that these features are formed by proteinaceous layers or polysaccharides could be ventured. In some bacterial types the assignment of surface features is unequivocal in cases where proteins form ordered crystalline layers (e.g. S-layer in *Corynebacterium*) [287], but this is not one of those cases.



(a) Height image

(b) Deflection image

**Figure 4.22:** *Rhodococcus 92* imaged with a DDT tip. The height scale is 250 nm. The bacterial cell appears double, a phenomenon due to the contamination of the tip, which leads to a double-tip effect.

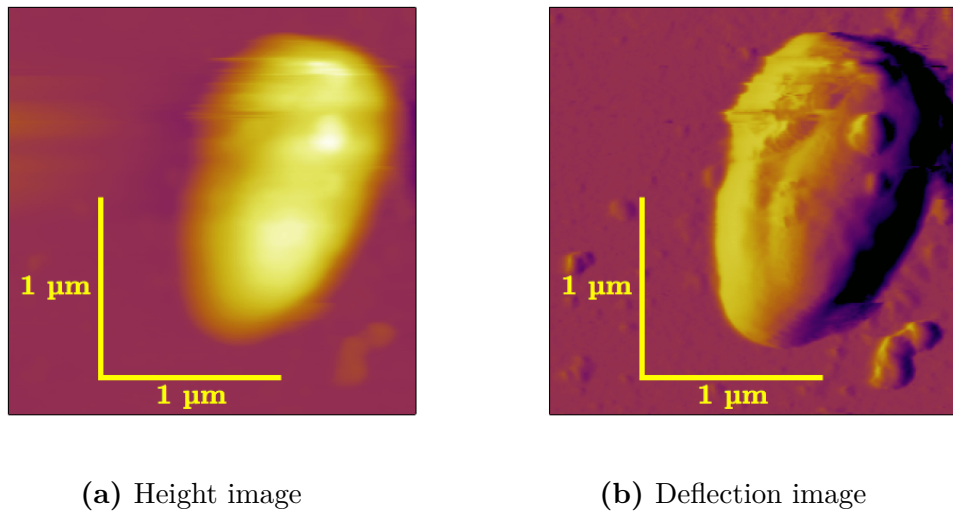


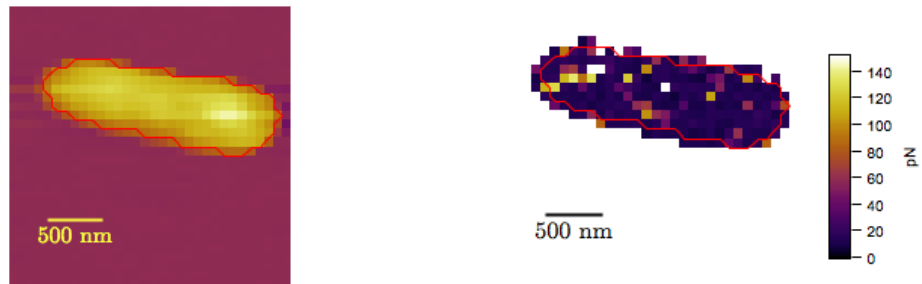
**Figure 4.23:** *Rhodococcus* 92 imaged with a MUA tip. The height scale is 400 nm. Clusters of organic material are present next to the cell and on its surface.

## 4.4 Force measurements

A considerable amount of force-volume maps were acquired during the course of the experimental process, and as a consequence, only some selected height and force maps will be presented in this section. It was decided to showcase the experiments conducted on Pse1 as a model experiment, and hence the majority of the examples portrayed here will be related to this strain. In Figures 4.24-4.27 four examples of Pse1 force-volume maps recorded with a  $\text{Si}_3\text{N}_4$  tip are shown. In Figures 4.28-4.35 maps traced with Au, DDT and MUA -functionalised tips are represented. Further examples of force-volume maps of the other three strains have been included in Appendix B.

In all cases, a *height map* is included, which is a low-resolution, colour coded representation of the cell topography. Each one of these pixels has an equivalent in the force map next to them. The colour scale of the force map is included.

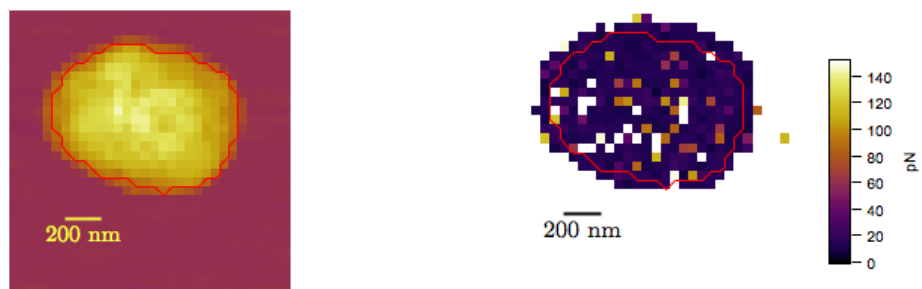
The data range controls the appearance of the force map, as it assigns a different interval of forces to a given colour. This data range was selected in such a way that the adhesion forces of the APTES background appeared mostly white, for the sake of clarity and contrast between the two surfaces.



(a) Height map, with a maximum height of 270 nm.

(b) Force-volume map

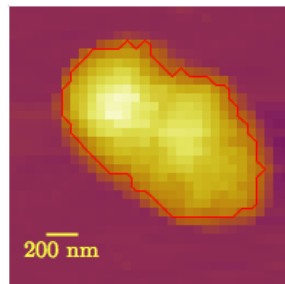
**Figure 4.24:** Pse1 mapped with a  $\text{Si}_3\text{N}_4$  tip.



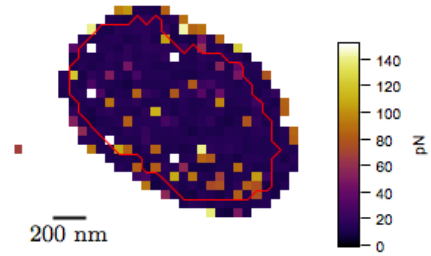
(a) Height map, with a maximum height of 170 nm.

(b) Force-volume map

**Figure 4.25:** Pse1 mapped with a  $\text{Si}_3\text{N}_4$  tip.

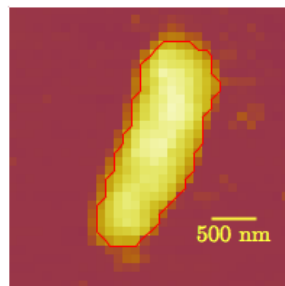


(a) Height map, with a maximum height of 220 nm.

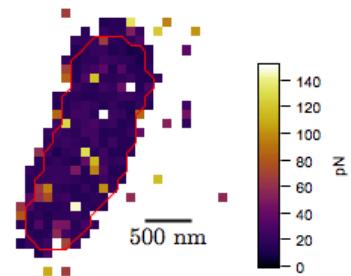


(b) Force-volume map

**Figure 4.26:** Pse1 mapped with a  $\text{Si}_3\text{N}_4$  tip.

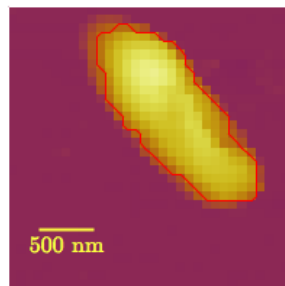


(a) Height map, with a maximum height of 270 nm.

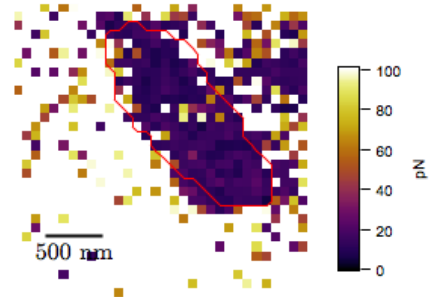


(b) Force-volume map

**Figure 4.27:** Pse1 mapped with a  $\text{Si}_3\text{N}_4$  tip.

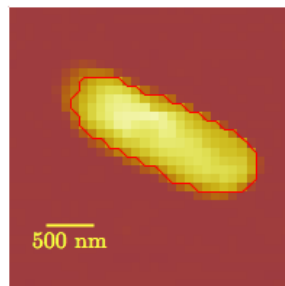


(a) Height map, with a maximum height of 550 nm.

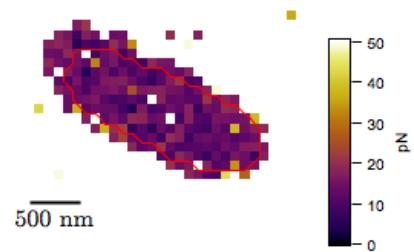


(b) Force-volume map

**Figure 4.28:** Pse1 mapped with an Au tip.

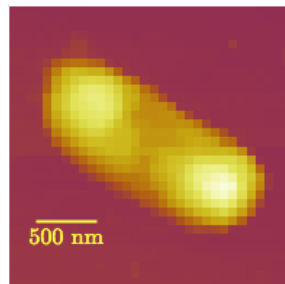


(a) Height map, with a maximum height of 550 nm.

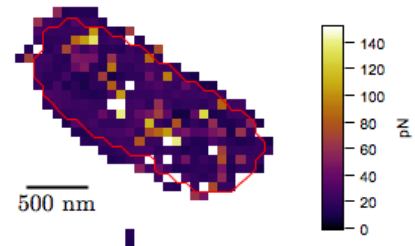


(b) Force-volume map

**Figure 4.29:** Pse1 mapped with an Au tip.

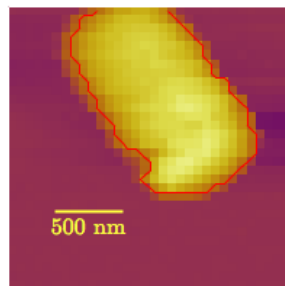


(a) Height map, with a maximum height of 350 nm.

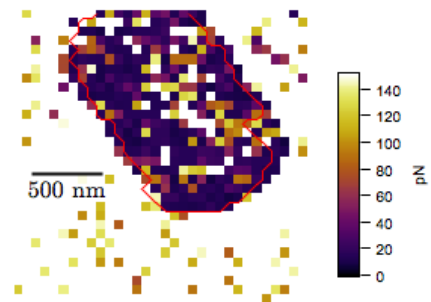


(b) Force-volume map

**Figure 4.30:** Pse1 mapped with an Au tip.

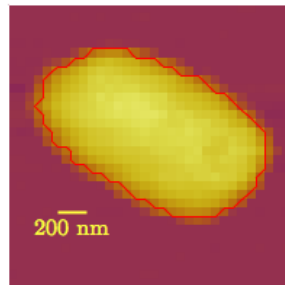


(a) Height map, with a maximum height of 280 nm.

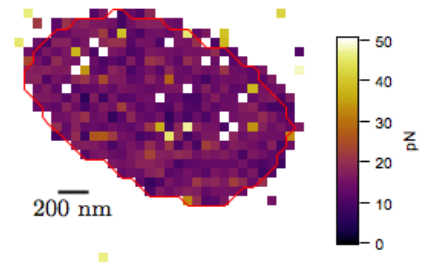


(b) Force-volume map

**Figure 4.31:** Pse1 mapped with a DDT tip.

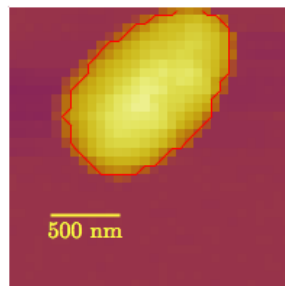


(a) Height map, with a maximum height of 280 nm.

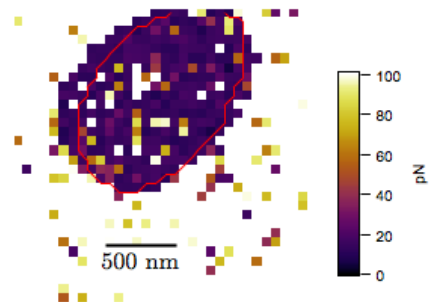


(b) Force-volume map

**Figure 4.32:** Pse1 mapped with a DDT tip.

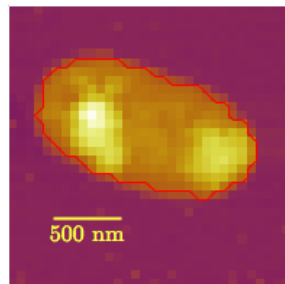


(a) Height map, with a maximum height of 280 nm.

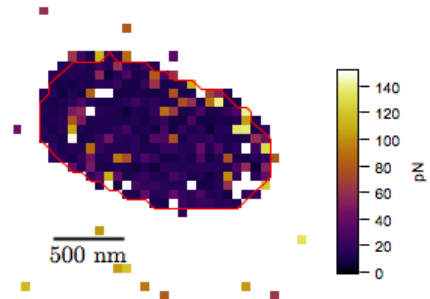


(b) Force-volume map

**Figure 4.33:** Pse1 mapped with a DDT tip.

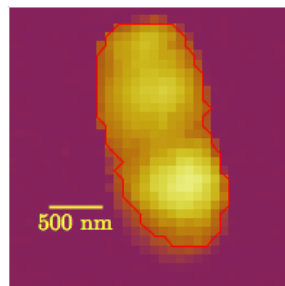


(a) Height map, with a maximum height of 200 nm.

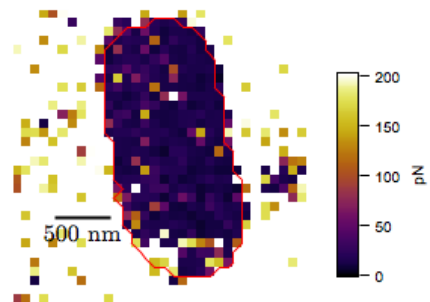


(b) Force-volume map

**Figure 4.34:** Pse1 mapped with a MUA tip.



(a) Height map, with a maximum height of 250 nm.

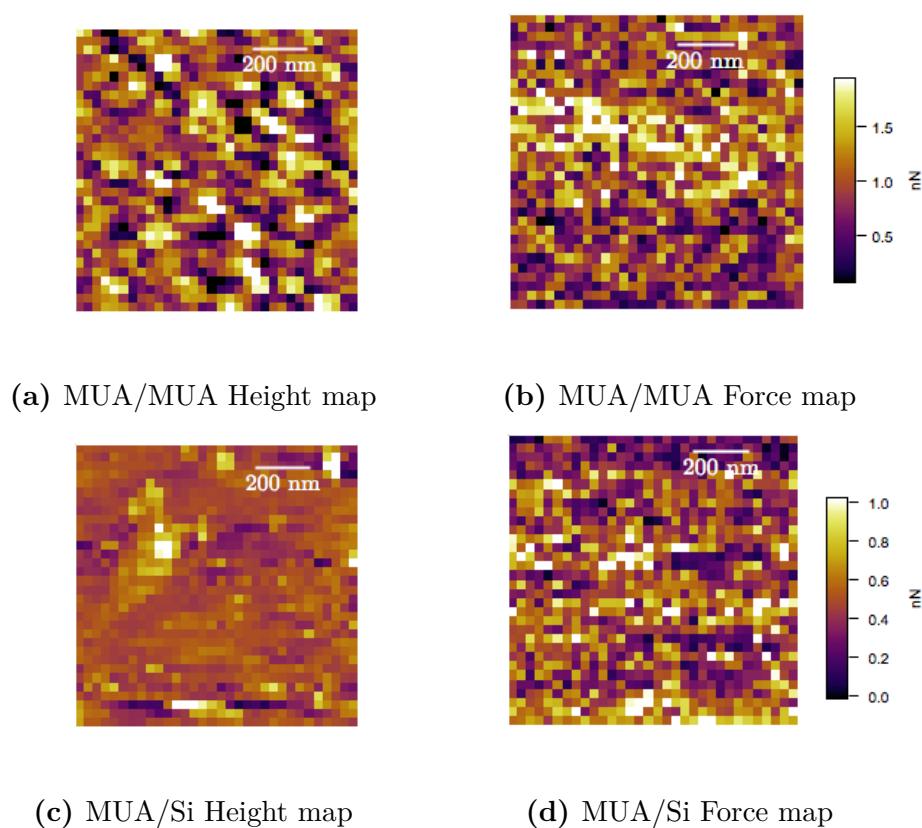


(b) Force-volume map

**Figure 4.35:** Pse1 mapped with a MUA tip.

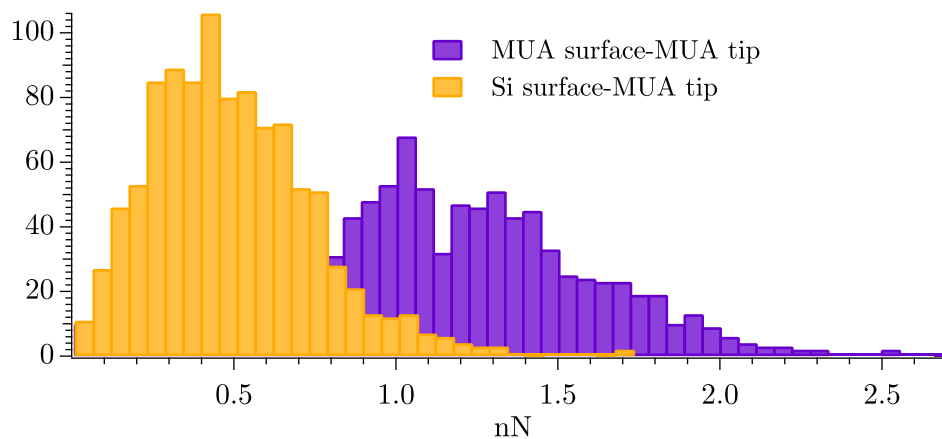
Some control experiments were also performed to ascertain the validity of the bacterial mapping. To that end, clean silicon wafers were coated with gold, following the exact same protocol that was used for tip functionalisation (§4.2.2, on page 124). The gold coated wafers and gold coated cantilevers were submerged overnight in thiol ethanolic solutions. After the designated time, both surfaces were rinsed with ethanol, air-dried and wetted with MOPS 20 mM on the microscope stage. Several force-volume maps were acquired for these systems.

Figure 4.36 shows height and force maps of a bare silicon wafer and an MUA-functionalised wafer, as probed by a MUA probe.



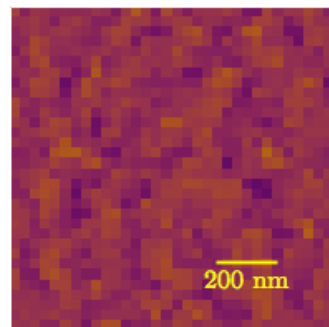
**Figure 4.36:** MUA-MUA and MUA-Si control experiments. In Figures 4.36a and 4.36b, a MUA-self assembled monolayer was probed using an MUA cantilever. Both substrate and probe, were assembled from the same solution. In Figures 4.36c and 4.36d, a silicon wafer is probed using a MUA-coated cantilever. The height scale is 120 nm.

Histograms of both of these events are portrayed in Figure 4.37. It can be seen that the interaction force between two MUA surfaces is higher than between the MUA-cantilever and a silicon surface. It is also noteworthy that the latter distribution appears to be normally distributed, whereas the former one shows some degree of bimodality.

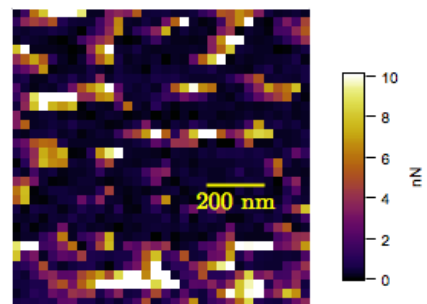


**Figure 4.37:** Histograms of the interaction forces between two MUA surfaces and between a MUA tip and a bare silicon surface.

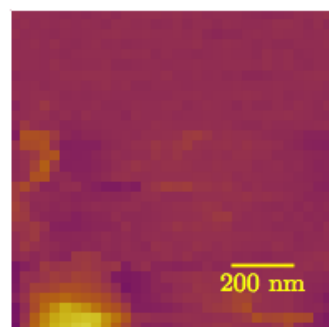
Similarly, the distribution of forces and histograms for the DDT controls are presented in Figure 4.38 and 4.39, respectively. The DDT-Si interaction appears to be monomodal and normally distributed, while the DDT-DDT experiment has a very different behaviour. The latter experiment has heavily skewed data, spanning along a higher force interval.



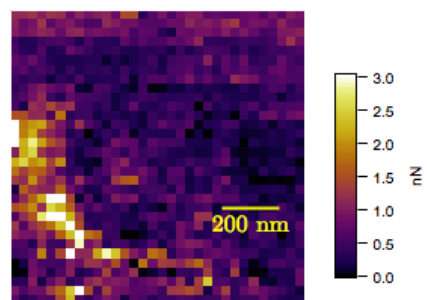
(a) DDT/DDT Height map



(b) DDT/DDT Force map



(c) DDT/Si Height map



(d) DDT/Si Force map

**Figure 4.38:** DDT-DDT and DDT-Si control experiments. In Figures 4.38a and 4.38b a DDT-self assembled monolayer was probed using an DDT cantilever. Both substrate and probe, were assembled from the same solution. In Figures 4.38c and 4.38d a silicon wafer was probed using a DDT-coated cantilever. The height scale is 40 nm.

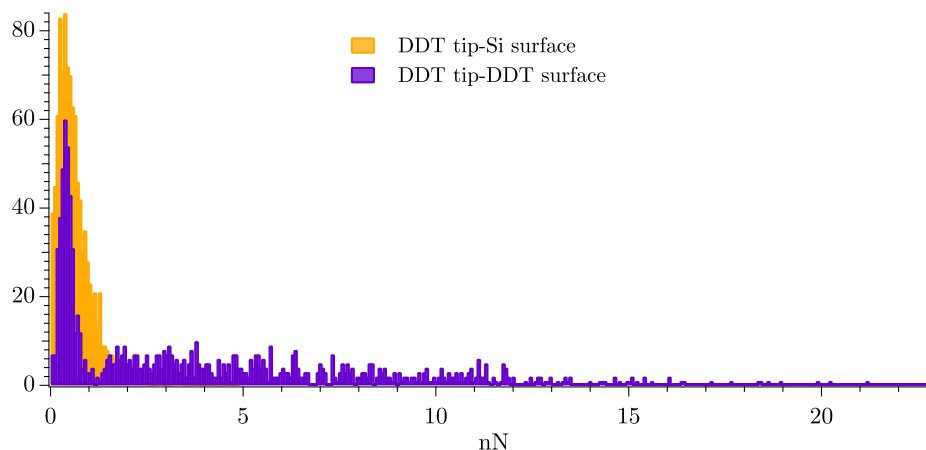


**Figure 4.39:** Histograms of the interaction forces between two DDT surfaces and between a DDT tip and a bare silicon surface. The bin sizes were minimised, to portray the distinction between the two conditions more appropriately.

## 4.5 Data Analysis

### 4.5.1 Statistical analysis

Diverse statistical methods have been applied in order to describe the adhesion values of these measurements. Often, for bacterial adhesion analysis, common statistical descriptors, such as the mean value are of little use, due to large standard deviations (the data range and median are better descriptors for highly heterogeneous data). This idea is supported by van der Mei, de Vries and Busscher [288], who have noticed that the measurement of bacterial adhesion is far from precise, as the standard deviation of the mean value is in the range of 50–70%, while the standard deviation of the adhesion between abiotic surfaces (e.g. silicon versus silicon nitride) is less disperse ( $\sim 13\%$ ).

In some cases, the data appears to be described better by non parametric distributions (Non parametric distributions are the ones that do not assume the data to have any structure or parameters. Non-parametric statistical tests do not suppose that the data are normally distributed.) In other cases, it is possible to describe the data using parametric models; for instance, Weibull distributions have successfully been used to describe the adhesion of bacteria to surfaces [288]. In Figure 4.40a a histogram of the interaction between a *R. terrigena* bacterial cell and a carbon particle mounted on a cantilever is shown. The distribution appears to be bimodal and was successfully fitted using a Weibull distribution.

In a similar way, other statistical analyses have been used to model bacterial adhesion to surfaces. For example, Poisson analysis has been used to describe the adhesion of *S. epidermis* to a glass surface [289]. Also, log-normal distributions have been employed to model the adhesion energies of *Listeria monocytogenes* to silicon nitride cantilevers [290].

Other authors have found possible to fit their adhesion histograms using a number of Gaussian histograms. Lorite *et al.* [291] studied the adhesion of the plant pathogen *Xylella fastidiosa* to silicon, ethyl cellulose and cellulose acetate. These researchers also immobilised one of *Xylella*'s adhesins (n.b. an adhesin is an adhesion protein) on an SFM tip and probed it against the same surfaces. They found a bimodal distribution that they fitted using two Gaussian curves for the ethyl cellulose and the acetate. For the silicon surface a skewed unimodal distribution was found. Similarly, Dupres *et al.* [292, 293] found a bimodal distribution between a *M. bovis* bacterial cell and a heparin-coated cantilever (Figure 4.40b). Other researchers [230, 294] have presented similar bimodal histograms. In some cases the curves have been fitted to a single Gaussian peak, despite the considerable skewness of the graph [295]. Trimodal distributions have also been reported: Busscher *et al.* [296] fitted three Gaussian peaks to a histogram of the adhesion forces of bacteria to protein coated SFM probes. Other authors, employing techniques different to SFM, have also suggested that the behaviour of cell populations towards adhesion appears to have a bimodal distribution [297–299].

Upon studying the profile of the histograms generated by force-volume maps of *Rhodococcus* Rc92 and Rc291, as well as the ones of *Pseudomonas* Pse1 and Pse2 probed by silicon nitride, gold, DDT and MUA cantilevers, it was clear that the distributions were heavily skewed towards high forces due to the presence of many outliers. It became apparent that the histograms could not have been fitted by a single Gaussian curve.

The force adhesion data were transformed using logarithms in an attempt to normalise the data, however the data continued to have a certain degree of skewness and the presence of a secondary peak of adhesion probability was made patent. Log-normal and Weibull functions were used to model the data, but the fits were not close. In order to normalise the data, the Box-Cox transformation was applied, but without successful results. The Box-Cox transformation is a function applied to transform the data in order to eliminate skewness and achieve normality. The expected outcome of this technique was to obtain a histogram of the transformed data that could have been fitted to a Gaussian distribution or given a straight line on a Q-Q plot (n.b. Q-Q plots, where Q stands for quantile, are probability plots that serve as a visual representation of normality). Since none of these results were achieved, the idea of normalising the data was abandoned, and another approach was taken.

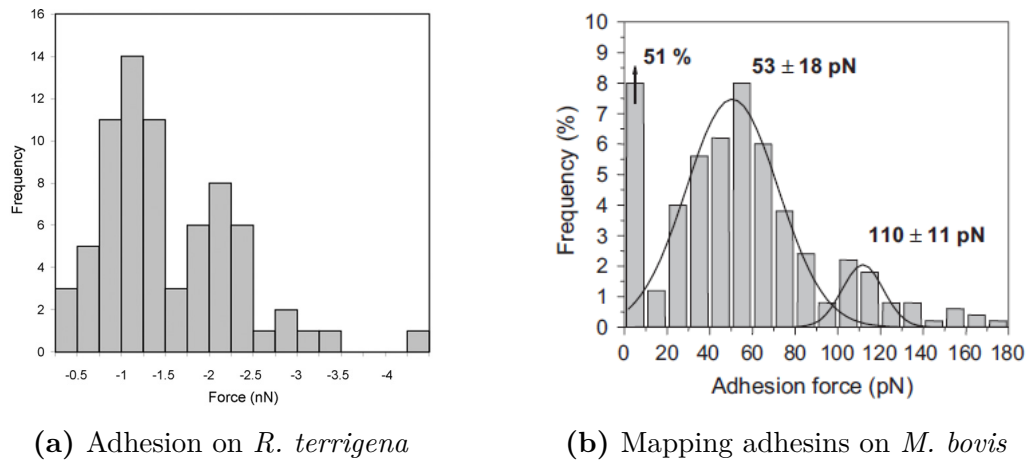


**Figure 4.40:** Examples of bimodal distributions in bacterial adhesion to SFM cantilevers. 4.40a shows the histogram of forces between a carbon coated cantilever and the bacterium *R. terrigena*. These data sets were fitted using Weibull distributions. Image used with permission of [288]. Copyright (2010) Elsevier. 4.40b shows the adhesion force between a cell of *M. bovis* as it is probed with a heparin-coated tip that probes specific interactions with the heparin-binding haemagglutinin adhesin that this strain produces. The histogram was fitted with two Gaussian curves. Image used with permission of [293]. Copyright (2007) Elsevier.

If a single Gaussian curve could not fit the data adequately, then it was hypothesised that a number of them might describe the distribution of adhesion forces more appropriately. Indeed, the best fit for the adhesion data histograms was obtained through the use of a number of Gaussian curves, which were fitted using the *mixtools* package on the R software. The details of this procedure will be detailed in the following section.

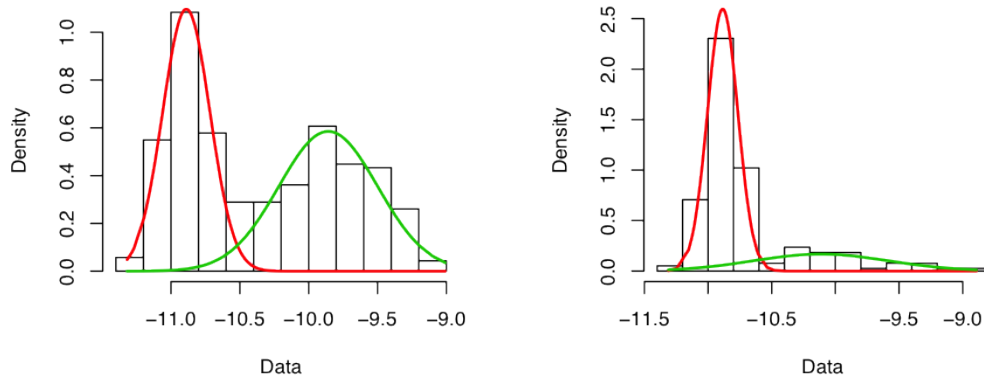
### 4.5.2 R and finite mixture models

The software R [300] was used for statistical analysis, using the *mixtools* package [301] that provides a set of functions to analyse finite mixture models. The main purpose of *mixtools* is to categorise a group of measurements and assign them into subgroups, even when there is not an obvious way to distribute measurements into categories; this process is known as *unsupervised clustering*. The finite mixture models give, thus, description of entire subgroups and often the assignment of individual measurements to such subgroups is not interesting per se (i.e. initially a data point is assigned to a cluster, without previous knowledge of the reasons for its membership to such category, and then using iterative methods, this datum is re-assigned to the cluster in which the items resemble this data point the most; as a result of this, the initial cluster assignment is arbitrary and meaningless until the iterations converge into the most stable solution). By combining the properties of two or more individual probability density functions, a finite mixture model can approximate any arbitrary distribution. *Mixtools* work under the assumption that the subgroups are distributed according to univariate or multivariate parametric forms. Often *mixtools* are used in cases where multivariate normality is apparent.

Finite mixture models are a common choice to study data that proceeds from heterogeneous sources. To begin a brief introduction about what these models entail, one needs to assume that the sample of interest consists of independently and identically distributed objects from a mixture of  $K$  subpopulations or components with different characteristics, specified by the set of parameters  $\theta_k$ , for  $k = 1, 2, \dots, K$ . Given that each cluster  $K$  is a probability density function, the probability that each data point  $x$  is a member of a certain cluster is written as  $p(x | \theta)$  and is formally defined as:

$$p(x | \theta) = \sum_{k=1}^K \lambda_k p_k(x | \theta_k), \quad (4.1)$$

where  $p_k(x | \theta_k)$  is the probability density function (pdf) of the  $k^{\text{th}}$  component,  $\lambda_k$  the mixing proportions (i.e. a descriptor of how likely it is that the data



(a) Highly overlapping bimodal density (b) Skewed unimodal density

**Figure 4.41:** Densities modelled by a mixture of two Gaussian probability density functions, represented by green and red lines. The distributions (black histogram) were modelled using mixture models on the R software.

are generated by the  $k^{th}$  component) and  $\theta = (\lambda_1, \dots, \lambda_k, \theta_1, \dots, \theta_k)$  is the set of parameters. Equation 4.1 is completely stochastic in nature.

A finite mixture model arises from the convex combination of a finite number of density functions (n.b. a convex combination is a linear combination of points where all coefficients are non-negative and their sum is equal to 1):

$$\lambda_k \geq 0, \text{ for } k \in \{1, \dots, K\}, \text{ and } \sum_{k=1}^K \lambda_k = 1. \tag{4.2}$$

It is possible to understand the mixture model as a scenario where the random variable  $x$  is generated from  $K$  random processes, each one being a mixture component. These processes are modelled according to a particular density  $p_k(x | \theta_k)$  and have a proportion of observations  $\lambda_k$ . For instance, as shown in Figure 4.41 two densities that have been generated using a mixture of two Gaussian probability density functions are presented. The left graph corresponds to a clearly bimodal distribution, whereas on the right graph, a skewed distribution is being modelled. These graphs and all of the subsequent fits generated by mixture models were calculated and plotted using the R software and the mixtools package, following the code presented in Appendix C.

For the particular case of the data set presented in this thesis, a parametric, univariate Gaussian family is being used, in which case the model parameter reduces to

$$\theta = (\lambda, (\mu_1, \sigma_1^2), \dots, (\mu_k, \sigma_k^2)). \tag{4.3}$$

The majority of the protocols that comprise within the mixtools packages represent the mixture in terms of the maximum likelihood estimation (MLE). Briefly, the way in which the algorithm works implies the use of two sample spaces, a sample space of *complete* observations and a sample space of *incomplete* observations. The observed data consists of  $n$  identically and independently distributed entries  $x = (x_1, \dots, x_n)$  from a density  $p(x | \theta)$  given by Equation 4.1. In the incomplete data set,  $p(\theta)$  is termed *incomplete-data density* and its associated log-likelihood is given by

$$L_x(\theta) = \sum_{i=1}^n \log p(\theta)(x_i). \tag{4.4}$$

The maximum likelihood estimation will aim to find the argument of the maximum (i.e. point of the given argument in which the function has its maximum value)

$$\widehat{\theta}_x = \operatorname{argmax}_{\theta \in \Phi} L_x(\theta), \tag{4.5}$$

or at least a local maximum value.

The aforementioned incomplete-data set has an associated *complete-data set*, denoted by  $c = (c_1, \dots, c_m)$ , whose density is given by

$$h_\theta = \prod_{j=1}^m h_\theta(c_j). \tag{4.6}$$

In the complete data set associated with Equation 4.1, each random vector  $C_i = (X_i, Z_i)$ , where  $Z_i = Z_{ij}, j = 1, \dots, m$ , and  $Z_{ij} \in \{0, 1\}$ , indicating that the value  $i$  comes from the component  $j$ . Since at this point it is not clear which component of the mixture generated each data point, one could access a hidden variable  $Z$  that assigns each data point to the component and then uses maximisation approaches to find the right fit. Using the hidden variable  $Z$  it is possible to define the complete-data set. Its log-likelihood function can be written as:

$$h_c(\theta | X, Z) = \sum_{i=1}^n \sum_{j=1}^m z_{ij} \log P(x_i | z_i; \theta) P(z_i; \theta). \tag{4.7}$$

Since  $Z$  is unknown, the previous expression cannot be solved and maximised directly. The complete data maximum likelihood estimation comes from maximising  $\log h_c$  (as defined in Equation 4.7) and such calculation will determine the best fit of the model to the data [301–303].

The maximisation is performed through the so-called expectation-maximisation (EM) algorithm, which iteratively maximises the likelihood estimates. Briefly, what the EM algorithm does is to give an initial guess of the component distributions (i.e.  $\theta_k$  and  $\lambda_k$ ). Then, the algorithm uses the current parameters to estimate

which component each point is most likely to come from and finally re-calculate the components using only the data associated to them, until everything converges. These starting parameters, if they are not specified, are selected randomly and thus, the number of iterations needed for convergence will differ every time the algorithm is run.

The algorithm runs by iteration in two steps:

$$\text{E step : } Q(\theta | \theta_k) = E [l_c(\theta | X, Z) | X, \theta_k] \quad (4.8)$$

$$\text{and M step : } \theta_{k+1} = \operatorname{argmax} Q(\theta | \theta_k), \quad (4.9)$$

where  $\mathbf{E}$  is the expectation that computes the expected log likelihood and  $\mathbf{M}$  is the maximisation, that finds the maximum likelihood [304, 305].

Since this is a stochastic model, the R program might give different answers every time, and consequently only *stable* solutions must be taken into account (i.e. the ones in which the final results are very similar to each other, regardless of the value of the initial parameters).

The EM algorithm cannot estimate the number of components, since it would provide an overfitted histogram (i.e. as many fits as observations). Thus, it is imperative to find a compromise between adequate fitting and generality. The user has to decide an appropriate number of components, not only based on the likelihood of these components, but also according to the best fits of the Gaussian functions, according to the data. In Figure 4.42 the same histogram was fitted with 2 and 25 components. Figure 4.42a shows the histogram being reasonably well fitted by two components, and underneath, the theoretical CDF (cumulative distribution function) versus the empirical CDF, showing a rather straight line. Figure 4.42b show 25 components, all overlapped and being distinguished with difficulty, and a much straighter theoretical versus empirical CDF line, indicating a better match between the models and the data. The solution with two components offers a better way to describe the data, because it avoids over-fitting. Figure 4.42c shows the log-likelihood on having a particular number of components in the mixture. It is clear that one component would not fit the histogram at all, but is dubious whether two, three or more components would be more appropriate to fit the data. It is evident that more components will allow fitting the distribution in a very precise way, but having many components also entails that more parameters are generated, and since there is a variance associated to each one of these parameters, the level of accuracy is diminished.

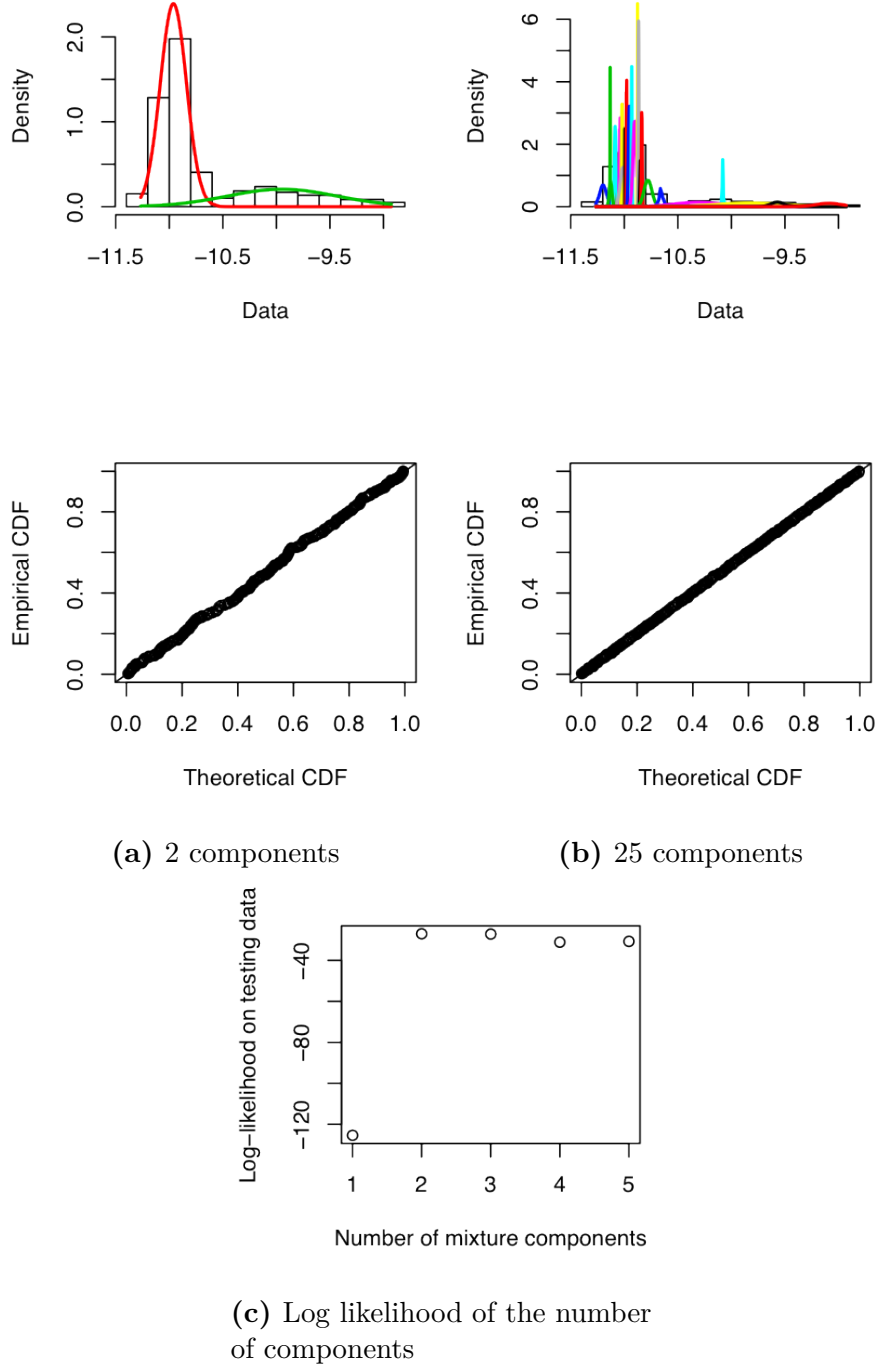
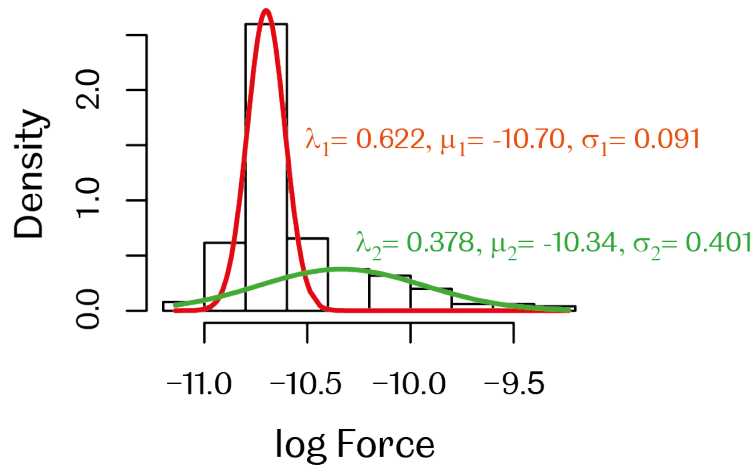


**Figure 4.42:** Example of histograms fitted with (a) 2 and (b) 25 components, with their respective theoretical versus empirical CDF. (c) Log-likelihood of number of components in the mixture.

If a number of graphs is generated, each one will have two components, that have associated a weight ( $\lambda$ , fraction of the data associated with each peak), a mean ( $\mu$ ) and a standard deviation ( $\sigma$ ) that are generated after a certain number of iterations. For the particular case of Figure 4.43, the histogram that shows the distribution of the logarithm of 284 values of adhesion forces has been fitted using two Gaussian curves and their parameters are written on the graph. The results were obtained after 35 iterations. The log-likelihood is a negative value, since the likelihood is a number between 0 and 1. The larger the log-likelihood, the better the fit is.



log-likelihood after 35 iterations = -75.10  
 Number of observations = 284

**Figure 4.43:** Histogram of 284 log-force values, calculated from a force-volume map and fitted with two Gaussian curves, alongside their values of mean, standard deviation and mixing proportions. Convergence in the algorithms was obtained after 35 iterations.

To check if a fit is satisfactory, R can generate a calibration plot that correlates the theoretical cumulative distribution function with the empirical CDF. The calibration graph allows to make probability forecasts by correlating events predicted to happen with a certain probability  $p$  should in fact happen with a frequency  $\sim p$ . For the case of the adhesion histograms, there is a cumulative distribution function  $F(x)$ , that states that the probability of finding a force adhesion event is  $\leq x$ . The CDF of a two component mixture is given by

$$F(x) = \lambda_1 F_1(x) + \lambda_2 F_2(x). \tag{4.10}$$

The R software produces a CDF plot like the ones shown in Figure 4.42a and b.

Visually it is possible to assess the departure of the plot from the main diagonal. A highly straight line would be indicative of an excellent fit. To select the best number of mixture components that would fit the data, R can perform a cross-validation algorithm, that calculates the log-likelihood of a number of components, like in Figure 4.42c. It is possible to see that there is a dramatic improvement between fitting the histogram with two components than with one component, but in this case there is no substantial difference between the use of two and five Gaussian curves. In cases like this, it is better to select the fewest components, to avoid over-fitting the data.

Force data from selected force-volume maps, acquired using different tips, was transformed using logarithms. These data were compiled in a single spread sheet and exported to the program R for fitting. A compendium of the statistical descriptors acquired by the models is presented in Tables 4.3 and 4.4 and a visual representation of the data is portrayed in Figures 4.44, 4.45, 4.46 and 4.47 (grouped by cantilever and with  $\sigma$  values included), and in Figures 4.48, 4.49, 4.50 and 4.51 (grouped by strain, only  $\mu$  values shown). Only stable solutions were considered for the calculations. From the analysis of the data presented on Tables 4.3 and 4.4, some conclusions can be drawn:

- The first component almost always has a larger weight ( $\lambda_1$ ) than the second component ( $\lambda_2$ ). The first component has always a larger value of  $\lambda$ , which indicates that the majority of the data are described by the first component of the mixture. Since the first component has a smaller value of  $\mu_1$ , it can be concluded that the majority of the data corresponds to low forces.
- The median value of the data has a magnitude which is intermediate between the means of the first ( $\mu_1$ ) and second ( $\mu_2$ ) components. The median value is closer to that of the first component, a second indication that the majority of the data lies at low forces.
- The difference between the means of the components, ( $\mu_1$ ) and ( $\mu_2$ ), might be indicative of the heterogeneity of the data. The difference of the peaks of the fitting models could be used as a descriptor of the variability of the data within the same cell. A comprehensive discussion of the reasons behind bacterial heterogeneity is given in §4.6 and a possible correlation between the value of the means of the fitting peaks with the existence of adhesion domains on the cells is presented by the end of this section.
- The second component is more disperse than the first (and third) components. The value of  $\sigma_2$  is in all cases larger than the values of  $\sigma_1$  and  $\sigma_3$ . The values that occurred at low forces were concentrated around the mean ( $\mu_1$ ), whereas the values that occurred at high forces, had a larger deviation.

	$\lambda_1$	$\mu_1$	$\sigma_1$	$\lambda_2$	$\mu_2$	$\sigma_2$	log median	
<b>Pse1</b>	Si <sub>3</sub> N <sub>4</sub>	0.812 ± 0.018	-10.845 ± 0.034	0.104 ± 0.006	0.188 ± 0.018	-10.144 ± 0.057	0.299 ± 0.022	-10.814 ± 0.029
	Au	0.762 ± 0.047	-10.851 ± 0.038	0.112 ± 0.005	0.238 ± 0.047	-10.185 ± 0.113	0.476 ± 0.036	-10.810 ± 0.039
	DDT*	0.649 ± 0.089	-10.833 ± 0.008	0.113 ± 0.020	0.320 ± 0.076	-10.212 ± 0.131	0.325 ± 0.044	-10.738 ± 0.045
	MUA	0.742 ± 0.041	-10.891 ± 0.011	0.132 ± 0.009	0.258 ± 0.041	-10.247 ± 0.069	0.330 ± 0.038	-10.836 ± 0.012
<b>Pse2</b>	Si <sub>3</sub> N <sub>4</sub>	0.741 ± 0.056	-10.754 ± 0.102	0.171 ± 0.063	0.259 ± 0.056	-10.284 ± 0.109	0.388 ± 0.026	-10.704 ± 0.090
	Au*	0.407 ± 0.064	-10.673 ± 0.024	0.096 ± 0.003	0.396 ± 0.073	-10.150 ± 0.054	0.327 ± 0.055	-10.344 ± 0.085
	DDT	0.471 ± 0.064	-11.006 ± 0.005	0.123 ± 0.008	0.529 ± 0.064	-9.974 ± 0.064	0.488 ± 0.020	-10.597 ± 0.129
	MUA	0.803 ± 0.029	-10.961 ± 0.004	0.113 ± 0.004	0.197 ± 0.029	-10.073 ± 0.034	0.458 ± 0.042	-10.918 ± 0.008
<b>Rc92</b>	Si <sub>3</sub> N <sub>4</sub>	0.586	-10.836	0.135	0.414	-9.914	0.533	-10.721
	Au*	0.411 ± 0.065	-10.960 ± 0.029	0.145 ± 0.016	0.265 ± 0.080	-10.168 ± 0.119	0.345 ± 0.078	-10.303 ± 0.193
	DDT	0.639 ± 0.085	-10.879 ± 0.024	0.129 ± 0.014	0.361 ± 0.085	-10.122 ± 0.045	0.390 ± 0.039	-10.713 ± 0.085
	MUA	0.849 ± 0.029	-10.942 ± 0.008	0.133 ± 0.006	0.151 ± 0.029	-9.902 ± 0.071	0.385 ± 0.051	-10.922 ± 0.007
<b>Rc291</b>	Si <sub>3</sub> N <sub>4</sub>	0.832 ± 0.008	-10.877 ± 0.049	0.201 ± 0.016	0.168 ± 0.008	-10.133 ± 0.074	0.231 ± 0.011	-10.730 ± 0.033
	Au *	0.483 ± 0.076	-10.822 ± 0.011	0.234 ± 0.121	0.294 ± 0.024	-10.148 ± 0.053	0.321 ± 0.035	-10.397 ± 0.140
	DDT	0.468 ± 0.132	-10.732 ± 0.035	0.107 ± 0.010	0.532 ± 0.132	-10.250 ± 0.016	0.350 ± 0.017	-10.623 ± 0.075
	MUA*	0.445 ± 0.057	-10.872 ± 0.020	0.153 ± 0.010	0.332 ± 0.076	-10.026 ± 0.108	0.272 ± 0.045	-10.344 ± 0.133

**Table 4.3:** Statistical descriptors of mixture model fits. The values of the weight ( $\lambda$ ), mean ( $\mu$ ) and standard deviation ( $\sigma$ ) of the first two components of the data are shown, alongside the logarithm of the median of the raw data for that experiment. The results are quoted stating the standard error of a number of observations ( $n = 2 - 7$ ). The experiments marked with (\*) indicate that the histogram was fitted with three components, whose descriptors are included in Table 4.4.

		$\lambda_3$	$\mu_3$	$\sigma_3$
<b>Pse1</b>	DDT	0.124	-9.505	0.087
<b>Pse2</b>	Au	$0.394 \pm 0.090$	$-9.528 \pm 0.205$	$0.223 \pm 0.044$
<b>Rc92</b>	Au	$0.325 \pm 0.077$	$-9.488 \pm 0.125$	$0.256 \pm 0.040$
<b>Rc291</b>	Au	$0.390 \pm 0.021$	$-9.483 \pm 0.071$	$0.221 \pm 0.012$
	MUA	$0.335 \pm 0.051$	$-9.867 \pm 0.162$	$0.253 \pm 0.053$

**Table 4.4:** Statistical descriptors of mixture model fits (Continuation from Table 4.3). Some systems required three Gaussian components to be fitted. The values of the weight ( $\lambda$ ), mean ( $\mu$ ) and standard deviation ( $\sigma$ ) of the third component of the data are shown in this table. The results are quoted stating the standard error of a number of observations ( $n = 2 - 4$ ). The first two components of these experiments are included in Table 4.3.

Now that the statistical model has been defined, it is important to relate these distributions to the actual pattern of forces within a bacterial cell wall. To this end, let us consider Figure 4.43. It is noteworthy that the two components have a very distinct appearance; the red one has a smaller mean ( $\mu_1$ ) and a smaller variance ( $\sigma_1$ ) and the green one, which appears at larger forces ( $\mu_2$ ) is more spread ( $\sigma_2$ ). The same behaviour was found for all of the histograms analysed in the course of these experiments: the four bacterial strains probed with the four cantilevers show a similar pattern. In principle, it is possible to think of two possible scenarios: two or three different regions of adhesion on a bacterial cell wall that give rise to two or three Gaussian distributions or the presence of a number of Gaussian distributions as a consequence of the statistical treatment. The first one supports the idea of biological heterogeneity. In this scenario it might be that indeed there are two distinct regimes of adhesion forces within the same bacterial cell. One could think that there are distinct regions in a microorganism in which the adhesion is somewhat greater, these regions would be represented by the second and third components. A larger percentage of the bacterial cell wall shows little affinity for the SFM cantilever and this is represented by the first component.

The existence of adhesive domains within a cell wall is not unheard of. For instance, Alsteens *et al.* [306] found adhesive domains of a few hundred nanometres on fungal cells (*Aspergillus fumigatus*) using DDT-coated cantilevers. These domains have been associated with the presence of rodlets composed of hydrophobic proteins, which are embedded into regions rich in hydrophilic polysaccharides. Similar approaches have been taken to study bacteria. Francius *et al.* [146] have localised polysaccharide-rich regions on *Lactobacillus rhamnosus* GG using SFM

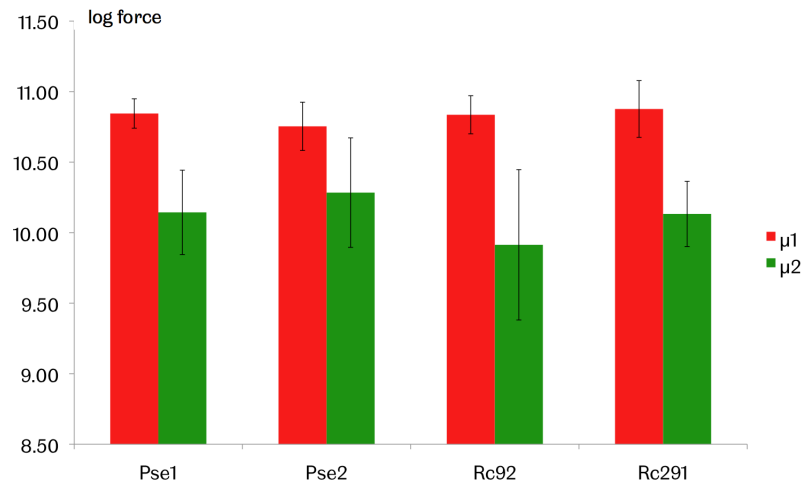


**Figure 4.44:** Visual representation of the means ( $\mu_1, \mu_2$ ) and standard deviations ( $\sigma_1, \sigma_2$ ) of the logarithms of the force data, acquired with a  $\text{Si}_3\text{N}_4$  tip. The absolute values of the logarithms have been used for simplicity.

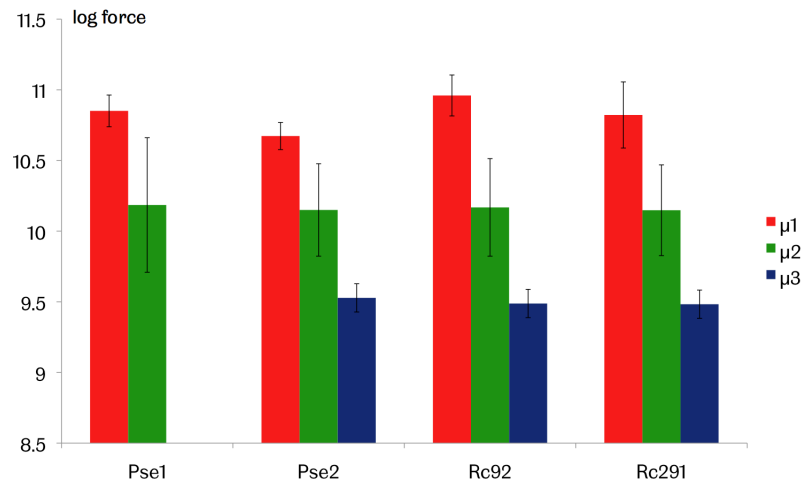


**Figure 4.45:** Visual representation of the means ( $\mu_1, \mu_2, \mu_3$ ) and standard deviations ( $\sigma_1, \sigma_2, \sigma_3$ ) of the logarithms of the force data, acquired with an Au tip. The absolute values of the logarithms have been used for simplicity.

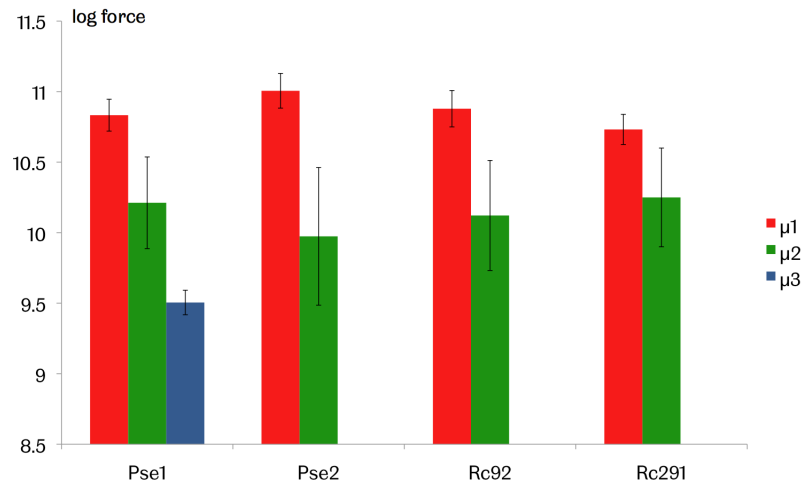


**Figure 4.46:** Visual representation of the means ( $\mu_1, \mu_2, \mu_3$ ) and standard deviations ( $\sigma_1, \sigma_2, \sigma_3$ ) of the logarithms of the force data, acquired with a DDT tip. The absolute values of the logarithms have been used for simplicity.

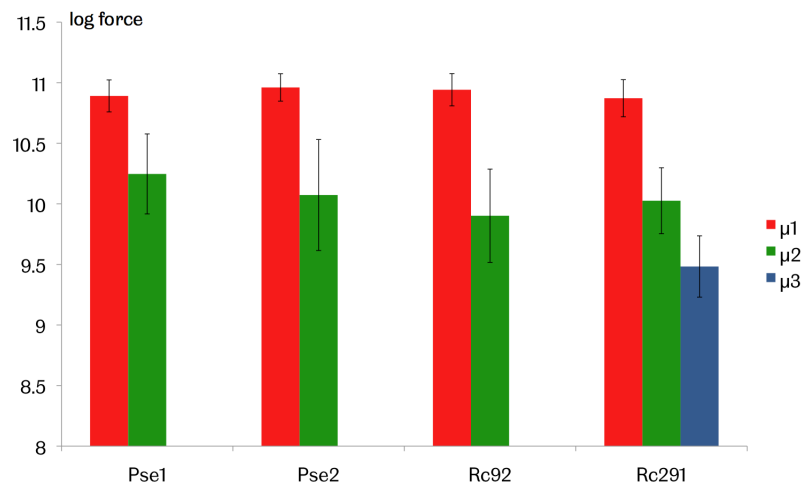


**Figure 4.47:** Visual representation of the means ( $\mu_1, \mu_2, \mu_3$ ) and standard deviations ( $\sigma_1, \sigma_2, \sigma_3$ ) of the logarithms of the force data, acquired with a MUA tip. The absolute values of the logarithms have been used for simplicity.

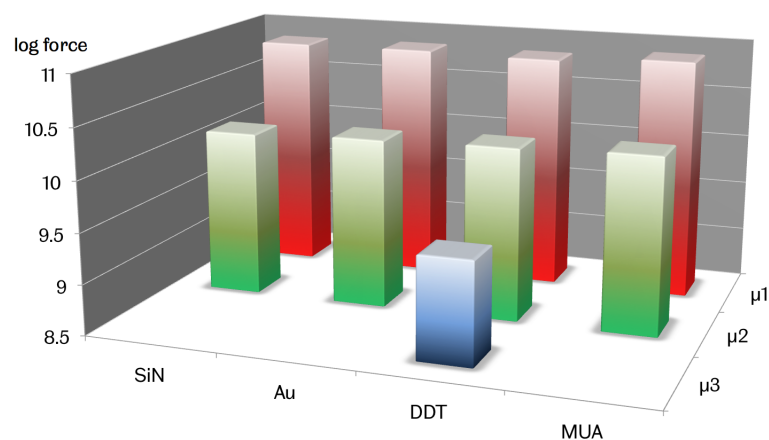


**Figure 4.48:** Means of the mixture components of Pse1 ( $\mu_1, \mu_2, \mu_3$ ), acquired with four different tips. The absolute values of the logarithms have been used for simplicity.

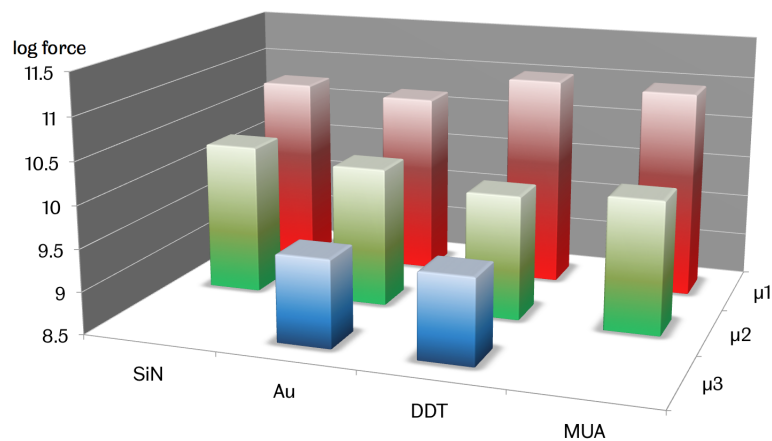


**Figure 4.49:** Means of the mixture components of Pse2 ( $\mu_1, \mu_2, \mu_3$ ), acquired with four different tips. The absolute values of the logarithms have been used for simplicity.

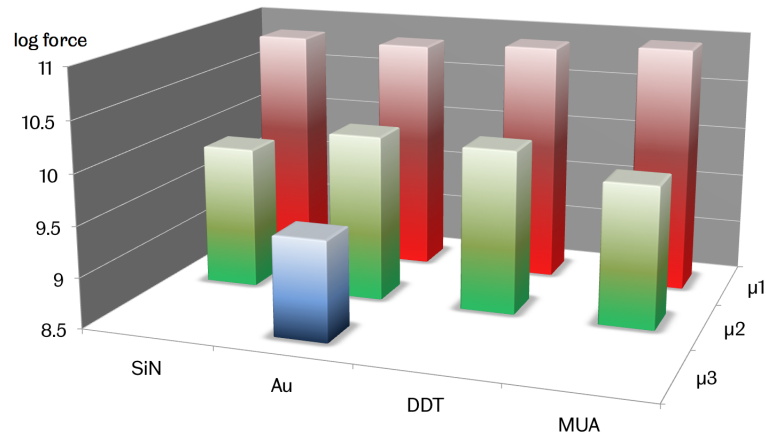


**Figure 4.50:** Means of the mixture components of Rc92 ( $\mu_1, \mu_2, \mu_3$ ), acquired with four different tips. The absolute values of the logarithms have been used for simplicity.

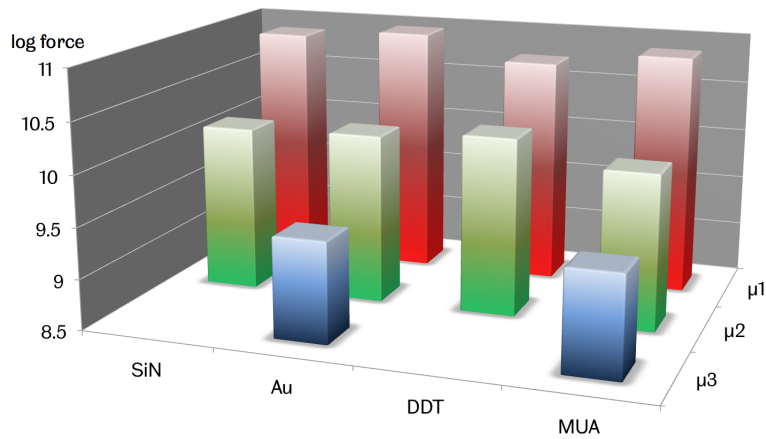


**Figure 4.51:** Means of the mixture components of Rc291 ( $\mu_1, \mu_2, \mu_3$ ), acquired with four different tips. The absolute values of the logarithms have been used for simplicity.

cantilevers functionalised with lectins (i.e. carbohydrate-binding proteins). Schär-Zammaretti and Ubbink [213] have also reported the existence of adhesive nanodomains in other *Lactobacillus* strains. In a very recent publication, El Kirat-Chatel *et al.* [307] mapped individual cells of *Pseudomonas fluorescens* using cantilevers functionalised with antibodies that selectively target LapA adhesion proteins. Such proteins are known to be involved in bacterial attachment in this strain and to accumulate at the cell-surface interface. Nanodomains rich in this protein were found using this technique. The literature gives plenty of evidence that microbial membranes are far from homogeneous and possess regions enriched with a particular biomolecule, a phenomenon that directs the way in which bacteria adhere to surfaces.

A second hypothesis to explain the presence of a number of fits on the histogram denies the existence of the adhesive nanodomains and suggests that the program is just using a number of Gaussian curves to approximate a completely different distribution. The cross-validation graph (Figure 4.42c) predicts that 2, 3, 4 or 5 models will fit the data, and that out of these, a 2-model system will have the best trade-off between approximation bias and estimation variance. Just from the statistics, it would not be sensible to affirm that indeed there are two (or more) regions on the cell that are chemically different.

To prove the validity of the first scenario it would be helpful to see the location of these low and high adhesion areas on a particular bacterial cell. It could be hypothesised that by clustering the data into two components, two groups with distinct biological attributes are being described. To visually assess the relationship between the distribution of forces in each one of the two components and their location within a bacterial cell, it was decided to colour code the force-volume maps. The pixels were coloured green or red, depending if the force belonged to the green or red component in the mixture model fit. In order to determine an appropriate cut-off point (i.e. the point in the  $x$  axis in which a particular data point starts belonging to one distribution), the  $x$ -coordinate where the two Gaussian curves crossed was calculated. The threshold value was determined using the Gaussian integral

$$\int_{-\infty}^{\infty} e^{-x^2} dx = \sqrt{\pi}, \quad (4.11)$$

and one obtains

$$\int_{-\infty}^{\infty} a e^{-\frac{(x-b)^2}{2c^2}} dx = ac \cdot \sqrt{2\pi}. \quad (4.12)$$

The integral is unity if and only if  $a = 1/c\sqrt{2\pi}$ , and in this case the Gaussian is the probability density function of a normally distributed random variable with

an expected value of  $b = \mu$  and  $c^2 = \sigma^2$

$$g(x) = \frac{1}{\sigma\sqrt{2\pi}} e^{-\frac{1}{2}\left(\frac{x-\mu}{\sigma}\right)^2}. \quad (4.13)$$

For a bimodal distribution the equations of distribution 1  $(\mu_1, \sigma_1)$  and distribution 2  $(\mu_2, \sigma_2)$  are combined into one expression

$$\frac{(x - \mu_2)^2}{2\sigma_2^2} - \frac{(x - \mu_1)^2}{2\sigma_1^2} = \ln \frac{\sigma_1}{\sigma_2}. \quad (4.14)$$

If the equation is solved for  $x$ , the result will be the point in the  $x$ -axis in which the distributions cross. Once the cut-off points were determined, the force-volume data of a number of bacterial cells were concentrated in an Excel worksheet. Each value was conditionally coloured red or green depending on their relative magnitude with respect to the calculated threshold result. Examples of the product of this exercise are portrayed in Figures 4.52–4.57.

The fact that the green pixels can sometimes be found clustered together suggests that there are effectively regions of low adhesion, and thus the bimodality that the mixture model shows is indeed a biological phenomenon, rather than just an statistical one. Nonetheless more statistical tests are needed to verify this claim. Perhaps finding a degree of data heterogeneity will suffice to support this idea.

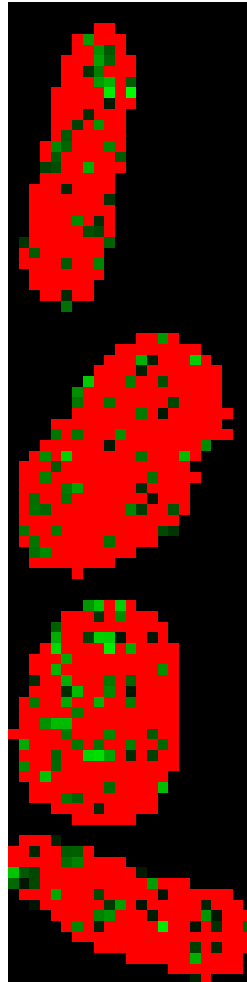


**Figure 4.52:** Force-volume maps of four Pse1 cells, probed with a silicon nitride tip. The red pixels correspond in average to the first distribution, whereas the green pixels correspond to the second distribution.

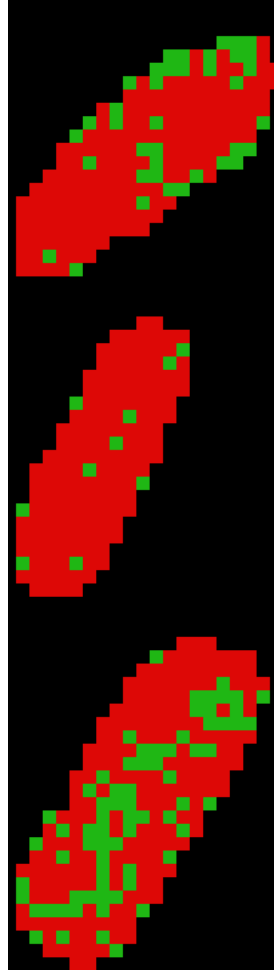


**Figure 4.53:** Force-volume maps of Pse1 cells, probed with an Au tip. The red pixels correspond in average to the first distribution, whereas the green pixels correspond to the second distribution.

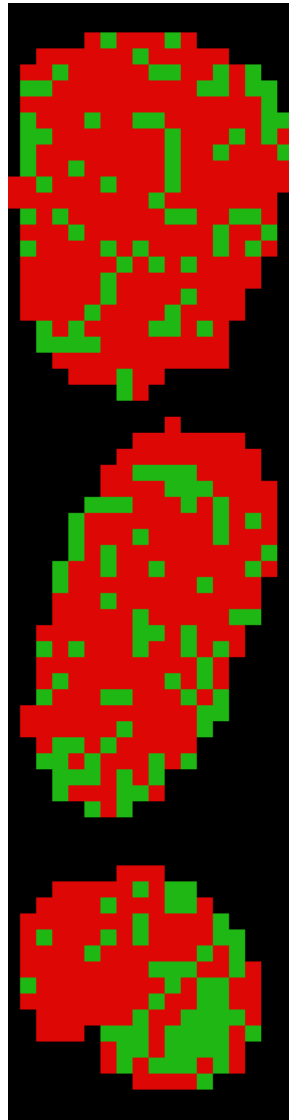


**Figure 4.54:** Force-volume maps of Pse1 cells, probed with an MUA tip. The red pixels correspond in average to the first distribution, whereas the green pixels correspond to the second distribution.

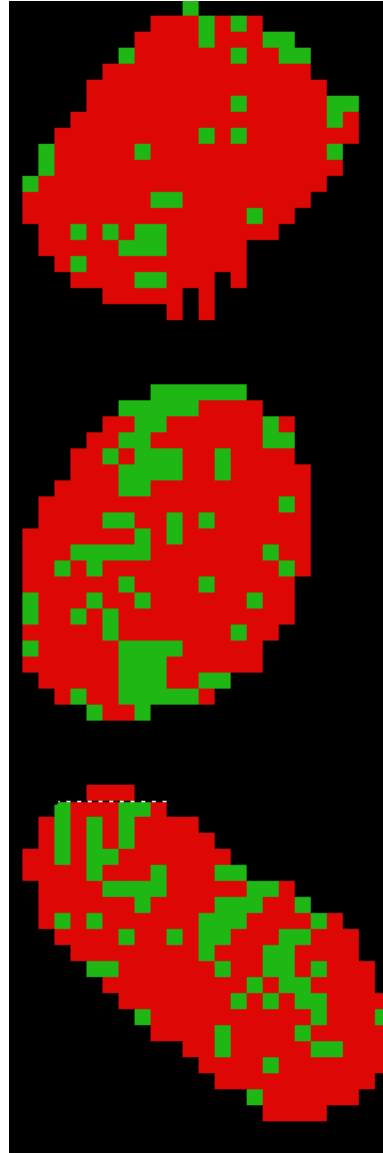


**Figure 4.55:** Force-volume maps of Pse2 cells, probed with an MUA tip. The red pixels correspond in average to the first distribution, whereas the green pixels correspond to the second distribution.

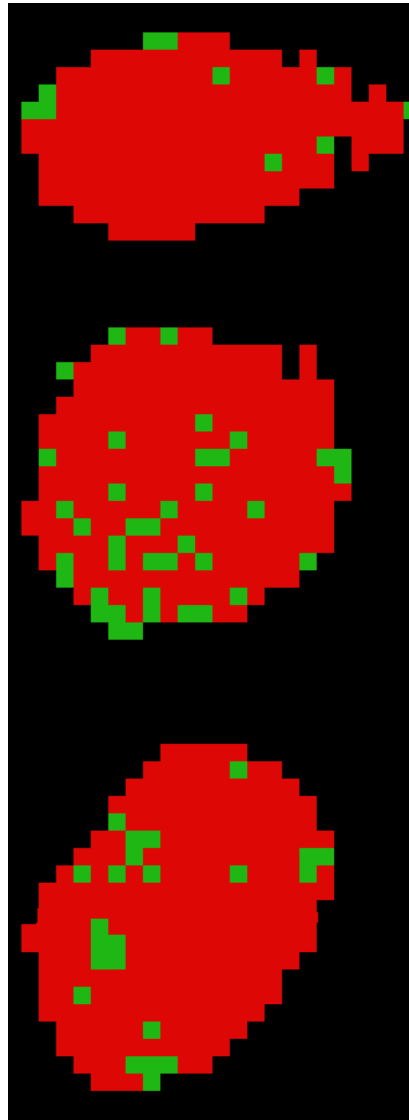


**Figure 4.56:** Force-volume maps of Rc92 cells, probed with an MUA tip. The red pixels correspond in average to the first distribution, whereas the green pixels correspond to the second distribution.

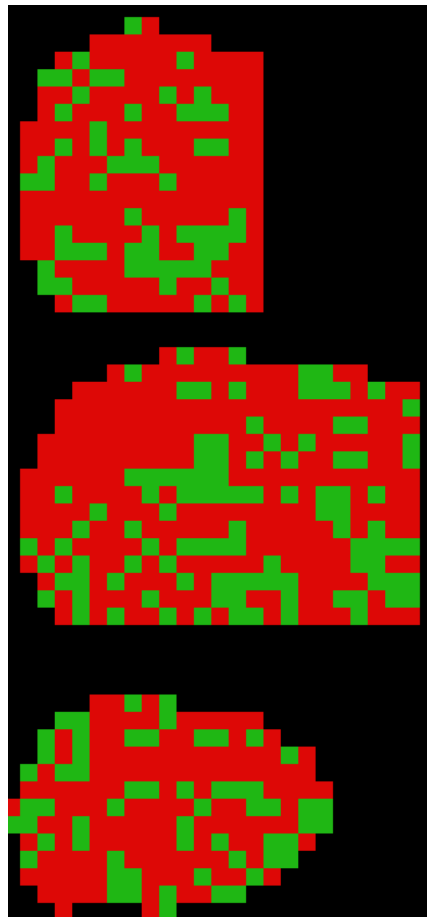


**Figure 4.57:** Force-volume maps of Rc291 cells, probed with an Au tip. The red pixels correspond in average to the first distribution, whereas the green pixels correspond to the second distribution.

### 4.5.3 Force-volume data fits

The mixture model bimodal fit for the four *Pseudomonas* Pse1 cells (Figures 4.24, 4.25, 4.26, 4.27) scanned using a silicon nitride tip is presented in Figure 4.58. The adhesion force histograms reveal a bimodal distribution with average rupture forces of approximately 13-20 pN for the first peak and 40-160 pN for the second peak. The multicomponent fits of Pse1 cells probed by Au, DDT and MUA cantilevers are shown in Figures 4.59, 4.60 and 4.61, respectively. Graphs of the fitted adhesion force distributions of Pse2, Rc92 and Rc291 have not been included.

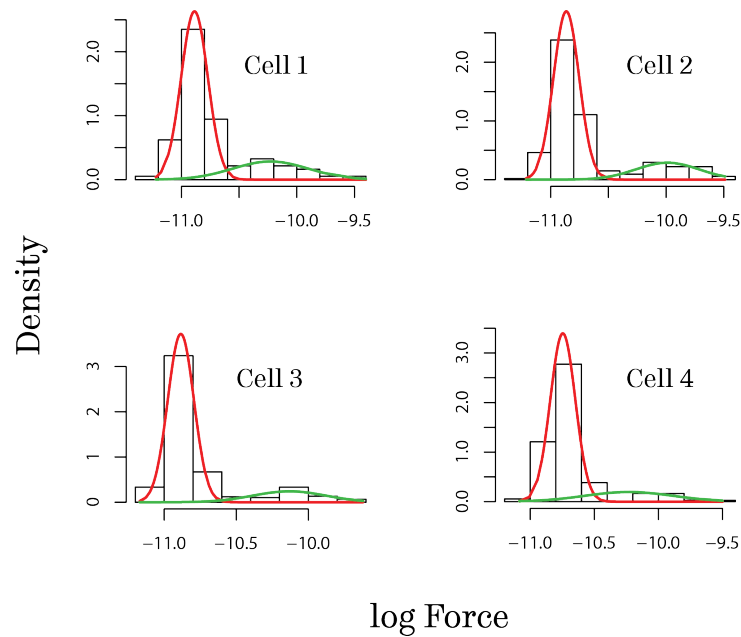


**Figure 4.58:** Bimodal fits for five Pse1 cells with a  $\text{Si}_3\text{N}_4$  tip.

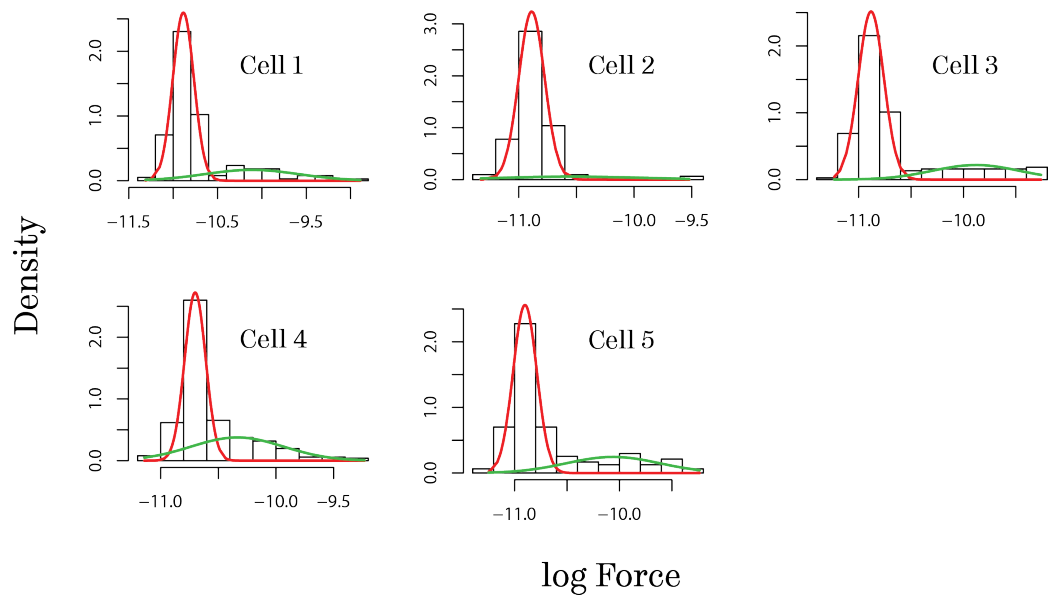


**Figure 4.59:** Bimodal fits for five Pse1 cells with an Au tip.

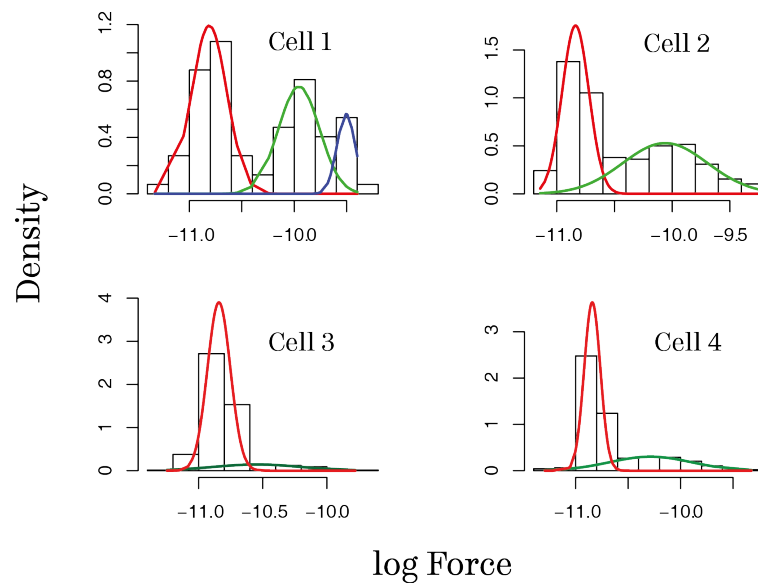


**Figure 4.60:** Bimodal fits for five Pse1 cells with a DDT tip. Notice that the distribution for Cell 1 is fitted with three Gaussian peaks.

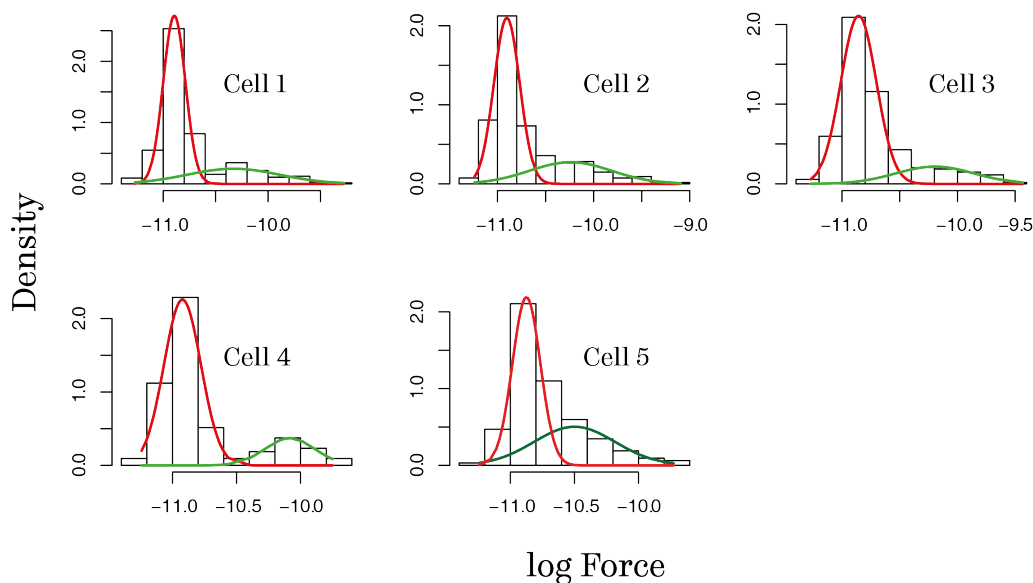


**Figure 4.61:** Bimodal fits for five Pse1 cells with an MUA tip.

#### 4.5.4 Tip-cell interactions

##### Tip properties

The first thing that needs to be considered in order to ensure that the CFM experiments produced the desired information, is the state of the probes. It has been noted by some authors [308] that the functionalisation of probes often does not occur in a perfectly repeatable manner. It is possible that the monolayers are defective, fact that could affect the comparison between different probes. Other possible factors are the contamination of the gold base and of the thiol layer [280] and the oxidation of the sulfur in the thiol molecules, circumstances that could reduce the degree of sorption on the tip and affect the quality of the experiments. Therefore, it is always a concern whether the reaction proceeded effectively, and the SAM was formed homogeneously on the tip. Moreover, any functionalisation reaction might alter the tip shape, which could complicate the calculations on the force-data (Figure 4.62).

Having considered these potential risks, care was taken in performing the experiments in the same conditions every time, to maximise the possibility of repeatability. The prepared probes were used immediately after preparation, to avoid their contamination or any possible degradation. Similarly, extreme care was taken during the preparation of the SAMs; as mentioned before, both the tips and the glassware were thoroughly cleaned with piranha solution before use, and

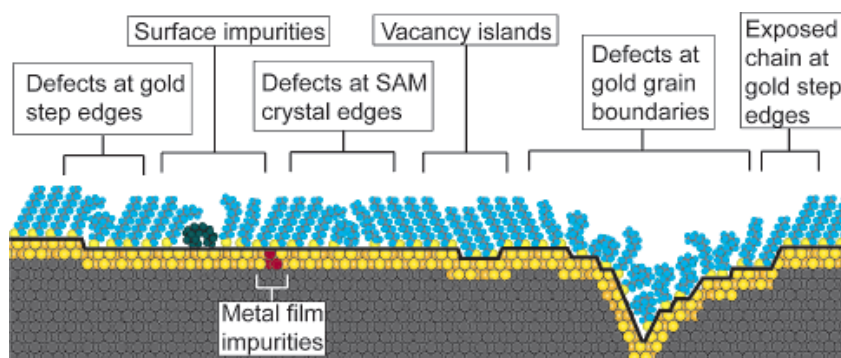


**Figure 4.62:** Typical defects found in SAMs assembled on polycrystalline substrates. Image taken from [280] with permission. Copyright (2005) American Chemical Society.

the reactants were kept sealed and only pipetted out of their bottles with dedicated instruments. Furthermore, the control experiments presented in Figures 4.38 and 4.36, confirm that the probes are able to tell two chemically distinct surfaces apart.

### Potential interactions

The interactions between the tip and the surface will be largely governed by xDLVO forces, which were reviewed in Chapter 2. The extended DLVO theory (xDLVO) proposes that the interaction between particles is a combination of Lifshitz-van der Waals (LW), electrostatic double layer (EL) and acid-base interactions (AB). LW forces are always present and their value depend on the properties of the interacting materials. In order to assess the value of LW forces, the Hamaker constant must be determined (Equation 2.2 on page 31). The value of this constant is often estimated from contact angle measurements with a variety of solvents. EL forces are highly dependent on the ionic strength of the surrounding medium, and thus the selection of the imaging buffer will determine the adhesive behaviour of the bacterial cells to the SFM cantilever. Acid-base interactions determine the hydrophobicity of the interacting surfaces, and on this account the role of the hydrophobic attraction has been considered.

The xDLVO model has been successful in describing abiotic colloidal systems and has approximated the adhesive behaviour of a number of microorganisms [309]. However, it is not always appropriate to describe the complex surfaces that surround bacterial cells [87].

Bacterial cells are rich in polymeric substances and extra-cellular structures, which can have varied sizes and chemical functionalities, and thus it is very com-

plicated to model their behaviour. The SFM tip, either bare, coated or functionalised with long alkyl chains, will come in contact with a myriad of extra-cellular polymeric substances and membrane components. As it indents the surface, such molecules will be forced into close contact and conformational changes will occur, compacting their chains. The molecules on the bacterial cell might experience repulsion or attraction to the surface of the tip or the molecules that this one carries. A visual summary of the potential interactions between molecules on the tip and molecules on the surface can be seen in Figure 4.63.

The tip and the bacterial cell surface could experience repulsive forces. Molecular repulsion could be provoked by similarly charged functional groups on the surface of the cell wall and on the cantilever. For instance, the pKa of MUA SAMs has been determined to be 4.8 [310], and therefore at the working pH it is expected that the acid groups are ionised. Since bacterial cell surfaces are normally negatively charged [311] an initial repulsion interaction between these two surfaces is expected (although in a solution that contains cations, these interactions are expected to be somewhat shielded).

Steric repulsion might occur due to the preference of the surface molecules for the liquid medium, in which case the molecules on both surfaces will compress, change conformation and repel each other. The steric repulsion between the tip and the surface has also been understood from the polymer physics point of view. Park and Abu-Lail [312] explain the interaction between the tip and the surface as a polymer brush interacting with a flat solid. They estimate the force per unit area, given the grafted polymer density in the brush layer and its thickness. The height of the polymer brush is dependent on the polymers' preference for the liquid medium and their elasticity. For instance, in water, hydrophilic molecules will extend towards the liquid medium, leaving the hydrophobic molecules collapsed near the bacterial surface.

Conversely, the tip and the bacterial cell can be attracted to each other. Bridging attraction might be present if the affinity between the molecules on both surfaces is high. For instance, long alkyl chains might have positive interactions due to a high number of hydrophobic interactions along their backbones. In an analogous manner, the formation of hydrogen bonds or other intermolecular interactions might bridge the molecules and promote their adhesion. Since all of these interactions happen in a stochastic fashion, it is imperative to acquire sufficient data, to draw significant conclusions from these events.

To enhance our understanding of the physics behind bond formation during the cantilever approach, it is convenient to picture a chemical bond under the circumstances where an external applied load is exerted upon it (Figure 4.64). The energy of bond formation, between molecules on the tip and the surface, is

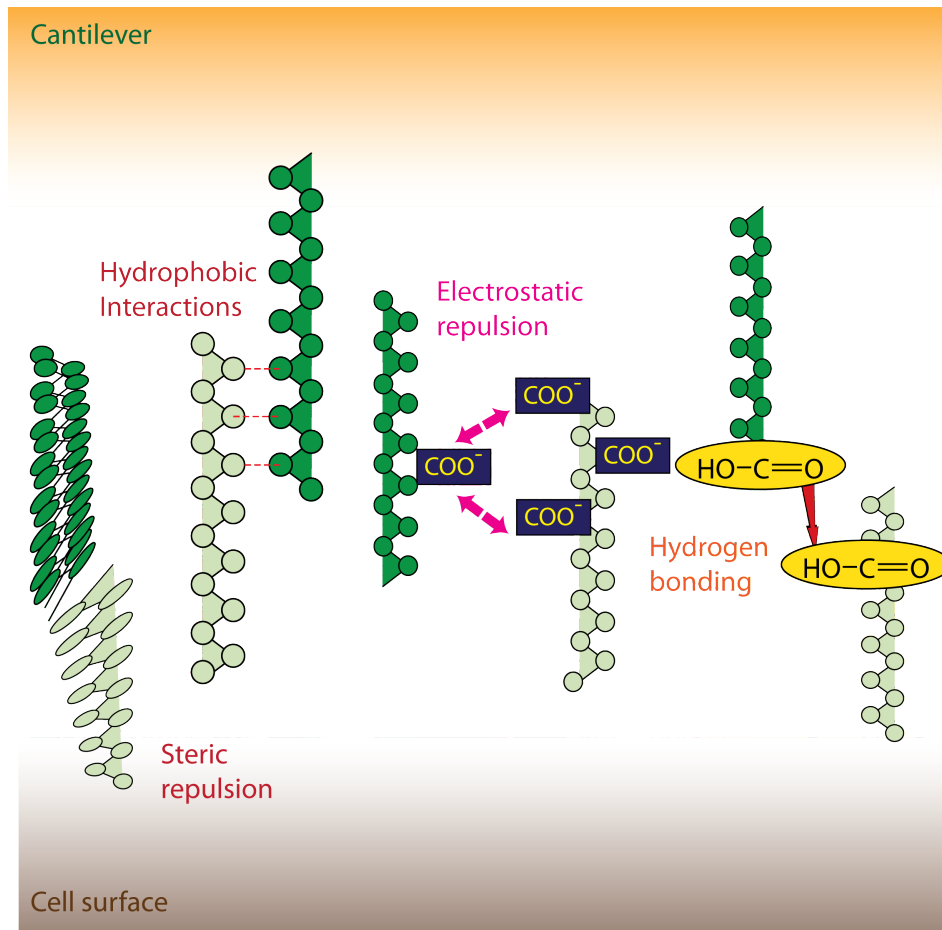


**Figure 4.63:** Potential tip-surface interactions. In this diagram, hydrophobic and hydrogen bonding attractive interactions are depicted, as well as repulsive steric hindrance and electrostatic interactions. The light green molecules belong to the cell surface and the dark green ones are anchored on the tip.

represented by a potential well in the graph. A second potential well, parabolic in shape, is associated with the equilibrium position of the SFM cantilever; here, the probe is represented as a *loading spring* and in this system performs the function of exerting a load upon the bond. The total interaction potential contains a primary and a secondary minimum: these represent two possible transition states that make attachment and detachment possible. It is evident from this figure that the load of the cantilever has the effect of lowering the energetic barrier for binding and increases the rebinding barrier. Consequently, the energy potential of the probe-cell system is not only determined by the interplay between a large quantity of binding molecules and the imaging environment but also the mechanics of the cantilever determine the attachment and detachment behaviour [313].

It is clear that a solid understanding of the data produced by CFM is based on the knowledge of the interactions between the functionalised tips and the bacterial surfaces. A model of the reciprocal action between molecules on the tip and on the surface has also been considered by other authors [87]. In Figure 4.65 the interaction between a thiolated tip and a bacterial cell surface has been represented. This particular cell also bears exo-polymeric structures such as pili and an EPS capsule. The authors propose that as the tip approaches the surface, the first points of contact will be these appendages. There is some evidence that the chemical composition of these appendages might vary from the main body of the cell. Pili tend to have a higher degree of hydrophobicity, an evolutionary advantage that allows the bacterial cells to dock onto solid surfaces more easily. As the tip continues its travel downwards, the appendages become compressed. Even at closer distances, the tip will start interacting with the extra-cellular polymeric layer, constricting the polymer brush that coats the bacterial cell. As the  $z$ -piezo continues its motion towards the cell, the molecules on the tip could potentially access the bacterial membrane. In the case of the *Rhodococcus* cells, the hydrophobic mycolic acids could, in principle, be adhering to other hydrophobic moieties on the tip.

In the force-distance experiments that were performed in this thesis, the cells have been indented through distances over 100 nm (as determined by the negative  $x$  coordinate in the force-distance curves), which leads to the conclusion that we are in contact with polymers on the EPS layer and the bacterial cell wall. Upon retraction, the profile of the force curves acquired on the selected cells often reveals the rupture of specific interactions, like the ones depicted in Figure 4.66. This is indicative of one or several polymers being detached from the surface in a stepwise fashion.

In the framework of this thesis, the description of the force curves is largely limited to qualitative parameters, since mathematical models, like the Hertz model

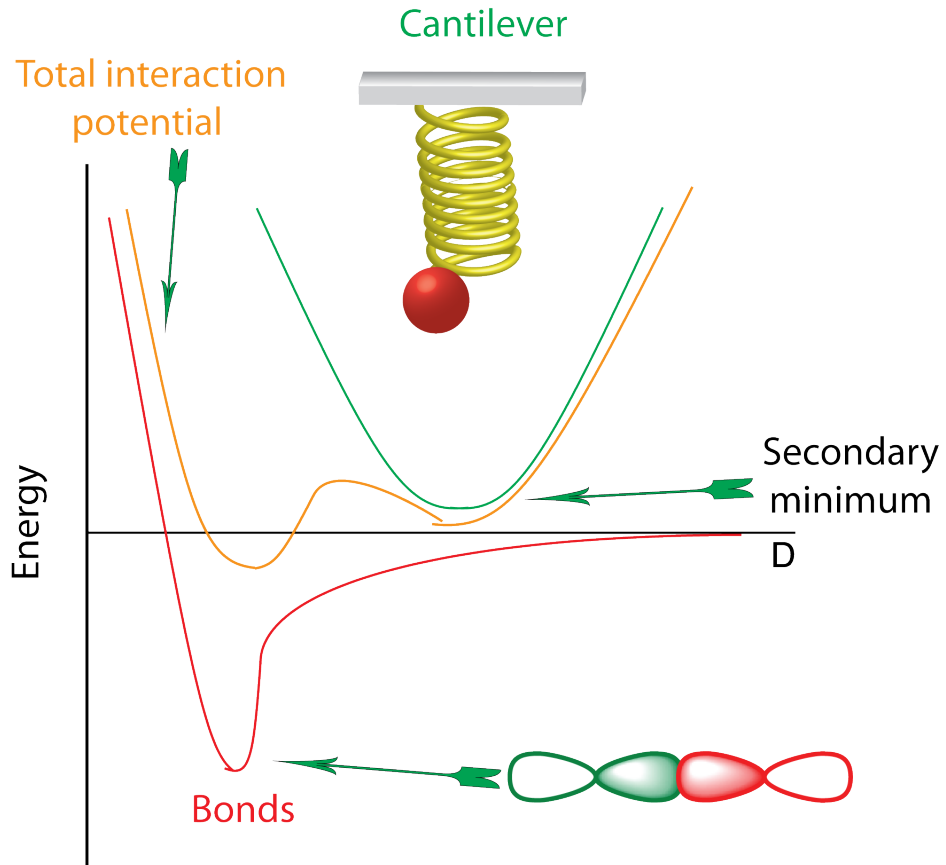


**Figure 4.64:** Potential energy profile for the tip-sample bond formation. The chemical bond is represented by the red curve and the cantilever by the green one. The orange line represents the total potential energy surface for the system. The primary and secondary minima on the latter line represent the regions for binding and rebinding events. Image adapted from reference [313].

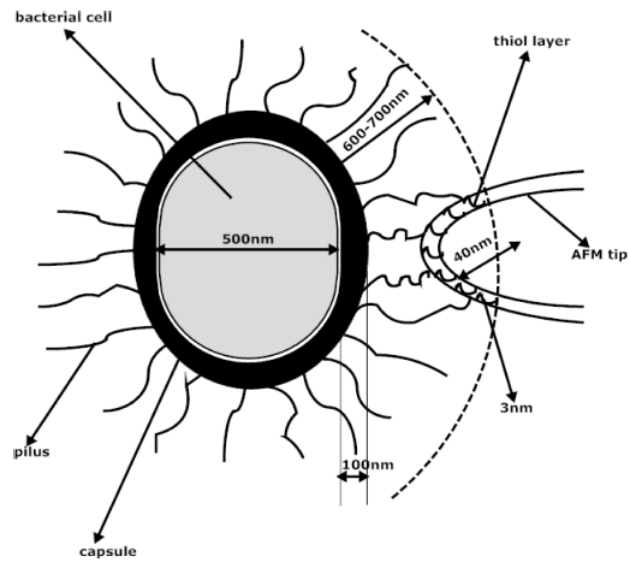


**Figure 4.65:** Interaction between the exopolymeric layer and appendages with a thiolated SFM tip. Image reproduced with permission of reference [87]. Copyright (2009) American Chemical Society.

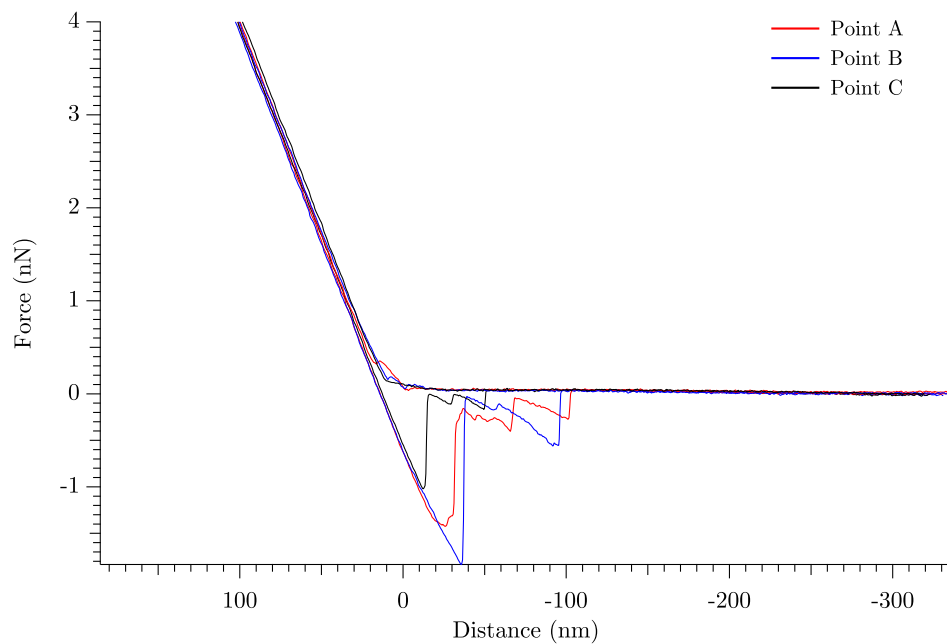


**Figure 4.66:** Force-distance curves for the interaction between Rc291 and Au, showing specific interactions.

[173] that calculates the deformation of the sample, were not used. The only parameter taken into account was the measurement of the force of detachment, that is calculated from the minimum value in the  $y$ -axis. (§2.6.5).

A tip that approaches a surface will first experience repulsive interactions and then it begins indenting the soft cellular envelope. The sample moulds around the shape of the tip and its outer polymers will be compressed. The indentation section of the curve gives information about the elastic modulus. When the probe is taken away, the outer molecules of the cell adhere to the surface of the tip. Each adhesion peak will give information about the force, work of adhesion and the distance of the interactions. The area bounded by the approach and retraction curves gives information about the work done to deform the sample. In Figure 4.67 a typical force-distance curve is shown, clearly separating the extension from the retraction part of the curve. The curves acquired on the same experiment are often very similar. In Figures 4.68 and 4.69, five curves taken on the same bacterial cell have been overlaid. All of them show approximately the same degree of indentation and sample stiffness, but their adhesive behaviour is somewhat different. The curve belonging to Point 5 in Figure 4.68 shows a fragment detaching at a distance of almost 150 nm, while the other curves detach at around 30 nm. It is hard to make any generalisations from these values as the adhesion forces and force profiles of the cells are very heterogeneous.

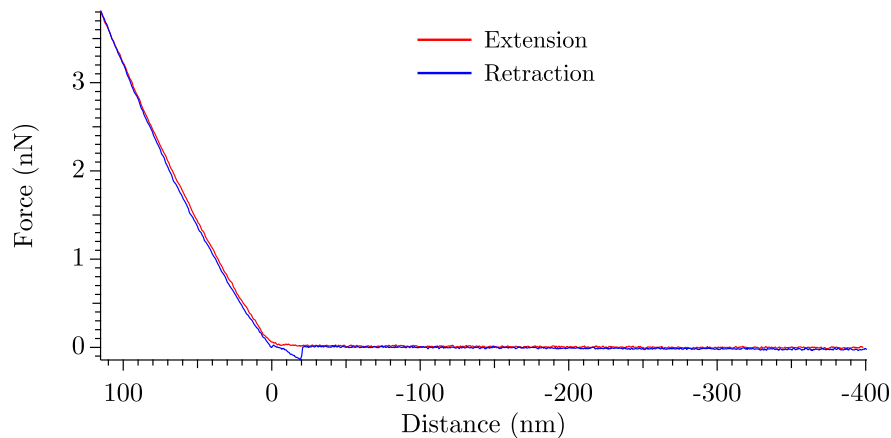


**Figure 4.67:** Force-distance curve of a Pse1 cell, using a silicon nitride probe.

The reason for the heterogeneity of adhesion force measurements on a particular bacterial cell has been attributed to the fact that the tip could be interacting with distinct molecules of the cell surface in an stochastic manner [290, 314]. Thus, the statistical model selected to describe the data must account for these differences.

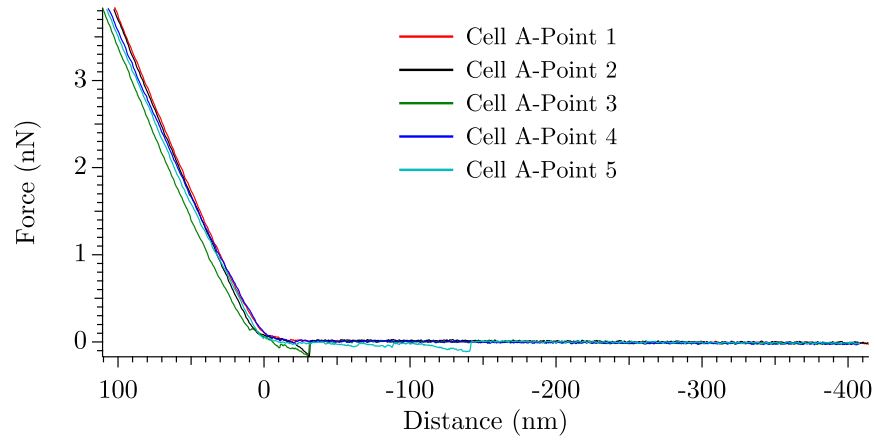


**Figure 4.68:** Retraction curves of five points of a Pse1 cell overlaid on the same plot. The FD curves were taken using a silicon nitride cantilever.

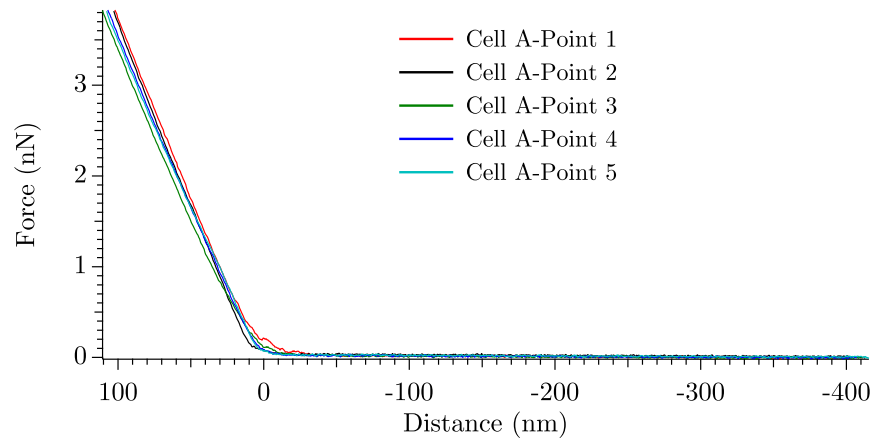


**Figure 4.69:** Extension curves of 5 different points on a Pse1 cell probed with a silicon nitride tip and overlaid on the same plot.

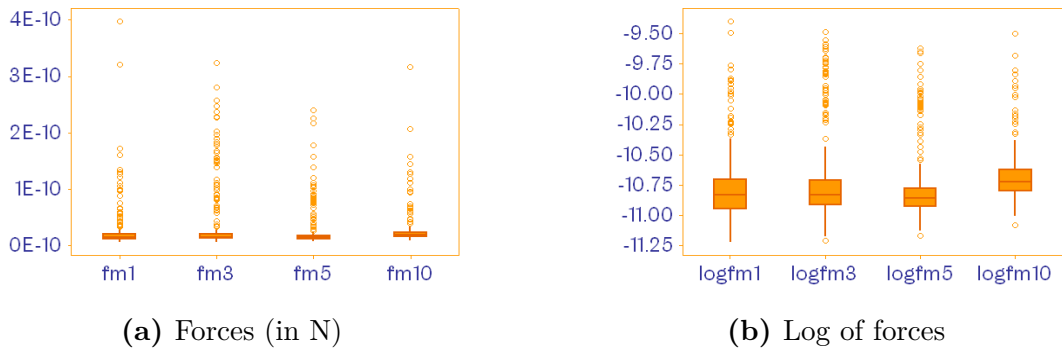
Due to the time invested in studying bacterial cells using force-volume maps (6 days of growth for *Rhodococcus* and *Pseudomonas* and approximately 7 hours of scanning per experimental session) only a limited number of cells could be studied. The data are heterogeneous within a particular cell membrane, and can also differ substantially between cells of the same sample, and also between cells of different cultures.

### 4.5.5 Differences between groups

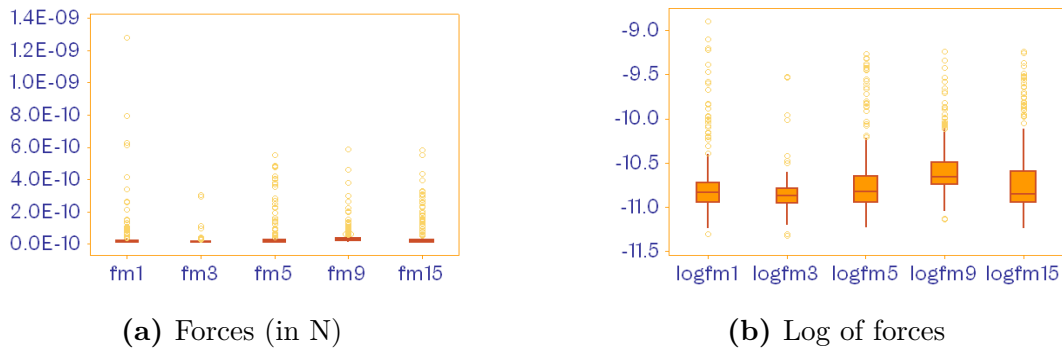
#### Differences between cells

Figure 4.70 shows the results of the adhesion forces of four Pse1 cells scanned with a silicon nitride tip. Each box plot corresponds to the measurements taken on one bacterial cell. The boundaries of the box represent the lower (Q1) and the higher quartiles (Q3) and the median (Q2) is represented as the horizontal line inside the box. The bottom vertical bars or *whiskers*, show the lowest datum still within 1.5 of the inter-quartile range (IQR) and the top whisker represents the maximum value within 1.5 IQR (n.b. the IQR is a measure of statistical dispersion that represents the difference between Q3 and Q1). The symbols indicate the outliers of the adhesion energy, which are values beyond 1.5 IQR. The asymmetry of the box reflects the fact that the data are skewed. The box plots on the raw data (Figure 4.70a) are hard to read, since the data are heavily skewed towards high forces. The box plots on the log-transformed data (Figure 4.70b) are considerably easier to compare. The box plots of Pse1 cells analysed with Au, DDT and MUA tips have been included in Figures 4.71, 4.72 and 4.73. The plots that compare the adhesion forces of individual cells of Pse2, Rc92 and Rc291 have been omitted in this thesis.

It is possible to observe a certain degree of heterogeneity among cells that belong to the same population, and that were probed using the same tip on a particular experiment.



**Figure 4.70:** Comparative adhesion forces of Pse1 cells with  $\text{Si}_3\text{N}_4$  tips. Four different force maps (fm) of cells are compared.



**Figure 4.71:** Comparative adhesion forces of Pse1 cells with Au tips. Five different force maps (fm) of cells are compared.

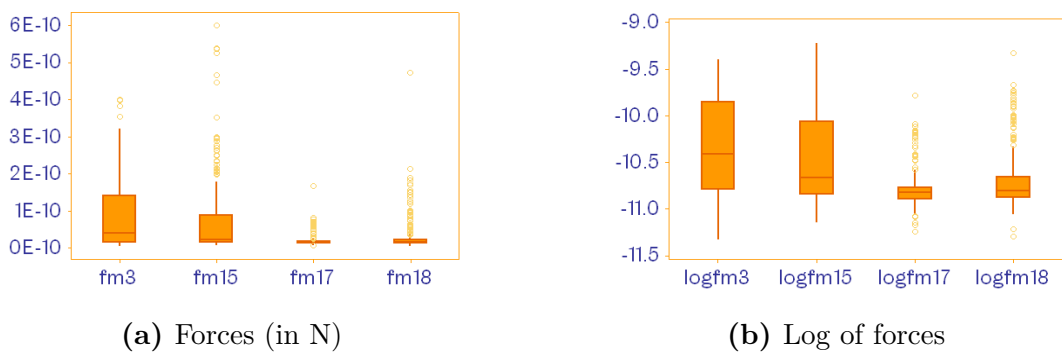


**Figure 4.72:** Comparative adhesion forces of Pse1 cells with DDT tips. Four different force maps (fm) of cells are compared.

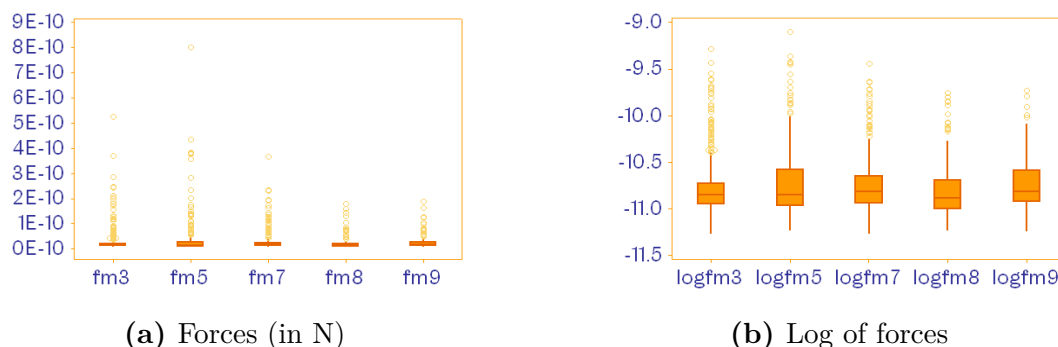


**Figure 4.73:** Comparative adhesion forces of Pse1 cells with MUA tips. Five different force maps (fm) of cells are compared.

### Differences between genera and strains

The median and standard deviations of the measurements were calculated and compared in order to detect differences in the data (Tables 4.5, 4.6). *Pseudomonas* Pse1 showed no statistical difference between the measurements acquired with the four cantilevers. The four probes gave rise to rather low adhesion values ( $\sim 15$  pN). This might be indicative that the molecules on the bacterial cell surface showed little affinity for the tip surface or for the thiol molecules that the probe bore.

Pse2 showed the highest adhesion to Au ( $36.57 \pm 4.98$  pN) and the lowest adhesion to MUA ( $11.93 \pm 3.92$  pN), a behaviour that was also found for Rc92, which had an adhesion force of  $37.47 \pm 5.71$  pN with the gold-coated cantilever and  $12.31 \pm 3.21$  pN with MUA.

For Rc291 the adhesion forces measured with Au, DDT and MUA were not statistically different from each other ( $\sim 25$  pN). Only the silicon nitride probe showed less affinity for the cell ( $\sim 14$  pN). Similar data sets have been obtained by other authors [87], who report roughly similar adhesion values between hydrophobic and hydrophilic strains and probes (Table 4.2). Furthermore, confidence in the validity of the results presented on this thesis arises from the observation of the control experiments, between functionalised cantilevers and bare or functionalised surfaces (Figures 4.38, 4.36). Such control trials proved that the tips used were indeed capable of recognising surfaces of varying chemistry.

High adhesion forces were found between the Au coated cantilever and the surface of Pse2 and Rc92, as well as Rc291 to a lesser extent. This behaviour was puzzling since gold was considered to have a rather neutral surface. It was expected that the hydrophilic strains (Pse1, Pse2) in principle would have a higher interaction with the MUA tip, and that the hydrophobic strains (Rc92, Rc291)

would have more affinity for the DDT tip. This was not the case, as the distribution of forces and adhesion values of the four strains with the four cantilevers looked rather similar.

Some tentative reasons of why the bacterial cells have a preference for gold have been hypothesised. It is known fact that bacteria form biofilms on metallic surfaces, a phenomenon that is a special case of concern since metals are important parts of prosthetic devices, which ought not to be contaminated to avoid infections. For instance *Pseudomonas fluorescens* [315] and *P. aeruginosa* [316] are known to form extensive biofilms on gold. Busalem and Sánchez [315] studied the attachment of *Pseudomonas* to gold, while varying the ionic strength and the surface potentials. The authors hypothesised that gold surfaces might be able to support the formation of bonds with the bacteria due to the metal's surface charge. The possibility exists that the negative charges on the bacterial cells induce a charge on the metallic cantilever coating, thus rearranging the electronic distribution on the gold [317]. This would provoke a mirroring of the charges on the tip and the sample and create a strong field between these two entities, favouring their adhesion (Figure 4.74a). This phenomenon has been seen, for instance, in the strong adhesion of DNA molecules to Au surfaces [318].

Additionally, it is known that thin layers of gold are known to display a hydrophobic behaviour when they have been exposed to ambient air for some time (Figure 4.74b) [319]; only extremely clean gold is hydrophilic [320]. The hydrophobic gold surface could be interacting with hydrophobic moieties on the cell surface. This contribution is probably less important than the surface charge, since the DDT cantilevers were substantially more hydrophobic, and their adhesive forces were not superior to those of gold. These properties might be part of the reason of why some strains had a slight preference for the gold surface, but these ideas remain uncertain.

Strain	Cantilever	Median (pN)	S. error (pN)
Pse1	Si <sub>3</sub> N <sub>4</sub>	15.01	1.40
	Au	15.82	2.85
	DDT	16.11	2.31
	MUA	14.46	1.49
Pse2	Si <sub>3</sub> N <sub>4</sub>	17.73	2.27
	Au	36.57	4.98
	DDT	16.04	9.17*
	MUA	11.93	3.92

**Table 4.5:** Median values of adhesion in *Pseudomonas*. \* large standard error associated with small number of data points.

Strain	Cantilever	Median (pN)	S. error (pN)
Rc 92	Si <sub>3</sub> N <sub>4</sub>	19.03	8.73*
	Au	37.47	5.71
	DDT	16.76	2.81
	MUA	12.31	3.21
Rc 291	Si <sub>3</sub> N <sub>4</sub>	14.35	1.09
	Au	25.28	4.84
	DDT	23.31	1.83
	MUA	27.43	3.15

**Table 4.6:** Median values of adhesion in *Rhodococcus*. \* large standard error associated with small number of data points.

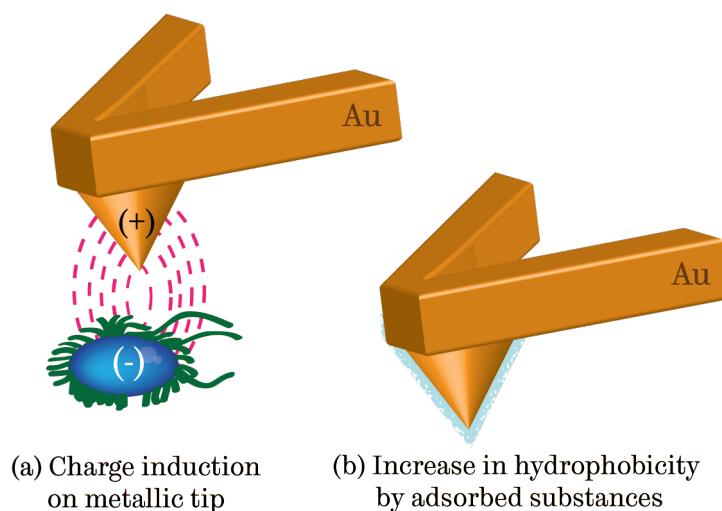


**Figure 4.74:** Possible reasons for the high adhesion between bacteria and Au-coated cantilevers

## 4.6 Heterogeneity in bacterial cell surfaces

It was observed that the heterogeneity within the same cell surface and between cells belonging to the same sample was, in some cases, greater than the differences between species and between genera. This is quite surprising, since the membrane architecture and composition of the Gram negative and positive selected strains is substantially different, and so was the chemical composition of the probe. The possible sources of this heterogeneity will be discussed on this section. Figure 4.76 summarises the possible sources of bacterial heterogeneity within the same cell, between different cells of the same culture and between cells prepared on different days.

Biological sources of heterogeneity are related to differences between cells prepared on different days. The growth phase and conditions are known to affect the properties of the bacterial cells. For instance, studies conducted by Stratton *et al.* [35] on the *Rhodococcus* cell wall composition revealed that the mycolic acid content (which controls, to some extent, the hydrophobicity) is affected by culture age and culture media. Moreover, *Rhodococcus* cells harvested in stationary phase have been found to be more hydrophobic than the ones in exponential phase. This effect can be attributed to the fact that as time goes by, the cells produce mycolic acids with longer alkyl chains [42, 45, 98].

For all the strains, there was a careful control of the bacterial growth procedure. Agar plates were prepared monthly from the frozen glycerol stocks, in order to

reduce the possibility of mutations and ensure that the bacteria had similar traits every time. To prepare the cells for a particular experiment, an overnight culture in a liquid medium was prepared by taking a single colony from the agar plates, in order to reduce variability. This overnight culture was used in turn, to inoculate a larger amount of medium, which was adjusted to a particular optical density and grown again. This was done to ensure that an equivalent number of cells were present on the final culture. The final culture was grown for the same amount of time in every case, to ensure that the cells were in a similar growth stage. All of these measures were taken to reduce the variability between experiments performed on different days.

Biological differences might be present even within the same bacterial cell. Membranes are not homogeneous, since their polymeric constituents are not evenly distributed. This distribution can be different to that of another cell, and hence variability between individuals of the same population is expected.

The preparation protocol might affect the surface composition of the cell walls. For instance, harsh washing steps could strip the EPS layer of the surface to some extent, compromising the repeatability of the experiment. A series of experiments designed to assess the effect of the washing protocols on the cell surface hydrophobicity of the cells is presented in Appendix D. These experiments suggested that the washing protocol did not change the contact angle of bacteria, a fact that is indicative that the bulk surface properties remained unchanged. In principle, if the same preparation protocols are followed, like they were, it is possible to obtain cells with similar characteristics.

Chemical and physical heterogeneity might arise from the interaction between polymers with different chemical functionalities and in different conformations. A large number of different intermolecular bonds can be formed during the course of a force experiment. The type of forces present in the bacteria-tip interaction, as well as their range of action are depicted in Figure 4.75. At distances around 50 nm, van der Waals interactions can be felt by the tip. As it gets closer, the electrostatic forces start to modify the energetic balance of the system. Finally, at close distances ( $\sim 5$  nm) specific interactions are felt by the tip. The stochastic nature of the latter has been mentioned before and are the main contributors to the heterogeneity of the measurements.

It is clear that the formation of these bonds also depends on the SFM parameters, like dwell time, loading rate, applied force, indentation distance, cantilever shape and functionalisation. These parameters can be controlled to some extent, but irregularities might arise from non-controlled variables (e.g. tip asperities, irregular SAM formation, tip contamination, etc.) Furthermore, every experiment will be subject to technical problems that can include change in environmental

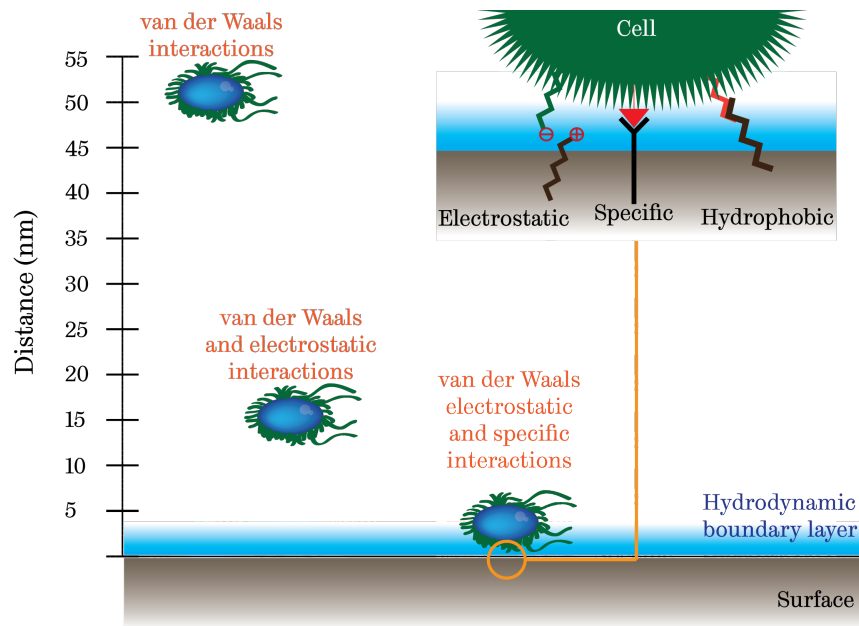


**Figure 4.75:** Interactions between a bacterium and a surface. Image inspired by reference [321].

conditions, imaging buffer evaporation (and concentration), drift in the photodetector and thermal, mechanical noise or instrumental noise. The manufacturer of the microscope in which the force measurements were performed, Asylum MFP-3D, claims that the noise in the optical lever is around 0.02 nm and a  $z$ -piezo noise of 0.25 nm. Even though the instrument was designed to have the least possible instrumental noise and the microscope is located over a floating table to reduce noise from the surroundings, sometimes the microscope detects vibrations caused by loud sounds or vibrations from the building. These factors are substantially more difficult to control and their effect on the measured adhesion forces is uncertain.

Finally, it is possible to introduce bias through an erroneous selection of the statistical models that describe the data. It is often difficult to directly compare data across publications from different authors, since the data treatment could be radically different. Much is done to ensure the repeatability of the experiments, but in the realm of biology complete homogeneity, in practice, cannot be achieved.

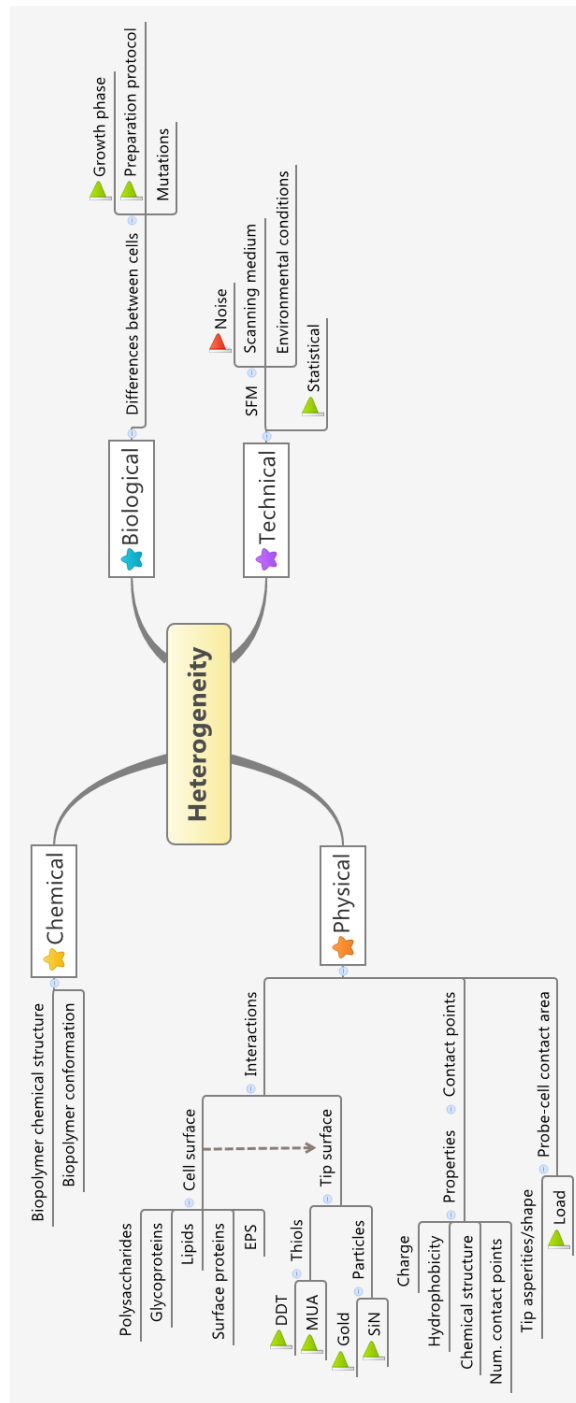


**Figure 4.76:** Sources of bacterial heterogeneity. The green flags mark sources of heterogeneity that can be controlled to a certain extent. The red flag indicates those that cannot.

## 4.7 Concluding remarks

### 4.7.1 Bacterial adhesion in context

Bacterial adhesion is undoubtedly important for a wide variety of reasons, many of which were reviewed in the introduction to this thesis. A deeper understanding of the mechanisms that bacteria use to attach to living organisms and abiotic surfaces is needed. It was mentioned that from the medical point of view it is interesting to decipher the interaction between the cell envelopes of pathogens and mammalian hosts. This knowledge will be key in the prevention of future illnesses, since we would have the knowledge to block the initial attachment to the surface and we would be in a position to manage microbial threats without resorting to antibiotics. It is evident that humanity is in dire need to find alternative methods to prevent or cure infections, in the light of the discovery of antibiotic resistant strains and with the emergence of new, or even forgotten lethal pathogens (e.g. bubonic plague, a deadly infection caused by the bacterium *Yersinia pestis* is still an impending threat [322] and could become an epidemic again).

On the other hand, it was mentioned that humans carry more bacterial cells than human cells, and thus we have established a careful symbiotic balance with them that is equally worthy of attention. Many research groups have tried to shed light to the interaction between lactic acid bacteria and human gut cells [323]; *Lactobacillus* bacteria contribute to our digestive health and are involved in the modulation of immune responses and it even has been proposed that they regulate emotional responses in other mammalian models [324]. Consequently, the knowledge of how probiotic bacteria bind to the intestines might even give us insights into how the *gut-brain axis* influences our emotions.

Similarly, it was mentioned that many metabolically diverse bacteria are used for bioremediation purposes. *Rhodococcus* and *Pseudomonas* are both known for having an excellent array of enzymes capable of degrading a high number of xenobiotic pollutants. Mature biofilms are widely used in waste-treatment plants, as opposed to their planktonic counterparts, since the former are capable of immobilising toxic compounds and are more effective at getting rid of recalcitrant substances. Furthermore, it has been observed that the degradation of pollutants can be enhanced by horizontal gene transfer within biofilms, and by the improved bio-availability of the pollutants due to chemotactic processes [325]. Thus, a careful understanding of the interaction between a group of bacterial cells and their surrounding medium will refine the current methods for pollution treatment.

### 4.7.2 The chemical maps of the future

Microbiologists know a great deal about the nature and composition of the cell surface, and have a clear understanding of the macromolecules present on the cell envelope. On the other hand, the mechanical and adhesive properties of these polymers are poorly understood. The key challenge in biophysical studies of bacterial cells is to understand the role that the surface polymeric substances play on the adhesion of cells to substrates. The localisation and association of surface molecules needs to be understood, along with their function and the way in which they specifically and non-specifically bind to the appropriate ligands on the surface of interest.

The fact that on a particular bacterial cell there are areas of higher adhesion is of high interest in microbiology, and with this observation many questions come to mind. Firstly it would be interesting to see if the distribution of adhesive areas varies with time. If so it would be possible to perform dynamic studies of bacterial surface behaviour, for instance during the process of cell division or in response to the presence of an antibiotic substance. With the advancement of SFM, now is possible to acquire images much faster, and this will allow us to study the dynamic processes of surface macromolecules in response to external stimuli. These experiments would give us a deeper insight into the functional roles and organisation of macromolecular assemblies.

Secondly, it would be interesting to know the chemical composition of the areas of high adhesion. The past decade has seen a tremendous development in the area of single-molecule force spectroscopy and now the study of the interaction and properties of single molecules has become a reality. In order to detect and manipulate single molecules, the SFM probe needs to be functionalised with specific antibodies or ligands (see §2.6.6). Through the use of these techniques, there have been a number of pioneering studies that have aimed to map the presence of polysaccharides, proteins and lipids on bacterial cell walls. For example, Lebeer *et al.* [146] have mapped the surface of lactobacilli and obtained force-volume maps that indicate the distribution of polysaccharides, using lectin decorated probes. Similarly, peptidoglycan has been mapped in *Lactococcus* bacteria using SFM probes functionalised with vancomycin, a substance that binds specifically to the D-Ala-D-Ala sites in this macromolecule [323]. In a recent study, Pfreundschuh *et al.* [326] were able to image, detect and map proteins in their native state using force-distance based SFM.

The experiments designed to map the distribution of lipids are less developed. For instance, Adams *et al.* [327] measured the interaction between *V. cholerae* bioprobes and lipid bilayers. Normally, bilayers are used as models of the cell

wall, since these are easy to produce, but these experiments do not use the single-molecule approach. After reviewing the literature, it was observed that the mapping of lipids *in vivo* is still in its infancy. The development of a technique that is able to map the distribution of lipids on a bacterial cell wall will be very beneficial for the current project. In the introduction, the work of Andrews *et al.* [24] on *Rhodococcus* was presented (§2.2.1 on page 14). In this paper, the attachment of strains Rc291 and Rc92 to polystyrene and other substrates was analysed. It was observed that whereas Rc291 formed extensive biofilms on polystyrene, Rc92 preferred to remain in suspension. Confocal microscopy studies were performed, in which the cell biofilms and aggregates were labelled with a fluorescent lipophilic dye that differentiates between polar and non-polar lipids. These studies led to the conclusion that these strains possessed a different ratio of polar to non-polar lipids, and that these substances associated in a different manner with the cell assemblies. It would be ideal if a SMFS experiment could be devised to map the distribution of these two lipids on a particular bacterial cells and on biofilms.

The optimal SFMS experiment would have the ability to map the presence of different chemical groups on a cell either simultaneously or in close succession. It is not too far fetched to envisage a system in which multiple cantilevers with specific functionalities could be easily exchanged to map a particular region of the sample.

### 4.7.3 The statistics of heterogeneity

This chapter presented the analysis of the adhesion forces of several individuals of Pse1, Pse2, Rc92 and Rc291 probed by four different types of probes: silicon nitride, gold, DDT and MUA. The measurements were taken using the force-volume functionality of the SFM, which yielded colour-coded maps in which each pixel has a colour associated according to the measurement of adhesive force on that particular point of the sample. The force-values on each cell were compiled and gathered into histograms. These histograms did not conform to the normal distribution, but appeared skewed towards high forces. These suggested the existence of regions on the surface of the cell which had a considerably higher adhesion than the rest of the cell. The data was described by fitting the histograms using a number of Gaussian functions using finite mixture models. Each Gaussian peak is represented by a value of mean, standard deviation and height, and these parameters were calculated for each one of the bacterial cells studied in this chapter.

These values were calculated with the aim of sorting the different strains according to their adhesive properties (i.e. a comparison of the means), but soon it became evident that the standard deviation on each cell was very large due to

the heterogeneity present in every bacterial cell. Thus, the comparison between experiments taken under different conditions is not straightforward. It is apparent that the mean value of adhesion is not a very valuable indicator of bacterial adhesion. Many authors [87, 140] use this descriptor to assess the differences between bacterial strains and conditions, but it is the hypothesis of this thesis that by only reporting this value, a lot of information is lost in the process. Since the SFM excels at providing spatially resolved adhesion data with an excellent lateral resolution, it is evident that the force-volume maps should be studied as a whole and not reduced to an individual number.

Two potential ways to reflect on the outcome of this project can be envisaged. The first one is from the perspective of the utility of the adhesion values and descriptors (i.e. mean, standard deviation and height of the Gaussian curves) for each one of the force-volume maps acquired in this chapter. These values could be put in context with the literature, aiming to sort the different bacterial strains according to their adhesive properties. Such effort would generate a repository, in which data produced by different research groups could compile all the information known about a large number of bacterial strains, in the hope to gather enough information to model the behaviour of new types of bacteria. The construction of a framework of these proportions would undoubtedly call for standards and conventions in the field that are currently non-existent, for instance, use of similar immobilisation methods, statistical descriptors, and instrumental parameters, to name a few. The adhesive forces in this repository should be quoted with their respective standard deviations to have an indication of the range of expected adhesion forces. But before embarking in the creation of this repository, one should wonder if these values are actually meaningful by themselves. A repository like this would require a high number of experiments and samples taken, which might be challenging with the current SFM methods that do not allow for high throughput experiments. It is not until faster SFM techniques and easier and reliable immobilisation methods appear that we will be able to study a large number of cells, in order to derive statistically significant data out of them.

There is a second way to analyse the data produced in this thesis, in which the main emphasis is not on the mean values of adhesion, but on the force-volume maps themselves. The distribution of adhesion regions could give us a deep insight into the way in which bacteria attach to surfaces. Mapping the distribution of adhesive sites on individual cells or in early-stage biofilms might help us identify which areas establish a contact first with the surface or other cells. A mass study of this type would help us to identify the molecules responsible for adhesion, and thus we would be in a better position to control bacterial behaviour.

## DNA interactions with mineral surfaces

The vast majority of microorganisms prefer to live in a sessile form, forming aggregates such as biofilms and flocs. An attached state is preferable to leading a solitary and perilous life in the *plancton*. A comprehensive review of biofilm formation was presented in §2.2 and only some key aspects of the theoretical background will be presented here.

Biofilms are the primordial form of growth in nature, and mixed conglomerates of a variety of species are distributed in aquatic and terrestrial environments. Biofilms are defined as accumulations of microorganisms, encased in a polymeric matrix made of extra-cellular polymeric substances (EPS). These substances are responsible for the biological and chemical properties of the matrix, forming a highly hydrated, three-dimensional, gel-like structure in which the cells are embedded. Such EPS are known to contain primarily water and dissolved substances such as ions, diverse polysaccharides, proteins, phospholipids and extra-cellular DNA [328].

Extra-cellular DNA (eDNA) is ubiquitous in soil (up to 2 µg/L) and aquatic environments (up to 44 µg/L) and constitutes a rich source of C, N and  $\text{PO}_4^{3-}$  [329]. It can also be found in the fluids of the human body, like mucus, blood, urine and amniotic liquid. It is produced by the lysis of cells, and membrane vesicles, and it accumulates throughout the EPS matrix.

It is known that some bacteria can use eDNA as a nutrient source [330]; if they possess the adequate enzymatic capabilities, they can cleave this polymer backbone, and use it as a source of N and  $\text{PO}_4^{3-}$ , and C at a lesser extent. The use of eDNA will normally take place in situations of nutritional stress; for instance, when  $[\text{PO}_4^{3-}]$  is low, the enzyme DNase is produced, in order to utilise it as a source of phosphate.

In §2.2.3 it was seen that the bacteria *P. aeruginosa* forms biofilms on the mucus and lung cells of cystic fibrosis patients. The conditions in this mucus can sometimes be anoxic and deficient in nutrients, but rich in eDNA, to a concentration of up to 20 µg/L. In these sub-optimal conditions, *P. aeruginosa* will develop virulence traits in order to survive. They undergo phenotypical changes and adopt a mucoidal form, characterised by the increased production of the polymer alginate. This deteriorates the condition of the host's lungs, causing cell lysis. The breakage of the cell membrane will release DNA that will be assimilated by the bacterial invaders in order to survive.

One of the proposed roles of eDNA in biofilm of pseudomonads is thus, as a nutrient source. The fact that this genus is capable of having such metabolic diversity ensures its success as a pathogen in the body. The presence of DNases facilitates the degradation of this polymer and their presence is related with the ability of a colony to support growth in the absence of any carbon source but DNA.

Extra-cellular DNA is also involved in the formation of biofilms of *Pseudomonas* Pse1 and Pse2. Andrews *et al.* [24] explored the role of this nucleic acid on biofilm formation by growing the aforementioned strains on polystyrene. In Figure 2.4 on page 14, it was shown that Pse1 attaches preferentially to substrates, whereas Pse2 does not form extensive biofilms.

Further experiments have been performed in order to assess the influence of eDNA on biofilm formation. Walton *et al.* [11] added the enzyme DNase throughout the growth period or at the end of the experiment. Figure 5.1a shows the growth curve in LB medium of Pse1, whose exponential phase occurs between 20-40 h after inoculation. The modification in the growth of Pse1, when DNase is added to the growth medium, can be observed with higher cell numbers present when the enzyme is added, one possible explanation being that DNase breaks cell assemblies, a phenomenon that increases the scatter of light. In Figure 5.1b it can be seen that a sharp increase in the concentration of DNA in the growth medium coincides with the exponential phase. Double-stranded DNA accumulated in solution and reached a concentration of 60-70 ng/mL, 46 h after inoculation. These DNA molecules had a high molecular weight (>20kbp) as revealed by gel electrophoresis.

To study the influence of DNase on the adhesion of Pse1, attachment assays were performed. Pse1 cells were grown until late exponential phase and harvested. The bacteria were incubated onto polystyrene and washed gently with PBS to remove unattached material. The enzyme DNaseI was either added at the beginning or the growth period or once harvested from the growth medium. Figure 5.2 shows the attachment of Pse1 and Pse2 to polystyrene [24].

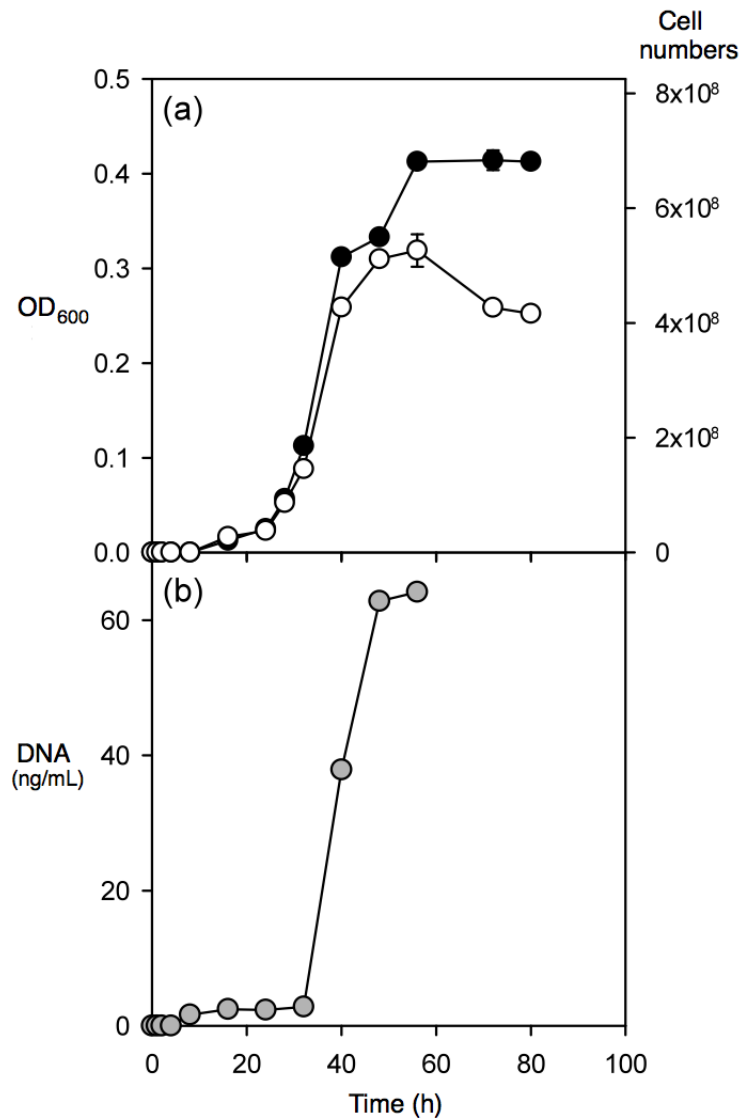


**Figure 5.1:** Growth of Pse1 in LB medium with and without DNase. Figure (a) shows the growth of Pse1 in LB medium without DNase (open symbols) and with DNase (dark symbols). The left-hand side scale shows the average values ( $n = 3$ ) of OD<sub>600</sub> and the right hand scale shows values of cell numbers. Figure (b) shows the concentration of DNA in the growth medium. Data acquired and plotted by Dr Rachel Walton [11].

For Pse1, the addition of DNase detached a considerable number of cells from the biofilm. The highest impact of this enzyme was seen when it was present during the entirety of the growth period, with only few cells attaching to the surface. Conversely the addition of DNase, both during or at the end of the experiment, did not have a significant effect on the number of attached Pse2 cells. These observations lead to the conclusion that eDNA is involved in the mechanism of biofilm formation of Pse1, but not for Pse2.

Since eDNA proved to be involved in the attachment of Pse1, this strain was studied further, by designing attachment experiments using fused quartz slides as the adhesion substrate, in the presence and absence of eDNA under varied conditions. Figure 5.3 shows the results of such investigations. Figure 5.3a shows the scenario in which the microbes have been washed, resuspended and deposited in PBS only, and it can be seen that a considerable amount of cells are attached to the substrate and the presence of cell aggregates is evident. In Figure 5.3b, which shows DNase treated cells, it becomes apparent that the enzymatic digestion of DNA led to a reduction in the number of attached cells as well as a dissolution of the conglomerates. However, when the eDNA is restored into the media (Figure 5.3c) the aggregates are restored. Similarly, the presence of DNase in the growth medium (i.e. since the beginning of the growth cycle) contributed to low attachment numbers (Figure 5.3d), but the binding was restored by the addition of eDNA (Figure 5.3e).

The source of the DNA is apparently not important in the restoration of the binding of DNase treated cells to the quartz substrates. DNA of 20-25 kbp in size, extracted from the supernatant (eDNA), genomic Pse1 DNA (gnDNA) and sheared salmon sperm DNA (ssDNA) were added at the same concentration (5 ng/ $\mu$ L) to DNase treated cells. The three types of DNA caused a greater number of cells to adhere to the surface as seen in Figure 5.4a. DNA fragments of ssDNA of different lengths increase the adhesion of Pse1 cells to substrates as seen in Figure 5.4b.

The presence of divalent cations, like  $\text{Ca}^{2+}$  also seem to influence the attachment of Pse1 to fused silica surfaces. Pse1 cells were treated with DNase and washed with the chelating agent EGTA (ethylene glycol tetraacetic acid), which complexes the cations and removes them from solution. EGTA is a compound similar to the well-known EDTA (ethylenediaminetetraacetic acid), but has a lower affinity for  $\text{Mg}^{2+}$ , making it more selective to calcium ions. Once the calcium ions were removed from the cell suspension, they were restored in known concentrations, in order to assess the effect that these have on bacterial attachment. In Figure 5.5 the effect of the chelating agent and different concentrations of  $\text{Ca}^{2+}$  can be appreciated.

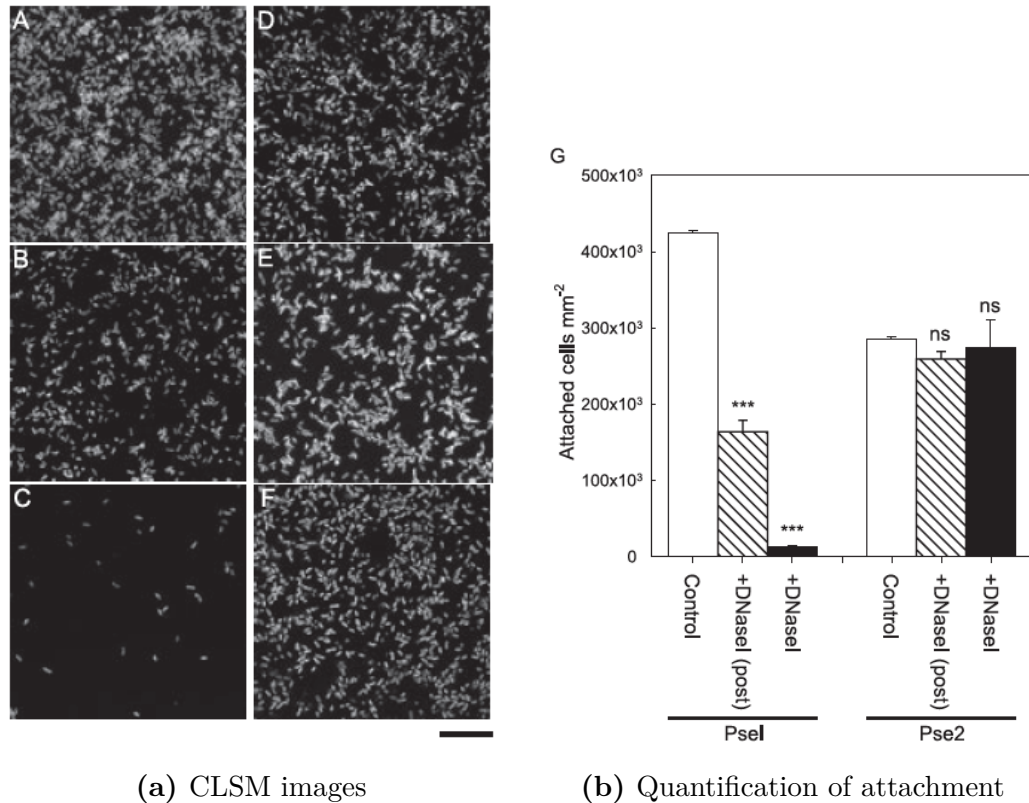


**Figure 5.2:** *Pseudomonas* Pse1 and Pse2 biofilms treated with DNase. Pse1 (A-C) and Pse2 (D-F) are shown attached to polystyrene, and dyed with SYTO9, as seen with confocal laser scanning microscopy (CLSM). A and D are control images, without DNase, after 96 h of growth. B and E show the effect of DNase added after the period of growth. C and F show the effect of DNase added throughout the period of growth. “ns” indicates that these values are not statistically different from the control. \*\*\* $p < 0.01$  (statistical significance). Scale bar=20  $\mu\text{m}$ . Images taken from [24] with permission. Copyright (2010) Wiley.

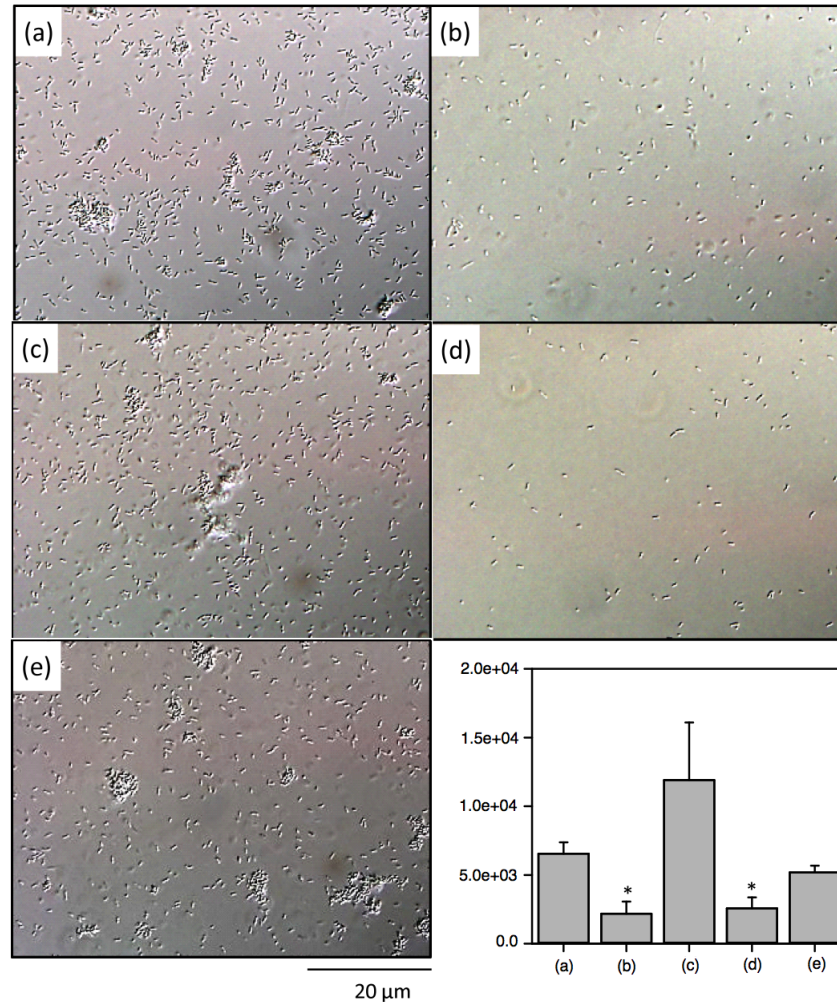


**Figure 5.3:** Pse1 attachment to fused quartz silica with and without DNase. (a) washed cells in PBS, (b) DNase-treated cells in PBS, (c) DNase-treated cells in PBS and 60 ng/mL eDNA, (d) DNase-treated growth medium, and (e) DNase-treated growth medium and 60 ng/mL of eDNA. The statistical results of the number of attached cells are represented in the graph in the bottom right corner, where the values of the averages and standard deviations of three samples are computed. Data acquired and analysed by Dr Rachel Walton [11].

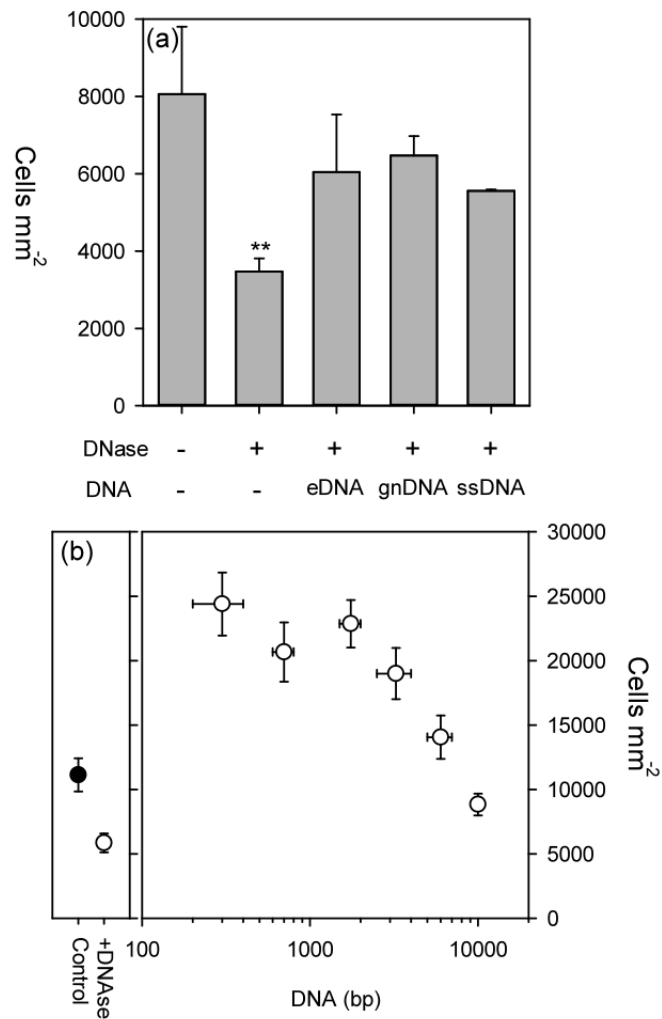


**Figure 5.4:** Influence of DNA sources and sizes on cell adhesion. Figure (a) shows the effect of DNA extracted from three different sources. When the cells are treated with DNase, the number of cells adhered decreases from around 8000 to under 4000 cells/ $\text{mm}^2$ , a value significantly different from the control experiment. Binding is restored with the adhesion of eDNA from the supernatant, genomic DNA (gnDNA) and salmon sperm DNA (ssDNA). Figure (b) shows the effect that different sizes of DNA have on the increase in attachment of Pse1/DNase treated cells to the quartz substrate. The control experiment (dark circle) and the DNase treated cells without DNA (open circle), are shown for comparison. Data acquired and analysed by Dr Rachel Walton [11].

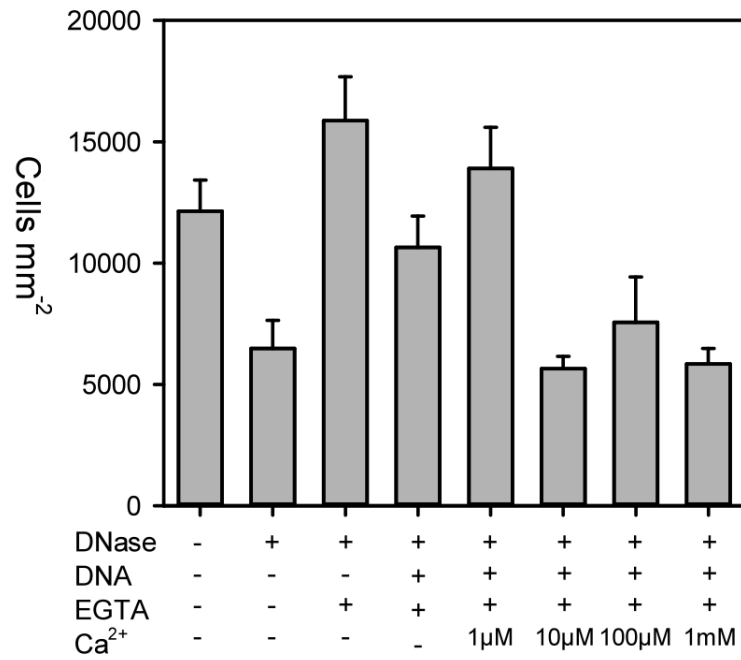


**Figure 5.5:** Pse1 attachment to fused silica surfaces under different  $\text{Ca}^{2+}$  concentrations. Cells were treated with DNase, and then with the chelating agent, EGTA, to remove calcium ions. DNA and  $\text{Ca}^{2+}$  were added into the suspension, and the ions were added in different concentrations to assess their effect on cell adhesion. The results presented are the means of three different experiments, and the error bars correspond to the standard deviations. Data acquired and analysed by Dr Rachel Walton [11].

It has been seen that in other *Pseudomonas* species the presence of divalent cations affects the production of EPS.  $\text{Ca}^{2+}$  and  $\text{Mg}^{2+}$  bind to several components of the biofilm matrix; calcium is involved in signalling processes [331], regulates enzymatic functions, and the presence of calcium can potentially increase the cohesion of the biofilm, as seen in marine environments, where the presence of this ion is high. Calcium ions are also involved in specific interactions between bacterial cells and substrates, as many calcium-binding proteins are related to adhesion and aggregation. Mangwani *et al.* [332] observed that the phenantrene-degrading strain *Pseudomonas mendocina* grows considerably larger biofilms in the presence of  $\text{Ca}^{2+}$  and  $\text{Mg}^{2+}$  20 mM, than without these ions. The presence of calcium increased the production of EPS and cell aggregates, whereas the effect of magnesium was seen as an increment in cell growth, albeit less notoriously. Similar studies [333] have been conducted with the pernicious strain *P. aeruginosa* where also thicker biofilms are obtained in the presence of  $\text{Ca}^{2+}$ .

## 5.1 Chapter overview

Having acknowledged the importance of eDNA in the biofilm formation process of Pse1, it became interesting to study the adherence of single molecules of DNA to solid surfaces using the SFM in its force mode. To this end SFM gold coated cantilevers, functionalised with very dilute solutions of thiolated DNA, were employed. Also, having established that the presence of divalent cations affects the adhesion of eDNA in Pse1 attachment experiments, the effect of the addition of calcium was also studied and compared to the effect caused by a monovalent ion. The DNA-cantilevers were probed against silicon surfaces under water and electrolytes containing  $\text{Ca}^{2+}$  and  $\text{Na}^+$ . The adhesion force of the distinct events was computed and the profile of the force-distance curves was analysed using the worm-like chain model of polymer elasticity. The data will also be compared to theoretical predictions made by computer simulations that model the adhesive behaviour of DNA in the presence of cations.

In the literature, a large number of publications that study the *stretching* of DNA are found. These experiments make use of the SFM and optical or magnetic tweezers. Little, however, has been said about the measurement of the adhesion force of molecules of DNA to abiotic surfaces. Hence, there is a need to understand the mechanisms that this biopolymer uses to attach to surfaces; knowledge that will also shed light into the more complex mechanisms of bacterial adhesion.

Before the experimental results are presented and discussed, several key concepts regarding the nature of the deoxyribonucleic acid and its study from the point of view of polymer physics, will be reviewed.

Ana Lorena Morales-García

## 5.2 Deoxyribonucleic acid

Deoxyribonucleic acid is composed by monomers or building blocks called nucleotides, which have three key components: a nitrogenous base, the sugar 2'-deoxy-D-ribose and a phosphate group (Figure 5.6). Nitrogenous bases are heterocyclic compounds that in nucleic acids can have two forms, named pyrimidines and purines. DNA has two purines, adenine and guanine, and two pyrimidines, cytosine and thymine. The neighbouring nucleotides in the nucleic acids are linked via phosphodiester bonds, forming a backbone of alternating phosphate and pentose residues that are covalently linked to each other. These backbones are of hydrophilic character, since the sugar residues have free hydroxyl groups that can form hydrogen bonds with water. The phosphate groups, at neutral pH, are ionised, thus bearing negative charges (DNA is one of the most charged polymers known) that in physiological environments are neutralised by metal ions, proteins and amines. A short nucleic acid (i.e. less than 50 nucleotides) is called an oligonucleotide, whereas a longer polymer is referred to as a polynucleotide.

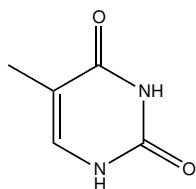
The pyrimidines and purines are highly conjugated and weakly basic molecules, properties that will determine their chemistry, structure, and electronic characteristics. The bases are of hydrophobic nature, and practically insoluble in water at neutral pH. Hydrophobic interactions, as well as other intermolecular forces between close base pairs, will cause their stacking and direct the three-dimensional structure of the DNA molecule. Hydrogen bonds between the amino and carbonyl groups between nitrogenous bases allow the association between two strands of nucleic acids. In 1953, James Watson and Francis Crick discovered the patterns of association between the bases, and determined that adenine-thymine and guanine-cytosine were complementary *base pairs*. Experiments developed by Erwin Chargaff proved that the base composition of DNA varies between species, but the number of purine residues is equal to the number of pyrimidine residues, a proof of the complementarity between the nitrogenous bases [334]. The guanine and cytosine molecules can form three hydrogen bonds between them ( $G \equiv C$ ) but the adenine-thymine pairs can form only two ( $A = T$ ) (Figure 5.7).

The three-dimensional structure of DNA was resolved with the aid of X-ray diffraction experiments conducted by Rosalind Franklin and Maurice Wilkins in the 1950s. From the patterns obtained, Watson and Crick deduced that DNA consisted in two helical and entwined chains, forming a double helix. The hydrophilic backbone, consisting in alternating pentose and phosphate moieties are located on the outside of the helix, facing the aqueous medium. The hydrophobic nitrogenous bases of both strands are facing inwards, stacked inside the double helix to minimise their interaction with water. The pairing of the two strands generates a *major groove* and a *minor groove*, as shown in Figure 5.8.

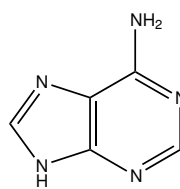
**DNA Bases**

**Pyrimidines**

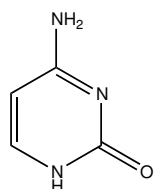
**Purines**



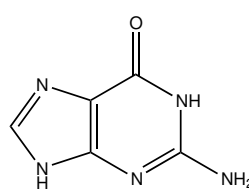
Thymine



Adenine



Cytosine



Guanine

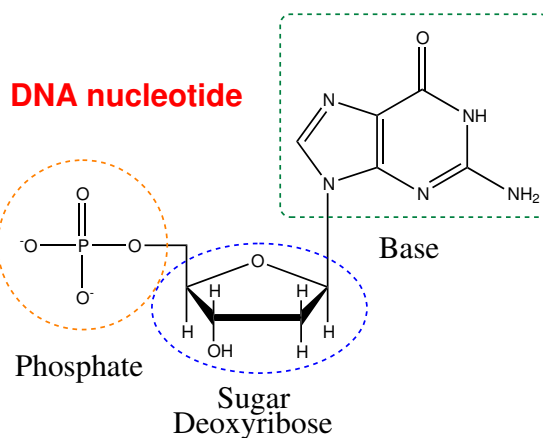


**Figure 5.6:** Structure of nucleotides. (a) Major purine and pyrimidine nitrogenous bases of DNA. (b) Covalent link between a phosphate group, deoxyribose (a pentose sugar) and a purine or pyrimidine base.

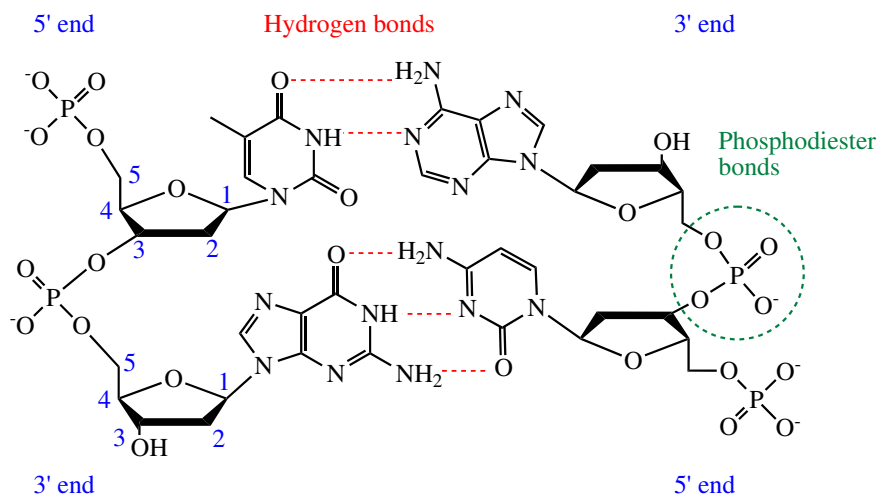


**Figure 5.7:** Hydrogen bonding between complementary base pairs: thymine and adenine form two hydrogen bonds, whereas cytosine and guanine form three. The nitrogenous bases are stacked in the inner section of the double helix. The outer section is flanked by a phosphate-pentose backbone. The 5' end of the strand lacks a nucleotide in the 5' position, and the 3' end lacks a nucleotide at the 3' position. All phosphodiester bonds have the same orientation along the chain, and thus the 5' and 3' markers help to identify the orientation of the strand.

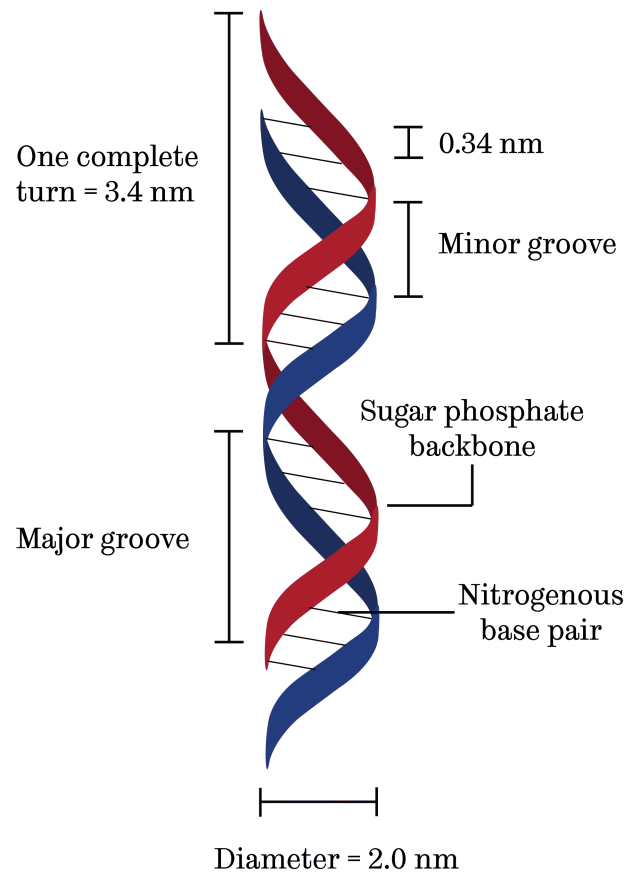


**Figure 5.8:** B-DNA Structure. Diagram not to scale.

DNA can exist in three main structural forms: B, A and Z. The best known is the B form, whose parameters are depicted in Figure 5.8. The A form, which is favoured in low water concentrations, has a larger diameter and is more compressed around the main axis; the involvement of A-DNA in metabolic pathways is uncertain. The Z form is left handed and narrower than the A or B forms and has been found in living organisms [334].

DNA can be flexible under some circumstances, and so is capable of bending, stretching and the un-pairing of the complementary strands. DNA can be bent smoothly, dividing the strain over long molecular sections, rather than folding abruptly at a particular location [335]. These mechanical properties are key to the roles that the nucleic acids play in metabolism.

### 5.3 Polymer physics of nucleic acids

Polymeric molecules are an assembly of hundreds or thousands of monomers, which makes them very complicated to study, unless simplifications are made. If we were to analyse the interaction forces that govern the behaviour of each monomer, in terms of its position and relation with other monomers and solvent molecules, the calculation would be unnecessarily complicated. This is why *mean-field* theory, which assumes that a polymer chain experiences a uniform environment regardless of its location in the medium, helps to simplify and model polymeric molecules [336]. For the particular case of nucleic acids, DNA is much longer than it is wide (it is approximately 2 nm in diameter), and is made up of thousands of base-pairs, approximately 0.34 nm long (Figure 5.8). DNA thus, can be described as a long cylinder and therefore it is reasonable to assume that its properties will not depend on the microscopic structure of the molecule (i.e. the particular order of the base pairs).

All polymers are flexible at a sufficiently long length scale but they can be considered as stiff on short length scales (i.e. one or few monomers). This length that describes the stiffness of a particular polymer, is directly related to its chemical nature and it is known as its *persistence length*. A second important concept in the description of polymeric molecules is the *contour length*, which is defined as the distance from end to end in a linear polymer chain [337].

Force spectroscopy experiments give an insight into the measurement of these parameters. At low pulling forces the conformation of a polymer chain can be described by a *random-walk* or Gaussian distribution. This approach omits the influence of the microscopic structure on the conformation of a chain. Since low pulling forces are being applied, the extension would be smaller than the contour

length. In the Gaussian model, only part of the molecule is being measured as the interaction between the molecule attached to the SFM tip and the surface, will not necessarily happen at the very end of the molecule, but a random section of the polymer will be the one that is probed instead. So in this case, the contour length,  $L$ , will represent a section of the molecule. Assuming that  $x$  is the distance between the tip and the sample and  $x \ll L$ , the relationship between the force and the distance can be expressed as in

$$F(x) = 3 \frac{k_B T x}{l_K L}, \quad (5.1)$$

where  $k_B$  is the Boltzmann constant and  $l_K$  the Kuhn length, which is related to the stiffness of the molecule. Since there is a linear relationship between the force  $F(x)$  and the pulling distance  $x$ , the molecule will behave as a linear spring [274, 338].

At higher pulling forces the molecule is no longer randomly oriented, but mainly aligned in the direction of the external force; in this case, ideal polymers can simply be described with a freely-jointed chain (FJC) model, that considers the polymer to be a chain formed by monomers connected by freely-rotating bonds. In this way the units of the polymer can have any orientation that does not depend on the orientation of its neighbours. In Figure 5.9a representation of an ideal chain is depicted. The FJC model is the simplest description that a polymer can have and constitutes a starting point to describe a polymer in an elementary manner. As shown in Figure 5.9a, the end-to-end distance of the polymer chain  $\vec{R}$  is the vector sum of the position of the individual monomers  $\vec{r}_i$  as in

$$R = \sum_i^N r_i, \quad (5.2)$$

since  $\langle R \rangle = 0$ , the chain size cannot be computed from 5.2, but  $\sqrt{\langle R^2 \rangle}$ , which is non-zero, and is calculated from

$$\langle R^2 \rangle = \left\langle \sum_{i,j}^N r_i \cdot r_j \right\rangle = Nl^2 + \left\langle \sum_{i \neq j}^N r_i \cdot r_j \right\rangle = Nl^2. \quad (5.3)$$

In the FJC model, the polymer chain is assumed to have  $n$  segments of length  $l_K$ , joined by flexible hinges that do not feel the influence of long range interactions. For this model, the chain extension  $x$  is expressed as a function of the pulling force  $F$  as in:

$$x(F) = L \left[ \coth \left( \frac{F l_K}{k_B T} \right) - \frac{k_B T}{F l_K} \right] = L \mathbf{L} \left( \frac{F l_K}{k_B T} \right) \quad (5.4)$$

where  $\mathbf{L}$  is the so-called Langevin function (i.e.  $\Lambda(x) \equiv \coth(x) - x^{-1}$ ) and the contour length  $L = n l_K$ . When the extension is small (i.e.  $x \ll L$ ), the polymer

still behaves like an ideal spring, but at large extension the behaviour stops being linear [339].

The conformation that an ideal polymer chain acquires when in a liquid medium, depends on the nature of the solvent; if the polymer is in a good solvent, it becomes thermodynamically favourable to make more monomer-solvent contacts than monomer-monomer interactions. This would result in an expansion of the polymer chain, where it would have the maximum number of contact points with the liquid medium, having a *self-avoiding* random walk. If on the other hand, the polymer is in a bad solvent the chain would collapse and increase the number of monomer-monomer contacts, reducing its size. The final form of the chain will consequentially depend on a compromise between enthalpic interactions and the entropic effects [336].

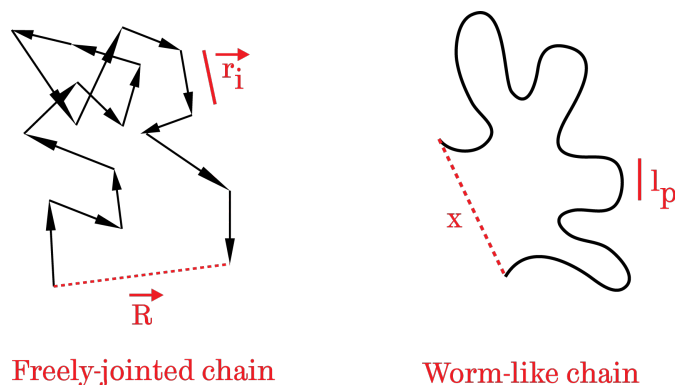


**Figure 5.9:** Polymer chain models. (a) Freely-jointed chain or ideal chain is the simplest model, where the monomers can have any orientation, which is independent of neighbouring units. The distance  $\vec{R}$  is the vector sum of the individual position of the monomers  $\vec{r}_i$ . (b) Worm-like chain model, which is a more suitable model for semiflexible polymers.  $l_p$  represents the persistence length of the polymer.

A more realistic view of a dsDNA molecule, instead of being described as discrete segments joined by freely rotating hinges, can be understood as a continuous elastic medium. The molecule of dsDNA is rather stiff, and consecutive segments are oriented in a similar general direction. Double-stranded DNA is among the stiffest known polymers (about 50 times more energy is needed to bend dsDNA into a circle than single-stranded DNA [335]), with a persistence length of around 50 nm ( $\sim 150$  base pairs, as measured in 0.1 M NaCl) but can have smaller persistence lengths ( $\simeq 15 - 30$  nm) at higher salt-concentrations or in presence of certain trivalent cations [338, 340–342]. Since stereochemistry directs the bond angles between monomers and given that the rotation of certain bonds has a high en-

ergy barrier, more sophisticated polymer models are needed to describe the elastic behaviour of DNA, such as the worm-like chain model.

A worm-like chain (WLC), continuously curved chain, or Porod-Kratky chain is a linear macromolecule with an infinitely thin chain of continuous curvature (Figure 5.9b). This model is used to represent stiff chains [337], especially at low pulling forces ( $< 10$  pN) [343]. This model takes into account entropic and enthalpic contributions, and considers the molecule to be inextensible, and thus, the contour length is a constant. The key characteristic of a chain in the WLC model is the persistence length, which quantifies the stiffness of the polymer, thus assessing the structural rigidity of a macromolecule and the energy cost of bending it. Formally, the persistence length is defined as the length over which correlations in the direction of the tangent are lost. For molecular sections which lengths are below the persistence length of the molecule, they behave like a flexible elastic rod, whereas for longer sections that surpass the persistence length the properties can only be described statistically.

The persistence length,  $l_p$ , is defined as

$$l_p = \frac{l}{1 - \cos \alpha} = \frac{l(1 + C_\infty)}{2}, \quad (5.5)$$

where  $\alpha$  is the angle between bond vectors (Figure 5.10) and  $C_\infty$  is the Flory characteristic ratio given by

$$C_\infty = \frac{\langle R^2 \rangle}{nl^2}, \quad (5.6)$$

for a chain of  $n$  bonds.

When  $\alpha$  in Figure 5.10 has a small value, the chains are stiff and can be described by the worm-like model. The force-distance relationship for the WLC model is described by

$$F(x) = \frac{(k_B T)^2}{B} \left[ \frac{1}{4} \left( 1 - \frac{x}{L} \right)^{-2} + \frac{x}{L} - \frac{1}{4} \right] = \frac{k_B T}{l_p} \left[ \frac{1}{4} \left( 1 - \frac{x}{L} \right)^{-2} + \frac{x}{L} - \frac{1}{4} \right], \quad (5.7)$$

where  $B$  is the bending modulus of the polymer. At lengths less than the persistence length, the directionality of the molecule is kept. For low extensions, both the FJC and the WLC have a similar behaviour. At low forces the relationship between the persistence and Kuhn length is

$$l_K = 2l_p. \quad (5.8)$$

Ana Lorena Morales-García

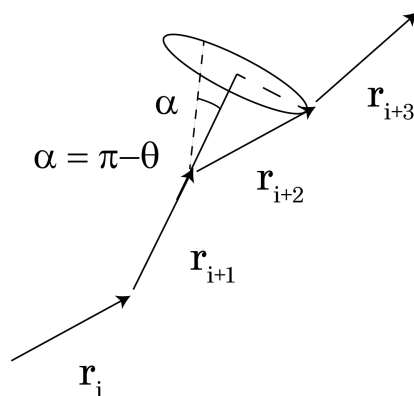


**Figure 5.10:** Azimuthal rotation of bonds. Even when bonds are stiff (i.e. the rotation around the bond has a high energy barrier) the bond does not constrict the chain completely and allows azimuthal rotation. The angle  $\alpha = \pi - \theta$  where  $\theta$  is the bond angle. Image adapted from reference [336].

It is important to point out that neither the persistence or the Kuhn lengths are directly related to the size of the monomer units. As stated before, the size of a DNA monomer is  $3.4 \text{ \AA}$ , whereas its  $l_p = 500 \text{ \AA}$ .

## 5.4 Single-molecule force spectroscopy

Single-molecule experiments allow the study of one molecule at a time. These measurements access the whole distribution of observable events that a molecule can have, in terms of its interaction with a surface and its surrounding environment. If several molecules were analysed at the same time, one would have to consider an average behaviour instead, so the mathematical treatment would become more complicated. Single-molecule experiments reveal information about the dynamics and conformation of molecules that cannot be attained otherwise, as well as strains and stresses that occur in biochemical reactions.

There is a range of techniques available to study single-molecular events, namely optical tweezers, magnetic tweezers and scanning force microscopy. They all rely on having the molecule of interest anchored to a fixed point and stretched over time, measuring its response [344].

Optical tweezers use laser radiation pressure to trap small particles. These traps can be applied in biological systems to attach macromolecules to dielectric particles and manipulate the molecules to measure diverse interactions and stretching forces, in the range of  $10^{-10} - 10^{-13} \text{ N}$ . Single nucleic acid molecules have been

attached to micron-sized polystyrene beads, which are trapped using optical tweezers. The anchored molecule can be analysed in such a way that it is possible to assess a diversity of its chemical and biophysical properties. Such parameters enhance our understanding of biological processes like DNA replication and repair or RNA translation and transcriptions, under controlled conditions. For instance, Williams and Rouzina [345] have stretched single dsDNA (double stranded DNA) beyond its B-form contour length ( $\sim 0.34 \text{ nm} \times \text{number of base pairs}$ ). At forces higher than 60 pN the applied force is no longer extending the molecule, but performing work and deforming the polymer), over-stretching it to a single stranded form, as the nucleic acid unwinds during the stretching. This is why, below the 60 pN threshold, the extensible WLC model describes the mechanical behaviour of DNA appropriately, but after this limit, the molecule can be stretched to twice its normal length. In such an experiment, a single molecule of DNA is stretched using a set-up similar to that of Figure 5.11. Optical tweezer experiments are ideal to measure the elasticity of nucleic acids. The mechanical properties of nucleic acids are of great interest since, in a cell, a particular gene must become accessible in order to be used in transcription or regulation processes, even when DNA is packed with proteins; thus, the fact that DNA is an entropic or extensible chain proves to be advantageous for it to perform all of its functions [274].

In a magnetic tweezers experiment, the molecule is attached to a magnetic bead at one end, and to a glass surface at the other end, and the molecule can be manipulated at the operator's will. Since the magnetic field exerts a constant force, it is possible to measure the force of molecular extension. A simple diagram explaining the main components of this technique is depicted in Figure 5.12.

An SFM experiment for stretching DNA, would have one end of the nucleic acid firmly attached to a glass surface and the other end attached to a cantilever. The probe is then retracted, and the force of extension is recorded as a function of the deflection of the cantilever.

The small masses used in optical and magnetic tweezers experiments, make them suitable for the measurement of very small forces, as illustrated in Figure 5.13. SFM spectroscopy, which uses heavier and stiffer probes, is better suited for experiments that involve higher forces, resolving shorter distances. This is why experiments that involve nucleic acids have been mostly developed using tweezers experiments. On the other hand, the fact that the SFM can access forces in the nanoNewton range, could be advantageous over tweezers experiments; most studies with optical and magnetic tweezers are limited to forces below 100 pN. Notwithstanding, significant conformational changes already occur at these low forces (e.g. the elongation of DNA at 65 pN) [274].

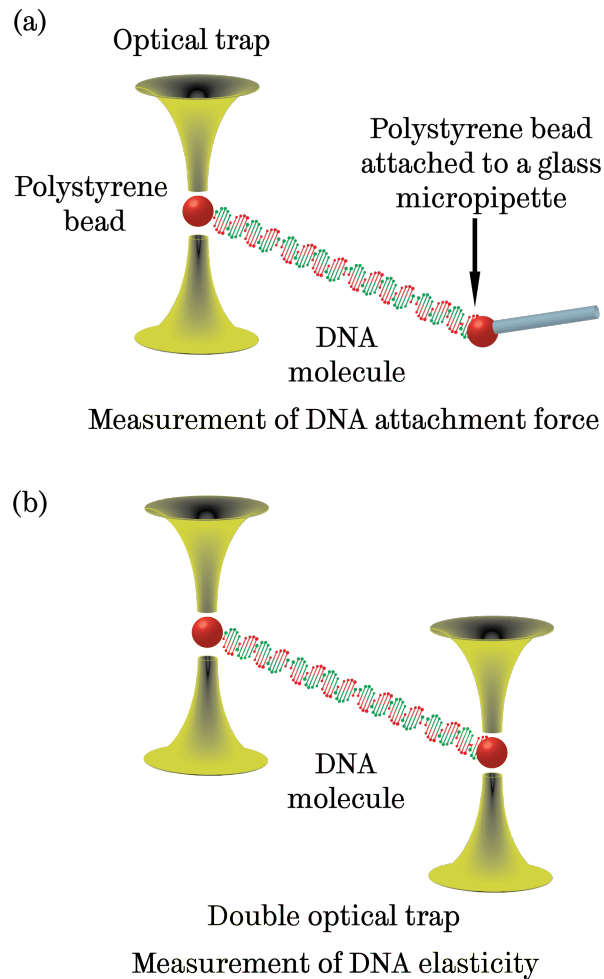
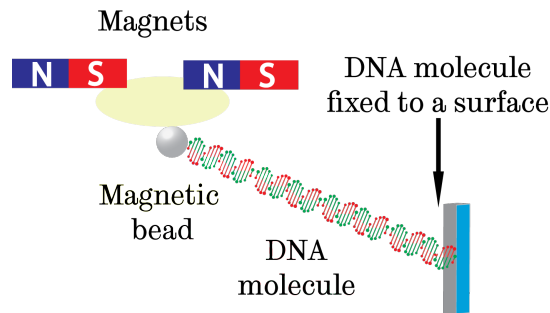


**Figure 5.11:** Classical DNA studies using optical tweezers. (a) Classic setup of an optical tweezers experiment, that employs an optical trap that fixes a polystyrene particle onto which a DNA molecule is firmly bound. The other end of the molecule is fixed to another bead, which is manipulated by a pipette tip. (b) Variation of the experiment that uses two optical traps. The DNA molecule can be stretched by positioning the beads further apart from the equilibrium distance.



Measurement of DNA elasticity

Figure 5.12: Magnetic tweezers.

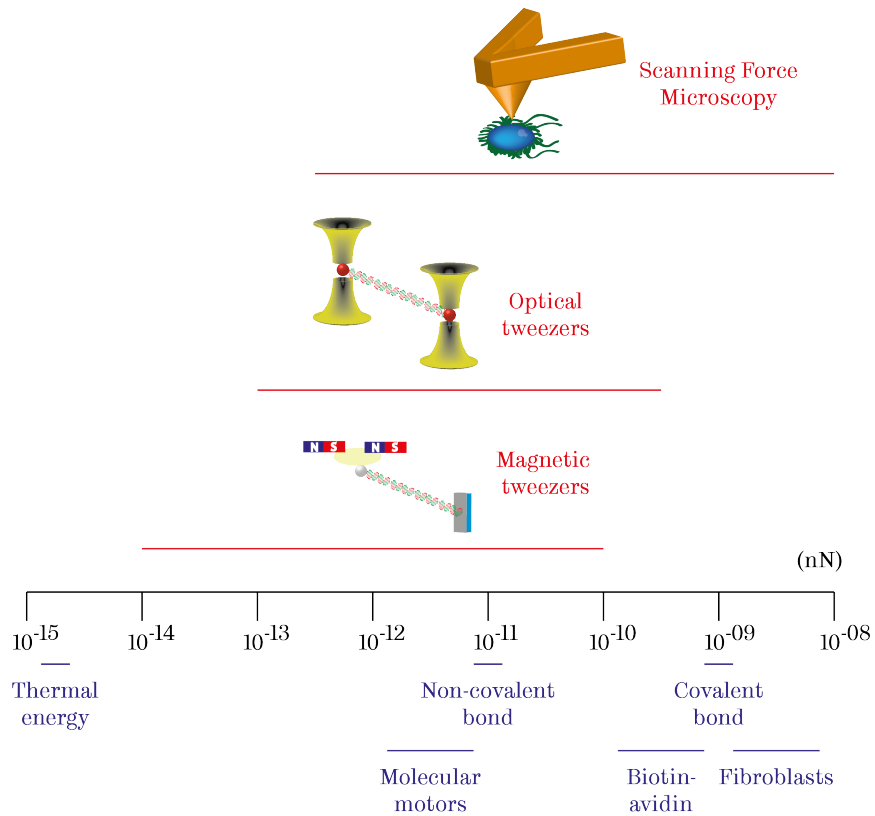


Figure 5.13: Force resolution of SMFS techniques. Image adapted from reference [344].

### 5.4.1 SFM as a tool for single molecular analysis

As reviewed in §2.6, the scanning force microscope has evolved from being an imaging device to one that measures molecular forces in interfaces with great precision. The cantilever acts as a sensor of the interaction forces at a given point in the sample. This information is extracted from force-distance curves, which are a product of the cantilever deflection, as the probe is moved towards or away from the surface (See §2.6.5). Force-distance curves have an approach and a retraction section, and in some cases the latter exhibits complex features and patterns that provide a wide variety of information about the nature of the forces that take place while retracting the probe. These interactions span from van der Waals forces in the range of tens of nN to forces that are entropic in nature and are in the range of tens to hundreds of pN. An entropic force, for instance, would arise from the stretching of a molecule that is fixed both in the probe and in the sample.

When a single molecule is anchored to the cantilever, retraction of the piezo device, at a constant velocity, gives rise to rupture events that are seen as a discontinuous slope in the retraction part of the force curve. Statistical analysis of the resultant pulling forces can relate their rupture values to the piezo position during the detachment event. The maximum peak usually represents the binding strength and sometimes multiples of a unit binding force  $n \times F$  can be detected in several systems. Thus, the shape of the rupture curve is indicative of the number of the molecules adhered or number of bonds broken and this information can be related to the chemical structure of the polymer that is being probed.

The interaction forces between the probe and the sample are strongly dependent on the chemical nature of the sample that is being studied, as well as on the nature of the probe, the fixing surface and the surrounding gaseous or liquid medium. The measured forces that predominate in a given experiment depend on the local medium; it has been stated earlier than when the experiment takes place in humid air, capillary forces dominate the measurements and obscure van der Waals interactions. This is why single-molecule experiments are carried out in a liquid medium, in which capillary forces are negligible.

Aqueous solutions are thus a convenient way in which to perform single-molecular analyses, in which biomolecules can reside in physiological conditions. Electrostatic forces are predominant in aqueous solution and consequently the ionic strength and the nature of the ions in solution will greatly affect the measurements taken.

The literature on single-molecular force experiments of nucleic acids is rich in stretching, twisting and unravelling experiments [338, 345, 346]. Experiments that involve detaching DNA molecules from a surface are far less common. In stretching experiments is important that the binding energy between the tip, the molecule

and the surface is stronger than the property that is to be measured. This is why strong ligand-receptor interactions are employed to firmly anchor the nucleic acid, and stretch it before it is detached.

The interpretation of force-distance curves that are produced by force-pulling experiments is rarely straightforward. It is seldom the case that only one molecule is anchored to the SFM probe apex and that only one molecule is interacting with the substrate at any given point in time. It often occurs that many molecules are interacting almost simultaneously, and thus it is important to learn to recognise the patterns that such interactions would provoke in a force curve.

In all the models that have been presented before, Gaussian, FJC and WLC, there is a relationship between the force  $F(x)$  and  $x/L$ , meaning that the elasticity of a polymer chain scales with its contour length. Hence, two polymeric molecules of different lengths will have different extension curves, since their stiffness values would be different. Due to the fact that properties like the persistence or Kuhn lengths, and the spring constant of particular segments of the polymer are parameters that are independent of the total length of the macromolecule, different polymers of the same type, but different size, can be described by a typical force-extension curve.

Single-molecule experiments are also subject to a wide variety of experimental hurdles, such as the SFM sensitivity, heterogeneity of the surface chemistry, susceptibility of contamination, tip radius, background noise and control of the pulling velocity, among others [274].

## 5.5 Experimental protocols

### 5.5.1 dsDNA fragment preparation

Salmon (*Oncorhynchus keta*) sperm DNA was obtained from Sigma-Aldrich UK (Dorset, England), extracted with 1:1 phenol:chloroform and precipitated using 50% (v/v) ethanol and 0.3 M sodium acetate and then resuspended in 50  $\mu$ L buffer containing 10 mM Tris and 1 mM EDTA at pH 8.0 (TE buffer). According to Tanaka and Okahata [347], the salmon sperm DNA supplied by Sigma-Aldrich, is approximately 2000 bp long, a value that was confirmed by [11] using gel electrophoresis.

The DNA was thiolated using the 5' EndTag nucleic acid system (Vector Laboratories, Burlingame, USA). This kit covalently attaches a variety of functionalities to the 5'-end of nucleotides, leaving the 3'-end untouched. The protocol in

the manufacturers' instruction was followed. The preparation started with a 10  $\mu\text{g}/\text{mL}$  DNA solution in water. In the first step, the DNA was dephosphorylated by mixing the DNA with the enzyme alkaline phosphatase in a universal reaction buffer. The mixture was incubated at 37 °C for 30 minutes. Once ready, the mixture was treated with adenosine-5'-O-(3-thiotriphosphate) (ATP- $\gamma$ -S) and T4 polynucleotide kinase. The mixture was incubated at 37 °C for 30 minutes. Details of the reaction scheme can be seen in Figure 5.14.

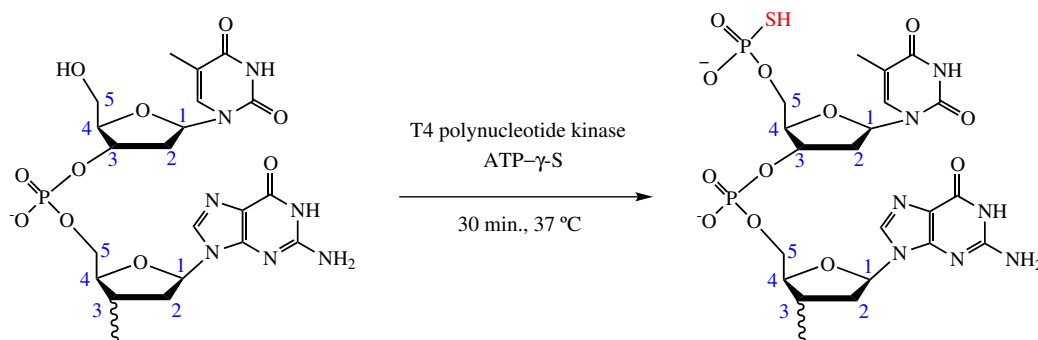


**Figure 5.14:** 5'EndTag labelling reaction that thiolates the 5'-end of the DNA.

After the DNA was thiolated, the mixture was diluted with water and purified through a mini quick spin DNA column (Roche Diagnostics, Indianapolis, USA) to remove any unattached ATP- $\gamma$ -S.

The concentration of the nucleotide was then measured using a Nanodrop 8000 Spectrophotometer (Thermo Fisher Scientific, Wilmington, USA) and was determined to be 4.6  $\text{ng}/\text{mL}$ . The solution was further diluted to 3  $\text{ng}/\text{mL}$  and stored at -18 °C until use. Both the DNA extraction and functionalisation were carried out by Dr Rachel Walton.

### 5.5.2 Cantilever functionalisation

The thiolated DNA was defrosted on the day of the experiment and diluted to a concentration of 3  $\mu\text{g}/\text{mL}$  with sterile filtered ultra pure water. This very low concentration was selected so as to have only a very small number of molecules attached to the SFM probe. A functionalised cantilever is represented in Figure 5.15.

MLTC  $\text{Si}_3\text{N}_4$  SFM probes (Bruker AFM Probes, Camarillo, USA) probes were used and gold coated as explained in §4.2.2. The cantilever was kept in a clean and sealed Petri dish until the day of the experiment. Then it was cleaned using a home-made oxygen plasma cleaner for 30 minutes before functionalisation.

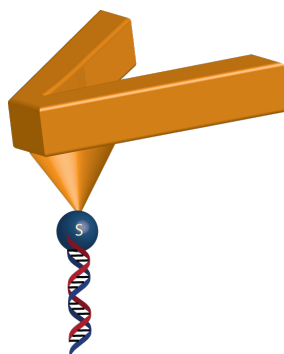


**Figure 5.15:** DNA-functionalised cantilever. A thiolated DNA molecule is attached to an Au coated cantilever.

The gold-coated cantilever was saturated with the thiolated-DNA solution for 2 minutes. After this time, it was rinsed with sterile and filtered water. The probe was air-dried and mounted onto the cantilever holder.

The imaging solutions were prepared using  $\text{CaCl}_2$  anhydrous and  $\text{NaCl}$  (both Sigma-Aldrich, Dorset, England) in analytical grade water (AnalaR Normapur Water, VWR International LTD, Lutterworth, England). These compounds were used exclusively for this experiment, to avoid cross-contamination. The solutions were diluted from a concentrated stock to final concentrations of 2 and 20 mM  $\text{NaCl}$  and 1 and 10 mM  $\text{CaCl}_2$ . The solutions were filtered immediately before use, using sterile syringe filters (0.20  $\mu\text{m}$  pore size, Minisart, Sartorius, Göttingen, Germany).

### 5.5.3 SFM experiments

Silicon wafers of  $425 \pm 25$   $\mu\text{m}$  thickness (Prolog Semicor, Kiev, Ukraine) were cut into rectangles of  $0.5 \times 1$  cm. The substrates were cleaned using piranha solution for 1 h (with a ratio of  $\text{H}_2\text{SO}_4:\text{H}_2\text{O}_2$  7:3) and then rinsed with copious amounts of deionised water. The wafers were then boiled in water for 1 h and the water was replaced 2–3 times during this process. Afterwards the wafers were rinsed with analytical grade ethanol (Sigma-Aldrich, Dorset, England) and sonicated in HPLC grade methanol (Fisher, Leicestershire, England). The wafers were kept in a sealed vial containing methanol until they were used.

A Molecular Force Probe 3D system (MFP-3D, Asylum Research, Santa Barbara, USA) was used to perform the force-pulling experiments. The microscope is equipped with IgorPro 6.22A for data acquisition and analysis.

The bare gold-coated cantilever was mounted on the SFM stage and both the probe and the clean silicon substrate were covered with sterile and filtered ultra pure water. The cantilever was engaged on the surface and its deflection sensitivity and spring constant were determined as described on page 127. Once the cantilever parameters were calibrated, 150 force distance curves were acquired. Once this set was finished, the same steps were repeated, and 150 curves were taken under  $\text{Na}^+$  2 mM,  $\text{Na}^+$  20 mM,  $\text{Ca}^{2+}$  1 mM and  $\text{Ca}^{2+}$  10 mM. All of these solutions were prepared and filtered on the day of the experiment.

The reason for doing this was that this experiment requires a meticulous control of the cleanliness. Since the objective of this experiment was to detect single-molecular interactions, the presence of foreign contaminants on the tip, the surface or the imaging liquid, could obscure the DNA-silicon interactions or be mistaken as one of them. The desired outcome of the force-distance curves between the bare gold cantilever and the clean silicon surface was to see all of the adhesion peaks presenting an *unspecific interaction* peak only. If multiple adhesion peaks had been seen, this would have indicated that the system was contaminated, and that the tip was probing the detachment of a molecular species. Unfortunately, contamination was an important hurdle during this experiment, and thus, these careful control tests were needed and repeated on many occasions until no contaminants were seen. The distinction between specific and non-specific interactions can be seen in Figure 5.16b.

Once the controls proved that only non-specific interactions were present, the cantilever holder, along with the gold-coated tip, were removed from the microscope head. A drop of the thiolated DNA ( $\sim 100 \mu\text{L}$ ) was added to the cantilever and left to bind for 2 minutes. After the time elapsed, the probe and cantilever holder were carefully rinsed with water several times. The cantilever holder was mounted again, and the probe and substrate were saturated with clean water.

The InvOLS and spring constant were determined again and their values recorded. A set of 500 force-distance curves were then recorded under water. The majority of the events appeared to have non-specific interactions only, but a few presented specific interactions as well. This observation led to the conclusion that there was at least one molecule of DNA that became immobilised near the apex of the cantilever and that it was occasionally interacting with the substrate.

After the water set had finished, the tip and cantilever holder were carefully, but profusely rinsed with fresh water. Then a drop of  $\text{Na}^+$  2 mM was added to the tip and substrate. The InvOLS and spring constant were determined again, and 500 force-distance curves were recorded. This process was repeated again for  $\text{Na}^+$  20 mM,  $\text{Ca}^{2+}$  1 mM and  $\text{Ca}^{2+}$  10 mM (in that order).

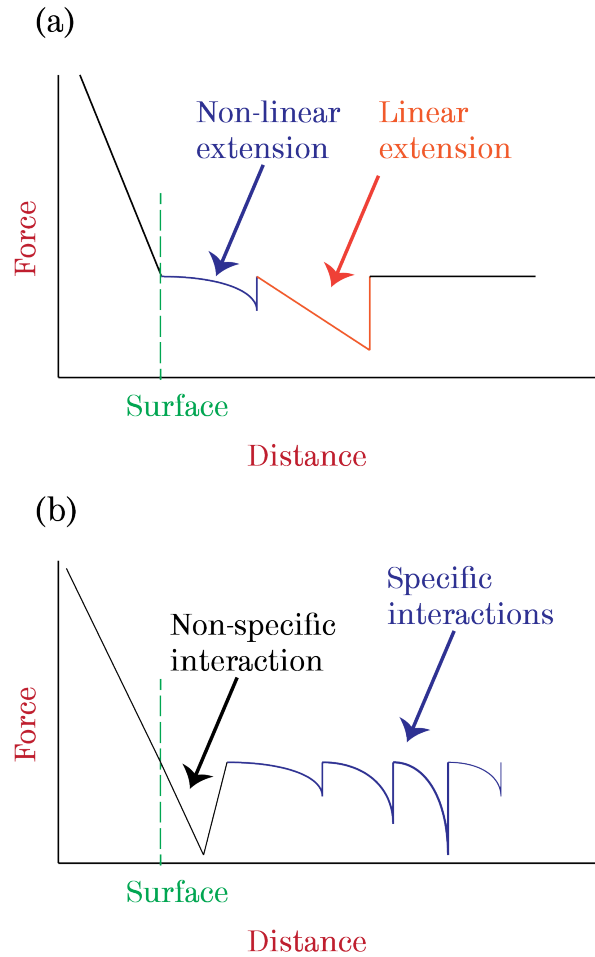


**Figure 5.16:** Typical areas in the retraction part of a force-distance curve. (a) Distinction between linear and non-linear extension retraction peaks. (b) Distinction between specific and non-specific interactions. Image adapted from reference [348].

Percentage of occurrence of multiple peaks	
Scanning medium	Percentage (%)
Water	8.4
Na <sup>+</sup> 2 mM	19.2
Na <sup>+</sup> 20 mM	22.0
Ca <sup>2+</sup> 1 mM	9.6
Ca <sup>2+</sup> 10 mM	19.0

**Table 5.1:** Percentage of occurrence of multiple peaks in a sample of 500 force-distance curves, acquired under water and ionic solutions of diverse strength and nature.

The force-distance curves were recorded between the DNA-functionalised cantilever and the clean silicon substrate at an approximate loading rate of 40,000 pN/s (spring constant  $\sim 40$  pN/nm, force distance = 500 nm, speed 0.99  $\mu\text{m/s}$ ) under a variety of solutions. Only a percentage of a total of 500 force curves per solution presented multiple (specific) adhesion peaks, the rest only presented the main (unspecific) peak of adhesion. The percentage of curves that presented a multiple peak is presented in Table 5.1. It is apparent that at higher ionic concentrations, the probability of finding a force-distance curve with a multiple peak increases. It also seems that it is more likely to find a multiple peak under a sodium solution than under a calcium solution. The lowest probability of finding a multiple peak occurs under water.

## 5.6 SMFS results

Force-distance curves were acquired using the force mode of the SFM. A typical specific force event is shown in Figure 5.17. The positions of the tip in relation to the surface, as well as the behaviour of the cantilever and the molecule have been represented here. Steps 1–3 represent the approach of the functionalised cantilever to the surface. On contact with the surface, the force increases substantially due to the repulsion forces exerted by the close contact on the cantilever with the surface. Upon retraction, on step 4 the cantilever overcomes its attachment to the surface, and in step 5 the molecule does as well. As the tip moves away from the surface, the interaction between the molecule and the surface ceases and the conformation of the molecule stops being dependent on its interaction with the surface.

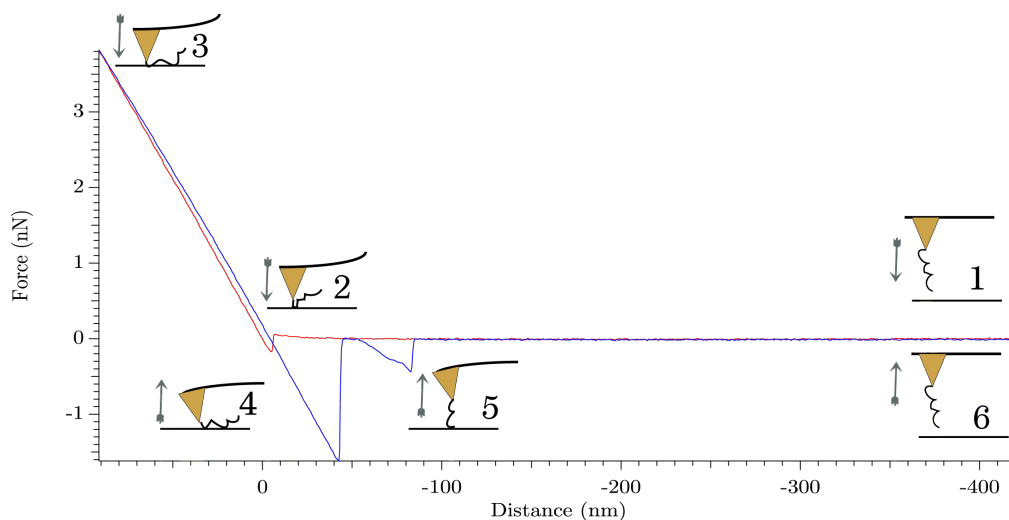


**Figure 5.17:** Typical force-distance curve, which includes the extension and retraction parts. The retraction profile shows the main peak of adhesion, product of the interaction between the tip and the surface, as well as a secondary peak of adhesion, caused by the attachment of the DNA molecule to the surface. The positions of the tip, DNA and surface have been indicated.

### 5.6.1 WLC fitting

The force-distance curves were analysed using the software PUNIAS (Protein unfolding and nano-indentation analysis software, version 1.0, Beta version, directly supplied by Dr Philippe Carl, author of the software [349]). The force data were analysed using the WLC model, based on the following equation:

$$F = \frac{k_B T}{l_p} \left( \frac{1}{4(1 - x/L)^2 - \frac{1}{4} + \frac{x}{L}} \right) \quad (5.9)$$

where  $F$  is the force,  $x$  the chain extension,  $l_p$  the persistence length,  $L$  the contour length,  $k_B$  the Boltzmann constant and  $T$  the absolute temperature.

After the raw data were converted into force-distance curves, the rupture length and force of every peak of adhesion was determined using PUNIAS (Examples in Figures 5.18 and 5.19). The values were recorded and arranged into histograms, which can be found in Figures 5.20-5.24.

A careful observation of all of the force-distance curves that presented specific adhesion peaks, revealed interesting details about the nature of the interactions between the DNA-tip and the surface. Firstly, not all the force experiments gave rise to an interaction between the DNA molecule and the surface, a phenomenon that suggests that the molecule had the freedom to acquire a conformation in

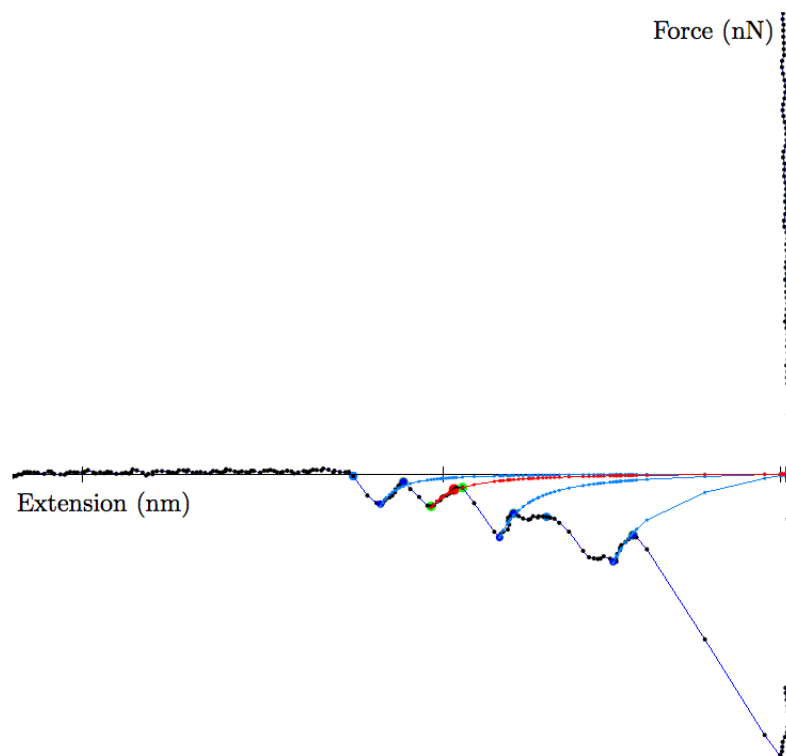


**Figure 5.18:** Force curve of DNA attaching to silicon acquired under water. This curve has been fitted using the WLC model (Equation 5.9).

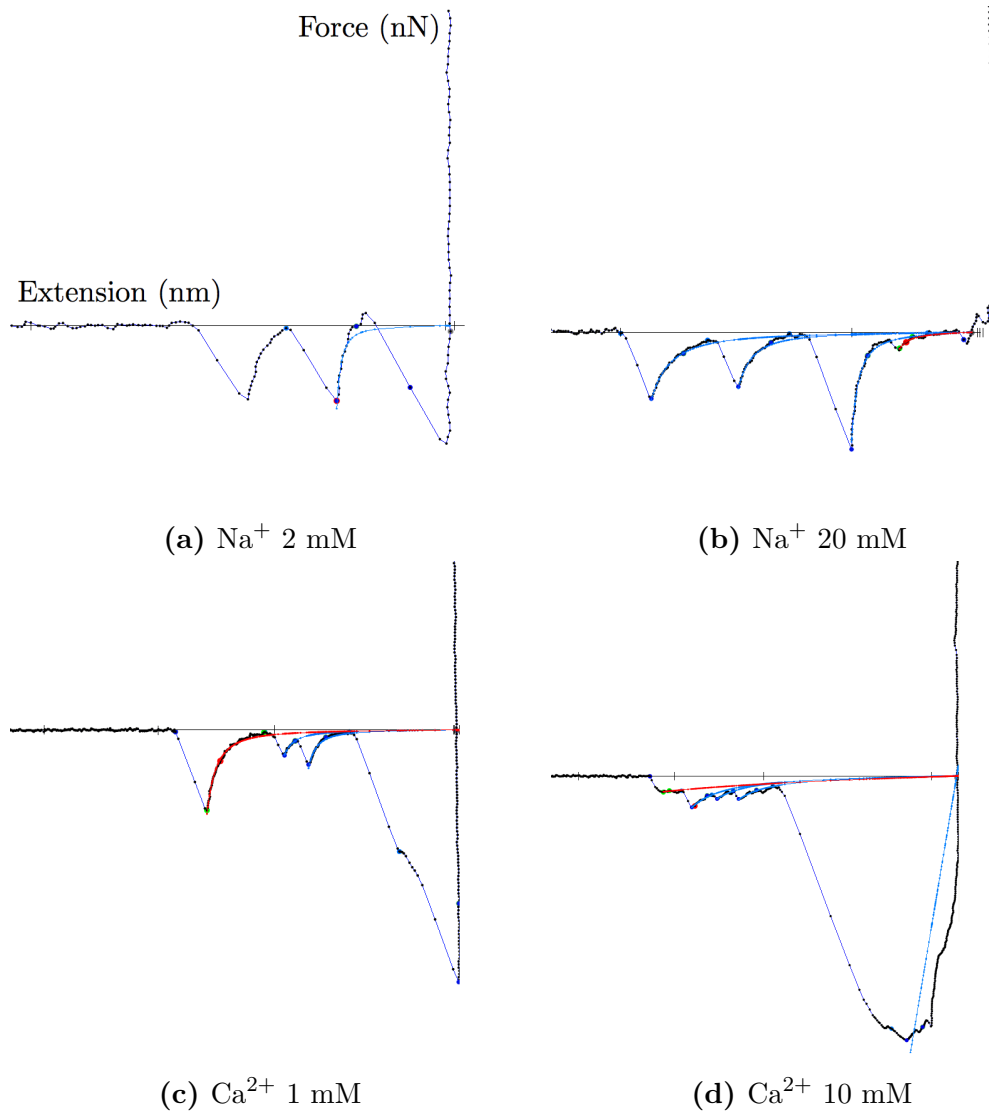


**Figure 5.19:** Force-distance curves of a thiolated DNA tip attaching to silicon under a variety of electrolytes. These curves have been fitted using the WLC model (Equation 5.9).

which it was not directly located between the tip and the surface. Out of the events that showed specific adhesion peaks, a variety of detachment profiles could be appreciated. Under the same experimental conditions, the DNA detached in a variety of ways and with an ample range of forces and extensions. Neither the force nor the extension values conform to a Gaussian distribution and some graphs give the impression of multimodality (Figure 5.23).

Despite the diversity of the data, some conclusions can be drawn when examining the measured force and extension parameters. From the force histograms it can be appreciated that the most probable detachment force is in the range of 80-200 pN for water and the sodium solutions. The maximum detachment force found on these experiments is around 800 pN for water and Na 2 mM, and somewhat lower (500 pN) for Na 20 mM (Figures 5.20, 5.21, 5.22).

It can be appreciated that the maximum detachment force augmented considerably when the experiments were performed under a calcium solution. The experiments under  $\text{Ca}^{2+}$  1 mM solution seem to have a bimodal behaviour, having the most probable detachment forces around 240 pN and 700 pN. The maximum detachment force occurred above 1.1 nN. For the case of  $\text{Ca}^{2+}$  10 mM solution, the most probable detachment force was around 100 pN, and no bimodal behaviour was seen unlike the case of the more diluted calcium solution. The maximum adhesion force was, however, larger than in any other instance, registering events superior to 1.2 nN (Figures 5.23, 5.24).

The study of the extension forces is equally interesting. The extension values of the peaks of detachment under water conform to a rather normal distribution, being 30-50 nm, the most probable range of detachment lengths, and the maximum 70 nm. The sodium electrolytes gave rise to DNA extensions, with the maximum probability of occurrence of  $\sim 20$  nm, and the maximum detachment extension at around 100 nm for both solutions (Figures 5.20, 5.21, 5.22).

Calcium solutions presented a different behaviour. The extension forces in calcium 1 mM showed bimodality, having the most probable extension force at around 20 nm and the second most common at around 60 nm. The maximum extension under these conditions was at 112 pN. Calcium 10 mM solution gave rise to the longest extensions recorded, having a maximum value of 240 nm and the most common value around 110 nm. Under  $\text{Ca}^{2+}$  10 mM, the highest forces and extensions were recorded (Figures 5.23, 5.24).

Reflecting back to the nature of the used DNA strand, it was said that it contained 2000 bp (§5.5.1). If each base pair has a length of 0.34 nm, it is expected that the total length of the fragment (when completely stretched) is 680 nm. Since the maximum detachment length is approximately 35% of the total DNA length, it leads to the supposition that either the molecule was not anchored directly on the apex of the cantilever, but further up, or that the molecule was coiled.

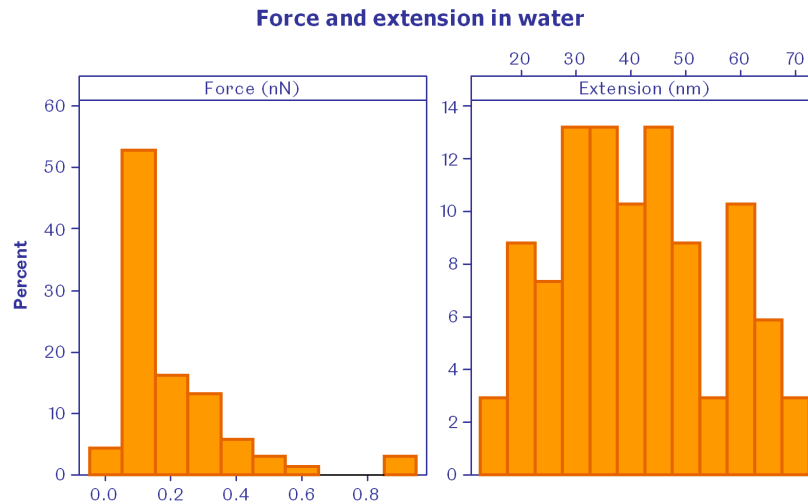


**Figure 5.20:** Histogram of force measurements in force-distance curves of a DNA functionalised tip attaching to silicon. The histogram records the percentage of events. Experiments taken under water.

Figures 5.25, 5.26 and 5.27 show scatter plots that relate the value of the rupture force with the rupture length of each adhesion peak. It is possible to appreciate that the data are similar for the experiments performed under water and sodium solutions. There seems to be a greater degree of variability for the experiments performed under calcium. In Figure 5.27 it can be seen that the rupture events that took place under calcium solutions are different not only to the ones measured under sodium, but also different between each other. Some of the events in  $\text{Ca}^{2+}$  1 mM occurred at higher forces for similar extension values (compared to  $\text{Na}^+$  2 mM and 20 mM). The events observed in the  $\text{Ca}^{2+}$  10 mM solution happened both at higher extensions and at higher forces, a phenomenon which leads to the idea that the presence of calcium aids in the attachment of DNA strands to silicon. This fact has been predicted by molecular simulations, which will be described on the next section.

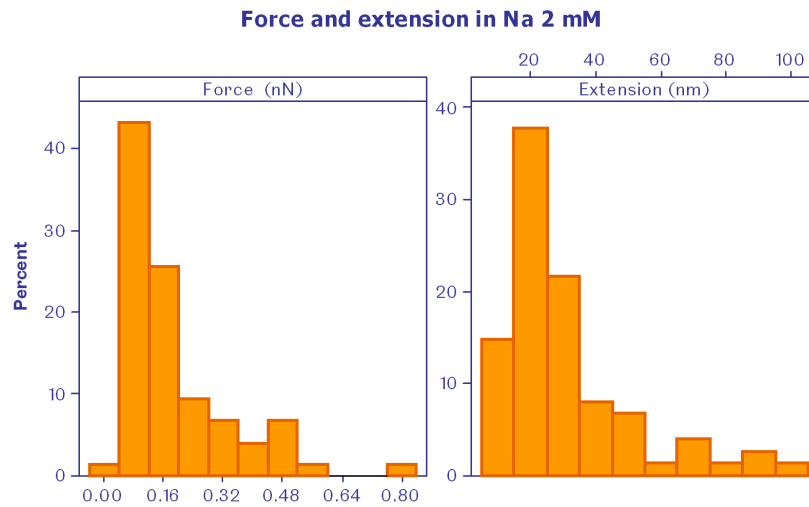


**Figure 5.21:** Histogram of force measurements in force-distance curves of a DNA functionalised tip attaching to silicon. The histogram records the percentage of events. Experiments taken under  $\text{Na}^+$  2 mM.

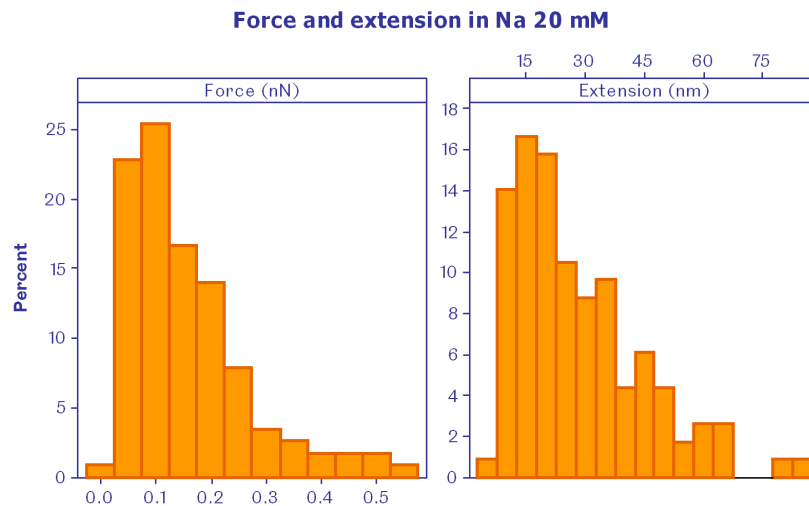


**Figure 5.22:** Histogram of force measurements in force-distance curves of a DNA functionalised tip attaching to silicon. The histogram records the percentage of events. Experiments taken under  $\text{Na}^+$  20 mM.

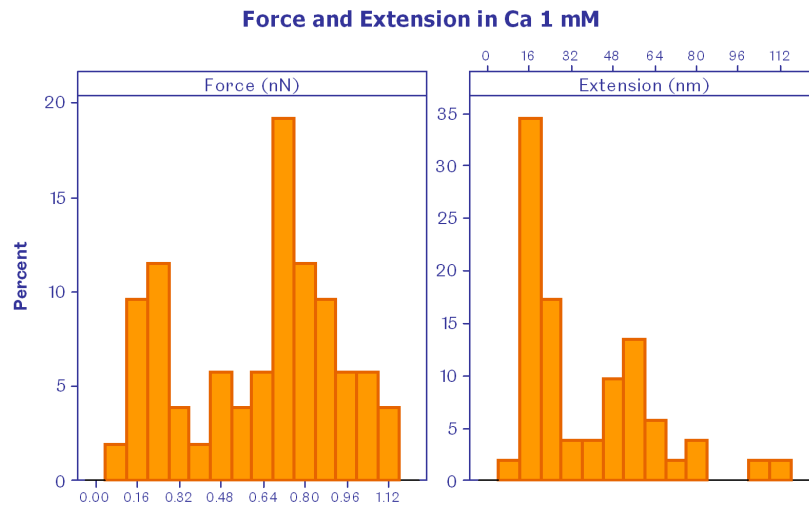


**Figure 5.23:** Histogram of force measurements in force-distance curves of a DNA functionalised tip attaching to silicon. The histogram records the percentage of events. Experiments taken under  $\text{Ca}^{2+}$  1 mM.

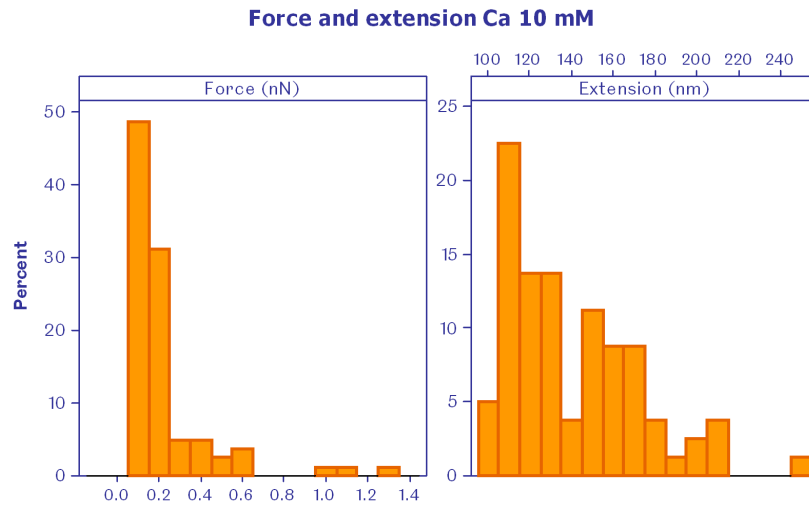


**Figure 5.24:** Histogram of force measurements in force-distance curves of a DNA functionalised tip attaching to silicon. The histogram records the percentage of events. Experiments taken under  $\text{Ca}^{2+}$  10 mM.

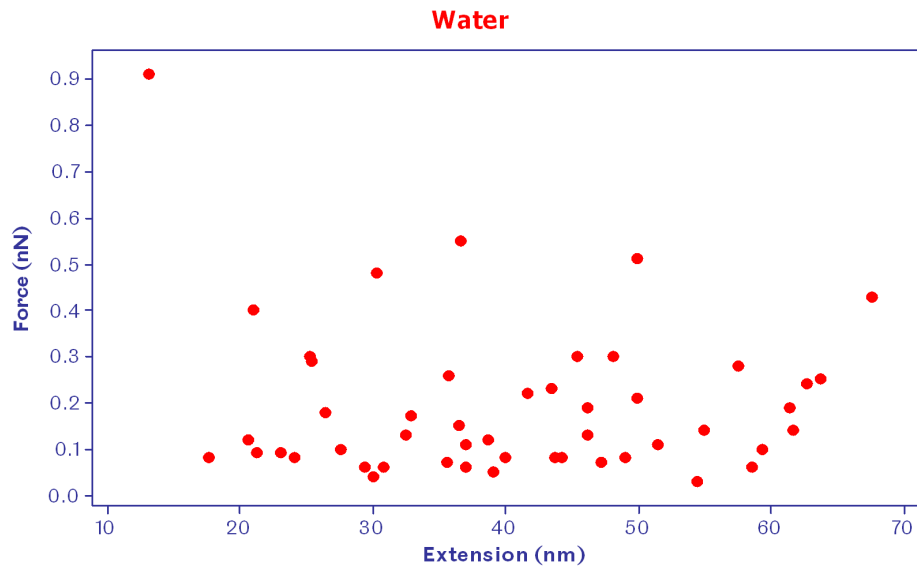


**Figure 5.25:** Scatter plot that relates the extension versus force of unspecific peaks of adhesion. Force-distance curves taken under water.

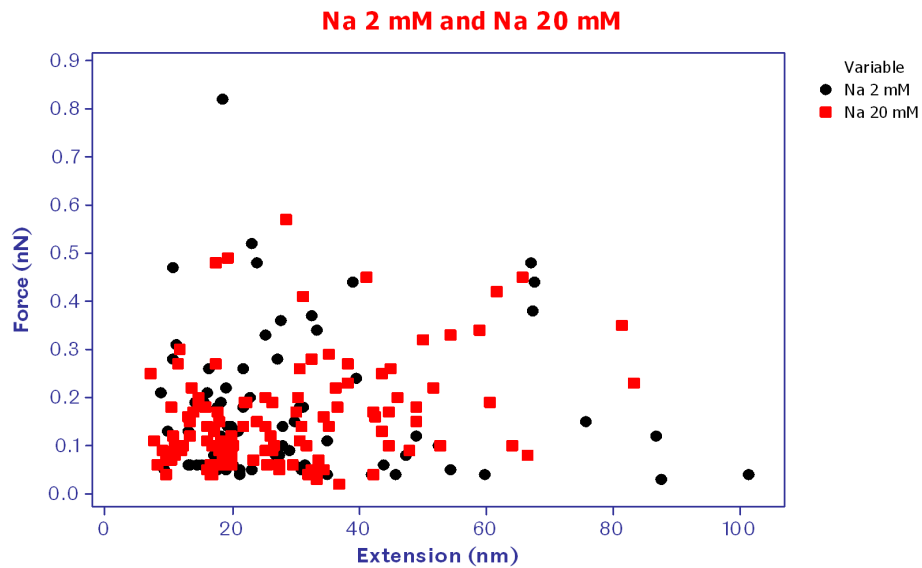


**Figure 5.26:** Scatter plot that relates the extension versus force of unspecific peaks of adhesion. Force-distance curves taken under  $\text{Na}^+$  2mM and  $\text{Na}^+$  20 mM.

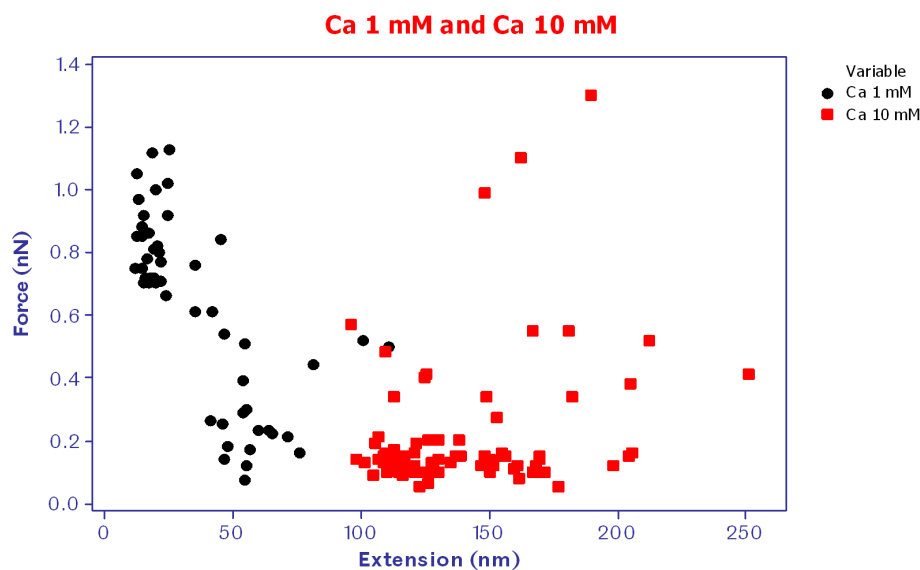


**Figure 5.27:** Scatter plot that relates the extension versus force of unspecific peaks of adhesion. Force-distance curves taken under  $\text{Ca}^{2+}$  1 mM and  $\text{Ca}^{2+}$  10 mM.

### Data relationship with mathematical simulation models

These results are in good agreement with the mathematical simulations performed by Dr Colin Freeman, of the Department of Materials Science and Engineering at the University of Sheffield [11]. The mathematical simulations were aimed to understand the mechanism in which negatively charged DNA interacts with a negatively charged silica surface, and the influence of the surrounding solution on this binding. It is known that the hydroxyl groups on the surface of silica surfaces can form strong interactions with biomolecules, which will be highly dependent on the presence of ions in solution [350].

Briefly, the simulation setup consisted on a randomly generated 13 bp dsDNA which was made to interact with an amorphous silica cell of sub-nanometre dimensions ( $8.0 \times 4.9 \times 4.0 \text{ nm}^3$ ). The two surfaces were placed in a periodic simulation box solvated by 1500 molecules of water and either 38  $\text{Na}^+$  ions or 19  $\text{Ca}^{2+}$  ions, to ensure charge neutrality. The experiments were simulated at 297 K and pH 7 for 0.1 ns. The DNA molecule was placed approximately parallel to the surface at different starting separations from the surface.

The simulations ran without DNA, show that there is an organised layer of calcium cations formed above the silica surface, and the majority of them are

lined up around 2.3 Å from the surface. Figure 5.28 shows a density profile for the molecular dynamics simulations. This positively charged layer forms part of a Stern or double layer (see §2.4 on page 31) that balances the charge from the negatively charged silica. The interaction between the two surfaces was proved to be completely dependent on the presence of the calcium ions, which generate a *potential well* in which the DNA has its maximum interaction with the surface.

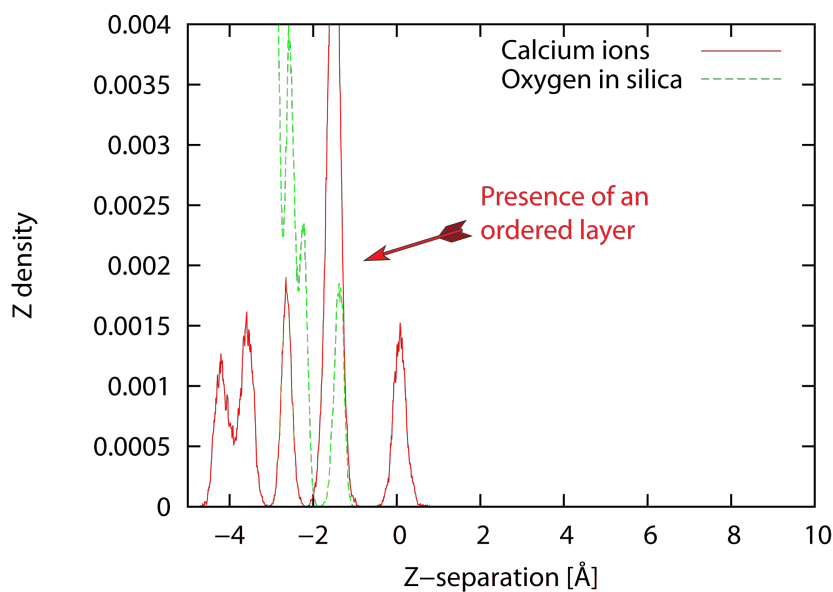


**Figure 5.28:** Number densities for calcium and silicon, without DNA. The  $x$ -axis represents the atomic coordinate within the simulation box, covering an interval of 16 Å. The  $z$  density gives an indication of where the atoms are present: if we refer to the green line, it is possible to see where the oxygen atoms in the silica are located. The red curve shows a narrow and ordered layer of calcium atoms above the silicon surface. This is indicative that the calcium ions are located roughly at the same separation above the surface. The features located on the right hand side of this green line are above the surface. It is possible to see calcium ions before the green line, but these are due to inhomogeneities of the surface and can be largely ignored. Image plotted and calculated by Dr Colin Freeman [11].

The model gives different outputs depending on the initial position of the DNA molecule. When this is placed at distances between 32–36 Å from the silicon surface, the oligonucleotide quickly moves to a separation of  $\sim 36$  Å. If, on the other hand, the DNA is placed further away ( $\sim 41$  Å), the molecule drifts away. This suggests that there is an optimal distance of interaction between the DNA and the surface, and that at longer separations no major forces are felt by the DNA. This is because the calcium ions act as a bridge between the oxygen atoms

on the silica surface and the oxygen atoms on the phosphate groups of the DNA (Figure 5.29). These oxygen atoms will be embedded within the first or second water shells of the ordered layer of calcium ions.

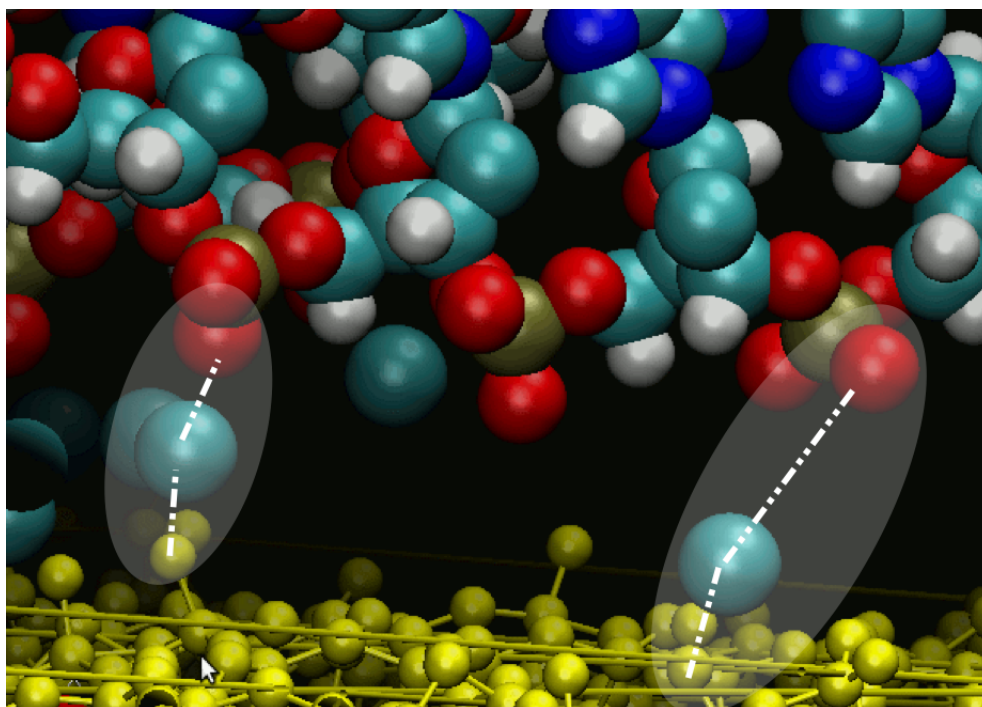


**Figure 5.29:**  $\text{Ca}^{2+}$  ion as a bridge between the oxygen atoms in the silica and the oxygen atoms in the phosphate groups of the DNA. Image generated by a computer simulation run by Dr Colin Freeman [11].

Figure 5.30 shows that there is a significant energy barrier ( $\sim 2000$  kJ/mol) at some point near the silicon surface. When the DNA molecule approaches the silicon, it has to undergo a considerable rearrangement to maximise its interactions with the calcium. Until this optimal configuration is achieved, the cationic layer is being disrupted and the system is in a high energy state.

It is also noteworthy the fact that the DNA has very little enthalpic gain from its association with the silicon surface. In Figure 5.30 it can be seen that the energy of the bound DNA is very similar to the energy of a DNA molecule located far from the surface.

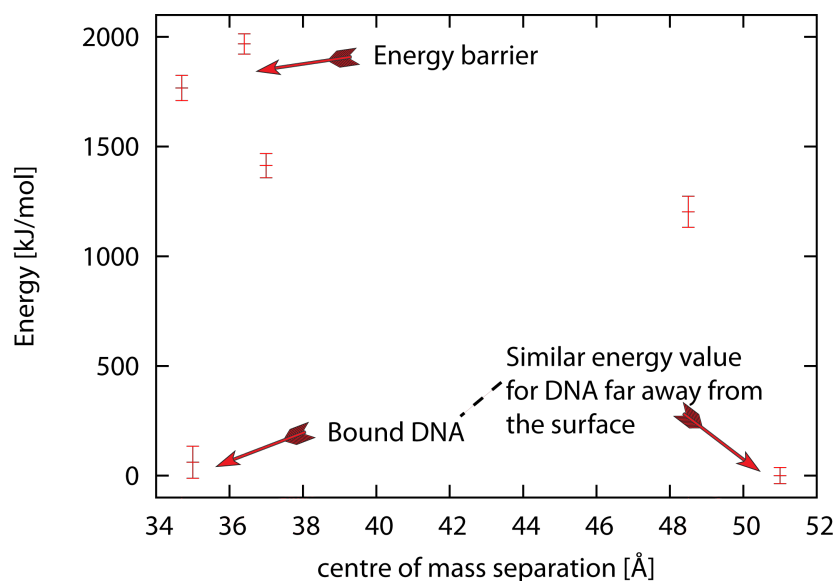


**Figure 5.30:** Energy configurations for DNA molecules located at different separation distances from the silicon surface. Simulations run in presence of  $\text{Ca}^{2+}$  ions. Image plotted and calculated by Dr Colin Freeman [11].

The influence that  $\text{Na}^+$  has on the system is substantially different to the effect of  $\text{Ca}^{2+}$ . For instance, unless the DNA molecule is located very near the surface in the initial simulation parameters ( $\sim 32 \text{ \AA}$ ), the molecule will invariably drift away, an observation that implies that the molecule does not feel long range interactions under these conditions. As Figure 5.31 reveals, the sodium ions do not form ordered layers above the silica surface. It is clear that the monovalent nature of  $\text{Na}^+$  reduces the strength of the electrostatic interactions with the surface. As a result of this, when the experiment is run in the presence of  $\text{Na}^+$  instead of  $\text{Ca}^{2+}$ , there is no potential well near the surface: effectively, the sodium is not aiding the adhesion of the DNA to the silicon surface. The sodium ions form considerably less O (DNA)– $\text{Na}^+$ –O (Silica) bridges, and when formed, these bridges are short lived. Direct interactions between the silicon atoms on the silica and the oxygen atoms on the phosphate groups of DNA were seen instead (Figure 5.32).

Figure 5.33 shows the energy profile of DNA molecules separated from the silicon surface by different lengths. When the oligonucleotide is far from the surface the simulation predicts a plateau on the energy measurements, and that as it gets closer to the surface, an energy barrier emerges. This barrier arises from the disruption of cation-surface interactions and the rearrangement of the DNA molecule to maximise its interaction with the cations. Note that this barrier is not as high as in the case of  $\text{Ca}^{2+}$ , an effect due to the fact that the sodium Stern layer is less structured. Close to the surface it is possible to find a stable

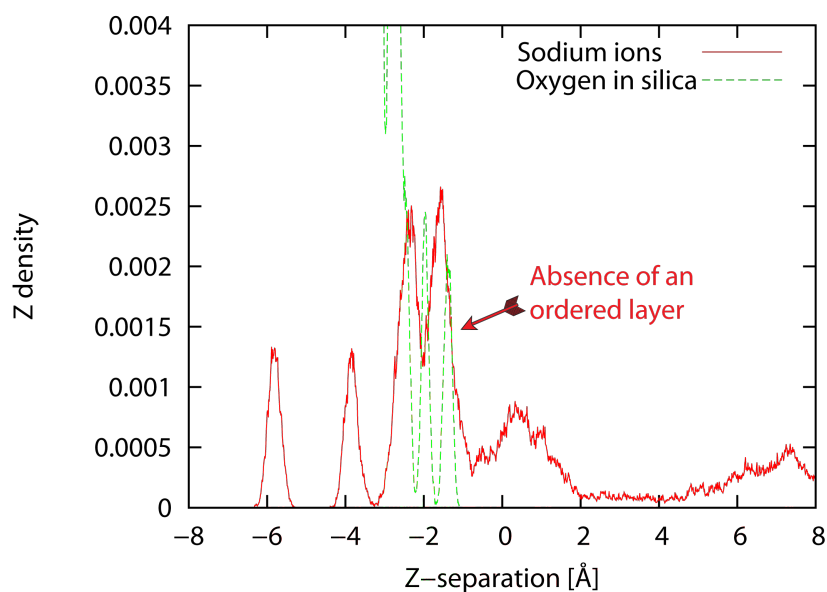


**Figure 5.31:** Number densities for sodium ions and siloxane oxygens, in the absence of DNA. The oxygen atoms on the silica surface are represented by the green line. The features to the right of this green line represent formations above the silica surface. It is possible to see a broad and disordered layer of sodium atoms (red line). The features to the right of the green line are due to inhomogeneities in the silica surface, and can be largely ignored. Image plotted and calculated by Dr Colin Freeman [11].

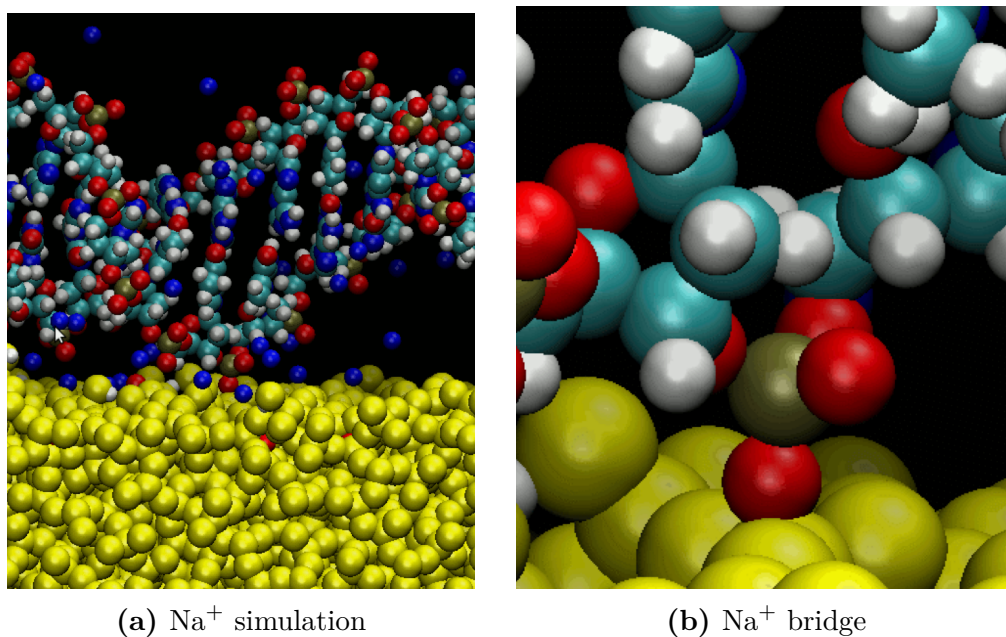


**Figure 5.32:** Molecular dynamics simulation run in the presence of  $\text{Na}^+$ . Figure 5.32a represents the molecule of DNA located close to the surface. Under these conditions O-Na-O bridges are less common than in the  $\text{Ca}^{2+}$  system, and direct interactions are favoured. Figure 5.32b shows a direct interaction between an oxygen atom on DNA and a silicon atom on the silica. Image generated by a computer simulation run by Dr Colin Freeman [11].

configuration. Unlike in Figure 5.30, the DNA-silicon interaction in the presence of  $\text{Na}^+$  is energetically favourable and there is some enthalpy gain of about 800 kJ, which is indicated by the arrows in Figure 5.33.

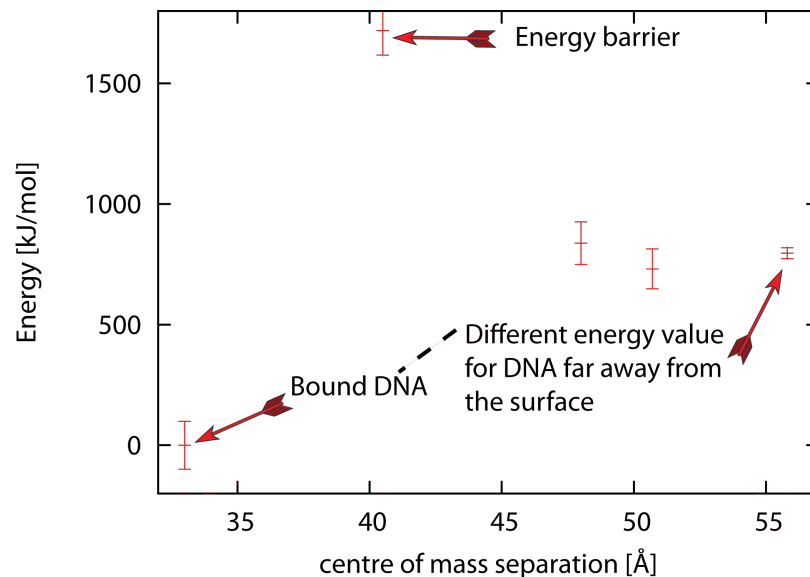


**Figure 5.33:** Energy configurations for DNA molecules located at different separation distances from the silicon surface. Simulations run in presence of  $\text{Na}^+$  ions. Image plotted and calculated by Dr Colin Freeman [11].

In summary, the simulations performed on the silicon/DNA/solvent system suggest that when the DNA is in the sodium solution, the DNA will preferentially bind to the surface, instead of remaining in solution, provided the molecule is very close to the substrate. In the calcium solution, however, the DNA shows no preference for the surface, a phenomenon due to the large adhesion barrier caused by the ordered Stern layer that the  $\text{Ca}^{2+}$  ions form. The energy barrier, works both ways, so more energy will be required to remove the DNA molecule from the surface when in a  $\text{Ca}^{2+}$  solution. The prediction made by this mathematical seems to be in agreement with SFM experimental data, where it was found that the detachment force of DNA molecules under calcium solutions gave rise to detachment peaks with higher forces.

### Other WLC model findings

Both the FJC and the WLC models were used in an attempt to model the retraction peaks, but the former did not mimic the retraction profiles at all (Data not shown), and thus all attempts to use the FJC model were abandoned.

The WLC model, on the other hand, was able to model the retraction peaks appropriately (as seen in Figures 5.18 and 5.19), and hence it was decided to use WLC fits for all the specific detachment peaks encountered under all the experimental conditions.

The contour lengths calculated by the program PUNIAS for the SFM experiments conducted under water and the ionic solutions have been computed in the histograms presented in Figure 5.34. The contour lengths were found to be in most cases only slightly larger than the rupture extensions. The persistence lengths appeared to be underestimated by the model, as the values obtained from the curves that were able to be fitted were  $1.09 \pm 2.05$  nm ( $n = 49$ ) for water,  $2.36 \pm 4.54$  nm ( $n = 74$ ) for  $\text{Na}^+$  2 mM,  $0.13 \pm 0.20$  nm ( $n = 114$ ) for  $\text{Na}^+$  20 mM,  $0.39 \pm 0.20$  nm ( $n = 21$ ) for  $\text{Ca}^{2+}$  1 mM and  $0.14 \pm 0.29$  nm ( $n = 80$ ) for  $\text{Ca}^{2+}$  10 mM. These results are neither in agreement with the values of  $\sim 50$  nm found in the literature or the claims of many authors that the persistence length increases with ionic strength.

If the WLC model is indeed the best choice to model the acquired data, then it is perhaps needed to fix, in the WLC model equation, a number of parameters with a reasonable estimate, in order to get closer to the value of the other variables. Similarly, the reason why the WLC model might not be fitting the data adequately might be due to the influence of neighbouring DNA chains that occasionally have also access to the surface. The effect of the adhesion of several polymeric chains to the surface could complicate the panorama and make the data analysis difficult. Zhang *et al.* [351] recommends to normalise the force profiles and seek to overlap the force-distance curves of all events; if this can be achieved, then the observed interactions are the product of only one chain, and the data can be fitted to the WLC model. More effort needs to be put in this respect to elucidate the nature of the system that is being studied.

Notwithstanding these results, it is important to remember that the experiments presented in this chapter differ considerably from the experiments of DNA extension reported in the literature. In these approaches, a DNA strand is fixed covalently to two surfaces and stretched with a controlled force. On the other hand, in the experiments shown in the present chapter, the interaction between the DNA molecule and the surface is feeble and only appears in selected data points. This experimental setup would not allow a study of true DNA extension because the molecule would detach before it has started to stretch. Therefore it would be unreasonable to compare the data produced by these experiments with the elasticity data that are obtained through optical and magnetic tweezers or other SFM systems.

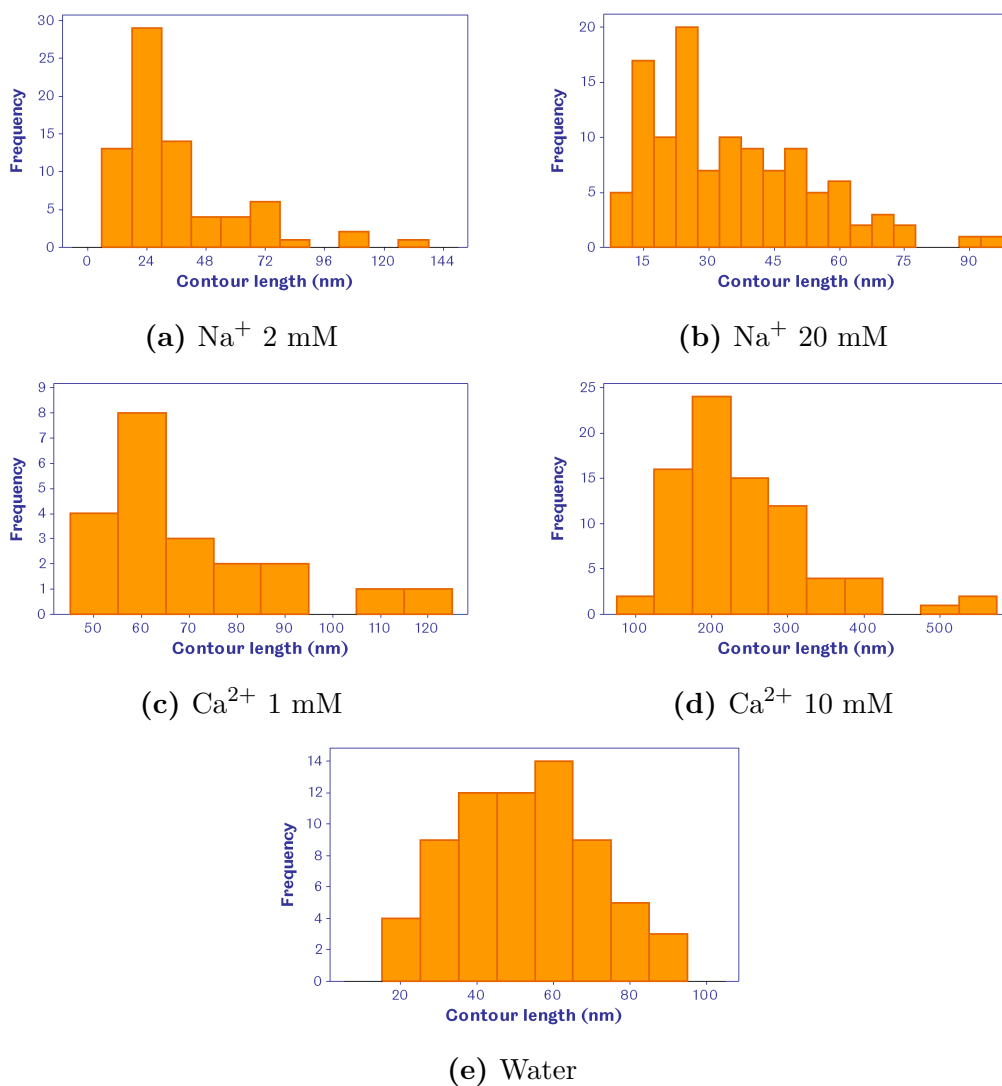


**Figure 5.34:** Histograms of contour lengths of unspecific adhesion events, taken in a variety of solvents. The histograms record the number of events.

### 5.6.2 Force-distance curve analysis

As was mentioned earlier in this chapter, not all of the force-distance curves acquired in each set (i.e. under a particular solvent) presented specific adhesion peaks. A considerable majority showed only tip-substrate interactions, characterised by a large and homogeneous peak of adhesion in the retraction curve, as shown in Figure 5.16b. The rest of the curves showed specific peaks of adhesion that were considered to have come from direct interactions between the grafted DNA molecule and the silicon surface, an interaction aided in some cases by the positive charges in solution.

A variety of specific adhesion peaks in the force-distance curves was found during the course of these experiments. Each peak represents a pulling event in which the DNA molecule is being extended until the strain is relieved and the molecule breaks free from the surface. These peaks correspond to non-linear extension events as seen in Figure 5.16a.

These specific events did not conform to any specific pattern and appeared randomly throughout the data set, but often clustered together in consecutive force-pulling events, suggesting that the molecule remained sometimes in the vicinity of the surface for a given amount of time, before changing conformation and ceasing its interaction with the silicon.

There was a variety of specific peaks of adhesion on the force-distance curves (Table 5.2), suggesting that the probing molecule was interacting with the surface in diverse conformations, which presented a different number of contact points with the surface. In Figures 5.35 and 5.36 the principal types of these force-distance curve profiles can be seen. Figure 5.35a shows a shoulder attached to the main peak of adhesion, suggesting that the majority of the interaction that is taking place is between the apex of the tip and the surface, and that the anchored molecule is only playing a minor role in the adhesion profile as shown in Figure 5.35b. This configuration was most commonly seen under  $\text{Ca}^{2+}$  1 mM. Figure 5.35c shows a plateau conformation, which was a common profile to be obtained, especially for the interaction in  $\text{Ca}^{2+}$  10 mM. A plateau profile suggests that the molecule is interacting through many neighbouring binding sites, and that the molecule is effectively being *peeled off* upon retraction of the cantilever. Plateau profiles are common for polyelectrolytes, since there are many ionic bonds between the charged entities on the molecule and the surface [352]. Other discrete multiple-adhesion peaks were detected, like the one shown in Figure 5.36a. This profile suggests that the molecule was coiled, and only certain points of the molecule were interacting with the surface, as portrayed in Figure 5.36b. This configuration was most commonly seen under  $\text{Na}^+$  20 mM.

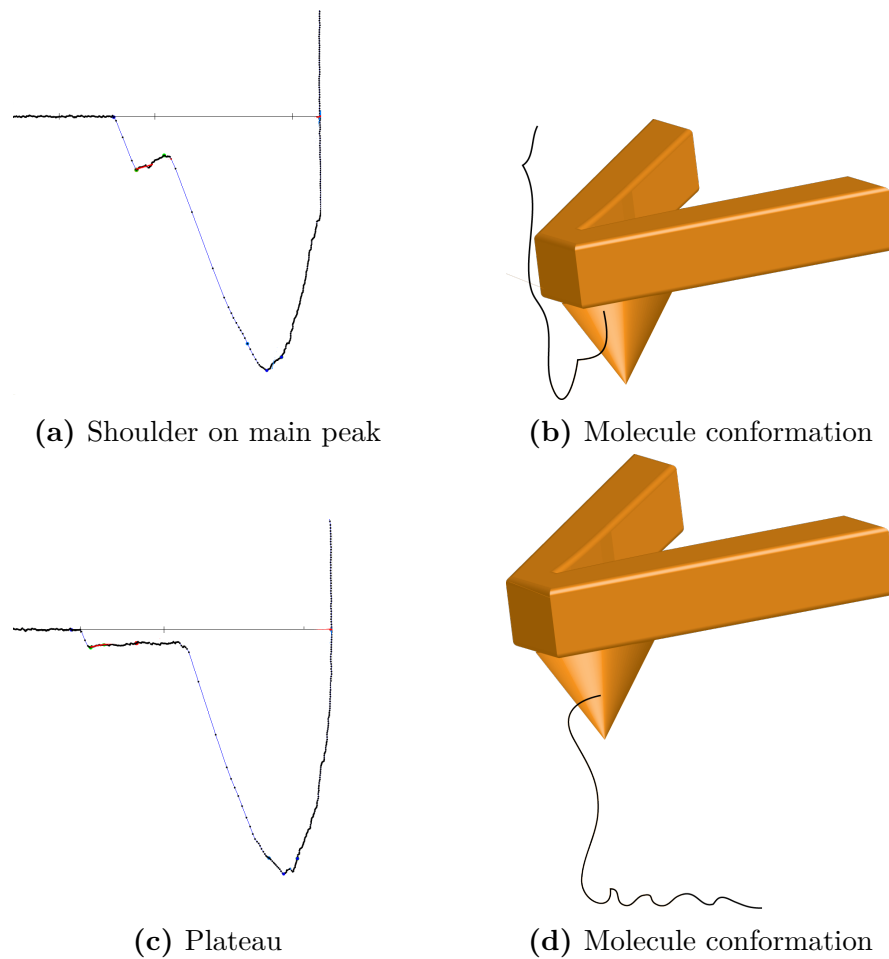


**Figure 5.35:** Types of force-distance retraction curves and possible conformations that the molecules acquire to produce them

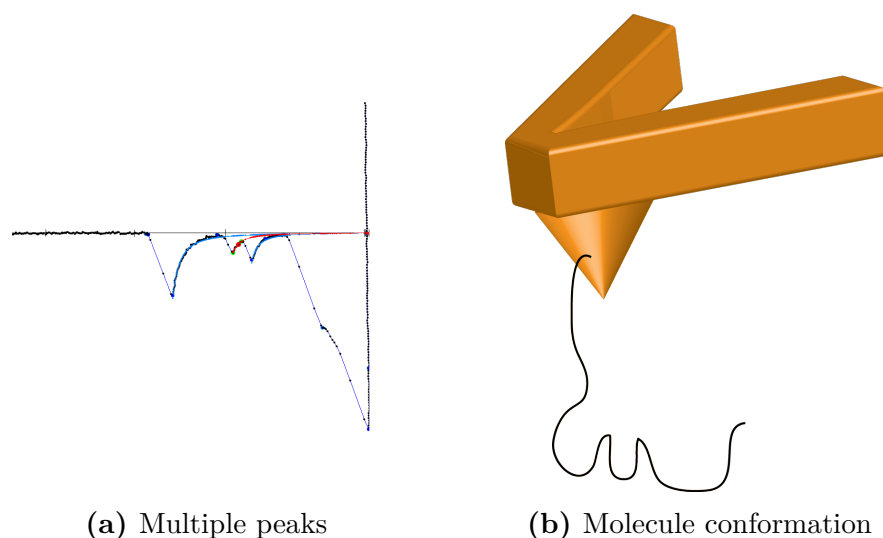


**Figure 5.36:** Types of force-distance retraction curves and possible conformations that the molecules acquire to produce them

Polymers can have strong interactions with surfaces; even if the adhesion force between individual monomers is low, once one has attached there is an increased probability that other monomers will adhere too. There might be an enthalpy gain for the polymer if it adsorbs to the surface, which could counterbalance the entropy loss, which arises as a product of the extension of the chain. It is not possible to control the amount of monomers that adhere to a surface and thus, the measured adhesion force is the product of the adhesion of a large part of the chain. Some chains will adhere more than others, as in the case of the plateau (Figure 5.35b), where there are more contact points between the DNA molecule and the silicon surface. Other chains will adhere less and will have discrete points of contact between the polymer and the substrate. These points will be separated by a few nm, a value that will be related to the flexibility of the polymer. For the case of the multiple detachment events (Figure 5.36), the inter-peak separation was of variable magnitude, a fact that revealed that the loops were formed by a different number of monomers after every approach [353].

Medium	Type of interaction	Percentage
Water	Shoulder	12.5%
	Multiple	69.6%
	Plateau	17.9%
Na <sup>+</sup> 2 mM	Shoulder	10.7%
	Multiple	78.7%
	Plateau	10.7%
Na <sup>+</sup> 20 mM	Shoulder	1.7%
	Multiple	<b>84.9%</b>
	Plateau	13.4%
Ca <sup>2+</sup> 1 mM	Shoulder	<b>72.5%</b>
	Multiple	25.0%
	Plateau	2.5%
Ca <sup>2+</sup> 10 mM	Shoulder	13.0%
	Multiple	32.5%
	Plateau	<b>54.5%</b>

**Table 5.2:** Percentage of occurrence of the distinct types of retraction profiles.

## 5.7 Concluding remarks

Single-molecule force spectroscopy has proven to be a powerful tool to understand the mechanics of polymeric molecules as well as their attachment properties. SMFS has given insight into the relationship between the force and extension in macromolecules, as well as the nature of folding and unfolding processes in biomolecules.

Single-molecule force spectroscopy experiments constitute a convenient exercise to understand the behaviour of one or few molecules. Traditionally, the majority of the efforts in the biophysics field have concentrated on understanding DNA bending and stretching properties using single-molecule approaches. This information is paramount in genetic studies: in prokaryotic organisms, the molecule of DNA is several orders of magnitude larger than the cell, and is tightly packed inside the bacterium through a process known as “supercoiling”. The DNA is twisted and experiences sharp bends due to the combined action of a group of proteins, like DNA topoisomerase I and DNA gyrase. Thus, the understanding of the mechanical response upon bending of this stiff polymer has naturally attracted the attention of polymer physicists. Furthermore, some processes such as DNA replication require this molecule to be stretched [354] and thus the knowledge of its elastic behaviour is key for genetic studies.

However, there is another aspect of DNA that remains poorly studied and this is its role as an adhesive polymer. It has been observed that certain strains of bacteria, like *Pseudomonas* Pse1, depend on the presence of eDNA to attach to surfaces [11]. Consequently, the study of the adhesion of DNA by itself might shed light into the role that this polymer plays on bacterial adhesion. SMFS hold the key to the behaviour of single molecules of DNA in close contact with surfaces.

The aim of the work presented in this chapter was to better understand how DNA interacts with silica surfaces under different ionic conditions using SMFS, and to relate the force spectroscopy findings to predictions made by molecular modelling.

It is evident that the ionic strength of the medium plays a very important role in the adhesive behaviour of single molecules of DNA. This effect was seen not only in the magnitude of the adhesive forces, but also on the shape of the retraction curves on the force-distance curves (see Table 5.2). Whereas the experiments obtained under water and sodium solutions displayed multiple adhesion peaks upon retraction, the calcium solutions prompted the molecule to behave in a different way. Under  $\text{Ca}^{2+}$  1 mM there was a prevalence of “shoulder” events, a fact that was attributed to the conformation in which the molecule was approaching the surface. In such conformation, the majority of the DNA strand was pointing away from the surface, and the tip established most of the contact with the silicon wafer,

as illustrated in Figure 5.35b. The  $\text{Ca}^{2+}$  10 mM solution, on the other hand, gave rise primarily to plateau interactions, profile that was attributed to a conformation in which a flat and large part of the DNA molecule was interacting with the surface and was “peeled off” during retraction, as shown in Figure 5.35d. The  $\text{Ca}^{2+}$  10 mM solution also presented a large proportion of multiple adhesion peaks.

The profile on the force-distance curves was reflected on the extension data. Shoulder and multiple peak-type events gave rise to short extension forces whilst plateau events gave much longer extensions. It was hypothesised that in plateaux, the surface was interacting with the DNA along the length of the molecule and that many adhesion contact points were present. This substantial interaction between the two entities could have been mediated by the calcium ions. It is believed that the differential behaviour of DNA in sodium and calcium solutions is due to a conformational effect.

The interaction of a model DNA strand with a surface was calculated using molecular modelling techniques. Basically, what these analyses predicted was that DNA would have a higher level of interaction with silica under a calcium ionic solution, since the divalent nature of the ions would help to bridge the negative centres on the DNA with the negative centres on the silicon substrate (see Figure 5.29). It was predicted that the ions would form an ordered layer above the silicon surface, and thus the approach of the DNA molecule would disrupt this order (see Figure 5.28). This disruption seems to generate a high energy barrier for the adhesion of DNA (Figure 5.30). But, since the energy barrier works both ways, it would also prevent the desorption. As a consequence of this, DNA in the presence of calcium solutions tends to adhere strongly to the surface. This effect was corroborated by looking at the detachment forces under calcium solutions. Particularly in the case of  $\text{Ca}^{2+}$  1 mM, high detachment forces were seen (Figure 5.27).

On the other hand, sodium 2 and 20 mM solutions did not seem to have a particularly different effect from doing the experiments under water, as similar force profiles, extensions and detachment force values were found under the three conditions. This was again, predicted by the molecular simulations in which it was discovered that sodium, being a monovalent ion did not help bridging the atoms of DNA and the surface. The negative phosphate groups on DNA, in the absence of divalent ions, seem to bind directly to the positive silicon ions on the substrate (Figure 5.32b). This interaction is not very strong and consequently the DNA molecules obtain only a little enthalpic gain from their association to the surface (see Figure 5.33). All in all, the comparison between data obtained using SMFS and the predictions made using molecular modelling is an exciting contribution to the field and seeking links between theory and practice should be pursued in future biophysical endeavours.

### 5.7.1 Future work in SMFS

#### Enhance repeatability

Single-molecule events are characterised by the presence of secondary peaks of adhesion (see Figure 5.16), so it is expected that when the probe has not been functionalised (i.e. gold coated probe), no secondary peaks will be seen. In order to prove that, control experiments were performed before the DNA functionalisation of the probe takes place. The curves generated by the control experiments should only present the non-specific peak of adhesion. Once the experimenter has ascertained that the probe is free of any contaminant, then the SMFS experiment can begin. This type of experiment is extremely challenging to perform, since it requires absolute cleanliness to avoid interaction from unwanted substances. This, in practice, is very difficult to attain and consequently it becomes complicated to perform the experiment repeatedly. So even though the experiment was repeated 500 times under each condition, all the force curves were taken using only one cantilever. Notwithstanding these limitations, it would be desirable to repeat this experiment using a greater number of probes.

#### Make better use of the WLC model

As stated in the introduction, polymer models are useful to describe DNA bending fluctuations. The double-helix persistence length is usually quoted as 50 nm, whereas each base pair has a length of 0.34 nm and the contour length is around 1000 nm for 3000 base pairs. DNA in physiological conditions is a semi-flexible polymer. Since there are only three base pairs per nanometre of contour length, a free molecule of DNA in solution bends in a way in which its local tangent re-orientates every 150 base pairs. However, if tension is applied, the molecule will re-orient in the direction of this tension, even at very low forces. The WLC model has been applied to describe the stretching of a DNA molecule in the 0.1-20 pN range. At higher forces, the double-helix undergoes overstretching [355].

There are plenty of publications (e.g. [343,356]) in which the application of the WLC model to the modelling of DNA bending and stretching have been described. However, there is surprisingly very little in the literature referring to the use of the WLC model to describe DNA attachment to surfaces. There is plenty of evidence that the WLC model is useful in the understanding of force-pulling events of single molecules (e.g. adhesion of single poly(N,N-dimethylacrylamide) chains by [352]) but so far this model has not been applied to describe the force pulling events of single DNA molecules on surfaces. Thus, it became interesting to apply this commonly used model in polymer physics to fit the generated force-distance curves.

It is evident that, for the set of experiments presented in this chapter, the outcome of the WLC fitting is a fallacy since the persistence lengths are nonsensical. Other authors have reported that the expected persistence length of DNA is around 50 nm in conditions of low salinity. This value is in accordance with the fact that DNA is an incredibly stiff molecule due to its double helix structure. The persistence lengths obtained in the present analysis are smaller than the length of a single base pair, and thus it is not credible that the molecule can bend at that length scale. A proposed way to improve the quality of the WLC analysis, would be to fix the value of the persistence length to a reasonable number (e.g. 50 nm) and derive the rest of the parameters, like molecule extension, from this assumption.

In general, it is the opinion of the author that the field of polymer physics has much to offer to the study of the adhesion of single molecules, and despite the failure of the WLC model to describe the data in the conditions presented in this thesis, more effort should be put to understand how the equations and the model can be used to describe the data.

## What is the relevance of the study of bacterial adhesion?

In most natural environments, the prevailing way of life for microbes it is to be attached to a surface in the form of biofilms. These conglomerates are far from static, as they are highly dynamic communities of organisms firmly anchored to surfaces and encased in a polymeric matrix that gives them enhanced protection against environmental threats. Microbes that belong to a biofilm are considerably more resistant to starvation and are better protected against antibiotics. Since many biofilm-driven illnesses are lethal to the human being, it is in our best interest to gather sufficient data to understand the mechanisms of bacterial adhesion. The assembly of bacteria inside our body is often one of the first steps in the infection process. Nowadays, as the threat of antibiotic resistance is impending, [357] it is vital to gather as much information as possible about the diverse mechanisms of bacterial attachment and devise mechanisms to tackle colonisation of pathogenic bacteria inside our body.

The relationship of bacteria and humans is not always pernicious. Through a deep understanding of bacterial biochemical pathways and clever engineering, it is possible to exploit their metabolism and use them for our benefit. Some strains of bacteria are an integral part in bioremediation systems, due to their capacity to degrade xenobiotic substances. Often, a careful control of their surface properties enhances their bioremediation capabilities.

Biofilm formation is a phenomenon that is interesting both from the physics and biology point of view. The initial approach of a microorganism to a surface can be understood in terms of the DLVO model of bacterial adhesion, and the

concepts used to study the behaviour of colloidal solutions can be extrapolated to the study of living organisms. In this junction lies the setting of the present thesis: an understanding of bacterial adhesion from the physics point of view. The main goal of this thesis was to gather more information about the mechanisms of bacterial adhesion, studying the bacterial membrane by means of scanning force microscopy. To gather what was thought to be contrasting information, two very different bacteria were selected for this study: the Gram-negative *Pseudomonas* (strains 1 and 2) and the Gram positive *Rhodococcus sp.* (strains Rc92 and Rc291).

Rhodococci are thought to be hydrophobic organisms, by means of their coverage by mycolic acids, which possess long carbonated chains. This hydrophobicity is manifested through large contact angles with water, and is translated as the microbes' capacity to adhere to hydrophobic surfaces and to degrade oil and other hydrophobic pollutants. The rhodococci studied in this thesis were found in a contaminated gasworks site, where plenty of oil-derived hydrophobic nutrients are available. Rhodococci are equipped with a fine chemical armamentarium that allows them to degrade a wide variety of substances, an evolutionary advantage that makes them ideal candidates for bioremediation. The understanding of their attachment must be expanded to make the best use of these bacteria.

Pseudomonads have been the subject of many studies due to the medical importance of *P. aeruginosa*, a pathogenic organism that affects patients suffering from cystic fibrosis. Other *Pseudomonas* strains are less pernicious and have also been used in bioremediation. The strains of *Pseudomonas* used in these thesis were found in a phenol contaminated aquifer, a demonstration of their remarkable nutritional versatility. *Pseudomonas* has been used in bioremediation and in other chemical processes, such as plastic production and biocatalysis.

Given the environmental importance of the selected strains and the need to understand the basic mechanisms of bacterial adhesion, it was considered relevant to assess the heterogeneity of adhesive forces throughout the bacterial cell wall using scanning force microscopy.

## How can the bacterial cell surface be studied?

The SFM has proven to be a key element in the development of biophysics as a whole, since it is capable of studying biological samples in physiological conditions. Not only is it capable of obtaining images of microscopic entities, but also excels at extracting mechanical information about the samples. One of the parameters that can be measured using the SFM is the adhesion forces between the probe and the surface of the bacteria.

Conventional SFM experiments make use of silicon or silicon nitride cantilevers, which are adequate to sense the surface and produce high quality images in air or in media. The use of silicon cantilevers for adhesion measurements might have some drawbacks, since the silicon surface might not be chemically consistent through a number of batches. To overcome this hurdle and to gather more meaningful adhesion data, a variant of SFM, chemical force microscopy, has been devised. This technique uses chemically functionalised cantilevers to favour the preferential interaction with a particular component or region of the cell surface. To this end, silicon nitride cantilevers were coated with a thin layer of gold, which acted as a support for a self-assembled monolayer. This SAM consisted of long-chained thiol molecules: DDT which bore a methyl group in the non-thiolated end and MUA, with an acid functionality in the non-thiolated end. These groups conferred the tips a hydrophobic and a hydrophilic character, respectively. These two functionalised cantilevers, along with Au-coated and simple silicon nitride ones, were used in spatially resolved force spectroscopy experiments. The microscope was driven in the force-volume mode, which correlates the bacterial topography with the measurement of the adhesion forces. The generated maps are a visual representation of the distribution of forces throughout the bacterial cell and they are aimed at analysing the heterogeneity of forces on a particular bacterial cell. A secondary output of these maps is a collection of force-distance curves, which are analysed statistically, and their results used to compare the overall adhesion forces between bacteria belonging to different genera and species, as well as differences that arise from the use of different cantilevers.

Before the final conclusions of these experiments are presented it is important to consider other experimental aspects of this project, to present an integral picture of the whole process.

## **How are the cells grown to ensure repeatability?**

The first step in the development of this project was the growth of the bacterial samples. The cells were preserved in glycerol stocks and plated onto a solid agar medium every month. This step diminished the chances of bacterial mutation and ensured that the cells were viable for further growth protocols. The cells were then cultured in a liquid medium, namely AB10, supplemented with glucose 2 mM. AB10 was selected for being a chemically defined minimal medium (i.e. a medium in which all the chemical components are known and that contains only minimal requirements for bacterial growth); knowing the exact chemical composition of the medium reduced the possibilities of variability between batches. The bacteria were grown at 20 °C ; this low temperature was selected in order to mimic the

conditions of growth of the bacteria in their natural environments. The growth medium selection, coupled to the low temperature of incubation, made the bacteria grow in low numbers and reach their stationary phase after an extended period of time.

The bacteria were grown in a three step protocol, which was detailed in §3.3.1. The protocol was repeated for every experiment, and although long and time-consuming, it ensured that the bacteria were in the same state before SFM scanning, reducing the number of variables that need to be taken into account while studying their heterogeneity. The control over the growth parameters is very relevant, since it has been proven that bacteria change their physicochemical characteristics in response to changes in the medium composition, time of growth and culture conditions, among other factors.

## How can cells be immobilised for SFM studies?

One of the pre-requisites for bacterial imaging and force-experiments is that the organisms ought to be firmly immobilised onto a flat support. This is easily achievable when the pictures are taken in air, but can be very challenging if the measurements are to be taken under a liquid medium. The literature is rich in methodologies for the attachment of bacterial cells for SFM imaging. These methodologies encompass adhesion via electrostatic interactions, hydrophobic forces, covalent bonds and polyphenolic proteins. These methods appear to be excellent for a particular strain under given conditions, but it is apparent that they lack universality. This is only logical, as bacterial membranes are highly diverse and their attachment is closely linked to the environmental conditions.

Chapter 3 gave an ample review of the common strategies that scientists use to immobilise bacteria to surfaces for SFM experiments. Broadly, the main approaches for cell attachment can be divided into mechanical entrapment into the pores of polycarbonate membranes, the use of polycationic surfaces to adhere negatively charged cells, the use of hydrophobic surfaces to instigate the attachment of hydrophobic organisms, the formation of covalent bonds to link bacteria to substrates, and the use of polyphenolic proteins to condition surfaces in order to promote cell attachment.

Hydrophobic and electrostatic interactions proved to be reasonably good options for the attachment of the studied strains. Both methods yielded good images in air, and occasionally produced cells that withstood the lateral forces of the SFM tip under liquid, however, these methods were not optimal when working under a liquid medium.

The use of polycarbonate membranes did not have very positive results in the immobilisation of *Pseudomonas* and *Rhodococcus* since both of these genera consist of rod-shaped cells, and the majority of the pores on polycarbonate membranes can only fit spherical-shaped cells. Undoubtedly, mechanical trapping is the way forward to analyse bacterial cells with the SFM, since is the least invasive protocol to anchor cells, as it does not modify the chemistry of the bacterial surface in any manner. More effort should be made in designing ways to make the pores of membranes coalesce into rod-shaped holes or engineer grids that can accommodate bacteria. For the time being, these approaches were not available during the course of the experimental work that led to this thesis and thus, other methods of immobilisation were sought.

The use of Cell-Tak<sup>®</sup>, a mixture of polyphenolic proteins produced by the marine mussel *Mytilus edulis* was thought to be the best method to condition the surface and strongly adhere the bacteria to it. It was, however, the worst method attempted to immobilise the studied strains. Despite the literature reports [166] of the applicability of this substance to a wide variety of bacterial cells, it was not found useful for these particular bacteria and imaging conditions.

Immobilisation using polystyrene Petri dishes and polycationic coated surfaces might have been unsuccessful in yielding a high number of cells that withstood scanning in liquid medium, but had very favourable outcomes in other respects. The firm immobilisation under ambient conditions (i.e. air) produced high resolution images of the bacterial membranes, in which details of their membranes were revealed. Bacteria, like the one shown in Figure 3.34 on page 105 shows a breadth of surface features, EPS and appendages. Furthermore, pictures like this show the first stages of biofilm formation and give an insight into the way in which suspended bacteria approach a surface, condition it and colonise it, setting the foundations of a biofilm.

The methodology developed by Professor Terri Camesano's group for the immobilisation of bacterial cells through covalent bonds (EDC/NHS/APTES) proved to be the best solution to fix the bacterial cells on the present thesis. Covalent fixing allowed the acquisition of high resolution images of Pse1, Pse2, Rc92 and Rc291 under physiological conditions. This milestone was reached after many experimental attempts and opened up the possibilities to further force experiments. Using this immobilisation approach it was also possible to record a high number of force maps per experiment. A typical SFM experimental session lasted eight hours, and it was possible to find immobilised cells all throughout the course of the experiment. Often, more than 20 force maps were recorded in each session, normally two of them per cell, meaning that each bacterium was interacting with the tip for about 40 minutes. Therefore, a firm cell immobilisation was key to the development of these experiments.

The covalent linkage methodology involved the coating of silicon wafers with APTES. These substrates were prepared every two weeks to diminish the possibility of contamination or surface degeneration. These substrates were characterised using contact angle measurements and ellipsometry. Once the substrates were ready, the bacterial cells were prepared for the covalent crosslinking by mixing them with EDC and NHS and incubating them for 20 minutes. After this time lapsed, the acid groups on the bacterial surfaces were activated (as shown in Figure 3.14) and were put in contact with the aminated surface for 6 h. After this time, the samples were ready for SFM scanning.

It has been discussed [257] that this method of immobilisation does not affect the surface of the bacterial cells, since the activated acid groups, when they are unable to interact with amine groups, revert back to their original form. The creators of this immobilisation method [167] claim that it does not affect the viability of the cells and that it does not interfere with the cells' biochemical reactions. In this thesis it was found that the viability of these cells is affected to some extent, and that the more time the cells are in contact with the crosslinkers, the higher the chances they will die. Nonetheless, it was found that a proportion of the cells were alive after the treatment. A way of knowing if a particular cell that is being scanned with the SFM is alive or not, would be by coupling the scanning force microscope with a fluorescent microscope, and using differential dyes for live and dead cells.

## What were the findings of the cell mapping experiments?

Spatially resolved force measurements were acquired on *Rhodococcus* Rc92 and Rc291 and *Pseudomonas* Pse1 and Pse2 using silicon nitride, gold, DDT and MUA coated tips. Each one of these sixteen types of experiments involved the scanning of several cells per sample.

The cell area of the force-volume map was extracted using an iterative mask, a way of selecting only the force points on top of the bacterial cell surface. These force points, often more than a hundred per cell, were analysed statistically, and plotted into histograms.

The histograms turned out to be highly skewed, thus being impossible to fit them to single Gaussian functions. Several normalisation approaches were attempted, to no avail. The data were transformed using logarithms and fitted to a number of Gaussian functions using finite mixture models, an approach that

was able to model the data appropriately. The majority of the force-volume maps were fitted with two curves and the distribution of forces was similar in most cases (e.g. Figures 4.58, 4.59, 4.60, 4.61). The fits showed that the majority of the force events fell into the first Gaussian curve, which had a lower adhesion force and whose data dispersion was narrower. The minority of the data fell into the second curve, which modelled the data at higher forces. This evidently shows heterogeneity of the adhesion measurements on a cell wall. The areas of high adhesion are often clustered in regions that span through many pixels, forming a domain with a size of around 100 nm. There was no evident difference in the distribution of these domains of high adhesion when the cells were probed with each one of the four cantilevers.

The analysis of the median values of the adhesion forces of the four bacterial strains, as measured by the four cantilevers, revealed little differences between the experiments. All the analysis revealed a similar degree of heterogeneity in the force measurements, and the differences in the data within a particular experiment were often greater than the differences with other strain or species. Highly heterogeneous microbial adhesion data is nothing unheard of. Other authors have reported skewed data that does not conform to normal distributions.

Pse1 had a very similar value of adhesion when probed by the four cantilevers ( $\sim 15$  pN). Pse2, on the other hand, showed a marked preference to gold ( $\sim 36$  pN), and was less likely to have high interaction forces with the MUA tip ( $\sim 12$  pN). The same trend was observed by Rc92 ( $\sim 37$  pN with Au and  $\sim 12$  pN with MUA). The preference for these cells for the gold surface could potentially be attributed to mirror charges induced onto the gold probe by the negatively charged bacterial cells.

Rc291, although considered to be the most hydrophobic of the studied bacterial strains (as determined by its MATH score), showed no statistical difference when probed by Au, DDT and MUA cantilevers (all around 25 pN). This strain only shows low adhesion with the silicon nitride cantilever ( $\sim 14$  pN). Analogous data sets have been obtained by other authors [87], who report roughly similar adhesion values between hydrophobic and hydrophilic strains and probes (Table 4.2). Furthermore, confidence in the validity of the results presented on this thesis arises from the observation of the control experiments, between functionalised cantilevers and bare or functionalised surfaces. Such control trials proved that the tips used were indeed capable of recognising surfaces of varying chemistry.

From the observation of these values it can be concluded that the heterogeneity between bacterial cells belonging to the same sample is often greater than the differences between strains, species or experimental conditions. A comprehensive list of the possible reasons for this heterogeneity was presented in §4.6.

## What was learnt from the DNA adhesion studies?

The study of *Pseudomonas* was also centred in the extra-cellular polymeric substances that they produce. It has been proven that eDNA is involved in the biofilm formation process of several *Pseudomonas* species but the way this polymer enhances bacterial adhesion remains poorly understood. Hence it was considered relevant to study the adhesion of DNA to surfaces. Many elegant techniques have been devised to study the behaviour of single polymer molecules when stretched or adhered to surfaces. Among them, the use of optical and magnetic tweezers, as well as the SFM were reviewed. Force spectroscopy has been used to study a variety of polymers, including DNA. All the experiments that were found in the literature, using either tweezers or SFM, have the molecule firmly anchored to two surfaces, and its extension is measured in terms of the applied force and loading rate. Very little information was found about the measurement of the detachment forces of DNA from solid surfaces.

In the experiment that we devised, a very diluted solution of thiolated DNA was put in contact with a gold surface. A low concentration was needed in order to obtain single molecule stretching, a condition that would suppress lateral interactions between neighbouring DNA chains, since this entanglement could complicate the system. A small number of these chains were chemisorbed onto the SFM cantilever, by virtue of the low concentration and the low adsorption time. The adsorption of the DNA onto the cantilever modified its behaviour during force-pulling experiments: before the tip was functionalised only unspecific adhesion events could be seen, whereas after the functionalisation, a proportion of the events showed specific adhesion events as well. This is indicative that the DNA molecule was in the region between the apex of the tip and the substrate, and that upon retraction of the tip the molecule had a bonding interaction with the surface. The surface was a silicon wafer (with a native top layer of  $\text{SiO}_2$ , which has a negatively charged surface by virtue of the oxygen atoms on the surface). DNA is a negatively charged polymer due to the oxygen atoms on the phosphate groups.

The frequency in which the specific interactions were seen increased with the addition of ions to the solution. Molecular simulations revealed that the calcium ions act as a bridge between the oxygen atoms on the DNA phosphates and the oxygen atoms on the silica. This allows a larger interaction between the two entities. Sodium on the other hand, was calculated to play a very minor role as a bridge between these two negative moieties. The adhesive interaction between a DNA molecule and a silicon surface under a sodium solution (and presumably in water too) arises from the direct interaction between the phosphate groups and the silicon atoms on the surface.

The number of specific adhesion events when the system was in sodium was slightly higher than in calcium, perhaps due to the enthalpic gain that the polymer in the former conditions gets when interacting with the silicon. It was hypothesised that there is a higher energy barrier to adhesion of DNA to silicon under a calcium solution, this translates to a higher interaction force between the polymer and the surface upon retraction. This idea was corroborated by experimental data in which higher adhesion forces were detected for the system under calcium, particularly when the concentration was at its highest (i.e. 10 mM).

Common models of polymer elasticity (FJC, WLC) were applied to the data in order to fit the retraction curve profiles. This approach was not altogether successful, since the persistence length is underestimated by the WLC model. The persistence length is an indicator of the flexibility of the molecule, and low values of this parameter are associated with very flexible polymers. Double-stranded DNA is stiff by virtue of the rigidity imposed by the double helix and it has been calculated that its persistence length is around 20-50 nm. The calculated persistence lengths were considerably lower than this value. The reasons for the inability of the WLC model to fit our data were discussed, one of them being the difference in our experimental approach. It is important to notice that although the DNA molecule is firmly anchored to the tip via the Au-S bond, the interaction between the DNA and the surface is feeble, rendering the experiment different from the typical stretching protocol found in the literature. Furthermore, the data obtained might be the product of the interaction of more than one DNA strand, a fact that can complicate the data analysis and cause deviations from the ideal WLC fits.

The results obtained during the SMFS part of this thesis are bridging the gap between the observations made on the macroscopic scale and the behaviour of individual atoms in the nanoscale. eDNA has been proven to be involved in the mechanism of biofilm formation in *Pse1* through diverse attachment assays. Moreover it has been seen that the addition of calcium promotes the attachment of cells at certain concentrations. The nature of the interactions between DNA and solid surfaces has been investigated further, and a considerable increase in the adhesion force between a DNA strand and a silica surface was seen when the SMFS experiment took place under a calcium solution at a concentration of 10 mM. Theoretical approaches support these results, as it was seen that there is a substantial energy barrier for the attachment and detachment of DNA to solid surfaces in the presence of calcium ions. In this respect, the experimental results gathered by our research group span over three levels: macroscopic observation on whole bacterial cells, study of the attachment of a discrete number of DNA molecules, and molecular simulations of the behaviour of the individual atoms that conform this system. This multidisciplinary approach points toward the same

conclusion: eDNA is involved in the biofilm formation process of Pse1, which is mediated by divalent cations.

## 6.1 Future work

The project presented in this thesis constitutes a systematic approach in which Gram positive and Gram negative organisms are compared. It contributes to the body of knowledge of bacterial adhesion, since it deals with bacterial strains with different cell envelopes and attachment strategies. Such direct comparisons were found to be rare in the literature, since these entail a tremendous amount of work. The frontal comparison between hydrophobic and hydrophilic probes remains relevant, since these are model molecules with interactions that are very clearly understood (see Figure 4.63). Additionally, there is plenty of compelling evidence that the hydrophobic effect is one of the main driving forces for bacterial attachment [358] and consequently the detection of hydrophobic and hydrophilic regions within a cell can shed light into the way in which bacteria adhere.

The present work contributes to the current understanding of bacterial adhesion by describing the data using strong statistical models. Future work will take this project beyond the descriptive stage and dwell on the chemical principles behind bacterial heterogeneity. Even though biologists are perfectly aware of the presence of distinct macromolecules on the cell substrate, it is still unclear which relationship they bear with the adhesive properties measured by SFM.

To that end, higher specificity in the SFM cantilevers is needed, to unequivocally probe specific components on the cell wall (e.g. lectin-decorated cantilevers to measure interaction forces with carbohydrates). It is envisaged that in the near future, an adhesive map will become a *chemical map*, where the localisation of regions rich in a particular component are known. An ideal breakthrough of chemical mapping will see multiple cantilevers with distinct chemical functionalities interacting with the *same* cell either simultaneously, or in close succession, to map the distribution of chemical groups in real time.

Better resolution on the cell wall is needed in order to perform a better correlation between morphology and composition, and eventually between morphology and function. With the fast paced evolution of single-molecule force spectroscopy and the advent of new techniques such as Peak-Force tapping [359], we are closer every day to reaching these goals. The latter technique allows the acquisition of high resolution images with a minimal applied force and also permits the collection of adhesion and nano-mechanical parameters coupled to high-resolution height maps. In other words, super-resolution force-volume mapping is available now in facilities all over the world, including this University.

Ana Lorena Morales-García

The field of bacterial biophysics is in dire need of standardisation methods and the establishment of conventions. For the measurement of adhesion force on bacterial cells, it would be useful if the analysis were done using comparable immobilisation techniques, scanning parameters and analysis protocols in order to compare directly the attachment of strains with data proceeding from different research groups. An effort of this nature would allow researchers to sort bacteria according to their adhesive properties and to build a knowledge database that would help us to enhance our predictive skills of bacterial adhesion to surfaces.

Much effort has been placed in understanding the mechanisms of bacterial adhesion. In the view of the impending threat of antibiotic resistance, which could potentially take us to a new era of microbe-induced morbidity and mortality similar to pre-antibiotic times, it is imperative to design new methods to prevent bacterial infection. For instance, recently (May 2014) de la Fuente-Núñez *et al.* [360] reported the efficacy of small peptides against biofilm formation in Gram positive and negative species. These peptides appear to inhibit signalling nucleotides, which are produced under conditions of stress. It is perhaps by preventing the adhesion of bacteria in the first place that we will be able to deal with threatening diseases, and thus the study of bacterial attachment should remain a central topic in biophysics.

## Final remarks

The study of bacterial adhesion and biomolecule interactions through SFM is gaining popularity among the scientific community, due to the increasing presence of this microscope in laboratories around the world. Additionally, it is becoming increasingly evident that the SFM has the potential of studying bacteria in a way that was not possible before: alive and in physiological conditions. Notwithstanding the resources availability and the keen interest of the scientific community, certain issues still need to be solved in order to establish universal protocols for these studies. These topics include a reliable method of bacterial immobilisation, adequate probe characterisation, reduction of noise in the measurements and seamless and widespread integration of the SFM to other techniques, such as fluorescent or confocal microscopy, to name a few.

This PhD thesis has increased the current knowledge database of the nature of bacterial adhesion of diverse strains and has presented a different approach to the analysis of force data, using finite mixture models, which has not been reported in the literature as a way to treat microbial adhesion data.

Other key contribution of the present PhD thesis is the pursuit of the link between macroscopic adhesion experiments with molecular simulations. SFM approaches bridge the gap between these two subjects and reinforce the knowledge obtained through dissimilar approaches. Hopefully, this research has contributed to the understanding of biological systems, through the analysis of probabilistic microbial entities, applying concepts that physical sciences designed for deterministic and less complex systems.

## Appendix A: Cell viability experiments

3.6  $\mu\text{L}$  of SYTO9 3.34 mM and 3  $\mu\text{L}$  of propidium iodide 20 mM were combined into 1 mL of phosphate buffer pH 7.1, to obtain final concentration of 12  $\mu\text{M}$  and 60  $\mu\text{M}$  respectively. The mixture was kept protected from light. 10  $\mu\text{L}$  of the dye mixture was added for each mL of cell suspension. The dyes were left to incubate for 10 minutes, before measuring 10  $\mu\text{L}$  of the stained cell suspension and putting it on a microscope slide, and covering it with a coverslip. The samples were analysed with an Olympus microscope (Olympus BX50W1, Olympus Optical Ltd., Watford, UK) equipped with SWB (super-wide band) and WB (wide band) filters. The first one allows a visualisation of the fluorescence of the green and red channels (i.e. alive and dead cells), whereas the second one only allows the visualisation of the red fluorescence. Representative images were captured using the CellB imaging software (Olympus Optical Ltd., Watford, UK).

Figure 6.1 shows the state of the cells after 6 hours of treatment with EDC and NHS. Figures 6.2 and 6.3 shows the viability of cells that have not been treated after 3 and 6 h., respectively. All the pictures shown were acquired through the SWB filter cube, and thus show both dead and alive cells.

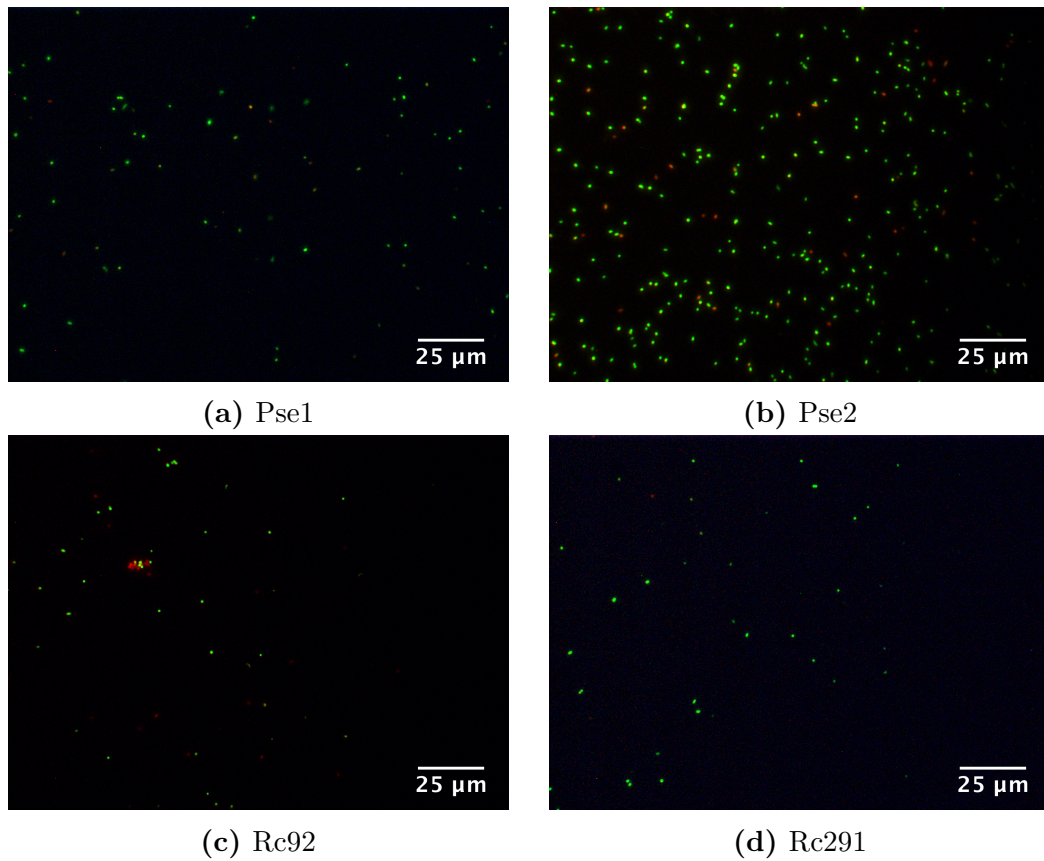


**Figure 6.1:** Bacterial cells after being treated with EDC/NHS, after 6 h of incubation. The cells were stained with BacLight<sup>®</sup>.

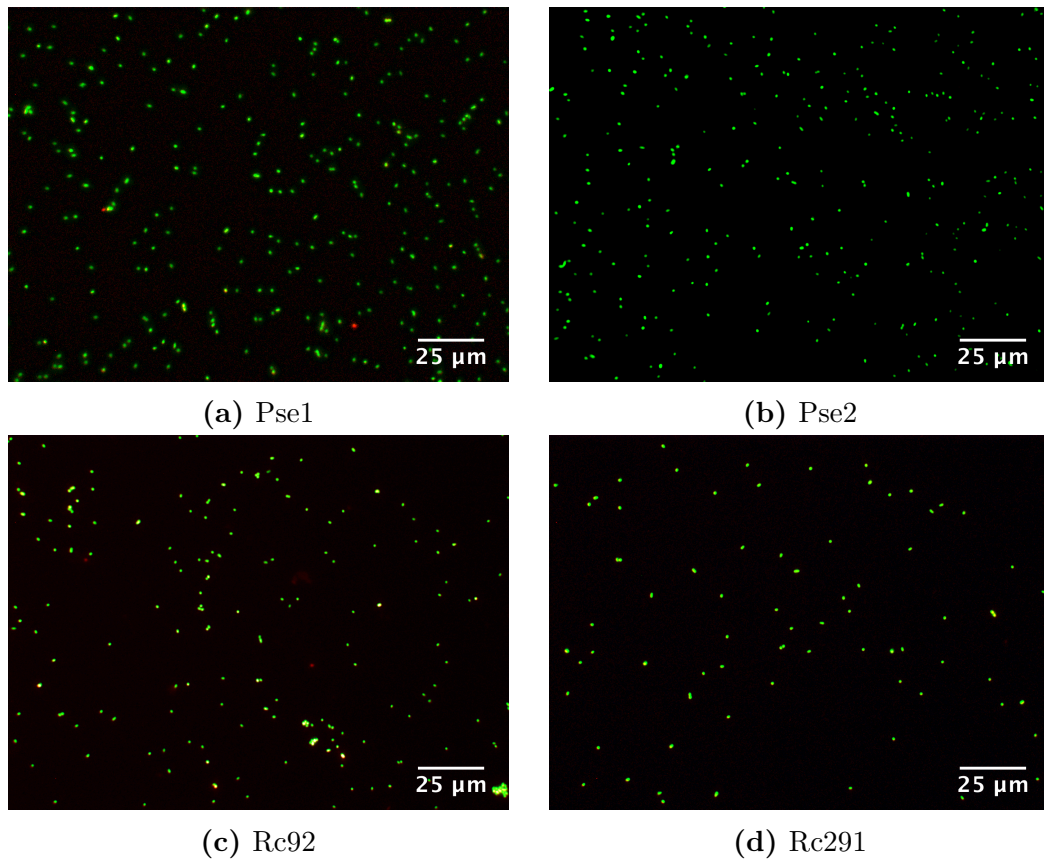


**Figure 6.2:** Bacterial cells without treatment, after 3 h of incubation. The cells were stained with BacLight®.

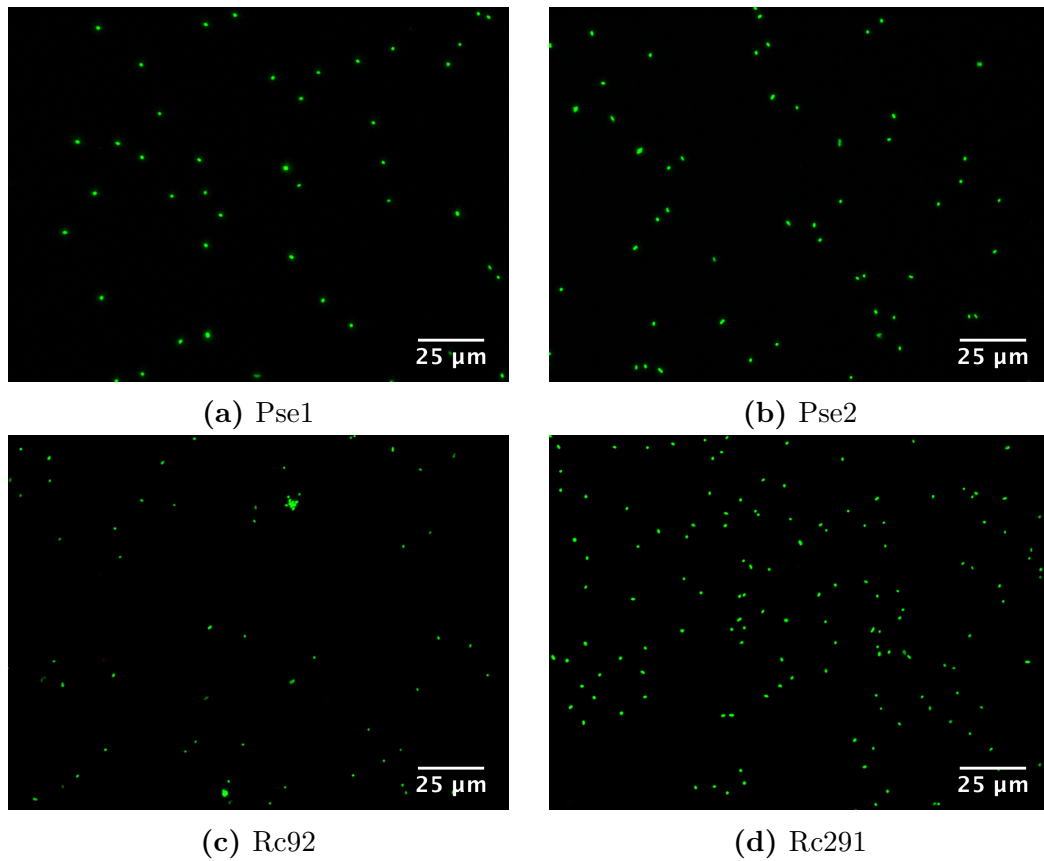


**Figure 6.3:** Bacterial cells without treatment, after 6 h of incubation. The cells were stained with BacLight®.

## Appendix B: Force-volume maps

The following force-volume maps are selected examples of Pse2 (Figure 6.4), Rc92 (Figure 6.5) and Rc291 (Figure 6.6) bacterial cells probed with 4 different types of cantilevers:  $\text{Si}_3\text{N}_4$ , Au, DDT and MUA. The maps associated to the experiments involving Pse1 and the four different cantilevers was presented in §4.4. The experimental protocols related to the acquisition of these maps has already been detailed in Chapter 4.

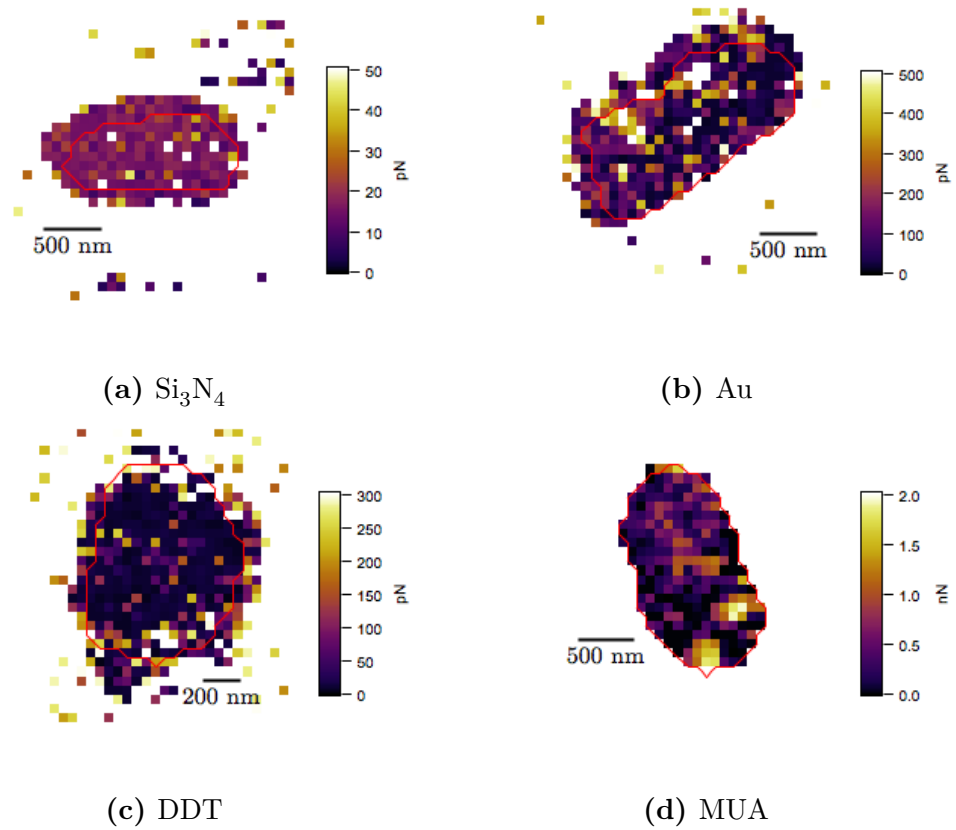


**Figure 6.4:** Force-volume maps of Pse2, imaged with 4 different cantilevers, under MOPS 20 mM.

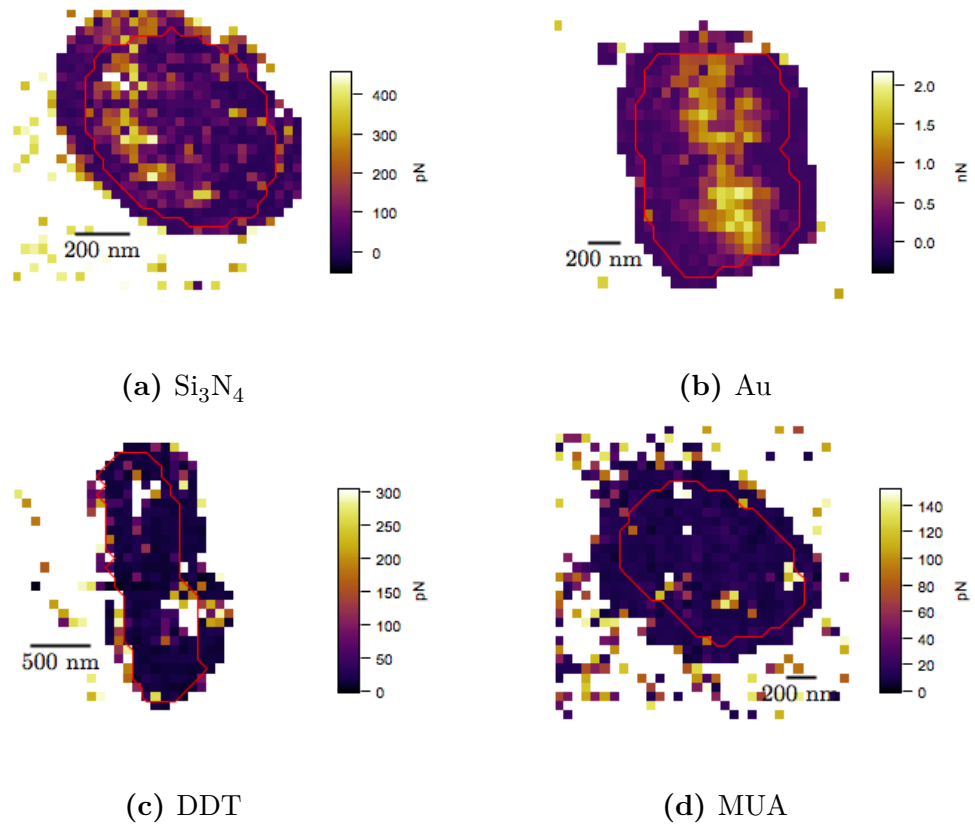


**Figure 6.5:** Force-volume maps of Rc92, imaged with 4 different cantilevers, under MOPS 20 mM.

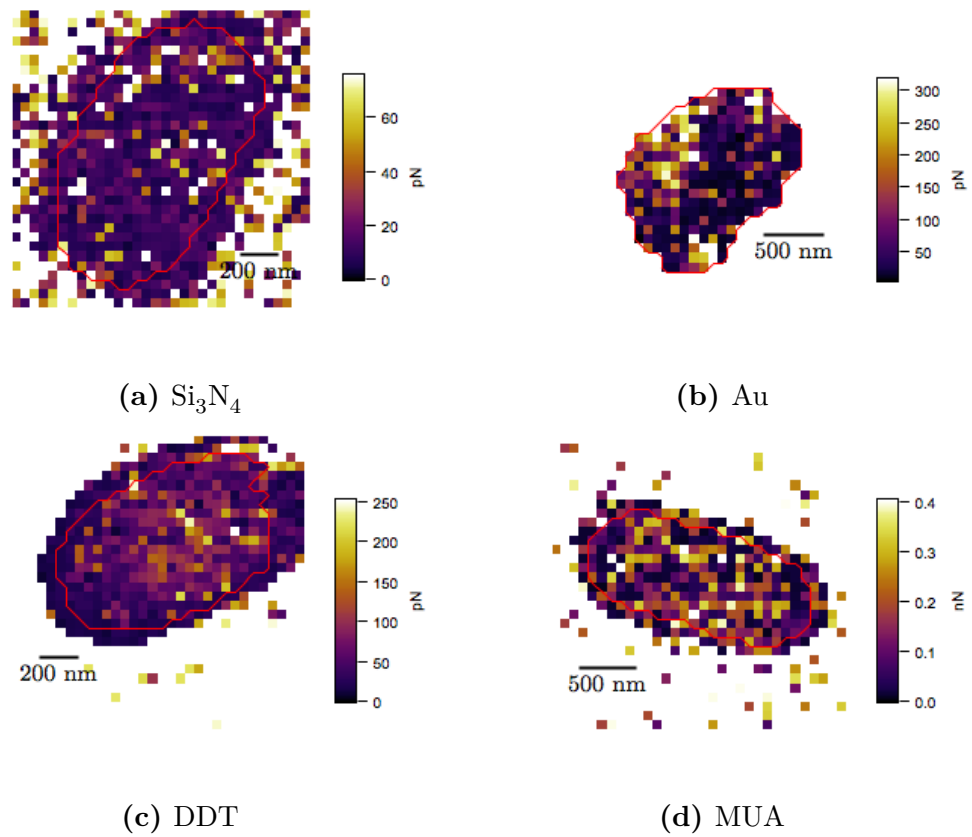


**Figure 6.6:** Force-volume maps of Rc291, imaged with 4 different cantilevers, under MOPS 20 mM.

## Appendix C: R code for bimodal fits

The following code was employed to fit the distribution of adhesion forces using finite mixture models. This code was written by Dr Stephen Rolfe.

```
#load the mixmodel package
library("mixtools")

#functions needed for various actions

pnormmix <- function(x,mixture) {
  lambda <- mixture$lambda
  k <- length(lambda)
  pnorm.from.mix <- function(x,component) {
    lambda[component]*pnorm(x,mean=mixture$mu[component],
                           sd=mixture$sigma[component])
  }
  pnorms <- sapply(1:k,pnorm.from.mix,x=x)
  return(rowSums(pnorms))
}

plot.normal.components <- function(mixture,component.number,...) {
  curve(mixture$lambda[component.number] *
        dnorm(x,mean=mixture$mu[component.number],
              sd=mixture$sigma[component.number]), add=TRUE, ...)
}
```

```
dnormalmix <- function(x,mixture,log=FALSE) {
  lambda <- mixture$lambda
  k <- length(lambda)
  # Calculate share of likelihood for all data for one component
  like.component <- function(x,component) {
    lambda[component]*dnorm(x,mean=mixture$mu[component],
                           sd=mixture$sigma[component])
  }
  # Create array with likelihood shares from all components
  over all data
  likes <- sapply(1:k,like.component,x=x)
  # Add up contributions from components
  d <- rowSums(likes)
  if (log) {
    d <- log(d)
  }
  return(d)
}

# Log likelihood function for a Gaussian mixture, potentially
on new data
loglike.normalmix <- function(x,mixture) {
  loglike <- dnormalmix(x,mixture,log=TRUE)
  return(sum(loglike))
}

#do the probability calculation
probCalc<-function(f){
  n <- length(f)
  data.points <- 1:n
  data.points <- sample(data.points) # Permute randomly
  train <- data.points[1:floor(n/2)] # First random half is training
  test <- data.points[-(1:floor(n/2))] # 2nd random half is testing
  candidate.component.numbers <- 2:5
  loglikes <- vector(length=1+length(candidate.component.numbers))
  # k=1 needs special handling
  mu<-mean(f[train]) # MLE of mean
  sigma <- sd(f[train])*sqrt((n-1)/n) # MLE of standard deviation
  loglikes[1] <- sum(dnorm(f[test],mu,sigma,log=TRUE))
  for (k in candidate.component.numbers) {
```

```
mixture <- normalmixEM(f[train],k=k,maxit=400,epsilon=1e-2)
loglikes[k] <- loglike.normalmix(f[test],mixture=mixture)
}
plot(x=1:5, y=loglikes,xlab="Number of mixture components",
      ylab="Log-likelihood on testing data")
}
#end of the functions needed

#load in the data
#set the working directory first and change the filename

data<-as.matrix(read.table("MINITAB.CSV",sep=" ",head=TRUE))

#here are a series of functions to allow things to be checked

#function viewHist(col,dataset) displays the histogram
and CDF of the column in the dataset

viewHist<-function(dataset,col){
  cnames<-colnames(data)
  ind<-is.na(dataset[,col])
  f<-dataset[!ind,col]
  plot.new()
  par(mfrow=c(2,2))
  hist(f,main=cnames[col])
  ef<-ecdf(f)
  plot(ef)
  probCalc(f)
}

calcHist<-function(dataset,col,k){
  cnames<-colnames(data)
  ind<-is.na(dataset[,col])
  f<-dataset[!ind,col]
  plot.new()
  par(mfrow=c(2,2))
  mixmdl = normalmixEM(f,k=k)
```

```
plot(mixmdl,which=2,main2=c(cnames[col]))
title<-c("lambda","mu","sigma")
print(mixmdl[title])
ef<-ecdf(f)
plot(ef)
#Distinct values in the data
distinct.f <- sort(unique(f))
# Theoretical CDF evaluated at each distinct value
tcdfs <- pnormmix(distinct.f,mixture=mixmdl)
# Empirical CDF evaluated at each distinct value
  # ecdf(f) returns an object which is a _function_,
  suitable for application
  # to new vectors
ecdfs <- ecdf(f)(distinct.f)
# Plot them against each other
plot(tcdfs,ecdfs,xlab="Theoretical CDF",ylab="Empirical CDF",xlim=c(0,1),
      ylim=c(0,1))
# Main diagonal for visual reference
abline(0,1)
return(mixmdl)
}

viewHist(data,1)

calcHist(data,1,2)
```

## Appendix D: Influence of preparation protocols on bacterial surface properties

In §2.2.2 and §2.2.3 the production of extracellular polymeric substances (EPS) by members of the *Rhodococcus* and *Pseudomonas* genus was reviewed. Since the EPS constitute the outermost layer of the bacterial cell, it is imperative to study the properties of these polymers in order to understand the mechanisms of bacterial adhesion to surfaces.

Many different assays have been developed with the aim of assessing bacterial properties, including MATH measurements, SFM experiments, electron microscopy, electrophoretic mobility and other forms of spectroscopy. Many of these techniques share in common the bacterial preparation methods: normally the bacteria grow in liquid nutrient broths, which have to be eliminated in order to simplify the analysis. These growth media often contain dozens of chemical components as well as cell debris accumulated during the incubation time. It is a common practice to wash the cells and resuspend them in a buffer or water before performing any other experiments. Marshall *et al.* [15] speculated about the dangers of using these widespread methodologies and suggested that they could be modifying the bacterial cell surfaces in such a way that the information extracted from them during the experiments could not be compared to the actual behaviour in natural environments. The washing techniques could be too harsh on the exo-polymers, which could be modified or removed from the bacterial surface. Pembrey *et al.* [14] have conducted methodical experiments in which they investigate the influence of resuspension medium, centrifugation speed and air-drying, among other parameters, on the attachment efficiency of a number of bacterial strains. They assessed the changes in hydrophobicity, viability and electrophoretic mobility as a func-

tion of the medium of re-suspension: water or NaCl 0.4 M. This is based on the assumption that cells might behave differently in a low-salt concentration than in a high-salt concentration, situation that could induce a conformational change in the cell envelope, cellular collapse or adsorption of ions on the cell surface. The researchers found that the measured properties varied significantly depending on the buffer into which the cells were re-suspended. The biggest changes were recorded when the cells were washed with water after having been washed with the saline solution. It was also shown that the speed of centrifugation also affected, to some extent, the measured properties. These changes are highly dependent on the investigated strain, thus, making it difficult to generalise their behaviour. The authors conclude that one must be careful while interpreting hydrophobicity and electrophoretic mobility studies with natural processes. One must ascertain that the preparation protocols do not significantly affect the nature of the cell walls.

With this in mind, it was decided to evaluate the effect on the suspension medium and centrifugation speed on the hydrophobicity of bacteria. Rc291 was selected for a pilot test, that involved measuring the contact angle of water droplets on bacterial lawns.

## Experimental protocols and results

Rc291 cells were incubated for 6 or 36 h in 50 mL of LB Broth (Sigma, Dorset, UK) at 25 °C, on an orbital shaker. After the incubation time, batches of 7 mL were prepared under different conditions

- **Unwashed:** The cells were pipetted out from the growth medium and received no further treatment.
- **Mild wash:** The cells were concentrated in 15 mL centrifuge tube at 1200  $g_n$  (MSE Centaur 2, MSE Ltd. London, England) for 10 minutes. The resultant pellet was re-suspended in 7 mL of PBS and washed two times with this buffer.
- **PBS:** The pellet was resuspended in 1 mL of PBS and washed three times through 2-minute centrifugation cycles at 12,100  $g_n$ .
- **Water:** The pellet was resuspended in 1 mL PBS and washed three times through 2-minute centrifugation cycles at 12,100  $g_n$ . Then it was resuspended in water and washed three times.

The cells were then filtered using a Millipore glass microanalysis filter holder with fritted glass, a vacuum pump and Isopore polycarbonate membrane filters,

0.2  $\mu\text{m}$ , GTTP (Merck Millipore, MA USA). The vacuum was kept on until the bacterial lawns were reasonably dry. The filters were left to dry further inside Petri dishes with filter paper bottoms for 30 min. The contact angle measurements were acquired with the static sessile method using distilled water and measured with a Theta optical tensiometer (Attension, Biolin Scientific, Espoo, Finland). The results of the contact angle measurements are shown in Figure 6.7.

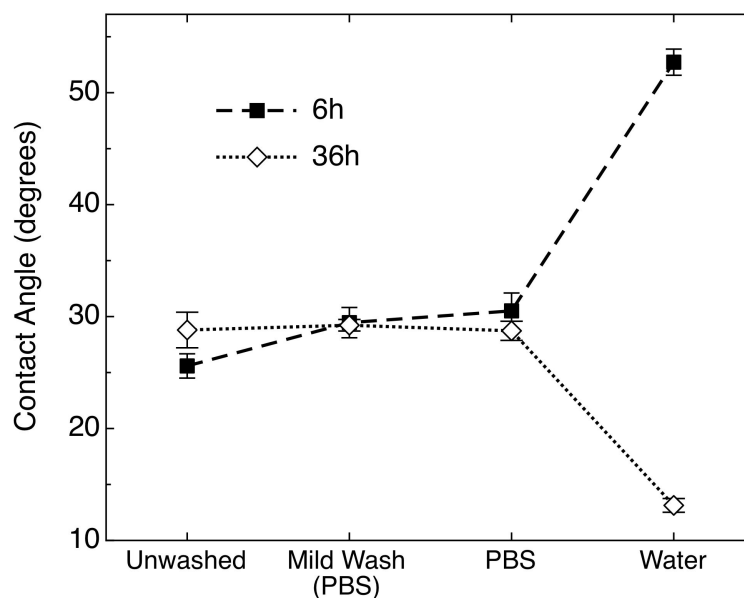


**Figure 6.7:** Contact angle measurements as a function of the washing protocol. The plotted results are the averages of 300 measurements taken by the high speed camera mounted on the goniometer. Three samples were measured for each condition. These data were analysed and plotted by Dr Matthew Mears.

In Figure 6.7 it can be seen that for cells grown either for 6 or 36 h, the speed of centrifugation with PBS has very little effect on their contact angle value as compared to the un-washed control (a contact angle of  $\sim 30^\circ$  was measured under the three conditions). The fact that the bacterial lawns have a similar contact angle has led to conclude that the nature of the surface of the bacterial cells has not been modified through the washing protocol. In contrast, when the cells are washed a further three times in water, the value of the contact angle is substantially modified.

In order to assess if the change in contact angle is due to the nature of the washing medium or the number of centrifugation cycles, a second experiment was performed. Rc291 cells were incubated for 6, 24 or 36 h in 50 mL of LB Broth (Sigma, Dorset, UK) at  $25^\circ\text{C}$ , on an orbital shaker. After the incubation time,

batches of 7 mL were concentrated at 1200  $g_n$  for 10 minutes. The pellets then were resuspended in PBS and washed either 7 times in 1 mL PBS or 3 times in 1 mL PBS and 3 times in 1 mL water, or 3 times in 1 mL PBS and 3 times in 1 mL water and 1 time in 1 mL of PBS with centrifugation at 12,100  $g_n$  for 2 minutes in each cycle. The cells were then filtered using a Millipore glass microanalysis filter holder with fritted glass, a vacuum pump and Isopore polycarbonate membrane filters, 0.2  $\mu$ m, GTTP (Merck Millipore, MA USA). The vacuum was kept on until the bacterial lawns were reasonably dry. The filters were left to dry further inside Petri dishes with filter paper bottoms for 30 min. The contact angle measurements were acquired with the static sessile method using distilled water and measured with a Theta optical tensiometer (Attension, Biolin Scientific, Espoo, Finland). The results of these measurements are depicted in Figure 6.8. In this second experiment

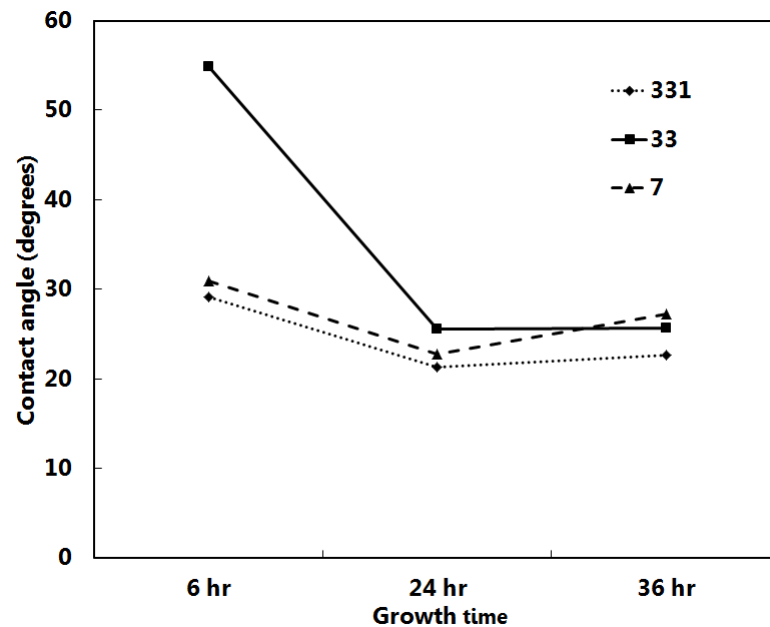


**Figure 6.8:** Contact angle measurements as a function of the washing protocol. These data were analysed and plotted by Dr Matthew Mears.

it can be seen that the contact angle remains at approximately 20-30° for the majority of the washing protocols. The only exception is again the PBS/Water treatment for the 6 h growth. Like in Figure 6.7 the contact angle for this set of experiments surpasses the 50° mark. It has been hypothesised that in the early stages of growth the cells are more sensitive to the washing conditions, and by washing them and re-suspending them in water an increase in hydrophobicity is caused.

## Appendix E: Growth curves

It is the nature of bacteria in general, to propagate effectively when put into a nutritive media with adequate concentrations of oxygen and ions and at a suitable temperature. Under these conditions, cells will divide or double at a specific rate and the growth can be described by:

$$N = N_0 e^{\mu t}, \quad (6.1)$$

where  $N$  is the number of cells after a division event,  $N_0$  is the initial number of cells in the culture,  $t$  is the time and  $\mu$  is a constant termed *growth rate* that comes from the division of  $\ln 2$  over the doubling time.

From this equation we can get a plot that relates  $N$  versus  $t$ . Experimentally it is not possible to determine  $N$  by counting all the cells. To overcome this issue, aliquots of the culture must be taken and the number of cells must be determined by indirect means. One of these methods involves the measurement of the cell concentration (density) using a spectrophotometer. The optical density (OD), or turbidity, will be proportional to the concentration of cells in the aliquot and a time versus OD curve can be plotted. A growth curve will look like the one shown in Figure 6.9.

The plot is not a perfect straight line because the cells do not grow with the same  $\mu$  all the time. During the *initial or lag phase*, they must first recognise their environment, express their genes and synthesise the substances that they will need to proliferate. In the exponential phase, the cells grow with the optimal  $\mu$  for some time and by the end of this phase the growth rate decreases, as new genes become operative, thus making the cells enter a stable phase where the population remains constant. During the stationary phase the cells stop growing due to the depletion

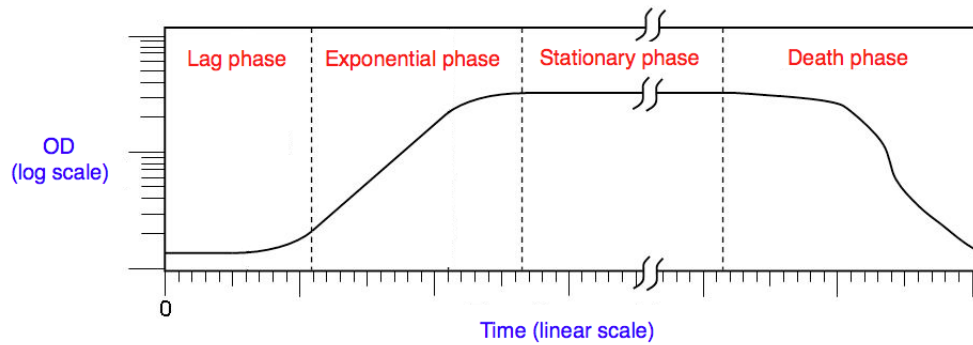


**Figure 6.9:** Typical bacterial growth curve appearance.

of nutrients and accumulation of waste products. Finally, if the environment that holds the bacteria does not provide means for the perfusion of toxic substances out and the introduction of fresh nutrients into the media, then the cells will eventually die and the decrease in members will be reflected as a decay in the OD, as shown in the final phase of Figure 6.9.

To ensure the repeatability of any experiment that we attempt it is vital to harvest the cells at the same point of the growth curve, since bacteria vary chemically and physiologically with time. The ideal time to harvest is generally the late exponential phase or early stationary phase because at this time the cells are in high concentration, the nutrients have not been depleted and the amount of excreted substances is minimal. Other variables that remain constant at this point are the volume, density and cell wall composition.

The growth curves were plotted from three bacterial cultures grown simultaneously. The samples were prepared and incubated as it was stated in §3.3.1 in page 86.

The vertical line in the following four graphs indicates the usual time of harvest. The exponential phase can be clearly seen approximately from 8-18 h after incubation. The stationary phase in this case is shown as an interval of slowed growth. The death phase cannot be appreciated in these plots (Figures 6.10, 6.11, 6.12 and 6.13).

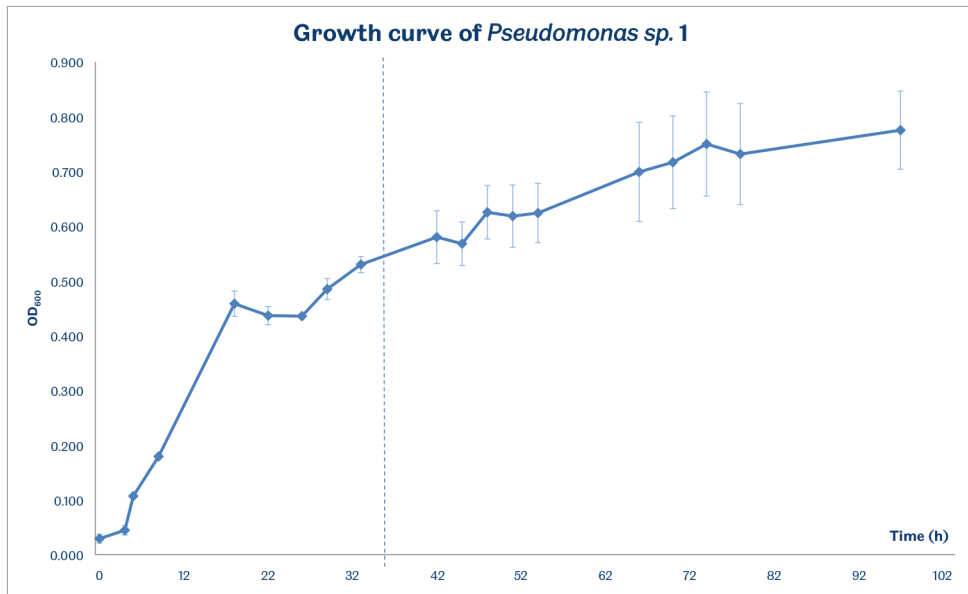


**Figure 6.10:** Growth curve of *Pseudomonas* Pse1 in AB10 media at 20°C. The data points are the average of three measurements.

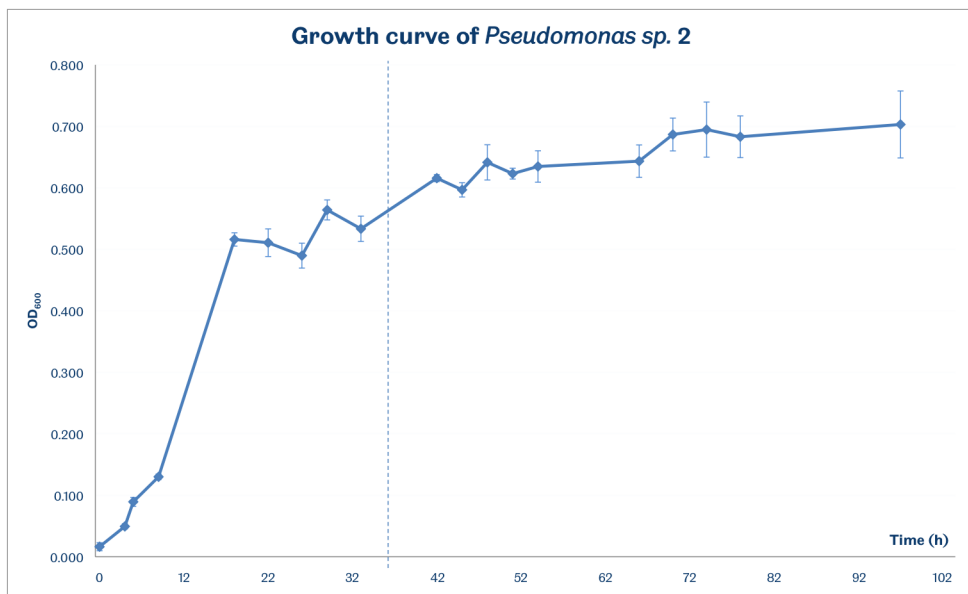


**Figure 6.11:** Growth curve of *Pseudomonas* Pse2 in AB10 media at 20°C. The data points are the average of three measurements.

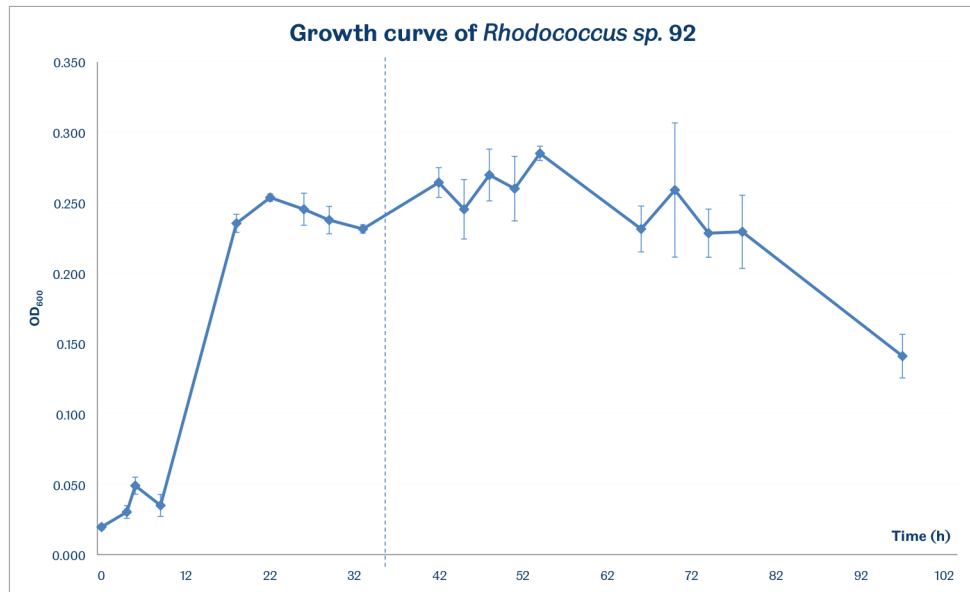


**Figure 6.12:** Growth curve of *Rhodococcus Rc92* in AB10 media at 20°C. The data points are the average of three measurements.

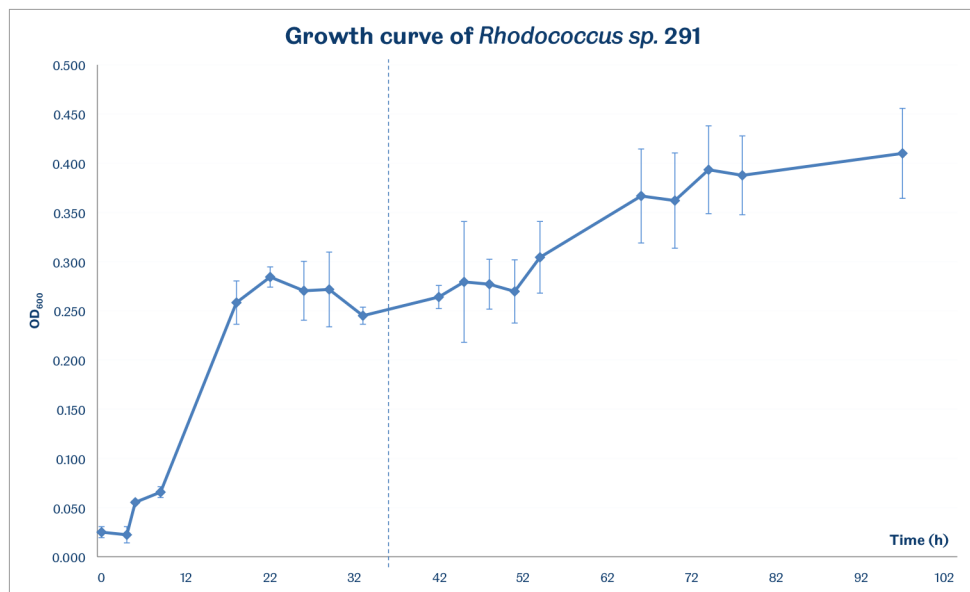


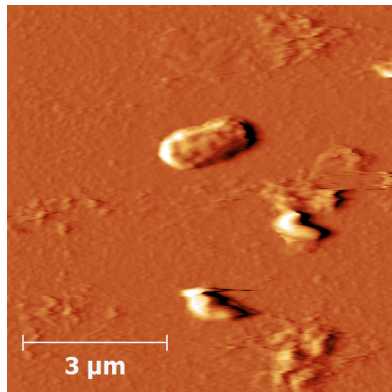
**Figure 6.13:** Growth curve of *Rhodococcus Rc291* in AB10 media at 20°C. The data points are the average of three measurements.

## Appendix F: Miscellaneous force-mapping experiments

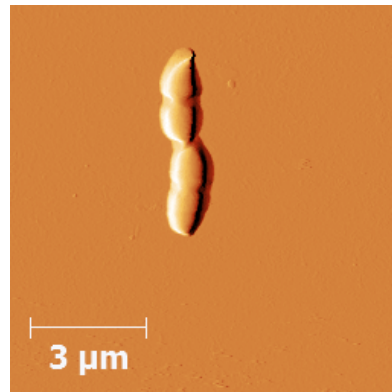
It is clear that the distribution of adhesion forces and their average magnitude is not circumscribed to the adhesion method or to the instrument used. In this Appendix, a different type of experiment is described, whose results support this idea.

Rc291 cells were immobilised onto a PEI coated glass following the methodology described in §3.3.4. A picture of such cells is shown in Figure 6.14. A series of 100 force-distance curves were acquired over 6 different points of the upper cell in Figure 6.14b. The measurements were taken under water using an MLTC probe, using the cantilever with a nominal value 0.01 N/m of spring constant. The experiment was performed on the Dimension 3100 system (Nanoscope IV, Digital Instruments, NY, USA). The data were analysed using the Carpick's toolbox routine on Matlab [361]. The results from such analysis are summarised in Figure 6.15.

This plot comprises six adhesion force histograms from a Rc291 adhered to a PEI surface in water. The distribution, however, looks remarkably similar to the one in which the cells are attached to a surface via the APTES/EDC/NHS chemistry under MOPS 20 mM. A more comprehensive study is needed to ascertain the validity of this claim.



(a) Rc291 attached to PEI.  
Imaged in water.  
The height scale is 300 nm.



(b) Rc291 attached to PEI.  
Imaged in water.  
The height scale is 700 nm.

**Figure 6.14:** *Rhodococcus* 291 imaged with a  $\text{Si}_3\text{N}_4$  tip, with a 0.01 N/m cantilever. Several sets of force-distance curves were acquired on these cells.

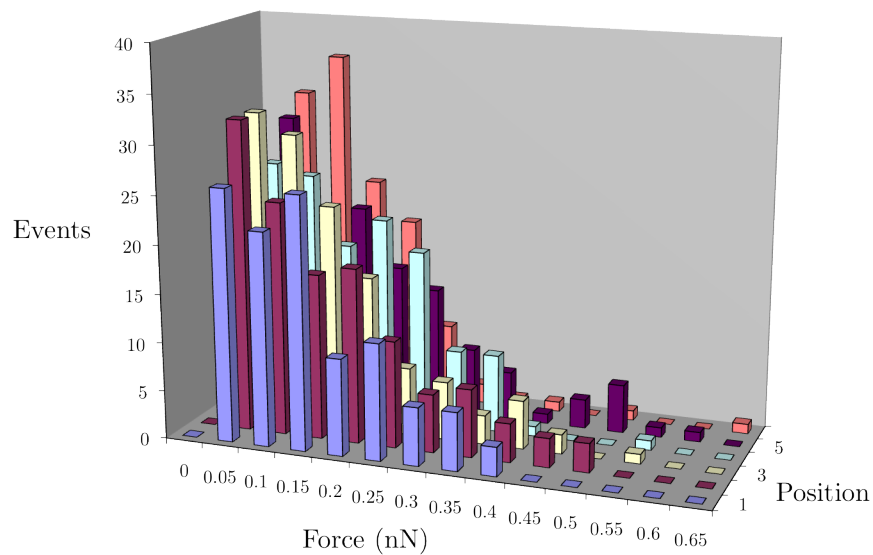


**Figure 6.15:** Histogram of the adhesion forces in 6 regions of a Rc291 cell. Forces taken in water using a 0.01 N/m cantilever.

## Appendix G: SFM images of adhesion surfaces

In this section, SFM deflection images of the substrates used for bacterial immobilisation are presented. The PEI surface (Figure 6.16) was prepared as detailed in §3.3.4, on page 100. The APTES surface (Figure 6.17) was prepared as in 3.3.4 on page 97.

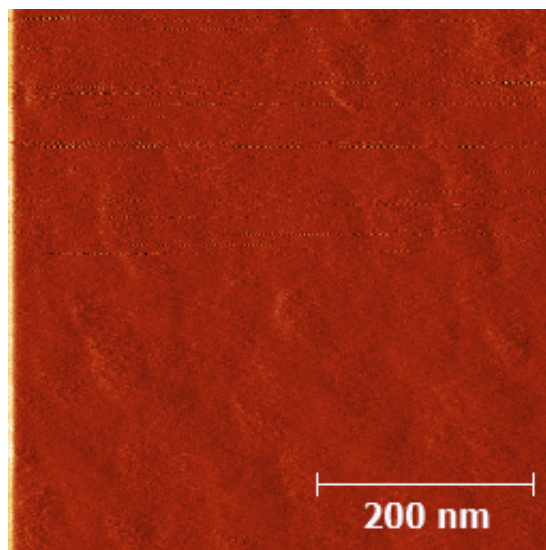


**Figure 6.16:** PEI surface. Imaged in contact mode, in air. 0.01 N/m cantilever.

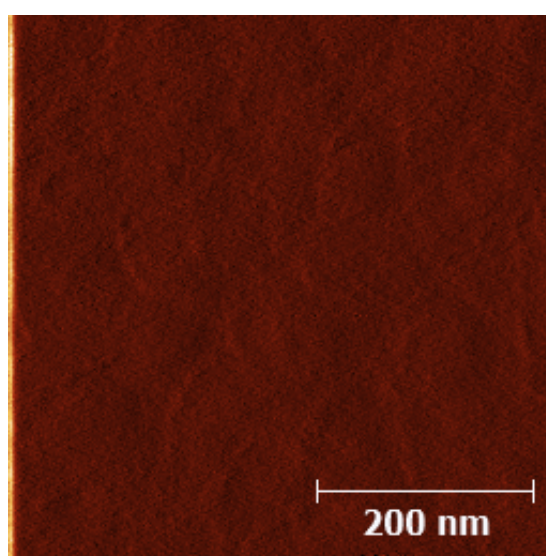


**Figure 6.17:** APTES surface. Imaged in intermittent contact mode, under MOPS 20 mM using a 0.03 N/m cantilever.

## Bibliography

- [1] S. G. Amyes, *Bacteria: A very short introduction*. Gosport, Great Britain: Oxford University Press, 1st ed., 2013.
- [2] J. T. O'Malley-James, J. S. Greaves, J. A. Raven, and C. S. Cockell, "Swan-song biospheres: refuges for life and novel microbial biospheres on terrestrial planets near the end of their habitable lifetimes," *Int. J. Astrobiol.*, vol. 12, no. 02, pp. 99–112, 2012. [http://www.journals.cambridge.org/abstract\\_S147355041200047X](http://www.journals.cambridge.org/abstract_S147355041200047X).
- [3] N. I. Abu-Lail and T. A. Camesano, "Role of lipopolysaccharides in the adhesion, retention, and transport of *Escherichia coli* JM109.," *Environ. Sci. Technol.*, vol. 37, no. 10, pp. 2173–83, 2003. <http://www.ncbi.nlm.nih.gov/pubmed/12785523>.
- [4] M. E. Cortés, J. C. Bonilla, and R. D. Sinisterra, "Biofilm formation, control and novel strategies for eradication," in *Science against microbial pathogens: communicating current research and technological advances* (A. Méndez-Vilas, ed.), pp. 896–905, Formatex Research Center, 2011. <http://www.formatex.info/microbiology3/book/896-905.pdf>.
- [5] S. K. Lower, M. F. Hochella, and T. J. Beveridge, "Bacterial recognition of mineral surfaces: nanoscale interactions between *Shewanella* and alpha-FeOOH.," *Science*, vol. 292, pp. 1360–3, 2001. <http://www.ncbi.nlm.nih.gov/pubmed/11359008>.
- [6] A. J. Francis, "Microbial dissolution and stabilization of toxic metals and radionuclides in mixed wastes," *Experientia*, vol. 46, pp. 840–851, 1990. <http://link.springer.com/article/10.1007%2F2FBF01935535>.

- [7] P. G. Falkowski, T. Fenchel, and E. F. Delong, "The microbial engines that drive Earth's biogeochemical cycles.," *Science*, vol. 320, no. 5879, pp. 1034–9, 2008. <http://www.ncbi.nlm.nih.gov/pubmed/18497287>.
- [8] J. Hughes, Y. C. Armitage, and K. C. Symes, "Application of whole cell rhodococcal biocatalysts in acrylic polymer manufacture.," *Anton. Leeuw. Int. J. G.*, vol. 74, no. 1-3, pp. 107–18, 1998. <http://www.ncbi.nlm.nih.gov/pubmed/10068794>.
- [9] J. Ubbink and P. Schär-Zammaretti, "Probing bacterial interactions: integrated approaches combining atomic force microscopy, electron microscopy and biophysical techniques," *Micron*, vol. 36, pp. 293–320, 2005. <http://www.ncbi.nlm.nih.gov/pubmed/15857770>.
- [10] D. V. Vezenov, A. Noy, and P. Ashby, "Chemical force microscopy : probing chemical origin of interfacial forces and adhesion," *J. Adhesion Sci. Technol.*, vol. 19, p. 313, 2005. [http://www.tandfonline.com/doi/abs/10.1163/1568561054352702#.UugrFXfFK\\_E](http://www.tandfonline.com/doi/abs/10.1163/1568561054352702#.UugrFXfFK_E).
- [11] R. Walton, C. L. Freeman, A. L. Morales-Garcia, J. Harding, S. A. Rolfe, M. Geoghegan, and S. A. Banwart, "The role of extracellular DNA in cellular adhesion to silica," *Manuscript in preparation*, 2013.
- [12] P. K. Sahu, P. S. Iyer, A. M. Oak, K. R. Pardesi, and B. A. Chopade, "Characterization of eDNA from the clinical strain *Acinetobacter baumannii* AIIMS 7 and its role in biofilm formation.," *TheScientificWorldJournal*, vol. 2012, p. 973436, 2012. <http://www.pubmedcentral.nih.gov/articlerender.fcgi?artid=3346689&tool=pmcentrez&rendertype=abstract>.
- [13] J. Azeredo and R. Oliveira, "The role of hydrophobicity and exopolymers in initial adhesion and biofilm formation," in *Biofilms in medicine, industry and environmental biotechnology* (P. Lens, V. O'Flaherty, A. P. Moran, P. Stoodley, and T. Mahony, eds.), ch. 2, p. 16, Padstow, England: IWA, 2003. [http://repositorium.sdum.uminho.pt/bitstream/1822/5519/1/Biofilms\\_in\\_Medicine\\_cap2%5B1%5D.pdf](http://repositorium.sdum.uminho.pt/bitstream/1822/5519/1/Biofilms_in_Medicine_cap2%5B1%5D.pdf).
- [14] R. S. Pembrey, K. C. Marshall, and R. P. Schneider, "Cell surface analysis techniques: What do cell preparation protocols do to cell surface properties?," *Appl. Environ. Microbiol.*, vol. 65, no. 7, pp. 2877–94, 1999. <http://www.pubmedcentral.nih.gov/articlerender.fcgi?artid=91432&tool=pmcentrez&rendertype=abstract>.
- [15] K. C. Marshall and R. P. Schneider, "The relevance of X-ray photoelectron spectroscopy for analysis of microbial cell surfaces : a critical view," *Coll. Surf. B*, vol. 2, no. 93, pp. 371–376, 1994. <http://www.sciencedirect.com/science/article/pii/0927776594800502>.

- [16] B. W. Peterson, P. K. Sharma, H. C. van der Mei, and H. J. Busscher, "Bacterial cell surface damage due to centrifugal compaction," *Appl. Environ. Microbiol.*, vol. 78, no. 1, pp. 120–5, 2012. <http://www.pubmedcentral.nih.gov/articlerender.fcgi?artid=3255633&tool=pmcentrez&rendertype=abstract>.
- [17] R. Austrian, "The Gram stain and the ethiology of lobar pneumonia, an historical note," *Bacteriol. Rev.*, vol. 24, pp. 261–265, 1960. <http://www.ncbi.nlm.nih.gov/pmc/articles/PMC441053/>.
- [18] G. O. Toole, H. B. Kaplan, and R. Kolter, "Biofilm formation as microbial development," *Annu. Rev. Microbiol.*, vol. 54, pp. 49–79, 2000. <http://www.ncbi.nlm.nih.gov/pubmed/11018124>.
- [19] H. Heukelekian and A. Heller, "Relation between food concentration and surface for bacterial growth," *J. Bacteriol.*, vol. 40, no. 4, pp. 547–58, 1940. <http://www.pubmedcentral.nih.gov/articlerender.fcgi?artid=374658&tool=pmcentrez&rendertype=abstract>.
- [20] C. E. ZoBell, "The effect of solid surfaces upon bacterial activity," *J. Bacteriol.*, vol. 46., no. 204, pp. 39–56, 1943. <http://www.ncbi.nlm.nih.gov/pmc/articles/PMC373789/>.
- [21] J. W. Costerton, G. G. Geesev, and C. K. J. How, "How bacteria stick," *Sci. Am.*, vol. 238, p. 86, 1978. <http://www.ncbi.nlm.nih.gov/pubmed/635520>.
- [22] B. Vu, M. Chen, R. J. Crawford, and E. P. Ivanova, "Bacterial extracellular polysaccharides involved in biofilm formation," *Molecules*, vol. 14, no. 7, pp. 2535–54, 2009. <http://www.ncbi.nlm.nih.gov/pubmed/19633622>.
- [23] H.-C. Flemming and J. Wingender, "The biofilm matrix," *Nat. Rev. Microbiol.*, vol. 8, no. 9, pp. 623–33, 2010. <http://www.ncbi.nlm.nih.gov/pubmed/20676145>.
- [24] J. S. Andrews, S. A. Rolfe, W. E. Huang, J. D. Scholes, and S. A. Banwart, "Biofilm formation in environmental bacteria is influenced by different macromolecules depending on genus and species," *Environ. Microbiol.*, vol. 9, p. 2496, 2010. <http://www.ncbi.nlm.nih.gov/pubmed/20406292>.
- [25] I. D. Auerbach, C. Sorensen, H. G. Hansma, and P. A. Holden, "Physical morphology and surface properties of unsaturated *Pseudomonas putida* biofilms," *J. Bacteriol.*, vol. 182, no. 13, p. 3809, 2000. <http://jb.asm.org/content/182/13/3809>.
- [26] G. A. O'Toole and R. Kolter, "Initiation of biofilm formation in *Pseudomonas fluorescens* WCS365 proceeds via multiple, convergent signalling pathways: a genetic analysis," *Mol. Microbiol.*, vol. 28, no. 3, pp. 449–61, 1998. <http://www.ncbi.nlm.nih.gov/pubmed/9632250>.

- [27] D. Wall and D. Kaiser, "MicroReview Type IV pili and cell motility," *Mol. Microbiol.*, vol. 32, pp. 1–10, 1999. <http://www3.interscience.wiley.com/journal/119078867/abstract>.
- [28] S. A. Makin and T. J. Beveridge, "The influence of A-band and B-band lipopolysaccharide on the surface characteristics and adhesion of *Pseudomonas aeruginosa* to surfaces.," *Microbiol.-SGM*, vol. 142, pp. 299–307, 1996. <http://www.ncbi.nlm.nih.gov/pubmed/8932703>.
- [29] P. Watnick and R. Kolter, "Biofilm , city of microbes," *J. Bacteriol.*, vol. 182, no. 10, pp. 2675–2679, 2000. <http://jlb.asm.org/content/182/10/2675.full>.
- [30] M. Gjermansen, P. Ragas, C. Sternberg, S. Molin, and T. Tolker-Nielsen, "Characterization of starvation-induced dispersion in *Pseudomonas putida* biofilms.," *Environ. Microbiol.*, vol. 7, pp. 894–906, 2005. <http://www.ncbi.nlm.nih.gov/pubmed/15892708>.
- [31] Y. V. Nancharaiah, V. P. Venugopalan, S. Wuertz, P. A. Wilderer, and M. Hausner, "Compatibility of the green fluorescent protein and a general nucleic acid stain for quantitative description of a *Pseudomonas putida* biofilm.," *J. Microbiol. Meth.*, vol. 60, no. 2, pp. 179–87, 2005. <http://www.ncbi.nlm.nih.gov/pubmed/15590092>.
- [32] A. Sivan, M. Szanto, and V. Pavlov, "Biofilm development of the polyethylene-degrading bacterium *Rhodococcus ruber.*," *Appl. Microbiol. Biotechnol.*, vol. 72, no. 2, pp. 346–52, 2006. <http://www.ncbi.nlm.nih.gov/pubmed/16534612>.
- [33] M. C. M. Van Loosdrecht, J. Lyklema, W. Norde, G. Schraa, and A. J. B. Zehnder, "Electrophoretic mobility and hydrophobicity as a measure to predict the initial steps of bacterial adhesion," *Appl. Environ. Microbiol.*, vol. 53, no. 8, pp. 1898–1901, 1987. <http://www.ncbi.nlm.nih.gov/pmc/articles/PMC204021/>.
- [34] L. G. Whyte, S. J. Slagman, F. Pietrantonio, L. Bourbonnière, S. F. Koval, J. R. Lawrence, W. E. Inness, and C. W. Greer, "Physiological adaptations involved in alkane assimilation at a low temperature by *Rhodococcus sp.* strain Q15.," *Appl. Environ. Microbiol.*, vol. 65, no. 7, pp. 2961–8, 1999. <http://www.pubmedcentral.nih.gov/articlerender.fcgi?artid=91443&tool=pmcentrez&rendertype=abstract>.
- [35] H. M. Stratton, P. R. Brooks, P. C. Griffiths, and R. J. Seviour, "Cell surface hydrophobicity and mycolic acid composition of *Rhodococcus* strains isolated from activated sludge foam," *J. Ind. Microbiol. Biotechnol.*, vol. 28, pp. 264 – 267, 2002. <http://www.ncbi.nlm.nih.gov/pubmed/11986930>.
- [36] M. Geoghegan, J. S. Andrews, C. A. Biggs, K. E. Eboigbodin, D. R. Elliott, S. Rolfe, J. Scholes, R. G. J. Edyvean, L. Swanson, R. Rutkaite,

- R. Fernando, Y. Pen, and S. A. Banwart, "The polymer physics and chemistry of microbial cell attachment and adhesion," *Faraday Discuss.*, vol. 139, pp. 85–103, 2008. <http://pubs.rsc.org/en/content/articlelanding/2008/fd/b717046g#!divAbstract>.
- [37] I. C. Sutcliffe, A. K. Brown, and L. G. Dover, "The rhodococcal cell envelope: composition, organisation and biosynthesis," in *Biology of Rhodococcus* (H. M. Alvarez, ed.), vol. 16 of *Microbiology Monographs*, pp. 29–72, Berlin: Springer Berlin Heidelberg, 2010. <http://link.springer.com/10.1007/978-3-642-12937-7>.
- [38] I. C. Sutcliffe, "Cell envelope composition and organisation in the genus *Rhodococcus*," *Anton. Leeuw. Int. J. G.*, vol. 74, no. 1-3, pp. 49–58, 1998. <http://www.ncbi.nlm.nih.gov/pubmed/10068788>.
- [39] T. J. Silhavy, D. Kahne, and S. Walker, "The bacterial cell envelope," *Cold Spring Harb. Perspect. Biol.*, vol. 2, no. 5, p. a000414, 2010. <http://www.pubmedcentral.nih.gov/articlerender.fcgi?artid=2857177&tool=pmcentrez&rendertype=abstract>.
- [40] B. Bendinger, H. H. M. Rijnaarts, K. Altendorf, and A. J. B. Zehnder, "Physicochemical cell surface and adhesive properties of coryneform bacteria related to the presence and chain length of mycolic acids," *Appl. Environ. Microbiol.*, vol. 59, no. 11, pp. 3973–3977, 1993. <http://www.ncbi.nlm.nih.gov/pmc/articles/PMC182562/>.
- [41] A. Zaragoza, F. J. Aranda, M. J. Espuny, J. A. Teruel, A. Marques, A. Manresa, and A. Ortiz, "Hemolytic activity of a bacterial trehalose lipid biosurfactant produced by *Rhodococcus sp.*: evidence for a colloid-osmotic mechanism," *Langmuir*, vol. 26, p. 8567, 2010. <http://www.ncbi.nlm.nih.gov/pubmed/20146489>.
- [42] S. Lang and J. C. Philp, "Surface-active lipids in rhodococci," *Anton. Leeuw. Int. J. G.*, vol. 74, pp. 59–70, 1998. <http://link.springer.com/article/10.1023%2FA%3A1001799711799>.
- [43] L. Martínková, B. Uhnáková, M. Pátek, J. Nešvera, and V. Křen, "Biodegradation potential of the genus *Rhodococcus*," *Environ. Int.*, vol. 35, pp. 162–177, 2009. <http://www.ncbi.nlm.nih.gov/pubmed/18789530>.
- [44] E. Y. Rosenberg and H. Nikaido, "Fluidity of the lipid domain of cell wall from *Mycobacterium chelonae*," *Proc. Natl. Acad. Sci. USA*, vol. 92, pp. 11254–11258, 1995. <http://www.ncbi.nlm.nih.gov/pmc/articles/PMC40610/>.
- [45] H. Bredholt, P. Bruheim, M. Potocky, and K. Eimhjellen, "Hydrophobicity development, alkane oxidation, and crude-oil emulsification in a *Rhodococcus* species," *Can. J. Microbiol.*, vol. 48, pp. 295–304, 2002. <http://www.ncbi.nlm.nih.gov/pubmed/12030701>.

- [46] F. G. Rie, M. Elflein, M. Benk, B. Schiffler, R. Benz, N. Garton, and I. Sutcliffe, "The cell wall of the pathogenic bacterium *Rhodococcus equi* contains two channel-forming proteins with different properties.," *J. Bacteriol.*, vol. 185, no. 9, pp. 2952–2960, 2003. <http://www.ncbi.nlm.nih.gov/pubmed/12700275>.
- [47] P. Rapp, H. Bock, V. Wray, and F. Wagner, "Formation, isolation and characterization of trehalose dimycolates from *Rhodococcus erythropolis* grown on n-alkanes," *J. Gen. Microbiol.*, vol. 115, no. 2, pp. 491–503, 1979. <http://mic.sgmjournals.org/cgi/doi/10.1099/00221287-115-2-491>.
- [48] M. Petrusma, G. Hessels, L. Dijkhuizen, and R. van der Geize, "Multiplicity of 3-ketosteroid-9 $\alpha$ -hydroxylase enzymes in *Rhodococcus rhodochrous* DSM43269 for specific degradation of different classes of steroids.," *J. Bacteriol.*, vol. 193, no. 15, pp. 3931–40, 2011. <http://www.pubmedcentral.nih.gov/articlerender.fcgi?artid=3147496&tool=pmcentrez&rendertype=abstract>.
- [49] J. S. Uotila, M. S. Salkinoja-Salonen, and J. H. Apajalahti, "Dechlorination of pentachlorophenol by membrane bound enzymes of *Rhodococcus chlorophenolicus* PCP-I.," *Biodegradation*, vol. 2, no. 1, pp. 25–31, 1991. <http://www.ncbi.nlm.nih.gov/pubmed/1368474>.
- [50] Z. Kang, A. Yeung, J. M. Foght, and M. R. Gray, "Mechanical properties of hexadecane – water interfaces with adsorbed hydrophobic bacteria," *Coll. Surf. B*, vol. 62, pp. 273–279, 2008. <http://www.ncbi.nlm.nih.gov/pubmed/18093811>.
- [51] S. Yamashita, M. Satoi, Y. Iwasa, K. Honda, Y. Sameshima, T. Omasa, J. Kato, and H. Ohtake, "Utilization of hydrophobic bacterium *Rhodococcus opacus* B-4 as whole-cell catalyst in anhydrous organic solvents.," *Appl. Microbiol. Biotechnol.*, vol. 74, no. 4, pp. 761–7, 2007. <http://www.ncbi.nlm.nih.gov/pubmed/17123076>.
- [52] W. R. Finnerty, "The biology and genetics of the genus *Rhodococcus*," *Annu. Rev. Microbiol.*, vol. 46, p. 193, 1992. <http://www.ncbi.nlm.nih.gov/pubmed/1444254>.
- [53] N. Iwabuchi, M. Sunairi, H. Anzai, H. Morisaki, and M. Nakajima, "Relationships among colony morphotypes, cell-surface properties and bacterial adhesion to substrata in *Rhodococcus*," *Coll. Surf. B*, vol. 30, pp. 51–60, 2003. <http://www.sciencedirect.com/science/article/pii/S0927776503000365>.
- [54] H. Stratton, B. Seviour, and P. Brooks, "Activated sludge foaming: what causes hydrophobicity and can it be manipulated to control foaming?," *Wat. Sci. Tech.*, vol. 37, p. 503, 1998. <http://www.sciencedirect.com/science/article/pii/S0273122398001528>.
- [55] J. Heard, B. B. Johnson, J. D. Wells, and M. J. Angove, "Measuring 'hydrophobicity' of filamentous bacteria found in wastewater treatment plants.," *Coll. Surf.*

- B*, vol. 72, no. 2, pp. 289–94, 2009. <http://www.ncbi.nlm.nih.gov/pubmed/19477105>.
- [56] M. Hermansson, “The DLVO theory in microbial adhesion,” *Coll. Surf. B*, vol. 14, pp. 105 – 119, 1999. <http://www.sciencedirect.com/science/article/pii/S0927776599000296>.
- [57] H. J. Busscher, W. Norde, P. K. Sharma, and H. C. van der Mei, “Interfacial re-arrangement in initial microbial adhesion to surfaces,” *Curr. Opin. Colloid Interface Sci.*, vol. 15, no. 6, pp. 510–517, 2010. <http://linkinghub.elsevier.com/retrieve/pii/S1359029410000567>.
- [58] H. Abbasnezhad, M. Gray, and J. M. Foght, “Influence of adhesion on aerobic biodegradation and bioremediation of liquid hydrocarbons,” *Appl. Microbiol. Biotechnol.*, vol. 92, no. 4, pp. 653–75, 2011. <http://www.ncbi.nlm.nih.gov/pubmed/21964551>.
- [59] S. S. Yoon, R. F. Hennigan, G. M. Hilliard, U. A. Ochsner, K. Parvatiyar, M. C. Kamani, H. L. Allen, T. R. DeKievit, P. R. Gardner, U. Schwab, J. J. Rowe, B. H. Iglewski, T. R. McDermott, R. P. Mason, D. J. Wozniak, R. E. W. Hancock, M. R. Parsek, T. L. Noah, R. C. Boucher, and D. J. Hassett, “*Pseudomonas aeruginosa* anaerobic respiration in biofilms: relationships to cystic fibrosis pathogenesis,” *Dev. Cell*, vol. 3, no. 4, pp. 593–603, 2002. <http://www.ncbi.nlm.nih.gov/pubmed/12408810>.
- [60] N. J. Palleroni and M. Doudoroff, “Some properties and taxonomic sub-divisions of the genus *Pseudomonas*,” *Annu. Rev. Phytopathol.*, vol. 10, p. 73, 1972. <http://www.annualreviews.org/doi/pdf/10.1146/annurev.py.10.090172.000445>.
- [61] W. Migula, “Über ein neues System der Bakterien,” *Arb. Bakteriolog. Inst. Karlsruhe*, vol. 1, p. 235, 1894.
- [62] L. den Dooren de Jong, *Bijdrage tot de kennis van het mineralisatieproces*. PhD thesis, Nijgh & van Ditmar Uitgevers-Mij., 1926.
- [63] N. J. Palleroni, “The *Pseudomonas* story,” *Environ. Microbiol.*, vol. 12, no. 6, pp. 1377–83, 2010. <http://www.ncbi.nlm.nih.gov/pubmed/20553550>.
- [64] Nosocomial Infection National Surveillance Service, “Surveillance of hospital-acquired bacteraemia in English hospitals,” tech. rep., Public Health Laboratory Service, 2002. [http://www.hpa.org.uk/webc/HPAwebFile/HPAweb\\_C/1194947379958](http://www.hpa.org.uk/webc/HPAwebFile/HPAweb_C/1194947379958).
- [65] J. C. Davies, “*Pseudomonas aeruginosa* in cystic fibrosis: pathogenesis and persistence,” *Paediatr. Resp. Rev.*, vol. 3, pp. 128–134, 2002. <http://www.ncbi.nlm.nih.gov/pubmed/12297059>.

- [66] G. Telford, D. Wheeler, P. Williams, P. T. Tomkins, P. Appleby, H. Sewell, G. S. Stewart, B. W. Bycroft, and D. I. Pritchard, "The *Pseudomonas aeruginosa* quorum-sensing signal molecule N-(3-oxododecanoyl)-L-homoserine lactone has immunomodulatory activity.," *Infect. Immun.*, vol. 66, no. 1, pp. 36–42, 1998. <http://www.pubmedcentral.nih.gov/articlerender.fcgi?artid=107855&tool=pmcentrez&rendertype=abstract>.
- [67] D. Balasubramanian, L. Schneper, H. Kumari, and K. Mathee, "A dynamic and intricate regulatory network determines *Pseudomonas aeruginosa* virulence.," *Nucleic Acids Res.*, vol. 41, no. 1, pp. 1–20, 2013. <http://www.pubmedcentral.nih.gov/articlerender.fcgi?artid=3592444&tool=pmcentrez&rendertype=abstract>.
- [68] K. E. Nelson, C. Weinel, I. T. Paulsen, R. J. Dodson, H. Hilbert, V. A. P. Martins dos Santos, D. E. Fouts, S. R. Gill, M. Pop, M. Holmes, L. Brinkac, M. Beanan, R. T. DeBoy, S. Daugherty, J. Kolonay, R. Madupu, W. Nelson, O. White, J. Peterson, H. Khouri, I. Hance, P. Chris Lee, E. Holtzapple, D. Scanlan, K. Tran, A. Moazzez, T. Utterback, M. Rizzo, K. Lee, D. Kosack, D. Moestl, H. Wedler, J. Lauber, D. Stjepandic, J. Hoheisel, M. Straetz, S. Heim, C. Kiewitz, J. A. Eisen, K. N. Timmis, A. Düsterhöft, B. Tümmler, and C. M. Fraser, "Complete genome sequence and comparative analysis of the metabolically versatile *Pseudomonas putida* KT2440.," *Environ. Microbiol.*, vol. 4, no. 12, pp. 799–808, 2002. <http://www.ncbi.nlm.nih.gov/pubmed/12534463>.
- [69] B. García, E. R. Olivera, B. Miñambres, M. Fernández-Valverde, L. M. Cañedo, M. A. Prieto, J. L. García, M. Martínez, and J. M. Luengo, "Novel biodegradable aromatic plastics from a bacterial source," *J. Biol. Chem.*, vol. 274, no. 41, pp. 29228–29241, 1999. <http://www.jbc.org/content/274/41/29228.full.pdf+html>.
- [70] E. Anaissie, V. Fainstein, P. Miller, H. Kassamali, S. Pitlik, G. P. Bodey, and K. Rolston, "*Pseudomonas putida*. Newly recognized pathogen in patients with cancer.," *Am. J. Med.*, vol. 82, no. 6, pp. 1191–4, 1987. <http://www.ncbi.nlm.nih.gov/pubmed/3605136>.
- [71] A. Kumar, S. Kumar, and S. Kumar, "Biodegradation kinetics of phenol and catechol using *Pseudomonas putida* MTCC 1194," *Biochem. Eng. J.*, vol. 22, no. 2, pp. 151–159, 2005. <http://linkinghub.elsevier.com/retrieve/pii/S1369703X04002323>.
- [72] G. Molin and I. Nilsson, "Degradation of phenol by *Pseudomonas putida* ATCC 11172 in continuous culture at different ratios of biofilm surface to culture volume.," *Appl. Environ. Microbiol.*, vol. 50, no. 4, pp. 946–50, 1985. <http://www.pubmedcentral.nih.gov/articlerender.fcgi?artid=291774&tool=pmcentrez&rendertype=abstract>.

- [73] K.-C. Loh and S.-S. Chua, "Ortho pathway of benzoate degradation in *Pseudomonas putida*: induction of meta pathway at high substrate concentrations," *Enzyme Microb. Tech.*, vol. 30, no. 5, pp. 620–626, 2002. <http://linkinghub.elsevier.com/retrieve/pii/S0141022902000169>.
- [74] A. Rosenhahn, S. Schilp, H. J. Kreuzer, and M. Grunze, "The role of "inert" surface chemistry in marine biofouling prevention," *Phys. Chem. Chem. Phys.*, vol. 12, no. 17, pp. 4275–4286, 2010. <http://www.ncbi.nlm.nih.gov/pubmed/20407694>.
- [75] Debstar, "Protein structure," 2007. [http://commons.wikimedia.org/wiki/File:Spombe\\_Pop2p\\_protein\\_structure\\_rainbow.png#filelinks](http://commons.wikimedia.org/wiki/File:Spombe_Pop2p_protein_structure_rainbow.png#filelinks).
- [76] C. Compère, M.-N. Bellon-Fontaine, P. Bertrand, D. Costa, P. Marcus, C. Poleunis, C. M. Pradier, B. Rondot, and M. G. Walls, "Kinetics of conditioning layer formation on stainless steel immersed in sea water," *Biofouling*, vol. 17, no. 2, pp. 129–145, 2001. <http://archimer.ifremer.fr/doc/2001/publication-1701.pdf>.
- [77] S. L. Hirsh, D. R. McKenzie, N. J. Nosworthy, J. A. Denman, O. U. Sezerman, and M. M. M. Bilek, "The Vroman effect: competitive protein exchange with dynamic multilayer protein aggregates.," *Coll. Surf. B*, vol. 103, pp. 395–404, 2013. <http://www.ncbi.nlm.nih.gov/pubmed/23261559>.
- [78] J. Lyklema, W. Norde, M. van Loosdrecht, and A. Zehnder, "Adhesion of bacteria to polystyrene surfaces," *Coll. Surf.*, vol. 39, no. 1, pp. 175–187, 1989. <http://linkinghub.elsevier.com/retrieve/pii/0166662289801866>.
- [79] N. P. Boks, W. Norde, H. van der Mei, and H. J. Busscher, "Forces involved in bacterial adhesion to hydrophilic and hydrophobic surfaces," *Microbiol.-SGM*, vol. 154, pp. 3122–3133, 2008. <http://www.ncbi.nlm.nih.gov/pubmed/18832318>.
- [80] C. J. van Oss, *Interfacial Forces in Aqueous Media*. New York, USA: Marcel Dekker Inc., 1st ed., 1994.
- [81] K. C. Marshall, R. Stout, and R. Mitchell, "Mechanism of the initial events in the sorption of marine bacteria to surfaces," *J. Gen. Microbiol.*, vol. 68, no. 3, pp. 337–348, 1971. <http://mic.sgmjournals.org/cgi/doi/10.1099/00221287-68-3-337>.
- [82] J. N. Israelachvili, *Intermolecular and Surface Forces*. London: Academic Press, 2nd ed., 1991.
- [83] G. Chen and S. L. Walker, "Role of solution chemistry and ion valence on the adhesion kinetics of groundwater and marine bacteria.," *Langmuir*, vol. 23, no. 13, pp. 7162–9, 2007. <http://www.ncbi.nlm.nih.gov/pubmed/17523680>.

- [84] L. Mauclair, E. Brombacher, J. D. Bunger, and M. Zinn, "Factors controlling bacterial attachment and biofilm formation on medium-chain-length polyhydroxyalkanoates ( mcl-PHAs )," *Coll. Surf. B*, vol. 76, pp. 104–111, 2010. <http://www.ncbi.nlm.nih.gov/pubmed/19914047>.
- [85] R. M. Donlan, "Biofilms: microbial life on surfaces.," *Emer. Infect. Dis.*, vol. 8, no. 9, pp. 881–90, 2002. <http://www.pubmedcentral.nih.gov/articlerender.fcgi?artid=2732559&tool=pmcentrez&rendertype=abstract>.
- [86] H. Wang, M. Sodagari, Y. Chen, X. He, B.-M. Z. Newby, and L.-K. Ju, "Initial bacterial attachment in slow flowing systems: effects of cell and substrate surface properties.," *Coll. Surf. B*, vol. 87, no. 2, pp. 415–22, 2011. <http://www.ncbi.nlm.nih.gov/pubmed/21715146>.
- [87] L. S. Dorobantu, S. Bhattacharjee, J. M. Foght, and M. R. Gray, "Analysis of force interactions between AFM tips and hydrophobic bacteria using DLVO theory," *Langmuir*, vol. 25, p. 6968, 2009. <http://pubs.acs.org/doi/abs/10.1021/la9001237>.
- [88] A. Méndez-Vilas, A. M. Gallardo-Moreno, R. Calzado-Montero, and M. L. González-Martín, "AFM probing in aqueous environment of *Staphylococcus epidermidis* cells naturally immobilised on glass: physico-chemistry behind the successful immobilisation.," *Coll. Surf. B*, vol. 63, no. 1, pp. 101–9, 2008. <http://www.ncbi.nlm.nih.gov/pubmed/18166445>.
- [89] M. Kuřec and T. Brányik, "The role of physicochemical interactions and FLO genes expression in the immobilization of industrially important yeasts by adhesion.," *Coll. Surf. B*, vol. 84, no. 2, pp. 491–7, 2011. <http://www.ncbi.nlm.nih.gov/pubmed/21367588>.
- [90] A. M. Gallardo-Moreno, M. L. Navarro-Pérez, V. Vadillo-Rodríguez, J. M. Bruque, and M. L. González-Martín, "Insights into bacterial contact angles: difficulties in defining hydrophobicity and surface Gibbs energy," *Coll. Surf. B*, vol. 88, no. 1, pp. 373–380, 2011. <http://linkinghub.elsevier.com/retrieve/pii/S092777651100419X>.
- [91] L. S. Dorobantu, S. Bhattacharjee, J. M. Foght, and M. R. Gray, "Analysis of force interactions between AFM tips and hydrophobic bacteria using DLVO theory.," *Langmuir*, vol. 25, no. 12, pp. 6968–76, 2009. <http://www.ncbi.nlm.nih.gov/pubmed/19334745>.
- [92] A. Kumar and Y.-P. Ting, "Effect of sub-inhibitory antibacterial stress on bacterial surface properties and biofilm formation.," *Coll. Surf. B*, vol. 111C, pp. 747–754, 2013. <http://www.ncbi.nlm.nih.gov/pubmed/23934235>.

- [93] B. W. Blokzijl and J. B. F. N. Engberts, "Hydrophobic effects. Opinions and facts," *Angew. Chem. Int. Ed.*, vol. 32, p. 1545, 1993. <http://onlinelibrary.wiley.com/doi/10.1002/anie.199315451/abstract>.
- [94] K. C. Marshall and R. H. Cruickshank, "Cell surface hydrophobicity and the orientation of certain bacteria at interfaces.," *Arch. Mikrobiol.*, vol. 91, no. 1, pp. 29–40, 1973. <http://www.ncbi.nlm.nih.gov/pubmed/4711456>.
- [95] R. J. Doyle, "Contribution of the hydrophobic effect to microbial infection.," *Microbes Infect.*, vol. 2, no. 4, pp. 391–400, 2000. <http://www.ncbi.nlm.nih.gov/pubmed/10817641>.
- [96] G. Di Bonaventura, R. Piccolomini, D. Paludi, V. D. Orio, A. Vergara, M. Conter, and A. Ianieri, "Influence of temperature on biofilm formation by *Listeria monocytogenes* on various food-contact surfaces : relationship with motility and cell surface hydrophobicity," *J. Appl. Microbiol.*, vol. 104, pp. 1552–1561, 2008. <http://www.ncbi.nlm.nih.gov/pubmed/18194252>.
- [97] M. A. Moorman, C. A. Thelemann, S. Zhou, J. J. Pestka, J. E. Linz, and E. T. Ryser, "Altered hydrophobicity and membrane composition in stress-adapted *Listeria innocua*," *J. Food Protect.*, vol. 71, no. 1, pp. 182–5, 2008. <http://www.ncbi.nlm.nih.gov/pubmed/18236681>.
- [98] C. C. C. R. de Carvalho, L. Y. Wick, and H. J. Heipieper, "Cell wall adaptations of planktonic and biofilm *Rhodococcus erythropolis* cells to growth on C5 to C16 n-alkane hydrocarbons.," *Appl. Microbiol. Biotechnol.*, vol. 82, no. 2, pp. 311–20, 2009. <http://www.ncbi.nlm.nih.gov/pubmed/19096838>.
- [99] H. M. Pouran, *The role of mineral surface properties on bacterial adhesion*. PhD thesis, The University of Sheffield, 2010.
- [100] Y. H. An and R. J. Friedman, "Concise review of mechanisms of bacterial adhesion to biomaterial surfaces.," *J. Biomed. Mater. Res.*, vol. 43, no. 3, pp. 338–48, 1998. <http://www.ncbi.nlm.nih.gov/pubmed/9730073>.
- [101] K. E. Eboigbodin and C. A. Biggs, "Characterization of the extracellular polymeric substances produced by *Escherichia coli* using infrared spectroscopic, proteomic, and aggregation studies.," *Biomacromolecules*, vol. 9, no. 2, pp. 686–95, 2008. <http://www.ncbi.nlm.nih.gov/pubmed/18186609>.
- [102] R. Bos, H. C. van Der Mei, and H. J. Busscher, "Physico-chemistry of initial microbial adhesive interactions—its mechanisms and methods for study.," *FEMS Microbiol. Rev.*, vol. 23, no. 2, pp. 179–230, 1999. <http://www.ncbi.nlm.nih.gov/pubmed/10234844>.
- [103] P. E. Kolenbrander, R. J. Palmer, S. Periasamy, and N. S. Jakubovics, "Oral multispecies biofilm development and the key role of cell-cell distance.," *Nat. Rev.*

- Microbiol.*, vol. 8, no. 7, pp. 471–480, 2010. <http://www.ncbi.nlm.nih.gov/pubmed/20514044>.
- [104] S. N. Ramakrishna, L. Y. Clasohm, A. Rao, and N. D. Spencer, “Controlling adhesion force by means of nanoscale surface roughness,” *Langmuir*, vol. 27, pp. 9972–9978, 2011. <http://www.ncbi.nlm.nih.gov/pubmed/21721580>.
- [105] L. Mei, H. J. Busscher, H. C. van der Mei, and Y. Ren, “Influence of surface roughness on streptococcal adhesion forces to composite resins,” *Dent. Mater.*, vol. 27, no. 8, pp. 770–8, 2011. <http://www.ncbi.nlm.nih.gov/pubmed/21524789>.
- [106] E. P. Ivanova, V. K. Truong, J. Y. Wang, C. C. Berndt, R. T. Jones, I. I. Yusuf, I. Peake, H. W. Schmidt, C. Fluke, D. Barnes, and R. J. Crawford, “Impact of nanoscale roughness of titanium thin film surfaces on bacterial retention,” *Langmuir*, vol. 26, no. 11, pp. 1973–1982, 2010. <http://www.ncbi.nlm.nih.gov/pubmed/19842625>.
- [107] I. M. Pelin, A. Piednoir, D. Machon, P. Farge, C. Pirat, and S. M. M. Ramos, “Adhesion forces between AFM tips and superficial dentin surfaces,” *J. Colloid Interf. Sci.*, vol. 376, no. 1, pp. 262–8, 2012. <http://www.ncbi.nlm.nih.gov/pubmed/22472512>.
- [108] G. S. Lorite, C. M. Rodrigues, A. A. de Souza, C. Kranz, B. Mizaikoff, and M. A. Cotta, “The role of conditioning film formation and surface chemical changes on *Xylella fastidiosa* adhesion and biofilm evolution,” *J. Colloid Interf. Sci.*, vol. 359, no. 1, pp. 289–95, 2011. <http://www.ncbi.nlm.nih.gov/pubmed/21486669>.
- [109] S. Montero-Pancera, V. Trouillet, A. Petershans, D. Fichtner, A. Lyapin, M. Bruns, T. Schimmel, D. Wedlich, S. Reichlmaier, P. G. Weidler, and H. Gliemann, “Design of chemically activated polymer microwells by one-step UV-lithography for stem cell adhesion,” *Langmuir*, vol. 26, no. 19, pp. 2050–2056, 2010. <http://www.ncbi.nlm.nih.gov/pubmed/19799401>.
- [110] T. Ishizaki, N. Saito, and O. Takai, “Correlation of cell adhesive behaviors on superhydrophobic, superhydrophilic, and micropatterned superhydrophobic/superhydrophilic surfaces to their surface chemistry,” *Langmuir*, vol. 26, no. 11, pp. 8147–54, 2010. <http://www.ncbi.nlm.nih.gov/pubmed/20131757>.
- [111] E. P. Ivanova, V. K. Truong, H. K. Webb, V. A. Baulin, J. Y. Wang, N. Mohammadi, F. Wang, C. Fluke, and R. J. Crawford, “Differential attraction and repulsion of *Staphylococcus aureus* and *Pseudomonas aeruginosa* on molecularly smooth titanium films,” *Sci. Rep.*, vol. 1, p. 165, 2011. <http://www.nature.com/doi/10.1038/srep00165>.
- [112] K. A. Whitehead, D. Rogers, J. Colligon, C. Wright, and J. Verran, “Use of the atomic force microscope to determine the effect of substratum surface topography

- on the ease of bacterial removal,” *Coll. Surf. B*, vol. 51, pp. 44–53, 2006. <http://www.ncbi.nlm.nih.gov/pubmed/16822658>.
- [113] G. Hauser, G. J. Curiel, H. W. Bellin, H. J. Cnossen, J. Hoffmann, J. Kastelein, E. Partington, Y. Peltier, and A. W. Timperley, “Hygienic equipment design criteria,” tech. rep., European Hygienic Engineering and Design Group, 2009. <http://www.ehedg.org/guidelines/doc8.htm#8>.
- [114] H. Gu, S. Hou, C. Yongyat, S. De Tore, and D. Ren, “Patterned biofilm formation reveals a mechanism for structural heterogeneity in bacterial biofilms,” *Langmuir*, vol. 29, pp. 11145–11153, 2013. <http://www.ncbi.nlm.nih.gov/pubmed/23919925>.
- [115] J. M. Meinders, H. C. V. D. Mei, and H. J. Busscher, “In situ enumeration of bacterial adhesion in a parallel plate flow chamber- elimination or in focus flowing bacteria from the analysis,” *J. Microbiol. Meth.*, vol. 16, pp. 119–124, 1992. <http://www.sciencedirect.com/science/article/pii/016770129290031X>.
- [116] M. Rosenberg, D. Gutnick, and E. Rosenberg, “Adherence of bacteria to hydrocarbons: a simple method for measuring cell-surface hydrophobicity,” *FEMS Microbiol. Lett.*, vol. 9, p. 29, 1980. <http://onlinelibrary.wiley.com/doi/10.1111/j.1574-6968.1980.tb05599.x/abstract>.
- [117] C. W. Zoueki, N. Tufenkji, and S. Ghoshal, “A modified microbial adhesion to hydrocarbons assay to account for the presence of hydrocarbon droplets,” *J. Coll. Int. Sci.*, vol. 344, no. 2, pp. 492–6, 2010. <http://www.ncbi.nlm.nih.gov/pubmed/20129613>.
- [118] J. S. Andrews and S. A. Rolfe, “MATH measurements of bacterial strains in n-decane,” *Personal Communication*, 2013.
- [119] D. Daffonchio, J. Thaveesri, and W. Verstraete, “Contact angle measurement and cell hydrophobicity of granular sludge from upflow anaerobic sludge bed reactors,” *Appl. Environ. Microbiol.*, vol. 61, no. 10, pp. 3676–3680, 1995. <http://www.ncbi.nlm.nih.gov/pubmed/16535148>.
- [120] W. W. Wilson, M. M. Wade, S. C. Holman, and F. R. Champlin, “Status of methods for assessing bacterial cell surface charge,” *J. Microbiol. Meth.*, vol. 43, pp. 153–164, 2001. <http://www.sciencedirect.com/science/article/pii/S0167701200002244>.
- [121] G. Binnig, C. F. Quate, and C. Gerber, “Atomic Force Microscope,” *Phys. Rev. Lett.*, vol. 56, p. 930, 1986. [http://prl.aps.org/abstract/PRL/v56/i9/p930\\_1](http://prl.aps.org/abstract/PRL/v56/i9/p930_1).
- [122] F. Moreno-Herrero and J. Gomez-Herrero, “AFM: basic concepts,” in *Atomic Force Microscopy in Liquid* (A. M. Baro and R. G. Reifengerger, eds.), pp. 3–34, Weinheim: Wiley-VCH, 2012.

- [123] W. F. Heinz and J. H. Hoh, "Getting physical with your chemistry : mechanically investigating local structure and properties of surfaces with the atomic force microscope," *J. Chem. Ed.*, vol. 82, no. 5, pp. 695–703, 2005. <http://pubs.acs.org/doi/abs/10.1021/ed082p695>.
- [124] "MFP-3D Manual," 2008.
- [125] C. S. Hodges, "Measuring forces with the AFM: polymeric surfaces in liquids.," *Adv. Colloid Interfac.*, vol. 99, no. 1, pp. 13–75, 2002. <http://www.ncbi.nlm.nih.gov/pubmed/12405400>.
- [126] I. Chasiotis, "Atomic force microscopy in solid mechanics," in *Springer Handbook of Experimental Solid Mechanics* (W. Sharpe, ed.), ch. 17, pp. 409–448, Springer, 2008. [http://download.springer.com/static/pdf/197/chp%253A10.1007%252F978-0-387-30877-7\\_17.pdf?auth66=1391123934\\_a09f284a7ce55db6062b5c986c20b009&ext=.pdf](http://download.springer.com/static/pdf/197/chp%253A10.1007%252F978-0-387-30877-7_17.pdf?auth66=1391123934_a09f284a7ce55db6062b5c986c20b009&ext=.pdf).
- [127] M. A. Hopcroft, W. D. Nix, and T. W. Kenny, "What is the Young's modulus of silicon?," *J. Microelectromech. S.*, vol. 19, no. 2, pp. 229–238, 2010. <http://ieeexplore.ieee.org/lpdocs/epic03/wrapper.htm?arnumber=5430873>.
- [128] M. J. Doktycz, C. J. Sullivan, N. P. Mortensen, and D. P. Allison, "Microbial cell imaging using atomic force microscopy," in *Life at the Nanoscale* (Y. F. Dufrène, ed.), ch. 3, pp. 45–70, Singapore: Pan Stanford Publishing, 1st ed., 2011.
- [129] Olympus, "Biolever." [http://probe.olympus-global.com/en/product/bl\\_rc150vb\\_hw/index.cfm](http://probe.olympus-global.com/en/product/bl_rc150vb_hw/index.cfm).
- [130] Bruker, "MLCT probes," 2013. <https://www.brukerafmprobes.com/Product.aspx?ProductID=3444>.
- [131] A. Noy, D. V. Vezenov, and C. M. Lieber, "Chemical force microscopy," *Annu. Rev. Mater. Sci.*, vol. 27, no. 1, pp. 381–421, 1997. <http://www.annualreviews.org/doi/abs/10.1146/annurev.matsci.27.1.381>.
- [132] C. D. Frisbie, L. F. Rozsnyai, A. Noy, M. S. Wrighton, and C. M. Lieber, "Functional group imaging by chemical force microscopy," *Science*, vol. 265, no. 5181, pp. 2071–4, 1994. <http://www.ncbi.nlm.nih.gov/pubmed/17811409>.
- [133] S. K. Lower, C. J. Tadanier, and M. F. Hochella, "Dynamics of the mineral – microbe interface : use of biological force microscopy in biogeochemistry and geomicrobiology," *Geomicrobiol. J.*, vol. 18, no. September 2000, pp. 63–76, 2001. [http://www.physics.uoguelph.ca/psi/papers/Bacteria%20&%20Biofilms/Bacteria\\_AFM/Lower\\_Geomicrobiol01.pdf](http://www.physics.uoguelph.ca/psi/papers/Bacteria%20&%20Biofilms/Bacteria_AFM/Lower_Geomicrobiol01.pdf).
- [134] R. Barattin and N. Voyer, "Chemical modifications of AFM tips for the study of molecular recognition events," *Chem. Comm.*, p. 1513, 2008. <http://pubs.rsc.org/en/Content/ArticleLanding/2008/CC/b614328h#!divAbstract>.

- [135] J. B. D. Green, A. Idowu, and S. S. F. Chan, "Modified tips: molecules to cells," *Mater. Today*, no. February, pp. 22–29, 2003. <http://www.materialstoday.com/characterization/articles/s1369702103002323/>.
- [136] E. Dague, D. Alsteens, J.-P. Latge, C. Verbelen, D. Raze, and Y. F. Dufrêne, "Chemical force microscopy of single live cells," *Nano Lett.*, vol. 7, no. 10, p. 3026, 2007. <http://www.ncbi.nlm.nih.gov/pubmed/17850167>.
- [137] Y. F. Dufrêne, "Direct characterization of the physicochemical properties of fungal spores using functionalized AFM probes," *Biophys. J.*, vol. 78, pp. 3286–3291, 2000. <http://linkinghub.elsevier.com/retrieve/pii/S0006349500768640>.
- [138] D. Alsteens, E. Dague, P. G. Rouxhet, A. R. Baulard, and Y. F. Dufrêne, "Direct measurement of hydrophobic forces on cell surfaces using AFM," *Langmuir*, vol. 23, pp. 11977–11979, 2007. <http://www.ncbi.nlm.nih.gov/pubmed/17941657>.
- [139] D. Alsteens, C. Verbelen, E. Dague, D. Raze, A. R. Baulard, and Y. F. Dufrêne, "Organization of the mycobacterial cell wall : a nanoscale view," *Pflugers Arch. Eur. J. Physiol.*, vol. 456, pp. 117–125, 2008. <http://www.ncbi.nlm.nih.gov/pubmed/18043940>.
- [140] V. Vadillo-Rodriguez, H. J. Busscher, W. Norde, J. D. Vries, and H. C. V. D. Mei, "Dynamic cell surface hydrophobicity of *Lactobacillus* strains with and without surface layer proteins," *J. Bacteriol.*, vol. 186, no. 19, pp. 6647–6650, 2004. <http://www.ncbi.nlm.nih.gov/pmc/articles/PMC516583/>.
- [141] V. Vadillo-Rodriguez, *Macroscopic and microscopic approaches toward bacterial adhesion*. PhD thesis, Rijksuniversiteit Groningen, 2004. <http://dissertations.ub.rug.nl/faculties/medicine/2004/v.vadillo.rodriguez/?pLanguage=en&pFullItemRecord=ON>.
- [142] L. S. Dorobantu, S. Bhattacharjee, J. M. Foght, and M. R. Gray, "Atomic force microscopy measurement of heterogeneity in bacterial surface hydrophobicity," *Langmuir*, vol. 24, pp. 4944–4951, 2008. <http://www.ncbi.nlm.nih.gov/pubmed/18355095>.
- [143] J. K. Gimzewski and C. Joachim, "Nanoscale science of single molecules using local probes," *Science*, vol. 283, p. 1683, 1999. <http://www.sciencemag.org/content/283/5408/1683>.
- [144] N. Liu, B. Peng, Y. Lin, Z. Su, Z. Niu, Q. Wang, W. Zhang, H. Li, and J. Shen, "Pulling genetic RNA out of tobacco mosaic virus using single-molecule force spectroscopy," *J. Am. Chem. Soc.*, vol. 132, no. 32, pp. 11036–8, 2010. <http://www.ncbi.nlm.nih.gov/pubmed/20698668>.
- [145] J. Alegre-Cebollada, R. Perez-Jimenez, P. Kosuri, and J. M. Fernandez, "Single-molecule force spectroscopy approach to enzyme catalysis," *J. Biol. Chem.*,

- vol. 285, no. 25, pp. 18961–6, 2010. <http://www.pubmedcentral.nih.gov/articlerender.fcgi?artid=2885171&tool=pmcentrez&rendertype=abstract>.
- [146] S. Lebeer, D. Alsteens, L. Wildling, H. J. Gruber, P. Hols, S. D. Keersmaecker, J. Vanderleyden, and Y. F. Dufrêne, “Conformational analysis of single polysaccharide molecules on live bacteria,” *ACS Nano*, vol. 2, no. 9, pp. 1921–1929, 2008. <http://pubs.acs.org/doi/abs/10.1021/nn800341b>.
- [147] C. Verbelen, V. Dupres, D. Raze, C. Bompard, C. Locht, and Y. F. Dufrêne, “Interaction of the mycobacterial heparin-binding hemagglutinin with actin, as evidenced by single-molecule force spectroscopy,” *J. Bacteriol.*, vol. 190, no. 23, pp. 7614–7620, 2008. <http://www.ncbi.nlm.nih.gov/pubmed/18835984>.
- [148] P. Hinterdorfer and Y. F. Dufrêne, “Detection and localization of single molecular recognition events using atomic force microscopy,” *Nat. Methods*, vol. 3, no. 5, p. 347, 2006. <http://www.nature.com/nmeth/journal/v3/n5/abs/nmeth871.html>.
- [149] J. W. Weisel, H. Shuman, and R. I. Litvinov, “Protein – protein unbinding induced by force : single-molecule studies,” *Curr. Opin. Struc. Biol.*, vol. 13, p. 227, 2003. <http://www.ncbi.nlm.nih.gov/pubmed/12727517>.
- [150] F. Kienberger, L. A. Chtcheglova, A. Ebner, T. Puntheeranurak, H. J. Gruber, and P. Hinterdorfer, “Single-molecule studies on cells and membranes using the atomic force microscope,” in *Applied Scanning Probe Methods* (B. Bushan and H. Fuchs, eds.), ch. 14, pp. 101–125, Berlin: Springer-Verlag, 1st ed., 2007. [http://link.springer.com/chapter/10.1007%2F978-3-540-37319-3\\_4](http://link.springer.com/chapter/10.1007%2F978-3-540-37319-3_4).
- [151] M. Leitner, G. E. Fantner, E. J. Fantner, K. Ivanova, T. Ivanov, I. Rangelow, A. Ebner, M. Rangl, J. Tang, and P. Hinterdorfer, “Increased imaging speed and force sensitivity for bio-applications with small cantilevers using a conventional AFM setup.,” *Micron*, vol. 43, no. 12, pp. 1399–407, 2012. <http://www.ncbi.nlm.nih.gov/pubmed/22721963>.
- [152] F. Quilès, P. Polyakov, F. Humbert, and G. Francius, “Production of extracellular glycogen by *Pseudomonas fluorescens*: spectroscopic evidence and conformational analysis by biomolecular recognition.,” *Biomacromolecules*, vol. 13, no. 7, pp. 2118–27, 2012. <http://www.ncbi.nlm.nih.gov/pubmed/22686500>.
- [153] Y. Pen, Z. Zhang, A. L. Morales-Garcia, M. Mears, D. S. Tarmey, R. G. Edyvean, S. A. Banwart, and M. Geoghegan, “Conformation and interactions of rhodococcal extracellular polymeric substances at the water-silicon interface,” *Preprint*, 2013.
- [154] S. Lower, C. J. Tadanier, and M. F. Hochella Jr., “Measuring interfacial and adhesion forces between bacteria and mineral surfaces with biological force microscopy,” *Geochim. Cosmochim. Ac.*, vol. 64, no. 18, pp. 3133–3139, 2000. <http://linkinghub.elsevier.com/retrieve/pii/S0016703700004300>.

- [155] T. L. Cail and M. F. Hochella Jr., “The effects of solution chemistry on the sticking efficiencies of viable *Enterococcus faecalis*: an atomic force microscopy and modeling study,” *Geochim. Cosmochim. Ac.*, vol. 69, no. 12, pp. 2959–2969, 2005. <http://www.sciencedirect.com/science/article/pii/S0016703705000682>.
- [156] M. Benoit, D. Gabriel, G. Gerisch, and H. E. Gaub, “Discrete interactions in cell adhesion measured by single-molecule force spectroscopy,” *Nat. Cell Biol.*, vol. 2, no. 6, pp. 313–7, 2000. <http://www.ncbi.nlm.nih.gov/pubmed/10854320>.
- [157] S. Kasas and A. Ikai, “A method for anchoring round shaped cells for atomic force microscope imaging,” *Biophys. J.*, vol. 68, pp. 1678–1680, 1995. <http://www.ncbi.nlm.nih.gov/pmc/articles/PMC1282070/>.
- [158] K. El Kirat, I. Burton, V. Dupres, and Y. F. Dufrêne, “Sample preparation procedures for biological atomic force microscopy,” *J. Microsc.*, vol. 218, no. January, pp. 199–207, 2005. <http://www.ncbi.nlm.nih.gov/pubmed/15958012>.
- [159] C. J. Sullivan, J. L. Morrell, D. P. Allison, and M. J. Doktycz, “Mounting of *Escherichia coli* spheroplasts for AFM imaging,” *Ultramicroscopy*, vol. 105, pp. 96–102, 2005. <http://www.ncbi.nlm.nih.gov/pubmed/16112809>.
- [160] R. D. Turner, N. H. Thomson, J. Kirkham, and D. Devine, “Improvement of the pore trapping method to immobilize vital coccoid bacteria for high-resolution AFM: a study of *Staphylococcus aureus*,” *J. Microsc.*, vol. 238, no. 2, pp. 102–10, 2010. <http://www.ncbi.nlm.nih.gov/pubmed/20529058>.
- [161] M. J. Doktycz, C. J. Sullivan, P. R. Hoyt, D. A. Pelletier, S. Wu, and D. P. Allison, “AFM imaging of bacteria in liquid media immobilized on gelatin coated mica surfaces,” *Ultramicroscopy*, vol. 97, no. 1-4, pp. 209–16, 2003. <http://www.ncbi.nlm.nih.gov/pubmed/12801673>.
- [162] Z. Hosseinidou, T. G. M. Van de Ven, and N. Tufenkji, “Bacterial capture efficiency and antimicrobial activity of phage-functionalized model surfaces,” *Langmuir*, vol. 27, no. 9, pp. 5472–80, 2011. <http://www.ncbi.nlm.nih.gov/pubmed/21452812>.
- [163] B. Y. Liu, G. M. Zhang, X. L. Li, and H. Chen, “Effect of glutaraldehyde fixation on bacterial cells observed by atomic force microscopy,” *Scanning*, vol. 34, no. 1, pp. 6–11, 2012. <http://www.ncbi.nlm.nih.gov/pubmed/21898456>.
- [164] L. Kailas, E. C. Ratcliffe, E. J. Hayhurst, M. G. Walker, S. J. Foster, and J. K. Hobbs, “Immobilizing live bacteria for AFM imaging of cellular processes,” *Ultramicroscopy*, vol. 109, pp. 775–780, 2009. <http://www.ncbi.nlm.nih.gov/pubmed/19268460>.
- [165] T. De, A. M. Chettoor, P. Agarwal, M. V. Salapaka, and S. Nettikadan, “Immobilization method of yeast cells for intermittent contact mode imaging using

- the atomic force microscope,” *Ultramicroscopy*, vol. 110, no. 3, pp. 254–8, 2010. <http://www.ncbi.nlm.nih.gov/pubmed/20080347>.
- [166] R. Louise Meyer, X. Zhou, L. Tang, A. Arpanaei, P. Kingshott, and F. Besenbacher, “Immobilisation of living bacteria for AFM imaging under physiological conditions,” *Ultramicroscopy*, vol. 110, no. 11, pp. 1349–57, 2010. <http://www.ncbi.nlm.nih.gov/pubmed/20619542>.
- [167] Y. Liu and T. A. Camesano, “Immobilizing bacteria for atomic force microscopy imaging of force measurements in liquids,” in *Microbial Surfaces*, ch. 10, p. 163, ACS Symposium Series, 2008. <http://pubs.acs.org/doi/abs/10.1021/bk-2008-0984.ch010>.
- [168] F. Gaboriaud, S. Bailet, E. Dague, and F. Jorand, “Surface structure and nanomechanical properties of *Shewanella putrefaciens* bacteria at two pH values (4 and 10) determined by atomic force microscopy,” *J. Bacteriol.*, vol. 187, pp. 3864–3868, 2005. [147-07d6-4704-8fe9-3538c15f2017](https://doi.org/10.1128/J. Bacteriol. 187.11.3864-3868.2005).
- [169] A. V. Bolshakova, O. I. Kiselyova, and I. V. Yaminsky, “Microbial surfaces investigated using atomic force microscopy,” *Biotechnol. Prog.*, vol. 20, pp. 1615–1622, 2004. <http://www.ncbi.nlm.nih.gov/pubmed/15575691>.
- [170] P. C. Braga and D. Ricci, “Atomic force microscopy: application to investigation of *Escherichia coli* morphology before and after exposure to cefodizime,” *Antimicrob. Agents Chemother.*, vol. 42, no. 1, pp. 18–22, 1998. <http://www.ncbi.nlm.nih.gov/pmc/articles/PMC105449/>.
- [171] A. V. Bolshakova, O. I. Kiselyova, A. S. Filonov, O. Y. Frolova, Y. L. Lyubchenko, and I. V. Yaminsky, “Comparative studies of bacteria with an atomic force microscopy operating in different modes,” *Ultramicroscopy*, vol. 86, pp. 121–128, 2001. <http://www.ncbi.nlm.nih.gov/pubmed/11215614>.
- [172] D. P. Allison, C. J. Sullivan, N. P. Mortensen, S. T. Retterer, and M. Doktycz, “Bacterial immobilization for imaging by atomic force microscopy,” *J. Vis. Exp.*, no. 54, pp. 5–7, 2011. <http://www.ncbi.nlm.nih.gov/pubmed/21860374>.
- [173] B. Cappella and G. Dietler, “Force-distance curves by atomic force microscopy,” *Surf. Sci. Rep.*, vol. 34, pp. 1–104, 1999. <http://www.see.ed.ac.uk/~vkoutsos/Force-distance%20curves%20by%20atomic%20force%20microscopy.pdf>.
- [174] B. L. Weeks, M. W. Vaughn, and J. J. DeYoreo, “Direct imaging of meniscus formation in atomic force microscopy using environmental scanning electron microscopy,” *Langmuir*, vol. 21, no. 18, pp. 8096–8, 2005. <http://www.ncbi.nlm.nih.gov/pubmed/16114907>.

- [175] B. van Der Aa, R. M. Michel, M. Ashter, M. Torrez-Zamora, P. G. Rouxhet, and Y. F. Dufrêne, “Stretching cell surface macromolecules by atomic force microscopy,” *Langmuir*, vol. 17, pp. 3116–3119, 2001. <http://pubs.acs.org/doi/abs/10.1021/la001573s>.
- [176] A. Denis, A. Touhami, B. Hoffmann, A. Vasella, and Y. F. Dufrêne, “Aggregation of yeast cells : direct measurement of discrete lectin – carbohydrate interactions,” *Microbiol.-SGM*, vol. 149, pp. 2873–2878, 2003. <http://www.ncbi.nlm.nih.gov/pubmed/14523119>.
- [177] J. J. Heinisch, V. Dupres, D. Alsteens, and Y. F. Dufrêne, “Measurement of the mechanical behavior of yeast membrane sensors using single-molecule atomic force microscopy,” *Nat. Protoc.*, vol. 5, no. 4, pp. 670–7, 2010. <http://www.ncbi.nlm.nih.gov/pubmed/20360762>.
- [178] H. C. van der Mei, H. J. Busscher, R. Bos, J. de Vries, C. J. Boonaert, and Y. F. Dufrêne, “Direct probing by atomic force microscopy of the cell surface softness of a fibrillated and nonfibrillated oral streptococcal strain,” *Biophys. J.*, vol. 78, no. 5, pp. 2668–74, 2000. <http://www.pubmedcentral.nih.gov/articlerender.fcgi?artid=1300855&tool=pmcentrez&rendertype=abstract>.
- [179] R. Bailey and J. Hobbs, “Entrapment of *Bacillus subtilis* using lithographically created pillars,” *Personal Communication*, 2013.
- [180] V. Dupres, F. D. Menozzi, C. Loch, B. H. Clare, N. L. Abbott, C. Bompard, D. Raze, and Y. F. Dufrêne, “Nanoscale mapping and functional analysis of individual adhesins on living bacteria,” *Nat. Methods*, vol. 2, no. 7, pp. 515–521, 2005. <http://www.ncbi.nlm.nih.gov/pubmed/15973422>.
- [181] M. A. Beckmann, S. Venkataraman, M. J. Doktycz, J. P. Nataro, C. J. Sullivan, J. L. Morrell-Falvey, and D. P. Allison, “Measuring cell surface elasticity on enteroaggregative *Escherichia coli* wild type and dispersin mutant by AFM,” *Ultramicroscopy*, vol. 106, pp. 695–702, 2006. <http://www.ncbi.nlm.nih.gov/pubmed/16682120>.
- [182] B. van Der Aa, M. Ashter, and Y. F. Dufrêne, “Surface properties of *Aspergillus oryzae* spores investigated by atomic force microscopy,” *Coll. Surf. B*, vol. 24, no. 3-4, pp. 277–284, 2002. <http://linkinghub.elsevier.com/retrieve/pii/S0927776501002776>.
- [183] Y. J. Oh, Y. Cui, H. Kim, Y. Li, P. Hinterdorfer, and S. Park, “Characterization of curli A production on living bacterial surfaces by scanning probe microscopy,” *Biophys. J.*, vol. 103, no. 8, pp. 1666–71, 2012. <http://www.pubmedcentral.nih.gov/articlerender.fcgi?artid=3475329&tool=pmcentrez&rendertype=abstract>.

- [184] S. Bagchi, H. Tomenius, L. M. Belova, and N. Ausmees, “Intermediate filament-like proteins in bacteria and a cytoskeletal function in *Streptomyces*,” *Mol. Microbiol.*, vol. 70, no. 4, pp. 1037–50, 2008. <http://www.pubmedcentral.nih.gov/articlerender.fcgi?artid=2680258&tool=pmcentrez&rendertype=abstract>.
- [185] F. Ahimou, M. J. Semmens, P. J. Novak, and G. Haugstad, “Biofilm cohesiveness measurement using a novel atomic force microscopy methodology,” *Appl. Environ. Microbiol.*, vol. 73, no. 9, pp. 2897–904, 2007. <http://www.pubmedcentral.nih.gov/articlerender.fcgi?artid=1892862&tool=pmcentrez&rendertype=abstract>.
- [186] S. Mangold, K. Harneit, T. Rohwerder, G. Claus, and W. Sand, “Novel combination of atomic force microscopy and epifluorescence microscopy for visualization of leaching bacteria on pyrite,” *Appl. Environ. Microbiol.*, vol. 74, no. 2, pp. 410–5, 2008. <http://www.pubmedcentral.nih.gov/articlerender.fcgi?artid=2223268&tool=pmcentrez&rendertype=abstract>.
- [187] Y. J. Oh, W. Jo, Y. Yang, and S. Park, “Influence of culture conditions on *Escherichia coli* O157:H7 biofilm formation by atomic force microscopy,” *Ultramicroscopy*, vol. 107, pp. 869–74, 2007. <http://www.ncbi.nlm.nih.gov/pubmed/17544218>.
- [188] A. N. Tsofigkas, J. Bowen, M. Winn, R. J. M. Goss, T. W. Overton, and M. J. H. Simmons, “Characterisation of spin coated engineered *Escherichia coli* biofilms using atomic force microscopy,” *Coll. Surf. B*, vol. 89, pp. 152–160, 2011. <http://www.ncbi.nlm.nih.gov/pubmed/21955509>.
- [189] C. B. Volle, M. A. Ferguson, K. E. Aidala, E. M. Spain, and M. E. Núñez, “Spring constants and adhesive properties of native bacterial biofilm cells measured by atomic force microscopy,” *Coll. Surf. B*, vol. 67, no. 1, pp. 32–40, 2008. <http://www.ncbi.nlm.nih.gov/pubmed/18815013>.
- [190] J. Otero, R. Baños, L. González, E. Torrents, A. Juárez, and M. Puig-Vidal, “Quartz tuning fork studies on the surface properties of *Pseudomonas aeruginosa* during early stages of biofilm formation,” *Coll. Surf. B*, vol. 102C, no. 2010, pp. 117–123, 2012. <http://www.ncbi.nlm.nih.gov/pubmed/23018019>.
- [191] Y. Hu, J. Zhang, and J. Ulstrup, “Interfacial electrochemical electron transfer processes in bacterial biofilm environments on Au(111),” *Langmuir*, vol. 26, no. 11, pp. 9094–103, 2010. <http://www.ncbi.nlm.nih.gov/pubmed/20334394>.
- [192] B. H. Liu, K.-L. Li, W.-K. Huang, and J.-D. Liao, “Nanomechanical probing of the septum and surrounding substances on *Streptococcus mutans* cells and biofilms,” *Coll. Surf. B*, vol. 110, pp. 356–362, 2013. <http://linkinghub.elsevier.com/retrieve/pii/S0927776513003238>.

- [193] C. Díaz, P. Schilardi, R. Salvarezza, and M. Fernández Lorenzo de Mele, “Have flagella a preferred orientation during early stages of biofilm formation?: AFM study using patterned substrates,” *Coll. Surf. B*, vol. 82, pp. 536–542, 2010. <http://linkinghub.elsevier.com/retrieve/pii/S0927776510005783>.
- [194] Y. Abe, S. Skali-Lami, J.-C. Block, and G. Francius, “Cohesiveness and hydrodynamic properties of young drinking water biofilms.,” *Water Res.*, vol. 46, no. 4, pp. 1155–66, 2012. <http://www.ncbi.nlm.nih.gov/pubmed/22221338>.
- [195] B. van Der Aa and Y. F. Dufrêne, “In situ characterization of bacterial extracellular polymeric substances by AFM,” *Coll. Surf. B*, vol. 23, pp. 173 – 182, 2002. <http://www.sciencedirect.com/science/article/pii/S0927776501002296>.
- [196] H. G. Silverman and F. F. Roberto, “Understanding marine mussel adhesion.,” *Mar. Biotechnol.*, vol. 9, no. 6, pp. 661–81, 2007. <http://www.pubmedcentral.nih.gov/articlerender.fcgi?artid=2100433&tool=pmcentrez&rendertype=abstract>.
- [197] Q. Ye, F. Zhou, and W. Liu, “Bioinspired catecholic chemistry for surface modification.,” *Chem. Soc. Rev.*, vol. 40, no. 7, pp. 4244–58, 2011. <http://www.ncbi.nlm.nih.gov/pubmed/21603689>.
- [198] J. L. Dalsin, L. Lin, S. Tosatti, J. Vörös, M. Textor, and P. B. Messersmith, “Protein resistance of titanium oxide surfaces modified by biologically inspired mPEG-DOPA.,” *Langmuir*, vol. 21, no. 2, pp. 640–6, 2005. <http://www.ncbi.nlm.nih.gov/pubmed/15641834>.
- [199] T. H. Anderson, J. Yu, A. Estrada, M. U. Hammer, J. H. Waite, and J. N. Israelachvili, “The contribution of DOPA to substrate-peptide adhesion and internal cohesion of mussel-inspired synthetic peptide films.,” *Adv. Funct. Mater.*, vol. 20, no. 23, pp. 4196–4205, 2010. <http://www.pubmedcentral.nih.gov/articlerender.fcgi?artid=3098815&tool=pmcentrez&rendertype=abstract>.
- [200] G. Bilic, C. Brubaker, P. B. Messersmith, A. S. Mallik, T. M. Quinn, C. Haller, E. Done, L. Gucciardo, S. M. Zeisberger, R. Zimmermann, J. Deprest, and A. H. Zisch, “Injectable candidate sealants for fetal membrane repair: bonding and toxicity in vitro.,” *Am. J. Obstet. Gynecol.*, vol. 202, no. 1, pp. 85.e1–9, 2010. <http://www.pubmedcentral.nih.gov/articlerender.fcgi?artid=2837921&tool=pmcentrez&rendertype=abstract>.
- [201] D. E. Fullenkamp, J. G. Rivera, Y.-K. Gong, K. H. A. Lau, L. He, R. Varshney, and P. B. Messersmith, “Mussel-inspired silver-releasing antibacterial hydrogels.,” *Biomaterials*, vol. 33, no. 15, pp. 3783–91, 2012. <http://www.pubmedcentral.nih.gov/articlerender.fcgi?artid=3367767&tool=pmcentrez&rendertype=abstract>.

- [202] J. Su, F. Chen, V. L. Cryns, and P. B. Messersmith, "Catechol polymers for pH-responsive, targeted drug delivery to cancer cells," *J. Am. Chem. Soc.*, vol. 133, no. 31, pp. 11850–3, 2011. <http://www.pubmedcentral.nih.gov/articlerender.fcgi?artid=3149454&tool=pmcentrez&rendertype=abstract>.
- [203] BD Biosciences, "BD Cell-Tak cell and tissue adhesive," 2010. Product manual.
- [204] J. H. Waite, "Evidence for a repeating 3,4-dihydroxyphenylalanine- and hydroxyproline-containing decapeptide in the adhesive protein of the mussel, *Mytilus edulis* L.," *J. Biol. Chem.*, vol. 258, no. 5, pp. 2911–5, 1983. <http://www.ncbi.nlm.nih.gov/pubmed/6298211>.
- [205] C. Ay, C. C. Lien, M. S. Hung, and C. C. Wang, "The study on mechanical response of human histiocytic lymphoma cells using an atomic force microscope," *J. Chin. Inst. Eng.*, vol. 32, no. 4, pp. 481–488, 2009. [http://www.tandfonline.com/doi/abs/10.1080/02533839.2009.9671530?journalCode=tcie20#.UupBvnd\\_vyc](http://www.tandfonline.com/doi/abs/10.1080/02533839.2009.9671530?journalCode=tcie20#.UupBvnd_vyc).
- [206] D. S. Hwang, S. B. Sim, and H. J. Cha, "Cell adhesion biomaterial based on mussel adhesive protein fused with RGD peptide.," *Biomaterials*, vol. 28, no. 28, pp. 4039–46, 2007. <http://www.ncbi.nlm.nih.gov/pubmed/17574667>.
- [207] E. S. Ovchinnikova, B. P. Krom, H. C. van der Mei, and H. J. Busscher, "Force microscopic and thermodynamic analysis of the adhesion between *Pseudomonas aeruginosa* and *Candida albicans*," *Soft Matter*, vol. 8, no. 24, p. 6454, 2012. <http://xlink.rsc.org/?DOI=c2sm25100k>.
- [208] A. Da Silva Jr and O. Teschke, "Effects of the antimicrobial peptide PGLa on live *Escherichia coli*," *BBA- Mol. Cell Res.*, vol. 1643, no. 1-3, pp. 95–103, 2003. <http://linkinghub.elsevier.com/retrieve/pii/S0167488903001629>.
- [209] T. Zhang, Y. Chao, K. Shih, X. Li, and H. Fang, "Quantification of the lateral detachment force for bacterial cells using atomic force microscope and centrifugation," *Ultramicroscopy*, vol. 111, no. 2, pp. 131–139, 2010. <http://linkinghub.elsevier.com/retrieve/pii/S0304399110002597>.
- [210] H. Xu, A. Murdaugh, W. Chen, K. E. Aidala, M. A. Ferguson, E. M. Spain, and M. E. Nuñez, "Characterizing pilus-mediated adhesion on biofilm-forming *E. coli* to chemically diverse surfaces using atomic force microscopy," *Langmuir*, vol. 29, p. 3000, 2013. <http://pubs.acs.org/doi/pdf/10.1021/la304745s>.
- [211] T. Das, P. K. Sharma, B. P. Krom, H. C. van der Mei, and H. J. Busscher, "Role of eDNA on the adhesion forces between *Streptococcus mutans* and substratum surfaces: influence of ionic strength and substratum hydrophobicity.," *Langmuir*, vol. 27, no. 16, pp. 10113–8, 2011. <http://www.ncbi.nlm.nih.gov/pubmed/21740034>.

- [212] T. Das, B. P. Krom, H. C. van der Mei, H. J. Busscher, and P. K. Sharma, "DNA-mediated bacterial aggregation is dictated by acid–base interactions," *Soft Matter*, vol. 7, no. 6, p. 2927, 2011. <http://xlink.rsc.org/?DOI=c0sm01142h>.
- [213] P. Schär-Zammaretti and J. Ubbink, "Imaging of lactic acid bacteria with AFM—elasticity and adhesion maps and their relationship to biological and structural data," *Ultramicroscopy*, vol. 97, no. 1-4, pp. 199–208, 2003. <http://linkinghub.elsevier.com/retrieve/pii/S0304399103000445>.
- [214] E. S. Ovchinnikova, B. P. Krom, H. J. Busscher, and H. C. van der Mei, "Evaluation of adhesion forces of *Staphylococcus aureus* along the length of *Candida albicans* hyphae," *BMC Microbiol.*, vol. 12, p. 281, 2012. <http://www.pubmedcentral.nih.gov/articlerender.fcgi?artid=3538519&tool=pmcentrez&rendertype=abstract>.
- [215] J. A. Younes, H. C. van der Mei, E. van den Heuvel, H. J. Busscher, and G. Reid, "Adhesion forces and coaggregation between vaginal staphylococci and lactobacilli," *PLoS ONE*, vol. 7, no. 5, p. e36917, 2012. <http://www.pubmedcentral.nih.gov/articlerender.fcgi?artid=3356358&tool=pmcentrez&rendertype=abstract>.
- [216] P. Loskill, H. Hähl, N. Thewes, C. T. Kreis, M. Bischoff, M. Herrmann, and K. Jacobs, "Influence of the subsurface composition of a material on the adhesion of staphylococci," *Langmuir*, vol. 28, no. 18, pp. 7242–8, 2012. <http://www.ncbi.nlm.nih.gov/pubmed/22475009>.
- [217] Y. Liu, J. Strauss, and T. A. Camesano, "Adhesion forces between *Staphylococcus epidermidis* and surfaces bearing self-assembled monolayers in the presence of model proteins," *Biomaterials*, vol. 29, pp. 4374–4382, 2008. <http://www.ncbi.nlm.nih.gov/pubmed/18760835>.
- [218] A. Atabek and T. A. Camesano, "Atomic force microscopy study of the effect of lipopolysaccharides and extracellular polymers on adhesion of *Pseudomonas aeruginosa*," *J. Bacteriol.*, vol. 189, no. 23, pp. 8503–9, 2007. <http://www.pubmedcentral.nih.gov/articlerender.fcgi?artid=2168939&tool=pmcentrez&rendertype=abstract>.
- [219] T. A. Camesano, M. J. Natan, and B. E. Logan, "Observation of changes in bacterial cell morphology using tapping mode atomic force microscopy," *Langmuir*, vol. 16, no. 20, pp. 4563–4572, 2000. <http://pubs.acs.org/doi/abs/10.1021/la990805o>.
- [220] G. L. Thompson, V. V. Reukov, M. P. Nikiforov, S. Jesse, S. V. Kalinin, and A. A. Vertegel, "Electromechanical and elastic probing of bacteria in a cell culture medium," *Nanotechnology*, vol. 23, no. 24, p. 245705, 2012. <http://www.ncbi.nlm.nih.gov/pubmed/22641388>.

- [221] A. Atabek, Y. Liu, P. A. Pinzón-Arango, and T. A. Camesano, “Importance of LPS structure on protein interactions with *Pseudomonas aeruginosa*,” *Coll. Surf. B*, vol. 67, no. 1, pp. 115–21, 2008. <http://www.ncbi.nlm.nih.gov/pubmed/18819781>.
- [222] A. Touhami, M. H. Jericho, J. M. Boyd, and T. J. Beveridge, “Nanoscale characterization and determination of adhesion forces of *Pseudomonas aeruginosa* pili by using atomic force microscopy,” *J. Bacteriol.*, vol. 188, no. 2, pp. 370–377, 2006. <http://jb.asm.org/content/188/2/370>.
- [223] Sigma-Aldrich, “Poly-D-lysine hydrobromide,” 2009. [http://www.sigmaaldrich.com/content/dam/sigma-aldrich/docs/Sigma/Product\\_Information\\_Sheet/1/p7886pis.pdf](http://www.sigmaaldrich.com/content/dam/sigma-aldrich/docs/Sigma/Product_Information_Sheet/1/p7886pis.pdf).
- [224] A. Razatos, Y. L. Ong, M. M. Sharma, and G. Georgiou, “Molecular determinants of bacterial adhesion monitored by atomic force microscopy,” *Proc. Natl. Acad. Sci. USA*, vol. 95, no. September, pp. 11059–11064, 1998. <http://www.ncbi.nlm.nih.gov/pubmed/9736689>.
- [225] S. B. Velegol, S. Pardi, X. Li, D. Velegol, and B. E. Logan, “AFM imaging artifacts due to bacterial cell height and AFM tip geometry,” *Langmuir*, vol. 19, pp. 851–867, 2003. <http://pubs.acs.org/doi/full/10.1021/la026440g>.
- [226] S. B. Velegol and B. E. Logan, “Contributions of bacterial surface polymers, electrostatics, and cell elasticity to the shape of AFM force curves,” *Langmuir*, vol. 18, pp. 5256–5262, 2002. <http://pubs.acs.org/doi/pdf/10.1021/la011818g>.
- [227] P. Polyakov, C. Soussen, J. Duan, J. F. L. Duval, D. Brie, and G. Francius, “Automated force volume image processing for biological samples,” *PLoS ONE*, vol. 6, no. 4, p. e18887, 2011. <http://www.pubmedcentral.nih.gov/articlerender.fcgi?artid=3084721&tool=pmcentrez&rendertype=abstract>.
- [228] M. N. Chandraprabha, P. Somasundaran, and K. A. Natarajan, “Modeling and analysis of nanoscale interaction forces between *Acidithiobacillus ferrooxidans* and AFM tip,” *Coll. Surf. B*, vol. 75, no. 1, pp. 310–8, 2010. <http://www.ncbi.nlm.nih.gov/pubmed/19800769>.
- [229] J. Zhu, Q. Li, W. Jiao, H. Jiang, W. Sand, J. Xia, X. Liu, W. Qin, G. Qiu, Y. Hu, and L. Chai, “Adhesion forces between cells of *Acidithiobacillus ferrooxidans*, *Acidithiobacillus thiooxidans* or *Leptospirillum ferrooxidans* and chalcopyrite,” *Coll. Surf. B*, vol. 94, pp. 95–100, 2012. <http://www.ncbi.nlm.nih.gov/pubmed/22341516>.
- [230] L. Arnal, D. O. Serra, N. Cattelan, M. F. Castez, L. Vázquez, R. C. Salvarezza, O. M. Yantorno, and M. E. Vela, “Adhesin contribution to nanomechanical properties of the virulent *Bordetella pertussis* envelope,” *Langmuir*, vol. 28, no. 19, pp. 7461–9, 2012. <http://www.ncbi.nlm.nih.gov/pubmed/22515332>.

- [231] E. Dague, D. T. L. Le, S. Zanna, P. Marcus, P. Loubiere, and M. Mercier-Bonin, "Probing in Vitro interactions between *Lactococcus lactis* and mucins using AFM," *Langmuir*, vol. 26, no. 4, pp. 11010–11017, 2010. <http://www.ncbi.nlm.nih.gov/pubmed/20540551>.
- [232] A. Razatos, Y.-l. Ong, M. M. Sharma, and G. Georgiou, "Evaluating the interaction of bacteria with biomaterials using atomic force microscopy," *J. Biomater. Sci. Polymer Edu.*, vol. 9, no. 12, p. 1361, 1998. <http://www.ncbi.nlm.nih.gov/pubmed/9860175>.
- [233] T. Cao, H. Tang, X. Liang, A. Wang, G. W. Auner, S. O. Salley, and K. Y. S. Ng, "Nanoscale investigation on adhesion of *E. coli* to surface modified silicone using atomic force microscopy," *Biotechnol. Bioeng.*, vol. 94, p. 167, 2006. <https://www.ncbi.nlm.nih.gov/m/pubmed/16538682/?i=2&from=/20932723/related>.
- [234] X. Li and B. E. Logan, "Analysis of bacterial adhesion using a gradient force analysis method and colloid probe atomic force microscopy," *Langmuir*, vol. 20, pp. 8817–22, 2004. <http://www.ncbi.nlm.nih.gov/pubmed/15379512>.
- [235] Y. L. Ong, A. Razatos, G. Georgiou, and M. M. Sharma, "Adhesion forces between *E. coli* bacteria and biomaterial surfaces," *Langmuir*, vol. 15, pp. 2719–2725, 1999. <http://pubs.acs.org/doi/abs/10.1021/la981104e>.
- [236] J. Burgain, C. Gaiani, G. Francius, a. M. Revol-Junelles, C. Cailliez-Grimal, S. Lebeer, H. L. P. Tytgat, J. Vanderleyden, and J. Scher, "In vitro interactions between probiotic bacteria and milk proteins probed by atomic force microscopy," *Coll. Surf. B*, vol. 104C, pp. 153–162, 2012. <http://www.ncbi.nlm.nih.gov/pubmed/23298601>.
- [237] G. Francius, R. Henry, J. F. L. Duval, E. Bruneau, J. Merlin, A. Fahs, and N. Leblond-Bourget, "Thermo-regulated adhesion of the *Streptococcus thermophilus* Δrgg0182 strain," *Langmuir*, vol. 16, p. 4847, 2013. <http://www.ncbi.nlm.nih.gov/pubmed/23530723>.
- [238] G. A. Burks, S. B. Velegol, E. Paramonova, B. E. Lindenmuth, J. D. Feick, and B. E. Logan, "Macroscopic and nanoscale measurements of the adhesion of bacteria with varying outer layer surface composition," *Langmuir*, vol. 19, pp. 2366–2371, 2003. <http://pubs.acs.org/doi/abs/10.1021/la026375a>.
- [239] D. Cunliffe, C. A. Smart, C. Alexander, and E. N. Vulfson, "Bacterial adhesion at synthetic surfaces," *Appl. Environ. Microbiol.*, vol. 65, no. 11, pp. 4995–5002, 1999. <http://www.pubmedcentral.nih.gov/articlerender.fcgi?artid=91672&tool=pmcentrez&rendertype=abstract>.
- [240] S. Karrasch, M. Dolder, F. Schabert, J. Ramsden, and A. Engel, "Covalent binding of biological samples to solid supports for scanning probe microscopy in buffer

- solution,” *Biophys. J.*, vol. 65, no. June, pp. 2437–2446, 1993. <http://www.ncbi.nlm.nih.gov/pmc/articles/PMC1225984/>.
- [241] G. Longo, L. M. Rio, C. Roduit, A. Trampuz, A. Bizzini, G. Dietler, and S. Kasas, “Force volume and stiffness tomography investigation on the dynamics of stiff material under bacterial membranes.,” *J. Mol. Recognit.*, vol. 25, no. 5, pp. 278–84, 2012. <http://www.ncbi.nlm.nih.gov/pubmed/22528189>.
- [242] D. Anselmetti, N. Griemla, W. Hellmich, K. Leffhalm, A. Ros, R. Ros, A. Sischka, and K. Tönsing, “Single cell analytics for nanobiology,” *Nanobiotechnology*, vol. 1, pp. 267–270, 2005. <http://link.springer.com/article/10.1007%2Fs12030-005-0036-6>.
- [243] A. Cerf, J.-C. Cau, C. Vieu, and E. Dague, “Nanomechanical properties of dead or alive single-patterned bacteria,” *Langmuir*, vol. 25, no. 19, pp. 5731–5736, 2009. <http://pubs.acs.org/doi/pdf/10.1021/la9004642>.
- [244] N. H. Thomson, “Atomic Force Microscopy of DNA Structure and Interactions,” in *Applied Scanning Probe Methods* (B. Bhushan and S. Kawata, eds.), ch. 15, p. 127, Springer Berlin Heidelberg, 1st ed., 2007. [http://link.springer.com/chapter/10.1007%2F978-3-540-37319-3\\_5](http://link.springer.com/chapter/10.1007%2F978-3-540-37319-3_5).
- [245] C. Stanford, M. Dagenais, J.-H. Park, and P. DeShong, “Real-time monitoring of siloxane monolayer film formation on silica using a fiber Bragg grating,” *Curr. Anal. Chem.*, vol. 4, no. 4, pp. 356–361, 2008. <http://www.eurekaselect.com/openurl/content.php?genre=article&issn=1573-4110&volume=4&issue=4&spage=356>.
- [246] M. Guillot, M. Richard-Plouet, and S. Vilminot, “Structural characterisations of a lamellar organic–inorganic nickel silicate obtained by hydrothermal synthesis from nickel acetate and (aminopropyl)triethoxysilane,” *J. Mater. Chem.*, vol. 12, no. 4, pp. 851–857, 2002. <http://xlink.rsc.org/?DOI=b110101c>.
- [247] V. K. Sarin, S. B. Kent, J. P. Tam, and R. B. Merrifield, “Quantitative monitoring of solid-phase peptide synthesis by the ninhydrin reaction.,” *Anal. Biochem.*, vol. 117, no. 1, pp. 147–57, 1981. <http://www.ncbi.nlm.nih.gov/pubmed/7316187>.
- [248] J.-L. Chen, S. Lin, and L.-P. Lin, “Rhizobial surface biopolymers and their interaction with lectin measured by atomic force microscopy,” *World J. Microb. Biot.*, vol. 22, no. 6, pp. 565–570, 2006. <http://link.springer.com/10.1007/s11274-005-9072-6>.
- [249] A. Atabek, *Investigating Bacterial Outer Membrane Polymers and Bacterial Interactions with Organic Molecules Using Atomic Force Microscopy*. PhD thesis, Worcester Polytechnic Institute, 2006. [http://www.wpi.edu/Pubs/ETD/Available/etd-082206-162049/unrestricted/Arzu\\_Atabek\\_MStthesis.pdf](http://www.wpi.edu/Pubs/ETD/Available/etd-082206-162049/unrestricted/Arzu_Atabek_MStthesis.pdf).

- [250] T. A. Camesano, *An investigation of bacterial interaction forces and bacterial adhesion to porous media*. PhD thesis, The Pennsylvania State University, 2000. <https://etda.libraries.psu.edu/paper/5811/1058>.
- [251] Y. F. Dufrêne, “Atomic force microscopy and chemical force microscopy of microbial cells,” *Nat. Protoc.*, vol. 3, no. 7, pp. 1132–8, 2008. <http://www.ncbi.nlm.nih.gov/pubmed/18600218>.
- [252] L. Abu-Lail, “Using atomic force microscopy to measure anti-adhesion effects on uropathogenic bacteria, observed in urine after cranberry juice consumption,” *J. Biomater. Nanobiotech.*, vol. 03, no. 04, pp. 533–540, 2012. <http://www.scirp.org/journal/PaperDownload.aspx?DOI=10.4236/jbnb.2012.324055>.
- [253] M. J. Doktycz, C. J. Sullivan, N. P. Mortensen, and D. P. Allison, “Microbial cell imaging using atomic force microscopy,” in *Life at the Nanoscale* (Y. F. Dufrêne, ed.), ch. 3, pp. 46–70, Singapore: Pan Stanford Publishing, 1st ed., 2011.
- [254] H. Butt, E. Wolff, S. Gould, B. Dixon Northern, C. Peterson, and P. Hansma, “Imaging cells with the atomic force microscope,” *Brit. J. Haematol.*, vol. 105, no. 3, p. 54, 1990. <http://www.ncbi.nlm.nih.gov/pubmed/22698505>.
- [255] S. Kang and M. Elimelech, “Bioinspired single bacterial cell force spectroscopy,” *Langmuir*, vol. 25, no. 21, pp. 9656–9659, 2009. <http://pubs.acs.org/doi/abs/10.1021/la902247w>.
- [256] N. I. Abu-Lail and T. A. Camesano, “Role of ionic strength on the relationship of biopolymer conformation, DLVO contributions, and steric interactions to bioadhesion of *Pseudomonas putida* KT2442,” *Biomacromolecules*, vol. 4, no. 4, pp. 1000–12, 2003. <http://www.ncbi.nlm.nih.gov/pubmed/12857085>.
- [257] J. M. Lee, H. H. L. Edwards, C. A. Pereira, and S. I. Samii, “Crosslinking of tissue-derived biomaterials in 1-ethyl-3-(3-dimethylaminopropyl)-carbodiimide (EDC),” *J. Mater. Sci.: Mat. Med.*, vol. 7, no. 9, pp. 531–541, 1996. <http://link.springer.com/10.1007/BF00122176>.
- [258] H. Mojarradi, *Coupling of substances containing a primary amine to hyaluronan via carbodiimide-mediated amidation*. PhD thesis, Uppsala Universitet, 2011. <http://www.diva-portal.org/smash/get/diva2:404392/FULLTEXT03>.
- [259] M.-J. Bañuls, R. Puchades, and A. Maquieira, “Chemical surface modifications for the development of silicon-based label-free integrated optical (IO) biosensors: a review,” *Anal. Chim. Acta*, vol. 777, pp. 1–16, 2013. <http://linkinghub.elsevier.com/retrieve/pii/S0003267013001736>.
- [260] N. E. Good, G. D. Winget, W. Winter, T. N. Connolly, S. Izawa, and R. M. M. Sing, “Hydrogen ion buffers for biological research,” *Biochemistry*, vol. 5, no. 2, p. 467, 1966. <http://pubs.acs.org/doi/pdf/10.1021/bi00866a011>.

- [261] L. Cabral, P. Giovanella, C. Gianello, F. M. Bento, R. Andrezza, and F. A. O. Camargo, "Isolation and characterization of bacteria from mercury contaminated sites in Rio Grande do Sul, Brazil, and assessment of methylmercury removal capability of a *Pseudomonas putida* V1 strain.," *Biodegradation*, vol. 24, no. 3, pp. 319–31, 2013. <http://www.ncbi.nlm.nih.gov/pubmed/22983740>.
- [262] D. J. Reasoner and E. E. Geldreich, "A new medium for the enumeration and subculture of bacteria from potable water.," *Appl. Environ. Microbiol.*, vol. 49, no. 1, pp. 1–7, 1985. <http://www.pubmedcentral.nih.gov/articlerender.fcgi?artid=238333&tool=pmcentrez&rendertype=abstract>.
- [263] A. T. Nielsen, T. Tolker-Nielsen, and K. B. Barken, "Role of commensal relationships on the spatial structure of a surface-attached microbial consortium," *Environ. Microbiol.*, vol. 2, pp. 59–68, 2000. <http://www.ncbi.nlm.nih.gov/pubmed/11243263>.
- [264] Thermo Scientific, "Sterilin™ Standard Petri Dishes, 90mm," 2013. [http://www.thermoscientific.com/ecom/servlet/productsdetail\\_11152\\_L10613\\_80492\\_14183637\\_-1](http://www.thermoscientific.com/ecom/servlet/productsdetail_11152_L10613_80492_14183637_-1).
- [265] Ibidi, "Micro-dish, 35 mm, low," 2011. <http://ibidi.com/xtproducts/en/ibidi-Labware/Open-Slides-Dishes:-ibidi-Standard-Bottom/m-Dish-35mm-low>.
- [266] M. F. D. Notter, "Selective attachment of neural cells to specific substrates including Cell-Tak, a new cellular adhesive," *Exp. Cell Res.*, vol. 177, pp. 237–246, 1988. <http://www.ncbi.nlm.nih.gov/pubmed/3391243>.
- [267] C. V. Benedict and P. T. Picciano, "Bioadhesives for cell and tissue adhesion," 1992. Patent found in <http://www.google.co.uk/patents/US5108923>.
- [268] F. Cuoq, A. Masion, J. Labille, J. Rose, F. Ziarelli, B. Prelot, and J.-Y. Bottero, "Preparation of amino-functionalized silica in aqueous conditions," *Appl. Surf. Sci.*, vol. 266, pp. 155–160, 2013. <http://linkinghub.elsevier.com/retrieve/pii/S0169433212020946>.
- [269] K. C. Vrancken, P. van der Voort, K. Possemiers, and E. F. Vansant, "Surface and structural properties of silica gel in the modification with gamma-aminopropyltriethoxysilane," *J. Colloid Interf. Sci.*, vol. 174, p. 86, 1995. <http://www.sciencedirect.com/science/article/pii/S0021979785713677>.
- [270] S. Ek, *Controlled preparation of amino-functionalized surfaces on porous silica by atomic layer deposition*. PhD thesis, Helsinki University of Technology, 2004. <http://lib.tkk.fi/Diss/2004/isbn9512274469/>.
- [271] J. Schindelin, I. Arganda-Carreras, E. Frise, V. Kaynig, M. Longair, T. Pietzsch, S. Preibisch, C. Rueden, S. Saalfeld, B. Schmid, J.-Y. Tinevez, D. J. White,

- V. Hartenstein, K. Eliceiri, P. Tomancak, and A. Cardona, "Fiji: an open-source platform for biological-image analysis," *Nat. Methods*, vol. 9, p. 676, 2012. <http://www.ncbi.nlm.nih.gov/pubmed/22743772>.
- [272] S. Dhahri, M. Ramonda, and C. Marlière, "In-situ determination of the mechanical properties of gliding or non-motile bacteria by atomic force microscopy under physiological conditions without immobilization.," *PLoS ONE*, vol. 8, no. 4, p. e61663, 2013. <http://www.pubmedcentral.nih.gov/articlerender.fcgi?artid=3625152&tool=pmcentrez&rendertype=abstract>.
- [273] A. Hall, "Personal communication on *Streptococcus pneumoniae*," *Personal Communication*, 2014.
- [274] A. Janshoff, M. Neitzert, Y. Oberdörfer, and H. Fuchs, "Force spectroscopy of molecular systems-single molecule spectroscopy of polymers and biomolecules.," *Angew. Chem. Int. Ed.*, vol. 39, no. 18, pp. 3212–3237, 2000. <http://www.ncbi.nlm.nih.gov/pubmed/11028062>.
- [275] L. S. Dorobantu and M. R. Gray, "Application of atomic force microscopy in bacterial research.," *Scanning*, vol. 32, no. 2, pp. 74–96, 2010. <http://www.ncbi.nlm.nih.gov/pubmed/20695026>.
- [276] G. J. Leggett, "Friction force microscopy of self-assembled monolayers: probing molecular organisation at the nanometre scale," *Analytica Chimica Acta*, vol. 479, no. 1, pp. 17–38, 2003. <http://linkinghub.elsevier.com/retrieve/pii/S0003267002015751>.
- [277] A. Noy, C. D. Frisbie, L. F. Rozsnyai, M. S. Wrighton, and C. M. Lieber, "Chemical force microscopy: exploiting chemically-modified tips to quantify adhesion, friction, and functional group distributions in molecular assemblies," *J. Am. Chem. Soc.*, pp. 7943–7951, 1995. [http://cmliris.harvard.edu/assets/JACS\\_117\\_7943.pdf](http://cmliris.harvard.edu/assets/JACS_117_7943.pdf).
- [278] Y.-S. Lo, N. D. Huefner, W. S. Chan, P. Dryden, B. Hagenhoff, and T. P. Beebe, "Organic and inorganic contamination on commercial AFM cantilevers," *Langmuir*, vol. 15, no. 7, pp. 6522–6526, 1999. <http://pubs.acs.org/doi/abs/10.1021/1a990371x>.
- [279] D. A. Lamprou, J. R. Smith, T. G. Nevell, E. Barbu, C. R. Willis, and J. Tsi-bouklis, "Self-assembled structures of alkanethiols on gold-coated cantilever tips and substrates for atomic force microscopy : Molecular organisation and conditions for reproducible deposition," *Appl. Surf. Sci.*, vol. 256, pp. 1961–1968, 2010. <http://eprints.port.ac.uk/1573/>.
- [280] J. C. Love, L. A. Estroff, J. K. Kriebel, R. G. Nuzzo, and G. M. Whitesides, "Self-assembled monolayers of thiolates on metals as a form of nanotechnology.,"

- Chem. Rev.*, vol. 105, no. 4, pp. 1103–69, 2005. <http://www.ncbi.nlm.nih.gov/pubmed/15826011>.
- [281] J. L. Hutter and J. Bechhoefer, “Calibration of atomic-force microscope tips,” *Rev. Sci. Instrum.*, vol. 64, p. 1868, 1993. <http://link.aip.org/link/RSINAK/v64/i7/p1868/s1&Agg=doi>.
- [282] T. W. Ridler and S. Calvard, “Picture thresholding using an iterative selection method,” *IEEE Trans. Systems, Man and Cybernetics*, vol. 8, pp. 630–632, 1978. [http://ieeexplore.ieee.org/xpls/abs\\_all.jsp?arnumber=4310039&tag=1](http://ieeexplore.ieee.org/xpls/abs_all.jsp?arnumber=4310039&tag=1).
- [283] Sigma-Aldrich, “Good’s buffers,” 2014. <http://www.sigmaaldrich.com/life-science/biochemicals/biochemical-products.html?TablePage=14572938>.
- [284] D. Ricci and P. C. Braga, “Recognizing and avoiding artifacts in AFM imaging,” in *Atomic Force Microscopy. Biomedical Methods and Applications*. (P. C. Braga and D. Ricci, eds.), vol. 242, ch. 3, pp. 25–37, Totowa, USA: Humana Press, 2004. <http://www.ncbi.nlm.nih.gov/pubmed/21660719>.
- [285] K. Sauer and A. K. Camper, “Characterization of phenotypic changes in *Pseudomonas putida* in response to surface-associated growth,” *J. Bacteriol.*, vol. 183, no. 22, pp. 6579–6589, 2001. <http://www.ncbi.nlm.nih.gov/pubmed/11673428>.
- [286] S. Takai, M. Iie, Y. Watanabe, S. Tsubaki, and T. Sekizaki, “Virulence-associated 15- to 17-kilodalton antigens in *Rhodococcus equi*: temperature-dependent expression and location of the antigens,” *Infect. Immun.*, vol. 60, no. 7, pp. 2995–7, 1992. <http://www.pubmedcentral.nih.gov/articlerender.fcgi?artid=257265&tool=pmcentrez&rendertype=abstract>.
- [287] V. Dupres, D. Alsteens, K. Pauwels, and Y. F. Dufrière, “In vivo imaging of S-layer nanoarrays on *Corynebacterium glutamicum*,” *Langmuir*, vol. 25, no. 17, pp. 9653–5, 2009. <http://www.ncbi.nlm.nih.gov/pubmed/19642621>.
- [288] H. C. van der Mei, J. de Vries, and H. J. Busscher, “Weibull analyses of bacterial interaction forces measured using AFM,” *Coll. Surf. B*, vol. 78, no. 2, pp. 372–5, 2010. <http://www.ncbi.nlm.nih.gov/pubmed/20399627>.
- [289] Y. Chen, H. J. Busscher, H. C. van der Mei, and W. Norde, “Statistical analysis of long- and short-range forces involved in bacterial adhesion to substratum surfaces as measured using atomic force microscopy,” *Appl. Environ. Microbiol.*, vol. 77, no. 15, pp. 5065–70, 2011. <http://www.pubmedcentral.nih.gov/articlerender.fcgi?artid=3147456&tool=pmcentrez&rendertype=abstract>.
- [290] B. J. Park and N. I. Abu-Lail, “Atomic force microscopy investigations of heterogeneities in the adhesion energies measured between pathogenic and non-pathogenic *Listeria* species and silicon nitride as they correlate to virulence and

- adherence,” *Biofouling*, vol. 27, no. 5, pp. 543–559, 2011. <http://www.ncbi.nlm.nih.gov/pmc/articles/PMC3172993/pdf/nihms-317997.pdf>.
- [291] G. S. Lorite, R. Janissen, J. a. H. Clerici, C. M. Rodrigues, J. P. Tomaz, B. Mizaikoff, C. Kranz, A. A. de Souza, and M. A. Cotta, “Surface physico-chemical properties at the micro and nano length scales: role on bacterial adhesion and *Xylella fastidiosa* biofilm development.,” *PLoS ONE*, vol. 8, no. 9, p. e75247, 2013. <http://www.pubmedcentral.nih.gov/articlerender.fcgi?artid=3779164&tool=pmcentrez&rendertype=abstract>.
- [292] V. Dupres, F. D. Menozzi, N. L. Abbot, and Y. F. Dufrêne, “AFM Imaging and Force Spectroscopy of Individual Bacterial Adhesins,” *Bruker*, 2005. <http://www.bruker.jp/axs/nano/imgs/pdf/AN092.pdf>.
- [293] V. Dupres, C. Verbelen, and Y. F. Dufrêne, “Probing molecular recognition sites on biosurfaces using AFM,” *Biomaterials*, vol. 28, pp. 2393–2402, 2007. <http://www.sciencedirect.com/science/article/pii/S0142961206009586>.
- [294] Y. Gilbert, M. Deghorain, L. Wang, B. Xu, P. D. Pollheimer, H. J. Gruber, J. Errington, B. Hallet, X. Haulot, C. Verbelen, P. Hols, and Y. F. Dufrêne, “Single-molecule force spectroscopy and imaging of the vancomycin / D -Ala-D -Ala interaction,” *Nano Lett.*, vol. 7, no. 3, p. 796, 2007. <http://pubs.acs.org/doi/abs/10.1021/nl0700853?journalCode=nalefd&quickLinkVolume=7&quickLinkPage=796&selectedTab=citation&volume=7>.
- [295] R. Afrin, T. Yamada, and A. Ikai, “Analysis of force curves obtained on the live cell membrane using chemically modified AFM probes,” *Ultramicroscopy*, vol. 100, pp. 187–195, 2004. <http://www.ncbi.nlm.nih.gov/pubmed/15231309>.
- [296] H. J. Busscher, W. Norde, and H. C. van der Mei, “Specific molecular recognition and nonspecific contributions to bacterial interaction forces,” *Appl. Environ. Microbiol.*, vol. 74, no. 9, pp. 2559–64, 2008. <http://www.pubmedcentral.nih.gov/articlerender.fcgi?artid=2394898&tool=pmcentrez&rendertype=abstract>.
- [297] S. F. Simoni, H. Harms, T. N. P. Bosma, and A. J. B. Zehnder, “Population heterogeneity affects transport of bacteria through sand columns at low flow rates,” *Environ. Sci. Technol.*, vol. 32, no. 14, pp. 2100–2105, 1998. <http://pubs.acs.org/doi/abs/10.1021/es970936g>.
- [298] J. C. Baygents, J. R. Glynn, O. Albinger, B. K. Biesemeyer, K. L. Ogden, and R. G. Arnold, “Variation of surface charge density in monoclonal bacterial populations: implications for transport through porous media,” *Environmental Science & Technology*, vol. 32, no. 11, pp. 1596–1603, 1998. <http://pubs.acs.org/doi/abs/10.1021/es9707116>.

- [299] C. H. Bolster, A. L. Mills, G. Hornberger, and J. Herman, “Effect of intra-population variability on the long-distance transport of bacteria,” *Ground Water*, vol. 38, pp. 370–375, 2000. [http://www.evsc.virginia.edu/~alm7d/pubs/71-Bolster\\_GW\\_00.pdf](http://www.evsc.virginia.edu/~alm7d/pubs/71-Bolster_GW_00.pdf).
- [300] R Core Team, “R: A language and environment for statistical computing,” 2013. <http://www.r-project.org/>.
- [301] T. Benaglia, D. R. Hunter, and D. S. Young, “mixtools : an R package for analyzing finite mixture models,” *J. Stat. Softw.*, vol. 32, p. 1, 2009. <http://cran.r-project.org/web/packages/mixtools/vignettes/mixtools.pdf>.
- [302] I. G. Costa-Filho, *Mixture models for the analysis of gene expression: integration of multiple experiments and cluster validation*. Phd, Freien Universität Berlin, 2007. <http://bioinformatics.rutgers.edu/Static/Publications/IvanGCosta-Dissertation.pdf>.
- [303] C. R. Shalizi, “Advanced data analysis,” 2012. <http://www.stat.cmu.edu/~cshalizi/uADA/12/lectures/ADafaEPoV.pdf>.
- [304] Z. Ghahramani and M. I. Jordan, “Supervised learning from incomplete data via an EM approach,” in *Advances in Neural Information Processing Systems 6* (J. D. Cowan, G. Tesauro, and J. Alspector, eds.), p. 120, San Francisco, USA: Morgan Kaufmann Publishers, 1994. <http://mlg.eng.cam.ac.uk/zoubin/papers/nips93.pdf>.
- [305] R. M. Freeman, *Analysis of avian navigation*. Phd, University of Oxford, 2008. [http://www.robots.ox.ac.uk/~parg/pubs/theses/RobinFreeman\\_thesis.pdf](http://www.robots.ox.ac.uk/~parg/pubs/theses/RobinFreeman_thesis.pdf).
- [306] D. Alsteens, V. Dupres, S. Yunus, J.-P. Latgé, J. J. Heinisch, and Y. F. Dufrêne, “High-resolution imaging of chemical and biological sites on living cells using peak force tapping atomic force microscopy,” *Langmuir*, vol. 28, no. 49, pp. 16738–44, 2012. <http://www.ncbi.nlm.nih.gov/pubmed/23198968>.
- [307] S. El-Kirat-Chatel, C. D. Boyd, G. A. O’Toole, and Y. F. Dufrêne, “Single-molecule analysis of *Pseudomonas fluorescens* footprints,” *ACS nano*, vol. Early view, 2014. <http://www.ncbi.nlm.nih.gov/pubmed/24509930>.
- [308] R. Luginbuhl, A. Szuchmacher, M. Garrison, J. Lhoest, R. Overney, and B. Ratner, “Comprehensive surface analysis of hydrophobically functionalized SFM tips,” *Ultramicroscopy*, vol. 82, no. 1-4, pp. 171–9, 2000. <http://www.ncbi.nlm.nih.gov/pubmed/10741668>.
- [309] M. Hermansson, “The DLVO theory in microbial adhesion,” *Coll. Surf. B*, vol. 14, no. 1-4, pp. 105–119, 1999. <http://linkinghub.elsevier.com/retrieve/pii/S0927776599000296>.

- [310] E. W. V. D. Vegte and G. Hadziioannou, "Scanning force microscopy with chemical specificity : an extensive study of chemically specific tip - surface interactions and the chemical imaging of surface functional groups," *Langmuir*, vol. 7463, no. 4, pp. 4357–4368, 1997. <http://pubs.acs.org/doi/pdf/10.1021/la970025k>.
- [311] J. S. Dickson and M. Koohmaraie, "Cell surface charge characteristics and their relationship to bacterial attachment to meat surfaces.," *Appl. Environ. Microbiol.*, vol. 55, no. 4, pp. 832–6, 1989. <http://www.ncbi.nlm.nih.gov/pmc/articles/PMC184210/>.
- [312] B. J. Park and N. I. Abu-Lail, "Variations in the nanomechanical properties of virulent and avirulent *Listeria monocytogenes*," *Soft Matter*, vol. 6, no. 16, pp. 3898–3909, 2011. <http://www.ncbi.nlm.nih.gov/pmc/articles/PMC2944262/>.
- [313] A. Noy, "Chemical force microscopy of chemical and biological interactions," *Surf. Interface Anal.*, vol. 38, pp. 1429–1441, 2006. [http://onlinelibrary.wiley.com/store/10.1002/sia.2374/asset/2374\\_ft.pdf?v=1&t=hqo86kac&s=440779ab6013d12802661f88d6795ad15f619984](http://onlinelibrary.wiley.com/store/10.1002/sia.2374/asset/2374_ft.pdf?v=1&t=hqo86kac&s=440779ab6013d12802661f88d6795ad15f619984).
- [314] T. A. Camesano and N. I. Abu-Lail, "Heterogeneity in bacterial surface polysaccharides, probed on a single-molecule basis," *Biomacromolecules*, vol. 3, pp. 661–667, 2002. <http://www.ncbi.nlm.nih.gov/pubmed/12099808>.
- [315] J. P. Busalmen and S. R. D. Sánchez, "Adhesion of *Pseudomonas fluorescens* (ATCC 17552 ) to nonpolarized and polarized thin films of gold," *Appl. Environ. Microbiol.*, vol. 67, pp. 3188–3194, 2001. <http://aem.asm.org/content/67/7/3188>.
- [316] A. T. A. Jenkins, R. French-Constant, A. Buckling, D. J. Clarke, and K. Jarvis, "Study of the attachment of *Pseudomonas aeruginosa* on gold and modified gold surfaces using surface plasmon resonance.," *Biotechnol. Prog.*, vol. 20, no. 4, pp. 1233–6, 2004. <http://www.ncbi.nlm.nih.gov/pubmed/15296453>.
- [317] T. Braun, N. Backmann, M. Vögtli, A. Bietsch, A. Engel, H.-P. Lang, C. Gerber, and M. Hegner, "Conformational change of bacteriorhodopsin quantitatively monitored by microcantilever sensors.," *Biophys. J.*, vol. 90, no. 8, pp. 2970–7, 2006. <http://www.pubmedcentral.nih.gov/articlerender.fcgi?artid=1414560&tool=pmcentrez&rendertype=abstract>.
- [318] R. Eckel, *Single molecules and nanocrystals: molecular recognition forces and optomechanical switching*. Phd, Bielefeld University, 2005. <http://d-nb.info/978888227/34>.
- [319] C. Sousa, P. Teixeira, S. Bordeira, J. Fonseca, and R. Oliveira, "*Staphylococcus Epidermidis* adhesion to modified polycarbonate surfaces: gold and SAMs coated," *J. Adhesion Sci. Technol.*, vol. 22, pp. 675–686, 2008. [http://www.tandfonline.com/doi/abs/10.1163/156856108X309657#.Uu1qW3d\\_vyc](http://www.tandfonline.com/doi/abs/10.1163/156856108X309657#.Uu1qW3d_vyc).

- [320] H. Ron, S. Matlis, and I. Rubinstein, "Self-assembled monolayers on oxidized metals. 2. Gold surface oxidative pretreatment, monolayer properties, and depression formation," *Langmuir*, vol. 14, no. 5, pp. 1116–1121, 1998. <http://pubs.acs.org/doi/abs/10.1021/la970785v>.
- [321] H. Busscher, "Specific and non-specific interactions in bacterial adhesion to solid substrata," *FEMS Microbiol. Lett.*, vol. 46, no. 2, pp. 165–173, 1987. [http://doi.wiley.com/10.1016/0378-1097\(87\)90062-0](http://doi.wiley.com/10.1016/0378-1097(87)90062-0).
- [322] D. M. Wagner, J. Klunk, M. Harbeck, A. Devault, N. Waglechner, J. W. Sahl, J. Enk, D. N. Birdsall, M. Kuch, C. Lumibao, D. Poinar, T. Pearson, M. Fourment, B. Golding, J. M. Riehm, D. J. D. Earn, S. DeWitte, J. M. Rouillard, G. Grupe, I. Wiechmann, J. B. Bliska, P. S. Keim, H. Scholz, E. Holmes, and H. Poinar, "*Yersinia pestis* and the Plague of Justinian 541–543 AD: a genomic analysis," *Lancet Infect. Dis.*, vol. 14, pp. 319–326, 2014. [http://www.thelancet.com/journals/laninf/article/PIIS1473-3099\(13\)70323-2/fulltext#article\\_upsell](http://www.thelancet.com/journals/laninf/article/PIIS1473-3099(13)70323-2/fulltext#article_upsell).
- [323] P. Tripathi, A. Beaussart, G. Andre, T. Rolain, S. Lebeer, J. Vanderleyden, P. Hols, and Y. F. Dufrêne, "Towards a nanoscale view of lactic acid bacteria.," *Micron* (, vol. 43, no. 12, pp. 1323–30, 2012. <http://www.ncbi.nlm.nih.gov/pubmed/22293169>.
- [324] J. A. Bravo, P. Forsythe, M. V. Chew, E. Escaravage, H. M. Savignac, T. G. Dinan, J. Bienenstock, and J. F. Cryan, "Ingestion of *Lactobacillus* strain regulates emotional behavior and central GABA receptor expression in a mouse via the vagus nerve.," *Proc. Natl. Acad. Sci. USA*, vol. 108, no. 38, pp. 16050–5, 2011. <http://www.pubmedcentral.nih.gov/articlerender.fcgi?artid=3179073&tool=pmcentrez&rendertype=abstract>.
- [325] R. Singh, D. Paul, and R. K. Jain, "Biofilms: implications in bioremediation.," *Trends Microbiol.*, vol. 14, no. 9, pp. 389–97, 2006. <http://www.ncbi.nlm.nih.gov/pubmed/16857359>.
- [326] M. Pfreundschuh, D. Martinez-Martin, E. Mulvihill, S. Wegmann, and D. J. Muller, "Multiparametric high-resolution imaging of native proteins by force-distance curve-based AFM," *Nat. Protoc.*, vol. 9, pp. 1113–1130, 2014. <http://www.nature.com/nprot/journal/v9/n5/pdf/nprot.2014.070.pdf>.
- [327] E. L. Adams, S. Almagro-Moreno, and E. F. Boyd, "An atomic force microscopy method for the detection of binding forces between bacteria and a lipid bilayer containing higher order gangliosides," *J. Microbiol. Meth.*, vol. 84, no. 2, pp. 352–4, 2011. <http://www.ncbi.nlm.nih.gov/pubmed/21192989>.
- [328] J. Wingender, T. R. Neu, and H. C. Flemming, "What are bacterial extra cellular polymeric substances?," in *Microbial Extracellular Polymeric Substances* (J. Win-

- gender, T. R. Neu, and H. C. Flemming, eds.), ch. 1, pp. 1–19, Springer Berlin Heidelberg, 1999. [http://dx.doi.org/10.1007/978-3-642-60147-7\\_1](http://dx.doi.org/10.1007/978-3-642-60147-7_1).
- [329] H. Mulcahy, L. Charron-Mazenod, and S. Lewenza, “*Pseudomonas aeruginosa* produces an extracellular deoxyribonuclease that is required for utilization of DNA as a nutrient source.,” *Environ. Microbiol.*, vol. 12, no. 6, pp. 1621–9, 2010. <http://www.ncbi.nlm.nih.gov/pubmed/20370819>.
- [330] S. E. Finkel and R. Kolter, “DNA as a nutrient: novel role for bacterial competence gene homologs,” *J. Bacteriol.*, vol. 183, no. 21, pp. 6288–6293, 2001. <http://www.ncbi.nlm.nih.gov/pmc/articles/PMC100116/>.
- [331] D. C. Dominguez, “Calcium signalling in bacteria.,” *Molecular microbiology*, vol. 54, no. 2, pp. 291–7, 2004. <http://www.ncbi.nlm.nih.gov/pubmed/15469503>.
- [332] N. Mangwani, S. K. Shukla, T. S. Rao, and S. Das, “Calcium-mediated modulation of *Pseudomonas mendocina* NR802 biofilm influences the phenanthrene degradation.,” *Coll. Surf. B*, vol. 114C, pp. 301–309, 2013. <http://www.ncbi.nlm.nih.gov/pubmed/24216621>.
- [333] S. Sarkisova, M. A. Patrauchan, D. Berglund, D. E. Nivens, and M. J. Franklin, “Calcium-induced virulence factors associated with the extracellular matrix of mucoid *Pseudomonas aeruginosa* biofilms,” *J. Bacteriol.*, vol. 187, p. 4327, 2005. <http://www.ncbi.nlm.nih.gov/pubmed/15968041>.
- [334] D. L. Nelson and M. M. Cox, “Nucleotides and nucleic acids,” in *Lehninger Principles of Biochemistry*, ch. 3rd, USA: Worth Publishers, 2000.
- [335] C. Bustamante, Z. Bryant, and S. B. Smith, “Ten years of tension: single-molecule DNA mechanics,” *Nature*, vol. 421, no. January, 2003. <http://www.nature.com/nature/journal/v421/n6921/abs/nature01405.html>.
- [336] M. Geoghegan and G. Hadziioannou, “The physics of polymers,” in *Polymer Electronics*, ch. 7, pp. 131–136, Oxford, England: Oxford University Press, 2013.
- [337] A. McNaught and A. Wilkinson, *IUPAC. Compendium of chemical terminology*. Oxford: Blackwell Scientific Publications, 2nd ed., 1997. <http://goldbook.iupac.org>.
- [338] C. Bustamante, S. B. Smith, J. Liphardt, and D. Smith, “Single-molecule studies of DNA mechanics.,” *Current opinion in structural biology*, vol. 10, no. 3, pp. 279–85, 2000. <http://www.ncbi.nlm.nih.gov/pubmed/10851197>.
- [339] G. Strobl, “Single chain conformations,” in *The Physics of Polymers*, ch. 2, pp. 15–67, Leipzig, Germany: Springer Berlin Heidelberg, 2007.

- [340] M. D. Frank-Kamenetskii, "Biophysics of the DNA molecule," *Physics Reports*, vol. 288, no. 1-6, pp. 13–60, 1997. <http://linkinghub.elsevier.com/retrieve/pii/S0370157397000203>.
- [341] N. I. Abu-Lail and T. A. Camesano, "Elasticity of *Pseudomonas putida* KT2442 surface polymers probed with single-molecule force microscopy," *Langmuir*, vol. 18, pp. 4071–4081, 2002. <http://pubs.acs.org/doi/abs/10.1021/la015695b>.
- [342] G. S. Manning, "The persistence length of DNA is reached from the persistence length of its null isomer through an internal electrostatic stretching force," *Biophys. J.*, vol. 91, no. 10, pp. 3607–16, 2006. <http://www.pubmedcentral.nih.gov/articlerender.fcgi?artid=1630458&tool=pmcentrez&rendertype=abstract>.
- [343] S. Brinkers, H. R. C. Dietrich, F. H. de Groote, I. T. Young, and B. Rieger, "The persistence length of double stranded DNA determined using dark field tethered particle motion.," *J. Chem. Phys.*, vol. 130, no. 21, p. 215105, 2009. <http://www.ncbi.nlm.nih.gov/pubmed/19508104>.
- [344] A. Galera-Prat, R. Hermans, R. Hervas, A. Gomez-Sicilia, and M. Carrion-Vazquez, "Single-molecule force spectroscopy," in *Atomic Force Microscopy in Liquid* (A. Baro and R. Reifengerger, eds.), ch. 6, pp. 157–187, Weinheim: Wiley-VCH, 1st ed., 2012.
- [345] M. C. Williams and I. Rouzina, "Force spectroscopy of single DNA and RNA molecules.," *Current opinion in structural biology*, vol. 12, no. 3, pp. 330–6, 2002. <http://www.ncbi.nlm.nih.gov/pubmed/12127451>.
- [346] J. A. Abels, F. Moreno-Herrero, T. van der Heijden, C. Dekker, and N. H. Dekker, "Single-molecule measurements of the persistence length of double-stranded RNA.," *Biophysical journal*, vol. 88, no. 4, pp. 2737–44, 2005. <http://www.pubmedcentral.nih.gov/articlerender.fcgi?artid=1305369&tool=pmcentrez&rendertype=abstract>.
- [347] K. Tanaka and Y. Okahata, "A DNA - lipid complex in organic media and formation of an aligned cast film," *J. Am. Chem. Soc.*, vol. 118, p. 10679, 1996. <http://pubs.acs.org/doi/abs/10.1021/ja9617855?journalCode=jacsat>.
- [348] R. D. Turner, *Development of Atomic Force Microscopy for Surface Analysis of Vital Bacteria*. Phd, The University of Leeds, 2009.
- [349] P. Carl, "Protein unfolding and nano-indentation analysis software," 2013. <http://punias.voila.net/>.
- [350] A. A. Hassanali and S. J. Singer, "Model for the water-amorphous silica interface: the undissociated surface.," *J. Phys. Chem. B.*, vol. 111, no. 38, pp. 11181–93, 2007. <http://www.ncbi.nlm.nih.gov/pubmed/17803296>.

- [351] W. Zhang and X. Zhang, "Single molecule mechanochemistry of macromolecules," *Prog. Polym. Sci.*, vol. 28, no. 8, pp. 1271–1295, 2003. <http://linkinghub.elsevier.com/retrieve/pii/S0079670003000467>.
- [352] Z. Zhang, M. R. Tomlinson, R. Golestanian, and M. Geoghegan, "The interfacial behaviour of single poly(N,N-dimethylacrylamide) chains as a function of pH.," *Nanotechnology*, vol. 19, no. 3, p. 035505, 2008. <http://www.ncbi.nlm.nih.gov/pubmed/21817573>.
- [353] C. Liu, W. Shi, S. Cui, Z. Wang, and X. Zhang, "Force spectroscopy of polymers: beyond single chain mechanics," *Curr. Opin. Solid State Mater. Sci.*, vol. 9, no. 3, pp. 140–148, 2005. <http://linkinghub.elsevier.com/retrieve/pii/S1359028605000343>.
- [354] K. E. Duderstadt, K. Chuang, and J. M. Berger, "DNA stretching by bacterial initiators promotes replication origin opening.," *Nature*, vol. 478, no. 7368, pp. 209–13, 2011. <http://www.pubmedcentral.nih.gov/articlerender.fcgi?artid=3192921&tool=pmcentrez&rendertype=abstract>.
- [355] J. F. Marko, "Mathematics of DNA Structure, Function and Interactions," in *Mathematics of DNA structure, functions and interactions* (C. J. Benham, S. Harvey, W. K. Olson, D. W. Sumners, and D. Swigon, eds.), vol. 150 of *The IMA Volumes in Mathematics and its Applications*, pp. 225–249, New York, NY: Springer New York, 2009. <http://link.springer.com/10.1007/978-1-4419-0670-0>.
- [356] C. Bouchiat, M. D. Wang, J. Allemand, T. Strick, S. M. Block, and V. Croquette, "Estimating the persistence length of a worm-like chain molecule from force-extension measurements.," *Biophys. J.*, vol. 76, no. 1 Pt 1, pp. 409–13, 1999. <http://www.pubmedcentral.nih.gov/articlerender.fcgi?artid=1302529&tool=pmcentrez&rendertype=abstract>.
- [357] Centers for Disease Control and Prevention (CDC), "Antibiotic resistance threats in the United States," tech. rep., U.S. Department of Health and Human Services, 2013. <http://www.cdc.gov/drugresistance/threat-report-2013/pdf/ar-threats-2013-508.pdf>.
- [358] R. J. Doyle and M. Rosenberg, *Microbial cell surface hydrophobicity*. Washington: American Society for Microbiology, 1990.
- [359] Bruker, "Introduction to Bruker's ScanAsyst and PeakForce tapping AFM technology," 2011. [http://www.bruker.com/fileadmin/user\\_upload/8-PDF-Docs/SurfaceAnalysis/AFM/ApplicationNotes/Introduction\\_to\\_Brukers\\_ScanAsyst\\_and\\_PeakForce\\_Tapping\\_Atomic\\_Force\\_Microscopy\\_Technology\\_AFM\\_AN133.pdf](http://www.bruker.com/fileadmin/user_upload/8-PDF-Docs/SurfaceAnalysis/AFM/ApplicationNotes/Introduction_to_Brukers_ScanAsyst_and_PeakForce_Tapping_Atomic_Force_Microscopy_Technology_AFM_AN133.pdf).

- [360] C. de la Fuente-Núñez, F. Reffuveille, E. F. Haney, S. K. Straus, and R. E. W. Hancock, “Broad-spectrum anti-biofilm peptide that targets a cellular stress response,” *PLoS Pathogens*, vol. 10, no. 5, p. e1004152, 2014. <http://dx.plos.org/10.1371/journal.ppat.1004152>.
- [361] R. W. Carpick, “Carpick’s Lab Software Toolbox,” 2008. <http://nanoprobenetwork.org/software-library/welcome-to-the-carpick-labs-software-toolbox>.

## Colophon

This thesis was typeset using L<sup>A</sup>T<sub>E</sub>X, TexMaker 4.02. The illustrations were designed by the author using Adobe Illustrator CS4 and CS5. The chemical formulae were designed with ChemDraw Std. 12. The SFM images and force-volume maps were acquired, formatted and analysed using IgorPro 6.22A and Gwyddion 2.34. The statistical analysis was carried out using Minitab 11 and Excel 2008 for Mac. The histograms were fit using the package *mixtools* in R 3.0.2, using a code written by Dr Stephen A. Rolfe. This thesis contains 204 figures, 351 pages, 361 references and **95500 words**. THE END.